



universität
wien

DISSERTATION / DOCTORAL THESIS

Titel der Dissertation / Title of the Doctoral Thesis

Matrix product operator symmetries
in topological phases of matter

verfasst von / submitted by

Dominic Joseph Williamson

angestrebter akademischer Grad / in partial fulfilment of the requirements for the degree of
Doktor der Naturwissenschaften (Dr. rer. nat.)

Wien, 2017

Studienkennzahl lt. Studienblatt /
Degree programme code as it appears on the student
record sheet:

A 796 605 411

Dissertationsgebiet lt. Studienblatt /
Field of study as it appears on the student record sheet:

Physik

Betreut von / Supervisor:

Univ. Prof. Dr. Frank Verstraete

*For my parents and grandparents
my teachers from the beginning
and Debra
my partner in life
I could not have done this without you.*

Contents

Zusammenfassung	11
Abstract	13
Acknowledgements	15
Introduction	17
1 Matrix product operators for symmetry-protected topological phases: gauging and edge theories	23
1.1 Introduction	24
1.2 Characterizing topological phases with matrix product operators	25
1.3 Global symmetry in PEPS	28
1.4 Symmetry-protected topological PEPS	30
1.4.1 Identifying SPT PEPS	30
1.4.2 Edge properties	31
1.5 Gauging SPT PEPS	33
1.5.1 Gauging SPT PEPS to topologically ordered PEPS	34
1.5.2 Gauging preserves the gap	35
1.6 Symmetry twists and monodromy defects	37
1.6.1 Symmetry twists in SPT PEPS	37
1.6.2 Gauging the symmetry twisted SPT PEPS	40
1.6.3 Modular transformations	40
1.6.4 Projective symmetry transformation of monodromy defects	41
1.7 Example: fixed-point SPT states	42
1.7.1 Fixed-point SPT PEPS	42
1.7.2 Gauging the fixed-point SPT PEPS	45
1.7.3 Perturbations away from fixed-points	48
1.8 Conclusions	48
Supplementary Material	50
1.9 Axioms for MPO-injectivity	50
1.10 Uniqueness of SPT PEPS ground state	51
1.11 Third cohomology class of a single block MPO group representation	53
1.12 Orientation dependencies of MPO group representations	55
1.12.1 Orientation reversing gauge transformation	55
1.12.2 Pivotal phases	56
1.13 Crossing tensors	60
1.13.1 Definitions	61
1.13.2 Composition rule	62
1.13.3 Symmetry action	63

1.13.4	Modular transformations	64
1.14	Gauging SPT PEPS yields topological PEPS	64
1.14.1	Quantum state gauging procedure	64
1.14.2	Gauging SPT PEPS	65
1.15	Generalizing the gauging procedure to arbitrary flat G-connections	66
1.15.1	Elementary definitions	67
1.15.2	Twisting and gauging operators and states	69
1.15.3	Gauging preserves the gap and leads to a topological degeneracy	71
1.16	Symmetry twists & monodromy defects	73
1.16.1	Symmetry twisted states	73
1.16.2	Topological ground states	75
1.16.3	Monodromy defects in SPT PEPS	76
1.16.4	Projective symmetry transformation of monodromy defects	77
1.17	Gauging symmetric Hamiltonians and ground states	79
1.17.1	Gauging the Hamiltonian	80
1.17.2	Disentangling the constraints	81
1.17.3	Gauging nontrivial SPT Hamiltonians	81
1.17.4	Gauging SPT groundstates	82
2	Anomalies and entanglement renormalization	85
2.1	Introduction	86
2.2	Symmetries and anomalies in MERA	87
2.2.1	Symmetries on the lattice	88
2.2.2	MERA and symmetry	89
2.2.3	On-site symmetry	90
2.2.4	Anomalous MPO symmetries	90
2.2.5	Physical data from MERA	91
2.3	Symmetry twists and topological sectors	92
2.3.1	Symmetry twist and topological correction to conformal spin	93
2.3.2	Projective representations and topological sectors	94
2.4	A class of MPO symmetric MERA	96
2.4.1	Disentangling an MPO	96
2.4.2	A class of anomalous \mathbb{Z}_N^3 MPO symmetries	97
2.4.3	Symmetric MERA tensors	98
2.5	Example: A \mathbb{Z}_2^3 symmetric model	99
2.5.1	Family of Hamiltonians	100
2.5.2	Scaling dimensions and topological sectors	100
2.5.3	Duality and domain walls	102
2.5.4	An anomaly protected gapless phase	103
2.6	Conclusions	103
	Supplementary Material	106
2.7	Conformal data in all topological sectors	106
2.8	MPO group representations and third cohomology	112
2.9	Ansatz for MERA tensors with type-III \mathbb{Z}_N^3 symmetry	115
2.9.1	4:2 MERA	115

2.9.2	Ternary MERA	116
2.10	Generalized \mathbb{Z}_N CZX model and its gapless boundary theory	117
2.10.1	Definitions	117
2.10.2	Hamiltonian and ground state	117
2.10.3	Symmetry	118
2.10.4	Boundary theory	118
2.10.5	General (1+1)D \mathcal{G} SPT duality at the edge of a (2+1)D $\mathcal{G} \times \mathcal{H}^2(\mathcal{G}, \text{U}(1))$ SPT	120

3 Symmetry-enriched topological order in tensor networks: gauging and anyon condensation 123

3.1	Introduction	124
3.2	A motivating example	125
3.2.1	Background: Constructing topological sectors in a tensor network	127
3.2.2	Symmetry-enriched tensor networks from anyon condensation	136
3.3	Symmetry-enriched string-net tensor networks	144
3.3.1	Input (graded) unitary fusion category data	144
3.3.2	Matrix product operator tensors and their fusion	147
3.3.3	String-net tensors and the pulling through equation	150
3.3.4	Symmetry-enriched string-net tensors, pulling through, and gauging	152
3.4	Oceanu's tube algebra and emergent topological order from matrix product operators	155
3.4.1	Definition of the tube algebra	155
3.4.2	Block diagonalizing the tube algebra with irreducible central idempotents	157
3.4.3	Minimally entangled states and modular matrices	158
3.4.4	Topological entanglement entropy of the superselection sectors	160
3.4.5	Fusion	161
3.4.6	Braiding	165
3.5	Symmetry-enriched topological order from matrix product operators	166
3.5.1	\mathcal{G} -graded MPO algebras	166
3.5.2	Classification via group extensions of MPO algebras	169
3.5.3	\mathcal{G} -graded MPO algebras satisfying the stronger zipper condition and \mathcal{G} -graded unitary fusion categories	172
3.5.4	SET tensor network states and the symmetry-enriched pulling through equation	178
3.5.5	Abstracting the calculus of \mathcal{G} -graded MPO algebras to diagrams	179
3.6	The defect tube algebra and emergent symmetry-enriched topological order	180
3.6.1	Definition of the tube algebra	181
3.6.2	Block diagonalizing sectors of the tube algebra with ICIs	182
3.6.3	Projective group actions on the defect ICIs	183
3.6.4	Symmetry-twisted minimally entangled states and \mathcal{G} -crossed modular matrices	186
3.6.5	Topological entanglement entropy of the defect superselection sectors	188
3.6.6	\mathcal{G} -graded fusion	189
3.6.7	\mathcal{G} -crossed braiding	192

3.6.8	Shifting by 2 and 3 cocycles	193
3.7	Gauging the global symmetry	194
3.7.1	Example: Gauging SPT orders	194
3.7.2	The general case	198
3.8	Anyon condensation phase transitions dual to gauging	200
3.8.1	MPO symmetry breaking perturbations and anyon condensation	200
3.8.2	Extracting the SET order that results from $\text{Rep}(\mathcal{G})$ anyon condensation	202
3.8.3	Using Morita equivalences to find all anyon condensation phase transitions	204
3.9	Further examples	205
3.9.1	\mathbb{Z}_2 -extension of $\text{Vec}_{\mathbb{Z}_2}$ and symmetry-enriched toric codes	205
3.9.2	Morita equivalent MPO algebras $\text{Vec}_{\mathbb{Z}_4} \sim \text{Vec}_{\mathbb{Z}_2 \times \mathbb{Z}_2}^{\omega_{\text{II}}}$ and condensation to the doubled semion model	207
3.9.3	Doubled Fibonacci model	210
3.9.4	$\mathcal{Z}(\text{Vec}_{S_3})$ and $\mathcal{Z}(\text{Rep}(S_3))$	211
3.10	Discussion and conclusions	216
4	Hamiltonian models for topological phases of matter in three spatial dimensions	221
4.1	Introduction	222
4.2	Background	223
4.2.1	State Sum TQFTs	223
4.2.2	Hamiltonians, Tensor Network Ground States and PEPO Symmetries	224
4.2.3	Review of the UGxBFC TQFT	225
4.2.4	Review of Kashaev's TQFT	234
4.3	Lattice Model for Kashaev's TQFT	235
4.3.1	The Hamiltonian	235
4.3.2	Degeneracy, Statistics, and the Ground State Wave Function	237
4.3.3	Example: \mathbb{Z}_2 Case	238
4.3.4	Back to the general case	241
4.4	Lattice Model for UGxBFC TQFT	242
4.4.1	Tensor Network Approach	242
4.4.2	Graphical Calculus Approach	243
4.4.3	Degeneracy, Statistics, and the Ground State Wave Function	249
4.5	Discussion	250
	Supplementary Material	255
4.6	Elementary combinatoric topology	255
5	Fractal symmetries: ungauging the cubic code	259
5.1	Introduction	260
5.2	Background	261
5.3	Gauging	262
5.3.1	Hamiltonian construction	263
5.3.2	Gauging procedure	264
5.3.3	Basic properties of the gauging procedure	266
5.3.4	Properties of the gauging complex	268

5.3.5	A construction from CSS stabilizer Hamiltonians	270
5.3.6	Cluster state construction & gauging	270
5.4	Fractal Symmetries	271
5.4.1	2D toric code - Ising model	271
5.4.2	3D cubic code - fractal symmetry Ising model	271
5.4.3	Self dual cluster models	272
5.5	Conclusions	272
Discussion and outlook		275
Bibliography		299
Lebenslauf		301

Zusammenfassung

Symmetrien — eine zentrales Konzept in der modernen Physik — spielen eine wichtige Rolle in der Formulierung vieler wichtiger physikalischen Theorien, wie z.B. der speziellen und allgemeinen Relativitätstheorie, der Quantenmechanik und diverser Feldtheorien bis hin zum Standardmodell der Teilchenphysik. Topologische Invarianz im Speziellen ist eine sehr starke Symmetrie, die dem tiefgreifenden Verständnis von kooperativen Phänomenen in kondensierter Materie (wie z.B. dem Quanten-Hall-Effekt), welche sich als erstaunlich robust gegenüber Störungen und Verunreinigungen erweisen, zugrunde liegt. In dieser Doktorarbeit wird ein theoretisches Grundgerüst entwickelt, das in der Lage ist, sowohl globale als auch topologische Symmetrien von sogenannten Tensornetzwerkzuständen zu beschreiben, und das Zugang zu universalen physikalischen Kenngrößen für die Klassifizierung von verschiedenen Phasen kondensierter Materie gewährt.

Zu Beginn wird ein allgemeiner Formalismus für die Beschreibung physikalischer und virtueller Symmetrien von Projected Entangled Pair State (PEPS)-Tensornetzwerken in zwei räumlichen Dimensionen entwickelt, welche aus der Kontraktion vieler Kopien ein und desselben elementaren, lokalen Tensors konstruiert werden. Dieser elementare Tensor verbindet physikalische, ortslokale Symmetrien mit virtuellen Matrixproduktoperator (MPO)-Symmetrien, welche auf die virtuellen Verschränkungsfreiheitsgrade wirken und die Grundbausteine des neuen Formalismus darstellen.

Insbesondere werden jene Systeme untersucht welche nur topologisch triviale Anregungen beinhalten um daraus die Klassifikation von symmetrie-geschützten topologischen Phasen herzuleiten. Ein Eichverfahren wird dann genau auf diese Zustände angewandt wobei gleichsam die globale Symmetrie auf eine Menge von lokalen Eichbedingungen transformiert wird. Weiters wird die daraus resultierende MPO-Symmetrietransformation dargelegt und die hieraus entstehende topologische Phase der Eichsysteme hergeleitet.

Im nächsten Schritt wird die Relevanz dieser MPO-Symmetrien für eindimensionale Oberflächenphysik untersucht. Es stellt sich heraus, dass die MPO's als Dualitätsabbildung zwischen gegapten Phasen, welche an kritischen Punkten zu Symmetrien werden, verstanden werden können. Solch ein Phasenübergang ist durch eine resultierende konforme Feldtheorie (CFT) beschrieben. Unter Verwendung der MPO Symmetrien werden topologische Sektoren, welche nichtlokale scaling Felder beinhalten können, von dieser CFT konstruiert und deren physikalische Eigenschaften studiert.

Wir entwickeln dann die allgemeine Theorie von MPO Symmetrien, welche wir mit den graduierten unitären Fusions-Kategorien identifizieren. Eine Methode zur Konstruktion von Tensor-Netzwerk-Darstellungen der Superauswahl-Sektoren, einschließlich der für extrinsische Symmetrie -Defekte, wird gegeben. Die universellen physikalischen Daten der emergenten Symmetrie-angereicherten topologischen Ordnung wird aus diesen Darstellungen abgeleitet. Der Effekt der Eichung der globalen Symmetrie wird berechnet und stellt sich als dual zum Prozess der Anyon-Kondensation, welcher von der Brechung der virtuellen MPO Symmetrie herrührt.

Ein Tensor-Netzwerk-Ansatz wird verwendet zur Konstruktion von Hamiltonians welche neue Phasen der Materie in drei räumlichen Dimensionen realisieren. Dies stellt ein Beispiel des allgemeinen Rahmens der Tensor-Netzwerk-Darstellungen von Zustandssummen, Hamiltonians, Grundzuständen, und deren Symmetrien der topologischen Quantenfeldtheorien (TQFT). Eine große Klasse von Beispielen wird abgeleitet aus einer TQFT welche kürzlich mit Hilfe der definierenden Daten einer Symmetrie-angereicherten topologischen Ordnung konstruiert wurde.

Zuletzt wird eine Verallgemeinerung der Eich-Prozedur gegeben für Symmetrien die auf Unterräumen des Gitters wirken, möglicherweise von fraktaler Dimension, welche diese auf lokale Eich-Constraints abbildet. Dies wirft neues Licht auf exotisch fracton topologische Phasen, einschließlich Haah's cubic code, welche in Termen von Symmetrien und Eichung verstanden werden können.

Abstract

Symmetry has played an essential role in the development of modern physics, from the theories of special and general relativity, to quantum mechanics, field theory and the standard model. Topological invariance is a very strong symmetry that underpins our profound understanding of emergent phenomena in condensed matter systems, such as the quantum Hall effect, that are remarkably robust to perturbation and impurity. In this thesis, we develop a theoretical framework that accommodates both global and topological symmetries of tensor network states and facilitates the extraction of universal physical data to classify the emergent phases of matter.

We begin by setting up a general formalism for the study of physical and virtual symmetries of projected entangled pair state (PEPS) tensor networks in two spatial dimensions, which are constructed by contracting many copies of a local tensor. The local tensor intertwines on-site physical symmetries to virtual matrix product operator (MPO) symmetries, acting on the entanglement degrees of freedom, which constitute the basic building blocks of our formalism.

The subclass of systems that support only topologically trivial excitations is treated in detail, from which the classification of symmetry-protected topological phases is recovered. A gauging procedure is applied directly to these states, thereby promoting the global symmetry to a set of local gauge constraints. The transformation thus induced upon the MPO symmetry is found and the emergent topological order of the gauged system is derived.

Next we study the role played by these MPO symmetries in the one-dimensional boundary physics. The MPOs are found to act as duality maps between gapped phases that become symmetries at a phase transition point. Such a phase transition is described by an emergent conformal field theory (CFT). We use the MPO symmetries to construct topological sectors of the CFT, which support nonlocal scaling fields, and derive their physical properties.

We proceed to develop the general theory of MPO symmetries, which we identify with unitary graded fusion categories. A method to construct tensor network representations of the superselection sectors, including those for extrinsic symmetry defects, is given. The universal physical data of the emergent symmetry-enriched topological order is derived from these representations. The effect of gauging the global symmetry is calculated and is found to be dual to an anyon condensation process that is induced by breaking the virtual MPO symmetry.

A tensor network approach is used to construct Hamiltonians that realize new phases of matter in three spatial dimension. This exemplifies a general framework for tensor network representations of topological quantum field theory (TQFT) partition functions, Hamiltonians, ground states, and their symmetries. A large class of examples are derived from a TQFT that was recently constructed using the defining data of a symmetry-enriched topological order.

Finally, a generalization of the gauging procedure is developed for symmetries that act on subsets of the lattice, possibly of fractal dimension, which maps them to local gauge constraints. This sheds new light on exotic fracton topological phases, including Haah's cubic code, allowing them to be understood in terms of symmetries and gauging.

Acknowledgements

“Where in the Schrödinger equation do you put the joy of being alive?”

—Eugene Wigner.

I would like to thank everyone who made the years of my PhD studies about far more than simply achieving a degree.

First, and foremost, I thank my girlfriend Debra, my family, and my friends in Sydney for their love and support. The revitalization I felt after each trip back home was invaluable for my drive to jump back into research.

I thank all the members of the Verstraete groups in Gent and Vienna, for fostering an exciting and open work environment. Particularly Damian Draxler, Martin Veznik, and Valentin Stauber for their help while I was preparing my PhD thesis.

Thanks to all my collaborators in the last few years: Stephen Bartlett, Jacob Bridgeman, Nick Bultinck, Jutho Haegeman, Michaël Mariën, Burak Şahinoğlu, Norbert Schuch, Frank Verstraete, Michael Walter, and Zhenghan Wang. Working together on various projects during my PhD was truly a pleasure.

Thanks to my fellow travelers (and tubers) Dave Aasen, Alex Turzillo, Ryan Thorngren, and numerous other PhD students I met along the way, for the hours spent shooting the breeze.

As the completion of this thesis marks the end of my institutional education, it seems fitting to thank all of the teachers who had to put up with me over the last twenty years. Although it may not have seemed like it at the time, some of the lessons did stick. I’d particularly like to thank Jason Ribbens for providing the encouragement that I needed to take my studies of mathematics as far as I could. I am also very grateful to my advisors throughout my undergraduate studies. Particularly Ross McPhedran, Yuriy Tyshetskiy, Roman Kompaneets, and Sergey Vladimirov for presenting me with the opportunity to undertake interesting research projects.

To my unofficial advisors in the Sydney quantum theory group: Stephen Bartlett, Andrew Doherty, and Steve Flammia, thanks for always making me feel welcome, and for the help with navigating various aspects of the physics life when I needed it. Thanks also to the current, and former, students of the Sydney group with whom I’ve had many an engaging discussion.

I am grateful to the Austrian Marshall Plan Foundation for providing me with the means to undertake a long term visit to UCSB, and Zhenghan Wang for his endless generosity in helping to arrange the visit and in sharing his ideas through many stimulating discussions while I was there. I would also like to thank the members of station Q, the quantum topology group and the theoretical physics students for their hospitality and some great discussions during the visit.

I am also grateful to Zhengcheng Gu, and Guifre Vidal for providing me with the opportunity to visit Perimeter institute as a graduate fellow. I appreciate the many interesting discussions I had with various residents and visitors at PI while I was there.

Last, but not least, I thank Frank Verstraete for the amazing experience of the last few years. I consider myself incredibly lucky to have landed in the group at the time I did. I am extremely grateful for the opportunity to pursue the research topics I was most interested in and for the freedom and means to follow them as far as they went. Above all, I will take away an enthusiastic approach to research which I hope to never lose.

Introduction

The consideration of symmetry has proven to be a valuable guide in the search for mathematical descriptions of natural law.

In classical physics, fundamental symmetries have been derived from the concept that the laws of physics should be the same for all observers. This is instantiated by the principle of Galilean invariance in Newtonian mechanics, invariance under the Poincaré group in special relativity, and diffeomorphism invariance in general relativity.

In quantum physics, considerations of symmetry brought about a dramatic change of course, with the proliferation of the so called “*Gruppenpest*” due to Wigner, Weyl and others. Once combined with the principle of linearity, symmetry provided powerful and explicit tools — in the form of representation theory — that led to the solution of hitherto intractable problems involving large numbers of identical particles.

In the Lagrangian formulation of physics, a famous theorem due to Noether shows that differentiable symmetries imply conservation laws. In this framework, field theories are described by systems of many degrees of freedom that interact in a purely local fashion. Symmetry considerations place strong constraints on the interactions that can occur. In the interest of harmony between symmetry and locality, the process of gauging can be used to turn a global symmetry into a local constraint. This is achieved via the introduction of gauge bosons to compensate for the transformation induced by the application of the symmetry to a local region. These ideas provided a significant boon en route to the standard model, a pinnacle amongst the achievements of modern physics.

A symmetry of the equations that govern a physical system does not necessarily translate into a symmetry of the observed solutions. Asymmetry is observed when the only symmetric solutions are given by macroscopic superpositions of distinguishable asymmetric states, which instantaneously decohere to break the symmetry. This phenomenon is known as spontaneous symmetry breaking, and it formed the basis for the discovery of Goldstone modes and, later, the Higgs boson.

Spontaneous symmetry breaking also underlies the general framework developed by Landau and Ginzburg for the description of second order phase transitions. This approach proved extremely successful in classifying phases of matter, in the presence of a global symmetry, in terms of how their low energy states spontaneously break that symmetry. The analysis is largely based on mean field theory, where the environment of each local degree of freedom is simply approximated by many copies of itself. In this decoupled description, all relevant physical information can be extracted from local measurements. The quantities that effectively diagnose these phase transitions are known as local order parameters.

Considerations of symmetries originating from the nontrivial topology of a configuration space led to new and previously unexpected phases and phase transitions, which were not predicted by mean field theory and spontaneous symmetry breaking. The Kosterlitz–Thouless transition¹ and the Haldane phase^{2,3} are notable examples — both of which went against the conventional wisdom that phase transitions could not occur in the relevant systems, as the Mermin-

Wagner theorem⁴ implies continuous symmetries cannot be spontaneously broken in two dimensions. An even stronger notion of topological symmetry, deformation invariance, underpins an elegant explanation of the astounding robustness of the quantum Hall effect⁵. The emergence of a precisely quantized value of Hall conductance from a system consisting of a vast number of interacting degrees of freedom boils down to a mathematical fact: the quantity being measured on the electronic wavefunction corresponds to a topological invariant^{6,7}. This sequence of developments, for which the 2016 Nobel prize in physics was awarded, played a large role in the reemergence of a new *Quantengruppenpest* that currently afflicts the community studying the condensed matter physics of strongly correlated quantum many-body systems^{8–10}.

The proliferation of the concept of topological symmetries also entered high energy and mathematical physics, culminating in the development of topological and conformal field theory^{11–13}. These are classes of field theories defined by a high degree of spatial symmetry, which led to the discovery of beautiful analytic and algebraic properties¹⁴. Such field theories play a key role in understanding fixed points of the renormalization group^{15,16}, which are defined by their high degree of symmetry under all renormalization transformations. For the unstable, gapless fixed points, this corresponds to a symmetry under conformal transformations. For stable, gapped fixed points — which are resilient to local deformations due to the spectral gap — this yields a stronger symmetry under arbitrary diffeomorphisms. Despite the extremely strong symmetry of topological quantum field theories — which essentially restricts their local properties to be trivial — they can exhibit extremely interesting topological features. In particular, they can yield nontrivial topological invariants, notably Witten’s formulation of the Jones polynomial^{17,18}.

The ideas of topological symmetry were brought into the newly developing field of quantum information by Kitaev, Preskill, Freedman, Wang, and others. They noticed that the topological degrees of freedom, which occur naturally in some condensed matter systems, yield good quantum error correcting codes due to their inherent robustness to local perturbations¹⁹. This observation led to the concept of topological quantum computation, where information is stored in topological degrees of freedom and all computations are implemented by changes of topology, whence robustness to local perturbations is preserved throughout arbitrary computations^{20–23}.

This inspired a new approach to the classification of quantum phases, in which gapped local Hamiltonians on the lattice — that are related by adiabatic deformation — are collected into equivalence classes^{24–27}. This mathematical formulation of the classification problem is intended to describe phases of matter, at extremely low temperatures, that are resilient to perturbations below a minimum energy scale. Although this formulation does not accurately capture all physical situations of interest, where the possibility of long wavelength phonon and photon excitations may imply there is no spectral gap²⁸, it does appear to capture the essence of the classification problem. Even in the absence of any global symmetry these equivalence classes yield distinct topological phases^{8–10}. The addition of a global symmetry further refines the classification, as the allowed adiabatic deformations must respect the symmetry property, and the topological phases split into symmetry-enriched topological (SET) phases^{29–33}. Even the trivial phase may split into nontrivial symmetry-protected topological (SPT)^{3,34–36} phases, which have neither intrinsic topological order, nor any broken symmetry.

The ground state wavefunctions in these strongly correlated quantum phases of matter are characterized by their entanglement patterns, that is, the structure of the quantum correlations

between the underlying degrees of freedom^{26,37,38}. The states in a nontrivial phase are said to be topologically ordered, a new type of ordering which cannot be detected by any local order parameter. This classification in terms of the way particles are ordered, relies little on the precise nature of the underlying degrees of freedom. This embodies the spirit of the Wilsonian renormalization group approach to physics through emergent phenomena.

A naive description of these ground state wavefunctions is marred by the curse of dimensionality, due to the exponential growth of Hilbert space dimension with the number of degrees of freedom. On a more subtle level, the resulting distributions over physical measurement outcomes cannot be efficiently sampled, in general. This is due to the notorious sign problem, a result of quantum interference, which diminishes the efficacy of the Monte Carlo methods that are ubiquitous for classical many-body systems. This has been addressed by extending the mean field approach to a more general ansatz class known as tensor network states^{39–41} which capture nontrivial local quantum correlations. This class of states maintains the crucial feature that the environment of a local degree of freedom can be efficiently approximated by a local object. This facilitates various approaches to the optimization of these ansatz states with respect to the energy of some local Hamiltonian.

The class of tensor network states forms a very general ansatz that captures many essential properties of the low energy states of local Hamiltonians^{42,43}. For gapped Hamiltonians this includes the entanglement area law⁴⁴, exponential decay of correlations and the existence of a local parent Hamiltonian^{45,46}. A single tensor from such an ansatz state provides a local window into the emergent physics, via the structure of its entanglement with the surrounding region. The use of such ansatz wavefunctions is reminiscent of the Laughlin and Moore-Read trial wavefunctions from condensed matter physics^{47,48}, although tensor networks aim to faithfully represent a more general class of groundstates.

The general efficacy of tensor network methods in condensed matter physics can be traced back to White’s famous DMRG algorithm for the optimization of spin chain ground states^{49,50}. It was later realized that the unprecedented success of this algorithm lay in the fact that it optimized over the class of matrix product states (MPS)⁵¹, which was shown to contain faithful representations of the ground states of one-dimensional Hamiltonians^{42,52}. MPS have also proven to be a useful tool in theoretical studies, including the discovery of the AKLT model^{53,54}, the formalism of finitely correlated states⁵⁵, and the recent classification of one-dimensional quantum phases^{27,56}.

This classification of quantum phases in one-dimension was based upon an analysis of how a physical symmetry could act on the virtual entanglement degrees of freedom^{27,56}. This approach was extended to the study of two-dimensional projected entangled pair states (PEPS), particularly those with topological order^{57–67}. We continue this line of inquiry by studying the interplay between physical and topological matrix product operator (MPO) symmetries on the virtual level of tensor networks in $(2 + 1)\text{D}$ and more generally. From this we construct a framework for the extraction of emergent physical data from these local symmetries.

Outline and summary of the results

The majority of this thesis focuses on the development of a formalism for the description of SET order in PEPS. Our formalism is founded on the principles of locality, linearity and symmetry, which coalesce in the form of an MPO symmetry algebra of a local PEPS tensor — the central object in our approach. We exercise this approach to study SPT states and their gapless edge theories, before moving on to general SET orders. A method to extract emergent physical data from the MPO symmetries is formulated. The effects of gauging the global symmetry, and the dual process of anyon condensation, are described. Tensor networks are used to construct new Hamiltonians for $(3 + 1)$ D topological phases of matter from the unitary G -crossed braided fusion category ($UG \times BFC$) data that describes an SET phase. Finally, we generalize the quantum state gauging procedure to symmetries that act on subsets of the lattice.

Chapter 1: In this chapter we lay a foundation for the study of global symmetry in PEPS. We expand the philosophy of MPO-injectivity⁶³, developed for the description of topological order, to capture the action of a global symmetry upon the entanglement degrees of freedom of a PEPS. The symmetry-enriched pulling through condition lies at the heart of this extension. Our formalism applies to non-injective PEPS, extending previous approaches^{68,69}, which is crucial for the description of nontrivial symmetry-protected and symmetry-enriched topological orders. We thus establish an approach to the classification of $(2 + 1)$ D SET phases in terms of the invariant labels of an MPO group representation.

We then specialize our study to SPT phases by focusing on PEPS that are MPO-injective with respect to an injective MPO. Interestingly a nontrivial MPO is still necessary for the description of nontrivial SPT phases⁶⁹. We show that such a PEPS is the unique ground state of its parent Hamiltonian⁴⁶ on any topology, and that the MPO group representation can also be picked to be injective. These MPO representations are labeled by an element of the third cohomology group, and hence the cohomology classification of $(2 + 1)$ D SPT phases³⁶ is recovered.

The MPO representation captures the action of the symmetry group upon the edge degrees of freedom of a symmetric PEPS⁷⁰. This MPO representation has an 't Hooft anomaly, specified by the third cohomology label, which constitutes an obstruction to an on-site realization of the group action. The presence of a nontrivial anomaly implies that the edge theory either spontaneously breaks the edge symmetry or is gapless.

We move on to apply the state gauging procedure, introduced in Ref. 71, to the SPT PEPS and find that the resulting PEPS falls into a twisted quantum double — or Dijkgraaf-Witten — topological phase of matter^{19,72}. This recovers the gauging approach to the classification of SPT phases⁷³.

We use our MPO group representation to construct symmetry-twisted states and monodromy defects, and to find the projective action of the global symmetry on these defects. We also calculate the transformation of symmetry-twisted states under the global symmetry and use the result to identify which states survive the gauging process.

We demonstrate our formalism with a general class of SPT fixed point PEPS examples.

Chapter 2: In this chapter we focus on the action of anomalous MPO representations of finite groups upon one-dimensional spin chains. Such models naturally arise at the boundary

of nontrivial SPT phases in $(2 + 1)\text{D}$, where the anomaly is said to be resolved by the SPT bulk^{74–76}. Such anomalous MPOs can implement dualities between distinct $(1 + 1)\text{D}$ SPT phases, that become symmetries at a critical phase transition point⁷⁷. Alternatively, they may be spontaneously broken throughout a gapped phase.

We focus our attention on MPO symmetric gapless spin chain Hamiltonians, which admit an emergent conformal field theory (CFT) description. We use the MPO representation to construct nontrivial topological superselection sectors, containing nonlocal scaling fields, and to derive general topological restrictions on conformal data that may be extracted from the lattice.

We formulate a variational subclass of the multi-scale entanglement renormalization ansatz (MERA)^{43,78} that is symmetric under an anomalous MPO representation, and apply this ansatz to numerically study an example with a symmetric critical line. The topological sectors of this model are constructed and nonlocal scaling fields are found, extending the approach taken in Ref. 79. The critical line is demonstrated to be a gapless phase protected by the anomalous MPO symmetry and translation, similar to Ref. 80. The same MPO representation is used to implement a duality between critical lines in a different parameter regime of the same example.

Chapter 3: In this chapter we develop the framework introduced in Chapter 1 to realize a constructive classification of $(2 + 1)\text{D}$ SET phases in terms of the emergent physical data extracted from a graded MPO symmetry algebra. We summarize the results of Refs. 63 and 64, explaining how the emergent topological order of a MPO-injective PEPS can be extracted from its MPO symmetry algebra. We build on this foundation to study graded MPO algebras that arise from group extensions of an underlying topological MPO symmetry algebra. We relate these graded MPO algebras to the theory of graded fusion categories⁸¹.

We extend the approach of Ref. 64 to construct a *defect tube algebra*, from which tensor network representations of the topological defect superselection sectors are derived. We describe how the physical data of the emergent SET can be extracted from our representations of the defect superselection sectors. This data specifies a G -crossed modular UGxBFC ³¹, which captures the permutation of defects, the projective symmetry action on each defect and the G -crossed modular S and T matrices.

We work out how a graded MPO algebra symmetry transforms when the state gauging procedure of Ref. 71 is applied to a SET PEPS. This is used to calculate the relationship between the physical data of an SET and that of the resulting topological order. We move on to analyze an anyon condensation phase transition, induced by MPO symmetry breaking, that is dual to the gauging transformation. Again, we work out the relationship between a topological order and the resulting SET. We describe a generalization of these MPO symmetry breaking phase transitions beyond cases that are dual to gauging a finite group. We conjecture that this captures all anyon condensation transitions between nonchiral topological phases in $(2 + 1)\text{D}$.

We work through several examples to demonstrate different aspects of our formalism. We write down PEPS representations of the recently introduced symmetry-enriched string-net^{32,33} ground states, and show that they satisfy a symmetry-enriched pulling through condition. We explicitly carry out the construction of defect superselection sectors, gauging, and condensation, for the electromagnetic duality enriched toric code. Further examples are also given to demonstrate the use of Morita equivalent MPO algebras to find different anyon condensation phase transitions.

Chapter 4: In this chapter we harness two recent constructions of state sum topological quantum field theories (TQFTs)^{82,83} to derive local commuting projector Hamiltonians for new topological phases of matter in three spatial dimensions. We follow a tensor network approach, introduced in Ref. 84, and also a diagrammatic calculus approach, similar to Refs. 24,85.

We introduce relevant background material on the definition of state sum TQFTs and the general machinery of Ref. 84 for the construction of Hamiltonians, tensor networks representations of ground states, and their virtual tensor network operator symmetries, from a state sum TQFT. We review Kashaev’s construction of a family of state sum TQFTs in Ref. 82. We also review the underlying data of a UGxBFC from which the state sum TQFTs in Ref. 83 are constructed.

We explicitly apply the machinery of Ref. 84 to construct local commuting projector Hamiltonians from Kashaev’s TQFTs. We compute the ground state degeneracies of these models on the 3-torus, which forms the basis for our conjecture that they realize a subset of the topological phase appearing in the Crane-Yetter-Walker-Wang (CYWW) models^{85,86}. We also explicitly write down local commuting projector Hamiltonians for the UGxBFC TQFTs, first by using the machinery of Ref. 84 and then by following a graphical calculus approach, generalizing the construction in Ref. 85.

We discuss how our Hamiltonians fit into the broader context of $(3 + 1)$ D topological phases that admit a TQFT description, which excludes so called *fracton*⁸⁷ phases which are discussed further in Chapter 5. We explain how the UGxBFC models — with the addition of a 2-group cocycle twist — capture previous constructions, including the CYWW models and 2-group gauge theory^{88,89} (which generalizes Dijkgraaf-Witten theory⁷² and Yetter’s 2-type TQFTs⁹⁰). We also speculate about the relation of our Hamiltonians to a general construction based on unitary fusion 2-categories, or 3-categories with a single object.

Chapter 5: In this chapter we generalize the quantum state gauging procedure of Ref. 71 to symmetries that act on subsets of the lattice. We refer to such symmetries as *submanifold symmetries* and we employ the polynomial language developed by Haah⁹¹ to describe them. This extends the toolbox of lattice gauge theory to exotic fracton topological phases of matter⁸⁷, which do not admit a conventional TQFT description. We derive general relations between a symmetric Hamiltonian and the Hamiltonian that results from gauging the symmetry. In particular, the existence of a uniform spectral gap is preserved by the gauging process.

For the special case of Calderbank-Shor-Steane code Hamiltonians we describe how the gauging process simplifies to shifting along a chain complex. We make use of this general phenomenon to construct novel cluster state Hamiltonians that are self dual under the gauging map. We also apply our formalism to several familiar examples, including the toric code¹⁹ and Haah’s cubic code⁹².

Chapter 1

Matrix product operators for symmetry-protected topological phases: gauging and edge theories

Synopsis:

Projected entangled pair states (PEPS) provide a natural ansatz for the ground states of gapped, local Hamiltonians in which global characteristics of a quantum state are encoded in properties of local tensors. We develop a framework to describe on-site symmetries, as occurring in systems exhibiting symmetry-protected topological (SPT) quantum order, in terms of virtual symmetries of the local tensors expressed as a set of matrix product operators (MPOs) labeled by distinct group elements. These MPOs describe the possibly anomalous symmetry of the edge theory, whose local degrees of freedom are concretely identified in a PEPS. A classification of SPT phases is obtained by studying the obstructions to continuously deforming one set of MPOs into another, recovering the results derived for fixed-point models [X. Chen *et al.*, Phys. Rev. B 87, 155114 (2013)]³⁶. Our formalism accommodates perturbations away from fixed point models, opening the possibility of studying phase transitions between different SPT phases. We also demonstrate that applying the recently developed quantum state gauging procedure to a SPT PEPS yields a PEPS with topological order determined by the initial symmetry MPOs. The MPO framework thus unifies the different approaches to classifying SPT phases, via fixed-points models, boundary anomalies, or gauging the symmetry, into the single problem of classifying inequivalent sets of matrix product operator symmetries that are defined purely in terms of a PEPS.

Based on: [93](#)

Dominic J. Williamson, Nick Bultinck, Michael Mariën, Mehmet B. Sahinoglu, Jutho Haegeman, and Frank Verstraete,

Phys. Rev. B **94**, 205150 (2016), [arXiv:1412.5604](#).

Changes compared to published version: Minor formatting changes.

Contributions of the author: This was a collaborative project, with significant contributions in the form of ideas and calculations by the first two authors. The included version was primarily written by the first author.

1.1 Introduction

The phase diagrams of quantum many-body systems become much richer when global symmetries are imposed. It has become clear of late that in the presence of a global symmetry there exist distinct phases which cannot be distinguished via local order parameters. These phases are referred to as *symmetry-protected topological* (SPT) phases³⁶. In contrast to topologically ordered systems¹⁰, all SPT phases become trivial if the symmetry is allowed to be explicitly broken. While this implies that SPT ground states possess only short-range entanglement, they cannot be adiabatically connected to a product state without breaking the symmetry. Furthermore they exhibit interesting edge properties when defined on a finite system with nontrivial boundary.

In recent years there has been a growing interplay between the theory of quantum many-body systems and quantum information. This has led to the development of tensor network ansatz for the ground states of local, gapped Hamiltonians^{39,41,42,46,55}. Tensor network methods have proven particularly useful in understanding the emergence of topological phenomena in quantum many-body ground states. In one dimension, Matrix Product States were used to completely classify SPT phases via the second cohomology group of their symmetry group^{27,35,56}. In two dimensions, Projected-Entangled Pair States (PEPS) have been used to characterize systems with intrinsic topological order^{59,62,63,94,95}, symmetry-protected topological order⁷⁰ and chiral topological insulators^{60,61,96}.

The first goal of this work is to present a general framework for the description of on-site symmetries within the PEPS formalism. The framework includes symmetry actions on states with topological order and thus provides a natural setting for the study of symmetry-enriched topological phases^{29–31,81,97–102} with PEPS¹⁰³, See Chapter 3 for more details. We then restrict to PEPS without topological order and provide a complete characterization of bosonic SPT order by formulating sufficient conditions to be satisfied by the individual PEPS tensors. Previously some powerful results for renormalization group (RG) fixed-point states with SPT order were presented by Chen *et al.*^{36,70}, the present work extends these results to systems with a finite correlation length. Furthermore, application of the quantum state gauging procedure of Ref. 71 within the framework presented here illuminates the correspondence between SPT phases and certain topologically ordered phases in the language of PEPS, providing a complementary description to the Hamiltonian gauging construction of Levin and Gu⁷³. This naturally brings together the classification of SPT phases via fixed-point models, gauging and anomalous boundary symmetries into a single unified approach that focuses only on MPOs which are properties of the ground states alone.

To achieve these goals we have developed tools to deal with orientation dependent MPO tensors. These tools allow us to calculate the symmetry action on monodromy defected and symmetry twisted states and also modular transformations, pre- and post- gauging, in a local way that is governed by a single tensor.

We first outline the general formalism for characterizing gapped phases in PEPS using matrix product operators (MPOs) in Section 1.2. Section 1.3 presents a set of local conditions that lead to a large class of PEPS with global symmetries which fit within the general formalism. Next, in Section 1.4, we identify a class of short-range entangled PEPS and discuss how SPT order manifests itself in these models via their anomalous edge physics. Section 1.5 explains

how gauging a SPT PEPS with a discrete symmetry group yields a long-range entangled PEPS with topological order. In Section 1.6 we study symmetry twists and monodromy defects of SPT PEPS. These concepts are then illustrated with a family of examples that fall within the framework of SPT PEPS in Section 1.7. We show explicitly that gauging these states yields ground states of the twisted quantum double models^{104,105}, which are the Hamiltonian formulations of Dijkgraaf-Witten discrete gauge theories^{72,106}.

The appendices are organized into sections that review relevant background and others that provide technical details of results which are used throughout the paper. We first review the relevant properties of MPO-injective PEPS in Appendix 1.9, provide an argument that a MPO-injective PEPS with a single block projection MPO is the unique ground state of its parent Hamiltonian in Appendix 1.10 and review the definition of the third cohomology of a single block MPO group representation in Appendix 1.11. In Appendix 1.12 we present results concerning possible orientation dependencies of MPO group representations. In Appendix 1.13 we discuss different crossing tensors, their composition and the effect of modular transformations. Appendix 1.14 contains a brief review of the quantum state gauging formalism and a proof that a gauged SPT PEPS is MPO-injective⁶³. In Appendix 1.15 we present an extension of the quantum state gauging procedure of Ref. 71 to arbitrary flat G-connections and use it to prove that the gauging procedure is gap preserving for arbitrary topologies and to furthermore construct the full topological ground space of a gauged SPT model. In Appendix 1.16 we develop a description of symmetry twisted states, topological ground states and monodromy defected states in terms of MPOs and calculate their transformation under the residual symmetry group. Finally in Appendix 1.17 we demonstrate that the quantum state gauging procedure for finite groups is equivalent to the standard minimal coupling scheme for gauging Hamiltonians.

1.2 Characterizing topological phases with matrix product operators

In this section we present a general framework for the classification of gapped phases with PEPS in terms of universal and discrete labels that arise directly from tensor network states. These discrete labels emerge from the set of MPO symmetries of the PEPS tensors and should remain invariant under continuous deformation of the MPOs.

A 2D PEPS can be defined on any directed graph Λ (most commonly a regular lattice) embedded in an oriented 2D manifold \mathcal{M} given a tensor

$$A_v := \sum_{i_v=1}^d \sum_{\{i_e\}=1}^D (A_v)_{\{i_e\}}^{i_v} |i_v\rangle \bigotimes_{e \in E_v} \langle i_e|$$

for every vertex $v \in \Lambda$, where E_v is the set of edges with v as an endpoint, see Fig. 1.1. Here i_v is the physical index running over a basis for the Hilbert space of a single site \mathbb{C}^d and each i_e is a virtual index of dimension D along an edge e adjacent to v in the graph Λ .

For any simply connected region $\mathcal{R} \subset \mathcal{M}$ whose boundary $\partial\mathcal{R}$ forms a contractible closed path in the dual graph Λ^* we define the PEPS map

$$A_{\mathcal{R}} : (\mathbb{C}^D)^{\otimes |\partial\mathcal{R}|_e} \rightarrow (\mathbb{C}^d)^{\otimes |\mathcal{R}|_v},$$



Figure 1.1: a) A PEPS tensor on a trivalent vertex. b) A right handed MPO tensor.

from $|\partial\mathcal{R}|_e$ virtual indices on the edges that cross $\partial\mathcal{R}$ to $|\mathcal{R}|_v$ physical indices on the vertices in \mathcal{R} , by taking the set of tensors $\{A_v | v \in \mathcal{R}\}$ and contracting each pair of indices that are assigned to an edge within \mathcal{R} , to yield

$$A_{\mathcal{R}} := \sum_{\{i_v\}_{v \in \mathcal{R}}} \sum_{\{i_e\}_{e \in \overline{\mathcal{R}}}} \bigotimes_{v \in \mathcal{R}} (A_v)^{i_v}_{\{i_e\}_{e \in E_v}} \bigotimes_{v \in \mathcal{R}} |i_v\rangle \bigotimes_{e \in \partial\mathcal{R}} (i_e|$$

where $\overline{\mathcal{R}} := \mathcal{R} \cup \partial\mathcal{R}$, see Fig.1.2.

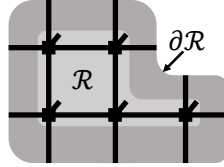


Figure 1.2: The PEPS map $A_{\mathcal{R}}$ from virtual indices on edges in $\partial\mathcal{R}$ to physical indices on vertices in \mathcal{R} .

Universal properties of the phase of matter containing the PEPS wave function are manifest in the local symmetries of $A_{\mathcal{R}}$. The specific symmetries we consider are of the form $U^{\otimes |\mathcal{R}|_v} A_{\mathcal{R}} = A_{\mathcal{R}} O^{\partial\mathcal{R}}$, where U is an on-site unitary corresponding to a physical symmetry that is respected in our classification of phases. Since physical symmetries necessarily form a group under multiplication, we henceforth use the notation $U(g)$, $g \in G$ (we do not consider non on-site symmetries such as lattice symmetries¹⁰⁷). $O^{\partial\mathcal{R}}$ is a MPO acting on the virtual space associated to the edges crossing $\partial\mathcal{R}$. In general,

$$O^{\partial\mathcal{R}} = \sum_{\{i_n\}, \{i'_n\}=1}^D \text{Tr}[B_{\sigma_1}^{i_1, i'_1} \dots B_{\sigma_N}^{i_N, i'_N}] |i_1 \dots i_N\rangle \langle i'_1 \dots i'_N|$$

where the edges crossing $\partial\mathcal{R}$ are ordered 1 to $N := |\partial\mathcal{R}|_e$, by fixing an arbitrary base point and following the orientation of $\partial\mathcal{R}$ (specifically the orientation induced by \mathcal{M}). Each $(B_{\sigma_n}^{i, i'})_{a, b}$ is a $\chi \times \chi$ matrix, see Fig.1.1, which can depend on the handedness $\sigma_n = \pm$ of the crossing of $\partial\mathcal{R}$ and edge n (+ for right, − for left).

Any truly topological symmetries should persist under arbitrary deformations of the region \mathcal{R} , hence the relevant task is to find a complete set \mathcal{S}_g of linearly independent single block⁴⁵ MPOs $O_{\alpha}^{\partial\mathcal{R}}(g)$ for every symmetry transformation $U(g)$ such that for every region \mathcal{R} (satisfying the conditions outlined above) we have

$$U(g)^{\otimes |\mathcal{R}|_v} A_{\mathcal{R}} = A_{\mathcal{R}} O_{\alpha}^{\partial\mathcal{R}}(g) \quad (1.1)$$

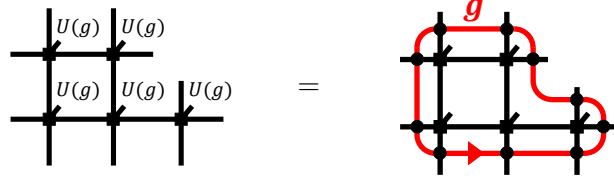


Figure 1.3: The symmetry of the PEPS map $A_{\mathcal{R}}$ on a region \mathcal{R} containing five sites.

see Fig.1.3. There is an important subtlety in finding inequivalent MPOs that satisfy Eq.(1.1) since two linearly independent solutions $O_1^{\partial\mathcal{R}}(g)$, $O_2^{\partial\mathcal{R}}(g)$ may coincide on the support of $A_{\mathcal{R}}$. This occurs precisely when they differ by an operator supported on the kernel of $A_{\mathcal{R}}$. To remove this redundancy one must first find the set of all single block MPO symmetries \mathcal{S}_1 for $U(1) = \mathbb{1}$. Assuming these MPOs are complete in the following sense $\sum_{\alpha} O_{\alpha}^{\partial\mathcal{R}}(1) = A_{\mathcal{R}}^+ A_{\mathcal{R}}$, where $A_{\mathcal{R}}^+$ is a distinguished generalized inverse of $A_{\mathcal{R}}$, any MPO $\hat{O}^{\partial\mathcal{R}}$ can be projected onto the support of $A_{\mathcal{R}}$ to yield another MPO $A_{\mathcal{R}}^+ A_{\mathcal{R}} \hat{O}^{\partial\mathcal{R}}$ with a (multiplicative) constant increase in the bond dimension. Hence the set of inequivalent single blocked MPO symmetries $\mathcal{S}_g := \{O_{\alpha}^{\partial\mathcal{R}}(g)\}_{\alpha}$ can be found by taking all linearly independent MPOs satisfying Eq.(1.1), projecting them onto the support subspace $A_{\mathcal{R}}^+ A_{\mathcal{R}}$ and collecting the linearly independent single block MPOs that result.

Eq.(1.1) implies that $\mathcal{S} := \bigcup_g \mathcal{S}_g$ has a G-graded algebra structure. This algebra structure and the number of elements in \mathcal{S} must be independent of \mathcal{R} . Note the MPO matrices $B_{\sigma_e, \alpha}^{ij}(g)$ also do not depend on \mathcal{R} hence for every region the MPO $O_{\alpha}^{\partial\mathcal{R}}(g)$ is constructed from the same local tensors. The symmetry relations of Eq.(1.1), the graded algebra structure of \mathcal{S} and any discrete labels of the MPO representation of this graded algebra provide universal labels of a quantum phase, independent of the details of the local tensors A_v .

Conjecture 1 (103). *A discrete set of labels that fully specify a symmetry-enriched topological phases of matter can be derived from \mathcal{S} , the MPO representation of G , in a purely local fashion and these labels remain invariant under continuous physical perturbations.*

This set of labels can be calculated by following a similar approach to Ref. 64, which is described in Chapter 3, and they describe the emergent symmetry defects and their G-graded fusion and G-crossed braiding properties. Note this data subsumes the underlying anyon theory and the possibly fractional symmetry transformation of the defects.

Intrinsic topological order is defined without reference to any symmetry and thus corresponds to the $G = \{1\}$ case, in which PEPS are classified by \mathcal{S}_1 . Injective PEPS⁴⁶ always posses trivial topological order and have $\mathcal{S}_1 = \{\mathbb{1} \otimes |\partial\mathcal{R}|\}$ whereas all known topological ordered PEPS^{59,62,63,94,95} satisfy Eq.(1.1) with a nontrivial \mathcal{S}_1 . This was formalized in the framework of MPO-injectivity in Ref. 63, which was shown to capture all Levin-Wen string-net models (the Hamiltonian version of Turaev-Viro state sum invariants¹⁰⁸). In Ref. 63 the independence of the MPO tensors from the region \mathcal{R} was guaranteed by the intuitive *pulling through* property and the more technical *generalized* and *extended inverse* properties, all of which were purely local conditions.

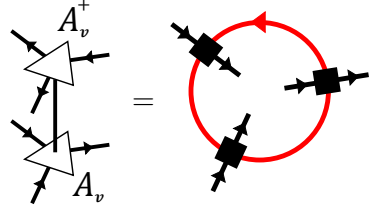
By taking a global symmetry G into account, a finer classification is achieved in terms of \mathcal{S} where $|\mathcal{S}_g| > 0 \forall g \in G$. This classification contains symmetry-protected phases for $|\mathcal{S}_1| = 1$

and symmetry-enriched topological phases for $|S_1| > 1$. In the next section we demonstrate how solutions of Eq.(1.1) can be obtained for nontrivial elements $g \in G$ in a similar fashion to Ref. 63.

1.3 Global symmetry in PEPS

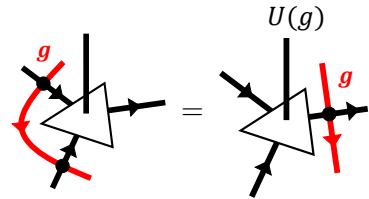
In this section we present a set of local conditions that lead to a general class of solutions to Eq.(1.1).

Consider a PEPS on a trivalent directed graph Λ embedded in an oriented manifold \mathcal{M} , built from four index tensors A which we interpret as linear maps from the virtual to physical indices $A : (\mathbb{C}^D)^{\otimes 3} \rightarrow \mathbb{C}^d$. Firstly, we require that the tensors A satisfy the axioms of MPO-injectivity⁶³, a framework describing general gapped phases without symmetry. Thus (potentially after some blocking of lattice sites, which we assume has already been carried out) the projection $P := A^+ A$ onto the subspace within which the tensor A is injective can be written as a matrix product operator

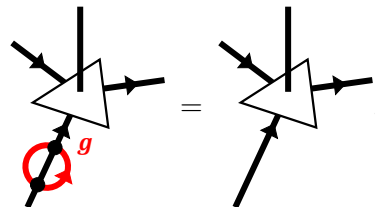

(1.2)

here the MPO tensors are denoted as black squares and satisfy the axioms listed in Ref. 63, see Appendix 1.9 for a brief review. These axioms ensure that the same MPO is obtained for any larger region, independent of the order in which the generalized inverses are applied, and furthermore that this closed MPO is a projector independent of its length.

We now describe purely local sufficient conditions for a PEPS to be invariant under the on-site action $U(g)$ of a global symmetry group G . Hereto, we introduce another set of closed MPOs $\{V^{\partial\mathcal{R}}(g) \mid g \in G\}$ which inherit an orientation from $\partial\mathcal{R}$. These MPOs are composed of four index tensors that depend on a group element g . The tensors are depicted by filled circles in the following diagrams and are defined by conditions (1.3) and (1.4)


(1.3)

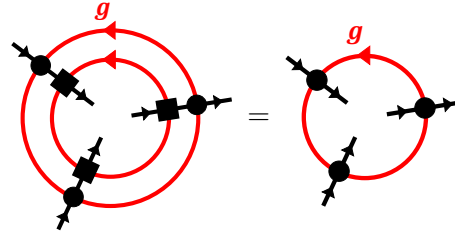
where $U(g)$ is a unitary representation of G , and


(1.4)

Note Eq.(1.4) with the directions reversed is implied by the above conditions. The orientation of the MPO tensors is significant as pulling the MPO through a PEPS tensor in a right handed fashion, as in Eq.(1.3), induces an action $U(g)$ on the physical index while pulling through in a left handed fashion results in a physical action $U^\dagger(g)$, this follows directly from Eq.(1.3) since U is a unitary representation.

With these two properties, it is clear that the ground space of a MPO-injective PEPS constructed from the tensor A on any closed system of arbitrary size is invariant under the global symmetry action $U(g)^{\otimes N}$. Hence such MPO-injective PEPS that are unique ground states must be eigenvectors of the global symmetry. For the special case of injective PEPS⁴⁶ the MPO P is simply the identity $P = \mathbb{1}$ (i.e. a MPO with bond dimension 1), the symmetry MPOs $V(g)$ can always be factorized into a tensor product of local gauge transformations⁶⁹ and the ground state is unique.

From Eqs.(1.3) and (1.4) it immediately follows that the PEPS tensors are intertwiners, i.e. $U(g)A = AV(g)$, where $V(g)$ denotes a closed MPO acting on the three virtual indices. Without loss of generality, and in accordance with the general framework of Section 1.2, we impose that the MPOs $V(g)$ act within the support space of A such that $PV(g) = V(g)$, i.e.


(1.5)

and in particular $V(1) = P$, for 1 the identity group element. Hence the MPOs $V(g)$ form a representation of G since we have $AV(g_1g_2) = U(g_1g_2)A = U(g_1)U(g_2)A = AV(g_1)V(g_2)$, and thus $PV(g_1g_2) = PV(g_1)V(g_2)$ where $P := A^+A$, see Eq.(1.2) (note $PV(g)P = A^+U(g)AP = PV(g)$). A similar argument shows that the symmetry MPO $V_{\text{rev}}(g)$ along the path with reversed orientation (inducing reversed arrows) equals $V(g^{-1})$ since $AV_{\text{rev}}(g) = U^\dagger(g)A = U(g^{-1})A = AV(g^{-1})$ which implies $PV_{\text{rev}}(g) = PV(g^{-1})$. The above two arguments extend to arbitrary contractible regions \mathcal{R} and boundary MPOs $P_{\partial\mathcal{R}}, V^{\partial\mathcal{R}}(g)$.

If we do not project the boundary symmetries onto the support subspace of A there are many equivalent choices for the symmetry action on the boundary. In particular, there might be choices for which the action is factorizable into a tensor product (see e.g. Ref. 70), even if the support projector is not. However, the resulting boundary actions will generically not form a representation of the relevant symmetry group G . The procedure we have outlined of projecting these actions onto the injectivity subspace provides an unambiguous recipe to identify the relevant set of boundary operators that form a MPO representation of the physical symmetry group G . For the particular case of renormalization group fixed-point models, our recipe matches the results of Ref. 70, as illustrated in Section 1.7.

With these properties it is clear that the class of symmetric PEPS satisfying Eqs.(1.3) and (1.4) constitute a special case of the general framework described in Section 1.2. Let $V^{\partial\mathcal{R}}(g)$ denote the MPO corresponding to group element g acting on the boundary of region \mathcal{R} then we have

$$U(g)^{\otimes |\mathcal{R}|_v} A_{\mathcal{R}} = A_{\mathcal{R}} V^{\partial\mathcal{R}}(g). \quad (1.6)$$

Note in the general case we may need to decompose $V^{\partial\mathcal{R}}(g)$ into a sum of single block MPOs to be consistent with Section 1.2.

This general class of solutions show that the formalism of Section 1.2 accommodates the description of both symmetries and topological order, and furthermore nontrivial actions of symmetries on states with topological order. Hence the formalism is well suited to describe symmetry-enriched topological phases within the PEPS framework. This is described in Ref. 103 and Chapter 3.

1.4 Symmetry-protected topological PEPS

Having discussed the general framework for gapped phases and global symmetries in PEPS, we now focus on the subclass corresponding to states with symmetry-protected topological order. In the first subsection we identify the characteristic properties of short-range entangled SPT PEPS. We proceed in the second subsection with an analysis of the edge properties of non-trivial SPT PEPS.

1.4.1 Identifying SPT PEPS

First we must identify the relevant set of PEPS that accurately capture the short-range entanglement property characteristic of SPT phases. As shown in Ref. 63 and argued in the previous sections, MPO-injective PEPS can describe topological phases with long-range entanglement. To single out the short-range entangled PEPS that are candidates to describe SPT states we require that the projection MPO P has a single block when brought into its canonical form. Let B_P^{ij} denote the MPO matrix with external indices i and j , the single block property is equivalent to the transfer matrix $\mathbb{E}_P := \sum_{ij} B_P^{ij} \otimes \bar{B}_P^{ij}$ having a unique eigenvalue of largest magnitude with a corresponding unique eigenvector of full rank. For RG fixed-point PEPS, which are injective on the support subspace of P , we argue that the single block property implies the topological entanglement entropy^{37,38} is zero.

Proposition 1. *For a RG fixed-point (zero correlation length) MPO-injective PEPS with a single blocked projector MPO P , the topological entanglement entropy of the PEPS is zero*

Note the rank of the reduced density matrix $\rho_{\mathcal{R}}$ on a finite homotopically trivial region \mathcal{R} of a MPO-injective PEPS on a sphere equals the rank of the projection MPO surrounding that region, i.e. $\text{rank}(\rho_{\mathcal{R}}) = \text{rank}(P_{\partial\mathcal{R}})$ ⁶³. Since the MPO P is a projection, we have $\text{rank}(P_{\partial\mathcal{R}}) = \text{tr}(P_{\partial\mathcal{R}}) = \text{tr}(P_{\partial\mathcal{R}}^2) = \text{tr}(\mathbb{E}_P^L)$, where $L = |\partial\mathcal{R}|_e$ is the number of virtual bonds crossing the boundary of the region \mathcal{R} under consideration. We then use the uniqueness of the largest eigenvalue λ_{\max} of \mathbb{E}_P to conclude that, for large regions, the rank of the reduced density matrix scales as λ_{\max}^L . This implies that the zero Rényi entropy has no topological correction and for RG fixed-points this furthermore implies that the topological entanglement entropy is zero¹⁰⁹. We expect this property to hold throughout the gapped phase containing the fixed-point.

A further crucial property of a SPT phase without symmetry breaking is the existence of a unique ground state on any closed manifold. For a PEPS to be a unique ground state its transfer matrix must have a unique fixed-point. This excludes both symmetry-breaking and topological degeneracy^{94,110}. By taking a PEPS sufficiently close to its isometric form^{59,62,63} we avoid the symmetry-breaking case (and assure the gap condition⁵⁶). Furthermore, in Appendix 1.10 we

present an argument showing that MPO-injective PEPS with single block projection MPOs do not lead to topological degeneracy.

We have argued above that SPT PEPS should be MPO-injective on the support subspace of a single blocked projection MPO. In the language of Section 1.2 this implies $|\mathcal{S}_1| = 1$ for SPT PEPS. We now show that in this case the symmetry MPOs are also single blocked.

Proposition 2. *For any MPO-injective PEPS with a single blocked projection MPO, all symmetry MPOs of that PEPS can be chosen to be single blocked.*

Assume $V(g)$ contains multiple blocks when brought into canonical form $V(g) = \sum_i V_i(g)$, then we have $PV(g) = \sum_i V_{\pi(i)}(g)$ in canonical form (for some permutation π) since $V(g) = PV(g)$ for all lengths. This follows from the fact that a pair of MPOs which are equal for all lengths exhibit the same blocks when brought into canonical form⁶⁷. Furthermore $\pi = 1$ since $V_i(g) = PV_{\pi^{-1}(i)}(g) = P^2 V_{\pi^{-1}(i)}(g) = V_{\pi(i)}(g)$.

We have

$$P = V(g^{-1})V(g) = \sum_i V(g^{-1})V_i(g)$$

and since this equality holds for all lengths and P has a single block, there can be only one block on the right hand side after bringing it into canonical form⁶⁷. Hence one term in the sum gives rise to a P block along with zero blocks in the canonical form and the others give rise only to zero blocks. Writing this out we have

$$P = V(g^{-1})V_i(g)$$

multiplying by $V(g)$ from the left and making use of the invariance under P implies

$$V(g) = V_i(g)$$

which has a single block (after throwing away the trivial zero blocks).

The arguments in this subsection show that the subclass of symmetric, MPO-injective PEPS satisfying Eqs.(1.3) and (1.4) which accurately describe SPT phases are precisely those with a single blocked projection MPO, provided they are taken sufficiently close to an isometric form to discount the possibility of a phase transition.

Hence the framework of Section 1.2 yields a classification of SPT phases in terms of the discrete labels of the (necessarily single blocked) MPO group representation $V(g)$ of the physical symmetry group G which include the group structure and the third cohomology class $[\alpha] \in H^3(G, U(1))$ ⁷⁰ (see Appendix 1.11 for a review).

1.4.2 Edge properties

We now focus on how the MPO symmetries affect the edge physics of a SPT PEPS and discuss how this can be used to diagnose nontrivial SPT order.

A short-range entangled PEPS with MPO symmetries $V(g)$ that satisfy Eqs.(1.3) and (1.4) has non-trivial SPT order if the third cohomology class $[\alpha]$ of the MPO representation is non-trivial. The existence of this non-trivial SPT order can be inferred by analyzing the edge physics when such a PEPS is defined on a finite lattice \mathcal{R} with a physical edge (boundary) $\partial\mathcal{R}$. In this case the PEPS has open (uncontracted) virtual indices along the physical boundary and

all virtual boundary conditions give rise to exact ground states of the canonical PEPS (bulk) parent Hamiltonian H_{PEPS} (note boundary conditions orthogonal to the support of $P_{\partial\mathcal{R}}$ yield zero). Hence the ground space degeneracy scales exponentially with the length of the boundary, which is a generic property of any PEPS (bulk) parent Hamiltonian. The physically relevant question is whether the Hamiltonian can be perturbed by additional local terms $H_{\text{pert}} = \sum_v H_v$, which are invariant under G , to gap out these edge modes and give rise to a unique symmetric ground state.

In Ref. 110 an isometry \mathcal{W} was derived that maps any operator O acting on the physical indices of the PEPS to an effective operator acting on the virtual indices of the boundary $O \mapsto \mathcal{W}_{\mathcal{R}}^A[O]$. Let $A_{\mathcal{R}} = WH$ be a polar decomposition of $A_{\mathcal{R}}$, where W is an isometry from the virtual to physical level $(\mathbb{C}^D)^{\otimes |\partial\mathcal{R}|_e} \rightarrow (\mathbb{C}^d)^{\otimes |\mathcal{R}|_v}$. This induces the following isometry $\mathcal{W}_{\mathcal{R}}^A[O] := W^\dagger O W$ that maps bulk operators to the boundary in an orthogonality preserving way. Note there is some freedom in choosing W precisely when $P_{\partial\mathcal{R}}$ is nontrivial, in this case we make the choice that best preserves locality. Regardless of our choice of W we always have $P_{\partial\mathcal{R}} \mathcal{W}_{\mathcal{R}}^A[O] P_{\partial\mathcal{R}} = H^+ A_{\mathcal{R}}^\dagger O A_{\mathcal{R}} H^+$, where H^+ is defined to be the pseudoinverse of H , see Fig.1.4. Away from an RG fixed-point, however, it has not been proven that this isometry

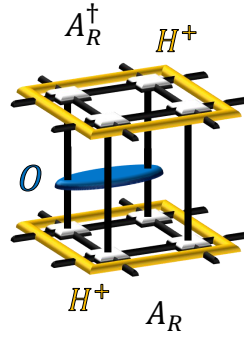


Figure 1.4: The bulk to boundary isometry, for a region \mathcal{R} containing four sites, projected onto the injectivity subspace $P_{\partial\mathcal{R}} \mathcal{W}_{\mathcal{R}}^A[O] P_{\partial\mathcal{R}} = H^+ A_{\mathcal{R}}^\dagger O A_{\mathcal{R}} H^+$.

preserves locality. To this point we venture the following conjecture, which was numerically illustrated for a particular non-topological PEPS in Ref. 111,

Conjecture 2. *The boundary isometry of any PEPS with exponentially decaying correlations maps a local operator O_v acting on the physical indices near the boundary to a (quasi-) local operator $\tilde{O}_e^v := \mathcal{W}_{\mathcal{R}}^A[O_v]$ acting on the virtual degrees of freedom along the boundary.*

From properties (1.3) and (1.4) it is clear that acting with $U(g)$ on every physical site is equivalent to acting with the MPO $V^{\partial\mathcal{R}}(g)$ on the virtual boundary indices of the PEPS, hence a G -symmetric local perturbation H_v to the Hamiltonian at the physical level H_{PEPS} is mapped to an effective (quasi-) local Hamiltonian term on the virtual boundary \tilde{H}_e^v that is invariant under $V^{\partial\mathcal{R}}(g)$. The full symmetric edge Hamiltonian is given by

$$\begin{aligned} \tilde{H}_{\text{edge}} &= P_{\partial\mathcal{R}} \mathcal{W}_{\mathcal{R}}^A[H_{\text{pert}}] P_{\partial\mathcal{R}} \\ &= V^{\partial\mathcal{R}}(1) \left(\sum_{e \in \partial\mathcal{R}} \sum_{v \mapsto e} \tilde{H}_e^v \right) V^{\partial\mathcal{R}}(1) \end{aligned} \quad (1.7)$$

where $v \mapsto e$ denotes that the bulk perturbation centered on site v becomes a (quasi-) local boundary term centered on virtual bond e .

Ground states of the perturbed physical Hamiltonian $H_{\text{bulk}} = H_{\text{PEPS}} + H_{\text{pert}}$ are given by contracting the virtual boundary indices of the ground state PEPS network with ground states of the effective edge Hamiltonian, i.e. $|\Psi_0^{\text{bulk}}\rangle = A_{\mathcal{R}}|\psi_0^{\text{edge}}\rangle$. If the edge Hamiltonian \tilde{H}_{edge} is gapped and does not exhibit spontaneous symmetry breaking then its ground state $|\psi_0^{\text{edge}}\rangle$ is well approximated by an injective MPS that is invariant under $V^{\partial\mathcal{R}}(g)$. However it was shown by Chen *et al.* that this results in a contradiction, since an injective MPS cannot be invariant under the action of a single blocked MPO group representation $V(g)$ with non-trivial third cohomology⁷⁰.

Consequently, the effective edge Hamiltonian \tilde{H}_{edge} either exhibits spontaneous symmetry breaking, in which case the MPS is not injective, or must be gapless, in which case its ground state cannot be well approximated by a MPS. In the former case, the physical state $A_{\mathcal{R}}|\psi_{0,i}^{\text{edge}}\rangle$ obtained by contracting the virtual boundary indices of the PEPS network with $|\psi_{0,i}^{\text{edge}}\rangle$, one of the symmetry breaking ground states of \tilde{H}_{edge} , also exhibits symmetry breaking and hence does not qualify as a symmetric state. The latter case, on the other hand, implies that a local symmetric perturbation to the physical Hamiltonian is unable to gap out the gapless edge modes, which is one of the hallmarks of non-trivial SPT order.

Here we have again relied on a form of Conjecture 2, specifically that a PEPS with exponentially decaying correlations has a gapped transfer matrix, which implies that the gapless modes on the virtual boundary of the PEPS network are approximately identified, via the PEPS map $A_{\mathcal{R}}$, with physical degrees of freedom that are an order of the correlation length from the boundary. Note this explicit identification of the gapless edge mode degrees of freedom is a major strength of the PEPS framework¹¹¹. Our conjecture is consistent with the intuition that as a SPT PEPS is tuned to criticality the gap of the transfer matrix shrinks and the edge modes extend further into the bulk, and is also supported by the results of Ref. 77 concerning phase transitions between symmetry-protected and trivial phases.

In this section we have identified a subclass of symmetric PEPS with short-range entanglement that are MPO-injective with respect to a single blocked projection MPO. This led to a classification of SPT phases within the framework of Section 1.2 in terms of the third cohomology class of the MPO symmetry representation. Finally we described the influence of the possibly anomalous MPO symmetry action on the boundary physics of the PEPS. In the next section we explore an alternative approach to classifying SPT phases with PEPS via gauging.

1.5 Gauging SPT PEPS

In this section we discuss how gauging a SPT PEPS yields a long range entangled PEPS whose topological order is determined by the symmetry MPOs. We then proceed to show that the gauging procedure preserves the energy gap of a symmetric Hamiltonian. Our approach explicitly identifies how the symmetry MPOs that determine the boundary theory of a SPT model are mapped to topological MPOs that describe the anyons of a topological theory⁶⁴.

1.5.1 Gauging SPT PEPS to topologically ordered PEPS

We first outline the application of the gauging procedure from Ref. 71 to SPT PEPS and the effect this has upon the MPO symmetries.

Conditions (1.3) and (1.4) ensure that the SPT PEPS described in Section 1.4 are invariant under the global action $U(g)^{\otimes |\mathcal{M}|_v}$ of a symmetry group G , hence the quantum state gauging procedure of Ref. 71 is applicable. It was shown in Ref. 71 that the virtual boundary action of the physical symmetry in an injective PEPS becomes a purely virtual topological symmetry of the gauged tensors, with a trivial physical action. More precisely, it was shown that the gauging procedure transforms an injective PEPS, with virtual bonds in \mathbb{C}^D and a virtual symmetry representation that factorizes as $V^{\partial\mathcal{R}}(g) = v(g)^{\otimes L}$ (with $v(g) : \mathbb{C}^D \rightarrow \mathbb{C}^D$), into a G -injective PEPS, with virtual bonds in $\mathbb{C}^D \otimes \mathbb{C}[G]$, that is injective on the support subspace of the projector $\sum_{g \in G} [v(g) \otimes R(g)]^{\otimes L}$. Here, $L := |\partial\mathcal{R}|_e$ is the number of virtual bonds crossing the boundary of the region \mathcal{R} under consideration and $R(g) |h\rangle := |hg^{-1}\rangle$ denotes the right regular representation of G on the new component $\mathbb{C}[G]$ of the virtual bonds. Let us recast this in the framework of Section 1.2. The ungauged symmetric injective PEPS map satisfies

$$A_{\mathcal{R}} V^{\partial\mathcal{R}}(g) = U(g)^{\otimes |\mathcal{R}|_v} A_{\mathcal{R}} \quad (1.8)$$

for any region $\mathcal{R} \subset \mathcal{M}$ and $g \in G$. Now let $O^{\partial\mathcal{R}}(g) := [v(g) \otimes R(g)]^{\otimes L}$, then the gauged PEPS map $A_{\mathcal{R}}^g$ for any region \mathcal{R} satisfies

$$A_{\mathcal{R}}^g O^{\partial\mathcal{R}}(g) = A_{\mathcal{R}}^g \quad (1.9)$$

for all $g \in G$, which implies that the gauged PEPS A^g is in the same phase as a quantum double model constructed from G , provided it is sufficiently close to a fixed-point to ensure there is no symmetry breaking^{19,59}.

The result of Ref. 71 can be extended to the general case outlined in Section 1.4 and Appendix 1.10 where the PEPS map $A_{\mathcal{R}}$ in region \mathcal{R} has a non-factorizable MPO representation of the symmetry on the virtual level, given by $V^{\partial\mathcal{R}}(g) : (\mathbb{C}^D)^{\otimes L} \rightarrow (\mathbb{C}^D)^{\otimes L}$, and is only injective on the support subspace of the projection MPO $P_{\partial\mathcal{R}} = V^{\partial\mathcal{R}}(1)$ which is required to be single blocked. Hence we have

$$A_{\mathcal{R}} P_{\partial\mathcal{R}} = A_{\mathcal{R}} \quad (1.10)$$

$$A_{\mathcal{R}} V^{\partial\mathcal{R}}(g) = U(g)^{\otimes |\mathcal{R}|_v} A_{\mathcal{R}} \quad (1.11)$$

for all $g \in G$; note we have explicitly separated the $g = 1$ case for emphasis. In the language of Section 1.2 we have $\mathcal{S}_g = \{V^{\partial\mathcal{R}}(g)\}$, $\forall g \in G$.

The gauged PEPS A^g obtained by applying the procedure of Ref. 71 to A has virtual bonds in $\mathbb{C}^D \otimes \mathbb{C}[G]$ and satisfies the axioms of MPO-injectivity⁶³, but is now injective on the support subspace of the projection MPO $P_{\partial\mathcal{R}}^g := \frac{1}{|G|} \sum_{g \in G} O^{\partial\mathcal{R}}(g)$, where $O^{\partial\mathcal{R}}(g) := V^{\partial\mathcal{R}}(g) \otimes R(g)^{\otimes L}$, see Appendix 1.14 for a detailed proof. Writing these conditions out, we have

$$A_{\mathcal{R}}^g O^{\partial\mathcal{R}}(g) = A_{\mathcal{R}}^g \quad (1.12)$$

for all $g \in G$, which implies $A_{\mathcal{R}}^g P_{\partial\mathcal{R}}^g = A_{\mathcal{R}}^g$. Note every MPO $O^{\partial\mathcal{R}}(g)$ is one of the original MPO symmetries $V^{\partial\mathcal{R}}(g)$ tensored with a tensor product representation on the new component

$\mathbb{C}[G]$ of the virtual space that was introduced by gauging. The MPO representation of $P_{\partial\mathcal{R}}^g$ thus has a canonical form with multiple blocks labeled by $g \in G$ that correspond to the single block MPOs $O^{\partial\mathcal{R}}(g)$. Hence for the gauged PEPS $\mathcal{S}_1 = \{O^{\partial\mathcal{R}}(g) | g \in G\}$. Importantly, tensoring with a local action $R(g)$ on the additional virtual space $\mathbb{C}[G]$ does not change the bond dimension nor the third cohomology class of the MPO representation.

The topological order of the gauged SPT PEPS is a twisted Dijkgraaf-Witten model (provided it is sufficiently close to a fixed-point to ensure there is no symmetry breaking) which is shown explicitly in Section 1.7.2. We emphasize that up to the trivial operators $R(g)^{\otimes L}$ the same MPOs determine both the gapless edge modes of the SPT phase and, as argued in Refs. 62,63, the topological order of the gauged model. This realizes the gauging map from SPT models with a finite symmetry group to models with intrinsic topological order, explored at the level of Hamiltonians by Levin and Gu⁷³, explicitly on the level of states. In Appendix 1.17 we apply the gauging procedure of Ref. 71 to families of SPT Hamiltonians with an arbitrary finite symmetry group, which yields an unambiguous gauging map to families of topologically ordered Hamiltonians.

We note that the PEPS gauging procedure can equally well be applied to gauge any normal subgroup $N \trianglelefteq G$ of the physical symmetry group G . This gives rise to states with symmetry-enriched topological order, where the topological component corresponds to a gauge theory with gauge group N and the global symmetry is given by the quotient group G/N ; this is investigated further in Ref. 103 and Chapter 3.

1.5.2 Gauging preserves the gap

We now show that the gauging procedure of Ref. 71 preserves the energy gap of a symmetric Hamiltonian, which implies by contrapositive that two SPT PEPS are in different phases when the corresponding gauged PEPS lie in distinct topological phases.

Let H_m denote a local gapped symmetric ‘matter’ Hamiltonian, which captures the particular case of parent Hamiltonians for SPT PEPS. The Hamiltonian is a sum of local terms $H_m := \sum_v h_v$, where each h_v acts on a finite region within a constant distance of vertex v . Without loss of generality we take the Hamiltonian to satisfy $[h_v, U(g)^{\otimes |\mathcal{M}|_v}] = 0, \forall g \in G$ and shift the lowest eigenvalue of H_m to 0. The gap to the first excited energy level is denoted by $\Delta_m > 0$. We now apply the gauging procedure of Ref. 71 to obtain the gauged matter Hamiltonian defined by $H_m^{\mathcal{G}} := \sum_v \mathcal{G}_{\Gamma_v}[h_v]$, for \mathcal{G}_{Γ_v} given in Eq.(1.112). This Hamiltonian is also local since each \mathcal{G}_{Γ_v} is locality preserving.

The gauging procedure introduces gauge fields on the links of the PEPS network and the full Hamiltonian of the gauged system contains local flux constraint terms $H_B := \sum_p (1 - \mathcal{B}_p)$ acting on these gauge fields by adding an energy penalty when the flux through a plaquette p is not the identity group element. Each local term \mathcal{B}_p is a Hermitian projector acting on the edges around plaquette p which has eigenvalue 1 on any gauge field configuration (G -connection) that satisfies the flux constraint and 0 otherwise, see Eq.(1.134). Furthermore \mathcal{B}_p is diagonal in the group basis on the edges, hence $[\mathcal{B}_p, \mathcal{B}_{p'}] = 0$.

The full Hamiltonian may also contain a sum of local commuting projections onto the gauge invariant subspace $H_P := \sum_v (1 - P_v)$, see Eq.(1.109), this corresponds to a model with an effective low energy gauge theory rather than a strict gauge theory. Hence the full Hamiltonian

on the gauge and matter system is given by the following sum

$$H_{\text{full}} = H_{\text{m}}^{\mathcal{G}} + \Delta_{\mathcal{B}} H_{\mathcal{B}} + \Delta_P H_P$$

where $\Delta_{\mathcal{B}}, \Delta_P \geq 0$. Note a strictly gauge invariant theory is recovered in the limit $\Delta_P \rightarrow \infty$. It is easy to verify that the components of the full Hamiltonian commute, i.e. $[H_{\text{m}}^{\mathcal{G}}, H_{\mathcal{B}}] = [H_{\text{m}}^{\mathcal{G}}, H_P] = [H_{\mathcal{B}}, H_P] = 0$, and hence are simultaneously diagonalizable. Furthermore, $H_{\mathcal{B}}$ and H_P each have lowest eigenvalue 0 and gap 1.

Assuming Δ_P is sufficiently large, the low energy subspace of H_{full} lies within the ground space of H_P and hence is spanned by states of the form $P[|\lambda\rangle_{\Lambda_v} \otimes |\phi\rangle_{\Lambda_e}]$, with $P = \prod_{v \in \Lambda} P_v$, for a basis $|\lambda\rangle$ of the matter (vertex) degrees of freedom (we will consider the eigenbasis of H_{m}) and a basis $|\phi\rangle$ of the gauge (edge) degrees of freedom (we will consider the group element basis).

Similarly, assuming $\Delta_{\mathcal{B}}$ is sufficiently large, the low energy subspace of H_{full} lies within the ground space of $H_{\mathcal{B}}$ which is spanned by states whose gauge fields form a flat G-connection on the edge degrees of freedom. Since we additionally have $[\mathcal{B}_p, P] = 0$ the common ground space of $H_{\mathcal{B}}$ and H_P is spanned by states of the form $P[|\lambda\rangle_{\Lambda_v} \otimes |\phi_{\text{flat}}\rangle_{\Lambda_e}]$, for a basis $|\phi_{\text{flat}}\rangle$ of the flat G-connections on the edge degrees of freedom (note these are product states).

G-connections form equivalence classes under the local gauge operations

$$a_v^g := \bigotimes_{e \in E_v^+} R_e(g) \bigotimes_{e \in E_v^-} L_e(g)$$

(see appendix 1.14 for a more detailed definition of a_v^g). On a 1-homotopy trivial manifold (no noncontractible loops) there is only 1 such equivalence class given by all connections of the form $|\phi_{\text{flat}}\rangle = \prod_i a_{v_i}^{g_i} |1\rangle_{\Lambda_e}$, where $|1\rangle_{\Lambda_e} := |1\rangle^{\otimes |\Lambda_e|}$.

Proposition 3. *For a 1-homotopy trivial manifold, the states $G|\lambda\rangle$ (for a basis $|\lambda\rangle$) span the common ground space of both $H_{\mathcal{B}}$ and H_P , where G is the quantum state gauging map defined in Eq.(1.111).*

Since $P_v = \int dg U_v(g) \otimes a_v^g$ one can easily see $P_v a_v^g = P_v U_v^\dagger(g)$ and hence for any state in the intersection of the ground spaces of $H_{\mathcal{B}}$ and H_P we have

$$\begin{aligned} P[|\psi\rangle_{\Lambda_v} \otimes |\phi_{\text{flat}}\rangle_{\Lambda_e}] &= P[|\psi\rangle_{\Lambda_v} \otimes \prod_i a_{v_i}^{g_i} |1\rangle_{\Lambda_e}] \\ &= P[\left[\prod_i U_{v_i}(g_i)\right]^\dagger |\psi\rangle_{\Lambda_v} \otimes |1\rangle_{\Lambda_e}] \\ &= G\left[\prod_i U_{v_i}(g_i)\right]^\dagger |\psi\rangle_{\Lambda_v} \end{aligned} \tag{1.13}$$

where we have started from our above characterization of the common ground space.

We now proceed to show that any eigenstate of H_{m} is mapped to an eigenstate of $H_{\text{m}}^{\mathcal{G}}$ by the quantum state gauging map G . See appendix 1.14 for the details about the operator and state gauging maps \mathcal{G} and G as constructed in Ref. 71.

Proposition 4 (71). *The identity $\mathcal{G}_\Gamma[O]G = GO$ holds for any symmetric operator O .*

Suppose O acts on the sites $v \in \Gamma \subset \Lambda$ where Γ is a subgraph of the full lattice which contains all the edges between its vertices, then we have

$$\begin{aligned}
\mathcal{G}_\Gamma[O]G &= \int \prod_{v \in \Gamma} dh_v \bigotimes_{v \in \Gamma} U_v(h_v) O \bigotimes_{v \in \Gamma} U_v^\dagger(h_v) \\
&\quad \bigotimes_{e \in \Gamma} |h_{v_e^-} h_{v_e^+}^{-1}\rangle \langle h_{v_e^-} h_{v_e^+}^{-1}| \int \prod_{v \in \Lambda} dg_v \bigotimes_{v \in \Lambda} U_v(g_v) \bigotimes_{e \in \Lambda} |g_{v_e^-} g_{v_e^+}^{-1}\rangle \\
&= \int \prod_{v \in \Lambda} dg_v \prod_{v \in \Gamma} dh_v \bigotimes_{v \in \Lambda} U_v(g_v) \bigotimes_{v \in \Gamma} U_v(g_v^{-1} h_v) \\
&\quad O \bigotimes_{v \in \Gamma} U_v^\dagger(g_v^{-1} h_v) \prod_{e \in \Gamma} \delta_{(g_{v_e^-}^{-1} h_{v_e^-}), (g_{v_e^+}^{-1} h_{v_e^+})} \bigotimes_{e \in \Lambda} |g_{v_e^-} g_{v_e^+}^{-1}\rangle \\
&= G O
\end{aligned} \tag{1.14}$$

where edge e runs from vertex v_e^+ to v_e^- . The last equality follows since the δ condition forces $(g_v^{-1} h_v)$ to be equal for all $v \in \Gamma$ (assuming Γ is connected) and the operator O is symmetric under the group action $[O, \bigotimes_{v \in \Gamma} U_v(g)] = 0$.

This implies that any eigenstate $|\psi_\lambda\rangle$ of H_m with eigenvalue λ gives rise to an eigenstate $G|\psi_\lambda\rangle$ of H_m^G with the same eigenvalue. Note we have assumed that $G|\psi_\lambda\rangle \neq 0$, which is the case when the representation under which $|\psi_\lambda\rangle$ transforms contains the trivial representation. This always holds for a unique ground state (possibly after redefining the matrices of the group representation by multiplicative phases $U(g) \mapsto e^{i\theta(g)}U(g)$).

If H_m has a unique ground state $|\lambda_0\rangle$ the ground state of the full Hamiltonian is given by $G|\lambda_0\rangle$ (since $H_m^G \geq 0$ for $H_m \geq 0$) and its gap satisfies $\Delta_{\text{full}} \geq \min(\Delta_m, \Delta_B, \Delta_P)$.

Hence if two local SPT Hamiltonians are connected by a gapped, continuous and symmetric path of local Hamiltonians then the gauged models are also connected by a gapped and continuous path of local Hamiltonians.

In Appendix 1.15 we extend this proof to SPT Hamiltonians on topologically nontrivial manifolds where the gauging procedure leads to a topological degeneracy of the ground space. Orthogonal topological ground states are obtained by gauging distinct symmetry twisted SPT states, which are the subject of the next section.

1.6 Symmetry twists and monodromy defects

In this section we argue that symmetry twists and monodromy defects have a natural description in the tensor network formalism in terms of symmetry MPOs that correspond to anyons in the gauged model. We harness this description to calculate the effect that modular transformations have upon symmetry twisted and topological ground states via their effect on a four index *crossing tensor*. Similarly we calculate the projective transformation of a monodromy defect by composing two *crossing tensors*. Our approach explicitly identifies how the symmetry MPOs that describe defects of a SPT model become topological MPOs that describe the anyons of a topological model⁶⁴.

1.6.1 Symmetry twists in SPT PEPS

We first describe the construction of a symmetry twisted SPT PEPS in terms of the original SPT PEPS, symmetry MPOs and a crossing tensor. We then calculate the transformation of this state

under the residual symmetry group.

For a flat gauge field configuration there is a well defined procedure for applying a corresponding symmetry twist to a local symmetric Hamiltonian, given by conjugating each local term by a certain product of on-site symmetries (see Appendix 1.15). On a trivial topology such a symmetry twist can be applied directly to a symmetric state by acting with a certain product of on-site symmetries. For example a symmetry twist on an infinite plane, specified by a pair of commuting group elements $(x, y) \in G \times G$ and oriented horizontal and vertical paths p_x, p_y in the dual lattice, acts on a state $|\psi\rangle$ in the following way

$$|\psi\rangle^{(x,y)} := \bigotimes_{v \in \mathcal{U}} U_v(x) \bigotimes_{v \in \mathcal{R}} U_v(y) |\psi\rangle$$

where \mathcal{R} is the half plane to the right of p_y , \mathcal{U} the half plane above p_x , see Fig.1.5. Note x and y must commute for the relevant gauge field configuration to be flat. One can also understand why they must commute by first applying the x -twist which reduces the symmetry group to $\mathbb{C}(x)$ (the centralizer of x) and hence it only makes sense to implement a second twist for $y \in \mathbb{C}(x)$. With this definition applying a symmetry twist to an eigenstate of a symmetric Hamiltonian (on a trivial topology) yields an eigenstate of the symmetry twisted Hamiltonian with the same eigenvalue.

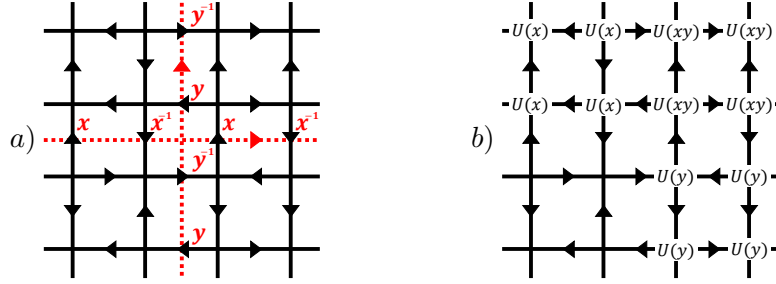


Figure 1.5: a) A symmetry twist (x, y) on an infinite plane. b) Physical action of the aforementioned symmetry twist.

The framework of SPT PEPS provides a natural prescription for the application of a symmetry twist directly to a PEPS on any topology, given by acting with symmetry MPOs on the virtual level of the PEPS. In the above example, assuming $|\psi\rangle$ is a SPT PEPS with local tensor A and symmetry MPOs $V(g)$, Eq.(1.3) implies that the symmetry twisted state $|\psi\rangle^{(x,y)}$ is given by acting on the virtual level of the PEPS $|\psi\rangle$ with the MPOs $V^{p_x}(x)$, $V^{p_y}(y)$ (with inner indices contracted with the four index *crossing tensor* $Q_{x,y}$ (1.15) where p_x, p_y intersect) see Fig.1.6.

The *crossing tensor* $Q_{x,y}$ is defined in terms of the local reduction tensor of the MPO rep-

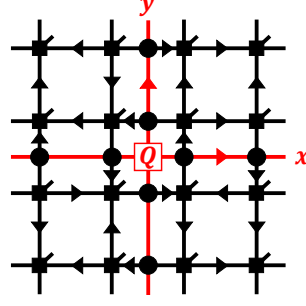


Figure 1.6: (x, y) symmetry twisted PEPS, for infinite or periodic boundary conditions.

representation $X(x, y)$ (see Eqs.(1.57,1.86))

$$\begin{aligned} Q_{x,y} &:= X(x, y)X^+(y, x) \\ &= W_R^x(y) \end{aligned} \quad (1.15)$$

$$x \text{---} \boxed{Q} \text{---} x \quad y \text{---} \boxed{Q} \text{---} y \quad := \quad \begin{array}{c} \nearrow X^+(y, x) \\ \nwarrow X(x, y) \end{array}$$

where $X^+(y, x)$ is the pseudoinverse of $X(y, x)$. Eq.(1.3) and the *zipper* condition (1.71) for $X(x, y)$ imply that the $Q_{x,y}$ tensor contracted with MPOs $V^{p_x}(x), V^{p_y}(y)$ can be moved through the PEPS on the virtual level by applying appropriate on-site symmetries to the physical level.

This prescription extends straightforwardly to an arbitrary topology (see Appendix 1.15) as we now demonstrate with the example of a symmetry twist on a torus for a pair of commuting group elements (x, y) along distinct noncontractible cycles p_x, p_y . The symmetry twisted SPT PEPS $|\psi\rangle^{(x,y)}$ is again given by applying the MPOs $V^{p_x}(x), V^{p_y}(y)$ (with inner indices contracted with the crossing tensor $Q_{x,y}$) to the virtual level of the untwisted PEPS $|\psi\rangle$. Importantly this prescription fulfills the condition that applying a symmetry twist to a PEPS groundstate of a symmetric frustration free Hamiltonian yields a groundstate of the symmetry twisted Hamiltonian due to Eq.(1.3). We note that similar tensor network techniques allow a construction of symmetry twists for time reversal symmetry¹¹².

A symmetry twisted state with conjugated group elements (x^g, y^g) is related, up to a phase, to the symmetry twisted state with group elements (x, y) via a global symmetry action as follows $\theta_g^{x,y} |\psi\rangle^{(x^g, y^g)} = U(g)^{\otimes |\mathcal{M}|_v} |\psi\rangle^{(x, y)}$. Similarly a symmetry twisted state for a local deformation of the paths $(p_x, p_y) \mapsto (\tilde{p}_x, \tilde{p}_y)$ is related to the symmetry twisted state for (p_x, p_y) by a product of on-site symmetries corresponding to the deformation via Eq.(1.3). Hence the number of distinct classes of symmetry twisted states on a torus, under local operations, is given by the number of conjugacy classes of commuting pairs of group elements, which equals the number of irreducible representation of the quantum double $D(G)$ ⁵⁹.

It is apparent that a symmetry twisted state $|\psi\rangle^{(x,y)}$ forms a 1D representation under the physical action of the residual symmetry group $C(x, y)$, where $C(S)$ denotes the centralizer of a subset $S \subseteq G$. Assuming that the untwisted ground state $|\psi\rangle$ is symmetric under G (which can always be achieved after rephasing the physical representation) the symmetry twisted states may still form nontrivial 1D representations of their respective residual symmetry groups, this

fact becomes important when counting the ground space dimension of the gauged model. Calculating these 1D representations explicitly within the PEPS framework yields the result $\theta_g^{x,y} = \alpha^{(x,y)}(g)$ the second slant product of the 3-cocycle α that arose from the MPO group representation (see Appendix 1.13, Eq.1.103). Hence an (x, y) symmetry twisted state is symmetric under $C(x, y)$ iff $\alpha^{(x,y)} \equiv 1$, in which case y is called $\alpha^{(x)}$ -regular. If this property is satisfied by a given $y \in C(x)$ it also holds for all conjugates of y . Furthermore the number of $\alpha^{(x)}$ -regular conjugacy classes is known to be equal to the number of irreducible projective representations with 2-cocycle $\alpha^{(x)}$ ⁷².

1.6.2 Gauging the symmetry twisted SPT PEPS

We now outline how the application of an appropriate gauging procedure to a symmetry twisted SPT PEPS yields a topological ground state.

There is a twisted version of the gauging procedure of Ref. 71 for each flat gauge field configuration which maps a symmetric Hamiltonian with the corresponding symmetry twist to a gauged Hamiltonian, the same one as obtained by applying the untwisted gauging procedure to the untwisted symmetric Hamiltonian (see Appendix 1.15 for more detail). For a fixed representative (x, y) the twisted gauging operator $G_{x,y}$ is given by contracting the tensor product operators $R(x)^{\otimes |p_x|}, R(y)^{\otimes |p_y|}$ with the virtual level of the original gauging operator G . The twisted versions of the state gauging map are orthogonal for distinct symmetry twists in general and furthermore the fixed representatives satisfy $G_{x',y'}^\dagger G_{x,y} = \delta_{[x',y'],[x,y]} \int dg U(g)^{\otimes |\mathcal{M}|_v} \delta_{g \in C(x,y)}$ (see Appendix 1.15.3 for a proof of this). Hence each conjugacy class of symmetry twisted states that are symmetric under the residual symmetry group is mapped to an orthogonal ground state, while those that form a nontrivial 1D representation are mapped to 0. Consequently the dimension of the ground space for the gauged model is given by the number of irreducible representations of the twisted quantum double $D^\alpha(G)$ which can not be larger than the ground space dimension of a gauged trivial SPT model with the same symmetry group.

Given a SPT PEPS ground state $|\psi\rangle$, the orthogonal ground states of the gauged model can be constructed by applying the gauging tensor network operator and acting with the SPT symmetry MPO and a product of on-site symmetry actions $[V(g) \otimes R(g)^{\otimes L}]$ along noncontractible cycles on the virtual level of the gauged tensor network $G|\psi\rangle$. For a fixed representative (x, y) of a symmetric class of symmetry twists the corresponding gauged ground state is given by contracting the MPOs $[V^{p_x}(x) \otimes R(x)^{\otimes |p_x|}], [V^{p_y}(y) \otimes R(y)^{\otimes |p_y|}]$ (with the crossing tensor $Q_{x,y}$ at the intersection point $p_x \cap p_y$ ⁶³) with the virtual level of the gauged PEPS $G|\psi\rangle$.

1.6.3 Modular transformations

We calculate the effect of modular transformation on symmetry twisted and topological ground states via their effect on a set of four index crossing tensors.

Symmetry twisted ground states have been used to identify non trivial SPT order via the matrix elements of modular transformations taken with respect to them^{113,114}. We have calculated the SPT \tilde{S} & \tilde{T} matrices, corresponding to a $\frac{\pi}{2}$ rotation and a Dehn twist respectively, using our framework to find (see Eq.(1.106))

$$\langle x', y' | \tilde{S} | x, y \rangle = \alpha^{(y)}(x^{-1}, x)^{-1} \langle x', y' | y, x^{-1} \rangle \quad (1.16)$$

$$\langle x', y' | \tilde{T} | x, y \rangle = \alpha(x, y, x) \langle x', y' | x, xy \rangle \quad (1.17)$$

where we have used the abbreviation $|x, y\rangle := |\psi\rangle^{(x,y)}$, $\alpha^{(y)}$ is the slant product of α (see Appendix 1.13, Eq.1.91) and note $y \in \mathbb{C}(x)$. The gauging procedure elucidates the precise correspondence between these matrix elements and the S & T -matrix of the gauged theory^{63,115,116} which we have also calculated within the ground space (again see Eq.(1.106))

$$S = \sum_{xy=yx} \alpha^{(y)}(x^{-1}, x)^{-1} |[y, x^{-1}]\rangle \langle [x, y]| \quad (1.18)$$

$$T = \sum_{xy=yx} \alpha(x, y, x) |[x, xy]\rangle \langle [x, y]| \quad (1.19)$$

where $|[x, y]\rangle := G_{x,y} |\psi\rangle^{(x,y)}$ denotes a ground state of the gauged model. Note in our framework we consider a fixed but arbitrary choice of representative for each conjugacy class, rather than group averaging over them.

We have explicitly verified that S & T generate a linear representation of the modular group in agreement with known results for lattice gauge theories (See Subsection 1.13.4).

1.6.4 Projective symmetry transformation of monodromy defects

Here we describe an explicit construction of the projective representation that acts upon a monodromy defect. We calculate the 2-cocycle of this projective representation by considering the composition of pairs of crossing tensors.

Monodromy defects can be understood as symmetry twists along paths with open end points and have proven useful for the identification of SPT phases^{117,118}. The prescription for applying symmetry twists to SPT PEPS extends naturally to a construction of a pair of monodromy defects at the ends of a path p_g , for $g \in G$. This is given by applying a symmetry MPO $V^{p_g}(g)$ to the virtual level of the PEPS with an open inner index at either end of the path, which may be contracted with defect tensors replacing the PEPS tensors at each of the defects, see Fig.1.7. A defect tensor must lie in the support subspace of the projector $\mathcal{V}^g(1)$ acting on its virtual indices, see Eq.(1.20). This may leave some freedom in choosing the tensor which correspond to internal degrees of freedom of the defect, see Ref. 64 for further details. Applying the twisted gauging procedure for the corresponding gauge field configuration (which is flat except near the defect points) explicitly maps the symmetry twisted PEPS to a PEPS that describes a pair of anyon excitations in the gauged theory, see Appendix 1.16 and Refs. 59,64.

We now study a pair of monodromy defects on a twice punctured sphere topology, with a defect in each puncture, see Fig.1.7. This captures the case of a symmetry twist g applied to a path p_g along a cylinder, from one boundary to the other, and also the case of a pair of monodromy defects on a sphere, where each puncture is formed by removing a PEPS tensor and replacing it with a tensor that describes the defect.

Treating a symmetry twisted SPT PEPS on a cylinder (of fixed radius) as a one dimensional system, it is clear that the bulk is invariant under the residual symmetry group $\mathbb{C}(g)$ since the symmetry twisted SPT PEPS on a torus formed by closing the cylinder (such that p_g becomes a noncontractible cycle) is symmetric. In this case the PEPS can be interpreted as a MPS and standard results in this setting imply that the global symmetry $U(h)^{\otimes |\mathcal{M}|_v}$ is intertwined by the PEPS to a tensor product of projective symmetry representations on the left and right virtual boundaries $\mathcal{V}_L^g(h) \otimes \mathcal{V}_R^g(h)$.

The projective boundary action $\mathcal{V}_R^g(h)$ of the symmetry can be explicitly constructed within the SPT PEPS framework. We find that it is given by a symmetry MPO acting on the PEPS

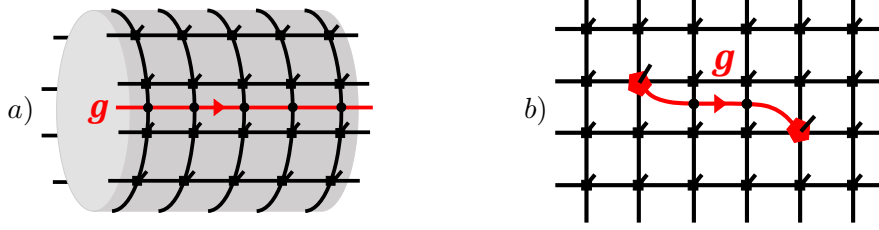


Figure 1.7: a) A symmetry twist along a cylinder PEPS. b) A pair of monodromy defects in a PEPS.

virtual bonds entering the puncture, with its inner indices at the intersection of p_g and the boundary of the puncture contracted with the tensor $Y_R^g(h)$ (see Eq.(1.88)) that acts on the inner index of the symmetry twist MPO $V^{p_g}(g)$ entering the puncture.

The diagram shows a vertical red oval with two horizontal lines passing through it. The left line has a red arrow pointing up, and the right line has a red arrow pointing down. A red arrow labeled g points to the right, and a red arrow labeled h points to the left. The equation $\mathcal{V}_R^g(h) =$ is written to the left of the diagram, and the equation number (1.20) is to the right.

$$\mathcal{V}_R^g(h) = \quad (1.20)$$

The multiplication of physical symmetries induces a composition rule for the $Y_R^g(\cdot)$ tensors, see Appendix 1.16 for details. Explicit calculation of these products yields the 2-cocycle factor set ω^g of the projective boundary representation $\mathcal{V}_R^g(k)\mathcal{V}_R^g(h) = \omega^g(k, h)\mathcal{V}_R^g(kh)$ in terms of the 3-cocycle α of the MPO symmetry representation $\omega^g(k, h) \sim \frac{\alpha(g, k, h)\alpha(k, h, g)}{\alpha(k, g, h)}$. This is consistent with the results of Ref. 118. Note that altering α by a 3-coboundary induces a 2-coboundary change to the 2-cocycle ω^g , which hence forms a robust label of the SPT phase. The projective symmetry action is closely related to the braiding of anyons in the gauged theory.

1.7 Example: fixed-point SPT states

Inspired by the illuminating examples in Refs. 36 and 70 we now present a family of SPT PEPS with symmetry group G and 3-cocycle α satisfying Eqs.(1.3) and (1.4), and explicitly demonstrate that gauging these states⁷¹ yields MPO-injective PEPS that are the ground states of twisted quantum double Hamiltonians^{72,105}.

1.7.1 Fixed-point SPT PEPS

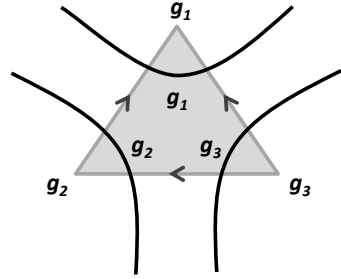
We describe our construction of fixed-point SPT PEPS and calculate the MPOs induced by the symmetry action on a site. We explicitly give the fusion tensors for these MPOs and verify that they satisfy the *zipper* condition before determining the 3-cocycle of the MPO representation.

Our short-range entangled PEPS are defined on any trivalent lattice embedded in an oriented 2-manifold (dual to a triangular graph). They realize states equivalent to a standard

SPT fixed-point construction on the triangular graph^{36,75}. To this end we specify an ordering on the vertices of the triangular graph which induces an orientation of each edge, pointing from larger to smaller vertex. With this information we assign the following PEPS tensor $A_\Delta : \mathbb{C}(G)^{\otimes 6} \rightarrow \mathbb{C}(G)^{\otimes 3}$ to each vertex of the trivalent lattice

$$A_\Delta := \int \prod_{v \in \Delta} dg_v \tilde{\alpha}_\Delta \bigotimes_{v \in \Delta} |g_v\rangle_{\Delta,v} \bigotimes_{e \in \Delta} (g_{v_e^-} |_{\Delta,e,v_e^-} (g_{v_e^+} |_{\Delta,e,v_e^+} \quad (1.21)$$

where edge e is oriented from v_e^+ to v_e^- (hence $v_e^- < v_e^+$) in the triangular graph. The phase $\tilde{\alpha}_\Delta$ is defined on a vertex of the trivalent PEPS lattice dual to plaquette Δ of the triangular lattice, whose vertices appear in the order v, v', v'' following the orientation of the 2-manifold (note the choice of starting vertex is irrelevant), by a 3-cocycle α as follows $\tilde{\alpha}_\Delta := \alpha^{\sigma_\pi}(g_1 g_2^{-1}, g_2 g_3^{-1}, g_3)$. Where $(g_1, g_2, g_3) := \pi(g_v, g_{v'}, g_{v''})$ with π the permutation that sorts the group elements into ascending vertex order and $\sigma_\pi = \pm 1$ is the parity of the permutation (equivalently the orientation of Δ relative to the 2-manifold). In the following example the tensor A_Δ , possessing six virtual and three physical indices, has non zero entries given by



$$= \alpha(g_1 g_2^{-1}, g_2 g_3^{-1}, g_3). \quad (1.22)$$

Note the tensor diagrams in this section use the convention that physical vertex indices are written within the body of the tensor. Moreover we only depict the virtual and physical index combinations that give rise to non-zero values of the tensor.

The global symmetry of the PEPS on a closed manifold is ensured by the following transformation property of each local tensor

$$R(h)^{\otimes 3} A_\Delta = A_\Delta \bigotimes_{e \in \Delta} [Z_e^{\sigma_{\Delta,e}}(h) R(h)^{\otimes 2}], \quad (1.23)$$

where $Z_e(h) := \int dg_{v_e^-} dg_{v_e^+} \alpha(g_{v_e^-} g_{v_e^+}^{-1}, g_{v_e^+}, h) |g_{v_e^-}, g_{v_e^+}\rangle (g_{v_e^-}, g_{v_e^+}|$, and $\sigma_{\Delta,e} = \pm 1$ is $+1$ if e is directed along the clockwise orientation of $\partial\Delta$, and -1 otherwise. With this definition one can check that Eq.(1.23) is equivalent to the cocycle condition (1.60). Note the boundary actions on the shared edge of two neighboring tensors $A_\Delta, A_{\Delta'}$, induced by group multiplication on the physical sites Δ, Δ' , cancel out since $\sigma_{\Delta,e} = -\sigma_{\Delta',e}$ from which it follows that the full PEPS (on a closed manifold) is invariant under the group action applied to all physical indices.

In our example the symmetry property is*

$$(1.24)$$

Where the left side of the equality depicts the physical symmetry acting on a single tensor, and the right side depicts the virtual representation of the symmetry.

Note that a tensor product of the virtual symmetry matrices $[Z_e^{\sigma\Delta,e}(h)R(h)^{\otimes 2}]$ in general do not constitute a representation of G . A representation of G on the virtual level, $V(g)$, is obtained by projecting these matrices onto the subspace on which the PEPS tensor is injective. By doing so we construct MPOs that cannot be factorized as a tensor product. For the current fixed-point example we project $[Z_e^{\sigma\Delta,e}(h)R(h)^{\otimes 2}]$ onto the subspace of virtual boundary indices corresponding to non-zero values of A_Δ , Eq.(1.21). This yields a MPO $V(h)$ constructed from the following tensors

$$(1.25)$$

note that for fixed h these MPOs possess a single block. We introduce the isometry $X(h_1, h_2)$

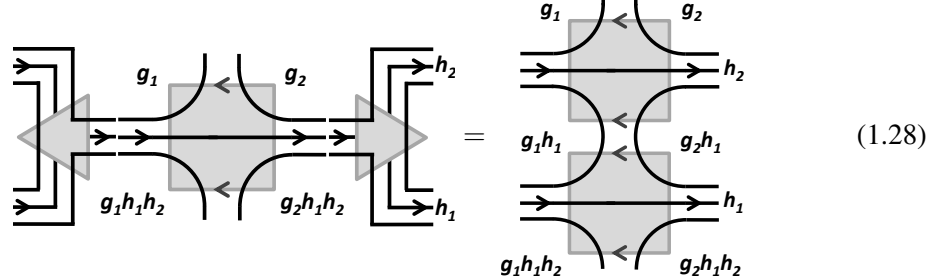
$$(1.26)$$

to describe the multiplication of two MPO tensors. With this isometry we have the following relation

$$(1.27)$$

* Note the following subtlety, our tensor diagrams depict the coefficients of the map A_Δ and hence the group action $R(h)$ on the physical kets is equivalent to $R(h^{-1})$ on the coefficients, i.e. $R(h) \int dg f(g) |g\rangle = \int dg f(gh) |g\rangle$.

where the left most tensor of Eq.(1.27) is $X^\dagger(h_1, h_2)$ and we have made use of the 3-cocycle condition (1.60). This implies that the MPOs $V(h)$ with fixed inner indices indeed form a representation of G . Note the stronger *zipper* condition



also holds for this MPO representation.

From Eq.(1.23) it is clear that the PEPS tensors A_Δ , Eq.(1.21), together with the MPOs $V(h)$, defined by Eq.(1.25), have SPT order described by the framework of Section 1.4. We now calculate the third cohomology class of the MPOs to determine which SPT phase the model belongs to. For this we see that X obeys the following associativity condition

$$X(h_1 h_2, h_3)[X(h_1, h_2) \otimes \mathbb{1}_{h_3}] = \alpha^{-1}(h_1, h_2, h_3) X(h_1, h_2 h_3)[\mathbb{1}_{h_1} \otimes X(h_2, h_3)], \quad (1.29)$$

which is again the 3-cocycle condition Eq.(1.60). From Eq.(1.29) we thus conclude that the short-range entangled states described by the tensors of Eq.(1.21) lie in a symmetry-protected topological phase labeled by the cohomology class $[\alpha^{-1}] \in H^3(G, U(1))$, see Appendix 1.9.

One may be surprised to notice that one layer of strictly local unitaries (equivalent to the local unitary circuit D_α (1.141)) acting on the vertices of the PEPS built from the tensors in Eq.(1.21) can remove the 3-cocycles, thus mapping it to a trivial product state. Superficially this seems to contradict the fact that SPT states cannot be connected to the trivial product state by low-depth local unitary circuits that preserve the symmetry. However, this is not the case as this definition requires every individual gate of the circuit to preserve the symmetry²⁶, which is not true for the circuit just described.

1.7.2 Gauging the fixed-point SPT PEPS

We now apply the quantum state gauging procedure of Ref. 71 to gauge the global symmetry of the fixed-point SPT PEPS defined in the previous subsection. For this we construct a gauging tensor network operator (matching that of Ref. 71 on the dual triangular graph) that couples gauge degrees of freedom to a given matter state. We proceed by applying a local unitary circuit to disentangle the gauge constraints and explicitly demonstrate that the resulting tensor describes the ground state of a twisted Dijkgraaf-Witten gauge theory.

The gauging map is defined by the following local tensors $G^\Delta : \mathbb{C}(G)^{\otimes 6} \otimes \mathbb{C}(G)^{\otimes 3} \rightarrow \mathbb{C}(G)^{\otimes 6}$

$$G^\Delta := \int \prod_{v \in \Delta} dh_v \bigotimes_{v \in \Delta} R_{\Delta, v}(h_v) \bigotimes_{e \in \Delta} [|h_{v_e^-} h_{v_e^+}^{-1}\rangle_{\Delta, e} \otimes (h_{v_e^+}|_{\Delta, e, v_e^+} (h_{v_e^-}|_{\Delta, e, v_e^-})], \quad (1.30)$$

note G^Δ introduces gauge degrees of freedom on the edges. For our example the gauging tensor

is

$$(1.31)$$

We can apply the gauging tensors locally to the SPT PEPS to form tensors for a gauge and matter PEPS

$$\bar{A}_\Delta := \int \prod_{v \in \Delta} dh_v dg_v \tilde{\alpha}_\Delta \bigotimes_{v \in \Delta} |g_v h_v^{-1}\rangle_{\Delta, v} \bigotimes_{e \in \Delta} |h_{v_e^-} h_{v_e^+}^{-1}\rangle_{\Delta, e} (g_{v_e^+}, h_{v_e^+}|_{\Delta, e, v_e^+} (g_{v_e^-}, h_{v_e^-}|_{\Delta, e, v_e^-} \quad (1.32)$$

in our example these are

$$= \alpha(g_1 g_2^{-1}, g_2 g_3^{-1}, g_3). \quad (1.33)$$

The gauged PEPS $|\psi_g\rangle$, built from the tensors \bar{A}_Δ , satisfies local gauge constraints $\tilde{P}_v |\psi_g\rangle = |\psi_g\rangle$ for every vertex v , where

$$\tilde{P}_v := \int dg_v \bigotimes_{\Delta \ni v} [R_{\Delta, v}(h) \bigotimes_{e \in E_v^+} R_{\Delta, e}(g_v) \bigotimes_{e \in E_v^-} L_{\Delta, e}(g_v)]$$

The gauge and matter tensor \bar{A}_Δ is MPO-injective with respect to a purely virtual symmetry inherited from the symmetry transformation of the SPT tensor A_Δ and it also intertwines a physical symmetry to a virtual symmetry due to the transformation of the gauging tensors

$$\begin{aligned} \bar{A}_\Delta \bigotimes_{e \in \Delta} [Z_e^{\sigma_{\Delta, e}}(h) R(h)^{\otimes 2}] \otimes R(h)^{\otimes 2} &= \bar{A}_\Delta \bigotimes_{v \in \Delta} R_{\Delta, v}(h) \bigotimes_{e \in \Delta} R_{\Delta, e}(h) L_{\Delta, e}(h) \bar{A}_\Delta \\ &= \bar{A}_\Delta \bigotimes_{e \in \Delta} \mathbf{1}^{\otimes 2} \otimes L(h)^{\otimes 2} \end{aligned} \quad (1.34)$$

the latter symmetry reflects the invariance of the full PEPS under the gauge constraints \tilde{P}_v .

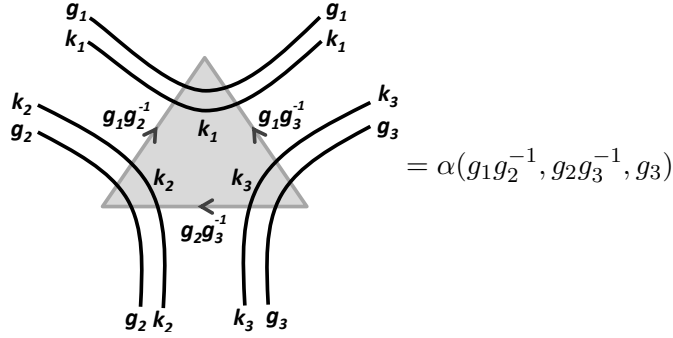
We next apply a local unitary circuit \tilde{C}_Δ to explicitly map the gauge and matter model to a twisted quantum double ground state on the gauge degrees of freedom alone. This circuit is given by the tensor product of the following local unitary on each site

$$\tilde{C}_\Delta := \int \prod_{v \in \Delta} dg_v \bigotimes_{v \in \Delta} |g_v\rangle \langle g_v|_v \bigotimes_{e \in \Delta} L_e(g_{v_e^-}) R_e(g_{v_e^+}),$$

which maps the gauge constraints to local rank one projectors on the matter degrees of freedom at each vertex $\tilde{C}_\Lambda \tilde{P}_v \tilde{C}_\Lambda = \int dg_v \otimes_{\Delta \ni v} R_{\Delta,v}(h)$, fixing the state of the matter to be $\int dg_v \otimes_{\Delta \ni v} |g_v\rangle_{\Delta,v}$. From this we infer that the circuit \tilde{C}_Λ disentangles the gauge from the matter degrees of freedom. To see this explicitly we apply the circuit locally to each PEPS tensor, along with a unitary change of basis on the virtual level (leaving the physical state invariant) to form the tensor $\bar{\bar{A}}_\Delta$ which is defined as follows

$$\begin{aligned} \bar{\bar{A}}_\Delta &:= \tilde{C}_\Delta \bar{A}_\Delta \bigotimes_{e \in \Delta} U_{\Delta,e,v_e^+} \otimes U_{\Delta,e,v_e^-} \\ &= \int \prod_{v \in \Delta} dk_v dg_v \tilde{\alpha}_\Delta \bigotimes_{v \in \Delta} |k_v\rangle_{\Delta,v} \bigotimes_{e \in \Delta} [|g_{v_e^-} g_{v_e^+}^{-1}\rangle_{\Delta,e} \otimes (g_{v_e^+}, k_{v_e^+} |_{\Delta,e,v_e^+} (g_{v_e^-}, k_{v_e^-} |_{\Delta,e,v_e^-}] \end{aligned} \quad (1.35)$$

where $U := \int dg |g\rangle \langle g| \otimes SL^\dagger(g)$, with $S|g\rangle := |g^{-1}\rangle$, satisfies $(g, h|U = (g, gh^{-1}|$. For our example this tensor is given by



$$= \alpha(g_1 g_2^{-1}, g_2 g_3^{-1}, g_3) \quad (1.36)$$

This disentangled PEPS tensor $\bar{\bar{A}}_\Delta$ is now MPO-injective on the support subspace of the projection MPO given by a normalized sum of the symmetry MPOs from the SPT PEPS. Moreover the intertwining condition maps the physical vertex symmetry to a trivial action on the virtual space

$$\bar{\bar{A}}_\Delta \bigotimes_{e \in \Delta} [Z_e^{\sigma_{\Delta,e}}(h) R(h)^{\otimes 2}] \otimes \mathbb{1}^{\otimes 2} = \bar{\bar{A}}_\Delta \bigotimes_{v \in \Delta} R_{\Delta,v}(h) \bar{\bar{A}}_\Delta \quad (1.37)$$

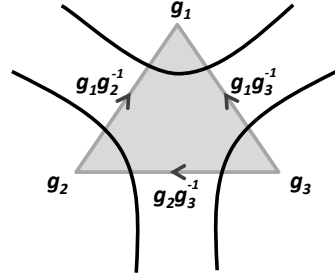
$$= \bar{\bar{A}}_\Delta \bigotimes_{e \in \Delta} \mathbb{1}^{\otimes 2} \otimes R(h)^{\otimes 2}. \quad (1.38)$$

From this we see that $\bar{\bar{A}}_\Delta$ separates into a trivial local component on the matter degrees of freedom yielding the state $\otimes_v \int dg_v \otimes_{\Delta \ni v} |g_v\rangle_{\Delta,v}$, and the following tensors on the gauge degrees of freedom

$$\int \prod_{v \in \Delta} dg_v \tilde{\alpha}_\Delta \bigotimes_{e \in \Delta} |g_{v_e^-} g_{v_e^+}^{-1}\rangle_{\Delta,e} (g_{v_e^+} |_{\Delta,e,v_e^+} (g_{v_e^-} |_{\Delta,e,v_e^-} \cdot \quad (1.39)$$

These tensors define a PEPS on the gauge degrees of freedom that is a ground state of a 2D twisted quantum double with 3-cocycle α . Note this PEPS matches the standard representation of the ground state on the subspace obtained by mapping $\otimes_{\Delta \ni v} |g\rangle_{\Delta,v} \mapsto |g\rangle_v$ and

$\otimes_{\Delta \ni e} |g\rangle_{\Delta, e} \mapsto |g\rangle_e$. For our example this tensor is



$$= \alpha(g_1 g_2^{-1}, g_2 g_3^{-1}, g_3) \quad (1.40)$$

note in the Abelian case the tensors in Eq.(1.40) reduce to the string-net tensors^{119,120} after a suitable mapping between 3-cocycles and F -symbols¹²¹ (in the non-Abelian case one has to change to the basis of irreducible representations to make the identification).

1.7.3 Perturbations away from fixed-points

The examples presented thus far in this section are all fixed-point states under a real space blocking renormalization group flow and have zero correlation length. This corresponds to the PEPS tensor that builds the state being of MPO-isometric type⁶³. More generally one could add an arbitrary perturbation that lies within the MPO-injectivity subspace (this can be constructed by applying the MPO projector to an arbitrary perturbation) to the MPO-isometric PEPS tensor to find a new MPO-injective PEPS that will generically have a finite correlation length. For a sufficiently small symmetric perturbation the resulting MPO-injective PEPS will lie in the same phase of matter as the fixed-point MPO-isometric PEPS^{62,122}.

The simplest explicit perturbations away from fixed-point tensors are given by local filtering operations on the physical indices. For a given MPO-injective PEPS tensor A local filtering by a projector P generates a family of MPO-injective deformations $\{P(\lambda)A \mid \lambda \in [0, 1]\}$ where $P(\lambda) := (1 - \lambda)\mathbb{1} + \lambda P$. For topological PEPS P can be an arbitrary projector on the physical index, while for SPT PEPS it must commute with the on-site symmetry action. This path of deformations can move from one phase of matter to another, for instance if we let $P = |0\rangle\langle 0|$ the deformation can induce an anyon condensation transition if A describes a topologically ordered ground state^{71,123,124}. In the SPT case with on-site group action $R(g)$ one can consider $P = |\tilde{e}\rangle\langle \tilde{e}|$, the projector onto the trivial representation, where $|\tilde{e}\rangle = \frac{1}{|G|} \sum_{g \in G} |g\rangle$ to find a symmetric interpolation to the trivial phase. A framework to understand these transitions in terms of symmetry breaking of the virtual symmetry is described in Refs. ^{123,124}.

1.8 Conclusions

We have presented a unified picture for the characterization of all gapped phases, possibly with respect to certain physical symmetries, within the framework of PEPS in terms of virtual MPO symmetries. To achieve this we developed a characterization of global symmetry in the framework of MPO-injective PEPS^{62,63}. In contrast to the injective case⁶⁹, where the symmetry representation on the virtual indices factorizes into a tensor product, a MPO-injective PEPS tensors can have a virtual symmetry representation given by unfactorizable MPOs. We subsequently identified the short-range entangled PEPS to be those having a single block in the projection

MPO onto the injectivity subspace. If the accompanying single block MPO virtual symmetry representation has a non-trivial third cohomology class it gives rise to unconventional edge properties and thus to symmetry-protected topological PEPS. Our identification of the virtual entanglement structure of PEPS with SPT order opens new routes to study transitions between SPT phases by utilizing methods that have been developed to study anyon condensation transitions of topological phases^{94,123}.

We demonstrated that applying the quantum state gauging procedure⁷¹ to a SPT PEPS transforms its MPO representation of G into a purely virtual symmetry of the gauged tensors. This implies that the resulting gauge-invariant PEPS also satisfies the axioms of MPO-injectivity, but with a projection MPO onto the injectivity subspace with a block structure labeled by the group elements $g \in G$. This block structure of the projection MPO, together with the third cohomology class label, characterizes the phases of the twisted quantum double models which are known to have intrinsic topological order. It was shown in Ref. 63 that the projection MPO determines all the topological properties of the gauged PEPS. This relation explains the mechanism behind the braiding statistics approach to SPT phases⁷³ at the level of the corresponding quantum states. It furthermore reveals that both the gauging and boundary theory approaches to classifying SPT phases are recast in the PEPS framework as the classification of a common set of MPOs. We have illustrated these concepts for a family of RG fixed-point states, containing a representative for all two-dimensional bosonic SPT phases with a finite on-site symmetry group.

To prove these results we developed new tools to deal with orientation dependent MPO tensors and used them to calculate the symmetry action on monodromy defected and symmetry twisted states and also modular transformations, before and after gauging, in terms of a single tensor.

The general formalism presented in this paper describes both local physical symmetries and topological order of PEPS with virtual MPO symmetries. Furthermore, it captures the general action of a symmetry on a PEPS with topological order and hence yields a natural framework for the study of symmetry-enriched topological phases (SET). The quantum state gauging procedure can be adapted to gauge only a normal subgroup of the global symmetry group of a SPT PEPS, which allows one to explicitly construct families of SET PEPS. An open question is how the corresponding MPOs encode the discrete, universal labels of the SET phase and how to extract them. We further expect that a better understanding of excitations in MPO-injective PEPS⁶⁴ will yield insights into the physical properties of SET phases such as symmetry fractionalization. These matters are studied in Ref. 103 and Chapter 3.

In this work we only explicitly consider finite on-site unitary symmetry actions. It is an interesting and relevant question to generalize this to time-reversal and continuous Lie group symmetries as well as lattice translation and point group symmetries. Progress has been made on incorporating these types of symmetries into PEPS in Ref. 107. In particular since time-reversal can be realized as a local action on the PEPS tensors¹¹² a similar approach to that used here should apply, with some extra care necessary due to the possible action of time reversal on the symmetry MPOs.

Another question which presents itself is how to generalize the constructions presented in this paper to fermionic systems. Partial progress has been made in the direction of applying the same principles to the formalism of fermionic PEPS¹²⁵. This has led to a (partial) classification

of fermionic SPT phases^{66,126} based on supercohomology¹²⁷ and the existence of Majorana-type defects¹²⁸. The quantum state gauging procedure works equally well for fermionic systems, but the gauge degrees of freedom are always bosonic. It would thus be interesting to see how fermionic SPT order can be probed in this way.

Our identification of SPT PEPS in 2D as being injective with respect to an injective MPO hints at a hierarchical definition of SPT PEPS in arbitrary dimension with an injective tensor network object associated to each codimension. This appears to recover the cohomological classification of bosonic SPT states in arbitrary dimensions by a generalization of the argument from⁷⁰. We plan to explore this further in future work.

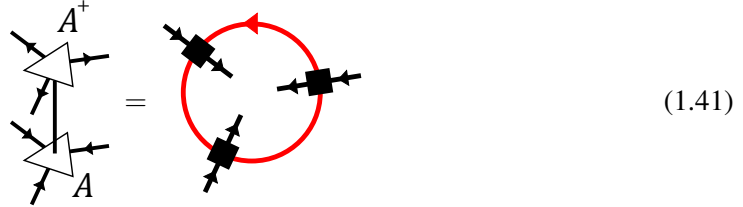
Acknowledgments — We acknowledge helpful discussions with N. Schuch. This work was supported by EU grant SIQS and ERC grant QUERG, the Odysseus grant from the Research Foundation Flanders (FWO) and the Austrian FWF SFB grants FoQuS and ViCoM. M.M. and J.H. further acknowledge the support from the Research Foundation Flanders (FWO).

Supplementary Material

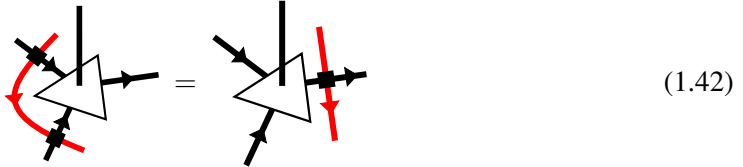
1.9 Axioms for MPO-injectivity

This section reviews the axioms of MPO-injectivity as presented in Ref. 63.

We interpret the tensors A of a MPO-injective PEPS as linear maps from the virtual to the physical space and apply a distinguished generalized inverse A^+ , which gives rise to a projector that can be written as a MPO:



We further require this MPO to satisfy the *pulling through* property shown in Eq.(1.42).



The same property should also hold where the MPO gets pulled from three virtual indices to one or vice versa. This makes the presence of this MPO locally undetectable in the PEPS. Using the pulling through property, it is easy to check that the requirement for the MPO to be a projector is equivalent to the property shown in Eq.(1.43)



We also need a technical requirement such that the properties of the PEPS grow in a controlled way with the number of sites. For example, we want two concatenated tensors to be injective on the support subspace of the projection MPO surrounding these two tensors. For this we need that there exists a tensor E , depicted in (1.44),

$$E := \text{[Diagram: A blue circle with a red line passing through it and a small black square on the line]} \quad (1.44)$$

such that we have the *extended inverse* property (1.45).

$$\text{[Diagram: A blue circle with a red line passing through it and a small black square on the line, surrounded by red arcs and black squares]} = \text{[Diagram: Two black squares connected by a red arc]} \quad (1.45)$$

The extended inverse property allows one to prove many useful things such as the intersection property or an explicit expression for the ground state manifold on a torus⁶³. It turns out that under very reasonable assumptions about the projection MPO the extended inverse condition is automatically satisfied⁶⁴.

1.10 Uniqueness of SPT PEPS ground state

In this appendix we demonstrate that the parent Hamiltonian of a MPO-injective PEPS with a single block projection MPO has a unique ground state on the torus (i.e. no topological degeneracy). A similar argument holds for higher genus surfaces.

For a Hermitian projection MPO there is no need to keep track of a direction on the internal leg of the MPO, we also ignore the explicit directions on the edges of the PEPS as they are irrelevant to our arguments. We require the following condition (stronger than Eq.(1.57))

We assume the projection MPO has been brought into a form satisfying the *zipper* condition, i.e. there are no off diagonal blocks in the product of two MPO tensors after it has been brought into canonical form, equivalently

$$\text{[Diagram: Two black squares stacked vertically with red lines]} = \text{[Diagram: A black square with red lines labeled } X \text{ and } X^+ \text{]} \quad (1.46)$$

where X is the reduction tensor for multiplication of copies of the MPO which forms a single block representation of the trivial group. This is true of the MPOs arising from fixed-point models. For this representation we have the following version of Eq.(1.58)

$$\text{[Diagram: A red line with a black square]} = \alpha \text{ [Diagram: A red line with a black square]} \quad (1.47)$$

We now rewrite this equality in a more suggestive fashion

$$\text{Diagram 1} = \alpha \text{Diagram 2} \quad (1.48)$$

In the above, and throughout the remainder of this appendix, we ignore explicit direction dependence as it does not affect the arguments made.

In the framework of MPO-injectivity different ground states of the PEPS parent Hamiltonian on the torus are spanned by tensor networks closed with different Q tensor solutions (see Ref. 63) connected to MPOs on the virtual level along the inequivalent noncontractible loops of the torus

$$\text{Diagram 1.49} \quad (1.49)$$

From the physical level one only has access to the Q tensor projected onto the support subspace of a MPO loop along the closure of the system.

$$\text{Diagram 1.50} \quad (1.50)$$

Note this closure gives rise to the same ground state as the closed loop is a symmetry of the closed MPO-injective tensor network. Using condition (1.46) repeatedly (within the closed tensor network) leads to the following crossing tensor

$$\text{Diagram 1.51} \quad (1.51)$$

which again gives rise to the same ground state. Following several more applications of Eqs.(1.46) & (1.48) we arrive at

$$\text{Diagram 1.52} \quad (1.52)$$

Note the overall phase of the ground state is irrelevant. Since the Q tensor can be placed anywhere in the tensor network we have that the following matrix

$$M_Q := \text{Diagram 1.53} \quad (1.53)$$

commutes through the virtual level of the single block (injective) projection MPO and hence must be proportional to the identity $M_Q = 1$. Plugging this in we have the crossing tensor


(1.54)

which, by Eq.(1.46), yields the same state as the following


(1.55)

and with several applications of Eqs.(1.46) & (1.48) one can verify that this is equivalent to

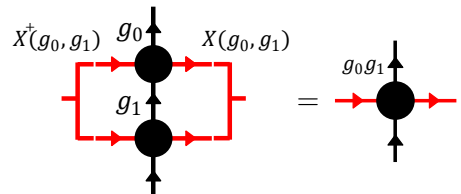

(1.56)

which is easily seen to be a symmetry of a closed MPO-injective tensor network which hence yields the trivial ground state. To summarize we have seen that any Q tensor solution gives rise to the unique ground state obtained by closing the tensor network without any MPOs on the virtual level.

1.11 Third cohomology class of a single block MPO group representation

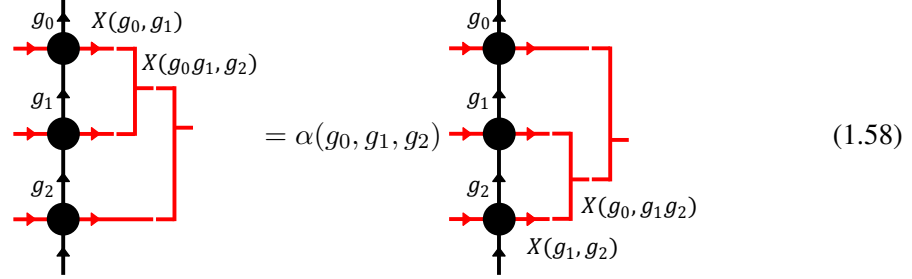
In this appendix we recount the definition of the third cohomology class of an injective MPO representation of a finite group G , as first introduced in Ref. 70. For details about group cohomology theory in the context of SPT order we refer the reader to Ref. 36.

In a MPO representation of G , multiplying a pair of MPOs labeled by the group elements g_0 and g_1 is equal to the MPO labeled by $g_0 g_1$ for every length. Since the MPOs are injective we again know there exists a gauge transformation on the virtual indices of the MPO that brings both representations into the same canonical form⁴⁵. This implies that there exists an operator (the reduction tensor) $X(g_0, g_1) : (\mathbb{C}^x)^{\otimes 2} \rightarrow \mathbb{C}^x$ such that Eq.(1.57) holds.


(1.57)

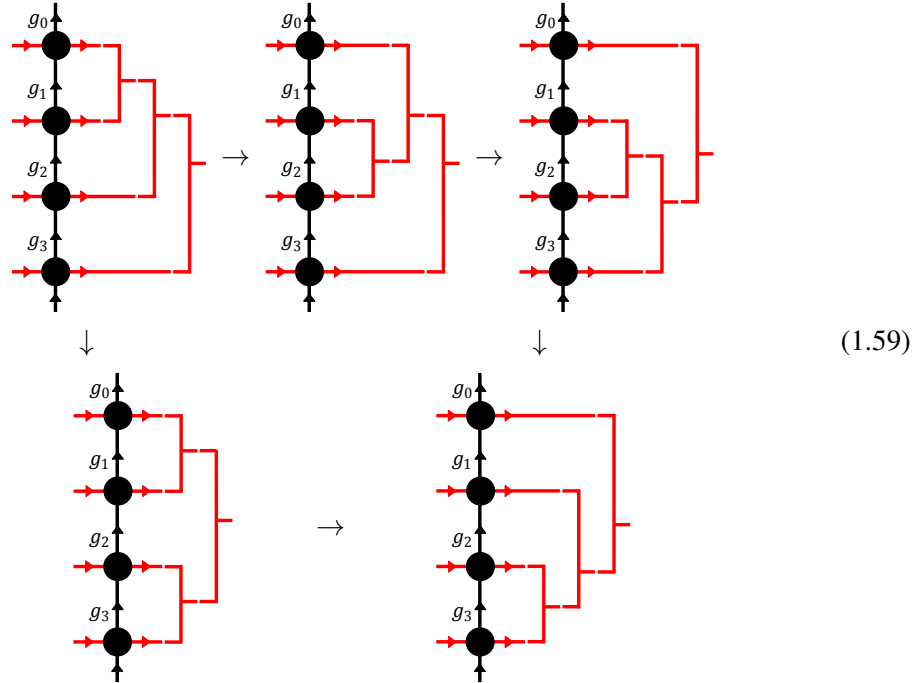
note $X(g_0, g_1)$ is only defined up to multiplication by a complex phase $\beta(g_0, g_1)$. If we now multiply three MPOs labeled by g_0 , g_1 and g_2 there are two ways to reduce the multiplied

MPOs to the MPO labeled by $g_0 g_1 g_2$. When only acting on the right virtual indices these two reductions are equivalent up to a nonzero complex number labeled by g_0 , g_1 and g_2 . This is shown in Eq.(1.58).



$$(1.58)$$

By multiplying four MPOs one sees that α has to satisfy certain consistency conditions as the two different paths achieving the same reduction, shown in Eq.(1.59), should give rise to the same complex number.



$$(1.59)$$

Using Eq.(1.58) one can easily verify that the consistency conditions are

$$\frac{\alpha(g_0, g_1, g_2)\alpha(g_0, g_1 g_2, g_3)\alpha(g_1, g_2, g_3)}{\alpha(g_0 g_1, g_2, g_3)\alpha(g_0, g_1, g_2 g_3)} = 1 \quad (1.60)$$

which are exactly the 3-cocycle conditions and hence α is a 3-cocycle. As mentioned above $X(g_0, g_1)$ is only defined up to a complex number $\beta(g_0, g_1)$. This freedom can change the 3-cocycle defined in Eq.(1.58) by

$$\alpha'(g_0, g_1, g_2) = \alpha(g_0, g_1, g_2) \frac{\beta(g_1, g_2)\beta(g_0, g_1 g_2)}{\beta(g_0, g_1)\beta(g_0 g_1, g_2)} \quad (1.61)$$

thus we see that α is only defined up to a 3-coboundary. For this reason the single block MPO group representation is endowed with the label $[\alpha]$ from the third cohomology group $H^3(G, \mathbb{C})$. Using the fact that $H^d(G, \mathbb{R}) = \mathbb{Z}_1$ ³⁶ (and that \mathbb{R} as an additive group is isomorphic to \mathbb{R}^+ as a multiplicative group), we thus obtain that the third cohomology class of the MPO representation $[\alpha]$ is an element of $H^3(G, U(1))$.

1.12 Orientation dependencies of MPO group representations

In this appendix we go beyond previous treatments of MPO group representations to consider subtleties that arise due to possible orientation dependencies of the tensors. We find a gauge transformation that reverses the orientation of MPO tensors, and use it to define the Frobenius-Schur indicator. We then find several *pivotal* phases and relate them to the 3-cocycle of the MPO group representation.

1.12.1 Orientation reversing gauge transformation

To describe the most general bosonic SPT phases one must use lattices with oriented edges, the internal index of the MPO also carries an orientation which leads to the definition of a pair of possibly distinct MPO tensors which depend on the handedness of the crossing upon which they sit

$$B_+(g) = \begin{array}{c} \uparrow \\ \text{---} g \text{---} \bullet \text{---} \\ \downarrow \end{array}, \quad B_-(g) = \begin{array}{c} \downarrow \\ \text{---} g \text{---} \bullet \text{---} \\ \uparrow \end{array} \quad (1.62)$$

As shown in Section 1.3 reversing the orientation of the internal MPO index corresponds to inverting the group element which the MPO represents, i.e. $V_{\text{rev}}(g) = V(g^{-1})$. Since this holds for any injective group MPO of arbitrary length standard results from the theory of MPS imply that the local tensors are related by an invertible gauge transformation which we denote Z_g

$$\begin{array}{c} \uparrow \\ \text{---} g \text{---} \bullet \text{---} \\ \downarrow \end{array} = \begin{array}{c} \uparrow \\ \text{---} g \text{---} \triangleleft \text{---} \end{array} \begin{array}{c} \uparrow \\ \text{---} g^{-1} \text{---} \bullet \text{---} \\ \downarrow \end{array} \begin{array}{c} \rightarrow \\ \text{---} \triangleleft \text{---} \end{array} \quad (1.63)$$

$$\begin{array}{c} \downarrow \\ \text{---} g \text{---} \bullet \text{---} \\ \uparrow \end{array} = \begin{array}{c} \downarrow \\ \text{---} g \text{---} \triangleleft \text{---} \end{array} \begin{array}{c} \downarrow \\ \text{---} g^{-1} \text{---} \bullet \text{---} \\ \uparrow \end{array} \begin{array}{c} \rightarrow \\ \text{---} \triangleleft \text{---} \end{array} \quad (1.64)$$

where we use the following graphical notation for Z_g and related matrices

$$Z_g = \begin{array}{c} \text{---} g \text{---} \triangleleft \text{---} \\ \text{---} g^{-1} \text{---} \end{array}, \quad Z_g^T = \begin{array}{c} \text{---} g^{-1} \text{---} \triangleleft \text{---} \\ \text{---} g \text{---} \end{array} \quad (1.65)$$

$$Z_g^{-1} = \begin{array}{c} \text{---} g^{-1} \text{---} \triangleleft \text{---} \\ \text{---} g \text{---} \end{array}, \quad (Z_g^{-1})^T = \begin{array}{c} \text{---} g \text{---} \triangleleft \text{---} \\ \text{---} g^{-1} \text{---} \end{array} \quad (1.66)$$

which satisfy the relations

$$\begin{array}{c} \text{---} g \text{---} \triangleleft \text{---} g^{-1} \text{---} \triangleleft \text{---} \\ \text{---} g \text{---} \end{array} = \begin{array}{c} \text{---} g^{-1} \text{---} \end{array} \quad (1.67)$$

$$\begin{array}{c} \text{---} g^{-1} \text{---} \triangleleft \text{---} g \text{---} \triangleleft \text{---} \\ \text{---} g^{-1} \text{---} \end{array} = \begin{array}{c} \text{---} g \text{---} \end{array} \quad (1.68)$$

note while it seems *a priori* that the gauge transformations in Eq.(1.64) could be independent, the fact that the equation $V_{\text{rev}}(g) = V(g^{-1})$ holds for arbitrary orientations of the PEPS bonds implies that they can be chosen to be the same.

Applying the gauge transformation twice we arrive at the equality

$$(1.69)$$

which implies $Z_g(Z_{g^{-1}}^{-1})^T = \chi_g \mathbb{1}$ for some $\chi_g \in U(1)$ since the MPO is injective. Hence $Z_g = \chi_g Z_{g^{-1}}^T$ i.e.

$$(1.70)$$

where χ_g is analogous to the Frobenius–Schur indicator and can be seen to satisfy $\chi_g = \chi_{g^{-1}}^{-1}$. Note χ_g can be absorbed by redefinition of Z_g whenever $g \neq g^{-1}$, but we will not do so at this point.

1.12.2 Pivotal phases

Since the multiplication of the injective MPOs forms a representation of G we have a local reduction as in Eq.(1.57). Again since this holds for arbitrary orientations of the PEPS bonds the reduction matrix $X(g_0, g_1)$ is the same for left and right handed MPOs. From here on we will work with a stronger restriction on the form of the MPOs such that the following *zipper* condition holds

$$(1.71)$$

this is equivalent to there being no off diagonal blocks in the product of two MPO tensors after it has been brought into canonical form, and is true for MPOs that arise from fixed-point models.

Let us now derive a relation between $\mathbb{1}_g \otimes (Z_h^{-1})^T X^+(g, h)$ and $X(gh, h^{-1})$ in terms of a *one-line pivotal phase* which we then proceed to calculate in terms of the three cocycle α of

the MPO group representation. Consider

Diagrammatic equation (1.72) showing the decomposition of a product of two MPOs into a single MPO with a loop. The equation is as follows:

$$\begin{aligned}
 & \begin{array}{c} X^\dagger(gh, h^{-1}) \quad gh \\ \text{---} \bullet \text{---} X(gh, h^{-1}) \\ \text{---} h^{-1} \text{---} \bullet \text{---} \\ \text{---} \end{array} = \begin{array}{c} g \\ \text{---} \bullet \text{---} \\ \text{---} \end{array} \\
 & = \begin{array}{c} g \\ \text{---} \bullet \text{---} \\ h \\ \text{---} \bullet \text{---} \\ h \\ \text{---} \bullet \text{---} \\ \text{---} \end{array} \\
 & = \begin{array}{c} g \\ \text{---} \bullet \text{---} \\ h \\ \text{---} \bullet \text{---} \\ h^{-1} \\ \text{---} \bullet \text{---} \\ \text{---} \end{array} \\
 & = \begin{array}{c} X(g, h) \quad gh \quad X^\dagger(g, h) \\ \text{---} \bullet \text{---} \\ \text{---} h^{-1} \text{---} \bullet \text{---} \\ \text{---} \end{array}
 \end{aligned} \tag{1.72}$$

which yields the desired equality

Diagrammatic equation (1.73) showing the separation of a phase into a product of a cocycle and a pivotal phase. The equation is as follows:

$$\begin{array}{c} X^\dagger(g, h) \\ \text{---} \text{---} \text{---} \\ \text{---} h^{-1} \text{---} \triangle \text{---} \\ \text{---} \end{array} = \gamma(gh, h^{-1}) \begin{array}{c} X(gh, h^{-1}) \\ \text{---} \text{---} \text{---} \\ \text{---} \end{array} \tag{1.73}$$

where $\gamma(gh, h^{-1})$ is some yet to be determined one-line pivotal phase. We now separate $\gamma(gh, h^{-1})$ into a product of a phase specified by the cocycle α and another phase $b(g, h)$

which we show to be trivial. Multiplying Eq.(1.73) by $X^{-1}(g_0 g_1, g_1^{-1})$ yields

$$\begin{aligned}
 \gamma(gh, h^{-1}) \xrightarrow{g} &= \text{Diagram 1} \\
 &= \alpha^{-1}(g, h, h^{-1}) \text{Diagram 2} \\
 &= \alpha^{-1}(g, h, h^{-1}) b(g, h) \xrightarrow{g} \text{Diagram 3}
 \end{aligned} \tag{1.74}$$

Now considering

$$\begin{aligned}
 &\text{Diagram 4} \\
 &= b(g, h) \xrightarrow{xg} \text{Diagram 5}
 \end{aligned} \tag{1.75}$$

after an application of Eq.(1.58) to the left most reductions tensors we see that $b(g, h) = b(xg, h)$, $\forall x$ and hence b has no dependence on the first input and can be absorbed into the definition of Z_h . Similar reasoning yields another useful equality

$$\begin{aligned}
 &\text{Diagram 6} = \alpha(g^{-1}, g, h) \text{Diagram 7}
 \end{aligned} \tag{1.76}$$

In summary we have calculated the one-line pivotal phases

$$\begin{aligned}
 \gamma(gh, h^{-1}) &= \alpha^{-1}(g, h, h^{-1}) \\
 \gamma'(gh, h^{-1}) &= \alpha(g^{-1}, g, h)
 \end{aligned} \tag{1.77}$$

We now proceed to define a *pivotal* phase relating the following different reductions of the

same left handed MPO tensors

$$(1.78)$$

Hence

$$(1.79)$$

for some pivotal phase $\beta(g, h) \in U(1)$. By making use of Eqs.(1.73,1.76,1.77) we calculate β directly to find

$$\beta(g, h) = \varepsilon(g)\varepsilon(h)\tilde{\beta}(g, h) \quad (1.80)$$

where

$$\begin{aligned} \varepsilon(g) &:= \chi_g \alpha(g, g^{-1}, g) \\ \tilde{\beta}(g, h) &:= \frac{\alpha(h, g, g^{-1})}{\alpha(hg, g^{-1}, h^{-1})} \end{aligned}$$

we proceed to show that $\varepsilon \cong 1$ and hence $\beta \cong \tilde{\beta}$.

Evaluating β in two different ways as follows

$$(1.81)$$

leads to the relation on ε

$$\varepsilon(k)\varepsilon(h)\varepsilon(hk) = 1 \quad (1.82)$$

after several applications of the 3-cocycle condition for α .

Using Eq.(1.58) we find

$$\text{Crossing Tensor} = \frac{\alpha(g^{-1}, h^{-1}, h^{-1})}{\alpha(k, h, g)} \text{Crossing Tensor} \quad (1.83)$$

applying Eq.(1.79) twice to both sides yields the further constraint on β

$$d\beta(a, b, c) := \frac{\beta(a, b)\beta(ab, c)}{\beta(b, c)\beta(a, bc)} = \frac{\alpha(a, b, c)}{\alpha(c^{-1}, b^{-1}, a^{-1})} \quad (1.84)$$

hence α forms a potential obstruction to β being a 2-cocycle. Note that $\tilde{\beta}$ also satisfies Eq.(1.84) as a consequence of the 3-cocycle condition for α and hence the function $\theta(a, b) := \varepsilon(a)\varepsilon(b)$ satisfies the 2-cocycle condition $d\theta(a, b, c) = 1$. This 2-cocycle condition, together with Eq.(1.82), implies that $\varepsilon(a) = \varepsilon(c)$, $\forall a, c \in G$ and since $\varepsilon(1) = 1$ consequently $\varepsilon \equiv 1$ is the constant function. This of course implies $\beta \equiv \tilde{\beta}$ which is the desired result

$$\beta(g, h) = \frac{\alpha(h, g, g^{-1})}{\alpha(hg, g^{-1}, h^{-1})}. \quad (1.85)$$

1.13 Crossing tensors

In this Appendix we define four crossing tensors and demonstrate that they are related by phases involving only the 3-cocycle of the MPO representation. We proceed to define a composition operation on the crossing tensors and calculate the resulting crossing tensor. Building upon this result we determine the transformation of a crossing tensor under the global symmetry. Finally we calculate the effect of modular transformations on the crossing tensors.

1.13.1 Definitions

We now introduce several different forms for the crossing tensor (see Eq.(1.15)) that are related by phases which play an important role in our calculations

$$W_R^g(h) := X(g, h)X^+(h, g) = \text{diagram} \quad (1.86)$$

$$W_L^g(h) := X(h, g)X^+(g, h) = \text{diagram} \quad (1.87)$$

$$Y_R^g(h) := X^+(gh, h^{-1})[X^+(h, g) \otimes Z_h^{-1}] = \text{diagram} \quad (1.88)$$

$$Y_L^g(h) := [X(h, g) \otimes Z_h]X(gh, h^{-1}) = \text{diagram} \sim \text{diagram} \quad (1.89)$$

note $h \in C(g)$ and each tensor above is treated as a representative of an equivalence class of all crossing tensors that give rise to equal PEPS. Using Eqs.(1.58,1.77) one finds $Y_L^g(h) = \alpha(g, h, h^{-1})W_L^g(h)$, $W_L^g(h) = \alpha^{(g)}(h, h^{-1})^{-1}W_R^g(h^{-1})$, and $W_R^g(h) = \alpha(g, h, h^{-1})Y_R^g(h)$, i.e.

$$\begin{array}{ccc} W_L^g(h) & \xrightarrow{\alpha^{(g)}(h, h^{-1})} & W_R^g(h^{-1}) \\ \alpha(g, h, h^{-1}) \downarrow & & \uparrow \alpha(g, h^{-1}, h) \\ Y_L^g(h) & \xrightarrow{\omega^g(h, h^{-1})} & Y_R^g(h^{-1}) \end{array} \quad (1.90)$$

where

$$\alpha^{(g)}(k, h) := \alpha(g, k, h)\alpha(k, h, g)\alpha^{-1}(k, g, h) \quad (1.91)$$

is the slant product of α (which is a 2-cocycle) and

$$\omega^g(k, h) := \alpha^{(g)}(k, h) \frac{\alpha(g, kh, (kh)^{-1})}{\alpha(g, k, k^{-1})\alpha(g, h, h^{-1})} \quad (1.92)$$

is an equivalent 2-cocycle, i.e. $[\omega^g] = [\alpha^{(g)}]$. One can easily verify that changing α by a 3-coboundary alters $\alpha^{(g)}$ by a 2-coboundary and hence the cohomology class $[\alpha]$ is mapped to $[\alpha^{(g)}]$ by the slant product.

There is a natural composition operation on the $Y_R^g(h)$ tensors induced by the action of a global symmetry $U(k)^{\otimes |\mathcal{M}|_v}$, $k \in \mathbb{C}(g, h)$, upon a symmetry twisted ground state as follows

which includes a reduction of the tensors by $X(k, h)$ and $X^+(k, h)$, note this product is associative but not commutative. The $Y_R^g(h)$ tensors in fact form a projective representation under this composition rule since

The diagram illustrates the derivation of the Reidemeister move $\beta(h, k)$ from the Reidemeister move $\alpha(k, gh, h^{-1})^{-1}$ and the Reidemeister move $\alpha(k, h, g)^{-1}$ using the Reidemeister move $\alpha(gkh, h^{-1}, k^{-1})$.

The diagram consists of five nodes representing string diagrams, connected by arrows labeled with the Reidemeister moves:

- Top Left Node:** A horizontal red line with two segments labeled g . Above the line, a red loop is formed by two segments labeled k and h . The top of the loop has an upward arrow labeled kh . Below the line, a red loop is formed by two segments labeled k and h . The bottom of the loop has a downward arrow labeled kh . Two blue triangles are on the line: the first is on the first g segment with its vertex pointing down, and the second is on the second g segment with its vertex pointing up.
- Top Right Node:** Similar to the top left node, but the blue triangles are swapped: the first is on the second g segment with its vertex pointing down, and the second is on the first g segment with its vertex pointing up.
- Middle Left Node:** Similar to the top left node, but the blue triangles are swapped: the first is on the second g segment with its vertex pointing down, and the second is on the first g segment with its vertex pointing up.
- Middle Right Node:** Similar to the top right node, but the blue triangles are swapped: the first is on the second g segment with its vertex pointing down, and the second is on the first g segment with its vertex pointing up.
- Bottom Node:** A horizontal red line with two segments labeled g . Above the line, a red loop is formed by two segments labeled k and h . The top of the loop has an upward arrow labeled kh . Below the line, a red loop is formed by two segments labeled k and h . The bottom of the loop has a downward arrow labeled kh . Two blue triangles are on the line: the first is on the first g segment with its vertex pointing down, and the second is on the second g segment with its vertex pointing up.

The arrows connecting the nodes are labeled with the Reidemeister moves:

- From Top Left to Top Right: $\alpha(k, gh, h^{-1})^{-1}$
- From Top Right to Middle Right: $\alpha(gkh, h^{-1}, k^{-1})$
- From Middle Right to Middle Left: $\alpha(k, h, g)^{-1}$
- From Middle Left to Bottom: $\beta(h, k)$

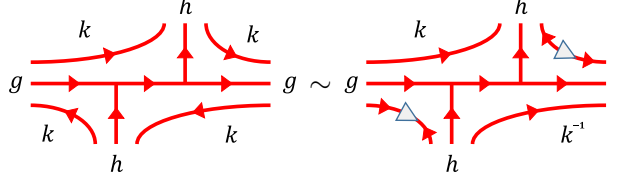
which yields

$$\begin{aligned}
Y_R^g(k) \times Y_R^g(h) &= \frac{\alpha(k, gh, h^{-1})\alpha(k, h, g)}{\alpha(gkh, h^{-1}, k^{-1})\beta(h, k)} Y_R^g(kh) \\
&= \alpha^{(g)}(k, h) \frac{\alpha(g, kh, h^{-1}k^{-1})}{\alpha(g, k, k^{-1})\alpha(g, h, h^{-1})} \\
&\quad \frac{\alpha(k, h, h^{-1}k^{-1})}{\alpha(h, h^{-1}, k^{-1})\beta(h, k)} Y_R^g(kh) \\
&= \omega^g(k, h) Y_R^g(kh)
\end{aligned} \tag{1.94}$$

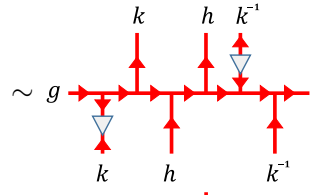
after several applications of the 3-cocycle condition for α , see Eq.(1.60).

1.13.3 Symmetry action

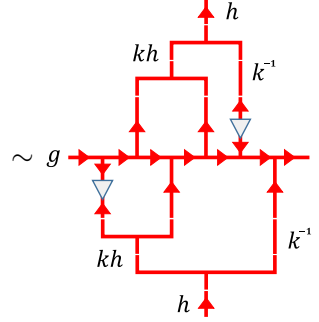
We are now in a position to calculate the effect of applying a global symmetry $k \in C(g, h)$ to an (x, y) symmetry twisted SPT PEPS on a torus as follows



$$(1.95)$$



$$(1.96)$$



$$(1.97)$$

$$= Y_R^g(k) \times W_R^g(h) \times Y_L^g(k) \quad (1.98)$$

$$= \frac{\alpha(g, h, h^{-1})}{\omega^g(k, k^{-1})} Y_R^g(k) \times Y_R^g(h) \times Y_R^g(k^{-1}) \quad (1.99)$$

$$= \frac{\alpha(g, h, h^{-1})\omega^g(k, h)}{\omega^g(k, k^{-1})} Y_R^g(kh) \times Y_R^g(k^{-1}) \quad (1.100)$$

$$= \frac{\omega^g(k, h)\omega^g(kh, k^{-1})\alpha(g, h, h^{-1})}{\omega^g(k, k^{-1})} Y_R^g(h) \quad (1.101)$$

$$= \frac{\omega^g(k, h)}{\omega^g(h, k)} W_R^g(h) \quad (1.102)$$

where we have made use of the 3-cocycle condition on α and the relations from Eq.(1.90). Hence we have found the group action $\pi_k[\cdot]$ induced on the crossing tensor by the physical symmetry to be

$$\begin{aligned} \pi_k[W_R^g(h)] &= (\omega^g)^{(h)}(k)^{-1} W_R^g(h) \\ &= \alpha^{(g, h)}(k)^{-1} W_R^g(h) \end{aligned} \quad (1.103)$$

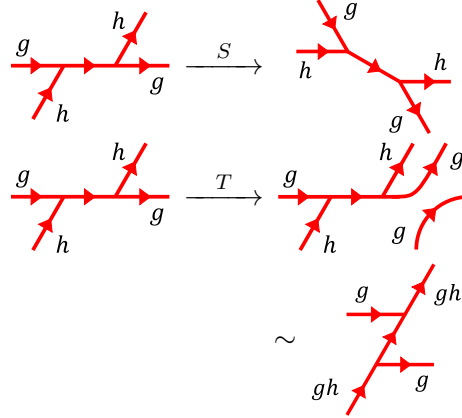
where $(\omega^g)^{(h)}$ is the slant product of ω^g (it is easy to see this equals the coefficient in Eq.(1.95)) and hence a 1D representation of $C(g, h)$ which equals the twice slant product of alpha, i.e. $(\omega^g)^{(h)} = \alpha^{(g, h)}$ (since the slant product maps cohomology classes to cohomology classes). Now by the orthogonality of characters we have that the projector $\Pi_{g, h}[\cdot] := \sum_{k \in C(g, h)} \pi_k[\cdot]$

maps a nonzero $W_R^g(h)$ to zero iff $\alpha^{(g,h)}$ is nontrivial i.e.

$$\Pi_{g,h}[W_R^g(h)] \neq 0 \iff \alpha^{(g,h)} \equiv 1. \quad (1.104)$$

1.13.4 Modular transformations

In this section we will calculate the effects of the S and T transformations ($\frac{\pi}{2}$ rotation and Dehn twist respectively) on the crossing tensor $W_R^g(h)$ which is relevant for both symmetry twisted and topological ground states. We use the following left handed convention



$$\begin{aligned} & \text{Crossing } W_R^g(h) \xrightarrow{S} \text{Rotated Crossing} \\ & \text{Crossing } W_R^g(h) \xrightarrow{T} \text{Twisted Crossing} \sim \text{Braided Crossing} \end{aligned} \quad (1.105)$$

Using Eqs.(1.60,1.73,1.76,1.77,1.90) and the 3-cocycle condition on α we find

$$S[W_R^g(h)] = \alpha^{(h)}(g^{-1}, g)^{-1} W_R^h(g^{-1}) \quad (1.106)$$

$$T[W_R^g(h)] = \alpha(g, h, g) W_R^g(gh) \quad (1.107)$$

with these formulas we have explicitly verified that the action of S and T generate a linear representation of the modular group, i.e. they satisfy the relations

$$S^4 = \mathbb{1}, \quad (ST)^3 = S^2. \quad (1.108)$$

It was sufficient to simply consider the multiplication of these generators since the gauge theories we deal with are doubled topological orders and consequently have zero modular central charge. We do not reproduce the tedious calculation here.

1.14 Gauging SPT PEPS yields topological PEPS

In this appendix we recount the definition of the quantum state gauging procedure of Ref. 71 and generalize their proof to show that gauging a SPT PEPS results in a MPO-injective PEPS with a projection MPO that has multiple blocks in its canonical form, labeled by the group elements.

1.14.1 Quantum state gauging procedure

Let us first recount the definition of the global projector onto the gauge invariant subspace. This is defined on a directed graph Λ in which the vertices are enumerated and the edges are directed from larger to smaller vertex. To each vertex $v \in \Lambda$ we associate a Hilbert space \mathbb{H}_v

together with a representation $U_v(g)$ of the group G and to each edge $e \in \Lambda$ we associate a Hilbert space isomorphic to the group algebra $\mathbb{H}_e \cong \mathbb{C}[G]$. We define the matter Hilbert space $\mathbb{H}_m := \bigotimes_{v \in \Lambda} \mathbb{H}_v$ and the gauge Hilbert space $\mathbb{H}_g := \bigotimes_{e \in \Lambda} \mathbb{H}_e$ which together form the full Hilbert space $\mathbb{H}_{g,m} := \mathbb{H}_g \otimes \mathbb{H}_m$. The states in $\mathbb{H}_{g,m}$ that are relevant for the gauge theory satisfy a local gauge invariance condition at each vertex. Specifically, they lie in the simultaneous $+1$ eigenspace of the following projection operators

$$P_v := \int dg_v U_v(g_v) \bigotimes_{e \in E_v^+} R_e(g_v) \bigotimes_{e \in E_v^-} L_e(g_v) \quad (1.109)$$

where E_v^+ (E_v^-) is the set of adjacent edges directed away from (towards) vertex v . $R(g), L(g)$ are the right and left regular representations, respectively. The projector onto the gauge invariant subspace is given by $P_\Lambda := \prod_v P_v$ and the analogous projector \mathcal{P}_Γ for any operator O supported on a subgraph $\Gamma \subset \Lambda$ (which contains the bounding vertices of all its edges) is defined to be

$$\mathcal{P}_\Gamma[O] := \int \prod_{v \in \Gamma} dg_v \left[\bigotimes_{v \in \Gamma} U_v(g_v) \bigotimes_{e \in \Gamma} L_e(g_{v_e^-}) R_e(g_{v_e^+}) \right] O \left[\bigotimes_{v \in \Gamma} U_v(g_v) \bigotimes_{e \in \Gamma} L_e(g_{v_e^-}) R_e(g_{v_e^+}) \right]^\dagger \quad (1.110)$$

where edge e points from v_e^+ to v_e^- .

We proceed to describe a gauging procedure for models defined purely on the matter degrees of freedom \mathbb{H}_m . To apply P_Λ and \mathcal{P}_Γ we first require a procedure to embed states and operators from \mathbb{H}_m into $\mathbb{H}_{g,m}$. For this we define the gauging map for matter states $|\psi\rangle \in \mathbb{H}_m$ by

$$G|\psi\rangle := P[|\psi\rangle \bigotimes_e |1\rangle_e], \quad (1.111)$$

and for matter operators $O \in \mathbb{L}(\mathbb{H}_m)$ acting on a subgraph $\Gamma \subseteq \Lambda$ (containing all edges between its vertices) by

$$\mathcal{G}_\Gamma[O] := \mathcal{P}_\Gamma[O \bigotimes_e |1\rangle \langle 1|_e]. \quad (1.112)$$

1.14.2 Gauging SPT PEPS

In this section we show that a gauged SPT PEPS satisfies the axioms of MPO-injectivity.

Consider a region \mathcal{R} of a SPT PEPS $|\psi\rangle \in \mathbb{H}_m$ built from local tensor A . The PEPS map $A_\mathcal{R}$ on this region satisfies $A_\mathcal{R}^\dagger A_\mathcal{R} = P_{\partial\mathcal{R}}$ and hence is injective on the support subspace of a single block projection MPO $P_{\partial\mathcal{R}} = V^{\partial\mathcal{R}}(1)$ given by $\text{supp}(P_{\partial\mathcal{R}}) \subseteq (\mathbb{V}_e)^{\otimes L}$ where \mathbb{V}_e denotes the Hilbert space of a virtual index and $L := |\partial\mathcal{R}|_e$.

For the gauged PEPS $G|\psi\rangle \in \mathbb{H}_{g,m}$, the region \mathcal{R} is defined to include only those edges between vertices within \mathcal{R} , i.e. excluding the edges $e \in \partial\mathcal{R}$. Note our proof is easily adapted to the case where the edge degrees of freedom are ‘doubled’ and absorbed into the neighboring vertex degrees of freedom, as in Section 1.7.

The gauged PEPS map on region \mathcal{R} , $A_\mathcal{R}^g : (\mathbb{V}_e \otimes \mathbb{C}[G])^{\otimes L} \rightarrow \mathbb{H}_v^{\otimes |\mathcal{R}|_v} \otimes \mathbb{H}_e^{\otimes |\mathcal{R}|_e}$, naturally decomposes into the original PEPS map and a gauging tensor network operator multiplying the physical degrees of freedom $A_\mathcal{R}^g = G_\mathcal{R} A_\mathcal{R}$ where

$$G_\mathcal{R} := \int \prod_{v \in \mathcal{R}} dg_v \bigotimes_{v \in \mathcal{R}} U_v(g_v) \bigotimes_{e \in \mathcal{R}} |g_{v_e^-} g_{v_e^+}^{-1}\rangle_e \bigotimes_{e \in \partial\mathcal{R}} (g_{v_e^\pm})_e \quad (1.113)$$

where $v_e^\pm \in \mathcal{R}$ denotes the unique vertex in \mathcal{R} adjacent to the edge $e \in \partial\mathcal{R}$.

Proposition 5. *A generalized inverse of the gauged PEPS is given by $(A_{\mathcal{R}}^g)^+ = A_{\mathcal{R}}^+ G_{\mathcal{R}}^\dagger$ which satisfies $(A_{\mathcal{R}}^g)^+ A_{\mathcal{R}}^g = \frac{1}{|\mathcal{G}|} \sum_{g \in \mathcal{G}} V^{\partial \mathcal{R}}(g) \otimes R(g)^{\otimes L}$. Furthermore, the gauged PEPS is MPO-injective with respect to the projection MPO $\frac{1}{|\mathcal{G}|} \sum_{g \in \mathcal{G}} V^{\partial \mathcal{R}}(g) \otimes R(g)^{\otimes L}$ which is a sum of single block injective MPOs labeled by $g \in \mathcal{G}$.*

Firstly we have

$$\begin{aligned} G_{\mathcal{R}}^\dagger G_{\mathcal{R}} &= \int \prod_{v \in \mathcal{R}} dh_v dg_v \bigotimes_{v \in \mathcal{R}} U_v(h_v^{-1} g_v) \bigotimes_{e \in \mathcal{R}} \langle h_{v_e^-} h_{v_e^+}^{-1} | g_{v_e^-} g_{v_e^+}^{-1} \rangle \bigotimes_{e \in \partial \mathcal{R}} |h_{v_e^\pm}\rangle (g_{v_e^\pm})_e \\ &= \int dg \bigotimes_{v \in \mathcal{R}} U_v(g) \bigotimes_{e \in \partial \mathcal{R}} R_e(g) \end{aligned} \quad (1.114)$$

since the delta conditions $\langle h_{v_e^-} h_{v_e^+}^{-1} | g_{v_e^-} g_{v_e^+}^{-1} \rangle$ force $h_{v_e^-}^{-1} g_{v_e^-} = h_{v_e^+}^{-1} g_{v_e^+}$ and hence $h_v^{-1} g_v =: g$ is constant across all $v \in \mathcal{R}$, assuming \mathcal{R} is connected. Hence

$$A_{\mathcal{R}}^+ G_{\mathcal{R}}^\dagger G_{\mathcal{R}} A_{\mathcal{R}} = P_{\partial \mathcal{R}} \int dg V^{\partial \mathcal{R}}(g) \bigotimes_{e \in \partial \mathcal{R}} R_e(g) \quad (1.115)$$

since $U(g)^{\otimes |\mathcal{R}|_v} A_{\mathcal{R}} = A_{\mathcal{R}} V^{\partial \mathcal{R}}(g)$ for a SPT PEPS (see Section 1.3) then the result follows as $P_{\partial \mathcal{R}} V^{\partial \mathcal{R}}(g) = V^{\partial \mathcal{R}}(g)$.

Let us now address the remaining conditions for MPO-injectivity. Most importantly the pulling through condition is easily seen to hold by Eq.(1.3) and since

$$P_v U_v^\dagger(g) = P_v \bigotimes_{e \in E_v^+} R_e(g) \bigotimes_{e \in E_v^-} L_e(g),$$

see Appendix 1.15, Proposition 13 for more detail. The trivial loops condition for the MPO $V^{\partial \mathcal{R}}(g) \otimes R(g)^{\otimes L}$ follows directly from the trivial loops condition for $V^{\partial \mathcal{R}}(g)$ and the convention that $R(g)$ is inverted depending on the orientation of the crossing of the MPO loop with the virtual bond edge of the PEPS graph, see Eqs.(1.3),(1.4). Finally, as discussed at the end of Appendix 1.9 the extended inverse condition is automatically satisfied when the projection MPO has a canonical form with injective blocks⁶⁴, which is the case for the MPO $V^{\partial \mathcal{R}}(g) \otimes R(g)^{\otimes L}$.

1.15 Generalizing the gauging procedure to arbitrary flat G-connections

In this section we outline a generalization of the gauging procedure defined in Ref. 71 to arbitrary flat G-connections. For equivalent G-connections the gauging maps are related by local operations while for inequivalent G-connections, which are necessary to construct the full ground space of a gauged model on a nontrivial manifold, the gauging maps are topologically distinct. The gauging maps for nontrivial flat G-connections take inequivalent symmetry twisted states of the initial SPT models to orthogonal ground states of the topologically ordered gauged models.

1.15.1 Elementary definitions

Definition 1. A G-connection ϕ on a directed graph Λ , embedded in an oriented 2-manifold \mathcal{M} , is given by specifying a group element $\phi_e \in G$ for each edge $e \in \Lambda$.

$$\begin{aligned}\phi : \Lambda_e &\rightarrow G \\ e &\mapsto \phi_e\end{aligned}$$

where Λ_e is the set of edges in Λ and ϕ can be thought of as a labeling $\{\phi_e\}$ of the edges in Λ by group elements $\phi_e \in G$. We view these connections as basis states $|\phi\rangle := \bigotimes_e |\phi_e\rangle_e \in \mathbb{C}[G]^{\otimes |\Lambda_e|}$.

Each G-connection ϕ defines a notion of transport along any oriented path (with origin and end point specified) $p \in \Lambda$ on the edges of the graph, the transport is specified by the group element

$$\phi_p := \prod_{i=|p|_e}^1 \phi_{e_i}^{\sigma_i} = \phi_{e_{|p|}}^{\sigma_{|p|}} \cdots \phi_{e_1}^{\sigma_1} \quad (1.116)$$

where the edges $e_i \in p$ are ordered as they occur following p along its orientation, and σ_i is 1 if the orientation of e_i matches that of p and -1 if it does not, see Fig. 1.8. Note for paths p^1 , from v_0 to v_1 , and p^2 , from v_1 to v_2 , we have the following relation $\phi_{p^2} \phi_{p^1} = \phi_{p^{12}}$, where $p^{12} := p^1 \cup p^2$ is given by composing paths 1 and 2.

A pair of G-connections ϕ, φ are considered equivalent if they are related by a sequence of local gauge transformations from the set

$$\begin{aligned}\{a_v^g := \bigotimes_{e \in E_v^+} R_e(g) \bigotimes_{e \in E_v^-} L_e(g) \mid \forall g \in G, v \in \Lambda\} \\ \text{i.e.} \quad \phi \sim \varphi \iff |\phi\rangle = \prod_i a_{v_i}^{g_i} |\varphi\rangle.\end{aligned} \quad (1.117)$$

One can easily verify that this constitutes an equivalence relation. Importantly, this equivalence relation preserves the conjugacy class of the G-holonomy ϕ_p of any closed path $p \in \Lambda$ with a fixed base point.

An important class of connections are the flat G-connections which are defined to have trivial holonomy along any contractible path.

Definition 2. A G-connection ϕ is flat iff $\phi_p = 1$ for any closed path $p \in \Lambda$ that is contractible in the underlying manifold \mathcal{M} .

This definition immediately implies that $\phi_p = \phi_{p'}$ for any pair of homotopic oriented paths p, p' with matching endpoints. It is easy to see that a G-connection is flat if and only if it satisfies the local condition $\phi_{\partial q} = 1$ for every plaquette q of the graph $\Lambda \subset \mathcal{M}$, where $\partial q \subset \Lambda$ is the boundary of q with the orientation inherited from \mathcal{M} . Moreover, one can easily verify that flatness is preserved under the equivalence relation (1.117) and hence the flat G-connections form equivalence classes under this relation. Note there can be multiple flat equivalence classes since it is possible for a flat G-connection to have a nontrivial holonomy $\phi_p \neq 1$ along a non-contractible loop $p \in \Lambda \subset \mathcal{M}$.

One can easily show that any contractible region $\Gamma \subseteq \Lambda \subset \mathcal{M}$ (formed by a set of vertices and the edges between them) of a flat G-connection $|\phi\rangle$ can be ‘cleaned’ by a sequence of operations $\prod_i a_{v_i}^{g_i}$, where each $v_i \in \Gamma$, such that the resulting equivalent connection $|\phi'\rangle := \prod_i a_{v_i}^{g_i} |\phi\rangle$

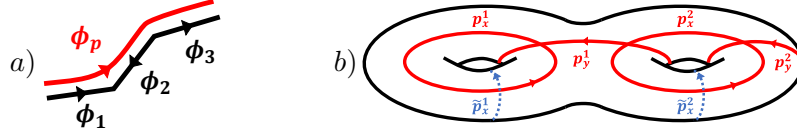


Figure 1.8: a) A simple example $\phi_p = \phi_3 \phi_2^{-1} \phi_1$. b) Noncontractible cycles of the 2-torus.

satisfies $\phi'_e = 1, \forall e \in \Gamma$.

Utilizing the cleaning procedure leads one to the following conclusion

Proposition 6. *The equivalence class $[\phi]$ of a flat G -connection ϕ on an oriented 2-manifold (w.l.o.g. a genus- n torus or n -torus) \mathcal{M} is labeled uniquely by the conjugacy class of n pairs of group elements that commute with their neighbors, i.e.*

$$\{[(x_1, y_1), \dots, (x_n, y_n)] \mid \exists x_i, y_i \in G, x_i y_i = y_i x_i, y_i x_{i+1} = x_{i+1} y_i\},$$

the set of such labels is henceforth referred to as $\mathcal{I}_{\mathcal{M}}$.

The argument proceeds as follows: any G -connection can be ‘cleaned’ onto the set of edges that cross any of the $2n$ closed paths $\{(p_x^i, p_y^i)\}$ in the dual graph Λ^* (where each (p_x^i, p_y^i) and (p_y^i, p_x^{i+1}) pair intersect once) that span the inequivalent noncontractible loops of the n -torus, see Fig.1.8. Now by the flatness condition the group elements along any loop must be the same (assuming w.l.o.g. the edges on that loop have the same orientation) and the group elements (x_i, y_i) and (y_i, x_{i+1}) of each pair of intersecting loops must commute. Furthermore, equivalence under the application of $\bigotimes_{v \in \Lambda} a_v^g, \forall g \in G$ implies that every set of labels in the same conjugacy class are equivalent.

Note there is a uniquely defined set of group elements

$$\{(x_1, y_1), \dots, (x_n, y_n) \mid x_i, y_i \in G, x_i y_i = y_i x_i, y_i x_{i+1} = x_{i+1} y_i\}, \quad (1.118)$$

for each flat G -connection ϕ which are specified by the G -holonomies $x_i := \phi_{\tilde{p}_x^i}, y_i := \phi_{\tilde{p}_y^i}$ of pairs of paths $(\tilde{p}_y^i, \tilde{p}_x^i)$ in the graph Λ , where \tilde{p}_x^i is defined to be a path that intersects p_x^i once and all other paths $p_y^j, p_x^j, j \neq i$, zero times (\tilde{p}_y^i is defined similarly). Moreover, the conjugacy class $[(x_1, y_1), \dots, (x_n, y_n)] := \{(x_1^h, y_1^h), \dots, (x_n^h, y_n^h) \mid \forall h \in G\}$ labels the equivalence class $[\phi]$ of the G -connection ϕ , where $x^h := h x h^{-1}$.

For a fixed representative $\gamma = \{(x_i, y_i)\}$ of conjugacy class $[\gamma] \in \mathcal{I}_{\mathcal{M}}$ and choice of paths $\{(p_x^i, p_y^i)\}$ spanning the inequivalent noncontractible cycles of the n -torus, we construct a particularly simple representative flat G -connection as follows

Definition 3. *The simple representative flat G -connection ϕ^γ is defined by setting $\phi_e^\gamma := x_i^{\sigma_e^i}$ if p_x^i crosses e and $\phi_e^\gamma := y_i^{\sigma_e^i}$ if p_y^i crosses e , where σ_e^i is $+1$ if the crossing is right handed and -1 if it is left handed, and otherwise $\phi_e^\gamma := 1$ for edges that are not crossed by either p_x^i, p_y^i .*

Note an arbitrary flat connection $|\phi\rangle$ is related to some $|\phi^\gamma\rangle$ by a sequence of local operations $|\phi\rangle = \prod_i a_{v_i}^{g_i} |\phi^\gamma\rangle$. In particular, the representative connection $|\tilde{\phi}^\gamma\rangle$ corresponding to a deformation of the paths $(p_x^i, p_y^i) \mapsto (\tilde{p}_x^i, \tilde{p}_y^i)$ that does not introduce additional intersections (a planar isotopy) is related to $|\phi^\gamma\rangle$ by a sequence of local operations $\prod_i a_{v_i}^{g_i}$ that implements the deformation.

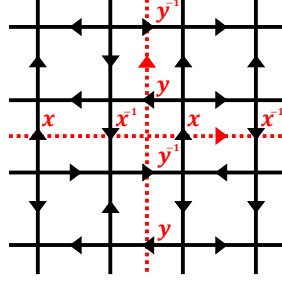


Figure 1.9: A representative flat G connection labeled by (x, y) .

1.15.2 Twisting and gauging operators and states

For any local operator O acting on the matter degrees of freedom in a contractible region $\Gamma \subseteq \Lambda$ there is a well defined notion of twisting O by a flat G-connection ϕ . Fixing a base vertex $v_0 \in \Gamma$ the twisted operator is given by

$$O^\phi := \int dg \bigotimes_{v \in \Gamma} U_v(\phi_{p_v} g) O \bigotimes_{v \in \Gamma} U_v^\dagger(\phi_{p_v} g) \quad (1.119)$$

where p_v is any path from v_0 to v within Γ (the choice does not matter since the connection is flat and Γ is contractible). The choice of distinguished base vertex v_0 is irrelevant since a change $v_0 \mapsto v'_0$ can be compensated by shifting $g \mapsto \phi_{p'}^{-1} g$, where p' is a path from v'_0 to v_0 , which has no effect since g is summed over. Note this definition of O^ϕ first projects O onto the space of symmetric operators, hence the sum over g is unnecessary if O is already symmetric. One can verify that O^ϕ commutes with the following twisted symmetry $\bigotimes_{v \in \Gamma} U_v(g^{\phi_{p_v}})$, $\forall g \in G$, where $g^h = hgh^{-1}$, independent of the choice of base point v_0 and paths $p_v \in \Gamma$ from v_0 to v .

The twisted state gauging map G_ϕ , for a flat G-connection ϕ , is defined by the following action

$$\begin{aligned} G_\phi |\psi\rangle &:= P[|\psi\rangle \otimes |\phi\rangle] \\ &= \int \prod_{v \in \Lambda} dg_v \left[\bigotimes_{v \in \Lambda} U_v(g_v) \right] |\psi\rangle \bigotimes_{e \in \Lambda} |g_{v_e^-} \phi_e g_{v_e^+}^{-1}\rangle_e \end{aligned} \quad (1.120)$$

where $|\psi\rangle \in \mathbb{H}_m$ is a state of the matter degrees of freedom. One can verify that

$$G_\phi^\dagger G_\phi = \int dg \bigotimes_{v \in \Lambda} U_v(g^{\phi_{p_v}}) \prod_i \delta_{gx_i, x_i g} \delta_{gy_i, y_i g},$$

is the projection onto the symmetric subspace of the twisted symmetry, where (x_i, y_i) are the pairs of commuting group elements that label ϕ , see Eq.(1.118). The δ conditions arise since the state overlaps force the conjugation of g by the transport group elements $\phi_{p_v}, \phi_{p'_v}$ to agree for non homotopic paths p_v, p'_v from v_0 to v . These δ conditions also ensure the choice of fixed base point v_0 is irrelevant.

The twisted operator gauging map \mathcal{G}_Γ^ϕ is defined similarly

$$\mathcal{G}_\Gamma^\phi[O] := \int \prod_{v \in \Gamma} dg_v \bigotimes_{v \in \Gamma} U_v(g_v) O \bigotimes_{v \in \Gamma} U_v^\dagger(g_v) \bigotimes_{e \in \Gamma} |g_{v_e^-} \phi_e g_{v_e^+}^{-1}\rangle \langle g_{v_e^-} \phi_e g_{v_e^+}^{-1}| \quad (1.121)$$

where O is an operator that acts on the matter degrees of freedom on sites $v \in \Gamma \subseteq \Lambda$, and Γ is defined to include all the edges between its vertices. \mathcal{G}_Γ^ϕ is invertible on the space of ϕ -twisted symmetric local operators O^ϕ in the following sense

$$\begin{aligned} \text{Tr}_{e \in \Gamma} [\mathcal{G}_\Gamma^\phi [O^\phi] \bigotimes_{e \in \Gamma} |\phi_e\rangle \langle \phi_e|_e] &= \int \prod_{v \in \Gamma} dg_v \bigotimes_{v \in \Gamma} U_v(g_v) \times O^\phi \bigotimes_{v \in \Gamma} U_v^\dagger(g_v) \prod_{e \in \Gamma} \delta_{g_{v_e^-} \phi_e g_{v_e^+}^{-1}, \phi_e} \\ &= \int dg_{v_0} \bigotimes_{v \in \Gamma} U_v(g_{v_0}^{\phi_{p_v}}) O^\phi \bigotimes_{v \in \Gamma} U_v^\dagger(g_{v_0}^{\phi_{p_v}}) \\ &= O^\phi \end{aligned} \quad (1.122)$$

where the final equality follows from the twisted symmetry of O^ϕ and the second equality follows since the δ conditions force $g_{v_e^-} = g_{v_e^+}^{\phi_e}$ which implies, after fixing a base point $v_0 \in \Lambda$, that $g_v = g_{v_0}^{\phi_{p_v}}$ for any path p_v from v_0 to v within Γ which is assumed to be contractible in the underlying manifold \mathcal{M} .

For the twisted gauging procedure we also have a version of Proposition 4, which states the useful equality $\mathcal{G}_\Gamma[O]G = GO$ for symmetric O . In the twisted case it must be modified in the following way

Proposition 7. *The identity $\mathcal{G}_\Gamma^\phi [O^\phi] G_\phi = G_\phi O^\phi$ holds for any symmetric operator O .*

We now proceed to show this

$$\begin{aligned} \mathcal{G}_\Gamma^\phi [O^\phi] G_\phi &= \int \prod_{v \in \Gamma} dh_v \bigotimes_{v \in \Gamma} U_v(h_v) O^\phi \bigotimes_{v \in \Gamma} U_v^\dagger(h_v) \bigotimes_{e \in \Gamma} |h_{v_e^-} \phi_e h_{v_e^+}^{-1}\rangle \langle h_{v_e^-} \phi_e h_{v_e^+}^{-1}| \\ &\quad \times \int \prod_{v \in \Lambda} dg_v \bigotimes_{v \in \Lambda} U_v(g_v) \bigotimes_{e \in \Lambda} |g_{v_e^-} \phi_e g_{v_e^+}^{-1}\rangle \\ &= \int \prod_{v \in \Lambda} dg_v \prod_{v \in \Gamma} dh_v \bigotimes_{v \in \Lambda} U_v(g_v) \bigotimes_{v \in \Gamma} U_v(g_v^{-1} h_v) O^\phi \bigotimes_{v \in \Gamma} U_v^\dagger(g_v^{-1} h_v) \\ &\quad \times \prod_{e \in \Gamma} \delta_{(g_{v_e^-}^{-1} h_{v_e^-}), (g_{v_e^+}^{-1} h_{v_e^+}) \phi_e} \bigotimes_{e \in \Lambda} |g_{v_e^-} \phi_e g_{v_e^+}^{-1}\rangle \\ &= G_\phi O^\phi \end{aligned} \quad (1.123)$$

the last equality follows since the δ condition forces $g_v^{-1} h_v = (g_{v_0}^{-1} h_{v_0})^{\phi_{p_v}}$ (for a fixed choice of vertex v_0 and path $p_v \in \Gamma$ from v_0 to v which has no effect on the outcome) implying $\bigotimes_{v \in \Gamma} U_v(g_v^{-1} h_v) = \bigotimes_{v \in \Gamma} U_v((g_{v_0}^{-1} h_{v_0})^{\phi_{p_v}})$ which is precisely a twisted symmetry that commutes with O^ϕ to yield the desired result.

For a symmetric local Hamiltonian that has been twisted by a flat G -connection ϕ , $H_m^\phi = \sum_v h_v^\phi$, we define the twisted gauged Hamiltonian $(H_m^\phi)^{\mathcal{G}^\phi} := \sum_v \mathcal{G}_{\Gamma_v}^\phi [h_v^\phi]$ in a locality preserving way similar to the untwisted case. With this definition we pose the following proposition

Proposition 8. *For all flat G -connections ϕ we have $(H_m^\phi)^{\mathcal{G}^\phi} = H_m^{\mathcal{G}}$.*

To prove this it suffices to consider a generic local term h_v^ϕ acting on the subgraph Γ_v

$$\begin{aligned}
\mathcal{G}_{\Gamma_v}^\phi[h_v^\phi] &= \int \prod_{v \in \Gamma} dg_v \bigotimes_{v \in \Gamma} U_v(g_v) U_v(\phi_{p_v}) h_v \bigotimes_{v \in \Gamma} U_v^\dagger(\phi_{p_v}) U_v^\dagger(g_v) \bigotimes_{e \in \Gamma} |g_{v_e^-} \phi_e g_{v_e^+}^{-1}\rangle \langle g_{v_e^-} \phi_e g_{v_e^+}^{-1}| \\
&= \int \prod_{v \in \Gamma} dg_v \bigotimes_{v \in \Gamma} U_v(g_v \phi_{p_v}) h_v \bigotimes_{v \in \Gamma} U_v^\dagger(g_v \phi_{p_v}) \bigotimes_{e \in \Gamma} |g_{v_e^-} \phi_{p_{v_e^-}} \phi_{p_{v_e^+}}^{-1} g_{v_e^+}^{-1}\rangle \langle g_{v_e^-} \phi_{p_{v_e^-}} \phi_{p_{v_e^+}}^{-1} g_{v_e^+}^{-1}| \\
&= \int \prod_{v \in \Gamma} d\tilde{g}_v \bigotimes_{v \in \Gamma} U_v(\tilde{g}_v) h_v \bigotimes_{v \in \Gamma} U_v^\dagger(\tilde{g}_v) \bigotimes_{e \in \Gamma} |\tilde{g}_{v_e^-} \tilde{g}_{v_e^+}^{-1}\rangle \langle \tilde{g}_{v_e^-} \tilde{g}_{v_e^+}^{-1}| \\
&= \mathcal{G}_{\Gamma_v}[h_v]
\end{aligned} \tag{1.124}$$

for the first equality we use the symmetry of h_v , for the second we use the fact $\phi_e = \phi_{p_{v_e^-}} \phi_{p_{v_e^+}}^{-1}$, note the choice of base point v_0 and paths p_v from v_0 to v in Γ have no effect since h_v is symmetric and Γ is contractible, for the third we use the invariance of the Haar measure under the change of group variables $g_v \mapsto \tilde{g}_v := g_v \phi_{p_v}$.

1.15.3 Gauging preserves the gap and leads to a topological degeneracy

We are now in a position to prove that gauging a SPT Hamiltonian defined on an arbitrary oriented 2-manifold \mathcal{M} preserves the energy gap, generalizing the proof presented in Section 1.5.2.

The full gauged Hamiltonian is given by $H_{\text{full}} := H_{\text{m}}^G + \Delta_B H_B + \Delta_P H_P$, see Section 1.5.2 for a discussion of each term in the Hamiltonian. Note by Proposition 8 the same full Hamiltonian H_{full} is achieved by gauging any ϕ -twist of a given SPT Hamiltonian.

As argued in Section 1.5.2, for Δ_B, Δ_P sufficiently large, the low energy subspace of H_{full} lies within the common ground space of H_B and H_P . This subspace is spanned by the states $P[|\lambda\rangle_{\text{m}} \otimes |\phi\rangle_{\text{g}}] = G_\phi |\lambda\rangle$, where the matter states $|\lambda\rangle$ form a basis of \mathbb{H}_{m} , and the gauge states $|\phi\rangle$ span the flat G-connections. This leads to a generalization of Proposition 3 to arbitrary 2-manifolds

Proposition 9. *For an oriented 2-manifold \mathcal{M} the set of states $\{G_{\phi^\gamma} |\lambda\rangle\}$, for $\{|\lambda\rangle\}$ a basis of \mathbb{H}_{m} and a fixed choice of representatives $\gamma \in [\gamma] \in \mathcal{I}_{\mathcal{M}}$, span the common ground space of H_B and H_P .*

Firstly, by Proposition 6, an arbitrary flat connection $|\phi\rangle$ is related to $|\phi^\gamma\rangle$, $\exists [\gamma] \in \mathcal{I}_{\mathcal{M}}$ by a sequence of local operations $|\phi\rangle = \prod_i a_{v_i}^{g_i} |\phi^\gamma\rangle$. Since $P_v = \int dg U_v(g) \otimes a_v^g$ one can easily see $P_v a_v^g = P_v U_v^\dagger(g)$ and hence we have

$$\begin{aligned}
G_\phi |\psi\rangle_{\text{m}} &= P[|\psi\rangle_{\text{m}} \otimes \prod_i a_{v_i}^{g_i} |\phi^\gamma\rangle_{\text{g}}] \\
&= P[\left[\prod_i U_{v_i}(g_i)\right]^\dagger |\psi\rangle_{\text{m}} \otimes |\phi^\gamma\rangle_{\text{g}}] \\
&= G_{\phi^\gamma} \left[\prod_i U_{v_i}(g_i)\right]^\dagger |\psi\rangle_{\text{m}}.
\end{aligned} \tag{1.125}$$

Therefore the common ground space of H_B and H_P is spanned by the states $\{G_{\phi^\gamma} |\lambda\rangle\}_{(\lambda, \gamma)}$ for a basis $\{|\lambda\rangle\}_\lambda$ of \mathbb{H}_{m} and a representative γ of each conjugacy class $[\gamma] \in \mathcal{I}_{\mathcal{M}}$.

We now bring together the definitions and propositions laid out thus far to show the following

Proposition 10. *Gauging a gapped SPT Hamiltonian on an arbitrary oriented 2-manifold \mathcal{M} yields a gapped local Hamiltonian with a topology dependent ground space degeneracy.*

Let $|\lambda^\gamma\rangle$ denote an eigenstate of the twisted SPT Hamiltonian $H_m^{\phi^\gamma}$ with eigenvalue λ . From Propositions 7 & 8 it follows that gauging an eigenstate of a ϕ -twisted SPT Hamiltonian yields an eigenstate of the gauged Hamiltonian, so we have $H_m^G G_{\phi^\gamma} |\lambda^\gamma\rangle = \lambda G_{\phi^\gamma} |\lambda^\gamma\rangle$.

If H_m has a unique ground state $|\lambda_0\rangle$ Proposition 9 implies the ground space of the full Hamiltonian H_{full} is spanned by the states $\{G_{\phi^\gamma} |\lambda_0^\gamma\rangle\}_\gamma$ and its gap satisfies $\Delta_{\text{full}} \geq \min(\Delta_m, \Delta_B, \Delta_P)$

In the above we have assumed that $G_{\phi^\gamma} |\lambda_0^\gamma\rangle \neq 0$, for some γ . Note $G |\lambda_0\rangle \neq 0$ always holds for a unique ground state $|\lambda_0\rangle$ of a symmetric Hamiltonian (possibly after rephasing the matrices of the physical group representation which is assumed to have occurred).

We now proceed to show that the ground space degeneracy is equal to the number of distinct equivalence classes of symmetry twists which are invariant under the residual physical symmetry. This relies on the assumption that the distinct symmetry twisted SPT Hamiltonians $H_m^{\phi^\gamma}$ each have a nonzero unique ground state $|\lambda_0^\gamma\rangle$ with the same energy λ_0 . We show this to be the case, when the original frustration free SPT Hamiltonian H_m has a SPT PEPS ground state, by explicitly constructing tensor network representations of the twisted ground states, see Definition 4.

Proposition 11. *The overlap matrix of the gauged ground states $M_{[\gamma'], [\gamma]} := \langle \lambda_0^{\gamma'} | G_{\phi^{\gamma'}}^\dagger G_{\phi^\gamma} | \lambda_0^\gamma \rangle$ is diagonal, where γ, γ' are drawn from a fixed set of representatives for the conjugacy classes in \mathcal{I}_M . Furthermore, $M_{[\gamma'], [\gamma]}$ is invariant under a change of representatives and $M_{[\gamma], [\gamma]} = 0$ iff $|\lambda_0^\gamma\rangle$ transforms as a nontrivial representation of the physical symmetry action of $C(\gamma)$.*

The operators $G_\phi^\dagger G_\phi$ that appear in the overlaps of the gauged twisted ground states imply that they are orthogonal. To see this consider the following

$$\begin{aligned} G_\phi^\dagger G_\phi &= \int \prod_{v \in \Lambda} dk_v dg_v \bigotimes_{v \in \Lambda} U_v(k_v^{-1} g_v) \prod_{e \in \Lambda} \langle k_{v_e^-} \varphi_e k_{v_e^+}^{-1} | g_{v_e^-} \phi_e g_{v_e^+}^{-1} \rangle \\ &= \int dg_{v_0} \bigotimes_{v \in \Lambda} U_v(\varphi_{p_v} g_{v_0} \phi_{p_v}^{-1}) \prod_i \delta_{x'_i g_{v_0}, g_{v_0} x_i} \delta_{y'_i g_{v_0}, g_{v_0} y_i} \end{aligned} \quad (1.126)$$

where we have fixed an arbitrary base vertex v_0 , p_v is any path from v_0 to v , and $\{(x'_i, y'_i)\}_i, \{(x_i, y_i)\}_i$ label the connections φ, ϕ respectively. The delta conditions arise since the overlaps in Eq.(1.126) force the transported group element $\varphi_{p_v} g_{v_0} \phi_{p_v}^{-1}$ to agree for any choice of path p_v (which may be homotopically distinct). This implies that $G_\phi^\dagger G_\phi = 0$ whenever the labels $\{(x'_i, y'_i)\}_i, \{(x_i, y_i)\}_i$ fall into distinct equivalence classes of \mathcal{I}_M .

For the particular case of the simple representative G-connections ϕ^γ we have

$$G_{\phi^{\gamma'}}^\dagger G_{\phi^\gamma} = \delta_{[\gamma'], [\gamma]} \int dg \bigotimes_{v \in \Lambda} U_v(g) \prod_i \delta_{x'_i g, g x_i} \delta_{y'_i g, g y_i}$$

for equivalence classes $[\gamma'], [\gamma] \in \mathcal{I}_M$. Furthermore, if $\gamma' \sim \gamma$ then there exists a group element $h \in G$ such that $(x'_i, y'_i) = (x_i^g, y_i^g), \forall i \iff g \in h C(\gamma)$, a left coset of the centralizer of $\gamma = \{x_i, y_i\}_i$. In this case

$$G_{\phi^{\gamma'}}^\dagger G_{\phi^\gamma} = \int dg \bigotimes_{v \in \Lambda} U_v(g) \delta_{g \in h C(\gamma)} \quad (1.127)$$

and $H_m^{\phi^{\gamma'}} = U(g)^{\otimes |\Lambda|_v} H_m^{\phi^\gamma} U^\dagger(g)^{\otimes |\Lambda|_v}$ for any $g \in h\mathcal{C}(\gamma)$, which implies $\theta_g^\gamma |\lambda_0^{\gamma'}\rangle = U(g)^{\otimes |\Lambda|_v} |\lambda_0^\gamma\rangle$ for some phase $\theta_g^\gamma \in \mathcal{U}(1)$. Hence

$$\langle \lambda_0^\gamma | G_{\phi^\gamma}^\dagger G_{\phi^\gamma} | \lambda_0^\gamma \rangle = \theta_h^\gamma \langle \lambda_0^\gamma | G_{\phi^\gamma}^\dagger G_{\phi^{\gamma'}} | \lambda_0^{\gamma'} \rangle \iff [\gamma] = [\gamma'].$$

Moreover since $|\lambda_0^\gamma\rangle$ is the unique groundstate of a $\mathcal{C}(\gamma)$ -symmetric Hamiltonian $\theta_{(\cdot)}^\gamma$ is a 1D representation of $\mathcal{C}(\gamma)$. By the orthogonality of characters we have $G_{\phi^\gamma}^\dagger G_{\phi^\gamma} | \lambda_0^\gamma \rangle \neq 0 \iff \theta_{(\cdot)}^\gamma \equiv 1$. Note $\theta_{(\cdot)}^\gamma \equiv 1$ is in fact a property of a conjugacy class as it does not depend on the choice of representative γ .

Consequently the choice of representative symmetry twist $\gamma \in [\gamma] \in \mathcal{I}_\mathcal{M}$ does not matter as all lead to the same gauged state $|\lambda_0, [\gamma]\rangle := G_{\phi^\gamma} | \lambda_0^\gamma \rangle$. Hence the overlap matrix of the gauged twisted SPT groundstates is given by

$$\begin{aligned} M_{[\gamma'], [\gamma]} &= \langle \lambda_0, [\gamma'] | \lambda_0, [\gamma] \rangle \\ &= \delta_{[\gamma'], [\gamma]} \delta_{\theta_{(\cdot)}^\gamma, 1} \frac{|\mathcal{C}(\gamma)|}{|G|} \langle \lambda_0^\gamma | \lambda_0^\gamma \rangle \end{aligned} \quad (1.128)$$

and the set of states $\{|\lambda_0, [\gamma]\rangle \mid [\gamma] \in \mathcal{I}_\mathcal{M}, \theta_{(\cdot)}^\gamma \equiv 1\}$ form an orthogonal basis for the ground space of the full gauged Hamiltonian H_{full} .

1.16 Symmetry twists & monodromy defects

In this appendix we describe a general and unambiguous procedure for applying symmetry twists to SPT PEPS using virtual symmetry MPOs. We furthermore demonstrate that the gauging procedure maps the symmetry MPOs to freely deformable topological MPOs on the virtual level and hence the gauged symmetry twisted PEPS are locally indistinguishable while remaining globally orthogonal, implying that they exhibit topological order. We move on to discuss how the same MPOs can be arranged along open paths to describe monodromy defects in SPT PEPS and anyons in the gauged PEPS. Moreover, we explicitly calculate the projective transformation of individual monodromy defects under the residual symmetry group using tensor network techniques.

1.16.1 Symmetry twisted states

In this section we discuss the ground states of symmetry twisted Hamiltonians in more detail and show that the PEPS framework naturally accommodates a simple construction of these states.

On a trivial topology a symmetry twist can be applied directly to a state by acting on some region of the lattice with the physical symmetry. For example on an infinite square lattice in the 2D plane a symmetry twist (x, y) along an oriented horizontal and vertical path p_x, p_y , in the dual lattice, acts on a state $|\psi\rangle$ via

$$\begin{aligned} |\psi\rangle^\phi &:= \int dg \bigotimes_{v \in \Gamma} U_v(\phi_{p_v} g) |\psi\rangle \\ &= \bigotimes_{v \in \mathcal{U}} U_v(x) \bigotimes_{v \in \mathcal{R}} U_v(y) \int dg \bigotimes_{v \in \Gamma} U_v(g) |\psi\rangle \end{aligned}$$

where ϕ is the simple representative connection with label (x, y) on paths p_x, p_y , see Definition 3, and \mathcal{R} is the half plane to the right of p_y , \mathcal{U} the half plane above p_x , see Fig. 1.5. Note this definition implicitly projects $|\psi\rangle$ onto the trivial representation and we have $O^\phi |\psi\rangle^\phi = (O |\psi\rangle)^\phi$ for symmetric operators O . Hence twisting an eigenstate $|\lambda\rangle$ of a SPT Hamiltonian H_m yields an eigenstate $|\lambda\rangle^\phi$ of the twisted Hamiltonian H_m^ϕ with the same eigenvalue. Note x and y must commute for ϕ to be a flat connection, equivalently if one thinks of first applying the x twist to a symmetric Hamiltonian, then the resulting operator will only be symmetric under the centralizer subgroup of x , $C(x) \leq G$, and hence it only makes sense to apply a second twist for an element $y \in C(x)$.

The effect of such a symmetry twist on a SPT PEPS $|\psi\rangle$ is particularly simple, it can be achieved by adding the virtual symmetry MPOs $V^{p_x}(x)$ and $V^{p_y}(y)$ (with inner indices contracted with the four index crossing tensor $Q_{x,y} = W_R^x(y)$ (1.15, 1.86) where p_x, p_y intersect, see Fig. 1.6) to the virtual level of the PEPS. Let us denote the resulting tensor network state $|\psi^{(x,y)}\rangle$, then by Eq. (1.3) we have $|\psi^{(x,y)}\rangle = |\psi\rangle^\phi$.

For nontrivial topologies the symmetry twist on a state $|\psi\rangle^{\phi^\gamma}$ is not well defined in terms of a physical symmetry action since two homotopically inequivalent paths p_v, p'_v can give rise to distinct transport elements $\phi_{p_v} \neq \phi_{p'_v}$. Note this problem does not arise when symmetry twisting local operators, such as the terms in a local Hamiltonian, since each operator acts within a contractible region. The PEPS formalism yields a simple resolution to this problem since the process of applying a symmetry twist ϕ^γ on the virtual level of a PEPS $|\psi^\gamma\rangle$ remains well defined, see Definition 4 and Fig. 1.10.

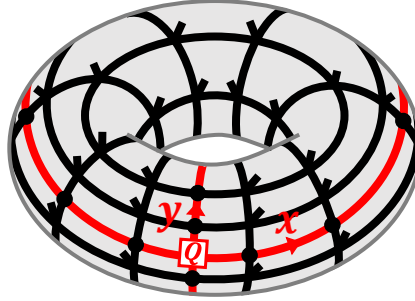


Figure 1.10: An (x, y) symmetry twisted PEPS on a torus.

The general scenario is as follows; we have a local gapped frustration free SPT Hamiltonian H_m defined on an oriented 2-manifold \mathcal{M} with a SPT PEPS $|\lambda_0\rangle$ as its unique ground state (note SPT PEPS parent Hamiltonians satisfy these conditions) and we want to apply a symmetry twist along paths p_x^i, p_y^i in the dual graph labeled by $\gamma = \{(x_i, y_i)\}_i$.

Definition 4 (Symmetry Twisted SPT PEPS). *For a SPT PEPS $|\psi\rangle$ and a symmetry twist γ , specified by a set of pairwise intersecting paths in the dual graph $\{p_x^i, p_y^i\}_i$ and pairwise commuting group elements $\{(x_i, y_i)\}_i$ in G , the symmetry twisted PEPS $|\psi^\gamma\rangle$ is constructed by taking the tensor network for $|\psi\rangle$ with open virtual indices on edges that cross $\{p_x^i, p_y^i\}_i$ and contracting these virtual indices with the MPOs $\{V^{p_x^i}(x_i), V^{p_y^i}(y_i)\}_i$. Moreover, at the intersection of the paths $p_x^i \cap p_y^i$ the internal indices of the MPOs $V^{p_x^i}(x_i), V^{p_y^i}(y_i)$ are contracted with four index crossing tensors $Q_{x_i, y_i} = W_R^{x_i}(y_i)$, defined in Eqs. (1.15, 1.86) and similarly with $Q_{y_{i-1}, x_i} = W_R^{y_{i-1}}(x_i)$ at the intersections $p_y^{i-1} \cap p_x^i$. This is depicted in Fig. 1.10.*

It follows from Eq.(1.3) and the *zipper* condition (1.71) for $X(x_i, y_i)$ that the symmetry twisted ground state SPT PEPS $|\lambda_0^\gamma\rangle$ is the ground state of the twisted SPT Hamiltonian $H_m^{\phi^\gamma}$. More generally for any SPT PEPS $|\psi\rangle$ that is an eigenstate of each local term in H_m , Eq.(1.3) implies that $|\psi^\gamma\rangle$ is an eigenstate of $H_m^{\phi^\gamma}$ with the same eigenvalue (thereby justifying the notation). Note the twisted SPT PEPS $|\psi^\gamma\rangle$ for different choices of representative γ from the same conjugacy class $[\gamma] \in \mathcal{I}_M$ are all related by the action of some global symmetry, which again follows from Eqs.(1.3),(1.71) and Proposition 6.

Proposition 12. *A γ -twisted SPT PEPS $|\psi^\gamma\rangle$ transforms as the following 1D representation*

$$\theta_{(\cdot)}^\gamma = \alpha^{(x_0, y_0)}(\cdot)^{-1} \prod_{i=1} [\alpha^{(y_{i-1}, x_i)}(\cdot) \alpha^{(x_i, y_i)}(\cdot)]^{-1} \quad (1.129)$$

under the physical action of the residual symmetry group $C(\gamma)$.

The physical action of the symmetry $U(k)^{\otimes |\mathcal{M}|_v}$ induces a local action π_k on each crossing tensor $\{W_R^{x_i}(y_i), W_R^{y_{i-1}}(x_i)\}_i$ and by Eq.(1.103) we find the combined action to be

$$\alpha^{(x_0, y_0)}(\cdot)^{-1} \prod_{i=1} [\alpha^{(y_{i-1}, x_i)}(\cdot) \alpha^{(x_i, y_i)}(\cdot)]^{-1}$$

as claimed.

1.16.2 Topological ground states

We now show that the twisted gauging procedure maps the virtual symmetry MPO to a freely deformable topological MPO on the virtual level.

Proposition 13. *Applying the twisted gauging map G_{ϕ^γ} to a nonzero twisted SPT PEPS $|\psi^\gamma\rangle$ yields the MPO-injective PEPS $G|\psi\rangle$ with a set of freely deformable MPOs joined by crossing tensors, specified by $[\gamma]$, acting on the virtual level. The gauged state is zero iff $|\psi^\gamma\rangle$ transforms nontrivially under the residual symmetry group $C(\gamma)$, this property depends only on $[\gamma]$ and $[\alpha]$.*

We will first show that the tensor network $G_{\phi^\gamma}|\psi^\gamma\rangle$ is given by contracting the MPOs $[V^{p_x^i}(x_i) \otimes_{e \in p_x^i} R_e(x_i)], [V^{p_y^i}(y_i) \otimes_{e \in p_y^i} R_e(y_i)]$ (contracted with the crossing tensor $Q_{x_i, y_i} = W_R^{x_i}(y_i)$ at $p_x^i \cap p_y^i$) with the virtual indices of $G|\psi\rangle$ on edges that cross the paths $\{p_x^i, p_y^i\}$.

In general G_ϕ is a projected entangled pair operator (PEPO) with vertex tensors

$$G_\phi^v = \int dg U_v(g) \bigotimes_{e \in E_v} (g| = G^v$$

and edge tensors⁷¹

$$G_\phi^e = \int dg_{v_e^+} dg_{v_e^-} L_e(g_{v_e^-}) R_e(g_{v_e^+}) |\phi_e\rangle \otimes (g_{v_e^+} | (g_{v_e^-} |.$$

Furthermore the edge tensors satisfy $G_\phi^e = G_1^e(R(\phi_e) \otimes \mathbb{1}) = G_1^e(\mathbb{1} \otimes R^\dagger(\phi_e))$. Hence the PEPO G_ϕ is given by the untwisted gauging map G with the tensor product operators $\{\bigotimes_{e \in p_x^i} R_e(x_i), \bigotimes_{e \in p_y^i} R_e(y_i)\}$ applied to the virtual indices that cross $\{p_x^i, p_y^i\}$.

Eqs.(1.3) and (1.71) together with $P_v a_v^g = P_v U_v^\dagger(g)$ imply $G_{\phi^\gamma}|\psi^\gamma\rangle = G_{\phi^{\tilde{\gamma}}}|\psi^{\tilde{\gamma}}\rangle$ for any deformation $\tilde{\gamma} = \{\tilde{p}_x^i, \tilde{p}_y^i\}$ of the paths $\gamma = \{p_x^i, p_y^i\}$ that does not introduce additional intersections (a planar isotopy). This furthermore implies that the MPOs $[V^p(g) \otimes_{e \in p} R_e(g)]$

satisfy the pulling through condition of Ref. 63 for any path p . Consequently, the MPO $\frac{1}{|G|} \sum_g [V^p(g) \otimes_{e \in p} R_e(g)]$, that was shown to be the projection onto the injectivity subspace of the gauged PEPS in Appendix 1.14, also satisfies the pulling through condition.

By Proposition 11 the gauged SPT PEPS $G_{\phi^\gamma} |\psi^\gamma\rangle$ is zero iff $\theta_{(\cdot)}^\gamma$ is nontrivial, which is a property of the conjugacy class $[\gamma]$. Now by Proposition 12 and the fact that the slant product maps cohomology classes to cohomology classes we have the stated result.

Hence the nonzero gauged symmetry twisted PEPS ground states $|\lambda_0, [\gamma]\rangle := G_{\phi^\gamma} |\lambda_0^\gamma\rangle$ are topologically ordered since the tensors Q_{x_i, y_i} that determine the ground state are locally undetectable, which follows from the pulling through condition satisfied by the topological MPOs and Eq.(1.71), while for $[\gamma] \neq [\gamma']$ the states are globally orthogonal $\langle \lambda_0, [\gamma] | \lambda_0, [\gamma'] \rangle = 0$, as shown above.

In fact there is a slight subtlety, as while the reduced density matrices for all $[\gamma], [\gamma'] \in \mathcal{I}_M$ are supported on the same subspace $\rho_{\mathcal{R}}^{\lambda_0, [\gamma]}, \rho_{\mathcal{R}}^{\lambda_0, [\gamma']} \in \text{Im}(A_{\mathcal{R}} \otimes A_{\mathcal{R}}^\dagger)$ for any contractible region \mathcal{R} , they are not necessarily equal⁵⁹ (or even exponentially close in the size of the region). One might also fret over the possibility that the state exhibits spontaneous symmetry breaking. However neither of these complications can occur for the gauged symmetry twisted SPT PEPS, since an exact isometric fixed-point SPT PEPS does not exhibit symmetry breaking and is gauged to a topologically ordered fixed-point state which also does not exhibit symmetry breaking (see Section 1.7). Furthermore the gauging map is gap preserving, hence gauging any SPT PEPS in the same phase as an SPT fixed-point maps it to a topological PEPS in the same phase as the gauged topological fixed-point PEPS.

1.16.3 Monodromy defects in SPT PEPS

Monodromy defects can be created in a SPT theory by applying a symmetry twist along an open ended path in the dual graph p_g from plaquette q_0 to q_1 , specified by a G-connection ϕ^{p_g} , where $\phi_e^{p_g} = 1$, for $e \notin p_g$ and $\phi_e^{p_g} = g^{\sigma_e}$ for $e \in p_g$ (σ_e is +1 if p_g crosses e in a right handed fashion and -1 for left handed crossings) hence ϕ^{p_g} is flat on every plaquette except q_0, q_1 , the end points of p_g , see Fig.1.11. The defect states can be realized as ground states of some twisted Hamiltonians $H_m^{\phi^{p_g}} = \sum_{q \in \Lambda \setminus \partial p_g} h_q^{\phi^{p_g}} + h'_{q_0} + h'_{q_1}$ where the choice of the end terms h'_{q_0}, h'_{q_1} is somewhat arbitrary. These monodromy defects can be introduced into a SPT PEPS $|\psi\rangle$ following the framework set up for symmetry twists.

Definition 5 (Monodromy defected SPT PEPS). *A monodromy defect specified by p_g in a SPT PEPS $|\psi\rangle$ is described by a set of tensor network states parametrized by a pair of tensors B_0, B_1 where $B_0 : (\mathbb{C}^D)^{\otimes |E_{v_0}|} \otimes \mathbb{C}^\chi \rightarrow \mathbb{C}^d$ is a local tensor associated to a vertex $v_0 \in \partial q_0$ with a set of indices matching those of the tensor A_{v_0} , and an extra virtual index of the same bond dimension χ as the internal index of the MPO (B_1 is defined similarly).*

The monodromy defected tensor network states $|\psi^{p_g}, B_0, B_1\rangle$ are constructed from the SPT PEPS $|\psi\rangle$ by replacing the PEPS tensors A_{v_0}, A_{v_1} with B_0, B_1 and contracting the extra virtual indices thus introduced with the open end indices of the MPO $V^{p_g}(g)$ which acts on the virtual indices of the PEPS that cross p_g . This is depicted in Fig. 1.12 b).

This provides an ansatz⁶⁴ for symmetry twists by choosing appropriate boundary tensors B_0, B_1 to close the free internal MPO indices at q_0, q_1 , the possibility of different boundary conditions corresponds to the ambiguity in the local Hamiltonian terms h'_{q_0}, h'_{q_1} , see Figs.1.11,1.12.

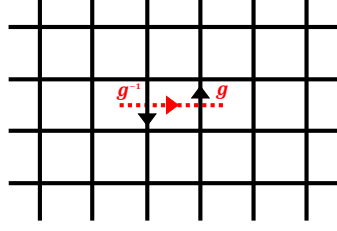


Figure 1.11: A symmetry twist g along an open path.

Eq.(1.3) implies that the defect state ansatz $|\psi^{p_g}, B_0, B_1\rangle$ is in the ground space of the sum of Hamiltonian terms away from the end points of p_g , $\sum_{q \in \Lambda \setminus \partial p_g} h_q^{\phi^{p_g}}$, for any choice of tensors B_0, B_1 .

Since the connection ϕ^{p_g} is flat everywhere but q_0, q_1 , the gauging map can be applied, in the usual way, to operators that are supported away from these plaquettes. Hence the twisted gauged defect Hamiltonian is $(H_m^{\phi^{p_g}})^{\mathcal{G}^{\phi^{p_g}}} := \sum_{q \in \Lambda \setminus \partial p_g} \mathcal{G}_{\Gamma_q}^{\phi^{p_g}}[h_q^{\phi^{p_g}}] + h''_{q_0} + h''_{q_1}$ where again there is an ambiguity in the choice of end terms h''_{q_0}, h''_{q_1} . The SPT PEPS with monodromy defect p_g can be gauged via the standard gauging procedure for the G-connection ϕ^{p_g} to yield the tensor network $G_{\phi^{p_g}} |\psi^{p_g}, B_0, B_1\rangle$. Similar to the case of symmetry twists on closed paths, the gauged defect SPT PEPS $G_{\phi^{p_g}} |\psi^{p_g}, B_0, B_1\rangle$ is constructed from the untwisted gauged SPT PEPS $G |\psi\rangle$ by removing the tensors $G^{v_0} A_{v_0}, G^{v_1} A_{v_1}$ and replacing them with the pair of tensors $G^{v_0} B_0, G^{v_1} B_1$ connected by a virtual MPO $[V^{p_g}(g) \otimes_{e \in p_g} R_e(g)]$ acting on the virtual indices of the PEPS that cross p_g . Note the dimension of the inner indices of this MPO match the extra indices of $G^{v_0} B_0, G^{v_1} B_1$ since the newly introduced component of the MPO $\otimes_{e \in p_g} R_e(g)$ has trivial inner indices. To achieve a more general ansatz one may want to replace $G^{v_0} B_0, G^{v_1} B_1$ by arbitrary tensors $\tilde{B}_0, \tilde{B}_1 : (\mathbb{C}^D \otimes \mathbb{C}[G])^{\otimes |E_v|} \otimes \mathbb{C}^X \rightarrow \mathbb{C}^d$.

As shown above, the MPO $[V^{p_g}(g) \otimes_{e \in p_g} R_e(g)]$ satisfies the pulling through condition of Ref. 63 and hence $G_{\phi^{p_g}} |\psi^{p_g}, B_0, B_1\rangle = G_{\phi^{p'_g}} |\psi^{p'_g}, B_0, B_1\rangle$ for p'_g an arbitrary, end point preserving, deformation of p_g . By Eq.(1.124) we have $\mathcal{G}_{\Gamma_q}^{\phi^{p_g}}[h_q^{\phi^{p_g}}] = \mathcal{G}_{\Gamma_q}[h_q]$ and hence the gauged defect SPT PEPS $G_{\phi^{p_g}} |\psi^{p_g}, B_0, B_1\rangle$, for all B_0, B_1 , is in the ground space of the sum of gauged Hamiltonian terms away from the end points $\sum_{q \in \Lambda \setminus \partial p_g} \mathcal{G}_{\Gamma_q}[h_q]$. Consequently $G_{\phi^{p_g}} |\psi^{p_g}, B_0, B_1\rangle$ must represent a superposition of anyon pairs, localized to the plaquettes q_0, q_1 , on top of the vacuum (ground state). Furthermore the freedom in choosing B_0, B_1 leads to a fully general anyon ansatz within the framework of MPO-injective PEPS⁶⁴.

1.16.4 Projective symmetry transformation of monodromy defects

We proceed to show that the internal degrees of freedom of a monodromy defect p_g transform under a projective representation of the residual global symmetry group $\mathbb{C}(g)$ via a generalization of the mechanism for virtual symmetry actions in MPS^{27,35,56}.

We consider a SPT PEPS on an oriented manifold \mathcal{M} with a twice punctured sphere topology and a symmetry twist p_g running from one puncture Π_0 to the other Π_1 . This captures both the case of a symmetry twisted SPT model defined on a cylinder (when the virtual bonds that enter the punctures are left open), and the case of a pair of monodromy defects on a sphere

(when the punctures are formed by removing a pair of PEPS tensors A_{v_0}, A_{v_1} and contracting the virtual indices thus opened with B_0, B_1), see Fig. 1.12.

The bulk of the symmetry twisted state is invariant under the physical on-site representation $U(h)^{\otimes |\mathcal{M}|_v}$ of $C(g) \leq G$, but this may have some action on the virtual indices that enter the punctures. Treating the SPT PEPS on a cylinder of fixed radius as a one dimensional symmetric MPS implies, by well established arguments^{27,56}, that the action of the symmetry on the virtual boundaries $\mathcal{V}_0^g(h) \otimes \mathcal{V}_1^g(h)$ forms a representation, while each individual boundary action $\mathcal{V}_0^g(h), \mathcal{V}_1^g(h)$ is free to form a projective representation.

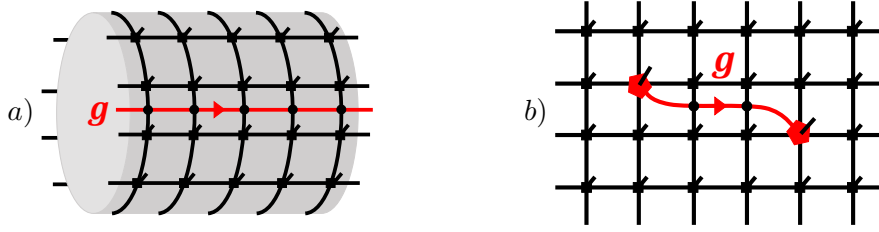


Figure 1.12: a) A symmetry twisted SPT PEPS on a cylinder. b) A pair of monodromy defects on a sphere.

Assuming the symmetry MPOs satisfy the *zipper* condition (1.71) one can directly calculate the effect that a physical symmetry action $U(h)^{\otimes |\mathcal{M}|_v}$, $h \in C(g)$ has on the virtual boundary, simultaneously demonstrating the symmetry invariance of the bulk.

$$\begin{array}{c}
 \text{Diagram 1} \\
 \text{Diagram 2}
 \end{array}
 = \begin{array}{c}
 \text{Diagram 3} \\
 \text{Diagram 4}
 \end{array} \quad (1.130)$$

The diagrams show the action of a symmetry h on a virtual boundary. Diagram 1 shows a grid of black arrows with a red arrow labeled g passing through. Diagram 2 shows the same grid with red arrows labeled h and h^{-1} at the boundaries. Diagram 3 shows the grid with red arrows labeled g and h at the boundaries. Diagram 4 shows the grid with red arrows labeled g and h^{-1} at the boundaries. The equations (1.130) and (1.131) show the equivalence of these diagrams.

$$\begin{array}{c}
 \text{Diagram 5} \\
 \text{Diagram 6}
 \end{array}
 = \begin{array}{c}
 \text{Diagram 7} \\
 \text{Diagram 8}
 \end{array} \quad (1.131)$$

The diagrams show the action of a symmetry h on a virtual boundary. Diagram 5 shows a grid of black arrows with a red arrow labeled g passing through. Diagram 6 shows the same grid with red arrows labeled h and h^{-1} at the boundaries. Diagram 7 shows the grid with red arrows labeled g and h at the boundaries. Diagram 8 shows the grid with red arrows labeled g and h^{-1} at the boundaries. The equations (1.130) and (1.131) show the equivalence of these diagrams.

Hence the symmetry action $\mathcal{V}_1^g(h)$ (see Eq.(1.20)) on the boundary of a single puncture Π_1 is given by the MPO $V^{\partial\Pi_1^-}(h)$, acting on the virtual indices along $\partial\Pi_1$, contracted with the crossing tensor $Y_R^g(h)$ (see Eq.(1.88)) acting on the inner MPO index of the symmetry twist $V^{p_g}(g)$ that enters the puncture. Similarly $\mathcal{V}_0^g(h)$, acting on the boundary of the other puncture Π_0 , is given by contracting the MPO $V^{\partial\Pi_0^-}(h)$ with the crossing tensor $Y_L^g(h)$.

There is a natural composition operation on the crossing tensors $Y_R^g(\cdot)$ that is induced by applying a product of global symmetries $U(k)^{\otimes |\mathcal{M}|_v} U(h)^{\otimes |\mathcal{M}|_v}$ and utilizing the reduction of Eq.(1.131) twice and then zipping the MPOs $V^{\partial\Pi_1^-}(k) V^{\partial\Pi_1^-}(h) = X(k, h) V^{\partial\Pi_1^-}(kh) X^+(k, h)$ by Eq.(1.71). This is nothing but the product $Y_R^g(k) \times Y_R^g(h)$ that was previously defined in Eq.(1.93).

Since the physical action $U(h)^{\otimes |\mathcal{M}|_v}$ forms a representation of the symmetry group $C(g)$ the simultaneous virtual action on both boundaries Π_0, Π_1 together $\mathcal{V}_0^g(h) \otimes \mathcal{V}_1^g(h)$ must also form a representation. However, there is a multiplicative freedom in the multiplication rule of

the representation on a single boundary

$$\mathcal{V}_1^g(k)\mathcal{V}_1^g(h) = \omega_1^g(k, h)\mathcal{V}_1^g(kh)$$

(and similarly for $\mathcal{V}_0^g(h)$), under the constraint $\omega_0^g(k, h)\omega_1^g(k, h) = 1$, allowing the possibility of projective representations.

Using the result of Eq.(1.94), $Y_R^g(k) \times Y_R^g(h) = \omega^g(k, h)Y_R^g(kh)$, we can pin down the 2-cocycle ω_1^g explicitly in terms of the 3-cocycle α of the injective MPO representation $V^{\partial\Pi_0^-}(\cdot)$ as follows $\omega_1^g(k, h) = \omega^g(k, h)$ (see Eq.(1.92) for definition of ω^g). Hence the cohomology class of the projective representation $\mathcal{V}_1^g(\cdot)$ is given by

$$[\omega_1^g(k, h)] = [\alpha^{(g)}(k, h)].$$

It was shown above that a gauged SPT PEPS with a pair of defects $G_{\phi^{p_g}} |\psi^{p_g}, B_0, B_1\rangle$ describes a superposition of anyon pairs in the resulting topological theory. The projective transformation of the monodromy defects is intimately related to the braiding of the resulting anyons, which can be inferred from the following process, depicted in Fig. 1.13. First consider an isolated anyon formed by creating a pair of anyons and then moving the other arbitrarily far away. Next create a second pair and move them to encircle the isolated anyon, at this point one should fuse these anyons, but the full description of such fusion requires a systematic anyon ansatz which is beyond the scope of the current paper (see Ref. 64). Instead we drag the pair arbitrarily far away as demonstrated in Fig. 1.13 and use the fact that this can be rewritten as some local action on the internal degrees of freedom of the isolated anyon, plus another locally undetectable action that can be moved arbitrarily far away.

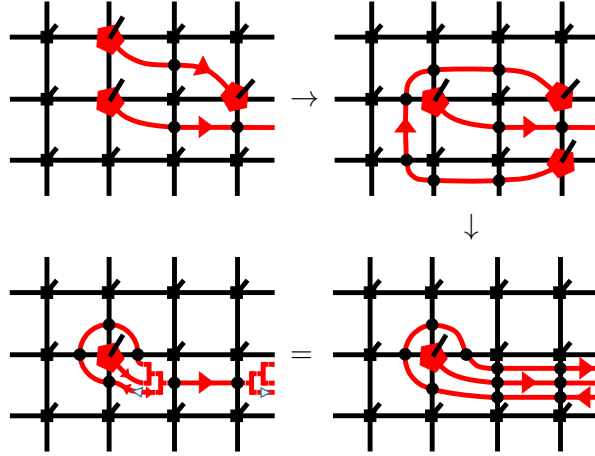


Figure 1.13: The process used to find the effect of braiding on the internal degrees of freedom of a single anyon.

1.17 Gauging symmetric Hamiltonians and ground states

In this appendix we apply the gauging procedure developed in Ref. 71 to families of trivial and SPT Hamiltonians with symmetric perturbations and find that they are mapped to perturbed

quantum double and twisted quantum double models respectively. We then go on to describe gauging the (unperturbed) fixed-point ground states.

1.17.1 Gauging the Hamiltonian

First we apply the gauging procedure to a symmetric Hamiltonian defined on the matter degrees of freedom, each with Hilbert space $\mathbb{H}_v \cong \mathbb{C}[G]$ and symmetry action $U_v(g) = R_v(g)$, associated to the vertices of a directed graph Λ embedded in a closed oriented 2-manifold \mathcal{M} . The Hamiltonian is given by

$$H_m = \alpha \sum_{v \in \Lambda} h_v^0 + \sum_{m \in G} \beta_m \sum_{e \in \Lambda} \mathcal{E}_e^m \quad (1.132)$$

the vertex terms are $h_v^0 := \int d\hat{g}_v dg_v |\hat{g}_v\rangle \langle g_v|$ while the edge interaction terms are

$$\mathcal{E}_e^m := \int dg_{v_e^-} dg_{v_e^+} \delta_{g_{v_e^-} g_{v_e^+}^{-1}, m} |g_{v_e^-}\rangle \langle g_{v_e^-}| \otimes |g_{v_e^+}\rangle \langle g_{v_e^+}|.$$

Each term in this Hamiltonian is symmetric under the group action $\otimes_v R_v(g)$. For $\alpha, \beta_m < 0$ and $|\alpha| \gg |\beta_m|$ this Hamiltonian describes a symmetric phase with trivial SPT order, while for $|\beta_m| \gg |\alpha|$ the Hamiltonian describes different symmetry broken phases.

We construct the gauge and matter Hamiltonian $H_{g,m}$ by first gauging the local terms h_v^0 , which leaves them invariant $\mathcal{G}_v[h_v^0] = h_v^0$. Next we gauge the interaction terms \mathcal{E}_e^m with the gauging map on \bar{e} (the closure of edge e)

$$\begin{aligned} \mathcal{G}_{\bar{e}}[\mathcal{E}_e^m] &= \int dg_{v_e^-} dg_{v_e^+} dh_{v_e^-} dh_{v_e^+} \delta_{g_{v_e^-} g_{v_e^+}^{-1}, m} |g_{v_e^-} h_{v_e^-}^{-1}\rangle \langle g_{v_e^-} h_{v_e^-}^{-1}| \\ &\quad \otimes |h_{v_e^-} h_{v_e^+}^{-1}\rangle \langle h_{v_e^-} h_{v_e^+}^{-1}|_e \otimes |g_{v_e^+} h_{v_e^+}^{-1}\rangle \langle g_{v_e^+} h_{v_e^+}^{-1}|. \end{aligned}$$

Finally we consider additional local gauge invariant Hamiltonian terms acting purely on the gauge degrees of freedom: symmetric local fields

$$\mathcal{F}_e^c := \int d\hat{g}_e dg_e \delta_{\hat{g}_e g_e^{-1} \in c} |\hat{g}_e\rangle \langle g_e| \quad (1.133)$$

where $c \in \mathfrak{C}(G)$ are conjugacy classes of G , and plaquette flux-constraints

$$\mathcal{B}_p^m := \int \prod_{e \in \partial p} dg_e \delta_{g_{e_1}^{\sigma_{e_1}} \dots g_{e_{|\partial p|}}^{\sigma_{e_{|\partial p|}}}, m} \bigotimes_{e \in \partial p} |g_e\rangle \langle g_e|, \quad (1.134)$$

where each plaquette p has a fixed orientation induced by the 2-manifold \mathcal{M} , and the group elements $\{g_{e_1}, \dots, g_{e_{|\partial p|}}\}$ are ordered as the edges are visited starting from the smallest vertex label and moving against the orientation of ∂p , then $\sigma_{e_i} = \pm 1$ is $+1$ if the edge e_i points in the same direction as the orientation of p and -1 otherwise. Finally we require that the group elements lie in the center of the group $m \in C(G)$ which renders the choice of vertex from which we begin our traversal of ∂p irrelevant.

The full gauge and matter Hamiltonian is thus given by

$$H_{g,m} = \alpha \sum_{v \in \Lambda} h_v^0 + \sum_{m \in G} \beta_m \sum_{e \in \Lambda} \mathcal{G}_{\bar{e}}[\mathcal{E}_e^m] + \sum_{c \in \mathfrak{C}(G)} \gamma_c \sum_{e \in \Lambda} \mathcal{F}_e^c + \sum_{m \in C(G)} \varepsilon_m \sum_{p \in \Lambda} \mathcal{B}_p^m. \quad (1.135)$$

Note that each term commutes with all local gauge constraints $\{P_v\}$, see Eq.(1.109), and the physics takes place within this gauge invariant subspace.

1.17.2 Disentangling the constraints

To see more clearly that this gauge theory is equivalent to an unconstrained quantum double model we will apply a local disentangling circuit to reveal a clear tensor product structure, allowing us to ‘spend’ the gauge constraints to remove the matter degrees of freedom.

We define the disentangling circuit to be the product of local unitaries $C_\Lambda := \prod_v C_v$, where $C_v := \int dg_v |g_v\rangle \langle g_v|_v \prod_{e \in E_v^+} R_e(g) \prod_{e \in E_v^-} L_e(g)$. Note the order in the product is irrelevant since $[C_v, C_{v'}] = 0$. This circuit induces the following transformation on the gauge projectors: $C_\Lambda P_v C_\Lambda^\dagger = \int dg R_v(g)$, hence any state $|\psi\rangle$ in the gauge invariant subspace (simultaneous $+1$ eigenspace of all P_v) is disentangled into a tensor product of symmetric states on all matter degrees of freedom with an unconstrained state $|\psi'\rangle \in \mathbb{H}_g$ on the gauge degrees of freedom $C_\Lambda |\psi\rangle = |\psi'\rangle \otimes_v \int dg_v |g_v\rangle$.

Now we apply the disentangling circuit to the Hamiltonian $H_{g,m}$. First note the pure gauge terms \mathcal{F}_e^c and \mathcal{B}_p^m are invariant under conjugation by C_v . The vertex terms are mapped to

$$C_v h_v^0 C_v^\dagger = \int dg_v R_v(g_v) \bigotimes_{e \in E_v^+} R_e(g_v) \bigotimes_{e \in E_v^-} L_e(g_v).$$

Since the disentangled vertex degrees of freedom are invariant under $R_v(g_v)$ we see that this Hamiltonian term acts as

$$\int dg_v \bigotimes_{e \in E_v^+} R_e(g_v) \bigotimes_{e \in E_v^-} L_e(g_v)$$

on the relevant gauge degrees of freedom. We recognize this as the vertex term of a quantum double model. Finally we examine the transformation of the interaction terms

$$C_v \mathcal{G}_e[\mathcal{E}_e^m] C_v^\dagger = \frac{1}{|\mathbb{G}|} |m\rangle \langle m|_e,$$

which yield local fields on the gauge degrees of freedom that induce string tension. Hence we see that the gauge plus matter Hamiltonian after disentangling becomes a local Hamiltonian $H_g := C_v H_{g,m} C_v^\dagger$ acting purely on the gauge degrees of freedom

$$\begin{aligned} H_g = \alpha \sum_v \int dg_v \bigotimes_{e \in E_v^+} R_e(g_v) \bigotimes_{e \in E_v^-} L_e(g_v) &+ \sum_{m \in \mathbb{G}} \frac{\beta_m}{|\mathbb{G}|} \sum_{e \in \Lambda} |m\rangle \langle m|_e \\ &+ \sum_{c \in \mathcal{C}(\mathbb{G})} \gamma_c \sum_{e \in \Lambda} \mathcal{F}_e^c + \sum_{m \in \mathcal{C}(\mathbb{G})} \varepsilon_m \sum_{p \in \Lambda} \mathcal{B}_p^m \end{aligned} \quad (1.136)$$

which describes a quantum double model with string tension and flux perturbations. Note that a spontaneous symmetry breaking phase transition in the ungauged model is mapped to a string tension induced anyon condensation transition by the gauging procedure.

1.17.3 Gauging nontrivial SPT Hamiltonians

The gauging procedure extends to nontrivial SPT Hamiltonians which are defined on triangular graphs embedded in closed oriented 2-manifolds \mathcal{M} . The only modification required is to replace the trivial vertex terms h_v^0 by nontrivial terms h_v^α which are defined by

$$\int d\hat{g}_v dg_v \prod_{v' \in L(v)} dg_{v'} \prod_{\Delta \in S(v)} \alpha_\Delta |\hat{g}_v\rangle \langle g_v| \bigotimes_{v' \in L(v)} |g_{v'}\rangle \langle g_{v'}| \quad (1.137)$$

where $S(v)$ is the star of v , $L(v)$ is the link of v and $\alpha_\Delta \in U(1)$ for plaquette Δ , whose vertices are given counterclockwise (relative to the orientation of the 2-manifold) by v, v', v'' , is defined by the 3-cocycle $\alpha_\Delta := \alpha^{\sigma_\pi}(g_1 g_2^{-1}, g_2 g_3^{-1}, g_3 g_4^{-1})$ where $(g_1, g_2, g_3, g_4) := \pi(\hat{g}_v, g_v, g_{v'}, g_{v''})$ for π the permutation that sorts the group elements into ascending vertex label order (with the convention that \hat{g}_v immediately precedes g_v) and $\sigma_\pi = \pm 1$ is the parity of the permutation. The terms h_v^α are clearly symmetric under global right group multiplication and are seen to be Hermitian since conjugation inverts the phase factor α_Δ and interchanges the role of \hat{g}_v and g_v which inverts the parity of π thereby compensating the conjugation of α_Δ .

We apply the gauging map on the region $\bar{S}(v)$ (the closure of the star of v) to h_v^α

$$\mathcal{G}_{\bar{S}(v)}[h_v^\alpha] = \int d\hat{g}_v dg_v dh_v \prod_{v' \in L(v)} dg_{v'} dh_{v'} \prod_{\Delta \in S(v)} \alpha_\Delta |\hat{g}_v h_v^{-1}\rangle \langle g_v h_v^{-1}| \bigotimes_{v' \in L(v)} |g_{v'} h_{v'}^{-1}\rangle \langle g_{v'} h_{v'}^{-1}| \bigotimes_{e \in \bar{S}(v)} |h_{v_e^-} h_{v_e^+}^{-1}\rangle \langle h_{v_e^-} h_{v_e^+}^{-1}|_e \quad (1.138)$$

followed by the disentangling circuit $C_\Lambda \mathcal{G}_{\bar{S}(v)}[h_v^\alpha] C_\Lambda^\dagger$ which yields

$$\int d\hat{g}_v dg_v dh_v \prod_{v' \in L(v)} dg_{v'} dh_{v'} \prod_{\Delta \in S(v)} \alpha_\Delta |\hat{g}_v h_v^{-1}\rangle \langle g_v h_v^{-1}| \bigotimes_{v' \in L(v)} |g_{v'} h_{v'}^{-1}\rangle \langle g_{v'} h_{v'}^{-1}| \bigotimes_{e \in E_v^+} |g_{v_e^-} \hat{g}_v^{-1}\rangle \langle g_{v_e^-} g_v^{-1}| \bigotimes_{e \in E_v^-} |\hat{g}_v g_{v_e^+}^{-1}\rangle \langle g_v g_{v_e^+}^{-1}| \bigotimes_{e \in L(v)} |g_{v_e^-} g_{v_e^+}^{-1}\rangle \langle g_{v_e^-} g_{v_e^+}^{-1}|. \quad (1.139)$$

Note, importantly, the phase functions α_Δ now depend only on the gauge degrees of freedom. Finally in Eq.(1.140) we rewrite the pure gauge Hamiltonian terms without reference to the matter degrees of freedom, which become irrelevant as the matter degrees of freedom in any gauge invariant state are fixed to be in the symmetric state $\int dg_v |g_v\rangle_v$ by the disentangling circuit

$$\int d\hat{g}_v dg_v \prod_{v' \in L(v)} dg_{v'} \prod_{\Delta \in S(v)} \alpha_\Delta \bigotimes_{e \in E_v^+} |g_{v_e^-} \hat{g}_v^{-1}\rangle \langle g_{v_e^-} g_v^{-1}| \bigotimes_{e \in E_v^-} |\hat{g}_v g_{v_e^+}^{-1}\rangle \langle g_v g_{v_e^+}^{-1}| \bigotimes_{e \in L(v)} |g_{v_e^-} g_{v_e^+}^{-1}\rangle \langle g_{v_e^-} g_{v_e^+}^{-1}| \quad (1.140)$$

This can be recognized as the vertex term of a 2D twisted quantum double model (the lattice hamiltonian version of a twisted Dijkgraaf Witten theory for the group G and cocycle α).

1.17.4 Gauging SPT groundstates

In this section we apply the gauging procedure directly to the ground states of the nontrivial SPT Hamiltonian that was defined in Eq.(1.137). These ground states are constructed using the following local circuit⁷⁵

$$D_\alpha := \int \prod_{v \in \Lambda} dg_v \prod_{\Delta \in \Lambda} \tilde{\alpha}_\Delta \bigotimes_{v \in \Lambda} |g_v\rangle \langle g_v| \quad (1.141)$$

where $\tilde{\alpha}_\Delta \in U(1)$ is a function of the degrees of freedom on plaquette Δ , whose vertices are given counterclockwise, relative to the orientation of the 2-manifold \mathcal{M} , by v, v', v'' (note the choice of starting vertex is irrelevant) and is defined by a 3-cocycle as follows

$$\tilde{\alpha}_\Delta := \alpha^{\sigma_\pi}(g_1 g_2^{-1}, g_2 g_3^{-1}, g_3)$$

where $(g_1, g_2, g_3) := \pi(g_v, g_{v'}, g_{v''})$ with π the permutation that sorts the group elements into ascending vertex label order and $\sigma_\pi = \pm 1$ is the parity of the permutation (equivalently the orientation of \triangle embedded within the 2-manifold \mathcal{M}). Note D_α is easily expressed as a product of commuting 3-local gates.

To define SPT fixed-point states we start with the trivial state

$$|\text{SPT}(0)\rangle := \bigotimes_v \int dg_v |g_v\rangle_v ,$$

which is easily seen to be symmetric under global right group multiplication. One can also check that D_α is symmetric under conjugation by global right group multiplication by utilizing the 3-cocycle condition satisfied by each $\tilde{\alpha}_\Delta$. With this we define nontrivial SPT fixed-point states

$$|\text{SPT}(\alpha)\rangle := D_\alpha |\text{SPT}(0)\rangle ,$$

which are symmetric by construction. To see that $|\text{SPT}(\alpha)\rangle$ is the ground state of the SPT Hamiltonian $\sum_v h_v^\alpha$ we note $h_v^\alpha = D_\alpha h_v^0 D_\alpha^\dagger$ which again is proved using the 3-cocycle condition.

We will now gauge the SPT fixed-point states by applying the state gauging map to D_α , since the input variables of the circuit carry the same information as the virtual indices of the fixed-point SPT PEPS we hope this makes the correspondence between the two pictures more clear

$$GD_\alpha = \int \prod_{v \in \Lambda} dg_v dh_v \prod_{\Delta \in \Lambda} \tilde{\alpha}_\Delta \bigotimes_{e \in \Lambda} |h_{v_e^-} h_{v_e^+}^{-1}\rangle \bigotimes_{v \in \Lambda} |g_v h_v^{-1}\rangle \langle g_v|. \quad (1.142)$$

Under the local disentangling circuit this transforms to

$$C_\Lambda GD_\alpha = \int \prod_{v \in \Lambda} dg_v \prod_{\Delta \in \Lambda} \tilde{\alpha}_\Delta \bigotimes_{e \in \Lambda} |g_{v_e^-} g_{v_e^+}^{-1}\rangle \bigotimes_{v \in \Lambda} \langle g_v| \bigotimes_{v \in \Lambda} \int dk_v |k_v\rangle , \quad (1.143)$$

where it is clear that the matter degrees of freedom have been disentangled into symmetric states and the cocycles $\tilde{\alpha}_\Delta$ depend on both the group variables on the edges and the inputs on the vertices (which correspond to the PEPS virtual degrees of freedom).

The explicit connection to the fixed-point SPT PEPS is made by replacing the basis at each vertex $|g_v\rangle_v$ by an analogous basis of the diagonal subspace of variables at each plaquette surrounding the vertex $\bigotimes_{\Delta \in S(v)} |g_v\rangle_{\Delta, v}$. This construction lends itself directly to a PEPS description where a tensor is assigned to each plaquette of the original graph (i.e. the PEPS is constructed on the dual graph). This in turn is why we must apply a seemingly modified version of the gauging operator of Ref. 71 to gauge the PEPS correctly and we note that on the subspace where redundant variables are identified the modified PEPS gauging operator becomes identical to the standard gauging operator.

Chapter 2

Anomalies and entanglement renormalization

Synopsis:

We study 't Hooft anomalies of discrete groups in the framework of (1+1)-dimensional multi-scale entanglement renormalization ansatz states on the lattice. Using matrix product operators, general topological restrictions on conformal data are derived. An ansatz class allowing for optimization of MERA with an anomalous symmetry is introduced. We utilize this class to numerically study a family of Hamiltonians with a symmetric critical line. Conformal data is obtained for all irreducible projective representations of each anomalous symmetry twist, corresponding to definite topological sectors. It is numerically demonstrated that this line is a protected gapless phase. Finally, we implement a duality transformation between a pair of critical lines using our subclass of MERA.

Based on: [129](#)

Jacob C. Bridgeman and Dominic J. Williamson,
submitted, [arXiv:1703.07782](#).

Changes compared to published version: Minor formatting changes.

Contributions of the author: Both authors contributed equally to this project as a whole, including the writing up. Section [2.5](#) was primarily due to the first author, whilst Section [2.3](#) was primarily due to the second author, the remaining sections received an equal contribution. This work will also appear in the first author's PhD thesis.

2.1 Introduction

Quantum many-body models of strongly interacting spins display surprisingly complex emergent physics. Understanding general classes of collective behaviors corresponds to understanding which phases of matter can be realized through local interactions. The universal behavior of phases, and their transitions, is determined by the fixed points under renormalization group (RG) flows^{15,16}.

Symmetries play a fundamental role in the understanding of phases, due to constraints they impose on RG. Indeed, the conventional classification of phases describes how a symmetry can be broken¹³⁰. Distinct quantum phases emerge even without a broken symmetry^{1,8–10,131}. In the absence of intrinsic topological order, these phases are known as *symmetry protected topological* (SPT) phases^{3,34–36}. Despite having no topological order and no local order parameter, SPT phases are resources for quantum computation^{132–136}.

On the lattice, symmetries are usually assumed to act independently on each site. More exotic symmetries, which cannot be made on-site, have recently been studied in chains of anyons^{80,137–140} and at the boundary of SPT phases^{70,74–76,93,141–145}. In fact, a classification of SPTs can be obtained by considering possible boundary actions of the symmetry. Equivalence classes of such symmetries are labeled by the ‘t Hooft anomalies¹⁴⁶ of a discrete group. Such anomaly labels are preserved by symmetric RG transformations, so restrict the possible fixed points¹⁴⁷.

Tensor network methods^{39–41} allow anomalous symmetries to be realized directly on the lattice. In $(1 + 1)$ dimensions, *matrix product operators* (MPOs) capture all ‘t Hooft anomalies of discrete groups^{70,74,93,141}. Within the framework of tensor networks, phases are classified at the level of states. For example, *matrix product states* (MPS) have proven particularly successful for the study of gapped spin chains^{27,45,49–51,53–56,67}. Despite substantial complications arising for tensor networks in higher dimensions; significant progress has been made, particularly in the study of topological states^{57–66}.

Imposing on-site symmetries on tensor network representations of quantum states is well understood^{68,69,148}. Far less effort has been made to study the effect of anomalous group actions on these states. Such group actions naturally arise as the effective edge symmetries of $(d + 1)$ D SPTs^{75,143,144}. In $(2 + 1)$ D, the edge theory must either spontaneously break this symmetry or be gapless. Since all MPS break the symmetry⁷⁰, to study gapless, symmetric edge theories we turn to another class of tensor networks known as *multiscale entanglement renormalization ansatz* (MERA)⁴³. These networks draw on ideas from RG to represent the low energy states of gapless Hamiltonians^{43,78,149}.

In this work we define a variational subclass of MERA which can be used to simulate SPT edge physics in a manifestly symmetric way. This subclass allows us to investigate the interplay between RG and anomalies in the framework of tensor networks. We use tensor network methods to derive general consequences of an anomalous symmetry on the conformal field theory (CFT) data of an RG fixed point. For a family of Hamiltonians, corresponding to a line of fixed points, we numerically optimize within our variational class to find the lowest energy states and extract conformal data^{150,151}. We observe the effects of the anomaly in these results. Furthermore, we demonstrate that as a consequence of the anomaly these Hamiltonians admit no relevant, symmetric perturbations. The Hamiltonians therefore support a gapless phase

which is protected by an anomalous symmetry.

More generally, RG fixed points may transform non-trivially under an anomalous group action. Our variational class accommodates this possibility, and hence permits the study of gapless models which are not symmetric. We utilize this in a numerical simulation of two critical lines that are related by a duality transformation, which we implement at the level of a single tensor.

This paper is organized as follows: In Section 2.2, we introduce background material on anomalies, symmetries and tensor networks. In particular, we introduce the 't Hooft anomaly of a discrete symmetry. We then briefly review the MERA and what it means for it to be symmetric under an on-site group action. The difficulties in enforcing anomalous MPO symmetries locally are then discussed. In Section 2.3, we derive general consequences of an anomalous symmetry on a MERA, which are later utilized in the numerical simulations. We study anomalous symmetry twists and the projective representations under which they transform. From these ingredients, projectors onto definite topological sectors are constructed. Consequences for fields within a sector are discussed. In Section 2.4, we define a variational subclass of MERA which is later used for manifestly symmetric simulations. We present a disentangling unitary capable of decoupling a local piece of an anomalous \mathbb{Z}_N^3 group action. This allows the unconstrained variational parameters of any symmetric MERA scheme to be isolated, and therefore optimized over. In Section 2.5, we bring together tools developed in the preceding sections to simulate a family of Hamiltonians with three critical lines. One of these lines possesses an anomalous symmetry, whilst the other two are dual under the anomalous group action. We present conformal data for these critical lines obtained from a numerically optimized MERA, including two nontrivial topological sectors for the symmetric line. Additionally, we demonstrate that the symmetric line is in fact a protected gapless phase. In Section 2.6 we summarize the results and suggest several possible extensions of this work.

We have included several appendices for completeness. In Appendix 2.7 we provide conformal data obtained from a symmetric MERA in all topological sectors for the symmetric line of our example model. Additionally, we present fusion rules for these topological sectors computed using a symmetric MERA. In Appendix 2.8 we review the notion of third cohomology for an MPO representation of a finite group. In Appendix 2.9 we provide details of our ansatz for MPO symmetric MERA including example tensors for two MERA schemes. In Appendix 2.10 we describe a generalization of the CZX model⁷⁰ to arbitrary finite groups \mathcal{G} , such that the bulk symmetry acts as an MPO duality of \mathcal{G} -SPT phases on the boundary.

2.2 Symmetries and anomalies in MERA

This section introduces the main tools and concepts utilized in the remainder of this manuscript. We begin by discussing 't Hooft anomalies of group actions, including some historical context. Lattice realizations of these anomalies, and their influence on tensor network states, are our primary objects of study. Readers unfamiliar with this terminology may skip to Section 2.2.1 for the definition of anomaly used throughout this work. We then review the MERA, the tensor network designed for critical behavior, and define what it means for it to be symmetric under a unitary group action. We briefly explain how one enforces an on-site symmetry via a local constraint before moving on to discuss the difficulties in enforcing an anomalous symmetry in

a similar fashion.

Recently anomalies have played an important role in the classification and study of topological phases of matter^{142,152,153}. Particularly relevant are 't Hooft anomalies, which describe obstructions to gauging a global symmetry¹⁴⁶. SPT phases, and their higher symmetry generalizations^{88,154,155}, can be classified by the possible 't Hooft anomalies on their boundaries^{75,76,143,144}. Conversely one can think of the possible 't Hooft anomalies as being classified by what is known as anomaly inflow from one dimension higher^{76,142–145}.

A global symmetry with an 't Hooft anomaly has an interesting interplay with the renormalization group (RG). For a connected Lie group symmetry, an 't Hooft anomaly restricts the possible RG fixed points, even if the symmetry is spontaneously broken^{156,157}. In the case of a broken discrete symmetry, this is no longer true. For a symmetry respecting RG flow, however, the 't Hooft anomaly can not change and hence constrains the possible fixed points¹⁴³.

Symmetry actions which can be realized independently on each site have trivial 't Hooft anomaly because they can be gauged directly on the lattice^{71,73,93}, see Chapter 1. Conversely, this gauging procedure cannot be applied directly to symmetries which cannot be made on site. Therefore, we treat the 't Hooft anomaly as an obstruction to making a symmetry action on-site^{74,142,145}.

For a discrete symmetry group \mathcal{G} in $(1+1)\text{D}$, all 't Hooft anomalies of bosonic unitary representations occur on the boundaries of $(2+1)\text{D}$ SPT phases, in other words they arise from anomaly inflow. The anomalies can therefore be classified by $\mathcal{H}^3(\mathcal{G}, \text{U}(1))$, the same set of labels as the SPT phases^{70,75,144}. In the next section, we describe how *matrix product operators* can be utilized to represent these anomalous actions.

2.2.1 Symmetries on the lattice

In this work, we consider unitary representations of finite groups on the lattice. We say a state $|\psi\rangle$ is *symmetric* under a group \mathcal{G} if $U_g |\psi\rangle = |\psi\rangle$ for all $g \in \mathcal{G}$, where U_g is some unitary representation of the group.

The symmetry is *on-site* if the representation can be decomposed as $U_g = \otimes_{j=1}^N (u_g)_j$, where each $(u_g)_j$ is a (local) unitary representation.

Although group actions are usually considered to be on-site, this is not the most general way a symmetry can be represented. A more general class of group actions can be represented by matrix product operators (MPOs). Using the conventional tensor network notation^{39–41}, these are denoted

$$U_g = \text{MPO}_g, \quad (2.1)$$

where g next to the MPO indicates which group element it represents. We refer to the dimension of the horizontal indices as the *bond dimension* of the MPO. The on-site case corresponds to bond dimension 1, whilst arbitrary bond dimension allows representation of any unitary. We consider the case of a constant bond dimension in the length of the MPO.

To form a representation, the MPOs must obey

$$\text{MPO}_g^h = \text{MPO}_{gh}, \quad (2.2)$$

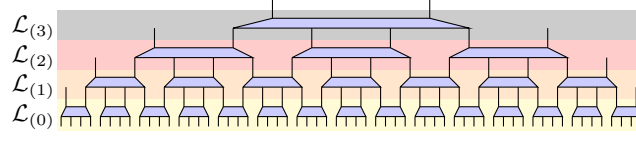


Figure 2.1: The MERA represents a quantum state using layers of isometric tensors. Together, these tensors define a quantum circuit of logarithmic depth which can be used to prepare an entangled state from a product state. If the tensors are chosen appropriately, the network is thought to be able to accurately represent the ground state of gapless one-dimensional Hamiltonians. Throughout the paper we use a convention such that tensor network diagrams read bottom-to-top correspond to matrix multiplication read left-to-right.

for all lengths. In contrast to on-site representations, for bond dimensions larger than one this does not hold at the level of the local tensors. Rather there is a tensor $X(g, h)$, referred to as the *reduction tensor*^{45,55,70} (Appendix 2.8) such that

$$X(g, h)^\dagger \begin{array}{c} \text{---} h \\ \text{---} g \\ \text{---} \end{array} X(g, h) = \begin{array}{c} \text{---} gh \\ \text{---} \end{array}. \quad (2.3)$$

The reduction procedure need not be associative. When reducing three tensors, there are two distinct orders of reduction which may differ by a phase ϕ

$$\begin{array}{c} \text{---} h \\ \text{---} g \\ \text{---} f \end{array} X(g, h) \begin{array}{c} \text{---} g \\ \text{---} f \end{array} X(f, gh) = \phi(f, g, h) \begin{array}{c} \text{---} h \\ \text{---} g \\ \text{---} f \end{array} X(fg, h) \begin{array}{c} \text{---} f \\ \text{---} g \end{array} X(f, g). \quad (2.4)$$

As discussed in Appendix 2.8, ϕ is a 3-cocycle with $[\phi] \in \mathcal{H}^3(\mathcal{G}, \text{U}(1))$. Since on-site representations are locally associative they have a trivial cocycle. Hence a nontrivial $[\phi]$ indicates an obstruction to making the symmetry action on-site. We can therefore regard a nontrivial $[\phi]$ as a nontrivial 't Hooft anomaly for \mathcal{G} in $(1+1)\text{D}$. We remark that each class of 't Hooft anomaly can be realized using MPOs in this way^{62,93}, see Chapter 1.

2.2.2 MERA and symmetry

In its most general form^{43,78}, the MERA can be thought of as a series of locality preserving isometric maps

$$\mathcal{L}_{(i)} : (\mathbb{C}^{d_{i+1}})^{\otimes N_{i+1}} \rightarrow (\mathbb{C}^{d_i})^{\otimes N_i}, \quad (2.5)$$

where $d_{i+1}^{N_{i+1}} \leq d_i^{N_i}$. Since the size of the lattice decreases at each step, these maps can be thought of as enacting a renormalization group on the real-space lattice. At the base (layer 0), the high energy, short-wavelength, lattice scale Hamiltonian $H^{(0)}$ is defined, with subsequent layers defining increasingly low-energy, long-wavelength effective theories

$$H^{(i+1)} := \mathcal{L}_{(i)}^\dagger H^{(i)} \mathcal{L}_{(i)}. \quad (2.6)$$

To correctly describe the physical RG fixed points, the MERA layers must be chosen to preserve the low-energy physics of $H^{(0)}$.

For concreteness, in this discussion we specialize to the MERA depicted in Fig. 2.1, which we refer to as the 4:2 MERA. This MERA is built from a single kind of tensor, an isometry from 4 sites to 2 sites. In general, these tensors may all contain distinct coefficients, although space-time symmetries such as scale invariance can be imposed by, for example, forcing the tensors on each layer to be identical. We remark that our results are not specific to this choice, rather they work for all MERA schemes. In particular, in Appendix 2.9, we describe how the results apply to the commonly used ternary MERA^{78,149}.

In the MERA the fundamental constraint that a symmetry is preserved under renormalization is that each coarse-graining circuit acts as an intertwiner of \mathcal{G} representations. That is, the renormalized symmetry

$$U_g^{(i+1)} := \mathcal{L}_{(i)}^\dagger U_g^{(i)} \mathcal{L}_{(i)}, \quad (2.7)$$

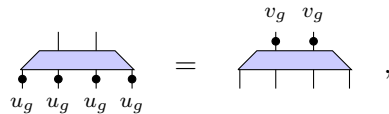
is again a representation of \mathcal{G} . When this condition is satisfied the third cohomology anomaly label of the symmetry does not change along the renormalization group flow^{76,143}. Hence the presence of an anomaly does not introduce any additional constraints on the renormalization process (which is to be expected for a discrete group).

For both practical and physically motivated reasons it is common to require further restrictions on the form of a symmetry throughout renormalization. For example, at a scale invariant renormalization group fixed point, the symmetry is also required to be scale invariant¹⁴⁹. Furthermore, along an RG flow one may require that the bond dimension of an MPO symmetry remain constant, or grow subexponentially with the renormalization step. An extreme case is that of an on-site symmetry where the bond dimension is always required to be one, such that the symmetry remains strictly on-site.

2.2.3 On-site symmetry

In the case of a trivial 't Hooft anomaly, a physical symmetry can be realized by an on-site representation. For a MERA satisfying Eqn. 2.7, the 't Hooft anomaly is preserved and hence it should remain possible to realize the symmetry in an on-site fashion at each RG step. This additional constraint is imposed by insisting that $U_g^{(i+1)}$ remains an on-site representation. Therefore the symmetry constraint becomes completely local¹⁴⁸.

The symmetry can then be enforced on a MERA state by ensuring that the local tensors are locality preserving *intertwiners* for the group action



$$= \quad (2.8)$$

where the representation on each bond may be distinct. Standard results in representation theory allow one to impose the conditions Eqn. 2.8.

2.2.4 Anomalous MPO symmetries

Generally $(2+1)$ D SPT states are gapped in the bulk (on a closed manifold), but, on a manifold with a boundary they either spontaneously break the ‘protecting’ symmetry, or possess gapless excitations in the vicinity of the boundary⁷⁰. Since the low energy physics is confined to the

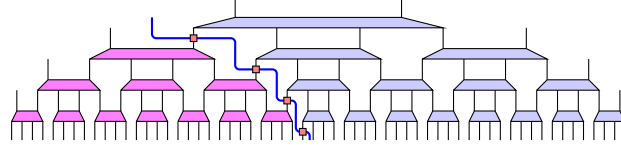


Figure 2.2: By applying the MPO to a half infinite chain, one can insert a domain wall between two dual theories. If the MPO acts as a symmetry, this corresponds to putting the theory on boundary conditions which have been twisted by the group element.

edge, it is interesting to consider the low energy, effective edge theory. When restricting the on-site bulk symmetry to the edge, it becomes anomalous with anomaly label $[\phi] \in \mathcal{H}^3(\mathcal{G}, \text{U}(1))$ matching the bulk SPT^{70,74,75}. An on-site representation of the bulk symmetry cannot be recovered by any local operations on the edge.

Since anomalous symmetries cannot be made on-site, the condition in Eqn. 2.7 is no longer strictly local. If the bond dimension of an MPO is allowed to grow at each renormalization step, the only constraint in Eqn. 2.7 is that the symmetry remains a global representation.

So long as this constraint is satisfied, the nontrivial anomaly label $[\phi] \in \mathcal{H}^3(\mathcal{G}, \text{U}(1))$ of an MPO representation, discussed in Appendix 2.8, is invariant under renormalization¹⁴³.

For anomalous symmetries the natural analogue to Eqn. 2.8 is

$$\begin{array}{c} \text{Diagram of a tensor with four legs, where the two bottom legs are connected by a red line labeled } g. \end{array} = \begin{array}{c} \text{Diagram of a tensor with four legs, where the two top legs are connected by a blue line labeled } g. \end{array}, \quad (2.9)$$

which is a sufficient condition for a symmetric MERA, but is not necessarily implied by Eqn. 2.7.

We remark that this condition does not correspond to a local group action unless further assumptions are made. Consequently conventional techniques from representation theory do not suffice to enforce the constraint. Despite this, in Section 2.4 we define a class of MERA which allow Eqn. 2.9 to be imposed via a strictly local condition.

Although Eqn. 2.9 generically allows the MPO to change one may wish to insist that the MPO is fixed under the RG. For instance, at an RG fixed point where identical tensors are used at each layer of the MERA.

Unlike an on-site symmetry, an MPO can act as a duality transformation between a pair of critical models. This can be realized in MERA by allowing the MERA tensors themselves to change in Eqn. 2.9. We demonstrate such an action in Section 2.5.3. One can also use the MPO to create a domain wall between the two critical theories by applying the MPO to a half-infinite chain. In the case where the dual theories coincide (i.e. the MPO acts as a symmetry) this corresponds to a symmetry twist (topological defect) or twisted boundary condition. This will be the subject of Section 2.3.

2.2.5 Physical data from MERA

Once a MERA has been obtained, a variety of physical data can be extracted. The most straightforward of these is the energy of the MERA, which simply requires evaluation of $\langle \psi | H | \psi \rangle$.

For a MERA representing the ground state of a gapless Hamiltonian, one can also extract a variety of data about the associated conformal field theory (CFT)^{150,151}. One can compute the central charge as discussed in Refs. 149,158 using the scaling of entanglement entropy in

the state. One can also obtain the scaling dimensions of the associated CFT^{149,158} by seeking eigenoperators of the scaling superoperator

$$\mathcal{S}_1(\text{---}\text{---}) = \text{---}\text{---} = \lambda \text{---}\text{---} . \quad (2.10)$$

The scaling dimensions describe the decay of correlations in the theory. We will refer to $\Delta = -\log_2(\lambda)$ as the *scaling dimension* corresponding to a particular *scaling field*.

The scaling fields obtained from the scaling superoperator correspond to local fields in the CFT. Given a symmetric MERA, one can also obtain nonlocal scaling fields by constructing the ‘symmetry twisted’ scaling superoperators

$$\mathcal{S}_g(\text{---}\text{---}) = \text{---}\text{---} = \lambda \text{---}\text{---} , \quad (2.11)$$

where --- is the symmetry MPO for the group element g . These fields correspond to a half infinite symmetry twist, as in Fig. 2.2, terminated by a local tensor. Previously, nonlocal scaling operators with a tensor product structure have been obtained in the same way⁷⁹, but this more general class involving an anomalous symmetry was not investigated.

2.3 Symmetry twists and topological sectors

Once a symmetric MERA is optimized to represent the ground state of a critical model, conformal data can be obtained as discussed in Section 2.2.5. In this section, we investigate the impact that an anomalous symmetry has on such conformal data. In particular, we use the properties of MPO group representations to obtain possible topological corrections to the conformal spins when a symmetry twist is applied. We observe these corrections in our example model, as shown in Table 2.1. Additionally, we construct the projective representations under which the nonlocal scaling fields (as defined in Eqn. 2.11) transform. These allow us to construct projectors onto irreducible topological sectors, extending the usual decomposition into symmetry sectors. We discuss the constraints that this decomposition imposes on the operator product expansion of the CFT. For our example model, we observe these constraints in Table 2.2.

Throughout this section, for simplicity of presentation, we treat the case of scale invariant MERA with scale invariant MPO symmetry. Furthermore, we assume the technical condition that the MPO representation satisfies the *zipper condition*⁹³

$$X(g, h) X(g, h)^\dagger = \text{---} . \quad (2.12)$$

These assumptions imply that the MPOs can be deformed freely through a symmetric MERA network. We remark that representative MPOs satisfying the zipper condition have been given for all anomalous discrete symmetries in $(1+1)\text{D}$ ⁹³. Additionally, we have suppressed possible orientation dependencies of the MPOs, although this effect is accounted for in our results. For a full treatment of the intricacies that arise due to orientation dependence see Ref. 93, Chapter 1. We note that similar reasoning applies to MPOs not satisfying these simplifying assumptions.

2.3.1 Symmetry twist and topological correction to conformal spin

For a model described by symmetric Hamiltonian H , a symmetry twist can be created by acting with an element of the group on a half-infinite chain. Hamiltonian terms far away from the end of the twist are left invariant and the only remnant is a single twisted Hamiltonian term crossing the end. This is captured by the MERA in Fig. 2.2 with uniform tensors.

The twisted Hamiltonian term can be used to close a chain into a ring of length L . In the case of a trivial (identity) twist this yields periodic boundary conditions. For a nontrivial group element this corresponds to a flux insertion through the ring as there is now a nontrivial monodromy around the ring given by the group element.

The introduction of an MPO twist by group element g leads to a twisted translation operator

$$\tau_g = \cdots \curvearrowright \curvearrowright \curvearrowright \text{[red box with } g \text{]} \curvearrowright \curvearrowright \curvearrowright \cdots, \quad (2.13)$$

which translates the system by one site without moving the end of the twist (previously noted in Refs. 159,160). We will see that this leads to corrections to the conformal spin.

The untwisted translation operator for periodic boundary conditions satisfies $\tau_1^L = \mathbb{1}$ which implies that local fields have integer conformal spin¹⁶¹. The twisted translation operator satisfies $\tau_g^L = T_g$ where

$$T_g = \cdots \text{[red box with } g \text{]} \text{[red box with } g \text{]} \text{[red box with } g \text{]} \text{[blue line]} \text{[red box with } g \text{]} \text{[red box with } g \text{]} \cdots \quad (2.14)$$

is the Dehn twist operator. For a faithful on-site representation of g the order of T_g is simply the order of g , denoted n_g . Hence the conformal spins of g -twisted fields may have a topological correction leading them to take values¹⁶¹ in $\frac{1}{n_g}\mathbb{Z}$.

We now consider anomalous representations and show that the order of T_g is $2n_g$ in some cases, reflecting a further correction due to the anomaly. We observe this additional correction in our numerical example, as shown in Table 2.1.

First we define

$$M_h^{(g)} = h \text{ [diagram with red boxes and blue lines] } . \quad (2.15)$$

which corresponds to the action of h on the g twisted MERA shown in Fig. 2.2. It was shown in Ref. 93 and Chapter 1 that

$$T_g M_h^{(g)} = \phi(g, h, g) M_{gh}^{(g)}, \quad (2.16)$$

where ϕ is the 3-cocycle of the MPO representation. Applying the Dehn twist n_g times results in a phase

$$T_g^{n_g} M_1^{(g)} = \prod_{i=1}^{n_g-1} \phi(g, g^i, g) M_1^{(g)}, \quad (2.17)$$

where again n_g denotes the order of g . Since g generates a subgroup $\mathbb{Z}_{n_g} \leq \mathcal{G}$ and

$$\phi_g(i, j, k) := \phi(g^i, g^j, g^k) \quad (2.18)$$

defines a 3-cocycle of \mathbb{Z}_{n_g} . Denote the relevant cohomology class by $[\phi_g] \in \mathcal{H}^3(\mathbb{Z}_{n_g}, \mathbb{U}(1)) \cong \mathbb{Z}_{n_g}$. For simplicity, assume it has been brought into the normal form¹⁰⁶

$$\phi_g(i, j, k) = \omega^{[\phi_g]i(j+k-j \oplus k)/n_g}, \quad (2.19)$$

where ω is a primitive n_g^{th} root of unity and \oplus denotes addition modulo n_g . Hence

$$\prod_{i=1}^{n_g-1} \phi(g, g^i, g) = \omega^{[\phi_g]} \quad (2.20)$$

and

$$T_g^{n_g} = \omega^{[\phi_g]} \mathbb{1}. \quad (2.21)$$

Consequently an anomaly $[\phi]$ for g -twisted fields may induce a further topological correction to their conformal spins. In particular, the correction to the conformal spins take values in

$$\frac{1}{n_g} \mathbb{Z}_{n_g} + \frac{[\phi_g]}{n_g^2}. \quad (2.22)$$

To make this argument we fixed a particular representative of ϕ , however the topological correction to conformal spin is a gauge invariant quantity and should not depend on this choice.

For the case of $\mathcal{G} = \mathbb{Z}_2^3$, we observe this anomalous correction in our numerical example, where we see quarter- and three-quarter- integer conformal spins (displayed in Table 2.1).

2.3.2 Projective representations and topological sectors

We proceed to construct topological sectors that have a definite topological correction to the conformal spin. These topological sectors are an extension of the usual symmetry sectors used to block diagonalize a Hamiltonian.

Topological sectors are labeled by a conjugacy class $\mathcal{C} \subset \mathcal{G}$, indicating twist symmetry twist, and a (projective) irreducible representation (irrep.) χ_g^μ of the centralizer of a representative element $g \in \mathcal{C}$. The topological sectors are mathematically described by $D^\phi(\mathcal{G})$, the quantum double of the symmetry group \mathcal{G} twisted by the 3-cocycle anomaly ϕ . This category determines all topological properties of the sectors.

Since the MPO symmetry commutes with the MERA tensors, one can simultaneously diagonalize the twisted scaling superoperator $\mathcal{S}_g(\cdot)$ and the action of the symmetry. The vector space spanned by g -twisted scaling fields (see Eqn. 2.11) transforms under a projective representation $V_h^{(g)}$ of the centralizer \mathcal{Z}_g . This projective representation has 2-cocycle $\phi^{(g)}$ defined by

$$\phi^{(g)}(h, k) = \frac{\phi(g, h, k)\phi(h, k, g)}{\phi(h, g, k)}, \quad (2.23)$$

which is the slant product of ϕ . The action is explicitly given by⁹³

$$V_h^{(g)} = \begin{array}{c} \text{Diagram: A blue loop with two red squares. The top square is labeled } h \text{ and the bottom square is labeled } h. \text{ An arrow labeled } X(h, h^{-1}gh) \text{ points to the top square. Another arrow labeled } X(g, h)^\dagger \text{ points to the bottom square.} \end{array}, \quad (2.24)$$

where $h^{-1}gh = g$ for $h \in \mathcal{Z}_g$.

The g -twisted scaling superoperator commutes with the projective representation

$$\mathcal{S}_g(V_h^{(g)}(\cdot)) = V_h^{(g)}(\mathcal{S}_g(\cdot)), \quad (2.25)$$

and hence can be block diagonalized into projective irreps.

Topological sectors that contribute a definite correction to the conformal spin can be constructed following the approach of Ref. 64. The first step is to form projectors $P_{g,\mu}$ onto the projective irreps of \mathcal{Z}_g . For a twist g and projective irrep μ with 2-cocycle $\phi^{(g)}$

$$P_{g,\mu} := \frac{d_\mu}{|\mathcal{Z}_g|} \sum_{h \in \mathcal{Z}_g} \bar{\chi}_g^\mu(h) V_h^{(g)}, \quad (2.26)$$

where d_μ its dimension, χ_g^μ its character and $\bar{\cdot}$ denotes complex conjugation.

The full scaling superoperator, taking into account all sectors, is given by

$$\mathcal{S}_\mathcal{G}(\cdot) := \bigoplus_g \mathcal{S}_g(\cdot). \quad (2.27)$$

This commutes with the full $|\mathcal{G}|^2$ dimensional algebra spanned by $V_h^{(g)}$ (note $V_l^{(k)} V_h^{(g)} = 0$ unless $k = h^{-1}gh$). This is a C^* algebra⁶⁴ and can be diagonalized into blocks. The simple central idempotents that project onto each irreducible block are given by

$$P_{\mathcal{C}_g,\mu} := \sum_{k \in \mathcal{C}_g} P_{k,\mu}, \quad (2.28)$$

where \mathcal{C}_g is the conjugacy class of g in \mathcal{G} . These projectors block diagonalize $\mathcal{S}_\mathcal{G}(\cdot)$ into irreducible topological sectors. For the numerical example in Appendix 2.7, all conformal data is decomposed into these sectors.

The topological sectors thus constructed have definite topological spin⁶⁴ (correction to conformal spin), which we observe in our example in Table 2.1. Additionally, these sectors obey a set of fusion rules, and support a notion of braiding monodromy and exchange statistics. The full set of topological data can be extracted from the idempotents constructed in Eqn. 2.28 via the procedure outlined in Ref. 64.

In the MERA, with an MPO symmetry, the operator product expansion (OPE)^{150,151} for scaling fields a and b in topological sectors labeled (\mathcal{C}_0, μ_0) and (\mathcal{C}_1, μ_1)

$$a \times b = \sum_{\substack{g \in \mathcal{C}_0 \\ h \in \mathcal{C}_1}} X(g, h)^\dagger \left(\text{Diagram} \right) = \sum_c C_{ab}^c c. \quad (2.29)$$

The fusion rules imply topological restrictions on the OPE of scaling fields, generalizing symmetry constraints on the local fields. In particular, $C_{ab}^c = 0$ unless the sector labeling c appears in the fusion product

$$(\mathcal{C}_0, \mu_0) \times (\mathcal{C}_1, \mu_1) = \sum_{(\mathcal{C}_2, \mu_2)} N_{(\mathcal{C}_0, \mu_0)(\mathcal{C}_1, \mu_1)}^{(\mathcal{C}_2, \mu_2)} (\mathcal{C}_2, \mu_2). \quad (2.30)$$

We observe the constraints directly in the numerical MERA in Table 2.2.

Technically the symmetry twists and their fusion structure are described by the unitary fusion category (UFC) Vec_G^ϕ while the topological sectors are given by its Drinfeld center $Z(\text{Vec}_G^\phi)$ — equivalently the twisted quantum double $D^\phi(G)$ — which is a modular tensor category (MTC) ^{14,162–166}. The mathematical structure of this MTC determines all topological properties of the fields in each sector, including the topological correction to their conformal spin (equivalently the exchange statistics), topological restriction on the OPE and monodromies (braiding).

Interestingly the fusion rules for the topological sectors can be nonabelian, even when the symmetry group is abelian. This requires a nontrivial anomaly ϕ . This occurs in our numerical example as discussed in Section 2.5 and Table 2.2.

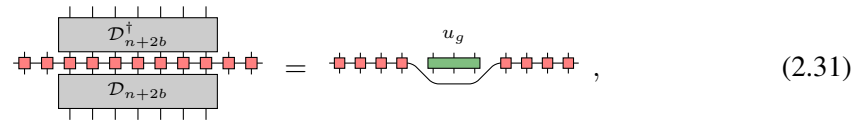
2.4 A class of MPO symmetric MERA

To enforce a constraint on a MERA state requires an identification of the remaining variational parameters in such a way that it is possible to optimize over them. In this section we describe an approach that relies on a property of the MPO symmetry: the existence of a local unitary capable of disentangling a contiguous region of each MPO into an inner part that forms a local representation of the symmetry and is decoupled from the original MPO on the outer section. Given such a local representation, conventional techniques can be used to ensure the MERA is symmetric. We construct a large class of MPOs with this property and find the resulting constraints on the form of symmetric MERA tensors.

2.4.1 Disentangling an MPO

For scale invariant MERA, where the MPO symmetry is required to be identical at all layers, the goal is to identify a family of MERA circuits which locally coarse grains each MPO to itself. If the MPOs form an on-site symmetry, standard techniques of representation theory allow this to be achieved. For MPOs with bond dimension greater than one it is unclear how to apply these techniques. Our approach involves disentangling a local piece out of each MPO. We can then use representation theory to coarse grain this piece, allowing us to identify the desired family of MERA circuits.

This approach may seem counter-intuitive since no local constant depth circuit is capable of disentangling an MPO representation with a nontrivial third cohomology label into an on-site representation. This does not rule out the possibility of disentangling a contiguous region without decoupling the tensors in its complement. More precisely, there may exist constants $b, k \in \mathbb{Z}^+$ such that for all $n \in k\mathbb{Z}^+$ (where k accounts for possible blocking of sites), and MPOs of arbitrary length N , sufficiently larger than n , there exists some unitary \mathcal{D}_{n+2b} acting on $n + 2b$ sites (where b is a buffer depending on the correlation length of the MPO) such that



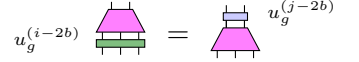
$$\text{Diagram showing a chain of sites with a unitary } \mathcal{D}_{n+2b}^\dagger \text{ and } \mathcal{D}_{n+2b} \text{ acting on a region, resulting in a local unitary } u_g \text{ acting on } n \text{ sites.} \quad (2.31)$$

for a local representation $u_g^{(n)}$ acting on n sites.

This leads to a special form for a MERA tensor that coarse grains i sites into j sites, given by


(2.32)

In this form the MPO symmetry condition in Eqn. 2.9 becomes


(2.33)

which can be handled using standard techniques from representation theory.

2.4.2 A class of anomalous \mathbb{Z}_N^3 MPO symmetries

We now define a class of anomalous symmetries for the groups \mathbb{Z}_N^3 . These symmetries exemplify the role played by an anomalous symmetry both at the boundary of a two dimensional SPT phase and as a duality of distinct one dimensional SPT phases^{77,167–169}. They occur as the boundary symmetry actions of \mathbb{Z}_N^3 SPTs labeled by a type-III anomaly in two spatial dimensions¹⁰⁶. In addition, they can be seen to act transitively on the set of one dimensional SPT phases with \mathbb{Z}_N^2 symmetry. This particular example is an instance of a more general relation between a two dimensional $\mathcal{G} \times \mathcal{H}^2(\mathcal{G}, \text{U}(1))$ SPT and the set of dualities of one dimensional \mathcal{G} SPTs. Further details about the specifics of the \mathbb{Z}_N^3 models, including a fixed point bulk model, bulk to boundary mapping and boundary Hamiltonian, as well as the more general case are contained in Appendix 2.10.

We consider a spin chain with a pair of N -dimensional spins at each site. For this discussion, we label the first spin in red and the second in blue. Let $\omega = \exp(2i\pi/N)$ and define the generalized Pauli operators via $ZX = \omega XZ$. Below we work in the basis where Z is the diagonal clock matrix and X is the shift matrix. We define the generalized controlled X and Z operators as

$$\blacktriangleleft \oplus = (\blacktriangleright \oplus)^\dagger = \frac{1}{N} \sum_{i,j=0}^{N-1} \omega^{ij} Z^i X^j \quad (2.34a)$$

$$\blacktriangleleft \blacktriangleleft = (\blacktriangleright \blacktriangleright)^\dagger = \frac{1}{N} \sum_{i,j=0}^{N-1} \omega^{ij} Z^i Z^j \quad (2.34b)$$

respectively.

Using the notation $(\alpha_1, \alpha_2, \alpha_3)$ for an element of \mathbb{Z}_N^3 , the group action is defined by the generators

$$(1, 0, 0) \rightarrow \bigotimes_j \textcolor{red}{X}_j \quad (2.35a)$$

$$(0, 1, 0) \rightarrow \bigotimes_j \textcolor{blue}{\tilde{X}}_j \quad (2.35b)$$

$$(0, 0, 1) \rightarrow \mathcal{C}, \quad (2.35c)$$

where \mathcal{C} is defined by the (periodic) circuit

$$\mathcal{C} = \begin{array}{c} \begin{array}{cccc} \uparrow & \downarrow & \uparrow & \downarrow \\ \downarrow & \uparrow & \downarrow & \uparrow \\ \uparrow & \downarrow & \uparrow & \downarrow \\ \downarrow & \uparrow & \downarrow & \uparrow \end{array} \\ \text{site} \end{array} . \quad (2.36)$$

The symmetry operators can be realized using a translationally invariant MPO with on-site tensor defined by

$$\begin{array}{c} i + \alpha_1 \quad j + \alpha_2 \\ \downarrow \quad \downarrow \\ \boxed{(\alpha_1, \alpha_2, \alpha_3)} \\ \uparrow \quad \uparrow \\ i \quad j \end{array} = \sum_{k=0}^{N-1} \omega^{j\alpha_3(k-i)} |i\rangle\langle k|, \quad (2.37)$$

with all other elements being zero. The reduction tensor (defined in Appendix 2.8) associated to these MPOs is given by

$$\boxed{X(\alpha, \beta)} = \sum_{x=0}^{N-1} \omega^{-x\alpha_2\beta_3} \begin{array}{c} x + \alpha_1 \\ x \end{array} \begin{array}{c} \rangle \\ \langle x| \end{array}. \quad (2.38)$$

From this, one can verify that this MPO representation has cocycle $\phi(\alpha, \beta, \gamma) = \omega^{\alpha_1\beta_2\gamma_3}$ which is a representative of the root ‘type-III’ anomaly¹⁰⁶.

2.4.3 Symmetric MERA tensors

The disentangling circuit, as defined in Eqn. 2.31, for this representation is given by

$$\mathcal{D}_{2K} = \prod_{j=1}^{K-1} CX_{1,2j+1}CX_{2K,2j}, \quad (2.39)$$

and the residual local symmetry is given by

$$u_{(\alpha_1, \alpha_2, \alpha_3)}^{(2K-2)} = \left(\prod_{j=1}^{K-1} CZ_{2j,2j+1} \prod_{j=2}^{K-1} CZ_{2j-1,2j}^\dagger \right)^{\alpha_3}. \quad (2.40)$$

For further details see Appendix 2.9. This leads to the ansatz for MERA tensors

$$\begin{array}{c} \text{blue trapezoid} \end{array} = \begin{array}{c} \text{red triangle with internal lines} \end{array}, \quad (2.41)$$

which allows the symmetry to be enforced by a local condition on each tensor.

The symmetry can then be enforced by ensuring the residual tensors obey the local conditions

$$\begin{array}{c} \text{red triangle with arrows} \end{array} = \begin{array}{c} \text{red triangle with vertical lines} \end{array}, \quad (2.42)$$

which can be achieved using standard techniques of representation theory. We remark that the on-site \mathbb{Z}_N^2 symmetry is automatically enforced, without any further constraints.

Since the action can be applied locally, this ansatz class can also be used to investigate how the group acts on numerically optimized states which have not been constrained to be invariant. This allows investigation of theories which are dual under anomalous group actions.

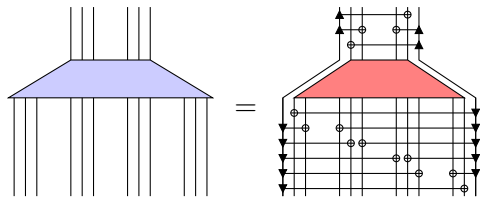
The constraint in Eqn. 2.41 was used in an exact renormalization scheme introduced in Ref. 170 for the case of a $\mathbb{Z}_2 \times \mathbb{Z}_2$ symmetry¹⁷¹. The form of the information transmitted to the next scale of renormalization is extremely restricted in this case. By considering more spins per site we find a less restrictive ansatz, described in Appendix 2.9, capable of attaining accurate results as demonstrated in Section 2.5. The scheme described in Ref. 170 does not see similar improvement at larger blocking on a model which is unitarily equivalent to the one considered here¹⁷¹. After blocking at least two spins per site, our ansatz cannot be captured by the approach of Ref. 170.

Analogous circuits exist for all MERA such that the number of ingoing/outgoing N -dimensional indices is even. This leads to a family of symmetric MERA with increasing bond dimension and a larger number of variational parameters. Eqn. 2.41 can also be generalized to other MERA schemes, such as the ternary MERA as discussed in Appendix 2.9.

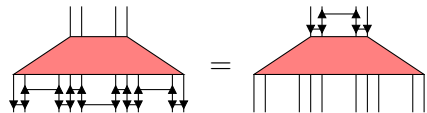
2.5 Example: A \mathbb{Z}_2^3 symmetric model

In this section we focus on the $N = 2$ case of the ansatz described in the previous section. We consider a particular Hamiltonian which transforms under the type-III anomalous \mathbb{Z}_2^3 group action. This Hamiltonian has three critical lines, one is symmetric and the other two are dual under the group action. We numerically optimize over the ansatz class presented in the previous section along these three lines. We present resulting conformal data for the local fields along each line, and for two nontrivial topological sectors along the symmetric line. Furthermore, we numerically implement the duality on the remaining pair of lines. Finally, we demonstrate that the symmetric line is a gapless phase protected by the anomalous symmetry and translation.

For a MERA with bond dimension 8 corresponding to three qubits per site, the ansatz for the tensors is


(2.43)

with symmetry constraint


(2.44)

This tensor contains all degrees of freedom which are not fixed by the symmetry, so can be optimized over.

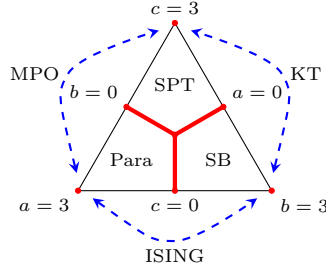


Figure 2.3: Phase diagram of the abc model where $a + b + c = 3$. SB=Symmetry breaking, ferromagnetic phase. SPT= $\mathbb{Z}_2 \times \mathbb{Z}_2$ symmetry protected topological phase. Para=Paramagnetic/disordered phase. RG fixed points are indicated in red, and the dashed blue lines indicate the unitary mappings between the phases. ISING=Ising duality map, KT=(Generalized) Kennedy-Tasaki transformation^{172,173}, MPO=action of (1,1,1) defined in Eqn. 2.35.

2.5.1 Family of Hamiltonians

The Hamiltonian we study is

$$H = -a \sum (\mathbf{X}_j + \tilde{\mathbf{X}}_j) - b \sum (\mathbf{Z}_j \mathbf{Z}_{j+1} + \tilde{\mathbf{Z}}_j \tilde{\mathbf{Z}}_{j+1}) - c \sum (\mathbf{Z}_j \tilde{\mathbf{X}}_j \mathbf{Z}_{j+1} + \tilde{\mathbf{Z}}_j \mathbf{X}_{j+1} \tilde{\mathbf{Z}}_{j+1}), \quad (2.45)$$

for positive values of (a, b, c) . Here $\mathbf{X}_j(\mathbf{Z}_j)$ and $\tilde{\mathbf{X}}_j(\tilde{\mathbf{Z}}_j)$ are the qubit Pauli operators action on the first and second qubit on site j . This model, which we refer to as the *abc model*, has a rich phase diagram as depicted in Fig. 2.3, possessing fully symmetric disordered and SPT phases, in addition to a fully symmetry breaking phase. For all values of (a, b, c) , this Hamiltonian has an on-site $\mathbb{Z}_2 \times \mathbb{Z}_2$ symmetry corresponding to Eqn. 2.35a and Eqn. 2.35b, whilst the anomalous action exchanges the terms with strength a and c , so is only a symmetry when $a = c$. The SPT phase is protected by the on-site symmetry.

We note that unitarily equivalent models have previously been studied^{174–179}. The critical lines in this model can all be exchanged by (nonlocal) unitary transformations, so all are known to be described by a conformal field theory (CFT) with central charge 1. Additionally, the ground state energy along each of these lines is known^{177–179}.

In Fig. 2.4, we study the model with $a = c$ (referred to as the b line) using a MERA with full anomalous symmetry enforced. For convenience, we allow a single transitional layer followed by a scale invariant portion. This leaves a pair of tensors which completely specify the state. After optimizing these residual degrees of freedom (2×16376 real parameters) within this symmetric manifold, we obtain a good approximation to the ground state for all values of b , as evidenced by the ground state energy in Fig. 2.4a (relative error $\mathcal{O}(10^{-4})$). When the symmetry operator is applied to the state, we see that the state is unchanged (a property which was explicitly enforced). The central charge remains within 4.2% of the analytic value for all values of b , comparable to that found in Ref. 179.

2.5.2 Scaling dimensions and topological sectors

From our optimized MERA tensors, we have obtained the scaling dimensions of the associated CFT in each symmetry sector using Eqn. 2.10. The data is shown in Fig. 2.4b. As expected, the scaling dimensions vary continuously with the parameter b .

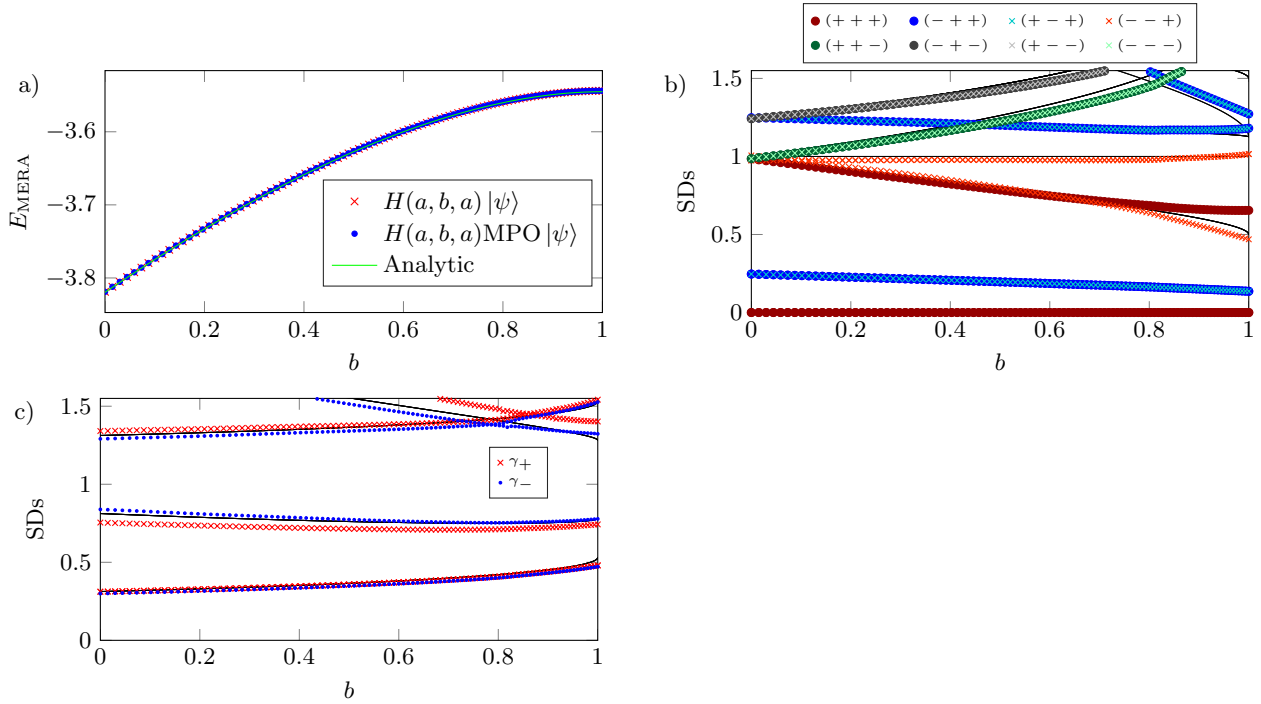


Figure 2.4: MERA data for the abc model along the ‘ b line’. This line is symmetric under the full \mathbb{Z}_2^3 . CFT data, including averaging process, is discussed in more detail in Appendix 2.7.

a) The energy of the optimized MERA state. The state remains a ground state when the anomalous symmetry operator is applied.

b) Scaling dimensions of the associated CFT. These vary continuously with the parameter b . Points are averaged MERA data, whilst black lines correspond to Eqn. 2.47a for integer e and m . Distinct colors/markers indicate under which irrep. the fields transform.

c) Scaling dimensions of nonlocal operators corresponding to applying an anomalous symmetry (for group element $(1, 1, 1)$ defined in Eqn. 2.35) twist to half of the chain. Points are averaged MERA data, whilst black lines correspond to Eqn. 2.47a for $e, m \in \mathbb{Z} + 1/2$. Distinct colors/markers indicate under which projective irrep. the fields transform.

The local fields are those of the compactified boson CFT at a radius

$$R^2 = \frac{\pi}{2 \cos^{-1}(\frac{2b}{b-3})}. \quad (2.46)$$

The fields can be labeled by a pair of integers, and have scaling dimension Δ and conformal spin s given by^{150,151}

$$\Delta_{e,m} = \frac{e^2}{R^2} + \frac{m^2 R^2}{4}, \quad (2.47a)$$

$$s_{e,m} = em, \quad (2.47b)$$

$$e, m \in \mathbb{Z}.$$

Finally, we investigate the effect of $(1, 1, 1)$ symmetry twist in Fig. 2.4c. By applying the symmetry to half of the infinite chain we create the twist, and a set of nonlocal (with respect to the original theory) twisted fields can be obtained⁷⁹. These operators correspond to eigenoperators of the ‘symmetry twisted’ scaling superoperator (Eqn. 2.11). Since the symmetry acts

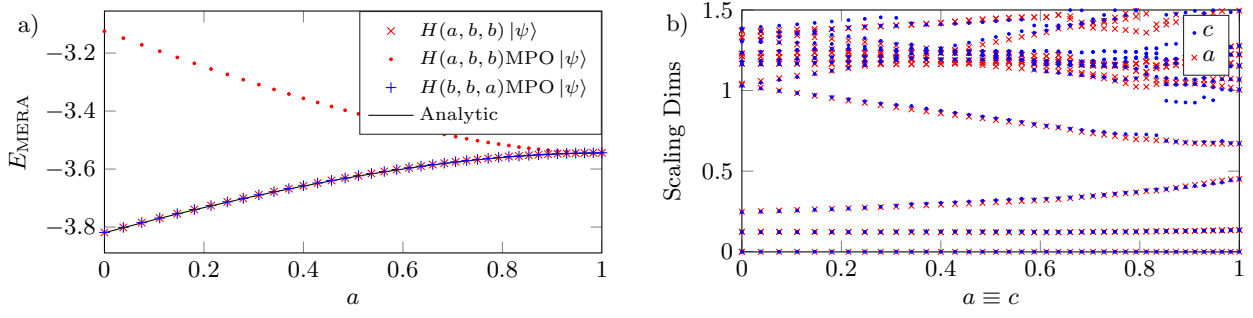


Figure 2.5: MERA data for the abc model along the ‘ a ’ and ‘ c ’ lines. These are exchanged by the symmetry action.

a) Ground state energy of the optimized MERA. By applying the symmetry operator to a state optimized for the Hamiltonian with (a, b, b) , we obtain a state which is the ground state of the Hamiltonian with parameters (b, b, a) . This demonstrates that the states are transforming properly.

b) The local fields in the CFTs describing these two lines are identical, but distinct from those on the ‘ b ’ line.

projectively on the twisted fields, they can be decomposed into projective irreps corresponding to definite topological sectors. We can then diagonalize $\mathcal{S}_g(\cdot)$ within each sector, allowing us to label the twisted fields by the projective irrep under which they transform.

Again we can compare the numerically calculated twisted scaling dimensions to the analytic results to identify conformal spins of the twisted fields. As displayed in Table 2.1, within each topological sector, all conformal spins receive the same correction.

From the MERA data, we can identify the fields with a $(1, 1, 1)$ twist as carrying scaling dimension and conformal spin given by Eqn. 2.47a and Eqn. 2.47b respectively, but with $e, m \in \mathbb{Z} + \frac{1}{2}$, leading to quarter- and three-quarter- integer spins in this sector.

To examine the effect of the anomalous symmetry on the OPE, we computed fusion rules for the topological sectors using Eqn. 2.29 for a symmetric MERA tensor. Despite the fact that the symmetry group is abelian, we observe nonabelian fusion for all sectors with nontrivial twist. For example, fusion of sectors with twist $(1, 1, 1)$ results in only half of the trivial twist sectors. The full set of fusion rules is given in Table 2.2 (Appendix 2.7).

In this example, the modular tensor category describing the topological sectors is $D^\phi(\mathbb{Z}_2^3)$. This category is known to be equivalent to $D(D_4)$, where D_4 is the symmetry group of a square. The fusion table obtained from MERA matches that of $D^\phi(\mathbb{Z}_2^3) \cong D(D_4)$ ^{106,180–183}.

The data for all topological sectors is displayed in full in Appendix 2.7.

2.5.3 Duality and domain walls

We have also studied the ‘ a ’ and ‘ c ’ lines which are not symmetric under the anomalous \mathbb{Z}_2 , but are exchanged by its action. We optimize over tensors of the form Eqn. 2.43, but do not enforce the symmetry constraint on the residual degrees of freedom.

The ground state energy obtained after optimization along the $b = c$ line is shown in Fig. 2.5a. If the symmetry MPO corresponding to group element $(1, 1, 1)$ is applied to the optimized state (via local application of Eqn. 2.44), the result is an excited state. If the energy of this state is measured using the Hamiltonian with parameters a and c switched, we see that it

is a ground state. This confirms that the state is transforming as expected under the anomalous action, that is, the MPO is acting as a duality transformation of the ‘ a ’ and ‘ c ’ critical lines.

We also show the scaling dimensions of the CFTs corresponding to the two dual lines (Fig. 2.5b). We observe that the local field content is identical, indicating that the same CFT describes these two lines. This CFT is distinct (in its local content) from that describing the ‘ b ’ line, although it still has central charge 1.

2.5.4 An anomaly protected gapless phase

In Ref. 70 it was shown that a phase with anomalous MPO symmetry can either be gapped and spontaneously break the symmetry, or be gapless. Furthermore it is known from Refs. 80,137,138,184,185 that a topological symmetry, together with translation, can protect a gapless phase. An anomalous MPO symmetry is in fact an example of a topological symmetry. Hence one may suspect that there exist gapless phases protected by such a symmetry.

Here we demonstrate that under an anomalous \mathbb{Z}_2^3 symmetry, along with translations, the gaplessness of the Hamiltonian along the ‘ b ’ line is protected. That is, there are no translation invariant terms which are both symmetric under the full anomalous symmetry and are relevant in the renormalization group sense, and would therefore gap the Hamiltonian.

Since the effect of translations cannot be tested in the MERA framework, we performed a finite size scaling analysis¹⁶¹ to test this. Using the ALPS MPS library^{186,187}, the lowest 40 eigenstates of the Hamiltonian (Eqn. 2.45) along the ‘ b ’ line were obtained. Bond dimensions were capped at 100 and lengths of between 6 and 55 sites (12-110 qubits) were considered. Scaling dimensions are obtained by first normalizing the Hamiltonian such that the ground state has energy 0 and the first excited state has energy corresponding to the smallest nonzero scaling dimension of the CFT¹⁸⁸. The energy levels are then fitted as a function of $1/N$ and extrapolated to $N = \infty$. This is shown in Fig. 2.6a for $b = .6$.

The Hamiltonian and symmetry operators were then simultaneously diagonalized within this subspace. In the fully symmetric sector (all symmetries acting as $+1$), the translation operator was diagonalized, allowing the momentum to be extracted.

Under the combined action of the anomalous symmetry group and translations by a single spin, there are no fully symmetric states with scaling dimension less than 2 (Fig. 2.6b). This implies there are no local symmetric terms which can gap the Hamiltonian, thus the gapless phase is protected. We remark that under the operator which translates by a full site; an RG relevant, fully symmetric state with momentum zero does exist and therefore the Hamiltonian can be gapped by a staggered term. A similar effect was observed in Ref. 80.

2.6 Conclusions

We have studied anomalous MPO symmetries in the framework of MERA. Following Ref. 143, the third cohomology class of an MPO representation of a finite group was identified with an ‘t Hooft anomaly.

The properties of a fully MPO symmetric MERA were derived, including anomalous symmetry twists and the projective representations they carry. These were used to construct all topological sectors. This construction allows the complete set of topological data to be extracted, including a definite topological correction to the conformal spins of the fields in each

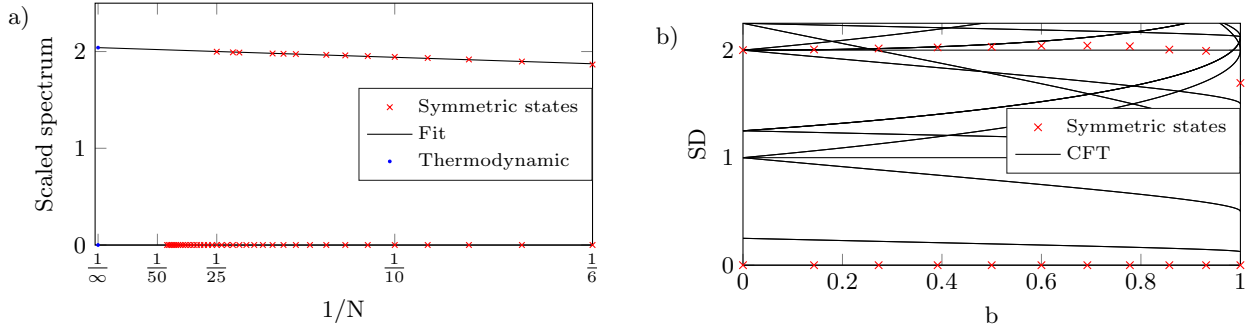


Figure 2.6: Finite size scaling data for the fully symmetric sector of the model.

a) After rescaling the spectrum so that the lowest excitation is consistent with the lowest nontrivial primary of the CFT, the fully symmetric states can be extracted. Fitting the data and extrapolating to the thermodynamic limit gives the scaling dimension.

b) For almost the whole ‘ b ’ line, we observe that there are no fully symmetric states with scaling dimension less than 2 (RG relevant). This implies that no local, symmetric, translationally invariant terms can be added to the Hamiltonian to gap it out, thus the gapless phase is protected.

sector and topological restrictions on the OPE.

A local condition to enforce the symmetry in the MERA was formulated, which allows for optimization of states with an anomalous symmetry. This ansatz works by locally disentangling the symmetry action, decoupling degrees of freedom on which the action can be expressed locally.

By way of an example, MERA states were optimized for a Hamiltonian with an anomalous \mathbb{Z}_2^3 symmetry. We have obtained accurate energy and conformal data for states optimized over our ansatz class, and demonstrated that the states transform as expected. All topological sectors were constructed and the resultant topological data was extracted. The conformal data was computed within each topological sector, and the projective action of the symmetry on the scaling fields was found. Furthermore, a correction to the conformal spin was identified, and shown to match the topological spin.

We applied the ansatz to study a duality of two critical lines. By extracting conformal data from optimized MERA the local content of the dual CFTs was shown to match. It was demonstrated that the action of the MPO mapped MERA ground-states optimized for Hamiltonians along one line to ground-states of the dual Hamiltonians. This required the ability to apply the MPO in a local fashion, which our ansatz permits.

We performed a finite size scaling analysis of the anomalous \mathbb{Z}_2^3 symmetric line for large system sizes. It was numerically demonstrated that the anomalous MPO symmetry, together with translation, protects a gapless phase.

There are several extensions of this work which suggest themselves. Our restricted MERA ansatz was only constructed for a particular class of anomalous group actions. It would be interesting to extend this to other MPOs, such as: nonabelian group representations with different cocycle anomalies, the Ising duality map or the translation operator.

The most general extension conceivable is to a set of MPOs described by a unitary fusion category^{64,189–194}. While the construction of topological sectors is known in this general case^{64,163,164,189,190,195–197}, an ansatz which allows the symmetry to be enforced locally in the MERA remains to be found.

It would be interesting to determine which of these general symmetries protects a gapless phase such as the one observed in this work and those in Refs. [80,137,138,184,185](#).

One could adapt these results to the recent tensor network renormalization (TNR) [198–201](#) scheme, constraining the RG flow to remain MPO symmetric. We remark that the Ising duality has previously been studied both numerically, using TNR but without manifestly enforcing the symmetry, in Ref. [159](#) and theoretically in Ref. [160](#).

It would also be interesting to consider the influence of an MPO symmetry on the entanglement entropy. We remark that by considering MPO symmetries of topologically ordered tensor network states in $(2 + 1)D$ one recovers the topological entanglement entropy [37,38,63,64,109](#).

A particularly interesting future direction is to generalize our MPO symmetric MERA ansatz to a $(2 + 1)D$ MERA describing a topologically ordered state that is symmetric under an anomalous PEPO symmetry.

Acknowledgments — The authors thank Dave Aasen, Matthias Bal, Stephen Bartlett, Nick Bultinck, Christopher Chubb, Andrew Doherty, Steve Flammia, Michaël Mariën, Sam Roberts, Thomas Smith, Ryan Thorngren, Frank Verstraete, Guifre Vidal and Juven Wang for useful discussions. DW especially thanks Dave Aasen for pointing out the connection between the tube algebra and topological defects. JB acknowledges support from the Australian Research Council via the Center of Excellence in Engineered Quantum Systems (EQuS), project number CE110001013. The authors acknowledge the University of Sydney HPC service at The University of Sydney for providing HPC resources. DW acknowledges The University of Sydney quantum theory group for their hospitality, and the Perimeter Institute Visiting Graduate Fellowship program.

Optimal contraction sequences of the networks used in this work were computed using the netcon package of Ref. [202](#).

Supplementary Material

2.7 Conformal data in all topological sectors

In this appendix, we present the full set of scaling dimensions extracted from the bond dimension 8 MERA with full anomalous symmetry enforced. The data is shown in Fig. 2.7 for the trivial twist, and Fig. 2.8 and Fig. 2.9 for the nontrivial twists. Each subplot in these figures corresponds to a distinct topological sector.

When examining the gray points, one notices a broken degeneracy. This was previously noted in Ref. 179. We conjecture that this occurs via coupling of states which, in the field theoretic limit, would be forbidden from coupling due to the full conformal symmetry. As such, we conjecture that the scaling dimensions corresponding to degenerate fields obtained from the MERA experience a splitting $\Delta_{\text{MERA}} = \Delta_{\text{CFT}} \pm \epsilon$, where the size of the splitting ϵ decreases with increased bond dimension as the full conformal symmetry is effectively recovered.

To combat this splitting, we average the MERA scaling dimensions in an attempt to recover the CFT values. When choosing which lines should be averaged together, we have taken all lines of similar gradient and position on the plot. The result of this procedure is indicated in red, and closely matches the CFT values.

The scaling dimensions and conformal spins in each topological sector are given in Table 2.1. Table 2.2 shows the fusion rules for the sectors, computed using the symmetric MERA.

The irreps are given explicitly in Eqn. 2.48. Those below the line are nontrivial projective representations.

$$\chi_{\pm}^1(100) = +1 \quad \chi_{\pm}^1(010) = +1 \quad \chi_{\pm}^1(001) = \pm 1 \quad (2.48a)$$

$$\chi_{\pm}^2(100) = -1 \quad \chi_{\pm}^2(010) = +1 \quad \chi_{\pm}^2(001) = \pm 1 \quad (2.48b)$$

$$\chi_{\pm}^3(100) = +1 \quad \chi_{\pm}^3(010) = -1 \quad \chi_{\pm}^3(001) = \pm 1 \quad (2.48c)$$

$$\chi_{\pm}^4(100) = -1 \quad \chi_{\pm}^4(010) = -1 \quad \chi_{\pm}^4(001) = \pm 1 \quad (2.48d)$$

$$\alpha_{\pm}^1(100) = \pm \mathbb{1} \quad \alpha_{\pm}^1(010) = X \quad \alpha_{\pm}^1(001) = Z \quad (2.48e)$$

$$\alpha_{\pm}^2(100) = Z \quad \alpha_{\pm}^2(010) = \pm \mathbb{1} \quad \alpha_{\pm}^2(001) = X \quad (2.48f)$$

$$\alpha_{\pm}^3(100) = X \quad \alpha_{\pm}^3(010) = Z \quad \alpha_{\pm}^3(001) = \pm \mathbb{1} \quad (2.48g)$$

$$\beta_{\pm}^1(100) = Z \quad \beta_{\pm}^1(010) = X \quad \beta_{\pm}^1(001) = \pm X \quad (2.48h)$$

$$\beta_{\pm}^2(100) = \pm X \quad \beta_{\pm}^2(010) = Z \quad \beta_{\pm}^2(001) = X \quad (2.48i)$$

$$\beta_{\pm}^3(100) = X \quad \beta_{\pm}^3(010) = \pm X \quad \beta_{\pm}^3(001) = Z \quad (2.48j)$$

$$\gamma_{\pm}(100) = \pm X \quad \gamma_{\pm}(010) = \pm Y \quad \gamma_{\pm}(001) = \pm Z \quad (2.48k)$$

Topological Sector		Topological spin	Scaling Dimension	Conformal spin	Parameters
Twist	Proj. Irrep.				
(000)	χ_+^1	0	$\frac{e^2}{R^2} + \frac{m^2 R^2}{4}$	em	$e, m \in 2\mathbb{Z}$
	χ_+^4	0	$\{\frac{e^2}{R^2} + \frac{m^2 R^2}{4}, 1\}$	em	$e, m \in 2\mathbb{Z}, em \neq 0$
	χ_+^2	0	$\frac{e^2}{R^2} + \frac{m^2 R^2}{4}$	em	$e \in 2\mathbb{Z}, m \in 2\mathbb{Z} + 1$
	χ_+^3	0			$e \in 2\mathbb{Z}, m \in 2\mathbb{Z} + 1$
	χ_-^1	0			$e \in 2\mathbb{Z} + 1, m \in 2\mathbb{Z}$
	χ_-^2	0			$e \in 2\mathbb{Z} + 1, m \in 2\mathbb{Z} + 1$
	χ_-^3	0			$e \in 2\mathbb{Z} + 1, m \in 2\mathbb{Z} + 1$
	χ_-^4	0			$e \in 2\mathbb{Z} + 1, m \in 2\mathbb{Z}$
(100)	α_+^1	0	$h + \bar{h}$	$h - \bar{h}$	$h, \bar{h} \in \{\frac{1}{16}, \frac{9}{16}\} \quad h - \bar{h} \in \mathbb{Z}$
	α_-^1	$\frac{1}{2}$			$h - \bar{h} \in \mathbb{Z} + \frac{1}{2}$
(010)	α_+^2	0	$h + \bar{h}$	$h - \bar{h}$	$h, \bar{h} \in \{\frac{1}{16}, \frac{9}{16}\} \quad h - \bar{h} \in \mathbb{Z}$
	α_-^2	$\frac{1}{2}$			$h - \bar{h} \in \mathbb{Z} + \frac{1}{2}$
(110)	β_+^3	0	$\frac{e^2}{R^2} + \frac{m^2 R^2}{4}$	em	$e \in \mathbb{Z} + \frac{1}{2}, m \in \mathbb{Z} \quad em \in \mathbb{Z}$
	β_-^3	$\frac{1}{2}$			$em \in \mathbb{Z} + \frac{1}{2}$
(001)	α_+^3	0	$\frac{e^2}{R^2} + \frac{m^2 R^2}{4}$	em	$e \in \mathbb{Z}, m \in \mathbb{Z} + \frac{1}{2} \quad em \in \mathbb{Z}$
	α_-^3	$\frac{1}{2}$			$em \in \mathbb{Z} + \frac{1}{2}$
(101)	β_+^2	0	$h + \bar{h}$	$h - \bar{h}$	$h, \bar{h} \in \{\frac{1}{16}, \frac{9}{16}\} \quad h - \bar{h} \in \mathbb{Z}$
	β_-^2	$\frac{1}{2}$			$h - \bar{h} \in \mathbb{Z} + \frac{1}{2}$
(011)	β_+^1	0	$h + \bar{h}$	$h - \bar{h}$	$h, \bar{h} \in \{\frac{1}{16}, \frac{9}{16}\} \quad h - \bar{h} \in \mathbb{Z}$
	β_-^1	$\frac{1}{2}$			$h - \bar{h} \in \mathbb{Z} + \frac{1}{2}$
(111)	γ_+	$\frac{3}{4}$	$\frac{e^2}{R^2} + \frac{m^2 R^2}{4}$	em	$e, m \in \mathbb{Z} + \frac{1}{2} \quad em \in \mathbb{Z} + \frac{3}{4}$
	γ_-	$\frac{1}{4}$			$em \in \mathbb{Z} + \frac{1}{4}$

Table 2.1: Primary fields in each topological sector labeled by a twist (an element of $\mathcal{G} = \mathbb{Z}_2^3$) and an irreducible (projective) representation. These sectors are the simple objects of $D^\phi(\mathbb{Z}_2^3) \cong D(D_4)$.

Note that the choices of e and m allowed for each representation under the trivial twist corresponds to $(-1)^e = \chi(001)$ and $(-1)^m = \chi(110)$, where χ is the representation being considered.

Projective representations in each topological sector are indicated in Eqn. 2.48, reproduced from Ref. 106.

The fusion table, computed using the symmetric MERA, for these sectors is explicitly presented in Table 2.2. All sectors with a nontrivial twist have quantum dimension 2, and so are nonabelian.

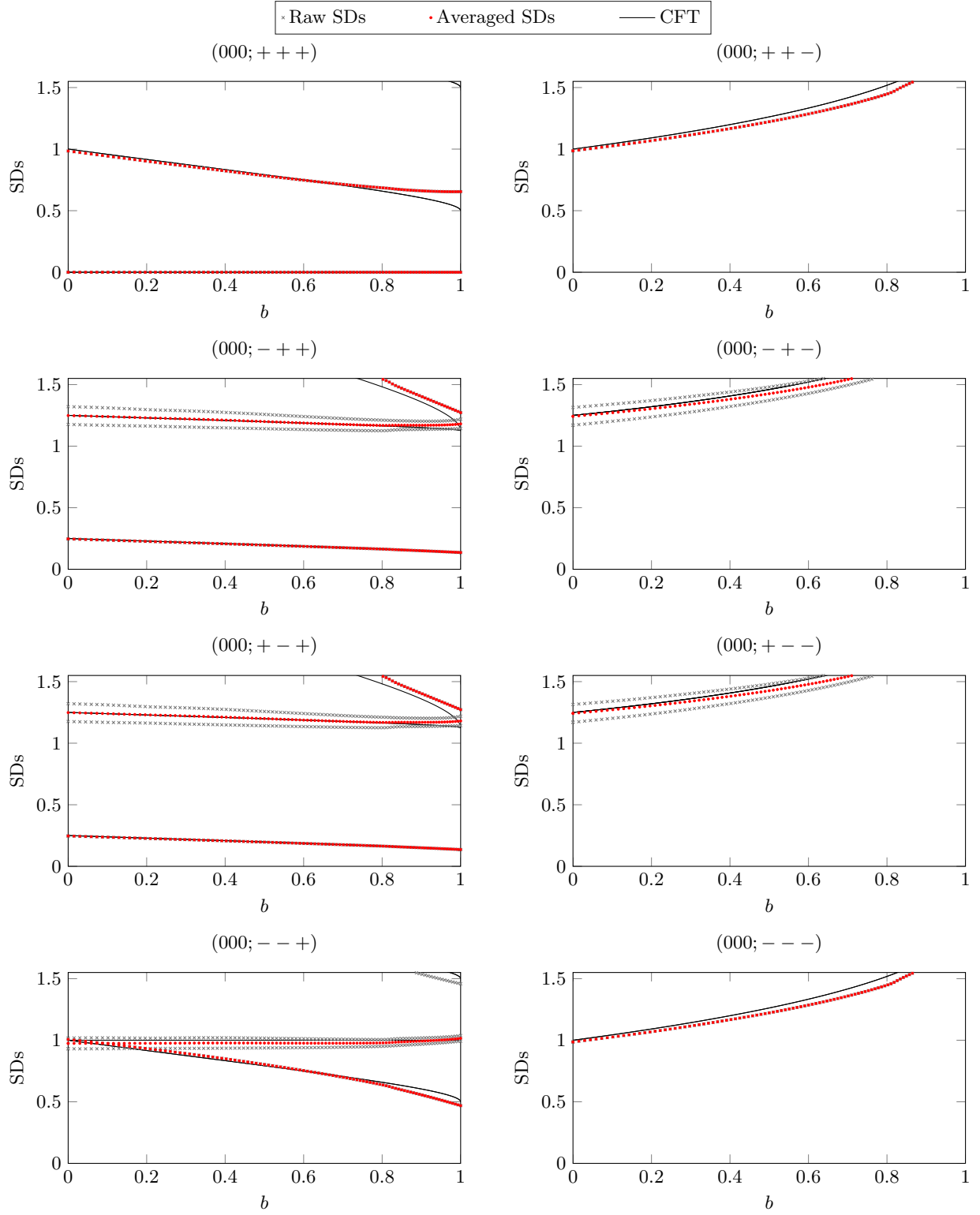


Figure 2.7: MERA scaling dimensions for the trivial twist of the abc model along the ‘b’ line. This line is symmetric under the anomalous action of \mathbb{Z}_2^3 .

Figure titles label: (twist label; irreducible representation label). Grey points are the raw data extracted from the MERA. Red points correspond to averaged data as discussed in Appendix 2.7. Black lines correspond to local fields of the compactified free boson CFT.

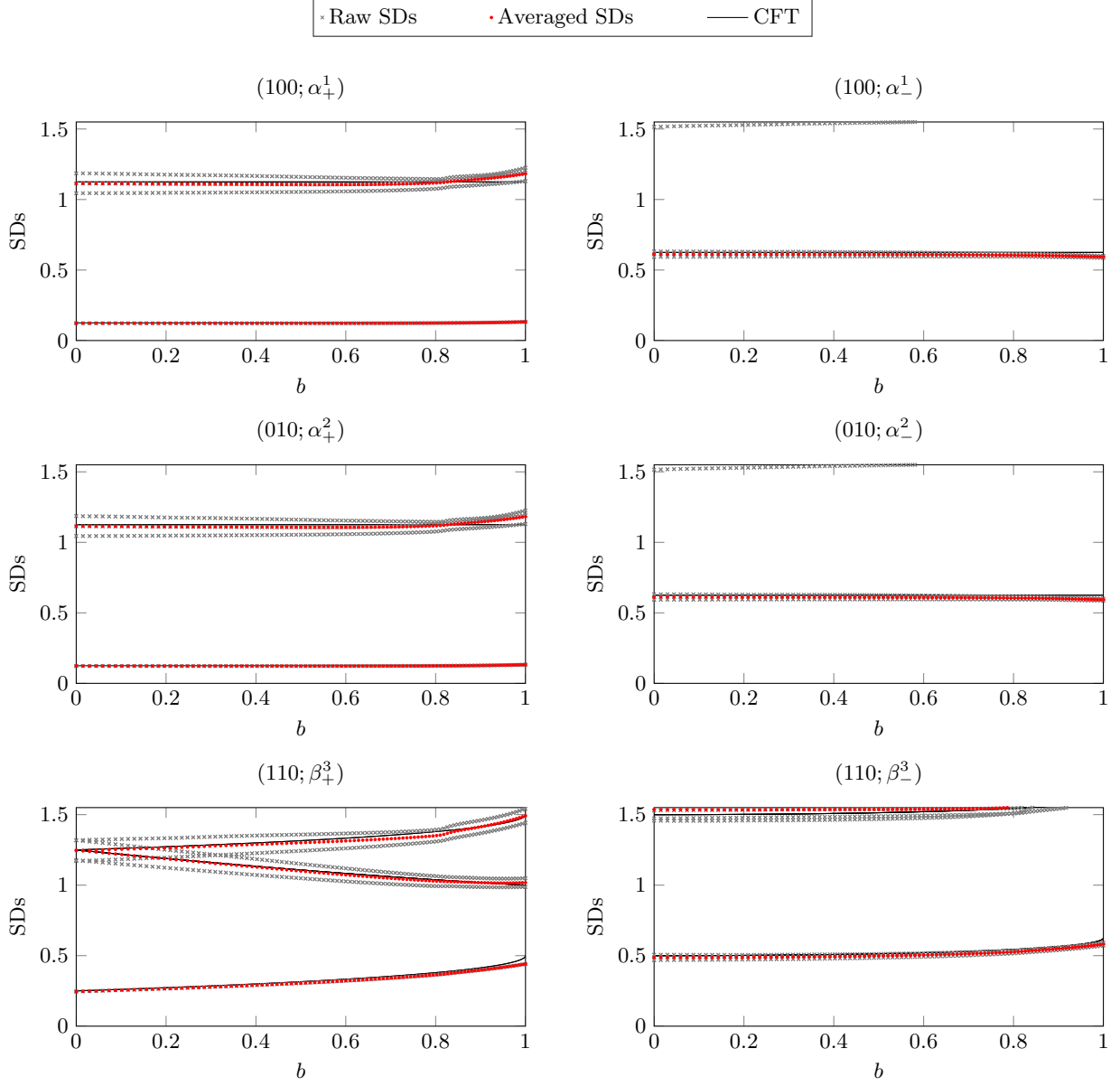


Figure 2.8: Scaling dimensions for topological sectors with twists of the form $(x, y, 0)$.

Figure titles label: (twist label; irreducible projective representation label).

Grey points are the raw data extracted from the MERA. Red points correspond to averaged data as discussed in Appendix 2.7. Black lines correspond to equations in Table 2.1.

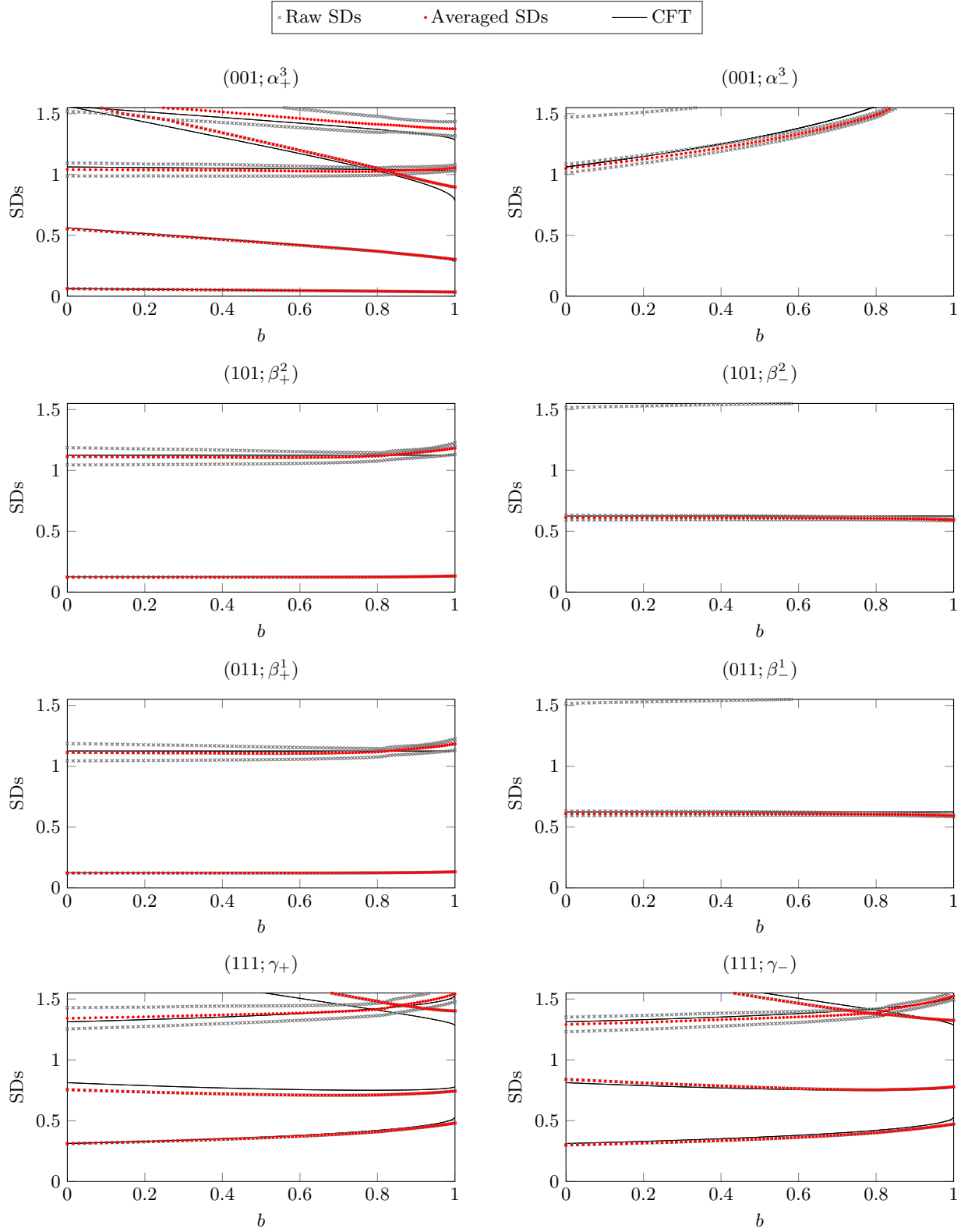


Figure 2.9: Scaling dimensions for topological sectors with twists of the form $(x, y, 1)$.

Figure titles label: (twist label; irreducible projective representation label).

Grey points are the raw data extracted from the MERA. Red points correspond to averaged data as discussed in Appendix 2.7. Black lines correspond to equations in Table 2.1.

$a \times b$	χ_+^1	χ_+^2	χ_+^3	χ_+^4	χ_-^1	χ_-^2	χ_-^3	χ_-^4	α_+^1	α_-^1	α_+^2	α_-^2	α_+^3	α_-^3	α_+^4	α_-^4	β_+^1	β_-^1	γ_+	γ_-
χ_+^1	χ_+^1	χ_+^2	χ_+^3	χ_+^4	χ_-^1	χ_-^2	χ_-^3	χ_-^4	α_+^1	α_-^1	α_+^2	α_-^2	α_+^3	α_-^3	α_+^4	α_-^4	β_+^1	β_-^1	γ_+	γ_-
χ_+^2	χ_+^2	χ_+^1	χ_+^4	χ_+^3	χ_-^2	χ_-^1	χ_-^4	χ_-^3	α_+^1	α_-^1	α_+^2	α_-^2	α_+^3	α_-^3	α_+^4	α_-^4	β_+^1	β_-^1	γ_-	γ_+
χ_+^3	χ_+^3	χ_+^4	χ_+^1	χ_+^2	χ_-^3	χ_-^4	χ_-^1	χ_-^2	α_+^1	α_-^1	α_+^2	α_-^2	α_+^3	α_-^3	α_+^4	α_-^4	β_+^1	β_-^1	γ_+	γ_-
χ_+^4	χ_+^4	χ_+^3	χ_+^2	χ_+^1	χ_-^4	χ_-^3	χ_-^2	χ_-^1	α_+^1	α_-^1	α_+^2	α_-^2	α_+^3	α_-^3	α_+^4	α_-^4	β_+^1	β_-^1	γ_-	γ_+
χ_-^1	χ_-^1	χ_-^2	χ_-^3	χ_-^4	χ_+^1	χ_+^2	χ_+^3	χ_+^4	α_-^1	α_+^1	α_-^2	α_+^2	α_-^3	α_+^3	α_-^4	α_+^4	β_-^1	β_+^1	γ_-	γ_+
χ_-^2	χ_-^2	χ_-^1	χ_-^4	χ_-^3	χ_+^2	χ_+^1	χ_+^4	χ_+^3	α_-^1	α_+^1	α_-^2	α_+^2	α_-^3	α_+^3	α_-^4	α_+^4	β_-^1	β_+^1	γ_+	γ_-
χ_-^3	χ_-^3	χ_-^4	χ_-^1	χ_-^2	χ_+^3	χ_+^4	χ_+^2	χ_+^1	α_-^1	α_+^1	α_-^2	α_+^2	α_-^3	α_+^3	α_-^4	α_+^4	β_-^1	β_+^1	γ_+	γ_-
χ_-^4	χ_-^4	χ_-^3	χ_-^2	χ_-^1	χ_+^4	χ_+^3	χ_+^2	χ_+^1	α_-^1	α_+^1	α_-^2	α_+^2	α_-^3	α_+^3	α_-^4	α_+^4	β_-^1	β_+^1	γ_-	γ_+
α_+^1	α_+^1	α_-^1	α_+^2	α_-^2	α_+^1	α_-^1	α_+^2	α_-^2	α_+^1	α_-^1	α_+^2	α_-^2	α_+^3	α_-^3	α_+^4	α_-^4	β_+^1	β_-^1	γ_+	γ_-
α_-^1	α_-^1	α_+^1	α_-^2	α_+^2	α_-^1	α_+^1	α_-^2	α_+^2	α_-^1	α_+^1	α_-^2	α_+^2	α_-^3	α_+^3	α_-^4	α_+^4	β_-^1	β_+^1	γ_-	γ_+
α_+^2	α_+^2	α_-^2	α_+^1	α_-^1	α_+^2	α_-^2	α_+^1	α_-^1	α_+^2	α_-^2	α_+^1	α_-^1	α_+^2	α_-^2	α_+^3	α_-^3	β_+^1	β_-^1	γ_+	γ_-
α_-^2	α_-^2	α_+^2	α_-^1	α_+^1	α_-^2	α_+^2	α_-^1	α_+^1	α_-^2	α_+^2	α_-^1	α_+^1	α_-^2	α_+^3	α_-^3	α_+^4	β_-^1	β_+^1	γ_-	γ_+
α_+^3	α_+^3	α_-^3	α_+^4	α_-^4	α_+^3	α_-^3	α_+^4	α_-^4	α_+^3	α_-^3	α_+^4	α_-^4	α_+^1	α_-^1	α_+^2	α_-^2	β_+^1	β_-^1	γ_+	γ_-
α_-^3	α_-^3	α_+^3	α_-^4	α_+^4	α_-^3	α_+^3	α_-^4	α_+^4	α_-^3	α_+^3	α_-^4	α_+^4	α_-^1	α_+^1	α_-^2	α_+^2	β_-^1	β_+^1	γ_-	γ_+
α_+^4	α_+^4	α_-^4	α_+^1	α_-^1	α_+^4	α_-^4	α_+^1	α_-^1	α_+^4	α_-^4	α_+^1	α_-^1	α_+^2	α_-^2	α_+^3	α_-^3	β_+^1	β_-^1	γ_+	γ_-
α_-^4	α_-^4	α_+^4	α_-^1	α_+^1	α_-^4	α_+^4	α_-^1	α_+^1	α_-^4	α_+^4	α_-^1	α_+^1	α_-^2	α_+^2	α_-^3	α_+^3	β_-^1	β_+^1	γ_-	γ_+
β_+^1	β_+^1	β_-^1	β_+^2	β_-^2	β_+^1	β_-^1	β_+^2	β_-^2	β_+^1	β_-^1	β_+^2	β_-^2	β_+^3	β_-^3	β_+^4	β_-^4	γ_+	γ_-	γ_+	γ_-
β_-^1	β_-^1	β_+^1	β_-^2	β_+^2	β_-^1	β_+^1	β_-^2	β_+^2	β_-^1	β_+^1	β_-^2	β_+^2	β_-^3	β_+^3	β_-^4	β_+^4	γ_-	γ_+	γ_-	γ_+
β_+^2	β_+^2	β_-^2	β_+^3	β_-^3	β_+^2	β_-^2	β_+^3	β_-^3	β_+^2	β_-^2	β_+^3	β_-^3	β_+^1	β_-^1	β_+^2	β_-^2	γ_+	γ_-	γ_+	γ_-
β_-^2	β_-^2	β_+^2	β_-^3	β_+^3	β_-^2	β_+^2	β_-^3	β_+^3	β_-^2	β_+^2	β_-^3	β_+^3	β_-^1	β_+^1	β_-^2	β_+^2	γ_-	γ_+	γ_-	γ_+
β_+^3	β_+^3	β_-^3	β_+^4	β_-^4	β_+^3	β_-^3	β_+^4	β_-^4	β_+^3	β_-^3	β_+^4	β_-^4	β_+^1	β_-^1	β_+^2	β_-^2	γ_+	γ_-	γ_+	γ_-
β_-^3	β_-^3	β_+^3	β_-^4	β_+^4	β_-^3	β_+^3	β_-^4	β_+^4	β_-^3	β_+^3	β_-^4	β_+^4	β_-^1	β_+^1	β_-^2	β_+^2	γ_-	γ_+	γ_-	γ_+
β_+^4	β_+^4	β_-^4	β_+^1	β_-^1	β_+^4	β_-^4	β_+^1	β_-^1	β_+^4	β_-^4	β_+^1	β_-^1	β_+^2	β_-^2	β_+^3	β_-^3	γ_+	γ_-	γ_+	γ_-
β_-^4	β_-^4	β_+^4	β_-^1	β_+^1	β_-^4	β_+^4	β_-^1	β_+^1	β_-^4	β_+^4	β_-^1	β_+^1	β_-^2	β_+^2	β_-^3	β_+^3	γ_-	γ_+	γ_-	γ_+
γ_+	γ_+	γ_-	γ_+	γ_-	γ_+	γ_-	γ_+	γ_-	γ_+	γ_-	γ_+	γ_-	γ_+	γ_-	γ_+	γ_-	γ_+	γ_-	γ_+	γ_-
γ_-	γ_-	γ_+	γ_-	γ_+	γ_-	γ_+	γ_-	γ_+	γ_-	γ_+	γ_-	γ_+	γ_-	γ_+	γ_-	γ_+	γ_+	γ_-	γ_+	γ_-

Table 2.2: Fusion rules for $D^\phi(\mathbb{Z}_3^3)$ sectors computed from symmetric MERA. Cell entries denote the allowed fusion outcome sectors for $a \times b$. The OPE coefficients defined in Eqn. 2.29 are zero if the resultant field c does not lie in an allowed sector.

$$\begin{aligned}
& \text{Diagram} = \phi(g_1, g_2, g_3) \text{Diagram} = \phi(g_1, g_2, g_3) \phi(g_0, g_1 g_2, g_3) \text{Diagram} \\
& = \phi(g_1, g_2, g_3) \phi(g_0, g_1 g_2, g_3) \phi(g_0, g_1, g_2) \text{Diagram} \quad (2.51)
\end{aligned}$$

$$\begin{aligned}
& \text{Diagram} = \frac{\phi(g_1, g_2, g_3) \phi(g_0, g_1 g_2, g_3) \phi(g_0, g_1, g_2)}{\phi(g_0 g_1, g_2, g_3)} \text{Diagram} \\
& = \frac{\phi(g_1, g_2, g_3) \phi(g_0, g_1 g_2, g_3) \phi(g_0, g_1, g_2)}{\phi(g_0 g_1, g_2, g_3) \phi(g_0, g_1, g_2 g_3)} \text{Diagram}, \quad (2.52)
\end{aligned}$$

implying that

$$\frac{\phi(g_0, g_1, g_2) \phi(g_0, g_1 g_2, g_3) \phi(g_1, g_2, g_3)}{\phi(g_0 g_1, g_2, g_3) \phi(g_0, g_1, g_2 g_3)} = 1. \quad (2.53)$$

This condition is known as the 3-cocycle conditions and identifies ϕ as a 3-cocycle. As mentioned above $X(g_0, g_1)$ is only defined up to a complex phase $\beta(g_0, g_1)$. This freedom can change the ϕ , giving the equivalence relation

$$\phi'(g_0, g_1, g_2) = \phi(g_0, g_1, g_2) \frac{\beta(g_1, g_2) \beta(g_0, g_1 g_2)}{\beta(g_0, g_1) \beta(g_0 g_1, g_2)}, \quad (2.54)$$

so ϕ is only defined up to a 3-coboundary. For this reason the single block MPO group representation is endowed with the label $[\phi]$ from the third cohomology group $\mathcal{H}^3(\mathcal{G}, \text{U}(1))$. One can check that multiplying any larger number of MPOs does not give additional conditions/equivalences on ϕ .

One can use a similar argument to demonstrate that no injective MPS can possess an anomalous symmetry. Assume an injective MPS with tensor A is symmetric under an MPO symmetry for all lengths, similar reasoning that lead to Eqn. 2.49 implies the existence of another reduction tensor $Y(g)$ satisfying

$$Y^\dagger(g) \text{Diagram} Y(g) = \text{Diagram} \quad (2.55)$$

Similar to Eqn. 2.50 we find that acting with multiple group elements leads to a complex phase $\beta(g_0, g_1)$

$$\begin{array}{c} \text{A} \\ | \\ g_1 \\ | \\ g_0 \end{array} \begin{array}{c} \text{---} Y(g_1) \\ \text{---} Y(g_0) \end{array} = \beta(g_0, g_1) \begin{array}{c} \text{A} \\ | \\ g_1 \\ | \\ g_0 \end{array} \begin{array}{c} \text{---} Y(g_0 g_1) \\ \text{---} X(g_0, g_1) \end{array} . \quad (2.56)$$

We now consider the application of three group elements

$$\begin{array}{c} \text{A} \\ | \\ g_2 \\ | \\ g_1 \\ | \\ g_0 \end{array} \begin{array}{c} \text{---} \\ \text{---} \\ \text{---} \end{array} = \beta(g_1, g_2) \begin{array}{c} \text{A} \\ | \\ g_2 \\ | \\ g_1 \\ | \\ g_0 \end{array} \begin{array}{c} \text{---} \\ \text{---} \\ \text{---} \end{array} = \beta(g_1, g_2) \beta(g_0, g_1 g_2) \begin{array}{c} \text{A} \\ | \\ g_2 \\ | \\ g_1 \\ | \\ g_0 \end{array} \begin{array}{c} \text{---} \\ \text{---} \\ \text{---} \end{array} \\
 = \beta(g_1, g_2) \beta(g_0, g_1 g_2) \phi(g_0, g_1, g_2) \begin{array}{c} \text{A} \\ | \\ g_2 \\ | \\ g_1 \\ | \\ g_0 \end{array} \begin{array}{c} \text{---} \\ \text{---} \\ \text{---} \end{array} \quad (2.57)$$

$$\begin{array}{c} \text{A} \\ | \\ g_2 \\ | \\ g_1 \\ | \\ g_0 \end{array} \begin{array}{c} \text{---} \\ \text{---} \\ \text{---} \end{array} = \frac{\beta(g_1, g_2) \beta(g_0, g_1 g_2) \phi(g_0, g_1, g_2)}{\beta(g_0 g_1, g_2)} \begin{array}{c} \text{A} \\ | \\ g_2 \\ | \\ g_1 \\ | \\ g_0 \end{array} \begin{array}{c} \text{---} \\ \text{---} \\ \text{---} \end{array} \\
 = \frac{\beta(g_1, g_2) \beta(g_0, g_1 g_2) \phi(g_0, g_1, g_2)}{\beta(g_0 g_1, g_2) \beta(g_0, g_1)} \begin{array}{c} \text{A} \\ | \\ g_2 \\ | \\ g_1 \\ | \\ g_0 \end{array} \begin{array}{c} \text{---} \\ \text{---} \\ \text{---} \end{array} , \quad (2.58)$$

which leads to a consistency equation

$$\phi(g_0, g_1, g_2) = \frac{\beta(g_0 g_1, g_2) \beta(g_0, g_1)}{\beta(g_1, g_2) \beta(g_0, g_1 g_2)}, \quad (2.59)$$

implying ϕ is a coboundary. Therefore $\phi \sim 1$, is in the trivial cohomology class. Hence no injective MPS can be symmetric under an anomalous MPO symmetry. This leaves open the possibility of a non-injective MPS, describing a state which spontaneously breaks the symmetry. Alternatively a symmetric state may be gapless and hence have no MPS description (with a fixed bond dimension).

2.9 Ansatz for MERA tensors with type-III \mathbb{Z}_N^3 symmetry

In this appendix, we describe an ansatz for the tensors in a MERA with type-III \mathbb{Z}_N^3 symmetry. Let $\mathcal{G} = \mathbb{Z}_N^3$, with action as defined in Eqn. 2.35. Let T be an isometric tensor with $2A$ upper indices and $2B$ ($B \geq A$) lower indices

$$T : (\mathbb{C}^N)^{\otimes 2A} \rightarrow (\mathbb{C}^N)^{\otimes 2B}, \quad (2.60)$$

$$T^\dagger T = \mathbb{1}_N^{\otimes 2A}. \quad (2.61)$$

Define the decoupling circuit on $2K$ indices as

$$\mathcal{D}_{2K} = \prod_{j=1}^{K-1} CX_{1,2j+1} CX_{2K,2j}. \quad (2.62)$$

Allowed MERA tensors are those given by

$$T = \mathcal{D}_{2B}^\dagger (\mathbb{1}_N \otimes t \otimes \mathbb{1}_N) \mathcal{D}_{2A}, \quad (2.63)$$

where

$$t : (\mathbb{C}^N)^{\otimes 2(A-1)} \rightarrow (\mathbb{C}^N)^{\otimes 2(B-1)}, \quad (2.64)$$

$$t^\dagger t = \mathbb{1}_N^{\otimes 2(A-1)}. \quad (2.65)$$

The X portion of the symmetry is automatically enforced by this circuit. To enforce the CZ part, one must ensure that

$$\left(\prod_{j=1}^{B-1} CZ_{2j-1,2j}^\dagger \right) \left(\prod_{j=1}^{B-2} CZ_{2j,2j+1} \right) t = t \left(\prod_{j=1}^{A-1} CZ_{2j-1,2j}^\dagger \right) \left(\prod_{j=1}^{A-2} CZ_{2j,2j+1} \right). \quad (2.66)$$

2.9.1 4:2 MERA

For clarity, we now include the form of the constraint on the 4:2 MERA (introduced in Fig. 2.1) with bond dimension N , N^2 and N^3 :

$$\text{Diagram 1} = \text{Diagram 2}, \quad (2.67a)$$

$$\text{Diagram 3} = \text{Diagram 4}, \quad (2.67b)$$

$$\text{Diagram 5} = \text{Diagram 6}. \quad (2.67c)$$

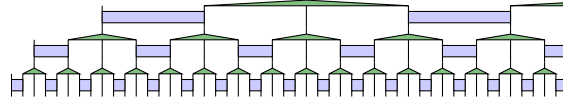


Figure 2.10: The ternary MERA represents a quantum state using two types of tensors; unitary ‘disentanglers’ (rectangles) and isometric tensors (triangles).

2.9.2 Ternary MERA

For completeness, we show how our ansatz is applied to the ternary MERA shown in Fig. 2.10. The ternary ansatz is commonly seen in the literature due to its relatively low optimization cost. A ternary MERA is built from two kinds of tensors; unitary ‘disentanglers’ v (rectangles in Fig. 2.10) and isometric tensors w (triangles in Fig. 2.10). In the general case, these tensors may all contain distinct coefficients, although symmetries such as scale invariance can be imposed by, for example, forcing the tensors on each layer to be identical.

For bond dimension N^2 and N^4 , the constraint on the tensors is

$$\begin{array}{c} \text{[Diagram of a blue rectangle with 3 input lines and 3 output lines]} \\ \text{[Diagram of a green triangle with 3 input lines and 1 output line]} \end{array} = \begin{array}{c} \text{[Diagram of a blue rectangle with 3 input lines and 3 output lines, with internal indices]} \\ \text{[Diagram of a green triangle with 3 input lines and 1 output line, with internal indices]} \end{array}, \quad (2.68a)$$

$$\begin{array}{c} \text{[Diagram of a blue rectangle with 9 input lines and 9 output lines]} \\ \text{[Diagram of a green triangle with 9 input lines and 3 output lines]} \end{array} = \begin{array}{c} \text{[Diagram of a blue rectangle with 9 input lines and 9 output lines, with internal indices]} \\ \text{[Diagram of a green triangle with 9 input lines and 3 output lines, with internal indices]} \end{array}, \quad (2.68b)$$

with the obvious generalization to other bond dimensions.

We remark that although our examples drawn here map χ dimensional sites to χ dimensional sites, this can be relaxed. This allows the effective dimension of the sites to be increased as desired.

2.10 Generalized \mathbb{Z}_N CZX model and its gapless boundary theory

The CZX model was introduced in Ref. 70 as a simple exactly solvable representative of the nontrivial \mathbb{Z}_2 SPT phase in two spatial dimensions. In this paper we have considered the larger symmetry group \mathbb{Z}_2^3 of the model for which it is a representative of the \mathbb{Z}_2^3 type-III SPT phase. In this appendix we describe a simple generalization of the CZX model to a Hamiltonian with \mathbb{Z}_N^3 symmetry that is a representative of the root type-III \mathbb{Z}_N^3 SPT. We then outline how this fits into the more general setting of $(1+1)$ D \mathcal{G} -SPT dualities at the edge of a particular $\mathcal{G} \times \mathcal{H}^2(\mathcal{G}, \text{U}(1))$ -SPT bulk in $(2+1)$ D.

2.10.1 Definitions

The model is defined on a two dimensional square lattice with four \mathbb{Z}_N spins per site. For concreteness we label them counterclockwise as follows



(2.69)

Before stating the Hamiltonian, ground-state, and symmetries of the model we establish some definitions:

$$P_2 = \sum_{i=0}^{N-1} |i\rangle^{\otimes 2} \langle i|^{\otimes 2} \quad (2.70)$$

$$X_4 = \sum_{i=0}^{N-1} |i+1\rangle^{\otimes 4} \langle i|^{\otimes 4} \quad (2.71)$$

$$|\text{GHZ}_4\rangle = \frac{1}{\sqrt{N}} \sum_{i=0}^{N-1} |i\rangle^{\otimes 4} \quad (2.72)$$

$$u_X^- = X_1 \otimes X_3 \quad (2.73)$$

$$u_X^+ = X_2 \otimes X_4 \quad (2.74)$$

$$u_{CZ} = CZ_{12} CZ_{23}^\dagger CZ_{34} CZ_{41}^\dagger, \quad (2.75)$$

where X, CZ are defined in Section 2.4.

2.10.2 Hamiltonian and ground state

The Hamiltonian is a sum of local terms acting on each plaquette of a square lattice $H = \sum_p h_p$. The terms are given by

$$h_p = - \sum_{i=0}^{N-1} X_4^i \otimes P_2 \otimes P_2 \otimes P_2 \otimes P_2, \quad (2.76)$$

which act on the lattice as


(2.77)

The ground state is unique for closed boundary conditions and is given by a tensor product of the state $|\text{GHZ}_4\rangle$ on the four spins around each plaquette

$$|\Psi_{\text{GS}}\rangle = \bigotimes_p |\text{GHZ}_4\rangle. \quad (2.78)$$

Note that this ground state is not a product state with respect the locality structure we have chosen by our grouping of spins into sites (if sites were instead defined to group the spins around each plaquette it would be a product state).

2.10.3 Symmetry

To describe the \mathbb{Z}_N^3 symmetry of the Hamiltonian in Eqn. 2.76 we first bipartition the lattice into black (b) and white (w) sites, as indicated in Fig. 2.11. The generators are then given by

$$U_{\text{X}} = \bigotimes_b u_{\text{X}}^- \bigotimes_w u_{\text{X}}^+ \quad (2.79)$$

$$U_{\text{X}} = \bigotimes_b u_{\text{X}}^+ \bigotimes_w u_{\text{X}}^- \quad (2.80)$$

$$U_{\text{CZ}} = \bigotimes_b u_{\text{CZ}}^\dagger \bigotimes_w u_{\text{CZ}}. \quad (2.81)$$

One can verify that each of these operators is of order N and that they mutually commute. Furthermore each local Hamiltonian term commutes with all symmetries and they leave the ground state invariant. Note the U_{CZ} symmetry is an on-site symmetry for our definition of site but would not be if sites were instead defined by grouping the spins around each plaquette.

2.10.4 Boundary theory

In the presence of an open boundary the bulk Hamiltonian is extensively degenerate as it only projects pairs of spins along the edge into the support subspace of P_2 . We identify effective \mathbb{Z}_N edge spins with the N states in this subspace via the projector $\sum_i |i\rangle \langle ii|$. This identification is indicated by \rightsquigarrow in Fig. 2.11. An edge site is formed by a pair of these spins, as shown in Fig. 2.11. This identification provides an exact mapping from bulk operators to the boundary.

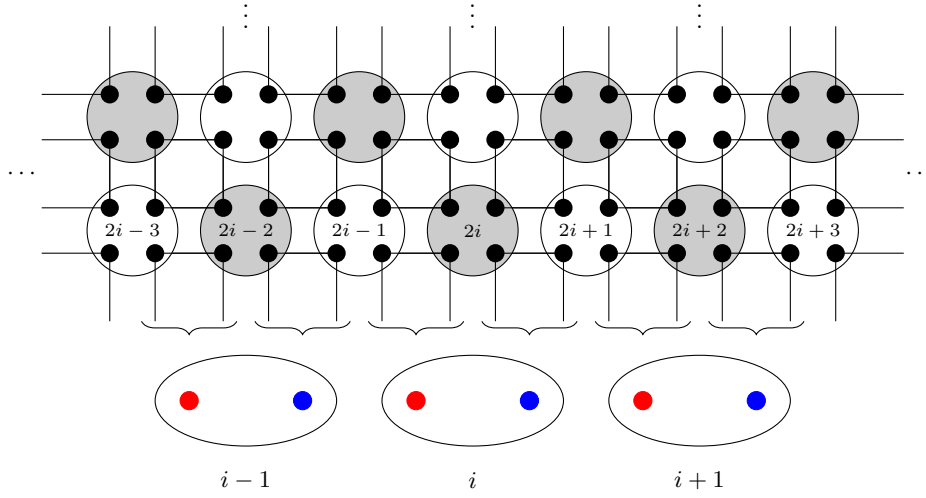


Figure 2.11: Identification of the edge degrees of freedom.

The symmetry acts on the edge as follows

$$U_X \mapsto \bigotimes_j X_j \quad (2.82)$$

$$U_{\tilde{X}} \mapsto \bigotimes_j \tilde{X}_j \quad (2.83)$$

$$U_{CZ} \mapsto \mathcal{C} = \underbrace{\begin{array}{c} \uparrow \downarrow \\ \uparrow \downarrow \\ \uparrow \downarrow \\ \uparrow \downarrow \end{array}}_{\text{site}} \quad (2.84)$$

Due to the grouping of edge spins into sites only the subgroup generated by U_X and $U_{\tilde{X}}$ acts on-site.

The bulk to boundary mapping can be used to find the edge action of certain operators that leave no residual effect on the bulk of the ground state. In particular

$$(Z_1)_{2i}^b \mapsto X_i \quad (2.85)$$

$$(Z_2)_{2i-1}^w \mapsto X_i \quad (2.86)$$

$$(Z_1)_{2i+1}^w \mapsto \tilde{Z}_i \quad (2.87)$$

$$(Z_2)_{2i}^b \mapsto \tilde{Z}_i \quad (2.88)$$

$$(X_2)_{2i-1}^w (X_1)_{2i}^b \mapsto X_i \quad (2.89)$$

$$(X_2)_{2i}^b (X_1)_{2i+1}^w \mapsto \tilde{X}_i, \quad (2.90)$$

where the numbering is indicated in Fig. 2.11. We find an effective edge Hamiltonian by considering symmetric perturbations in the bulk with minimal support.

$$(Z_1^\dagger Z_3)_{2i}^b (Z_2^\dagger Z_4)_{2i+1}^w \mapsto X_i^\dagger X_{i+1} \quad (2.91)$$

$$(Z_1 Z_3)_{2i+1}^w (Z_2 Z_4)_{2i+2}^b \mapsto \tilde{Z}_i \tilde{Z}_{i+1}^\dagger \quad (2.92)$$

$$(X_2)_{2i-1}^w (X_1)_{2i}^b + (Z_1 X_2 Z_3)_{2i-1}^w (X_1 Z_2^\dagger Z_4)_{2i}^b \mapsto X_i + \tilde{Z}_{i-1}^\dagger X_i \tilde{Z}_i^\dagger \quad (2.93)$$

$$(X_2)_{2i}^b (X_1)_{2i+1}^w + (Z_1^\dagger X_2 Z_3)_{2i}^b (X_1 Z_2^\dagger Z_4)_{2i+1}^w \mapsto \tilde{X}_i + X_i^\dagger \tilde{X}_i X_{i+1}. \quad (2.94)$$

The edge Hamiltonian is given by

$$H_{\text{Edge}} = - \sum_i \sum_{k=0}^{N-1} c_k \sum_{j=0}^{N-1} (\tilde{Z}_i^{\dagger jk} \tilde{X}_i^j Z_{i+1}^{jk} + \tilde{Z}_{i-1}^{jk} X_i^j \tilde{Z}_i^{\dagger jk}) - \sum_i \sum_{k=0}^{N-1} b_k (\tilde{Z}_i^{\dagger k} Z_{i+1}^k + \tilde{Z}_i^k \tilde{Z}_{i+1}^{\dagger k}). \quad (2.95)$$

where $b_k = b_{N-k}$. The Hamiltonian is fully symmetric under U_X and $U_{\tilde{X}}$ while the parameters transform as follows under \mathcal{C}

$$c_k \mapsto c_{k-1}, \quad (2.96)$$

$$b_k \mapsto b_k. \quad (2.97)$$

When c_k is the only nonzero parameter the Hamiltonian is in the $[k] \in \mathcal{H}^2(\mathcal{G}, \text{U}(1))$ SPT phase, while for $b_k = b_{N-k}$ the only nonzero parameters it describes a symmetry broken phase. Hence the \mathcal{C} operator cycles the SPT phases $[k] \mapsto [k+1]$ and the Hamiltonian is fully symmetric when all $c_k = c_0$. This may correspond to an SPT critical point or a symmetry breaking point depending upon the relative strength of the b_k parameters.

2.10.5 General $(1+1)\text{D } \mathcal{G}$ SPT duality at the edge of a $(2+1)\text{D } \mathcal{G} \times \mathcal{H}^2(\mathcal{G}, \text{U}(1))$ SPT

The above construction for \mathbb{Z}_N^3 is a specific instance of a general connection between duality of $(1+1)\text{D}$ edge \mathcal{G} SPT phases and a $(2+1)\text{D}$ bulk $\mathcal{G} \times \mathcal{H}^2(\mathcal{G}, \text{U}(1))$ SPT phase. This connection may be of independent interest. The action of the bulk $\mathcal{H}^2(\mathcal{G}, \text{U}(1))$ symmetry can be thought of as pumping \mathcal{G} SPTs onto the edge.

Similarly to the case above, the Hilbert space of each spin is given by $\mathbb{C}[\mathcal{G}]$ and 4 spins are grouped per site of a square lattice. R_g denotes the right regular representation, we fix a choice of representative for a set of generators of $\mathcal{H}^2(\mathcal{G}, \text{U}(1)) \cong \prod_k \mathbb{Z}_{N_k}$ (their products fix all other representatives) and

$$R_g^{\otimes 4} P_4 := \sum_{g \in \mathcal{G}} |hg^{-1}\rangle^{\otimes 4} \langle h|^{\otimes 4} \quad (2.98)$$

$$C\omega_{12} := \sum_{g_0, g_1} \omega(g_0 g_1^{-1}, g_1) |g_0, g_1\rangle \langle g_0, g_1| \quad (2.99)$$

$$u_\omega := C\omega_{12} C\omega_{23} C\omega_{34} C\omega_{41} \quad (2.100)$$

for $[\omega] \in \mathcal{H}^2(\mathcal{G}, \text{U}(1))$.

The local Hamiltonian terms are given by

$$h_p = - \sum_{g \in \mathcal{G}} R_g^{\otimes 4} P_4 \otimes P_2 \otimes P_2 \otimes P_2 \otimes P_2 \quad (2.101)$$

acting on the square lattice similarly to the term in Eqn. 2.77. The ground state is again given by

$$|\Psi_{\text{GS}}\rangle = \bigotimes_p |GHZ_4\rangle. \quad (2.102)$$

The global on-site symmetry is generated by

$$U_g = \bigotimes R_g^{\otimes 4} \quad (2.103)$$

$$U_\omega = \bigotimes_b u_\omega^\dagger \bigotimes_w u_\omega \quad (2.104)$$

which can be seen to mutually commute and also commute with h_p . These symmetries also leave the ground state invariant.

As above, the effective edge spins are identified with the ground state subspace of plaquettes crossing the boundary, via the projector $\sum_g |g\rangle \langle gg|$. The action of the symmetry on the edge is given by

$$U_g \mapsto \bigotimes_i R_g \quad (2.105)$$

$$U_\omega \mapsto \prod_i C\omega_{2i,2i+1} C\omega_{2i-1,2i}^\dagger. \quad (2.106)$$

This forms a matrix product operator representation of $\mathcal{G} \times \mathcal{H}^2(\mathcal{G}, \text{U}(1))$ with 3-cocycle

$$\alpha((g_0, \omega_0), (g_1, \omega_1), (g_2, \omega_2)) = \omega_2(g_0, g_1). \quad (2.107)$$

The edge action of U_ω maps a \mathcal{G} SPT phase $[\beta]$ to $[\beta + \omega]$. This can be seen by examining the effect of U_ω on a fixed point local Hamiltonian such as the \mathcal{G} -paramagnet

$$H = - \sum_v \sum_g (R_g)_v. \quad (2.108)$$

Alternatively, note the edge action of U_ω restricted to an open chain is an MPO with two dangling virtual indices associated to its boundaries. Denote this MPO M_ω . M_ω obeys the following commutation rules $R_g^{\otimes L} M_\omega R_g^{\dagger \otimes L} = V_g M_\omega V_g^\dagger$. Here V_g is a projective representation of \mathcal{G} , with cocycle ω , given by

$$V_g = \sum_h \omega(h, g) |hg\rangle \langle h|, \quad (2.109)$$

which acts on one dangling virtual bond of the MPO. Hence applying M_ω to a unique symmetric ground state, such as $|+\rangle^{\otimes N}$, maps it to a state in the SPT phase $[\omega]$.

Chapter 3

Symmetry-enriched topological order in tensor networks: gauging and anyon condensation

Synopsis:

We study symmetry-enriched topological order in two-dimensional tensor network states using graded matrix product operator algebras. A close connection to the theory of graded unitary fusion categories is established. Tensor network representations of the topological defect superselection sectors are constructed. The emergent symmetry-enriched topological order is extracted from these representations, including the symmetry action on the underlying anyons. Dual phase transitions, induced by gauging a global symmetry, and condensation of a bosonic subtheory, are analyzed and the relationship between topological orders on either side of the transition is derived. Several explicit examples are worked through.

Based on: [103](#)

Dominic J. Williamson, Nick Bultinck, Jutho Haegeman, and Frank Verstraete, in preparation.

Changes compared to published version: Minor formatting changes.

Contributions of the author: This is part of a larger collaboration between all the authors, the calculation and writing for this particular work was done by the first author. It includes a summary of Refs. [63](#) and [64](#) which are fruits of the same collaboration.

3.1 Introduction

Symmetry plays a fundamental role in the classification of phases of matter. From spontaneous symmetry breaking in the Landau-Ginzburg theory of second-order phase transitions¹³⁰ to the homeomorphism invariance of topological quantum field theories (TQFTs)^{11–13}. Even in the absence of a global symmetry, equivalence classes of gapped Hamiltonians under adiabatic deformation break up into inequivalent topological phases^{1,8–10,131}. These phases have topological symmetries inherited from the TQFTs that describe their low energy behavior, which are often realized by nontrivial string operators. Enforcing a global symmetry drastically refines the classification of phases that is found. Even the trivial phase splits into a set of SPT phases, which cannot be adiabatically connected while preserving the symmetry^{3,34–36}. Nontrivial topological phases also split into symmetry-enriched topological phases which are distinguished by the interplay of the global symmetry with their topological superselection sectors^{29–33,81,97–102,203}.

The interplay of a global symmetry with topological degrees of freedom has also received attention from the quantum information community due to its relevance for topological quantum codes and computation^{100,204–210}. Transversal gates on topological codes are generated by the action of on-site symmetries on superselection sectors, and symmetry defects have been used to alter the code properties of a topological order. In the quantum information approach to many-body condensed matter systems, tensor networks^{39–41} are used to describe ground states and excitations. These provide efficient representations that faithfully capture the local entanglement structure of the many-body states. In one spatial dimension, matrix product states (MPS) have been used to classify gapped phases by studying the way a global symmetry acts on the auxiliary entanglement degrees of freedom^{27,45,49–51,53–56,67}. In two spatial dimensions, projected entangled pair states (PEPS) have been used to study topological phases^{57–59,62–66}. A classification of nonchiral phases has been obtained from the algebra of matrix product operator (MPO) symmetries on the entanglement degrees of freedom of a local PEPS tensor that satisfy a pulling through equation. The resulting topological phases are given by Morita equivalence²¹¹ classes of MPO symmetry algebras. This class of tensor networks includes all the string-net states²⁴, for which explicit PEPS and MPO representations have been found^{63,119,120}. Chiral phases have also been studied^{60,61,95}, however a complete coherent theoretical framework is lacking.

In this work, we study PEPS representations of symmetry-enriched nonchiral topological phases. We focus on the interplay of a global symmetry with an MPO algebra symmetry on the entanglement degrees of freedom. To this end we consider the generalized symmetry-enriched pulling through equation⁹³ introduced in Chapter 1. The resulting SETs are classified by graded Morita equivalence classes of MPO symmetry algebras. We demonstrate that this class of tensor networks includes the recently introduced symmetry-enriched string-net models^{32,33} by constructing the local PEPS and MPO tensors. We generalize Ocneanu’s tube algebra^{163,212} to include nontrivial defect sectors, from which we construct the superselection sectors of the emergent SET order. We explain how the physical data of the SET can be extracted from this construction. We calculate the effects of gauging the global symmetry^{71,73,213,214}, and the relation of the SET to the resulting topological phase. We also find an anyon condensation phase transition²¹⁵ — dual to gauging — that is induced by breaking a graded MPO symmetry algebra, and calculate the relation of the topological order to the resulting SET. The nonchiral

case of many of the general results shown in Ref. 31 follow directly from our construction. The mathematical contribution of our work includes an explicit construction of the automorphism induced on the Drinfeld center (double) by a given extension of a UFC⁸¹, this is only part of our more general construction of the defect tube algebra and graded Drinfeld center from a graded UFC. Several explicit examples are provided to illustrate various aspects of our formalism.

The paper is organized as follows: In Section 3.2, we present a detailed analysis of the electromagnetic duality symmetry-enriched toric code: including a summary of relevant background results from Refs. 63 and 64, a \mathbb{Z}_2 gauging procedure that maps it to the doubled Ising model, and a dual $\text{Rep}(\mathbb{Z}_2)$ anyon condensation phase transition. In Section 3.3, we write down explicit tensor network representations of the symmetry-enriched string-net ground states and their \mathcal{G} -graded MPO symmetry algebras, and show that they satisfy the symmetry-enriched pulling through equation. In Section 3.4, we summarize the results of Ref. 64 including a derivation of Ocneanu's tube algebra from the MPO symmetry algebra of a tensor network, a construction of the emergent topological superselection sectors from the tube algebra, and the extraction of physical data from superselection sectors thus constructed. In Section 3.5, we describe the theory of \mathcal{G} -graded matrix product operator algebras in terms of \mathcal{G} -extensions of an underlying MPO algebra, we draw an analogy to the theory of \mathcal{G} -graded unitary fusion categories, and define the symmetry-enriched pulling through equation for a tensor network. In Section 3.6, we generalize the tube algebra to include nontrivial \mathcal{G} -defect sectors, which are constructed from a \mathcal{G} -graded MPO symmetry algebra of a tensor network, we describe a construction of the emergent SET order, and the extraction of its physical data. In Section 3.7, we calculate the effect that gauging a global \mathcal{G} symmetry has upon a \mathcal{G} -graded MPO symmetry algebra, derive the relationship between the emergent SET and the topological order that results from gauging, and demonstrate the gauging procedure explicitly for SPT phases. In Section 3.8, we describe the $\text{Rep}(\mathcal{G})$ anyon condensation phase transitions that are induced by \mathcal{G} -graded MPO algebra symmetry breaking, these phase transitions are dual to gauging a global \mathcal{G} symmetry, we derive the relation between the emergent topological order and the SET that results from the condensation. In Section 3.9, we present several examples that demonstrate different aspects of our formalism, particularly the interplay between Morita equivalence and anyon condensation phase transitions induced by MPO algebra symmetry breaking. In Section 3.10, we present conclusions and future directions.

3.2 A motivating example

We begin with a concrete example that demonstrates the methods developed throughout the paper. In this example we study the relation between the *doubled Ising model*²⁴ and the *toric code*¹⁹ enriched by \mathbb{Z}_2 electromagnetic duality symmetry^{32,33,100}. These models are related by the dual processes of gauging the \mathbb{Z}_2 electromagnetic duality symmetry or condensing a $\text{Rep}(\mathbb{Z}_2)$ subtheory, as follows

$$\begin{array}{ccccc} \text{Toric code} & \xrightleftharpoons[\text{Confine } \mathbb{Z}_2 \text{ defects}]{\text{Add } \mathbb{Z}_2 \text{ defects}} & \mathbb{Z}_2 \text{ symmetry-enriched} & \xrightleftharpoons[\text{Condense } \text{Rep}(\mathbb{Z}_2)]{\text{Gauge } \mathbb{Z}_2 \text{ symmetry}} & \text{Doubled Ising model.} \\ & & \text{toric code} & & \end{array} \quad (3.1)$$

Each of the steps in this diagram can be calculated concretely in the language of tensor networks. To achieve this we summarize the mathematical objects, known as *unitary fusion categories*, from which the toric code and doubled Ising model are built^{166,216}. Using this data, we recount the tensor network description of the toric code and doubled Ising model string-net ground states^{119,120} and the algebras of matrix product operator symmetries they possess⁶³. We present an extension of the fixed point tensor network construction to the recently defined class of symmetry-enriched string-net models^{32,33}, and demonstrate the interplay of the MPO symmetries with the physical symmetry. This extension is based upon the notion of graded unitary fusion categories^{81,97,98}. By viewing the Ising fusion category as a \mathbb{Z}_2 -graded fusion category the authors of Refs. 32,33 were able to construct a local commuting projector Hamiltonian, in two spatial dimensions, with a \mathbb{Z}_2 -enriched toric code topological order where an on-site group action implements the electromagnetic duality of the toric code anyons.

To calculate the action of the symmetry explicitly with the tensor network approach we build upon the anyon ansatz presented in Ref. 64, which is summarized in Section 3.4. In that work, a second algebra — corresponding to *Ocneanu's tube algebra*^{163,212} — was derived from the matrix product operator symmetry algebra of the local tensors. By diagonalizing this tube algebra into irreducible blocks, the topological sectors are constructed. From the projectors onto these blocks, the full set of topological data — characterizing the emergent anyonic excitations — can be extracted. This set of data forms a mathematical object known as a *modular tensor category*^{99,165,166,203,216} which includes an underlying set of anyons, their fusion rules and F -symbols, R matrices which describe braiding processes, as well as the gauge invariant Frobenius-Schur indicators, and the modular S and T matrices.

We extend the tube algebra to a set of $|\mathcal{G}|$ *defect tube algebras* whose irreducible blocks describe the definite topological \mathcal{G} -defect sectors. Similar to the anyon tubes, all topological data of the emergent symmetry-enriched theory can be extracted from the defect tubes. This data constitutes a \mathcal{G} -crossed modular tensor category^{31,81,97,98}, and includes the underlying set of topological defects, their fusion rules and F -symbols, the \mathcal{G} action on the set of defects, the \mathcal{G} -crossed R matrices which describe the braiding of defects, the projective representation carried by each defect and its 2-cocycle $\eta_{a_g}(\mathbf{h}, \mathbf{k})$, and the projective representation on the fusion and splitting spaces $U_g(a_{\mathbf{h}}, b_{\mathbf{k}}; c_{\mathbf{hk}})$, as well as the Frobenius-Schur indicators, and the \mathcal{G} -crossed modular S and T matrices.

Rather than calculating the topological defect sectors of the EM duality enriched toric code directly, we develop an extremely simple recipe to find the effect of $\text{Rep}(\mathbb{Z}_2)$ *anyon condensation* on the tubes of the doubled Ising model. This approach yields the pair of inequivalent topological defect sectors, known as¹⁰⁰ σ_+ , σ_- . We also describe a recipe to calculate the effects of *gauging* the \mathbb{Z}_2 EM duality symmetry on the defect tubes to recover the tubes of the doubled Ising model. We derive relations between the topological data of the models related by the dual gauging and condensation procedures.

3.2.1 Background: Constructing topological sectors in a tensor network

Toric code

The toric code is based on a very simple unitary fusion category $\mathcal{C} = \text{Vec}_{\mathbb{Z}_2}$ built from the algebra $\mathbb{C}[\mathbb{Z}_2]$. We denote the simple objects $\{0, \psi\}$ with abelian multiplication

$$0 \times a = a, \quad \psi \times \psi = 0, \quad (3.2)$$

for $a \in \{0, \psi\}$. The F -symbols are trivial, containing only the fusion constraints

$$F_{def}^{abc} = \delta_{ab}^e \delta_{ec}^d \delta_{bc}^f \delta_{af}^d, \quad (3.3)$$

which are defined by

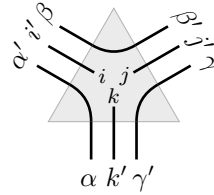
$$\delta_{ab}^c := \begin{cases} 1 & \text{when } a \text{ appears in the fusion product } b \times c \\ 0 & \text{otherwise.} \end{cases} \quad (3.4)$$

A tensor network representation of the toric code ground state on a trivalent lattice can be constructed from these F -symbols, see Eq.(3.6) left. This is a specific instance of the more general tensor network representation of string-net ground states^{63,119,120}. This tensor network specifies a state in a Hilbert space where the qubit degrees of freedom that usually live on edges live in the diagonal subspace of a pair of qubits living on the neighbouring vertices

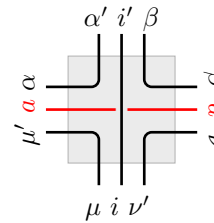
$$\mathbb{C}[\mathbb{Z}_2]_e \cong \text{span}\{|00\rangle, |11\rangle\} \subseteq \mathbb{C}[\mathbb{Z}_2]_u \otimes \mathbb{C}[\mathbb{Z}_2]_v, \quad (3.5)$$

where $\partial e = \{u, v\}$. This convention is used as it avoids the need to define separate tensors on the edges of the tensor network.

This tensor network has a \mathbb{Z}_2 MPO symmetry specified by the tensor on the right of Eq.(3.6).




$$= \delta_{ii'} \delta_{jj'} \delta_{kk'} \delta_{\alpha\alpha'} \delta_{\beta\beta'} \delta_{\gamma\gamma'} F_{\gamma\beta k}^{\alpha ij}, \quad (3.6)$$



$$= \delta_{\alpha\alpha'} \delta_{\beta\beta'} \delta_{\mu\mu'} \delta_{\nu\nu'} \delta_{ii'} \delta_{aa'} F_{\beta\alpha\nu}^{a\mu i}, \quad (3.7)$$

where all labels lie in \mathbb{Z}_2 . Here $a \in \mathbb{Z}_2 \cong \{0, \psi\}$ controls which element of \mathbb{Z}_2 the MPO represents

$$\text{MPO}_a :=$$


$$, \quad (3.8)$$

Furthermore the toric code tensor network is MPO-injective, in the terminology of Ref. 63, with respect to the MPO projector onto the symmetric subspace: $\frac{1}{2}(\text{MPO}_0 + \text{MPO}_\psi)$.

The framework developed in Refs. 63,64,160 demonstrated that calculations involving an algebra of MPO symmetries on the virtual level of an MPO-injective tensor network follow the same rules as the planar isotopy invariant, diagrammatic calculus for unitary fusion categories described in Refs. 203,217,218 and elsewhere. In other words, the properties of an MPO algebra on the virtual level of an MPO-injective tensor network can be abstracted to the diagrammatic calculus for anyons (without braiding).

To see this from another perspective, recall that the vector space associated to a manifold by the Turaev-Viro *topological quantum field theory* (TQFT)^{108,219} — for a given unitary fusion category — is defined to be the space of allowed pictures modulo local relations^{220,221} (this is isomorphic to the ground space of the string net model on that manifold). In this way a tensor network satisfying MPO-injectivity, together with its MPO symmetry algebra, can be thought of as an explicit representation of all pictures that can be reduced to the empty diagram via local relations. In this representation the local relations are implemented by the pulling through equation, together with the local conditions satisfied by the MPOs. We remark that one can construct the full set of different ground states by closing the tensor network using different MPOs, as described below.

The upshot of the previous paragraph is: for the purposes of calculations involving elements of the MPO algebra within an MPO-injective tensor network, we can work at the level of the diagrammatic UFC calculus^{203,217,218}. The MPO-injective tensor network itself can be thought of as a sort of background, and MPOs on the virtual level will become loops on top of this background. For example

The diagrammatic equation (3.16) consists of two rows of diagrams. The top row shows a square grid of circular nodes connected by lines, representing a tensor network background. An equals sign is placed between two such grids. The right grid has a red squiggly line labeled ψ drawn over it. Below each grid is a downward arrow. The bottom row shows two gray squares. The left square is empty, and the right square contains a single squiggly loop. These two squares are separated by a tilde symbol \sim . The equation is labeled (3.16) on the right.

where the ψ loop is depicted as a squiggly line in the diagrammatic calculus. As demonstrated

by this example local relations in the diagrammatic calculus correspond to equalities in the tensor network representation. For this reason we will work with the vector space of diagrams modulo local relations, hence the equivalence above becomes an equality.

As was mentioned above, on a topologically nontrivial manifold the vector space of the Turaev-Viro TQFT may have dimension greater than one. Equivalently the string-net model may have a ground state degeneracy. This appears in the tensor network formalism when one considers closing a disc to form a nontrivial topology. It was shown in Ref. 63 that the MPO-injectivity property is stable under concatenation. That is, one can contract arbitrarily many MPO-injective tensors on a disc and the resulting tensor will maintain the MPO-injectivity property. The resulting tensor network is a PEPS, and hence comes equipped with a frustration free, local, parent Hamiltonian for which it is a ground state⁴⁶. It was also shown in Ref. 63, that the ground space of this Hamiltonian on a disc is spanned by the tensor network on the disc contracted with an arbitrary boundary tensor, see Eq.(3.17), LHS. We remark that the local relations in the bulk give rise to an action of the MPO algebra on the boundary tensor which project it onto the symmetric subspace.

The local tensor in Eq.(3.6) can be used to build a unique state on a closed manifold. However there may be linearly independent states on the same manifold that are constructed from the same tensor on any disc, but also contain virtual level MPOs that are free to move through the tensor network. As a matter of terminology, we will refer to a spanning set of ground states of the local parent Hamiltonian on a given manifold as the set of tensor networks assigned to that manifold by the local tensor.

To form a closed manifold one can consider adding handles to a disc. The simplest choice is to close the disc into a sphere. Even in this case one finds a closure tensor, located on a single link, that is free to move throughout the tensor network⁶³. The different choices for this closure tensor pick out different ground states in an unstable TQFT. Here unstable means that the TQFT has a ground state degeneracy on the sphere. For a stable TQFT, which is always the case when the MPO algebra yields a unitary fusion category, there is a single ground state on the sphere and the closure tensor is trivial. Since an unstable TQFT can be written as a sum of stable TQFTs we will only consider the stable case from here on.

The next example we consider is attaching a 1-handle to a disc to form a cylinder. Before the closure, the class of states we are considering corresponds to the tensor network with arbitrary boundary conditions A , depicted below on the left. After taking the closure we are guaranteed that any disc must look like the original tensor network. Hence the only boundary conditions along the attaching edge that survive are the ones that can be freely deformed through the tensor network. This implies that these boundary condition must be a linear combination of the irreducible MPOs, shown below on the right. This argument was given explicitly in Ref. 63.

The diagram shows an equality between two tensor network expressions. On the left, a grey-shaded disc is shown with a horizontal cut. The top and bottom edges of the cut are labeled A . Dotted lines with arrows indicate a periodic identification of the boundaries. On the right, the same disc is shown, but the cut is now a solid line labeled p . The top and bottom edges of the cut are labeled B_μ and C_μ respectively. The entire expression is equated to a sum over p, μ of c_p times the right-hand side expression.

$$A = \sum_{p, \mu} c_p B_\mu \overset{p}{\text{---}} C_\mu, \quad (3.17)$$

where the dotted lines indicate a periodic identification of the boundaries and the solid line connecting the caps indicates that they are part of the same tensor. Hence all boundary conditions on the cylinder can be divided into an arbitrary tensor $A' := \sum_\mu B_\mu \otimes C_\mu$, acting on the open

left and right boundaries, joined by a linear combination of MPOs along the closure edge. More specifically, the virtual indices of the MPO are contracted with indices of A' .

Similarly, when closing a disc to form a torus, the most general boundary condition is given by a linear combination of MPOs along the cycles of the torus. Furthermore the tensor at their intersection point can be resolved into a linear combination of fusion and splitting vertices, shown below on the right.

$$\begin{array}{c} \text{Diagram: A square with a cross of thick lines. The four quadrants are shaded gray. Arrows on the boundary lines point outwards. } \end{array} B = \sum_{xyz} c_{xy}^z \begin{array}{c} \text{Diagram: A central vertex with four lines extending to the corners. Top-left: x, top-right: y, bottom-left: z, bottom-right: x. The quadrants are shaded gray. Arrows on the boundary lines point outwards. } \end{array} = \sum_{xyz} c_{xy}^z |xyz\rangle. \quad (3.18)$$

For the toric code, a basis for the ground space on the torus is given by

$$|000\rangle = \begin{array}{c} \text{Diagram: A square with a dashed boundary. A dotted line forms a path from the top-left to the bottom-right corner. The quadrants are shaded gray. Arrows on the boundary lines point outwards. } \end{array}, \quad |0\psi\psi\rangle = \begin{array}{c} \text{Diagram: A square with a dashed boundary. A wavy line forms a path from the top-left to the bottom-right corner. The quadrants are shaded gray. Arrows on the boundary lines point outwards. } \end{array}, \quad (3.19)$$

$$|\psi 0\psi\rangle = \begin{array}{c} \text{Diagram: A square with a dashed boundary. A wavy line forms a path from the top-left to the bottom-right corner. The quadrants are shaded gray. Arrows on the boundary lines point outwards. } \end{array}, \quad |\psi\psi 0\rangle = \begin{array}{c} \text{Diagram: A square with a dashed boundary. A wavy line forms a path from the top-left to the bottom-right corner. The quadrants are shaded gray. Arrows on the boundary lines point outwards. } \end{array}. \quad (3.20)$$

To find the superselection sectors within this tensor network, we consider a well separated pair of pointlike excitations on a sphere. This sphere can be stretched out to a cylinder with an excitation at each end. Away from these excitation points the tensor network locally looks the same, hence the whole tensor network is of the form in Eq.(3.17) with A' now also containing physical indices located around each excitation. The local relations in the bulk of the tensor network on the cylinder give rise to an MPO action on each boundary.

$$\begin{array}{c} \text{Diagram: A rectangle with a horizontal line. The top half is shaded gray. Arrows on the boundary lines point outwards. } \end{array} \quad (3.21)$$

$$= \sum_q \delta_{rs}^q \begin{array}{c} \text{Diagram: A rectangle with a horizontal line. The top half is shaded gray. A small square loop is in the bottom half. Arrows on the boundary lines point outwards. } \end{array} = \sum_{qr} \delta_{rs}^q \delta_{sq}^p \begin{array}{c} \text{Diagram: A rectangle with a horizontal line. The top half is shaded gray. A small square loop is in the bottom half. Arrows on the boundary lines point outwards. } \end{array}. \quad (3.22)$$

This defines an algebra acting on each of the punctures. In fact, this is Ocneanu's famous *tube algebra*. We remark that the tube algebra contains a copy of the fusion algebra, generated by \mathcal{T}_{0s0}^s , but is generally distinct from the fusion algebra. The irreducible superselection sectors within a puncture are given by the irreducible blocks of the tube algebra. Projecting onto a superselection sector fixes a definite anyon flux through the puncture. A particular sector can be constructed by projecting onto the corresponding block of the tube algebra using the *irreducible central idempotent* (ICI) that acts as the identity within that block.

We use the following labeling convention for basis elements of the tube algebra

$$\mathcal{T}_{pqr}^s = \begin{array}{c} \text{Diagram: A central vertex with four edges. Top-left edge is labeled } p, \text{ top-right is } s, \text{ bottom-left is } q, \text{ bottom-right is } r. \text{ The top and bottom edges are dashed with arrows pointing outwards. The left and right edges are solid.} \end{array}, \quad (3.23)$$

which corresponds to the minimal tensor network

$$\begin{array}{c} \text{Diagram: A central vertex with four edges. Top-left edge is labeled } p, \text{ top-right is } s, \text{ bottom-left is } q, \text{ bottom-right is } r. \text{ The top and bottom edges are dashed with arrows pointing outwards. The left and right edges are solid.} \end{array}, \quad (3.24)$$

note \mathcal{T}_{pqr}^s is only nonzero when $\delta_{qs}^r \delta_{sq}^p = 1$, hence the dimension of the algebra is given by

$$\sum_{pqrs} \delta_{qs}^r \delta_{sq}^p < |\mathcal{C}|^4,$$

where $|\mathcal{C}|$ is the number of simple objects in the fusion algebra, in this case $|\mathcal{C}| = 2$.

Multiplication of tubes is defined by the stacking operation

$$\mathcal{T}_{pqr}^s \mathcal{T}_{p'q'r'}^{s'} = \delta_{rp'} \begin{array}{c} \text{Diagram: A central vertex with four edges. Top-left edge is labeled } p, \text{ top-right is } s, \text{ bottom-left is } q, \text{ bottom-right is } r. \text{ The top and bottom edges are dashed with arrows pointing outwards. The left and right edges are solid.} \end{array} = \delta_{rp'} \sum_{q''s''} F_{q'rq''}^{sq's'} F_{pq's''}^{q''s's'} F_{r'q's''}^{s'sq''} \mathcal{T}_{pq''r'}^{s''}, \quad (3.25)$$

where the only tubes $\mathcal{T}_{pq''r'}^{s''}$ that appear on the RHS with nonzero coefficients satisfy $\delta_{ss'}^{s''}$. Hermitian conjugation is given by

$$(\mathcal{T}_{pqr}^s)^\dagger = \begin{array}{c} \text{Diagram: A central vertex with four edges. Top-left edge is labeled } s, \text{ top-right is } p, \text{ bottom-left is } r, \text{ bottom-right is } q. \text{ The top and bottom edges are dashed with arrows pointing outwards. The left and right edges are solid.} \end{array} = \sum_{q'} F_{pq'q}^{sr's} \mathcal{T}_{rq'p}^s. \quad (3.26)$$

With this notation Eq.(3.21) becomes

$$\mathcal{T}_{rrr}^0 = \sum_{pq} (\mathcal{T}_{pqr}^s)^\dagger \mathcal{T}_{ppp}^0 \mathcal{T}_{pqr}^s. \quad (3.27)$$

We have verified that the tube algebra is closed under multiplication and Hermitian conjugation. Hence the tube algebra is a C^* algebra, spanned by the tubes in Eq.(3.23) and can be block diagonalized.

The toric code tube algebra is spanned by the following basis elements

$$\mathcal{T}_{000}^0 = \begin{array}{c} \text{Diagram: A central vertex with four edges. Top-left edge is dashed with an arrow pointing outwards, top-right is dotted, bottom-left is dotted, bottom-right is dashed with an arrow pointing outwards.} \end{array}, \quad \mathcal{T}_{0\psi 0}^\psi = \begin{array}{c} \text{Diagram: A central vertex with four edges. Top-left edge is dashed with an arrow pointing outwards, top-right is wavy, bottom-left is dotted, bottom-right is wavy.} \end{array}, \quad (3.28)$$

$$\mathcal{T}_{\psi\psi\psi}^0 = \begin{array}{c} \text{Diagram: A central vertex with four edges. Top-left edge is dotted, top-right is wavy, bottom-left is wavy, bottom-right is dotted.} \end{array}, \quad \mathcal{T}_{\psi 0 \psi}^\psi = \begin{array}{c} \text{Diagram: A central vertex with four edges. Top-left edge is wavy, top-right is dotted, bottom-left is dotted, bottom-right is wavy.} \end{array}. \quad (3.29)$$

We remark that this tube algebra splits into two copies of $\mathbb{C}[\mathbb{Z}_2]$ and hence is diagonalized by a set of projectors onto the irreps of each \mathbb{Z}_2 . These projectors are summarized in the following table

Anyons	\mathcal{T}_{000}^0	$\mathcal{T}_{0\psi 0}^\psi$	$\mathcal{T}_{\psi\psi\psi}^0$	$\mathcal{T}_{\psi 0\psi}^\psi$
0	1	1		
e	1	-1		
m			1	1
em			1	-1

(3.30)

which contains the coefficients of each ICI. In this table — and for all superselection sector tables throughout the paper — we suppress a normalization by the quantum dimension squared \mathcal{D}^2 , which gives 2 in this case. Hence the ICIs of the toric code are given by

$$\underline{0} = \frac{1}{2}(\mathcal{T}_{000}^0 + \mathcal{T}_{0\psi 0}^\psi), \quad \underline{e} = \frac{1}{2}(\mathcal{T}_{000}^0 - \mathcal{T}_{0\psi 0}^\psi), \quad (3.31)$$

$$\underline{m} = \frac{1}{2}(\mathcal{T}_{\psi\psi\psi}^0 + \mathcal{T}_{\psi 0\psi}^\psi), \quad \underline{em} = \frac{1}{2}(\mathcal{T}_{\psi\psi\psi}^0 - \mathcal{T}_{\psi 0\psi}^\psi). \quad (3.32)$$

We remark that the vacuum $\underline{0}$ superselection sector is always given by the projector onto the symmetric subspace of the fusion algebra generated by \mathcal{T}_{0s0}^s . To justify the labeling of the other superselection sectors, we need a method to extract the physical data characterizing the anyon theory from the ICIs. The S and T matrices of the emergent topological theory are independent of any gauge choice in defining the input fusion category. These invariants are conjectured to be complete for non-chiral theories, which are precisely those arising from the double construction we have described.

On the tube algebra S and T are defined as

$$S(\mathcal{T}_{pqr}^s) := \delta_{pr} \text{ (diagram)} = \sum_{q'} F_{pq'q}^{sps} \mathcal{T}_{sq's}^p, \quad T(\mathcal{T}_{pqr}^s) := \mathcal{T}_{p1p}^p \mathcal{T}_{pqr}^s, \quad (3.33)$$

$$S(\underline{a}) = \sum_{\underline{b}} S_{ab} \underline{b}, \quad T(\underline{a}) = \theta_a \underline{a}, \quad (3.34)$$

in writing the second formula for S we have assumed that all idempotents have dimension one, which is true for the toric code example. The general formula is given in Section 3.3, Eq.(3.146). We remark that S corresponds to changing basis on the torus from a definite flux through the y -cycle to a definite flux through the x -cycle. Similarly T corresponds to a Dehn twist along the y -cycle of the torus with definite flux through the y -cycle, or equivalently a 2π rotation of a superselection sector.

For toric code S and T are given by

$\mathcal{D}^2 S$	0	e	m	em
0	1	1	1	1
e	1	1	-1	-1
m	1	-1	1	-1
em	1	-1	-1	1

T	0	e	m	em
0	1			
e		1		
m			1	
em				-1

(3.35)

We remark the normalization of the S matrix by \mathcal{D}^2 refers to the quantum dimension of the input fusion category which satisfies $\mathcal{D}^2 = \mathcal{D}_{\text{out}}$. In this example the normalization is $\mathcal{D}^2 = 2$. The T matrix uniquely identifies the em sector as it is the only fermion in the theory. However one can see that the choice of e and m sectors is arbitrary as the data is invariant under swapping e with m . This is an EM duality \mathbb{Z}_2 symmetry of the toric code. In the next section we will construct the symmetry enriched toric code, including the EM duality defects.

In fact we can also extract the full set of gauge-variant data, the F and R symbols, that define the emergent topological theory from the ICIs. The ICIs can be used to construct a realization of the emergent theory, which may be of use for topological quantum computation in wavefunctions that admit a tensor network description.

Throughout this subsection all explanations were given with the toric code in mind and hence many subtleties have been left out. In particular we neglected orientation dependence, factors of the quantum dimension, pivotal phases, Frobenius-Schur indicators and possible fusion degeneracy. These subtleties are covered in Section 3.3.

Doubled Ising model

The Ising fusion category is based on an algebra of three objects which we denote $\{0, \psi, \sigma\}$ with commutative multiplication rules

$$0 \times a = a, \quad \psi \times \psi = 0, \quad \sigma \times \psi = \sigma, \quad \sigma \times \sigma = 0 + \psi, \quad (3.36)$$

for $a \in \{0, \psi, \sigma\}$. The quantum dimensions are $d_0 = 1, d_\psi = 1, d_\sigma = \sqrt{2}$, hence $\mathcal{D}^2 = 4$. The nontrivial F -symbols are given by

$$[F_\sigma^{\sigma\sigma\sigma}]_i^j = \frac{1}{\sqrt{2}} \begin{bmatrix} 1 & 1 \\ 1 & -1 \end{bmatrix}, \quad [F_\psi^{\sigma\psi\sigma}]_\sigma = [F_\sigma^{\psi\sigma\psi}]_\sigma = -1, \quad (3.37)$$

for $i, j \in \{0, \psi\}$. The remaining F -symbols are either 0 or 1, which is completely determined by the convention that $[F_d^{abc}]_e^f$ contains the constraint $\delta_{ab}^e \delta_{ec}^d \delta_{bc}^f \delta_{af}^d$, defined in Eq.(3.4). One can check that these F -symbols satisfy the pentagon equation. We remark that $\text{Vec}_{\mathbb{Z}_2}$ is contained as a subcategory of Ising, generated by the objects $\{0, \psi\}$. This observation is the basis of the construction in Section 3.2.2.

The tensor network and MPO algebra for the Ising model are defined in a similar fashion to the toric code example. Both examples fall under the general case that covers all string-net models^{63,64}, which is described in Section 3.3. Here we will skip directly to the tube algebra. The construction of the tube algebra proceeds similarly to the toric code, but one must also deal with the appearance of quantum dimensions. For an explanation of the explicit details we have skipped over see Section 3.3.

The Ising tube algebra is twelve dimensional and is spanned by the tubes in Eq.(3.28),

together with the following

$$\mathcal{T}_{\sigma\sigma\sigma}^0 = \text{diagram}, \quad \mathcal{T}_{\sigma\sigma\sigma}^\psi = \text{diagram}, \quad \mathcal{T}_{0\sigma 0}^\sigma = \text{diagram}, \quad (3.38)$$

$$\mathcal{T}_{\psi\sigma\psi}^\sigma = \text{diagram}, \quad \mathcal{T}_{\sigma 0\sigma}^\sigma = \text{diagram}, \quad \mathcal{T}_{\sigma\psi\sigma}^\sigma = \text{diagram}, \quad (3.39)$$

$$\mathcal{T}_{\psi\sigma 0}^\sigma = \text{diagram}, \quad \mathcal{T}_{0\sigma\psi}^\sigma = \text{diagram}, \quad (3.40)$$

The coefficients of the ICIs that determine the superselection sectors of the tensor network are given by

Anyons	\mathcal{T}_{000}^0	$\mathcal{T}_{0\psi 0}^\psi$	$\mathcal{T}_{\psi\psi\psi}^0$	$\mathcal{T}_{\psi 0\psi}^\psi$	$\mathcal{T}_{\sigma\sigma\sigma}^0$	$\mathcal{T}_{\sigma\sigma\sigma}^\psi$	$\mathcal{T}_{0\sigma 0}^\sigma$	$\mathcal{T}_{\psi\sigma\psi}^\sigma$	$\mathcal{T}_{\sigma 0\sigma}^\sigma$	$\mathcal{T}_{\sigma\psi\sigma}^\sigma$
0	1	1					$\sqrt{2}$			
$\psi\bar{\psi}$	1	1					$-\sqrt{2}$			
ψ			1	-1				$-i\sqrt{2}$		
$\bar{\psi}$			1	-1				$i\sqrt{2}$		
$\sigma\bar{\sigma}$	2	-2	2	2						
σ					1	$-i$		$e^{-\frac{\pi i}{8}}$	$e^{\frac{3\pi i}{8}}$	
$\sigma\bar{\psi}$					1	$-i$		$e^{\frac{7\pi i}{8}}$	$e^{-\frac{5\pi i}{8}}$	
$\bar{\sigma}$					1	i		$e^{\frac{\pi i}{8}}$	$e^{-\frac{3\pi i}{8}}$	
$\psi\bar{\sigma}$					1	i		$e^{-\frac{7\pi i}{8}}$	$e^{\frac{5\pi i}{8}}$	

(3.41)

where we have suppressed a normalization by $\mathcal{D}^2 = 4$. To be explicit, the table should be read as follows

$$\underline{a_i} = \frac{1}{\mathcal{D}^2} \sum_j t_i^j (\mathcal{T}_{pqr}^s)_j, \quad (3.42)$$

where a_i is the i -th anyon row label, $(\mathcal{T}_{pqr}^s)_j$ is the j -th tube column label, and t_{ij} is the (i, j) -th table entry. We remark that our normalization convention for the tubes \mathcal{T}_{pqr}^s differs slightly from that in Ref. 64 by a factor $\sqrt{d_s}$, after adjusting for this difference our results match those reported in Ref. 64.

In the Ising tube algebra the $\sigma\bar{\sigma}$ block is two dimensional. The full block, including off diagonal elements, is given by

$$\begin{aligned} \underline{\sigma\bar{\sigma}}_{00} &= \frac{1}{2}(\mathcal{T}_{000}^0 - \mathcal{T}_{0\psi 0}^\psi) & \underline{\sigma\bar{\sigma}}_{01} &= \frac{1}{\sqrt{2}}\mathcal{T}_{0\sigma\psi}^\sigma \\ \underline{\sigma\bar{\sigma}}_{10} &= \frac{1}{\sqrt{2}}\mathcal{T}_{\psi\sigma 0}^\sigma & \underline{\sigma\bar{\sigma}}_{11} &= \frac{1}{2}(\mathcal{T}_{\psi\psi\psi}^0 + \mathcal{T}_{\psi 0\psi}^\psi). \end{aligned} \quad (3.43)$$

To justify the labeling of the particles we have calculated the S and T matrices from the ICIs using the formula in Section 3.3, Eq.(3.146). Note that since $\underline{\sigma\bar{\sigma}}$ is a two dimensional block, the S matrix is defined in terms of its action on the normalized ICI $\frac{1}{2}\underline{\sigma\bar{\sigma}}$.

$$\mathcal{D}^2 S = \begin{array}{c|ccc} & 0 & \psi & \sigma \\ \hline 0 & 1 & 1 & \sqrt{2} \\ \psi & 1 & 1 & -\sqrt{2} \\ \sigma & \sqrt{2} & -\sqrt{2} & 0 \end{array} \otimes \begin{array}{c|ccc} & \bar{0} & \bar{\psi} & \bar{\sigma} \\ \hline 0 & 1 & 1 & \sqrt{2} \\ \bar{\psi} & 1 & 1 & -\sqrt{2} \\ \bar{\sigma} & \sqrt{2} & -\sqrt{2} & 0 \end{array} \quad (3.44)$$

$$T = \begin{array}{c|ccc} & 0 & \psi & \sigma \\ \hline 0 & 1 & & \\ \psi & & -1 & \\ \sigma & & & e^{\frac{\pi i}{8}} \end{array} \otimes \begin{array}{c|ccc} & \bar{0} & \bar{\psi} & \bar{\sigma} \\ \hline 0 & 1 & & \\ \bar{\psi} & & -1 & \\ \bar{\sigma} & & & e^{-\frac{\pi i}{8}} \end{array} \quad (3.45)$$

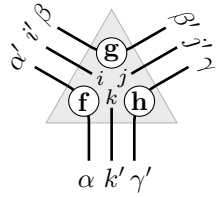
We remark the S and T matrices have a tensor product structure since the input Ising fusion category admits a modular braiding. This implies $\mathcal{Z}(\text{Ising}) \cong \text{Ising}^{(1)} \boxtimes \overline{\text{Ising}}^{(1)}$, where $\text{Ising}^{(1)}$ denotes the Ising theory equipped with the modular braiding³¹.

3.2.2 Symmetry-enriched tensor networks from anyon condensation

\mathbb{Z}_2 -paramagnet from the toric code

To demonstrate the condensation procedure we note the toric code trivially has a \mathbb{Z}_2 -grading $\mathcal{C}_1 \oplus \mathcal{C}_x = \{0\} \oplus \{\psi\}$, where we use the following presentation $\mathbb{Z}_2 \cong \langle \mathbf{x} \mid \mathbf{x}^2 = \mathbf{1} \rangle$. We make use of the notation $\psi_{\mathbf{x}}$ to indicate $\psi \in \mathcal{C}_{\mathbf{x}}$ and $[\psi] = \mathbf{x}$ to indicate the sector containing ψ . In this example each sector contains only a single simple object, so there is no need to keep track of the sector label separately. However, we will explicitly keep track of the sectors to prepare the reader for more complicated examples.

The tensors for the symmetry-enriched model^{32,33} are given by a simple modification of the string-net tensors, which amounts to promoting the sector label of the virtual indices to a physical degree of freedom.



$$= \delta_{\mathbf{f}[\alpha]} \delta_{\mathbf{g}[\beta]} \delta_{\mathbf{h}[\gamma]} \delta_{ii'} \delta_{jj'} \delta_{kk'} \delta_{\alpha\alpha'} \delta_{\beta\beta'} \delta_{\gamma\gamma'} F_{\gamma\beta k}^{\alpha i j}, \quad (3.46)$$

The set of MPOs for the SET string-net tensor are still given by Eq.(3.6), we simply reinterpret them in light of the additional \mathcal{G} -grading structure. Hence the $\mathbf{1}$ sector of the MPO algebra is given by MPO_0 and the \mathbf{x} sector is given by MPO_{ψ} . Since we are using the same MPOs they still satisfy the zipper condition, F -move, and the bubble popping relation introduced in Section 3.2.1.

The pulling through equation must be modified in accordance with the \mathcal{G} -grading. That is,

pulling through an MPO in sector \mathbf{g} results in a \mathbf{g} action on the physical indices

$$(3.47)$$

where

$$(3.48)$$

Similar to the purely topological case, the calculations involving MPOs within a tensor network that satisfies the SET pulling through condition can be abstracted to a diagrammatic calculus. This calculus additionally involves discs that are labeled by group elements, which represent the application of the on-site symmetry to the tensor network within the labeled region. For example

$$(3.49)$$

where the $\mathbf{1}$ label, corresponding to the action of the trivial element, remains implicit. This corresponds to a diagrammatic calculus for a 2-category²²² where the set of objects is \mathcal{G} , the morphisms from \mathbf{g} to \mathbf{h} are given by the objects in $\mathcal{C}_{\mathbf{g}\mathbf{h}}$, and the 2-morphisms are given by the 1-morphisms of $\mathcal{C}_{\mathcal{G}}$.

The emergent SET order of the tensor network is described by a unitary \mathcal{G} -crossed braided fusion category. This mathematical structure captures the topological properties of monodromy defects as they braid and fuse. The inequivalent monodromy defects for a given $\mathbf{g} \in \mathcal{G}$ correspond to the superselection sectors at the end point of a \mathbf{g} domain wall. The defect superselection sectors can be calculated using a modification of the tube algebra, which is described in Section 3.6.

The SET is intimately related to a topological order obtained by gauging the \mathcal{G} symmetry^{31,102}, which can be done directly on the lattice^{71,93,223}, see Chapter 1. The superselection sectors of the gauged topological order can be derived from the defect superselection sectors and the action of the group upon them. Alternatively, the defect sectors of the SET can be found via a $\text{Rep}(\mathcal{G})$ condensation²¹⁵ procedure on the gauged topological order.

Here we demonstrate the effect of condensing $\text{Rep}(\mathbb{Z}_2)$ on the toric code tubes. This is implemented by dividing the tube algebra into $\mathbf{1}$ and \mathbf{x} sectors, according to the group element $[p] = [r]$ in \mathcal{T}_{pqr}^s . Next we simply drop the basis elements \mathcal{T}_{pqr}^s with $[s] = \mathbf{x}$, corresponding

to a ψ line wrapping the tube, from the tube algebra. The ICIs in the $\mathbf{1}$ sector correspond to anyons or $\mathbf{1}$ -defects, while those in the \mathbf{x} sector correspond to \mathbf{x} -defects. Since the defect tube algebra in each sector becomes one dimensional, we find only the vacuum anyon and a single \mathbf{x} -defect, $\Delta_{\mathbf{x}}$.

Anyons	\mathcal{T}_{000}^0	$\mathcal{T}_{0\psi 0}^\psi$	$\mathcal{T}_{\psi\psi\psi}^0$	$\mathcal{T}_{\psi 0\psi}^\psi$
0	1	1		
e	1	-1		
m			1	1
em			1	-1

\Downarrow

(3.50)

Sectors	Defects	Condensed anyons	\mathcal{T}_{000}^0	$\mathcal{T}_{\psi\psi\psi}^0$	\mathbb{Z}_2 -action	
					$\mathcal{T}_{0\psi 0}^\psi$	$\mathcal{T}_{\psi 0\psi}^\psi$
$\mathbf{1}$	0	0	1		1	
		e	1			
\mathbf{x}	$\Delta_{\mathbf{x}}$	m		1		1
		em		1		

In the lower table we retain the implicit normalization of $\mathcal{D}^2 = 2$, from the toric code, in the coefficients of the ICIs. However, we also have multiple contributions to each defect ICI from the different anyon ICIs that condense into it. In this case the factors cancel and we simply have

$$\underline{0} = \mathcal{T}_{000}^0 \quad \underline{\Delta_{\mathbf{x}}} = \mathcal{T}_{\psi\psi\psi}^0. \quad (3.51)$$

From the table we see that the $\text{Rep}(\mathbb{Z}_2)$ boson which condensed was the e particle of the toric code. By picking a different tensor network representation of the toric code one can also realize the equivalent condensation of m . The result is a trivial topological order with a single \mathbb{Z}_2 defect. Since the underlying topological order is trivial, the model is an SPT which is classified by the cohomology class of the associator for the defects. This label lies in $\mathcal{H}^3(\mathcal{G}, \text{U}(1))$ and for this example it is trivial. Hence we have found a trivial \mathbb{Z}_2 -paramagnet as expected.

The tubes that were dropped to make the defect tube algebra can now be used to realize the action of the symmetry on the defect sectors. This is achieved by projecting the collection of discarded tubes onto each defect ICI. Hence we find the action $\mathcal{T}_{0\psi 0}^\psi$ on the vacuum, as expected, and $\mathcal{T}_{\psi 0\psi}^\psi$ acting on the $\Delta_{\mathbf{x}}$ defect. These actions generate linear representations of \mathbb{Z}_2 , note the identity in each sector is given by the corresponding defect ICI.

With the representation of the symmetry for each defect we can also calculate the effect of gauging the \mathbb{Z}_2 symmetry. Specifically there is a simple recipe to calculate the full set of anyon ICIs of the gauged theory. For each defect the post-gauging anyon ICIs are given by the projectors onto the irreps of the group action on that defect. In the toric code example this implies

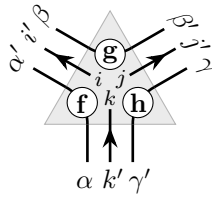
$$\underline{0} \mapsto \begin{aligned} \frac{1}{2}(\mathcal{T}_{000}^0 + \mathcal{T}_{0\psi 0}^\psi) &= \underline{0} \\ \frac{1}{2}(\mathcal{T}_{000}^0 - \mathcal{T}_{0\psi 0}^\psi) &= \underline{e} \end{aligned} \quad \underline{\Delta_{\mathbf{x}}} \mapsto \begin{aligned} \frac{1}{2}(\mathcal{T}_{\psi\psi\psi}^0 + \mathcal{T}_{\psi 0\psi}^\psi) &= \underline{m} \\ \frac{1}{2}(\mathcal{T}_{\psi\psi\psi}^0 - \mathcal{T}_{\psi 0\psi}^\psi) &= \underline{em} \end{aligned}. \quad (3.52)$$

We remark that there are much simpler ways to analyze the condensation / gauging procedure for the toric code, we have included it here to demonstrate our general approach on a familiar example.

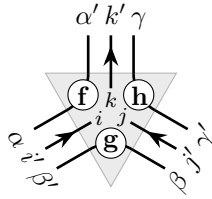
Symmetry-enriched toric code from the doubled Ising model

The Ising fusion category has a \mathbb{Z}_2 -graded structure $\mathcal{C}_1 \oplus \mathcal{C}_x = \{0, \psi\} \oplus \{\sigma\}$. In this case there are two simple objects in the trivial sector, so it is necessary to keep track of the object and sector index separately.

A tensor network representation of the recently introduced SET string-net models^{32,33} is given by the following tensors



$$= \delta_{\mathbf{f}[\alpha]} \delta_{\mathbf{g}[\beta]} \delta_{\mathbf{h}[\gamma]} \delta_{ii'} \delta_{jj'} \delta_{kk'} \delta_{\alpha\alpha'} \delta_{\beta\beta'} \delta_{\gamma\gamma'} \frac{d_i^{\frac{1}{4}} d_j^{\frac{1}{4}} F_{\gamma\beta k}^{\alpha ij}}{d_k^{\frac{1}{4}} \sqrt{d_\beta}}, \quad (3.53)$$

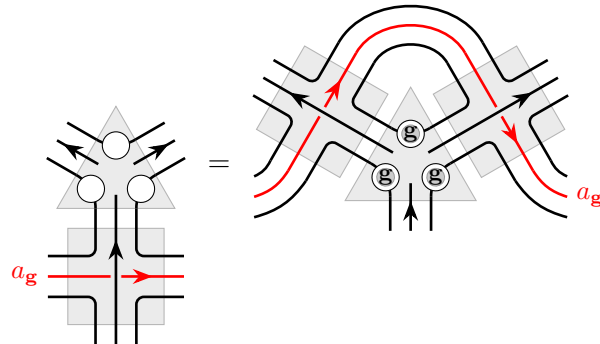


$$= \delta_{\mathbf{f}[\alpha]} \delta_{\mathbf{g}[\beta]} \delta_{\mathbf{h}[\gamma]} \delta_{ii'} \delta_{jj'} \delta_{kk'} \delta_{\alpha\alpha'} \delta_{\beta\beta'} \delta_{\gamma\gamma'} \frac{d_i^{\frac{1}{4}} d_j^{\frac{1}{4}} F_{\gamma\beta k}^{\alpha ij*}}{d_k^{\frac{1}{4}} \sqrt{d_\beta}}, \quad (3.54)$$

where the F -symbols are those of the input \mathcal{G} -graded fusion category. For the current example they are given in Eq.(3.37). We remark that the tensors are related by a combination of reflection and complex conjugation.

The MPOs for this tensor network are the same as those for the usual string-net²⁴, which are described in Section 3.3. However, the MPOs in the \mathbf{g} -sector now represent \mathbf{g} -domain walls. The multiplication of these MPOs is \mathbb{Z}_2 -graded, and in particular $\{\frac{1}{2}(\text{MPO}_0 + \text{MPO}_\psi), \frac{1}{\sqrt{2}}\text{MPO}_\sigma\}$ forms a representation of \mathbb{Z}_2 .

These domain walls require a group action to be moved through the lattice. This is captured by the symmetry-enriched pulling through equation



$$= \quad (3.55)$$

The diagram shows an equality between two tensor network configurations. On the left, a network of black and red strings (labeled a_g) is shown, with some strings passing through shaded gray regions. On the right, the same network is simplified into a configuration where the strings are straight and pass through circles labeled g . The equation is labeled (3.56).

We have used the notation defined in Eq.3.47 for the group action on the physical indices. The second equation is obtained from the first via complex conjugation and reflection. All other pulling through configurations can be derived from Eq.(3.55) by using properties of the string-net MPO given in Section 3.3.

The defect tube algebra is spanned by the subset of Ising tubes \mathcal{T}_{pqr}^s , given in Section 3.2.1, with $s \in \{0, \psi\}$. The algebra is \mathbb{Z}_2 -graded, with the $\mathbf{1}$ sector containing tubes with $[p] = [q] = \mathbf{1}$, and the \mathbf{x} sector containing those with $[p] = [q] = \mathbf{x}$. The ICIs can be found by condensing the $\text{Rep}(\mathbb{Z}_2)$ boson in doubled Ising, corresponding to the \mathbb{Z}_2 grading of the input Ising fusion category. First the — possibly non-central — irreducible idempotents of the defect tube algebra are derived from those of the doubled Ising model, given in Eq.(3.41), by simply dropping the elements \mathcal{T}_{pqr}^s with $s = \sigma$. In this case all the resulting idempotents turn out to be central in the defect tube algebra. In particular the two non-central irreducible idempotents in the $\sigma\bar{\sigma}$ block of doubled Ising split into distinct sectors after condensation. The results are summarized in the following table.

Sectors	Defects	Condensed anyons	\mathcal{T}_{000}^0	$\mathcal{T}_{0\psi 0}^\psi$	$\mathcal{T}_{\psi\psi\psi}^0$	$\mathcal{T}_{\psi 0\psi}^\psi$	$\mathcal{T}_{\sigma\sigma\sigma}^0$	$\mathcal{T}_{\sigma\sigma\sigma}^\psi$
1	0	0	1	1				
		$\psi\bar{\psi}$	1	1				
	em	$\frac{\psi}{\bar{\psi}}$			1	-1		
	e	$\sigma\bar{\sigma}_{00}$	2	-2	1	-1		
	m	$\sigma\bar{\sigma}_{11}$			2	2		
x	σ_+	$\frac{\sigma}{\sigma\bar{\psi}}$					1	$-i$
		$\bar{\sigma}$					1	$-i$
	σ_-	$\bar{\sigma}$					1	i
		$\psi\bar{\sigma}$					1	i

The left table carries over the implicit normalization of $\mathcal{D}^2 = 4$ from Eq.(3.41), but there are also two contributions to each of the condensed defects, except e and m . For example we have $\underline{0} = \frac{1}{2}(\mathcal{T}_{000}^0 + \mathcal{T}_{0\psi 0}^\psi)$.

Each defect sector, \underline{a} , carries a \mathbb{Z}_2 action, \mathcal{B}_a^g . This is found by projecting the Ising tubes that were thrown away onto the ICI of each sector and normalizing the results so that they satisfy the unitarity condition $(\mathcal{B}_a^g)^\dagger \mathcal{B}_a^g = \underline{a}$.

$$K (c_0 \mathcal{T}_{0\sigma 0}^\sigma + c_1 \mathcal{T}_{\psi\sigma\psi}^\sigma + c_2 \mathcal{T}_{\psi\sigma 0}^\sigma + c_3 \mathcal{T}_{0\sigma\psi}^\sigma + c_4 \mathcal{T}_{\sigma 0\sigma}^\sigma + c_5 \mathcal{T}_{\sigma\psi\sigma}^\sigma) \underline{a} = \mathcal{B}_a^x, \quad (3.58)$$

for arbitrary constants $c_i \in \mathbb{C}$ and some positive constant normalization K that depends on the c_i . We remark that certain specific choices of c_i can result in a zero projection, but any generic choice will lead to a nonzero result. There is a gauge freedom in the definition of $\mathcal{B}_a^{\mathbf{x}}$ corresponding to multiplication by a coboundary. In particular, one can always choose $\mathcal{B}_a^1 = \underline{a}$ for all \underline{a} .

Sectors	Defects	\mathbb{Z}_2 -action							
		$\mathcal{T}_{0\sigma 0}^\sigma$	$\mathcal{T}_{\psi\sigma\psi}^\sigma$	$\mathcal{T}_{0\sigma\psi}^\sigma$	$\mathcal{T}_{\psi\sigma 0}^\sigma$	$\mathcal{T}_{\sigma 0\sigma}^\sigma$	$\mathcal{T}_{\sigma\psi\sigma}^\sigma$		
1	0	$\sqrt{2}$							
	em	$\sqrt{2}$							
	e	$\sqrt{2}$							
	m	$\sqrt{2}$							
x	σ_+					$e^{-\frac{\pi i}{4}}$	$e^{\frac{\pi i}{4}}$		
	σ_-					$e^{\frac{\pi i}{4}}$	$e^{-\frac{\pi i}{4}}$		

(3.59)

The resulting $\mathcal{B}_a^{\mathbf{x}}$ for the symmetry-enriched toric code are contained in Eq.(3.59), note there is an implicit normalization by $\mathcal{D}_1^2 = 2$ there. We remark that the tubes which were thrown away correspond to an **x** domain wall, hence projecting them onto a defect captures the action of the **x** domain wall.

The nontrivial group element **x** may permute each defect \underline{a} , resulting in a defect ${}^{\mathbf{x}}\underline{a}$, this permutation is found by considering

$$\mathcal{B}_a^{\mathbf{x}}(\mathcal{B}_a^{\mathbf{x}})^\dagger = {}^{\mathbf{x}}\underline{a}. \quad (3.60)$$

In our example we find the only permutation corresponds to the EM duality ${}^{\mathbf{x}}\underline{e} = \underline{m}$, ${}^{\mathbf{x}}\underline{m} = \underline{e}$ as expected. This is summarized in the following table

$\rho_{\mathbf{x}}$	${}^{\mathbf{x}}0$	${}^{\mathbf{x}}em$	${}^{\mathbf{x}}e$	${}^{\mathbf{x}}m$	${}^{\mathbf{x}}\sigma_+$	${}^{\mathbf{x}}\sigma_-$
0	1					
em		1				
e				1		
m			1			
σ_+					1	
σ_-						1

(3.61)

For each defect, the action of the subgroup that does not permute it may form a projective representation. For our example we find

$$(\mathcal{B}_0^{\mathbf{x}})^2 = \mathcal{B}_0^1, \quad (\mathcal{B}_{em}^{\mathbf{x}})^2 = -\mathcal{B}_{em}^1, \quad (\mathcal{B}_{\sigma_+}^{\mathbf{x}})^2 = e^{-\frac{\pi i}{4}} \mathcal{B}_{\sigma_+}^1, \quad (\mathcal{B}_{\sigma_-}^{\mathbf{x}})^2 = e^{\frac{\pi i}{4}} \mathcal{B}_{\sigma_-}^1. \quad (3.62)$$

Note, the symmetry groups preserving \underline{e} and \underline{m} are trivial. In this case the projective phases of the **x**-defect sectors can be trivialized by a gauge transformation.

The $\mathcal{B}_{ag}^{\mathbf{h}}$ domain walls determine a basis of minimally entangled states for each symmetry twisted sector on the torus. The state $|\mathcal{B}_{ag}^{\mathbf{h}}\rangle$ is given by a linear combination of states derived

from basis elements of the tube algebra

$$|p_{\mathbf{g}} s_{\mathbf{h}} q_{\mathbf{g}\bar{\mathbf{h}}}\rangle = \text{Diagram} \quad (3.63)$$

The coefficient of each state is determined by those of $\mathcal{B}_{a_{\mathbf{g}}}^{\mathbf{h}}$ expanded in the tube basis. For a more detailed description see Eq.(3.280). For this state to be nonzero we must have $^{\mathbf{h}}a = a$, as the periodic boundary conditions imply that the following tubes yield the same state

$$\mathcal{B}_{a_{\mathbf{g}}}^{\mathbf{h}} = \mathcal{B}_{a_{\mathbf{g}}}^{\mathbf{h}} \underline{a} \sim \underline{a} \mathcal{B}_{a_{\mathbf{g}}}^{\mathbf{h}} = \delta_{^{\mathbf{h}}a a} \mathcal{B}_{a_{\mathbf{g}}}^{\mathbf{h}}. \quad (3.64)$$

Hence the dimension of the (\mathbf{g}, \mathbf{h}) -twisted sector is equal to the number of \mathbf{h} -invariant \mathbf{g} -defects.

The $\mathcal{B}_{a_{\mathbf{g}}}^{\mathbf{h}}$ domain walls, satisfying $^{\mathbf{h}}a = a$, give rise to \mathcal{G} -crossed S and T matrices. These matrices are defined by their action on tube basis elements, which is described in Eq.(3.146). They satisfy

$$\frac{1}{D_a} S(\mathcal{B}_{a_{\mathbf{g}}}^{\mathbf{h}}) = \sum_{b_{\mathbf{h}}} \frac{S_{a_{\mathbf{g}} b_{\mathbf{h}}}}{D_b} \mathcal{B}_{b_{\mathbf{h}}}^{\bar{\mathbf{g}}}, \quad T(\mathcal{B}_{a_{\mathbf{g}}}^{\mathbf{h}}) = \theta_a \mathcal{B}_{a_{\mathbf{g}}}^{\mathbf{g}\mathbf{h}}, \quad (3.65)$$

$$S_{a_{\mathbf{g}} b_{\mathbf{h}}} = \frac{D_b \text{Tr}[(\mathcal{B}_{b_{\mathbf{h}}}^{\bar{\mathbf{g}}})^\dagger S(\mathcal{B}_{a_{\mathbf{g}}}^{\mathbf{h}})]}{D_a \text{Tr}[(\mathcal{B}_{b_{\mathbf{h}}}^{\bar{\mathbf{g}}})^\dagger \mathcal{B}_{b_{\mathbf{h}}}^{\bar{\mathbf{g}}}]}, \quad \theta_a \delta_{ab} = \frac{D_b \text{Tr}[(\mathcal{B}_{b_{\mathbf{h}}}^{\bar{\mathbf{g}}})^\dagger T(\mathcal{B}_{a_{\mathbf{g}}}^{\mathbf{h}})]}{D_a \text{Tr}[(\mathcal{B}_{b_{\mathbf{h}}}^{\bar{\mathbf{g}}})^\dagger \mathcal{B}_{b_{\mathbf{h}}}^{\bar{\mathbf{g}}}]}, \quad (3.66)$$

where we have assumed that the defect ICIs are one dimensional for the top left equality for S , which is true for the current example.

For the current example the \mathcal{G} -crossed modular matrices are given by

$\mathcal{D}_1^2 S$	$(\mathbf{1}, \mathbf{1})$				$(\mathbf{1}, \mathbf{x})$		$(\mathbf{x}, \mathbf{1})$		(\mathbf{x}, \mathbf{x})	
	0	em	e	m	$\mathcal{B}_0^{\mathbf{x}}$	$\mathcal{B}_{em}^{\mathbf{x}}$	σ_+	σ_-	$\mathcal{B}_{\sigma_+}^{\mathbf{x}}$	$\mathcal{B}_{\sigma_-}^{\mathbf{x}}$
$(\mathbf{1}, \mathbf{1})$	0	1	1	1						
	em	1	-1	-1						
	e	1	1	-1						
	m	1	-1	1						
$(\mathbf{1}, \mathbf{x})$	$\mathcal{B}_0^{\mathbf{x}}$						$\sqrt{2}$	$\sqrt{2}$		
	$\mathcal{B}_{em}^{\mathbf{x}}$						$i\sqrt{2}$	$-i\sqrt{2}$		
$(\mathbf{x}, \mathbf{1})$	σ_+				$\sqrt{2}$	$-i\sqrt{2}$				
	σ_-				$\sqrt{2}$	$i\sqrt{2}$				
(\mathbf{x}, \mathbf{x})	$\mathcal{B}_{\sigma_+}^{\mathbf{x}}$								$e^{\frac{\pi i}{4}}$	
	$\mathcal{B}_{\sigma_-}^{\mathbf{x}}$								$e^{-\frac{\pi i}{4}}$	

(3.67)

T	0	em	e	m	$\mathcal{B}_0^{\mathbf{x}}$	$\mathcal{B}_{em}^{\mathbf{x}}$	σ_+	σ_-	$\mathcal{B}_{\sigma_+}^{\mathbf{x}}$	$\mathcal{B}_{\sigma_-}^{\mathbf{x}}$
0	1									
em		-1								
e			1							
m				1						
$\mathcal{B}_0^{\mathbf{x}}$					1					
$\mathcal{B}_{em}^{\mathbf{x}}$						-1				
σ_+									1	
σ_-										1
$\mathcal{B}_{\sigma_+}^{\mathbf{x}}$							$e^{\frac{\pi i}{4}}$			
$\mathcal{B}_{\sigma_-}^{\mathbf{x}}$							$e^{-\frac{\pi i}{4}}$			

(3.68)

We remark that these matrices are not gauge invariant quantities. However, they do contain gauge invariant data, in particular the S and T matrices of the underlying toric code, and the quantum dimensions of the defects. Unitarity of the S -matrix implies that the number of \mathbf{h} -invariant \mathbf{g} -defects equals the number of \mathbf{g} -invariant \mathbf{h} -defects, in particular the number of \mathbf{g} -defects equals the number of \mathbf{g} -invariant anyons³¹. It also allows one to use the \mathcal{G} -crossed Verlinde formula to calculate the fusion rules³¹.

The ICIs of the gauged model can be recovered from the full set of domain walls, the projective representations they form, and their permutation action on the defects. First, a set of idempotents (a, μ) are constructed by forming projectors onto the projective irreps of the stabilizer group of each defect. The ICIs $[a, \mu]$ are then found by taking a sum over projectors in the orbit of each defect

$$(a, \mu) = \frac{d_\mu}{|Z_a|} \sum_{\mathbf{h} \in Z_a} \bar{\chi}_a^\mu(\mathbf{h}) \mathcal{B}_a^{\mathbf{h}}, \quad [a, \mu] = \sum_{\mathbf{k} \in \mathcal{G}/Z_a} (\mathbf{k} a, \mathbf{k} \mu) \quad (3.69)$$

For example

$$\underline{\sigma_+} \mapsto \begin{aligned} \frac{1}{2}(\mathcal{B}_{\sigma_+}^{\mathbf{1}} + e^{\frac{\pi i}{8}} \mathcal{B}_{\sigma_+}^{\mathbf{x}}) &= \underline{\sigma} \\ \frac{1}{2}(\mathcal{B}_{\sigma_+}^{\mathbf{1}} - e^{\frac{\pi i}{8}} \mathcal{B}_{\sigma_+}^{\mathbf{x}}) &= \underline{\sigma\psi} \end{aligned}, \quad \underline{\frac{e}{m}} \mapsto \mathcal{B}_e^{\mathbf{1}} + \mathcal{B}_m^{\mathbf{1}} = \underline{\sigma\sigma}. \quad (3.70)$$

note the projective irreps $\chi_{\sigma_+}^{\pm}$ of the representation $\{\mathcal{B}_{\sigma_+}^{\mathbf{1}}, \mathcal{B}_{\sigma_+}^{\mathbf{x}}\}$ are given by $\chi_{\sigma_+}^{\pm}(\mathbf{1}) = 1$, $\chi_{\sigma_+}^{\pm}(\mathbf{x}) = \pm e^{-\frac{\pi i}{8}}$.

The full set of gauged ICIs is once again given by Eq.(3.41), and the resulting topological order is the Ising model. In this case, knowing the topological order post-gauging is enough to diagnose that the SET must be the EM duality enriched toric code $\{0, e, m, em\} \oplus \{\sigma_+, \sigma_-\}$ where σ_{\pm} have trivial FS indicator.

The S and T matrix of the gauged theory can be derived from their \mathcal{G} -crossed counterparts³¹ by using the the gauged ICIs, see Section 3.7,

$$S_{[a_g, \mu][b_h, \nu]}^{\mathcal{Z}(\text{Ising})} = \frac{1}{|\mathcal{G}|} \sum_{\substack{\mathbf{r} \in \mathcal{G}/Z_a \\ \mathbf{s} \in \mathcal{G}/Z_b}} \mathbf{r} \bar{\chi}_a^{\mu}(\mathbf{s} \mathbf{h}) \mathbf{s} \chi_b^{\nu}(\mathbf{r} \mathbf{g}) S_{r_a g s b_h}, \quad T_{[a_g, \mu][b_h, \nu]}^{\mathcal{Z}(\text{Ising})} = \delta_{[a_g, \mu][b_h, \nu]} \frac{\chi_a^{\mu}(\mathbf{g})}{\chi_a^{\mu}(\mathbf{1})} \theta_a, \quad (3.71)$$

where $S_{a_g b_h}$ denotes an element of the SET S matrix, and θ_a an element of the SET T matrix. We have also used the notation

$$\mathbf{r} \chi_a^{\mu} := \chi_{\mathbf{r} a}^{\mu}, \quad (3.72)$$

to denote the action of an element $\mathbf{r} \in \mathcal{G}/Z_a$, which permutes a , on a character of Z_a . Note the permutation action induces a fixed choice of irrep $\mathbf{r} \mu$ on $\mathbf{r} a$ which specifies the aforementioned character. By using Eq.(3.71), one can diagnose the gauged theory once the \mathcal{G} -crossed S and T matrices have been calculated, without needing to carry out the gauging procedure explicitly. In the current example we recover the S and T matrices of the doubled Ising model.

We remark that one can go further, and use the defect ICIs and domain walls to construct a realization of the full emergent $UG \times \text{BFC}$, including the full gauge variant, $\{N, F, R, \rho, U, \eta\}$ data. For the purposes of diagnosing the SET this does not appear to be particularly useful, but we anticipate that it may have applications to analyzing topological quantum computation^{19–23} with defects in a tensor network.

3.3 Symmetry-enriched string-net tensor networks

In this section we present the PEPS and MPO tensors for the class of symmetry-enriched string-net examples^{32,33}. These include the conventional string-nets as a subcase²⁴. We first introduce the unitary fusion category data^{166,216} that is the input for the string-net construction. We then present the MPOs that are used in both the string-nets and their symmetry-enriched counterparts. The local tensors for the (symmetry-enriched) string nets are then given, along with the (symmetry-enriched) pulling through equation that they satisfy. The global symmetry of the symmetry-enriched string-net tensors is explicitly gauged, which is shown to recover the regular string-net tensor.

3.3.1 Input (graded) unitary fusion category data

We give a pedestrian description of the algebraic data^{14,224} of a unitary fusion category (UFC) \mathcal{C} that is taken as input to the string-net construction. The skeleton of this data is given by a fusion algebra of a finite set of simple objects $a \in \mathcal{C}$

$$a \times b = \sum_{c \in \mathcal{C}} N_{ab}^c c, \quad (3.73)$$

where $N_{ab}^c \in \mathbb{N}$ are a set of fusion coefficients. We define $\delta_{ab}^c \in \mathbb{Z}_2$ to be 0 when $N_{ab}^c = 0$ and 1 otherwise.

For a \mathcal{G} -graded UFC $\mathcal{C}_{\mathcal{G}}$ the simple objects are organized into sectors $\mathcal{C}_{\mathbf{g}}$ and the fusion respects the \mathcal{G} -grading

$$\mathcal{C}_{\mathbf{g}} = \bigoplus_{\mathbf{g} \in \mathcal{G}} \mathcal{C}_{\mathbf{g}} , \quad N_{a_{\mathbf{g}} b_{\mathbf{h}}}^{c_{\mathbf{k}}} = \delta_{\mathbf{k}, \mathbf{gh}} N_{a_{\mathbf{g}} b_{\mathbf{h}}}^{c_{\mathbf{k}}} , \quad (3.74)$$

where $a_{\mathbf{g}}$ is shorthand for $a \in \mathcal{C}_{\mathbf{g}}$.

There is a distinguished unit element 0, corresponding to the vacuum in a physical theory, that satisfies $N_{0a}^b = \delta_{a,b} = N_{a0}^b$. Each simple object a has a unique conjugate simple object \bar{a} that satisfies $N_{ab}^0 = \delta_{\bar{a},b} = N_{ba}^0$, and $\bar{\bar{a}} = a$. For a graded fusion category $0 \in \mathcal{C}_{\mathbf{1}}$ and $\bar{a}_{\mathbf{g}} \in \mathcal{C}_{\bar{\mathbf{g}}}$.

Each simple object a is assigned a quantum dimension d_a , given by the Perron-Frobenius eigenvalue of the matrix obtained by fixing a in N_{ab}^c . These quantum dimensions satisfy

$$d_a d_b = \sum_c N_{ab}^c d_c , \quad d_0 = 1 \quad \text{and} \quad d_a = d_{\bar{a}} . \quad (3.75)$$

The total quantum dimension \mathcal{D} of a UFC \mathcal{C} is defined by

$$\mathcal{D}^2 = \sum_a d_a^2 . \quad (3.76)$$

For \mathcal{G} -graded UFCs the quantum dimension of $\mathcal{C}_{\mathbf{g}}$ is defined by

$$\mathcal{D}_{\mathbf{g}}^2 = \sum_{a_{\mathbf{g}}} d_{a_{\mathbf{g}}}^2 , \quad (3.77)$$

they satisfy $\mathcal{D}_{\mathbf{g}} = \mathcal{D}_{\mathbf{1}}$ for all $\mathbf{g} \in \mathcal{G}$, and hence $\mathcal{D}_{\mathcal{G}}^2 = |\mathcal{G}| \mathcal{D}_{\mathbf{1}}^2$.

The following sum is a projector known as the ω_0 -loop of \mathcal{C}

$$\omega_0 := \sum_{a \in \mathcal{C}} \frac{d_a}{\mathcal{D}^2} a . \quad (3.78)$$

For a \mathcal{G} -graded UFC the ω_0 -loop of $\mathcal{C}_{\mathbf{1}}$ plays the role of the unit element in a representation of \mathcal{G} given by

$$\pi_{\mathbf{g}} := \sum_{a \in \mathcal{C}_{\mathbf{g}}} \frac{d_{a_{\mathbf{g}}}}{\mathcal{D}^2} a_{\mathbf{g}} , \quad (3.79)$$

hence the ω_0 -loop of $\mathcal{C}_{\mathcal{G}}$ is the projector onto the symmetric subspace of this representation.

In a UFC the fusion coefficients are promoted to N_{ab}^c -dimensional vector spaces over \mathbb{C} . These vector spaces V_{ab}^c (and their duals V_c^{ab}) appear on fusion (and splitting) vertices. Basis states for V_c^{ab} are denoted

$$\begin{array}{c} a \quad b \\ \swarrow \quad \searrow \\ \mu \\ \uparrow \\ c \end{array} , \quad (3.80)$$

where $\mu \in \{1, \dots, N_{ab}^c\}$.

The fusion algebra is associative and the fusion coefficients satisfy

$$\sum_{e \in \mathcal{C}} N_{ab}^e N_{ec}^d = \sum_{f \in \mathcal{C}} N_{bc}^f N_{af}^d. \quad (3.81)$$

However, the composition of fusion or splitting vertices is not strictly associative. Rather, two different orders of fusion or splitting are related by an associator matrix known as the F -symbol.

At this point, for clarity of exposition, we restrict our discussion to multiplicity free UFCs. That is, we assume $N_{ab}^c = \delta_{ab}^c \in \mathbb{Z}_2$. It is straightforward, although cumbersome, to extend the whole construction to include fusion multiplicity, but we will not cover that here.

The F -symbol associators satisfy

$$\begin{array}{c} a \quad b \quad c \\ \swarrow \quad \searrow \quad \nearrow \\ e \quad \quad \quad \\ \downarrow \\ d \end{array} = \sum_f [F_d^{abc}]_e^f \begin{array}{c} a \quad b \quad c \\ \swarrow \quad \searrow \quad \nearrow \\ \quad \quad f \quad \\ \downarrow \\ d \end{array}. \quad (3.82)$$

The F -symbols are only defined upon the allowed splitting vertices, we use the convention that they are 0 outside of this subspace

$$[F_d^{abc}]_e^f = \delta_{ab}^e \delta_{ec}^d \delta_{bc}^f \delta_{af}^d [F_d^{abc}]_e^f. \quad (3.83)$$

The F -symbols are invertible matrices on the splitting spaces for which they are defined

$$\sum_f [F_d^{abc}]_e^f [(F_d^{abc})^{-1}]_f^{\tilde{e}} = \delta_{e\tilde{e}} \delta_{ab}^e \delta_{ec}^d. \quad (3.84)$$

The quantum dimension and Frobenius-Shur indicator can be extracted from the F -symbol

$$d_a = \frac{1}{|F_{a00}^{a\bar{a}a}|}, \quad \varkappa_a = \frac{F_{a00}^{a\bar{a}a}}{|F_{a00}^{a\bar{a}a}|}. \quad (3.85)$$

Since the associativity constraint of an algebra was relaxed to a nontrivial associator, we find a higher order constraint on the composition of associators known as the pentagon equation. The pentagon equation can be derived by equating two inequivalent paths of associators that relate a pair of splitting diagrams on four objects.

$$\begin{array}{ccccc} \begin{array}{c} a \quad b \quad c \quad d \\ \swarrow \quad \searrow \quad \nearrow \quad \nearrow \\ p \quad q \quad \quad \quad \\ \downarrow \\ e \end{array} & \xrightarrow{\quad} & \begin{array}{c} a \quad b \quad c \quad d \\ \swarrow \quad \searrow \quad \nearrow \quad \nearrow \\ \quad \quad x \quad \quad \\ \downarrow \\ e \end{array} & \xrightarrow{\quad} & \begin{array}{c} a \quad b \quad c \quad d \\ \swarrow \quad \searrow \quad \nearrow \quad \nearrow \\ \quad \quad \quad \quad s \quad \\ \downarrow \\ e \end{array} \\ & \searrow & & \nearrow & \\ & \begin{array}{c} a \quad b \quad c \quad d \\ \swarrow \quad \searrow \quad \nearrow \quad \nearrow \\ \quad \quad p \quad \quad r \quad \\ \downarrow \\ e \end{array} & & \begin{array}{c} a \quad b \quad c \quad d \\ \swarrow \quad \searrow \quad \nearrow \quad \nearrow \\ \quad \quad \quad \quad r \quad \\ \downarrow \\ e \end{array} \end{array} \quad (3.86)$$

Which can be written in terms of matrix elements as

$$F_{eqr}^{pcd} F_{eps}^{abr} = \sum_x F_{qpx}^{abc} F_{eqs}^{axd} F_{srx}^{bcd}, \quad \text{where} \quad F_{def}^{abc} := [F_d^{abc}]_e^f. \quad (3.87)$$

A result known as MacLane's coherence theorem²²⁵ implies that the pentagon equation alone is enough to ensure that any path of associators between a pair of splitting diagrams are consistent. Another fundamental result known as Ocneanu rigidity^{166,203}, implies that a continuous deformation of a solution to the pentagon equation can be absorbed into a gauge transformation of the associator.

The fusion categories that lead to Hermitian string-net Hamiltonians have unitary F -symbols on the relevant splitting subspace

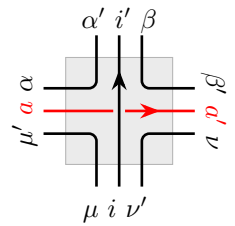
$$[(F_d^{abc})^{-1}]_f^e = [(F_d^{abc})^\dagger]_f^e = (F_{def}^{abc})^*, \quad \sum_f F_{def}^{abc} (F_{\tilde{e}f}^{abc})^* = \delta_{e\tilde{e}} \delta_{ab}^e \delta_{ec}^d. \quad (3.88)$$

3.3.2 Matrix product operator tensors and their fusion

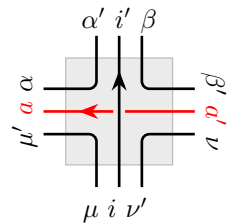
The string-net examples considered here are defined on oriented lattices, which give rise to both left and right handed MPO tensors. These tensors are related by a combined reflection and complex conjugation. A factor of the quantum dimension must be included for each variable that is summed over to achieve a correct overall normalization. The variables being summed over appear as closed loops in the tensor network diagrams and we use the convention established in Ref. 63, that such a sum over a variable s is weighted by the quantum dimensions d_s . We remark that the weighting by quantum dimension can also be incorporated into the local tensors directly, by making use of the planar geometry, which was done in Refs. 64,119,120. We do not take this approach here.

The MPOs described in this section are for both the string-nets and their symmetry-enriched variants. The only difference in the symmetry-enriched case is the inclusion of a \mathcal{G} -grading on the objects of the input fusion category $\mathcal{C}_{\mathcal{G}}$.

The left and right handed MPO tensors are given by



$$= \delta_{\alpha\alpha'} \delta_{\beta\beta'} \delta_{\mu\mu'} \delta_{\nu\nu'} \delta_{ii'} \delta_{aa'} \frac{F_{\beta\alpha\nu}^{a\mu i}}{\sqrt{d_\alpha d_\nu}}, \quad (3.89)$$



$$= \delta_{\alpha\alpha'} \delta_{\beta\beta'} \delta_{\mu\mu'} \delta_{\nu\nu'} \delta_{ii'} \delta_{aa'} \frac{F_{\nu\mu\beta}^{a\alpha i *}}{\sqrt{d_\mu d_\beta}}, \quad (3.90)$$

where the indices take values in the set of simple objects of the input category, and d and F are also taken from the input category. Each index of the tensor is $|\mathcal{C}|^3$ dimensional, and red is used to indicate the virtual indices. The MPO tensors have some redundancy, as they are only nonzero on the subspace of the bond indices that satisfy $\delta_{\beta'a'}^\nu$ and $\delta_{\alpha a}^\mu$, they are injective once projected onto this subspace. Here a corresponds to the block label of the MPO.

These MPO tensors satisfy an equation that corresponds to dragging an MPO string off a tensor network bond, this leads to a bubble popping equation that replaces a loop of MPO a with the quantum dimension d_a

$$\begin{aligned} \text{Diagram 1} &= \frac{1}{d_i} \delta_{ii'} \delta_{ik}^j \delta_{al}^{i'} & \text{Diagram 2} &= d_a \delta_{ik}^j \end{aligned} \quad (3.91)$$

The factor of $\frac{1}{d_i}$ in the left equation corrects for an excess quantum dimension that arises when two separate loops are merged. This can be seen by imagining the equation as part of a larger, closed, tensor network diagram in which the $\delta_{ii'}$ condition becomes redundant. Reflecting and conjugating the above equations, leads to analogous relations with reversed orientations.

The matrices constructed by contracting a periodic chain of L local tensors, with block label a and virtual index pointing left to right, are denoted MPO_a^L . These matrices form an MPO representation of the input fusion algebra

$$\text{MPO}_a^L \text{MPO}_b^L = \sum_{c \in \mathcal{C}} N_{ab}^c \text{MPO}_c^L. \quad (3.92)$$

In the symmetry-enriched case this algebra is \mathcal{G} -graded.

For open boundary conditions the MPOs only obey the algebra multiplication up to boundary fusion and splitting tensors

$$\text{Diagram 1} = \delta_{\alpha\alpha'} \delta_{\beta\beta'} \delta_{\gamma\gamma'} \frac{d_a^{\frac{1}{4}} d_b^{\frac{1}{4}} F_{\alpha c \beta}^{ab \gamma}}{d_c^{\frac{1}{4}} \sqrt{d_\beta}}, \quad (3.93)$$

$$\text{Diagram 2} = \delta_{\alpha\alpha'} \delta_{\beta\beta'} \delta_{\gamma\gamma'} \frac{d_a^{\frac{1}{4}} d_b^{\frac{1}{4}} F_{\alpha c \beta}^{ab \gamma*}}{d_c^{\frac{1}{4}} \sqrt{d_\beta}}. \quad (3.94)$$

These tensors are again related by a combined reflection and complex conjugation. We have chosen a particular normalization of the fusion and splitting tensors such that the following

equations hold

$$\begin{array}{c} a \\ \downarrow \\ \text{---} \\ \uparrow \\ b \end{array} = \sum_c \delta_{ab}^c \sqrt{\frac{d_c}{d_a d_b}} \begin{array}{c} a \\ \downarrow \\ \text{---} \\ \uparrow \\ b \end{array} \quad , \quad (3.95)$$

$$\begin{array}{c} \alpha c \beta \\ \downarrow \\ \text{---} \\ \uparrow \\ \alpha c' \beta \end{array} = \delta_{c,c'} \delta_{ab}^c \delta_{c\beta}^\alpha \sqrt{\frac{d_a d_b}{d_c}} \begin{array}{c} \alpha c \beta \\ \downarrow \\ \text{---} \\ \uparrow \\ \alpha c' \beta \end{array} \quad , \quad (3.96)$$

where the right equation reduces to bubble popping for $b = \bar{a}$ and $c = 0$.

While the multiplication of closed MPOs are clearly associative, as they are matrices, for open boundary conditions the multiplication is not strictly associative. Rather, two different orders of multiplication are related by an associator, that is given by the F -symbol of the input category

$$\begin{array}{c} a \quad b \quad c \\ \downarrow \quad \downarrow \quad \downarrow \\ \text{---} \\ \uparrow \quad \uparrow \quad \uparrow \\ d \end{array} = \sum_f F_{def}^{abc} \begin{array}{c} a \quad b \quad c \\ \downarrow \quad \downarrow \quad \downarrow \\ \text{---} \\ \uparrow \quad \uparrow \quad \uparrow \\ d \end{array} . \quad (3.97)$$

An analogous equation for the fusion tensors is obtained by a combined reflection and complex-conjugation. The resulting F symbols satisfy the pentagon equation, as the input was a consistent UFC. Since we are working with the tensor product of tensors over \mathbb{C} there is no difference between taking a left or right trace, which is analogous to the *spherical* property of UFCs.

In our examples we assume that the F symbols have been brought into a gauge where

$$F_{def}^{0bc} = F_{def}^{a0c} = F_{def}^{ab0} = 1 . \quad (3.98)$$

We remark that, in general, these elements may be arbitrary complex phases. This constraint is equivalent to the following *triangle equations*, which allow a vacuum line to be added or removed at fusion and splitting vertices

$$\begin{array}{c} 0 \\ \downarrow \\ \text{---} \\ \uparrow \\ \alpha b \beta \end{array} = \begin{array}{c} \alpha' a \beta' \\ \downarrow \\ \text{---} \\ \uparrow \\ \alpha b \beta \end{array} = \begin{array}{c} \alpha b \beta \\ \downarrow \\ \text{---} \\ \uparrow \\ \alpha' a \beta' \end{array} = \begin{array}{c} \alpha b \beta \\ \downarrow \\ \text{---} \\ \uparrow \\ \alpha' a \beta' \end{array} = \delta_{ab} \delta_{\alpha\alpha'} \delta_{\beta\beta'} \delta_{a\beta}^\alpha \begin{array}{c} \alpha a \beta \\ \downarrow \\ \text{---} \\ \uparrow \\ \alpha a \beta \end{array} . \quad (3.99)$$

In the above equations we have used the following states to terminate a vacuum line

$$\begin{array}{c} \alpha a \beta \\ \downarrow \\ \text{---} \\ \uparrow \\ 0 \end{array} := \delta_{a0} \delta_{\alpha\beta} \sqrt{d_\beta} , \quad \begin{array}{c} 0 \\ \downarrow \\ \text{---} \\ \uparrow \\ \alpha a \beta \end{array} := \delta_{a0} \delta_{\alpha\beta} \sqrt{d_\beta} . \quad (3.100)$$

Terminating a vacuum line that splits into (results from the fusion of) a particle-antiparticle pair leads to an orientation reversing “flag” matrix, corresponding to a cup (cap)

$$\begin{array}{c} \alpha \beta \\ \leftarrow \text{flag} \rightarrow \\ \beta' \bar{\alpha}' \end{array} := \begin{array}{c} \alpha \beta \\ \leftarrow \text{flag} \rightarrow \\ \beta' \bar{\alpha}' \\ \text{cup} \end{array}, \quad \begin{array}{c} \beta \alpha \alpha \\ \leftarrow \text{flag} \rightarrow \\ \beta' \bar{\alpha}' \end{array} := \begin{array}{c} \beta \alpha \alpha \\ \leftarrow \text{flag} \rightarrow \\ \beta' \bar{\alpha}' \\ \text{cap} \end{array}. \quad (3.101)$$

The absolute orientation chosen for the flag matrices is not important, as they already define their oppositely oriented variants via transposition and swapping $a \leftrightarrow \bar{a}$.

The closed MPOs satisfy $\text{MPO}_a^\dagger = \text{MPO}_{\bar{a}} = \text{MPO}_a^-$, where $-$ indicates orientation reversal. The orientation reversing flag matrices implement this at the level of the local tensors

$$\begin{array}{c} a \leftarrow \bar{a} \rightarrow a \\ \leftarrow \text{flag} \rightarrow \end{array} = \begin{array}{c} a \leftarrow \bar{a} \rightarrow a \\ \rightarrow \text{flag} \leftarrow \end{array}, \quad \begin{array}{c} \beta \alpha \alpha \\ \leftarrow \bar{a} \rightarrow \bar{a} \\ \beta' \bar{\alpha}' \end{array} = \delta_{\alpha\alpha'} \delta_{\beta\beta'} \delta_{\alpha\beta}^\alpha \begin{array}{c} \alpha \beta \alpha \\ \leftarrow \bar{a} \rightarrow \bar{a} \\ \beta' \bar{\alpha}' \end{array}. \quad (3.102)$$

From the above we see that the relative orientation of the flags does matter. Changing this orientation leads to the FS indicator $\varkappa_a \in \text{U}(1)$, which is a piece of gauge invariant physical data — given by $\varkappa_a = \pm 1$ — for $a = \bar{a}$

$$\begin{array}{c} \beta \alpha \alpha \\ \leftarrow \bar{a} \rightarrow \bar{a} \\ \beta' \bar{\alpha}' \end{array} = \varkappa_a \delta_{\alpha\alpha'} \delta_{\beta\beta'} \delta_{\alpha\beta}^\beta \begin{array}{c} \alpha \beta \alpha \\ \leftarrow \bar{a} \rightarrow \bar{a} \\ \beta' \bar{\alpha}' \end{array}, \quad \begin{array}{c} a \leftarrow \bar{a} \rightarrow a \\ \leftarrow \text{flag} \rightarrow \end{array} = \varkappa_a \begin{array}{c} a \leftarrow \bar{a} \rightarrow a \\ \rightarrow \text{flag} \leftarrow \end{array}. \quad (3.103)$$

The orientation reversing flag matrices can be used to derive a relation between the fusion and splitting spaces

$$\begin{array}{c} \bar{a} \rightarrow a \leftarrow a \\ \leftarrow \text{flag} \rightarrow \end{array} = A_c^{ab} \begin{array}{c} \bar{a} \rightarrow a \leftarrow a \\ \rightarrow \text{flag} \leftarrow \end{array}, \quad \begin{array}{c} a \leftarrow b \rightarrow b \\ \leftarrow \text{flag} \rightarrow \end{array} = B_c^{ab} \begin{array}{c} a \leftarrow b \rightarrow b \\ \rightarrow \text{flag} \leftarrow \end{array}, \quad (3.104)$$

with the normalization we have chosen these maps are unitary. They can be used to show a version of the *pivotal* identity satisfied by UFCs. For the case of no fusion multiplicity these maps are simply phases

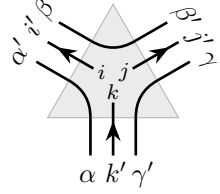
$$A_c^{ab} = \sqrt{\frac{d_a d_b}{d_c}} F_{b0c}^{\bar{a}ab*}, \quad B_c^{ab} = \sqrt{\frac{d_a d_b}{d_c}} F_{ac0}^{abb}. \quad (3.105)$$

Furthermore, the flag matrices allow one to derive a version of Eqs.(3.91), and (3.95) with the orientation of only the red lines reversed.

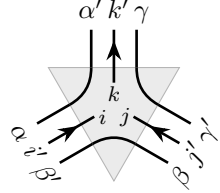
3.3.3 String-net tensors and the pulling through equation

The string-net models are defined on a trivalent lattice that is dual to a triangulation endowed with branching structure. A PEPS representation of the ground state is specified by the local

tensors



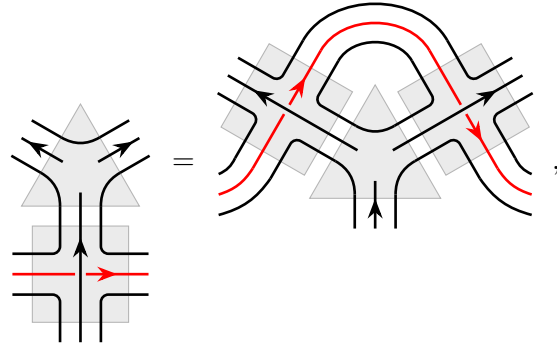
$$= \delta_{ii'} \delta_{jj'} \delta_{kk'} \delta_{\alpha\alpha'} \delta_{\beta\beta'} \delta_{\gamma\gamma'} \frac{d_i^{\frac{1}{4}} d_j^{\frac{1}{4}} F_{\gamma\beta k}^{\alpha ij}}{d_k^{\frac{1}{4}} \sqrt{d_\beta}}, \quad (3.106)$$



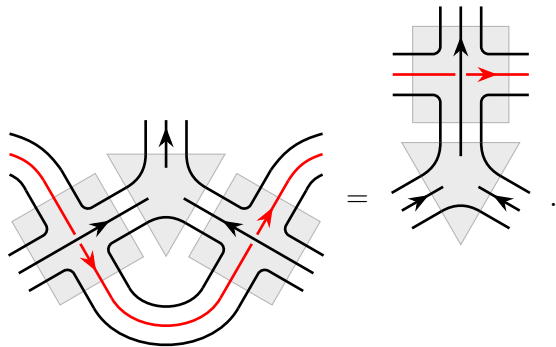
$$= \delta_{ii'} \delta_{jj'} \delta_{kk'} \delta_{\alpha\alpha'} \delta_{\beta\beta'} \delta_{\gamma\gamma'} \frac{d_i^{\frac{1}{4}} d_j^{\frac{1}{4}} F_{\gamma\beta k}^{\alpha ij*}}{d_k^{\frac{1}{4}} \sqrt{d_\beta}}, \quad (3.107)$$

which are related by a combined reflection and complex conjugation. Each of the indices is $|\mathcal{C}|^3$ dimensional, the physical indices are depicted within the tensors. In our representation of the string-nets each edge degree of freedom appears twice on the adjacent triangles. This convention, although redundant, is used for convenience and is equivalent to other conventions where the redundancy is removed.

The string-net PEPS was found to be MPO-injective in Ref. 63 with respect to the MPO defined by the same UFC \mathcal{C} . The pulling through equations for the string-nets are given by



$$= \text{[Diagram of the tensor with the red line moved to the other side]}, \quad (3.108)$$



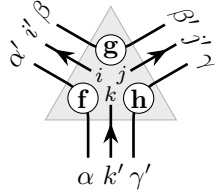
$$= \text{[Diagram of the tensor with the red line moved to the other side]}. \quad (3.109)$$

We emphasize the inclusion of a factor of the quantum dimension d_a on the index that is summed over, which appears as a closed loop. These equations are implied by the pentagon equation for the F -symbol used to define both the PEPS and the MPO tensors. The two equations are related by a combined reflection and complex conjugation. All other pulling through equations,

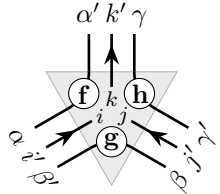
involving different combinations of indices and orientations, can be derived from the above by using Eqs.(3.91), and (3.102).

3.3.4 Symmetry-enriched string-net tensors, pulling through, and gauging

For the \mathcal{G} symmetry-enriched string-nets the simple objects of the input UFC are equipped with a \mathcal{G} -grading. We use the shorthand notation $[a] = \mathbf{g}$ to denote the sector $a \in \mathcal{C}_{\mathbf{g}}$, i.e. $[a_{\mathbf{g}}] = \mathbf{g}$. The PEPS tensors only differ from the ungraded string-nets via the inclusion of the sector information of the virtual indices in the physical index



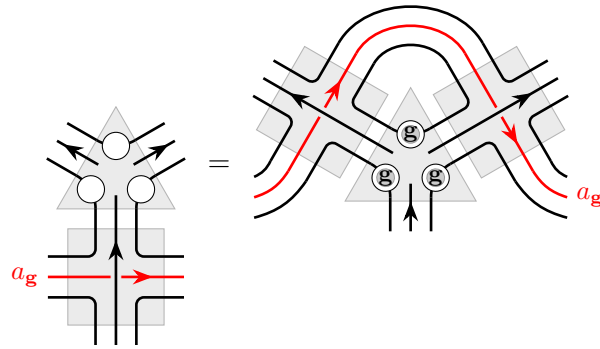
$$= \delta_{\mathbf{f}[\alpha]} \delta_{\mathbf{g}[\beta]} \delta_{\mathbf{h}[\gamma]} \delta_{ii'} \delta_{jj'} \delta_{kk'} \delta_{\alpha\alpha'} \delta_{\beta\beta'} \delta_{\gamma\gamma'} \frac{d_i^{\frac{1}{4}} d_j^{\frac{1}{4}} F_{\gamma\beta k}^{\alpha ij}}{d_k^{\frac{1}{4}} \sqrt{d_\beta}}, \quad (3.110)$$



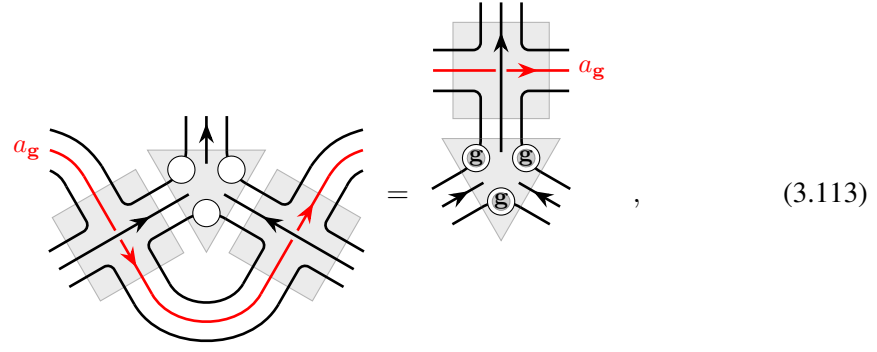
$$= \delta_{\mathbf{f}[\alpha]} \delta_{\mathbf{g}[\beta]} \delta_{\mathbf{h}[\gamma]} \delta_{ii'} \delta_{jj'} \delta_{kk'} \delta_{\alpha\alpha'} \delta_{\beta\beta'} \delta_{\gamma\gamma'} \frac{d_i^{\frac{1}{4}} d_j^{\frac{1}{4}} F_{\gamma\beta k}^{\alpha ij*}}{d_k^{\frac{1}{4}} \sqrt{d_\beta}}. \quad (3.111)$$

The tensor that copies the sector information is depicted as a circle. Again the tensors are related by combined reflection and complex conjugation. Similar tensors were described in Refs. 222,226.

These tensors are MPO-injective with respect to the MPO constructed from \mathcal{C}_1 . They further satisfy the symmetry-enriched pulling through equations defined by the MPOs constructed from $\mathcal{C}_{\mathcal{G}}$



$$= \text{[Diagram with red line and tensor]}, \quad (3.112)$$



where the shaded circle containing \mathbf{g} denotes the application of the on-site left regular group action

$$\textcircled{\mathbf{g}} := \mathbf{g} \times \textcircled{t} = \textcircled{\mathbf{g}t} . \quad (3.114)$$

Again a factor of the quantum dimension is included on the summed variable, which appears as a closed loop. These equations are implied by the pentagon equation, and the \mathcal{G} -grading of the fusion algebra for $\mathcal{C}_{\mathcal{G}}$. The two pulling through equations are related by a combined reflection and Hermitian conjugation. All other instances of the symmetry-enriched pulling through equation can be derived from the above by using Eqs.(3.91), and (3.102). The symmetry-enriched pulling through equation⁹³, together with the properties of the MPOs, imply that the PEPS is symmetric under the on-site left regular representation of \mathcal{G} , see Chapter 1.

Gauging the \mathcal{G} symmetry

The state gauging procedure defined in Ref. 71 can be applied to the PEPS tensors of a fixed-point model, such as the symmetry-enriched string-nets, to produce PEPS tensors for the gauged model. This was explained in detail in Ref. 93, and Chapter 1, which focused on SPT tensor networks, but the results generalize straightforwardly. For a system of $\mathbb{C}[\mathcal{G}]$ degrees of freedom on the vertices of a directed graph, in state $|\psi\rangle_V$, and a global symmetry given by a tensor product of the left regular representation on every vertex, the gauging map is given by

$$G|\psi\rangle_V := \prod_v \left(\frac{1}{|\mathcal{G}|} \sum_{\mathbf{g}_v} L_v(\mathbf{g}_v) \otimes_{e_v^+} L_{e_v^+}(\mathbf{g}_v) \otimes_{e_v^-} R_{e_v^-}(\mathbf{g}_v) \right) |\psi\rangle_V \otimes_e |\mathbf{1}\rangle_e , \quad (3.115)$$

where e_v^\pm is a neighboring edge that points away from (towards) vertex v . The resulting states $G|\psi\rangle_V$ are only defined on the subspace that satisfies the local gauge constraints, which does not have an immediately obvious tensor product structure.

For the on-site left regular representation the following isometry disentangles the gauge constraints, and maps back to a tensor product Hilbert space

$$Y := \left(\bigotimes_v \langle + |_v \right) \prod_v \prod_{e_v^+} CL_{v,e_v^+}^{-1} \prod_{e_v^-} CR_{v,e_v^-}^{-1} , \quad \text{where} \quad |+\rangle := \sum_{\mathbf{g}} |\mathbf{g}\rangle , \quad (3.116)$$

and $CL(R)$ is the controlled left (right) multiplication. Hence $YG|\psi\rangle_V$ is a state on the edge degrees of freedom alone.

The composition of the global gauging projector followed by the disentangling isometry, CG , can be implemented directly on the local tensors

$$\langle +|_0 \langle +|_1 \langle +|_2 CL_{0,01}^{-1} CL_{0,02}^{-1} CL_{1,12}^{-1} CR_{1,01}^{-1} CR_{2,02}^{-1} CR_{2,12}^{-1} |\mathbf{1}\rangle_{01} |\mathbf{1}\rangle_{12} |\mathbf{1}\rangle_{23} \quad \begin{array}{c} 1 \\ \diagup \quad \diagdown \\ \text{---} \text{---} \text{---} \\ \diagdown \quad \diagup \\ 0 \quad \quad 2 \end{array} = \begin{array}{c} \text{---} \text{---} \text{---} \\ \diagdown \quad \diagup \\ \text{---} \text{---} \text{---} \\ \diagup \quad \diagdown \\ \text{---} \text{---} \text{---} \end{array}, \quad (3.117)$$

where 0, 1, 2 labels the closest $\mathbb{C}[\mathcal{G}]$ degree of freedom, and 01, 12, 02 labels the newly introduced $\mathbb{C}[\mathcal{G}]$ degree of freedom on the relevant edge.

Every edge degree of freedom of the tensor network now carries a redundant copy of the sector information i.e. $|s_g\rangle |\mathbf{g}\rangle$. A further local isometry W can be applied to each edge to disentangle and project out this redundancy

$$W_{01} W_{12} W_{02} \quad \begin{array}{c} \text{---} \text{---} \text{---} \\ \diagdown \quad \diagup \\ \text{---} \text{---} \text{---} \\ \diagup \quad \diagdown \\ \text{---} \text{---} \text{---} \end{array} = \begin{array}{c} \text{---} \text{---} \text{---} \\ \diagdown \quad \diagup \\ \text{---} \text{---} \text{---} \\ \diagup \quad \diagdown \\ \text{---} \text{---} \text{---} \end{array}, \quad (3.118)$$

where $W |s_g\rangle |\mathbf{h}\rangle := (\mathbb{1} \otimes |\mathbf{1}\rangle) |s_g\rangle |\mathbf{gh}\rangle$. We find that this results in the string-net tensor for the full UFC \mathcal{C}_G , given in Eq.(3.106). A similar equation holds for the positively oriented tensor given in Eq.(3.107).

- In summary, the effect of gauging can be captured by simply projecting each local tensor onto the trivial representation of the on-site symmetry, in this case $|+\rangle$. This explains the results observed in Ref. 227.
- The inverse operation to gauging \mathcal{G} corresponds to a $\text{Rep}(\mathcal{G})$ anyon condensation. This can simply be implemented on the string-net tensors by copying the sectors of the virtual degrees of freedom to the physical index. This effectively ungauges the flat \mathcal{G} -connection defined by the \mathcal{G} -grading of the virtual indices.
- Similarly, confining the \mathcal{G} -defects of the SET can be implemented directly on the local tensors by projecting the sector information onto the $|\mathbf{1}\rangle$ state.
- The inverse operation corresponds to allowing \mathcal{G} -defects and can be implemented on the local tensors by allowing the sector degree of freedom to fluctuate freely.

These relations are summarized as follows

$$\text{SNTN}(\mathcal{C}) \xrightleftharpoons[\text{Project sector d.o.f. onto } \mathbf{1}]{\text{Fluctuate sector d.o.f.}} \text{SESNTN}(\mathcal{C}_G) \xrightleftharpoons[\text{Copy } [a] \text{ to phys. index}]{\text{Project sector d.o.f. onto } +} \text{SNTN}(\mathcal{C}_G) \quad (3.119)$$

where $\text{SNTN}(\mathcal{C})$ refers to the string-net tensor network constructed from the UFC \mathcal{C} , and $\text{SESNTN}(\mathcal{C}_G)$ refers to the symmetry-enriched string-net tensor network.

3.4 Ocneanu's tube algebra and emergent topological order from matrix product operators

In this section, we describe a construction known as Ocneanu's *tube algebra*^{163,164,212}. The derivation of the tube algebra from MPOs was first explained in Ref. 64, similar lattice constructions of the tube algebra have appeared in Refs. 195,196. By block diagonalizing this tube algebra we find tensor network representations of the emergent superselection sectors. We are able to extract gauge invariant observable physical data by using these representations to construct minimally entangled states, this includes the modular S and T matrices as well as the topological entanglement entropies of the superselection sectors. Furthermore we outline how the full emergent anyon theory, which is known to be the Drinfeld center (or double) $\mathcal{Z}(\mathcal{C})$ of the MPO UFC \mathcal{C} , can be constructed by finding the gauge variant fusion and braiding, F and R symbols. The tube algebra construction can be performed for the string-net examples tensors of the previous section.

3.4.1 Definition of the tube algebra

Throughout this section we work on the level of abstraction explained in Eq.(3.16), where the specifics of the underlying lattice are neglected. We use a diagrammatic notation in which grey shaded areas denote the PEPS tensor network, and black lines denote MPOs contracted with the virtual indices of the PEPS.

The tube algebra is found by considering a puncture in the tensor network and calculating the action of the topological MPO symmetry on the virtual indices of the puncture. To this end we consider a cylinder (or twice punctured sphere) as there is a global constraint that forces the charge in a unique puncture on a sphere to be trivial. As explained in Eq.(3.17) the MPO-injective tensor network states on the cylinder are found by closing the tensor network with an MPO. Hence it suffices to consider the action of the topological MPO symmetry algebra on the states

$$\begin{aligned}
 \text{Diagram 1} &= \frac{1}{d_s} \text{Diagram 2} = \frac{1}{d_s} \text{Diagram 3} = \sum_q \sqrt{\frac{d_q}{d_r d_s^3}} \text{Diagram 4} \\
 &= \sum_{pq} \frac{1}{d_s^2} \sqrt{\frac{d_p}{d_r}} \text{Diagram 5} = \sum_{pq} B_q^{r\bar{s}} (B_q^{r\bar{s}})^\dagger \frac{1}{d_s^2} \sqrt{\frac{d_p}{d_r}} \text{Diagram 6},
 \end{aligned} \tag{3.120}$$

where we have used Eqs.(3.91), (3.95), (3.102), and (3.104), or rather, the analogous equations for a general MPO algebra. The dashed lines indicate periodic boundary conditions.

Hence the basis elements that span the tube algebra are given by

$$\mathcal{T}_{pqr}^s = d_p^{\frac{1}{4}} d_r^{-\frac{1}{4}} \begin{array}{c} \text{---} p \text{---} \\ \text{---} q \text{---} \\ \text{---} s \text{---} \end{array} \begin{array}{c} \text{---} s \text{---} \\ \text{---} r \text{---} \\ \text{---} s \text{---} \end{array} , \quad (3.121)$$

which corresponds to the minimal tensor network

$$d_p^{\frac{1}{4}} d_r^{-\frac{1}{4}} \begin{array}{c} \text{---} p \text{---} \\ \text{---} q \text{---} \\ \text{---} s \text{---} \end{array} \begin{array}{c} \text{---} s \text{---} \\ \text{---} r \text{---} \\ \text{---} s \text{---} \end{array} , \quad (3.122)$$

we will often refer to these basis elements simply as tubes. There is some gauge freedom in the definition of these tubes which is similar to a 1-cochain. Eq.(3.120) can be rewritten as

$$\mathcal{T}_{rrr}^0 = \frac{1}{d_s^2} \sum_{pq} (\mathcal{T}_{pqr}^s)^\dagger \mathcal{T}_{ppp}^0 \mathcal{T}_{pqr}^s, \quad \text{and hence} \quad \mathbb{1} := \sum_r \mathcal{T}_{rrr}^0 = \frac{1}{\mathcal{D}^2} \sum_{pqrs} (\mathcal{T}_{pqr}^s)^\dagger \mathcal{T}_{pqr}^s, \quad (3.123)$$

where $\mathbb{1}$ denotes the identity matrix on a relevant subspace corresponding to virtual indices of a cylinder PEPS.

Multiplication of tubes is defined by the stacking operation

$$\mathcal{T}_{pqr}^s \mathcal{T}_{p'q'r'}^{s'} = \delta_{rp'} d_p^{\frac{1}{4}} d_{r'}^{-\frac{1}{4}} \begin{array}{c} \text{---} p \text{---} \\ \text{---} q \text{---} \\ \text{---} s \text{---} \end{array} \begin{array}{c} \text{---} s' \text{---} \\ \text{---} r' \text{---} \\ \text{---} s' \text{---} \end{array} \quad (3.124)$$

$$= \delta_{rp'} \sum_{q''s''} \varkappa_s \sqrt{\frac{d_s d_{s'}}{d_{s''}}} B_{q''}^{q'\bar{s}} (B_r^{qs})^\dagger F_{qrq''}^{s'q'\bar{s}} (F_{r's''q'}^{q''s's'})^* (F_{pq's''}^{ss's'})^* \mathcal{T}_{r'q''p}^{s''}, \quad (3.125)$$

only tubes, $\mathcal{T}_{pq''r'}^{s''}$, satisfying $\delta_{ss'}^{s''} \neq 0$ have nonzero coefficients in this expansion. The tube algebra is a C^* algebra as Hermitian conjugation is given by

$$(\mathcal{T}_{pqr}^s)^\dagger = d_p^{\frac{1}{4}} d_r^{-\frac{1}{4}} \begin{array}{c} \text{---} s \text{---} \\ \text{---} q \text{---} \\ \text{---} p \text{---} \end{array} \begin{array}{c} \text{---} p \text{---} \\ \text{---} q \text{---} \\ \text{---} s \text{---} \end{array} = \sqrt{\frac{d_p}{d_r}} \sum_{q'} B_{q'}^{ps} (A_p^{sq})^\dagger F_{rq'q'}^{\bar{s}ps} \mathcal{T}_{pq'r}^{\bar{s}}. \quad (3.126)$$

Each tube defines a state on the torus, which is identically zero when $p \neq r$

$$|\mathcal{T}_{pqr}^s\rangle := \delta_{pr} \begin{array}{c} \text{---} p \text{---} \\ \text{---} q \text{---} \\ \text{---} s \text{---} \end{array} \begin{array}{c} \text{---} s \text{---} \\ \text{---} p \text{---} \\ \text{---} s \text{---} \end{array} =: \delta_{pr} |psq\rangle. \quad (3.127)$$

As explained in Eq.(3.18), the above states span the ground space on the torus.

These states are not always independent, due to the relation induced by growing an ω_0 -loop over the whole torus and fusing it into the MPOs along the 1-skeleton

$$|\mathcal{T}_{pqr}^s\rangle = \frac{1}{\mathcal{D}^2} \sum_{pqs} |\mathcal{T}_{pqr}^s \mathcal{T}_{pqr}^s (\mathcal{T}_{pqr}^s)^\dagger\rangle. \quad (3.128)$$

3.4.2 Block diagonalizing the tube algebra with irreducible central idempotents

We have demonstrated that the tube algebra is a C^* algebra and hence can be block diagonalized. Since the tubes in Eq.(3.121) span the algebra we have

$$D = \sum_{pqr s} \delta_{sq}^p \delta_{qs}^r = \sum_{\underline{a}} D_a \times D_a, \quad (3.129)$$

where the sum is over all blocks \underline{a} of the tube algebra, D is the dimension of the tube algebra, and D_a is the dimension of the \underline{a} block (which consists of $D_a \times D_a$ -matrices).

The irreducible central idempotents (ICI) of the tube matrix algebra correspond to Hermitian projectors onto each irreducible block. These ICIs determine the set of inequivalent topological sectors for a disc in the tensor network that may be used to fill in a puncture. A constructive algorithm to find these ICIs was explained in Ref. 64. Alternatively, several exact formulas exist when the input category has additional structure such as a modular braiding²²⁸.

The irreducible central idempotents can be expressed as linear combinations of the tube basis elements

$$\underline{a} = \frac{1}{\mathcal{D}^2} \sum_{pqr s} t_a^{pqrs} \mathcal{T}_{pqr}^s, \quad (3.130)$$

$$\begin{array}{c} \text{Diagram: A square box labeled } a \text{ with four arrows pointing outwards (up, down, left, right).} \end{array} = \frac{1}{\mathcal{D}^2} \sum_{pqr s} t_a^{pqrs} \begin{array}{c} \text{Diagram: A vertex with four outgoing arrows labeled } p, q, r, s. \end{array}, \quad (3.131)$$

note the coefficients satisfy $t_a^{pqrs} = \delta_{pr} t_a^{pqps}$ as only basis elements \mathcal{T}_{pqr}^s with $r = p$ can occur in the construction of central idempotents. The ICIs are defined by the conditions, $\underline{a}, \underline{b} \neq 0$

$$\underline{a} \underline{b} = \delta_{ab} \underline{a}, \quad \mathcal{T}_{pqr}^s \underline{a} = \underline{a} \mathcal{T}_{pqr}^s, \quad \underline{a} \neq \underline{b} + \underline{c}, \quad (3.132)$$

for $\underline{a}, \underline{b}$ ICIs and \underline{c} a nonzero central idempotent. These idempotents realize the superselection sectors of the emergent anyon theory, or modular tensor category (MTC), which is the Drinfeld center $\mathcal{Z}(\mathcal{C})$ of the input UFC \mathcal{C} . The crossing tensor for \underline{a} , containing the weights t_a^{pqrs} , can be directly interpreted as the simple objects of the center MTC $\mathcal{Z}(\mathcal{C})$.

There is always a unique ICI corresponding to the vacuum

$$\underline{0} = \sum_{s \in \mathcal{C}} \frac{d_s}{\mathcal{D}^2} \mathcal{T}_{0s0}^s, \quad (3.133)$$

which is easily verified to be an ICI.

Each irreducible central idempotent that projects onto a block, a , of the matrix algebra with dimension D_a can be written as a sum of D_a non-central irreducible idempotents that partition the identity within the block

$$\underline{a} = \sum_{i=1}^{D_a} (\underline{a})_{ii}. \quad (3.134)$$

These non-central irreducible idempotents satisfy, $(\underline{a})_{ii} \neq 0$

$$(\underline{a})_{ii} (\underline{b})_{jj} = \delta_{ab} \delta_{ij} (\underline{a})_{ii}, \quad (\underline{a})_{ii} \neq (\underline{b})_{jj} + \underline{c}, \quad (3.135)$$

for $(b)_{jj}, c \neq 0$ idempotents and $(b)_{jj}$ irreducible. There are also $D_a(D_a - 1)$ off-diagonal, nilpotent elements $(a)_{ij} \neq 0$ in each degenerate block that satisfy

$$(a)_{ij}(a)_{kl} = \delta_{jk}(a)_{il}, \quad (a)_{ij}^\dagger = (a)_{ji}. \quad (3.136)$$

The irreducible idempotents are mixed by the conjugation action of the tube algebra $\mathcal{T}_{pqr}^s(a)_{ii}(\mathcal{T}_{pqr}^s)^\dagger$. In particular

$$(a) = \sum_j (a)_{ji}(a)_{ii}(a)_{ji}^\dagger. \quad (3.137)$$

We remark that the irreducible idempotents $(a)_{ii}$, together with the off-diagonal elements $(a)_{ij}$ within each block, define a basis for the tube algebra. Hence we can define the change of basis matrix

$$(a)_{ij} = \frac{1}{\mathcal{D}^2} \sum_{pqrs} t_{a_{ij}}^{pqrs} \mathcal{T}_{pqr}^s, \quad (3.138)$$

which includes expressions for the off-diagonal elements as well as for the irreducible idempotents. Similarly we have the inverse change of basis matrix

$$\mathcal{T}_{pqr}^s = \sum_{a_{ij}} \bar{t}_{pqrs}^{a_{ij}} (a)_{ij}, \quad \text{which implies} \quad (\mathcal{T}_{pqr}^s)^\dagger = \sum_{a_{ij}} (\bar{t}_{pqrs}^{a_{ij}})^* (a)_{ji}. \quad (3.139)$$

These coefficients satisfy

$$\frac{1}{\mathcal{D}^2} \sum_{pqrs} t_{a_{ij}}^{pqrs} \bar{t}_{pqrs}^{b_{kl}} = \delta_{ab} \delta_{ik} \delta_{jl}, \quad \frac{1}{\mathcal{D}^2} \sum_{a_{ij}} \bar{t}_{pqrs}^{a_{ij}} t_{a_{ij}}^{xyzw} = \delta_{px} \delta_{qy} \delta_{rz} \delta_{sw}. \quad (3.140)$$

The columns of the inverse change of basis matrix are orthogonal

$$\frac{1}{\mathcal{D}^2} \sum_{pqrs} \bar{t}_{pqrs}^{a_{ij}} (\bar{t}_{pqrs}^{b_{kl}})^* = \delta_{ab} \delta_{ik} \delta_{jl} \frac{1}{|a_{ij}|^2}, \quad (3.141)$$

for some positive weights $|a_{ij}|$.

It follows from Eqs.(3.120) and (3.141) that

$$\mathbb{1} = \sum_r \mathcal{T}_{rrr}^0 = \frac{1}{\mathcal{D}^2} \sum_{pqrs} (\mathcal{T}_{pqr}^s)^\dagger \mathcal{T}_{pqr}^s = \sum_{a_{ij}} \frac{1}{|a_{ij}|^2} (a)_{ij}^\dagger (a)_{ij}. \quad (3.142)$$

Multiplying by $(a)_{ii}$ implies

$$\sum_j \frac{1}{|a_{ij}|^2} = 1, \quad \text{and hence} \quad \mathbb{1} = \sum_p \mathcal{T}_{ppp}^0 = \sum_a a, \quad (3.143)$$

which is a partition of the identity, on the virtual indices of the cylinder tensor network, by ICIs.

3.4.3 Minimally entangled states and modular matrices

To diagnose the emergent topological order of the Drinfeld center $\mathcal{Z}(\mathcal{C})$ described by the ICIs, we want to calculate gauge invariant observable quantities. In this section we describe how to extract the modular S and T matrices by using the ICIs to define minimally entangled states

(MES)²²⁹. These modular matrices are conjectured to be complete invariants for non-chiral, equivalently Drinfeld center^{230,231}, topological orders.

Each irreducible idempotent defines a state on the torus

$$|a_{ij}\rangle := \delta_{ij} \frac{1}{\mathcal{D}^2} \sum_{pqs} t_{a_{ii}}^{pqps} |psq\rangle . \quad (3.144)$$

Due to the relation $(\underline{a})_{ii} = (\underline{a})_{ij}(\underline{a})_{ji} \sim (\underline{a})_{ji}(\underline{a})_{ij} = (\underline{a})_{jj}$, all irreducible idempotents $(\underline{a})_{ii}$ within the same block give rise to the same state, i.e. $|a_{ii}\rangle = |a_{jj}\rangle$.

In particular we take the following set of representatives as our definition

$$|a\rangle := \frac{1}{D_a} \sum_i |a_{ii}\rangle , \quad (3.145)$$

which yields a basis of minimally entangled states with a definite anyonic flux a threading the y -cycle of the torus. With this choice of normalization we have $|a\rangle = |a_{ii}\rangle$.

Since the ground space on the torus is spanned by states of the form $|psq\rangle$, see Eq.(3.18), we recover the well known fact that the ground space dimension of the torus equals $|\mathcal{Z}(\mathcal{C})|$ the number of emergent anyons or ICIs.

The modular S and T matrices are defined on the tubes as follows

$$S(\mathcal{T}_{pqr}^s) := \delta_{pr} \quad T(\mathcal{T}_{pqr}^s) := \mathcal{T}_{p0p}^p \mathcal{T}_{pqr}^s \quad (3.146)$$


$$= \sum_{q'} \varkappa_s B_p^{q'\bar{s}} B_{q'}^{sp} (B_p^{qs})^\dagger (A_{q'}^{ps})^\dagger (F_{pq'q}^{sp\bar{s}})^* \mathcal{T}_{sq's}^{\bar{p}} . \quad (3.147)$$

For the normalized MES and ICIs they satisfy

$$|S(a)\rangle = \sum_b S_{ab} |b\rangle , \quad T(\underline{a}) = \theta_a \underline{a} . \quad (3.148)$$

The quantity $\theta_a \in \text{U}(1)$ is known as the topological spin of sector \underline{a} . The equation defining it follows from Schur's lemma and the observations

$$\sum_a \mathcal{T}_{a0a}^a \mathcal{T}_{pqr}^s = \mathcal{T}_{pqr}^s \sum_a \mathcal{T}_{a0a}^a , \quad \text{and} \quad \left(\sum_a \mathcal{T}_{a0a}^a \right)^\dagger \left(\sum_a \mathcal{T}_{a0a}^a \right) = \sum_a \mathcal{T}_{aaa}^0 = \mathbb{1} , \quad (3.149)$$

which imply that T acts as the identity times a phase on each irreducible block of the matrix algebra. The S and T matrices just defined match those derived from state overlaps of MES for fixed point models such as the string-nets.

As a technical aside, note that S was defined on MES — rather than directly on ICIs — as the relation $|a_{ii}\rangle = |a\rangle$ is necessary to find the correct S matrix elements. This already shows up in the doubled Fibonacci example, see Section 3.9. An equivalent definition would be to look at the action of S on ICIs up to equivalence by conjugation $(\underline{a})_{ii} \sim (\underline{a})_{ji}(\underline{a})_{ii}(\underline{a})_{ij}^\dagger = (\underline{a})_{jj}$. Another useful equivalent definition of the matrix elements for S and T is given by

$$S_{ab} = \frac{D_b \text{Tr}[\underline{b}^\dagger S(\underline{a})]}{D_a \text{Tr}[\underline{b}^\dagger \underline{b}]} , \quad \theta_a \delta_{ab} = \frac{D_b \text{Tr}[\underline{b}^\dagger T(\underline{a})]}{D_a \text{Tr}[\underline{b}^\dagger \underline{b}]} , \quad (3.150)$$

where the trace now ensures that we have the necessary relation

$$\text{Tr}[(\underline{a})_{ii}] = \text{Tr}[(\underline{a})_{jj}] = \frac{1}{D_a} \text{Tr}[\underline{a}]. \quad (3.151)$$

We remark that the formulas in Eq.(3.150) were written with some unnecessary redundancies (such as the hermitian conjugation). We chose to present them in this way as it makes their generalization to the symmetry-enriched case more clear.

The S and T matrices constructed above are unitary, as the emergent theory is the Drinfeld center $\mathcal{Z}(\mathcal{C})$, which is known to be modular. Furthermore, since all such theories can be realized by local commuting projector Hamiltonians — via the string-net construction — they have zero chiral central charge and do not support robust gapless edge modes. Consequently S and T satisfy the modular relations

$$(ST)^3 = S^2, \quad S^4 = \mathbb{1}. \quad (3.152)$$

One can also verify that our definition of S and T must satisfy the above modular relations via direct manipulation of MPOs. Without using the previously known results it is clear that our definition of T must be unitary. It should also be possible to directly show that our definition of S is unitary. However we will not labor to reproduce this known result here.

One can find an explicit formula for S in terms of matrix elements $t_{a_{ij}}^{pqrs}, \bar{t}_{pqrs}^{a_{ij}}$ of the tube basis change matrix, and F_{def}^{abc} from the UFC data. This leads to a convenient formula for the quantum dimensions

$$d_a = \sum_p \frac{d_p t_a^{ppp0}}{D_a}, \quad (3.153)$$

which follows from

$$\frac{d_a}{\mathcal{D}^2} = S_{a0} = \frac{\text{Tr}[\underline{0}S(\underline{a})]}{D_a \text{Tr}[\underline{0}]} = \frac{1}{\mathcal{D}^2} \sum_{pqs} t_a^{pqps} \frac{\text{Tr}[\underline{0}S(\mathcal{T}_{pq}^s)]}{D_a \text{Tr}[\underline{0}]} = \sum_p \frac{d_p t_a^{ppp0}}{\mathcal{D}^2 D_a}. \quad (3.154)$$

Where we have used the relation $S(\mathcal{T}_{pq}^s) \underline{0} = d_p \delta_{s0} \delta_{pq} \underline{0}$, which is implied by Eq.(3.167).

3.4.4 Topological entanglement entropy of the superselection sectors

Our tensor network representation of the ICIs \underline{a} , that project onto each superselection sector, can be used to calculate the topological correction to the entanglement entropy for these sectors^{37,38,232}. We first calculate the scaling of the rank of each sector, given by the trace of the relevant ICI, to find the topological correction. We then argue that this correction should be independent of the Rényi index for an RG fixed point model¹⁰⁹ and, furthermore, that the value of topological entanglement entropy (TEE) should be robust throughout a gapped phase³⁷.

Using Eq.(3.153), we find that the topological correction to the 0-Rényi entropy H_0 (i.e. the entanglement rank) for the \underline{a} sector is given by

$$\gamma_a = \log(\mathcal{D}_{\text{out}}) - \log(d_a), \quad \text{where} \quad \mathcal{D}_{\text{out}} = \mathcal{D}^2, \quad (3.155)$$

\mathcal{D}_{out} is the total quantum dimension of the emergent theory. Note, this differs from the TEE of the MES, as reported in Ref. 229, since we are considering a disk topology rather than a torus.

For gapped, fixed point models — such as the string-nets — the 0-Rényi entropy is equal to the entanglement entropy as the Schmidt spectrum is flat. Hence, for fixed point models, the topological correction γ_a we have calculated corresponds to the topological entanglement entropy (TEE) of the a superselection sector^{37,38}. Furthermore, Ref. 109 argued that the result for the TEE calculated at a fixed point, via the 0-Rényi entropy, should hold throughout the gapped phase containing that fixed point model.

The 0-Rényi entropy H_0 of the a superselection sector can be calculated by taking the trace of the ICI \underline{a} . To extract the topological correction we need to access the regime of asymptotic scaling in the size of the perimeter L . Hence we consider an ICI formed by an MPO of length L contracted with the crossing tensor containing the weights t_a^{pqps}

$$H_0 = \log \left(\frac{1}{D_a \mathcal{D}^2} \sum_{pqps} t_a^{pqps} \text{Tr} \left[\begin{array}{c} \begin{array}{c} \text{---} s \text{---} q \text{---} p \text{---} \\ \text{---} p \text{---} s \text{---} \end{array} \\ \text{---} s \text{---} \end{array} \begin{array}{c} \text{---} s \text{---} \\ \text{---} s \text{---} \end{array} \begin{array}{c} \text{---} s \text{---} \\ \text{---} s \text{---} \end{array} \cdots \begin{array}{c} \text{---} s \text{---} \\ \text{---} s \text{---} \end{array} \end{array} \right] \right). \quad (3.156)$$

1 2 ... L

The factor of D_a^{-1} is included due to an argument presented in Ref. 64 that for a pair of charges a, \bar{a} on a sphere, each basis vector in the degenerate block appears with the same weight. To produce a correctly normalized state, this weight should be D_a^{-1} .

It was argued in Ref. 64 that the trace of a projector MPO of length L (assuming the existence of a unique unit element) is dominated by the leading eigenvector of the 0 block, $\lambda_0 > \lambda_s$ for $s \neq 0$. This contributes a factor of λ_0^L and picks out the elements of the crossing tensor t_a^{ppp0} satisfying $s = 0$. To be consistent with a faithful MPO representation of the UFC calculus, the traced crossing tensor must yield the quantum dimension of the closed loop it forms, i.e. d_p for the entry of the crossing tensor with coefficient t_a^{ppp0} . Using Eq.(3.153) we find that H_0 scales as

$$H_0 \approx \log(\lambda_0)L - \gamma_a, \quad \text{where} \quad \gamma_a = -\log \left(\sum_p \frac{d_p t_a^{ppp0}}{D_a \mathcal{D}^2} \right) = \log(\mathcal{D}_{\text{out}}) - \log(d_a). \quad (3.157)$$

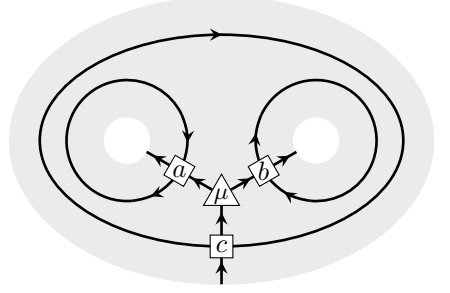
This provides a general method to extract the TEE of superselection sectors directly on the lattice, including the well known vacuum TEE $\gamma_0 = \log(\mathcal{D}_{\text{out}})$.

3.4.5 Fusion

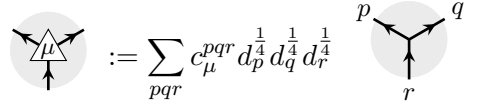
The fusion spaces of the emergent theory are found by considering the tensor network on a thrice-punctured sphere. To construct these fusion spaces we make a slight change of notation for the tubes

$$\begin{array}{c} \text{---} p \text{---} s \text{---} \\ \text{---} q \text{---} r \text{---} \\ \text{---} s \text{---} \end{array} = \begin{array}{c} \text{---} s \text{---} \\ \text{---} r \text{---} \\ \text{---} q \text{---} \\ \text{---} p \text{---} \end{array}, \quad \begin{array}{c} \text{---} \text{---} \\ \text{---} a \text{---} \\ \text{---} \text{---} \end{array} = \begin{array}{c} \text{---} \text{---} \\ \text{---} a \text{---} \\ \text{---} \text{---} \end{array}. \quad (3.158)$$

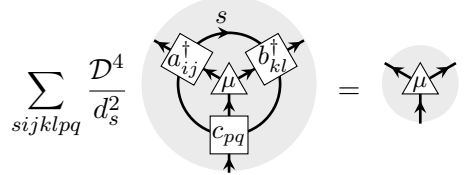
Now the splitting space V_c^{ab} is constructed from tensor networks of the form


(3.159)

where


(3.160)

There is an important subtlety in calculating the basis vectors of the spanning set, due to the local relation induced by growing an ω_0 -loop over the thrice punctured sphere and fusing it into the skeleton. Hence the splitting space is spanned by vertex tensors μ_{ab}^c in the support subspace of the following projector


(3.161)

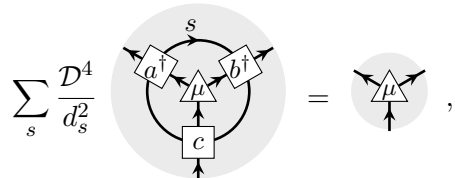
where μ_{ab}^c indicates $\mu \in V_c^{ab}$. More specifically, the relation is induced by creating an ω_0 -loop between \underline{c} and $\underline{a}, \underline{b}$ and fusing it into the edges around the μ_{ab}^c vertex. This also results in a correlated action by $(\underline{a})_{ij}, (\underline{b})_{kl}$ and $(\underline{c})_{pq}^\dagger$ on the $\underline{a}, \underline{b}$ and \underline{c} sectors, respectively. These actions permute the internal states within each degenerate block.

Considering Eq.(3.136), and the fact that the ω_0 -loop is a projector, one finds that the action in Eq.(3.161) is also a projector. By taking the trace of this projector we should find N_{ab}^c , the dimension of its support subspace. After using the tube S -matrix to expand $\underline{a}, \underline{b}, \underline{c}$ in a complementary tube basis, we find a formula that is tantalizingly close to the well known Verlinde formula ^{233,234}

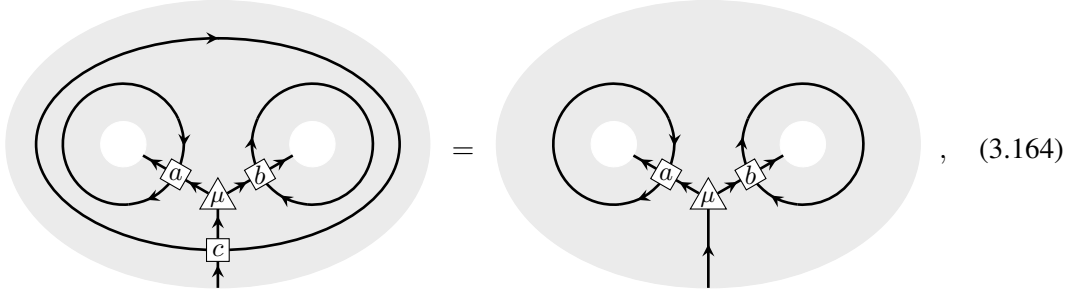
$$N_{ab}^c = \sum_x \frac{S_{ax} S_{bx} S_{\bar{c}x}}{S_{0x}}. \quad (3.162)$$

This formula holds for any modular theory, which includes all the theories we consider as they are Drinfeld centers. We expect that our formula should recover Verlinde, after some massaging, although we do not pursue this direction any further here.

In the case that $\underline{a}, \underline{b}$, and \underline{c} are nondegenerate, c_μ^{pqr} is a delta function that determines a unique fusion vertex, μ_{ab}^c . This fusion vertex, μ_{ab}^c , must satisfy

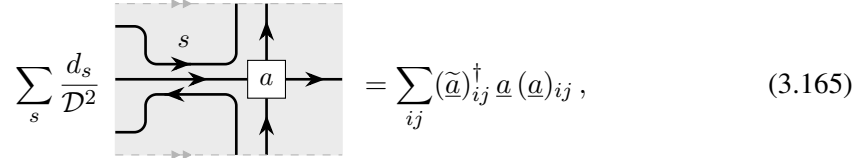

(3.163)

which allows one to absorb the \underline{c} ICI into \underline{a} , \underline{b} and μ_{ab}^c . More explicitly, for nondegenerate ICIs \underline{a} , \underline{b} , \underline{c} , one has

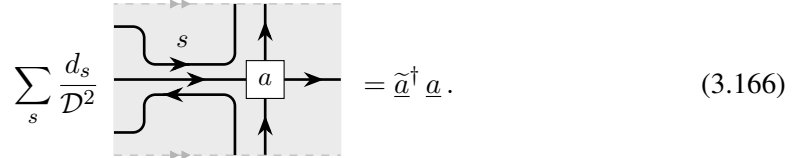


for the unique vertex μ_{ab}^c that satisfies Eq.(3.163).

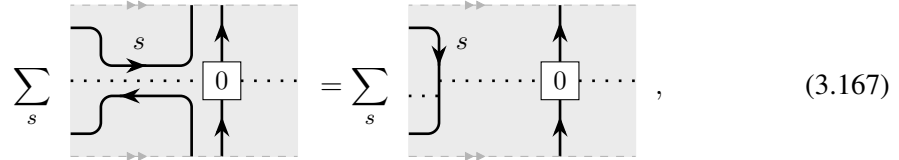
Eq.(3.161) follows from the identity



which takes a slightly more illuminating form for a nondegenerate block

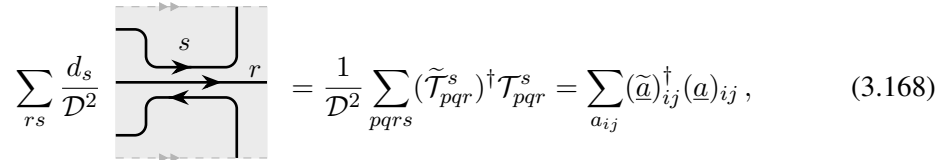


The special case of this equation for $\underline{a} = \underline{0}$, corresponds to sliding an MPO over an ω_0 -loop

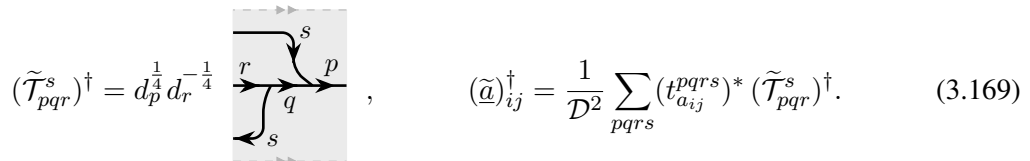


which can be intuitively understood as follows: the $\underline{0}$ ICI simply projects onto a disc of unaltered tensor network, through which the MPO is free to move.

The above identities are a consequence of the following slight generalization of Eq.(3.142), which is proved in much the same way,



where



Similar to Eq.(3.165), we have

with analogous definitions of $\tilde{\mathcal{T}}_{pqr}^s$ and $(\tilde{a})_{ij}$ to those in Eq.(3.169).

The special case of pair fusion (creation) to (from) the vacuum is captured by the cap (cup) tube

respectively. Where \bar{a} is the ICI for which the above tubes are nonzero. The FS indicator can be found by composing a cup and a cap²²⁸, which corresponds to unbending an anyon worldline

We remark that the the FS indicator only has an invariant meaning for self inverse particles, $\bar{a} = a$, in which case $\varkappa_a \pm 1$.

Assuming no block degeneracy, the F -symbols for the doubled theory, denoted \mathcal{F} , are given by

$$\sum_{pqrst} \text{Diagram 1} = \sum_{pqrstu \atop f\rho\sigma} F_{stu}^{pqr} c_{\mu}^{pqt} c_{\nu}^{trs} \bar{c}_{qru}^{\rho} \bar{c}_{pus}^{\sigma} \text{Diagram 2}, \quad (3.174)$$

where, due to the no degeneracy assumption, c_{pqt}^μ and \bar{c}_ρ^{gru} are delta functions. We remark that the above equation should be interpreted as part of a larger diagram, involving a sphere with four punctures, that have been projected onto idempotents $\underline{a}, \underline{b}, \underline{c}$ and \underline{d} respectively, similar to the thrice punctured sphere depicted in Eq.(3.159). The LHS of the above equation has an implicit \underline{e} idempotent between the fusion vertices, which was absorbed into the μ vertex using Eq.(3.163). Similarly, the line connecting the fusion vertices on the RHS has been resolved into a sum over idempotents \underline{f} , using Eq.(3.143), which have been absorbed into the ρ vertex using Eq.(3.163).

There is a similar, although somewhat more involved equation for F when degenerate blocks are involved. By considering a sphere with five punctures one can check that the emergent F -symbols satisfy the pentagon equation.

3.4.6 Braiding

The exchange of superselection sectors can be implemented by a deformation of the tensor network

(3.175)

$$= \sum_{ijs} \frac{\mathcal{D}^2}{d_s} \text{ (diagram) }, \quad (3.176)$$

where we have used Eq.(3.165) to find a tensor corresponding to the R^{ab} matrix. We remark that there is a correlated action $(\underline{a})_{ij}$ on the internal states of the \underline{a} block, if it is degenerate, which we do not explicitly depict.

R -matrix

If the \underline{a} ICI is nondegenerate, there is no summation over i, j and we simply have the above formula with \underline{a}^\dagger in place of $(\underline{a})_{ij}^\dagger$. Hence for nondegenerate \underline{a} and \underline{b} we have a formula for the

R matrix

$$R^{ab} = \text{diag}(a^\dagger)_{s^a s^b} = \sum_q \frac{(t_a^{s^a q} s^a s^b)^*}{d_{s^b}}, \quad (3.177)$$

where s^a is defined by the equation $\underline{a} \mathcal{T}_{ppp}^0 = \delta_{p,s^a} \underline{a}$.

The R matrix can be resolved into sectors of definite charge to find the R_c^{ab} symbols. For nondegenerate ICIs $\underline{a}, \underline{b}, \underline{c}$, and the unique fusion vertices μ_{ba}^c , and ν_{ab}^c , we have

$$\text{diag}(a^\dagger)_{\mu_{ba}^c \nu_{ab}^c} = R_c^{ab} \text{diag}(\nu_{ab}^c)_{\mu_{ba}^c}, \quad (3.178)$$

which should be interpreted as part of a larger fusion diagram such as Eq.(3.159). An explicit formula for R_c^{ab} can be derived from Eq.(3.177). We remark that a similar line of reasoning applies to degenerate ICIs, but the analysis becomes more complicated.

3.5 Symmetry-enriched topological order from matrix product operators

In Ref. 93, and Chapter 1, a formalism was introduced for the classification of symmetry-enriched topological order in two spatial dimensions using \mathcal{G} -graded matrix product operator algebras. The formalism was based on finding MPO representations $\text{MPO}_{\mathbf{g}}$ of the physical symmetry group \mathcal{G} . These MPOs correspond to \mathcal{G} -domain walls. Only unitary, on-site representations of finite groups were explicitly considered, but this turns out to capture the same SET phases without making the on-site assumption⁸¹ and there is a simple extension to also include anti-unitary elements³³.

In this section we develop the theory of \mathcal{G} -graded MPO algebras, drawing on the previous results derived for MPO algebras in Ref. 64. We find that the \mathcal{G} -graded MPO algebras, with a given underlying $\mathbf{1}$ -sector MPO algebra, correspond to \mathcal{G} extensions of that $\mathbf{1}$ -sector MPO algebra. We establish a close analogy between \mathcal{G} -graded MPO algebras and \mathcal{G} -graded UFCs, for which the extension problem has been thoroughly analyzed in Ref. 81. The \mathcal{G} -graded MPOs are used to define a symmetry-enriched pulling through condition for PEPS tensors that lead to symmetric tensor networks under the global symmetry. Finally we describe how calculations involving the \mathcal{G} -graded MPOs can be abstracted to a diagrammatic calculus that only keeps track of the relevant topological information.

3.5.1 \mathcal{G} -graded MPO algebras

We consider MPO representations of a finite group \mathcal{G} consisting of translation invariant elements of the form

$$\text{MPO}_{\mathbf{g}}^L = \sum_{\substack{i_1 \dots i_L \\ j_1 \dots j_L}} \text{Tr}[\Delta_{\mathbf{g}} B_{\mathbf{g}}^{i_1 j_1} B_{\mathbf{g}}^{i_2 j_2} \dots B_{\mathbf{g}}^{i_L j_L}] |i_1 \dots i_L\rangle \langle j_1 \dots j_L|, \quad (3.179)$$

for arbitrary length L . The object $B_{\mathbf{g}}^{ij}$ is a $\chi_{\mathbf{g}} \times \chi_{\mathbf{g}}$ matrix for each value of $i, j \in \mathbb{Z}_D$, where $\chi_{\mathbf{g}}$ is the bond dimension of the MPO and D corresponds to the bond dimension of a PEPS. $\Delta_{\mathbf{g}}$ is also a $\chi_{\mathbf{g}} \times \chi_{\mathbf{g}}$ matrix. In the conventional tensor network notation, we have

$$(B_{\mathbf{g}}^{ij})_{\alpha\beta} = \alpha \text{ --- } \boxed{\mathbf{g}} \text{ --- } \beta, \quad \text{MPO}_{\mathbf{g}} = \text{---} \boxed{\Delta_{\mathbf{g}}} \text{---} \boxed{\mathbf{g}} \text{---} \boxed{\mathbf{g}} \text{---} \cdots \text{---} \boxed{\mathbf{g}} \text{---}, \quad (3.180)$$

where dashed lines are used to denote periodic boundary conditions.

We restrict our attention to MPOs that can be brought into canonical form^{45,67} after insertion of $\Delta_{\mathbf{g}}$. Hence the tensors have a block diagonal structure

$$B_{\mathbf{g}}^{ij} = \bigoplus_{a \in \mathcal{C}_{\mathbf{g}}} B_a^{ij}, \quad \Delta_{\mathbf{g}} = \bigoplus_{a \in \mathcal{C}_{\mathbf{g}}} w_a \mathbb{1}_{\chi_a}, \quad (3.181)$$

where B_a^{ij} are a set of $\chi_a \times \chi_a$ matrices that generate the full matrix algebra, w_a are nonzero complex numbers, and $\mathcal{C}_{\mathbf{g}}$ refers to the collection of MPOs appearing in the decomposition of $\text{MPO}_{\mathbf{g}}$. These MPOs are referred to as *single block*, since they cannot be decomposed further. The full collection of single block MPOs in all sectors is denoted $\mathcal{C}_{\mathcal{G}}$. We remark that $\Delta_{\mathbf{g}}$ decomposes into a direct sum of multiples of the identity since it must commute with the full matrix algebra on each block, as the MPO is translationally invariant.

In tensor network notation Eq.(3.181), left, is written as

$$\boxed{\mathbf{g}} = \sum_{a_{\mathbf{g}}} \boxed{a_{\mathbf{g}}}, \quad \text{where} \quad \alpha \text{ --- } \boxed{a_{\mathbf{g}}} \text{ --- } \beta = (B_{a_{\mathbf{g}}}^{ij})_{\alpha\beta}, \quad (3.182)$$

and the shorthand notation $a_{\mathbf{g}}$ indicates $\text{MPO}_{a_{\mathbf{g}}} \in \mathcal{C}_{\mathbf{g}}$. We also use the shorthand $[a] \in \mathcal{G}$ to indicate $\text{MPO}_a \in \mathcal{C}_{[a]}$, i.e. $[a_{\mathbf{g}}] = \mathbf{g}$. We remark that each $a_{\mathbf{g}}$ MPO tensor is only nonzero within the relevant $\chi_a \times \chi_a$ block of the virtual index, hence a direct sum is implicit in the equation above, left.

The *single block* MPOs are then

$$\text{MPO}_{a_{\mathbf{g}}} = \text{---} \boxed{a_{\mathbf{g}}} \text{---} \boxed{a_{\mathbf{g}}} \text{---} \cdots \text{---} \boxed{a_{\mathbf{g}}} \text{---}, \quad \text{which satisfy} \quad \text{MPO}_{\mathbf{g}} = \sum_{a_{\mathbf{g}}} w_{a_{\mathbf{g}}} \text{MPO}_{a_{\mathbf{g}}}. \quad (3.183)$$

Since the \mathbf{g} MPOs form a representation of \mathcal{G} we have $\text{MPO}_{\mathbf{g}} \text{MPO}_{\mathbf{h}} = \text{MPO}_{\mathbf{gh}}$. The MPO algebra must have a faithful \mathcal{G} -grading, i.e. $|\mathcal{C}_{\mathbf{g}}| > 0$ for all \mathbf{g} , otherwise application of the physical symmetry to a tensor network can annihilate the state. If $|\mathcal{C}_1| = 1$ there is no underlying topological order, and the formalism recovers the cohomology classification of SPT phases^{36,70,73} in $(2+1)\text{D}$, this case was thoroughly analyzed in Ref. 93, Chapter 1. In general this representation yields a Hermitian MPO projector onto the symmetric subspace

$$\frac{1}{|\mathcal{G}|} \sum_{\mathbf{g} \in \mathcal{G}} \text{MPO}_{\mathbf{g}}^L, \quad (3.184)$$

for all lengths L . In Ref. 64 such MPO projectors were analyzed extensively, and it was found that many concepts from the theory of fusion categories naturally emerge. At an intuitive level,

such MPO projectors correspond to a representation of a fusion category. In particular, the theory of MPOs and the fact that we have a representation, implies

$$\text{MPO}_{a_g} \text{MPO}_{b_h} = \sum_{c \in \mathcal{C}_G} N_{a_g b_h}^c \text{MPO}_c = \sum_{c_{gh} \in \mathcal{C}_{gh}} N_{a_g b_h}^{c_{gh}} \text{MPO}_{c_{gh}}, \quad (3.185)$$

$$\sum_{a_g b_h} N_{a_g b_h}^{c_{gh}} w_{a_g} w_{b_h} = w_{c_{gh}}, \quad (3.186)$$

since $N_{a_g b_h}^c$ vanishes unless $c \in \mathcal{C}_{gh}$. Remarkably it also implies a local version of this condition on the level of individual MPO tensors. That is, there exists a set of independent *fusion tensors*, and their left inverses

$$[X_{a_g b_h}^{c_{gh} \mu}]_{\alpha\beta}^{\gamma} = \begin{array}{c} \alpha \\ \nearrow a \\ \mu \\ \nwarrow b \\ \beta \end{array} \xrightarrow{c_{gh} \gamma}, \quad [(X_{a_g b_h}^{c_{gh} \mu})^{-1}]_{\gamma}^{\alpha\beta} = \begin{array}{c} \alpha \\ \nwarrow c \\ \mu \\ \nearrow b \\ \beta \end{array} \xleftarrow{\gamma}, \quad (3.187)$$

where $\mu \in \mathbb{Z}_{N_{ab}^c}$, such that

$$\begin{array}{c} \nearrow a_g \\ \mu \\ \nwarrow b_h \end{array} \xrightarrow{c_{gh}} = \delta_{ab}^c \begin{array}{c} \uparrow \\ c \\ \downarrow \end{array}, \quad \begin{array}{c} \nearrow a_g \\ \mu \\ \nwarrow b_h \end{array} \xrightarrow{c_{gh}} = \delta_{ab}^c \delta_{\mu\nu} \delta_{cd} \xrightarrow{c_{gh}}, \quad (3.188)$$

where the c_{gh} line on the right indicates the identity on the c_{gh} block of the virtual index. We remark that the fusion tensor are only defined up to an invertible gauge transformation on the degeneracy index, μ ,

$$X_{a_g b_h}^{c_{gh} \mu} \mapsto \tilde{X}_{a_g b_h}^{c_{gh} \nu} := \sum_{\mu} (Y_{ab}^c)_{\nu\mu} X_{a_g b_h}^{c_{gh} \mu}. \quad (3.189)$$

For a symmetric PEPS on a sphere, a second type of MPO arises that has a reversed orientation of the virtual bond. These MPO are not independent from those introduced earlier, and lead to an arrow reversing gauge transformation. Consider a sphere and partition the on-site site representation into an action on the northern and southern hemispheres,

$$U(\mathbf{g}) = U_N(\mathbf{g}) \otimes U_S(\mathbf{g}), \quad (3.190)$$

respectively. Applying $U_S(\mathbf{g})$ to a symmetric PEPS — see Section 3.5.4 — leads to a domain wall along the equator, represented by $\text{MPO}_{\mathbf{g}}$. Applying $U_N(\mathbf{g})$ instead, leads to a different MPO

$$\text{MPO}_{\mathbf{g}}^- = \sum_{a_g} w_{a_g} \text{MPO}_{a_g}^-, \quad (3.191)$$

$$\text{where } \text{MPO}_{a_g}^- = \begin{array}{c} \uparrow \\ \leftarrow a_g \end{array} \cdots \begin{array}{c} \uparrow \\ \leftarrow a_g \end{array}, \quad \text{and } (B_{a_g}^-)^{ij}_{\alpha\beta} = \begin{array}{c} i \\ \uparrow \\ \leftarrow a_g \\ \downarrow \\ j \end{array} \begin{array}{c} \alpha \\ \beta \end{array}. \quad (3.192)$$

This is simply because the boundary of the southern disc has the opposite orientation to the boundary of the northern disc. Hence, by applying $U_N(\mathbf{g}) = (\mathbb{1} \otimes U_S(\bar{\mathbf{g}})) U(\mathbf{g})$ to a symmetric PEPS on the sphere we find

$$\text{MPO}_{\mathbf{g}}^- = \text{MPO}_{\bar{\mathbf{g}}} . \quad (3.193)$$

The theory of MPS implies that there is a unique label $\bar{a}_{\mathbf{g}}$, for each $a_{\mathbf{g}}$, such that

$$\text{MPO}_{a_{\mathbf{g}}}^- = \text{MPO}_{\bar{a}_{\mathbf{g}}} , \quad \text{and} , \quad w_{a_{\mathbf{g}}} = w_{\bar{a}_{\mathbf{g}}} , \quad (3.194)$$

which also satisfies $\bar{\bar{a}} = a$. Furthermore, there exists a local gauge transformation

$$Z_a = \begin{array}{c} \text{red arrow } a \text{ pointing left} \\ \text{grey triangle pointing right} \\ \text{red arrow } \bar{a} \text{ pointing right} \end{array} , \quad Z_a^{-1} = \begin{array}{c} \text{red arrow } \bar{a} \text{ pointing left} \\ \text{grey triangle pointing right} \\ \text{red arrow } a \text{ pointing right} \end{array} , \quad (3.195)$$

such that

$$\begin{array}{c} \text{red arrow } a \text{ pointing left} \\ \text{grey triangle pointing right} \\ \text{red arrow } \bar{a} \text{ pointing right} \end{array} = \begin{array}{c} \text{red arrow } a \text{ pointing left} \\ \text{grey triangle pointing right} \\ \text{red arrow } \bar{a}_{\bar{a}} \text{ pointing right} \\ \text{grey triangle pointing right} \\ \text{red arrow } a \text{ pointing right} \end{array} , \quad \text{and} \quad \begin{array}{c} \text{red arrow } \bar{a} \text{ pointing left} \\ \text{grey triangle pointing right} \\ \text{red arrow } a \text{ pointing right} \end{array} = \begin{array}{c} \text{red arrow } \bar{a} \text{ pointing left} \\ \text{grey triangle pointing right} \\ \text{red arrow } \bar{a}_{\bar{a}} \text{ pointing right} \\ \text{grey triangle pointing right} \\ \text{red arrow } a \text{ pointing right} \end{array} . \quad (3.196)$$

Note the same gauge transformation must work for both orientations in a consistent MPO representation⁹³. By applying Eq.(3.196) twice, we find that $Z_a(Z_{\bar{a}}^{-1})^T$ must commute with the set of matrices B_a^{ij} . Hence $Z_a(Z_{\bar{a}}^{-1})^T = \kappa_a \mathbb{1}_{\chi_a}$, for some complex number κ_a . This implies

$$\begin{array}{c} \text{red arrow } a \text{ pointing left} \\ \text{grey triangle pointing right} \\ \text{red arrow } \bar{a} \text{ pointing right} \end{array} = \kappa_a \begin{array}{c} \text{red arrow } a \text{ pointing left} \\ \text{grey triangle pointing right} \\ \text{red arrow } \bar{a} \text{ pointing right} \end{array} , \quad \text{and} \quad \begin{array}{c} \text{red arrow } \bar{a} \text{ pointing left} \\ \text{grey triangle pointing right} \\ \text{red arrow } a \text{ pointing right} \end{array} = \kappa_{\bar{a}} \begin{array}{c} \text{red arrow } \bar{a} \text{ pointing left} \\ \text{grey triangle pointing right} \\ \text{red arrow } a \text{ pointing right} \end{array} , \quad (3.197)$$

we also find $\kappa_{\bar{a}} = \kappa_a^{-1}$. The magnitude $|\kappa_a|$ can be absorbed into the definition of Z_a and the phase $\frac{\kappa_a}{|\kappa_a|}$ can also be absorbed unless $a = \bar{a}$, in which case we have $\kappa_a = \pm 1$. It will be shown later that this quantity corresponds to the familiar Frobenius-Schur indicator from the theory of fusion categories.

3.5.2 Classification via group extensions of MPO algebras

\mathcal{G} -graded matrix product operator algebras can be classified by \mathcal{G} extensions of an underlying MPO algebra, that corresponds to the **1**-sector of the resulting graded algebra.

Summary of the problem

\mathcal{G} -graded MPO algebras $\mathcal{C}_{\mathcal{G}}$ occur as group extensions of the ungraded MPO algebra \mathcal{C} that forms the **1** sector. This is a generalization of the more familiar group extension problem, where \mathcal{C} plays the role of the normal subgroup, and \mathcal{G} the quotient group. For the class of MPO algebras that correspond to fusion categories, which we focus on, one can apply the thorough analysis of the group extension problem for fusion categories given in Ref. 81.

The first step in the search for faithful \mathcal{G} extensions of an MPO algebra \mathcal{C} can intuitively be thought of as a hunt for \mathcal{G} -graded MPO algebras $\mathcal{C}_{\mathcal{G}}$ that make

$$1 \rightarrow \mathcal{C} \rightarrow \mathcal{C}_{\mathcal{G}} \rightarrow \mathcal{G} \rightarrow 1 , \quad (3.198)$$

into a short exact sequence. From left to right, the arrows correspond to: a map from unit to the 0 MPO (defined more precisely below), an injection that maps \mathcal{C} to $\mathcal{C}_1 \subseteq \mathcal{C}_{\mathcal{G}}$, a surjection that maps $\mathcal{C}_{\mathcal{G}}$ down to \mathbf{g} , and a map from all elements of \mathcal{G} to 1, respectively.

This extension problem includes the group extension problem as a special case in the following way: for $\mathcal{C} = \text{Vec}_N$ and $\mathcal{G} = Q$, any group G that is an extension of Q by N yields a solution $\mathcal{C}_G = \text{Vec}_G$. There are solutions beyond these group extensions, as demonstrated by the example $\mathcal{C} = \text{Vec}_{\mathbb{Z}_2}$ and $\mathcal{G} = \mathbb{Z}_2$, for which we find solutions where \mathcal{C}_G has Ising fusion rules, along with solutions that have $\mathbb{Z}_2 \times \mathbb{Z}_2$ and \mathbb{Z}_4 fusion rules. This example is explored further in Section 3.9.

There is a potential obstruction to finding an associative set of \mathcal{G} graded fusion rules which lies in the third cohomology group $\mathcal{H}^3(\mathcal{G}, \mathbb{Z}_1)$, explained in detail below. If this obstruction vanishes, we have a consistent set of \mathcal{G} -extended fusion rules. These form a torsor over $\mathcal{H}^2(\mathcal{G}, \mathbb{Z}_1)$ as shifting by such a 2-cocycle leads to another consistent solution.

A consistent \mathcal{G} -graded fusion algebra alone does not solve the extension problem. Since the fusion of open MPOs is only associative up to some boundary operator, we need to solve a categorification of the underlying algebra problem. Hence we must also check whether a consistent set of associators can be found, to relate the fusion of open MPOs in different orders. This amounts to finding F -symbols that solve the pentagon equation for the previously constructed \mathcal{G} -graded fusion algebra. Any such solution can be realized by a \mathcal{G} -graded MPO algebra via the fixed point construction in Section 3.3. It was shown in Ref. 81 that there is a potential obstruction to finding a consistent set of associators which lies in $\mathcal{H}^4(\mathcal{G}, \text{U}(1))$. We find that this obstruction vanishes for the class of MPOs considered here, and the resulting solutions form $\mathcal{H}^3(\mathcal{G}, \text{U}(1))$ torsors. That is, multiplying any solution by a 3-cocycle results in another — possibly distinct — solution. Physically this corresponds to the fact that a classification of SET phases depends upon the choice of on-site symmetry with respect to which they are classified.

For the above example, where $\mathcal{C} = \text{Vec}_N$, $\mathcal{G} = Q$, and the fusion rules are given by $\mathcal{C}_G = \text{Vec}_G$ — for G a group extension of Q by N — the potential $\mathcal{H}^4(\mathcal{G}, \text{U}(1))$ obstruction disappears as the trivial F -symbols are a valid solution to the pentagon equation. Shifting by an element $[\alpha] \in \mathcal{H}^3(\mathcal{G}, \text{U}(1))$ corresponds to twisting the extension by a 3-cocycle to obtain $\mathcal{C}_G = \text{Vec}_G^\alpha$.

This example captures the formalisms of Ref. 29,235–237. Refs. 236,237 corresponds to further restricting the 3-cocycle α to lie in the trivial cohomology class. They differ in so far as Ref. 237 captures the case where the restriction of the cocycle to N may be nontrivial in cohomology, while Ref. 236 requires this restriction to be trivial. It is clear that restricting \mathcal{C}_G to have the fusion rules of a finite group is very restrictive and misses many interesting cases, such as the Ising fusion rules needed to describe the EM duality enriched toric code, see Sections 3.9.1, 3.2.2. Furthermore, all such MPOs can be generated by an on-site representation times a diagonal local unitary circuit, see Refs. 70,74,93, while the more general MPOs may require a linear depth unitary circuit, for instance the Ising MPO.

MPO representations satisfying the group zipper condition

At this point we assume that a stronger version of the local fusion condition holds for the MPO group representation. This allows us to make contact with the theory of group extensions of fusion categories⁸¹. The MPO representation of a \mathcal{G} domain wall correspond to an invertible bimodule in the language of Ref. 81. We restrict to the case where the full group MPOs satisfy

the *group zipper condition*: that there exist tensors, together with left inverses

$$X_{\mathbf{g},\mathbf{h}} = \begin{array}{c} \text{g} \\ \swarrow \quad \searrow \\ \text{h} \end{array} \quad , \quad X_{\mathbf{g},\mathbf{h}}^{-1} = \begin{array}{c} \text{gh} \quad \text{g} \\ \swarrow \quad \searrow \\ \text{h} \end{array} \quad , \quad (3.199)$$

such that

$$\begin{array}{c} \uparrow \\ \text{g} \\ \downarrow \\ \text{h} \end{array} = \begin{array}{c} \text{g} \quad \text{gh} \quad \text{g} \\ \swarrow \quad \downarrow \quad \searrow \\ \text{h} \end{array} . \quad (3.200)$$

These tensors define a left and right group action on the $\chi_g \times \chi_g$ matrix algebra of the \mathbf{g} virtual bond

$$\mathbf{h} \circ M_{\mathbf{g}} = \begin{array}{c} \text{hg} \quad \text{h} \\ \swarrow \quad \searrow \\ M_{\mathbf{g}} \end{array} , \quad M_{\mathbf{g}} \circ \mathbf{h} = \begin{array}{c} \text{gh} \quad M_{\mathbf{g}} \\ \swarrow \quad \searrow \\ \text{h} \end{array} . \quad (3.201)$$

The subset of matrices — modulo multiples of the identity — that commute with $B_{\mathbf{g}}^{ij}$ for all ij , define the group of autoequivalences of the \mathbf{g} domain wall, $Z_{\mathbf{g}}$. The right and left actions in Eq.(3.201) imply isomorphisms $Z_{\mathbf{hg}} \cong Z_{\mathbf{g}} \cong Z_{\mathbf{gh}}$, due to the zipper condition, and hence $Z_{\mathbf{g}} \cong Z_1$. It was shown in Ref. 81 that $Z_1 \cong \mathcal{A}$, the group of abelian anyons of the emergent topological order $\mathcal{A} \subseteq \mathcal{Z}(\mathcal{C}_1)$. It is beyond the scope of this paper to rigorously establish that our definition of Z_1 matches that of Ref. 81, but they are analogous.

The $X_{\mathbf{g},\mathbf{h}}$ tensors define a matrix

$$T(\mathbf{g}, \mathbf{h}, \mathbf{k}) = \begin{array}{c} \text{g} \\ \swarrow \quad \searrow \\ \text{h} \quad \text{k} \end{array} , \quad (3.202)$$

that lies in $Z_{\mathbf{ghk}}$ and satisfies the 3-cocycle equation

$$\mathbf{g}_0 \circ T(\mathbf{g}_1, \mathbf{g}_2, \mathbf{g}_3) T(\mathbf{g}_0, \mathbf{g}_1 \mathbf{g}_2, \mathbf{g}_3) T(\mathbf{g}_0, \mathbf{g}_1, \mathbf{g}_2) \circ \mathbf{g}_3 = T(\mathbf{g}_0, \mathbf{g}_1, \mathbf{g}_2 \mathbf{g}_3) T(\mathbf{g}_0 \mathbf{g}_1, \mathbf{g}_2, \mathbf{g}_3) . \quad (3.203)$$

If we modify our choice of $X_{\mathbf{g},\mathbf{h}}$, by an element $M_{\mathbf{g},\mathbf{h}} \in Z_{\mathbf{gh}}$, to $X'_{\mathbf{g},\mathbf{h}} = X_{\mathbf{g},\mathbf{h}} M_{\mathbf{g},\mathbf{h}}$ we find that

$$T'(\mathbf{g}, \mathbf{h}, \mathbf{k}) = M_{\mathbf{gh},\mathbf{k}}^{-1} (M_{\mathbf{g},\mathbf{h}}^{-1} \circ \mathbf{k}) T(\mathbf{g}, \mathbf{h}, \mathbf{k}) (\mathbf{g} \circ M_{\mathbf{h},\mathbf{k}}) M_{\mathbf{g},\mathbf{hk}} , \quad (3.204)$$

which corresponds to a transformation by a coboundary.

Hence $X_{\mathbf{g},\mathbf{h}}$ yields an element $[T] \in \mathcal{H}^3(\mathcal{G}, Z_1)$, that is invariant under modifying the choice of $X_{\mathbf{g},\mathbf{h}}$ by an element of $Z_{\mathbf{gh}}$. This element $[T]$ constitutes an obstruction to a consistent MPO representation of a set of \mathcal{G} domain walls. Intuitively, the obstruction can be thought of as an anomalous anyonic charge appearing from the fusion of domain walls. It is unclear at this point whether an MPO group representation can be found with $[T] \neq 0$. If they were to be found, these MPOs would be relevant to the understanding of tensor network representations of SETs with anomalous symmetry fractionalization, such as those occurring on the boundary of a $(3+1)$ D higher form SPT^{155,238}.

Consistent fusion of the MPO representation requires $[T] = 0$ and that T has been transformed, by a coboundary, into a multiple of the identity. Tensor solutions $X_{\mathbf{g},\mathbf{h}}$ that satisfy $[T] = 0$, form $\mathcal{H}^2(\mathcal{G}, \mathbb{Z}_1)$ torsors. That is, we can modify any solution $X_{\mathbf{g},\mathbf{h}}$ by a 2-cocycle $M_{\mathbf{g},\mathbf{h}} \in \mathbb{Z}_{\mathbf{gh}}$ satisfying

$$(M_{\mathbf{g},\mathbf{h}} \circ \mathbf{k}) M_{\mathbf{gh},\mathbf{k}} = (\mathbf{g} \circ M_{\mathbf{h},\mathbf{k}}) M_{\mathbf{g},\mathbf{hk}}, \quad (3.205)$$

to find a new solution $X'_{\mathbf{g},\mathbf{h}} = X_{\mathbf{g},\mathbf{h}} M_{\mathbf{g},\mathbf{h}}$

Hence we have $T(\mathbf{g}, \mathbf{h}, \mathbf{k}) = \alpha(\mathbf{g}, \mathbf{h}, \mathbf{k}) \mathbb{1}_{\mathbf{ghk}}$, where we may take $\alpha(\mathbf{g}, \mathbf{h}, \mathbf{k}) \in \mathbb{U}(1)$ by normalizing the $X_{\mathbf{g},\mathbf{h}}$ tensors. This yields an associator

$$= \alpha(\mathbf{g}, \mathbf{h}, \mathbf{k}) \quad (3.206)$$

Considering the reduction of $\mathbf{g}_0 \mathbf{g}_1 \mathbf{g}_2 \mathbf{g}_3$, one finds a relation

$$, \quad (3.207)$$

leading to the phase

$$\nu(\mathbf{g}_0, \mathbf{g}_1, \mathbf{g}_2, \mathbf{g}_3) := \frac{\alpha(\mathbf{g}_1, \mathbf{g}_2, \mathbf{g}_3) \alpha(\mathbf{g}_0, \mathbf{g}_1 \mathbf{g}_2, \mathbf{g}_3) \alpha(\mathbf{g}_0, \mathbf{g}_1, \mathbf{g}_2)}{\alpha(\mathbf{g}_0, \mathbf{g}_1, \mathbf{g}_2 \mathbf{g}_3) \alpha(\mathbf{g}_0 \mathbf{g}_1, \mathbf{g}_2, \mathbf{g}_3)}, \quad (3.208)$$

which is a 4-cocycle. This constitutes an $\mathcal{H}^4(\mathcal{G}, \mathbb{U}(1))$ obstruction⁸¹ to finding a solution to the pentagon equation for the MPO representation. We find that this obstruction always vanishes for the MPOs we consider, due to the zipper condition we have assumed. It would be interesting to generalize our framework to capture a nontrivial $\mathcal{H}^4(\mathcal{G}, \mathbb{U}(1))$ obstruction, which is relevant for the understanding of tensor network representations of anomalous SETs such as those occurring on the boundary of a $(3+1)\text{D}$ SPT^{239–241}.

Since this obstruction vanishes, the possible solutions to the pentagon equation form an $\mathcal{H}^3(\mathcal{G}, \mathbb{U}(1))$ torsor. That is, any F -symbol solution may be multiplied by a 3-cocycle to obtain another solution which may or may not be distinct.

3.5.3 \mathcal{G} -graded MPO algebras satisfying the stronger zipper condition and \mathcal{G} -graded unitary fusion categories

We move on by narrowing our focus to the class of MPOs that are relevant for the description of anomaly free SET phases in $(2+1)\text{D}$. The properties thus introduced allow for an identification of these MPOs with \mathcal{G} -graded UFCs. In the process, we recount many results shown in Ref. 64

and put them into the context of \mathcal{G} -graded MPO algebras, which are relevant for the description of domain walls in SET ordered states.

From this point on we assume that the stronger *zipper condition* holds for the single block MPOs, and the fusion tensors defined in Eq.(3.187)

$$\begin{array}{c} \uparrow \\ \boxed{a_g} \\ \uparrow \\ \boxed{b_h} \\ \uparrow \end{array} = \sum_{c_{gh}\mu} \begin{array}{c} a_g \\ \swarrow \mu \\ b_h \end{array} \begin{array}{c} \uparrow \\ \boxed{c} \\ \uparrow \end{array} \begin{array}{c} a_g \\ \swarrow \mu \\ b_h \end{array}. \quad (3.209)$$

The class of MPOs satisfying the zipper condition is sufficiently general to capture representations of all \mathcal{G} -graded fusion categories, via the fixed point construction explained in Section 3.3.

The associativity of the product $(\text{MPO}_{a_g} \text{MPO}_{b_h}) \text{MPO}_{c_k} = \text{MPO}_{a_g} (\text{MPO}_{b_h} \text{MPO}_{c_k})$ implies

$$\sum_{e_{gh}} N_{a_g b_h}^{e_{gh}} N_{e_{gh} c_k}^{d_{ghk}} = \sum_{f_{hk}} N_{a_g f_{hk}}^{d_{ghk}} N_{b_h c_k}^{f_{hk}}. \quad (3.210)$$

The addition of the zipper condition further implies the existence of F -symbol associators⁶⁴

$$\begin{array}{c} a_g \quad b_h \quad c_k \\ \swarrow \alpha \quad \searrow \beta \\ e \quad d \end{array} = \sum_{f_{\mu\nu}} [F_d^{abc}]_{e\alpha\beta}^{f_{\mu\nu}} \begin{array}{c} a_g \quad b_h \quad c_k \\ \swarrow \mu \quad \searrow \nu \\ f \quad d \end{array}, \quad (3.211)$$

where

$$[F_d^{abc}]_{e\alpha\beta}^{f_{\mu\nu}} = \frac{1}{\chi_d} \begin{array}{c} a_g \quad b_h \quad c_k \\ \swarrow e \quad \searrow \alpha \quad \searrow \beta \\ \quad \quad \quad \mu \quad \nu \\ \quad \quad \quad f \quad d \end{array}, \quad (3.212)$$

that satisfy the *pentagon equation*

$$\begin{array}{c} a_g \quad b_h \quad c_k \quad d_l \\ \swarrow p \quad \searrow q \quad \searrow e \\ p \quad q \quad e \end{array} \rightarrow \begin{array}{c} a_g \quad b_h \quad c_k \quad d_l \\ \swarrow x \quad \searrow e \\ x \quad e \end{array} \rightarrow \begin{array}{c} a_g \quad b_h \quad c_k \quad d_l \\ \swarrow s \quad \searrow e \\ s \quad e \end{array} \rightarrow \begin{array}{c} a_g \quad b_h \quad c_k \quad d_l \\ \swarrow p \quad \searrow r \quad \searrow e \\ p \quad r \quad e \end{array}, \quad (3.213)$$

$$\sum_{\nu} [F_e^{pcd}]_{q\beta\gamma}^{r_{\mu\nu}} [F_e^{abr}]_{p\alpha\nu}^{s\sigma\tau} = \sum_{x\kappa\lambda\eta} [F_q^{abc}]_{p\alpha\beta}^{x\kappa\lambda} [F_e^{axd}]_{q\lambda\gamma}^{s\eta\tau} [F_s^{bcd}]_{x\kappa\eta}^{r_{\mu\sigma}}. \quad (3.214)$$

Hence all obstructions vanish for MPO representations satisfying this zipper condition, and we have a consistent fusion theory. It was shown in Ref. 64 that MPO algebras satisfying the zipper condition correspond closely to fusion categories. Hence the structure of \mathcal{G} -graded MPO algebras that satisfy the zipper condition correspond closely to \mathcal{G} -graded fusion categories.

The classification of \mathcal{G} SET phases for a given underlying topological order is given by \mathcal{G} -graded MPO algebras containing the MPO algebra of the underlying topological order as \mathcal{C}_1 . There is a subtlety in this classification as different MPO algebras may give rise to the same emergent SET. We say that a pair of \mathcal{G} -graded MPO algebras are *\mathcal{G} -graded Morita equivalent* if they lead to the same emergent SET. A method to calculate the emergent SET from the \mathcal{G} -graded MPO algebra is described in Section 3.6. Hence, for the SET phase classification, one should consider \mathcal{G} extensions of all representatives in the Morita equivalence class of the underlying topological order, up to \mathcal{G} -graded Morita equivalence.

Imposing further restrictions to isolate the \mathcal{G} -graded MPO algebras that describe SET orders

Thus far we have seen the structure of associative fusion rules arise from MPO algebras. We proceed to restrict our attention to MPO algebras that satisfy a range of further conditions, derived from structures in a unitary fusion category.

Firstly, we restrict to irreducible projector MPOs, i.e. those where MPO_1 cannot be written as a sum of inequivalent nonzero projector MPOs

$$\text{MPO}_1 \neq \text{PMPO} + \text{PMPO}' . \quad (3.215)$$

This excludes the possibility of cat state projectors that occur for spontaneous symmetry breaking phases. It corresponds to restricting to stable TQFTs, and we note the nonreducible case can be reconstructed by taking a sum of irreducible PMPOs.

Next we further restrict our attention to MPO representations that satisfy $\text{MPO}_g^\dagger = \text{MPO}_{\bar{g}}$. Equivalently, MPO representations that are unitary within the support subspace of a Hermitian unit MPO. This implies the MPO projector in Eq.(3.184) is also Hermitian. For a consistent unitary MPO representation we must have $\text{MPO}_{a_g}^\dagger = \text{MPO}_{\bar{a}_g} = \text{MPO}_{a_g}^-$, that is, the conjugate particle defined by Hermitian conjugation must match that defined by orientation reversal. In this case the tensor for the left handed tensor is defined by reflecting and complex conjugating the right handed tensor $(B_a^-)^{ij}_{\alpha\beta} = (B_a^{ij})_{\beta\alpha}^*$. Graphically

$$\begin{array}{c} i \\ \uparrow \\ \alpha \leftarrow a_g \rightarrow \beta \\ \downarrow \\ j \end{array} = \begin{array}{c} i \\ \uparrow \\ \beta \leftarrow a_g^* \rightarrow \alpha \\ \downarrow \\ j \end{array} , \quad (3.216)$$

i.e. complex conjugation is equivalent to reflection of the tensor. This implies

$$N_{ab}^c = N_{\bar{a}\bar{b}}^{\bar{c}} \quad (3.217)$$

Additionally, we have $w_{\bar{a}} = w_a^*$ and hence the w_a are real numbers. Moreover, $w_a > 0$ follows from Eq.(3.186), and the fact that N_{ab}^c has only nonnegative entries.

We further assume that the single block MPOs have been brought into a canonical form^{45,67} that admits unitary gauge transformation matrices Z_a and isometric fusion matrices X_{ab}^c .

It was shown in Ref. 64 that, for projector MPOs satisfying our assumptions, each block a has an element e_a that satisfies $N_{aa}^{e_a} = 1$. We further assume that there is a unique, single block

unit MPO 0 satisfying $N_{a\bar{a}}^0 = 1$ for all $a \in \mathcal{C}$. It was shown⁶⁴ that, with this assumption, $\bar{0} = 0$ and $\varkappa_0 = 1$. Furthermore, $N_{ab}^0 = \delta_{ab}$ and

$$N_{ab}^c = N_{b\bar{c}}^{\bar{a}} = N_{\bar{c}a}^{\bar{b}}, \quad \text{which implies} \quad \delta_{ab} = N_{a0}^b = N_{0a}^b, \quad (3.218)$$

and hence 0 plays the role of the trivial element under fusion, as expected. We do not expect all irreducible projector MPOs to be unital, as the existence of a unit is posited as an assumption in the theory of fusion categories.

Given the definition of the unit element, we require that the F -symbols have been brought into a gauge where

$$\delta_{ab}^c \delta_{\mu\nu} = [F_c^{a0b}]_{a0\mu}^{b0\nu} = [F_c^{ab0}]_{b\mu 0}^{a0\nu} = [F_c^{0ab}]_{b0\mu}^{a\nu 0}, \quad (3.219)$$

where the first equality corresponds to the *triangle equation* and the latter equalities follow by combining it with the pentagon equation. Then it was shown⁶⁴ that the F -symbols can be brought into a compatible gauge satisfying

$$[F_a^{a\bar{a}a}]_{000}^{000} = \frac{\varkappa_a}{d_a}, \quad (3.220)$$

with $d_a = d_{\bar{a}} > 0$, and \varkappa_a matching the definition given in Eq.(3.197).

Consistent fusion of the MPOs within a tensor network requires that removing an infinitesimal loop of MPO _{a} results in a weight d_a . A local sufficient condition for this is

$$\begin{array}{c} \uparrow \\ \boxed{a_g} \\ \uparrow \\ \boxed{a_g} \\ \uparrow \end{array} = d_a \begin{array}{c} \uparrow \\ \textcircled{P} \\ \uparrow \end{array}, \quad (3.221)$$

where P corresponds to the projector onto the support subspace of the PEPS virtual index. This implies that d_a match the definition of quantum dimension via the Perron-Frobenius vector, i.e.

$$d_a d_b = \sum_c N_{ab}^c d_c. \quad (3.222)$$

For a consistent MPO representation of \mathcal{G} domain walls within a tensor network, we furthermore require that an infinitesimal loop of domain wall \mathcal{G} can be removed. This corresponds to a local sufficient condition

$$\begin{array}{c} \uparrow \\ \boxed{g} \\ \uparrow \\ \boxed{g} \\ \uparrow \end{array} = \begin{array}{c} \uparrow \\ \textcircled{P} \\ \uparrow \end{array}, \quad (3.223)$$

which implies

$$w_{a_g} = \frac{d_{a_g}}{\mathcal{D}_{\mathbf{g}}^2}, \quad \text{where} \quad \mathcal{D}_{\mathbf{g}}^2 := \sum_{a_g} d_{a_g}^2. \quad (3.224)$$

Hence the MPO representation of \mathcal{G} is given by

$$\text{MPO}_{\mathbf{g}} = \sum_{a_g} \frac{d_{a_g}}{\mathcal{D}_{\mathbf{g}}^2} \text{MPO}_{a_g}, \quad (3.225)$$

in particular, MPO_1 corresponds to what is known as the ω_0 -projector for \mathcal{C}_1 .

At this point we renormalize the fusion and splitting tensors

$$\begin{array}{c} \alpha \\ \nearrow a \\ \mu \\ \nwarrow b \\ \beta \end{array} \gamma = d_a^{\frac{1}{4}} d_b^{\frac{1}{4}} d_c^{-\frac{1}{4}} [X_{a_g b_h}^{c_{gh} \mu}]_{\alpha\beta}^{\gamma}, \quad \begin{array}{c} \alpha \\ \nwarrow a \\ \mu \\ \nearrow b \\ \beta \end{array} \gamma = d_a^{\frac{1}{4}} d_b^{\frac{1}{4}} d_c^{-\frac{1}{4}} ([X_{a_g b_h}^{c_{gh} \mu}]_{\alpha\beta}^{\gamma})^*. \quad (3.226)$$

This is to ensure that removing a loop of $\text{MPO}_a \text{MPO}_{\bar{a}}$ fusing to the vacuum MPO_0 , matches the removal of an MPO_a loop within a tensor network

$$\begin{array}{c} \uparrow a_g \\ \downarrow b_h \end{array} = \sum_{c_{gh}\mu} \sqrt{\frac{d_c}{d_a d_b}} \begin{array}{c} a_g \\ \nwarrow \mu \\ \nearrow b_h \end{array} \begin{array}{c} \uparrow c \\ \downarrow c \end{array} = \delta_{ab}^c \delta_{\mu\nu} \delta_{cd} \sqrt{\frac{d_a d_b}{d_c}} \begin{array}{c} a_g \\ \nwarrow \mu \\ \nearrow b_h \end{array} \begin{array}{c} \uparrow c \\ \downarrow c \end{array}. \quad (3.227)$$

We focus on the class of MPOs admitting a set of unitary matrices A_c^{ab}, B_c^{ab} that satisfy *pivotal identities* relating the fusion and splitting tensors

$$\begin{array}{c} \bar{a} \\ \nwarrow a \\ \mu \\ \nearrow b \\ c \end{array} = \sum_{\nu} [A_c^{ab}]_{\mu}^{\nu} \begin{array}{c} \bar{a} \\ \nwarrow \nu \\ \nearrow b \\ c \end{array}, \quad \begin{array}{c} a \\ \nwarrow \mu \\ \nearrow b \\ c \end{array} = \sum_{\nu} [B_c^{ab}]_{\mu}^{\nu} \begin{array}{c} a \\ \nwarrow \nu \\ \nearrow b \\ c \end{array}. \quad (3.228)$$

This requires $N_{ab}^c = N_{ac}^b$, which follows from Eqs.(3.217) and (3.218). These pivotal identities are related to the existence of a pivotal structure in the theory of fusion categories. We believe that the above pivotal identities can be derived for the class of MPOs we are considering, however a proof is beyond the scope of this paper. We remark that such a proof was given in Ref. 93, Chapter 1, for the SPT case where $|\mathcal{C}_1| = 1$.

For the fixed point examples in Section 3.3 we found

$$[A_c^{ab}]_{\mu}^{\nu} = \sqrt{\frac{d_a d_b}{d_c}} ([F_b^{\bar{a}ab}]_{000}^{c\mu\nu})^*, \quad [B_c^{ab}]_{\mu}^{\nu} = \sqrt{\frac{d_a d_b}{d_c}} [F_a^{abb}]_{c\mu\nu}^{000}, \quad (3.229)$$

and we suspect that these formulas still hold for the full class of MPOs considered here.

Implications of the \mathcal{G} -grading

The existence of a \mathcal{G} -grading for the fusion structure implies further restrictions on the algebraic data of an MPO algebra, similar to results shown in Ref. 31.

Since each element $a_{\mathbf{g}}$ satisfies $N_{ab}^0 = N_{a0}^b = N_{0a}^b = \delta_{ab}$, for all $b_{\mathbf{g}}$ there must exist some c_1, c'_1 such that $N_{ab}^c = N_{ca}^b \neq 0$, and $N_{ba}^{c'} = N_{ac'}^b \neq 0$. That is, for any single block $\text{MPO}_{a_{\mathbf{g}}}$, any other single block $\text{MPO}_{b_{\mathbf{h}}}$ appears in the product $\text{MPO}_{a_{\mathbf{g}}} \text{MPO}_{c'_1}^{\bar{c}_1}$ and also $\text{MPO}_{c_1} \text{MPO}_{a_{\mathbf{g}}}$ for some c_1, c'_1 . However, we do not generally have $|\mathcal{C}_{\mathbf{g}}| = |\mathcal{C}_{\mathbf{h}}|$ for $\mathbf{g} \neq \mathbf{h}$.

The MPO algebras we consider are faithfully \mathcal{G} -graded, hence Eq.(3.222) implies that $\mathcal{D}_0^2 = \mathcal{D}_{\mathbf{g}}^2$ for all \mathbf{g} . The argument for this is identical to that given in Ref. 31. Consequently we have

$$\mathcal{D}_{\mathcal{G}}^2 = |\mathcal{G}| \mathcal{D}_1^2, \quad \text{where} \quad \mathcal{D}_{\mathcal{G}}^2 = \sum_{\mathbf{g}} \mathcal{D}_{\mathbf{g}}^2. \quad (3.230)$$

Hence the MPO projector onto the symmetric subspace in Eq.(3.184) corresponds to the ω_0 -loop of \mathcal{C}_G , since

$$\frac{w_a}{|\mathcal{G}|} = \frac{d_a}{\mathcal{D}_G^2}. \quad (3.231)$$

The ω_0 -MPO loop of \mathcal{C}_1 satisfies an equation, generalizing Eq.(3.167), that allows us to move a \mathbf{g} -MPO through an MPO_1 loop by transforming it to an $\text{MPO}_{\mathbf{g}}$ loop. That is,

$$\begin{aligned} \text{Diagram 1} &= \frac{1}{\mathcal{D}_1^2} \sum_{\substack{a_g s_1 \\ b_g \mu}} \sqrt{\frac{d_b d_s}{d_a}} \text{Diagram 2} \end{aligned} \quad (3.232)$$

$$= \frac{1}{\mathcal{D}_1^2} \sum_{\substack{a_g b_g \\ s_1 \nu \mu}} \sqrt{\frac{d_b d_s}{d_a}} ([B_b^{sa}]_\mu^*) [B_b^{sa}]_\mu^\nu \text{Diagram 3} \quad (3.233)$$

$$= \frac{1}{\mathcal{D}_1^2} \sum_{\substack{a_g b_g \\ s_1 \nu}} d_b \sqrt{\frac{d_s}{d_a d_b}} \varkappa_a \varkappa_{\bar{a}} \text{Diagram 4} = \frac{1}{\mathcal{D}_1^2} \sum_{a_g b_g} d_b \text{Diagram 5} \quad (3.234)$$

$$= \text{Diagram 6}, \quad (3.235)$$

where we have used the zipper condition, the pivotal identities, and properties of the FS indicator. A similar equation holds for a $\mathbf{1}$ MPO of arbitrary length and with arbitrary orientations of the black indices. By applying orientation reversing gauge transformations, Z_g , on the open red indices and noting that reversal of the orientation of the $\mathbf{1}$ MPO has no effect, $\text{MPO}_1^- = \text{MPO}_1$, the equation can also be seen to hold for all orientations of the red indices. Furthermore, the same argument applies for pulling through an open MPO from any contiguous subregion of a circle to its complement.

3.5.4 SET tensor network states and the symmetry-enriched pulling through equation

The \mathcal{G} -graded MPO algebras that were just introduced yield representations of domain walls in SET tensor network states. We proceed to introduce a condition on the local tensors of a PEPS that ensures it is symmetric under an on-site representation of \mathcal{G} , and furthermore that the domain walls are described by a \mathcal{G} -graded MPO algebra.

The local tensors of a two dimensional PEPS on a directed trivalent lattice, dual to a triangulation with branching structure, are specified by

$$T_p^{ijk} = \begin{array}{c} \text{triangle with } p \text{ in center} \\ \text{top edge } k \text{ (outgoing)} \\ \text{bottom-left edge } i \text{ (incoming)} \\ \text{bottom-right edge } j \text{ (incoming)} \end{array}, \quad T_p^{ijk} = \begin{array}{c} \text{triangle with } p \text{ in center} \\ \text{top edge } i \text{ (incoming)} \\ \text{bottom-left edge } j \text{ (incoming)} \\ \text{bottom-right edge } k \text{ (outgoing)} \end{array}. \quad (3.236)$$

We assume that this PEPS is MPO-injective and hence describes a state with some underlying topological order. The MPO w.r.t. which the PEPS is MPO-injective corresponds to MPO_1 in the MPO representation of \mathcal{G} .

The PEPS is symmetric under an on-site representation of \mathcal{G} if it satisfies the *symmetry-enriched pulling through equation*⁹³

$$\begin{array}{c} \text{triangle with } g \text{ in center} \\ \text{top edge } g \text{ (outgoing)} \\ \text{bottom-left edge } g \text{ (incoming)} \\ \text{bottom-right edge } g \text{ (incoming)} \end{array} = \begin{array}{c} \text{triangle with } g \text{ in center} \\ \text{top edge } g \text{ (outgoing)} \\ \text{bottom-left edge } g \text{ (incoming)} \\ \text{bottom-right edge } g \text{ (incoming)} \end{array}, \quad \begin{array}{c} \text{triangle with } g \text{ in center} \\ \text{top edge } g \text{ (outgoing)} \\ \text{bottom-left edge } g \text{ (incoming)} \\ \text{bottom-right edge } g \text{ (incoming)} \end{array} = \begin{array}{c} \text{triangle with } g \text{ in center} \\ \text{top edge } g \text{ (outgoing)} \\ \text{bottom-left edge } g \text{ (incoming)} \\ \text{bottom-right edge } g \text{ (incoming)} \end{array}. \quad (3.237)$$

Where we have used the following graphical notation for the on-site group action

$$g = U_g, \quad \text{hence} \quad \begin{array}{c} \text{triangle with } g \text{ in center} \\ \text{top edge } g \text{ (outgoing)} \\ \text{bottom-left edge } g \text{ (incoming)} \\ \text{bottom-right edge } g \text{ (incoming)} \end{array} := \sum_q [U_g]_p^q T_q^{ijk}. \quad (3.238)$$

By the properties of the MPOs described above, Eq.(3.237) implies that all the similar pulling through equations, involving MPO_g acting on a different choice of indices, also hold. While the tensors considered above can be used to build a PEPS on any triangulation with branching structure. Similar considerations apply for regular lattices, such as the square lattice, or more generally for locally planar directed graphs.

Due to Eqs.(3.223) and (3.232), the symmetry-enriched pulling through equation is equivalent to the following group intertwiner property

$$\begin{array}{c} \text{triangle with } g \text{ in center} \\ \text{top edge } g \text{ (outgoing)} \\ \text{bottom-left edge } g \text{ (incoming)} \\ \text{bottom-right edge } g \text{ (incoming)} \end{array} = \begin{array}{c} \text{triangle with } g \text{ in center} \\ \text{top edge } g \text{ (outgoing)} \\ \text{bottom-left edge } g \text{ (incoming)} \\ \text{bottom-right edge } g \text{ (incoming)} \end{array}, \quad \begin{array}{c} \text{triangle with } g \text{ in center} \\ \text{top edge } g \text{ (outgoing)} \\ \text{bottom-left edge } g \text{ (incoming)} \\ \text{bottom-right edge } g \text{ (incoming)} \end{array} = \begin{array}{c} \text{triangle with } g \text{ in center} \\ \text{top edge } g \text{ (outgoing)} \\ \text{bottom-left edge } g \text{ (incoming)} \\ \text{bottom-right edge } g \text{ (incoming)} \end{array}, \quad (3.239)$$

which we expect to be more practical for numerical purposes.

ω_0 -loop fixed-point tensors

The ω_0 -loop of \mathcal{C}_1 , MPO_1 , defines an MPO-injective PEPS tensor⁶⁴ which we refer to as an MPO fixed-point PEPS tensor

$$(3.240)$$

The physical degree of freedom is identified with a subspace of the three MPO indices that enter the circle, given by the support of $\text{MPO}_1^{L=3}$. The on-site group action is given by $U_g = \text{MPO}_g^{L=3}$, which is unitary on the support subspace of $\text{MPO}_1^{L=3}$, corresponding to the local physical degree of freedom. The application of the group action to the PEPS tensors results in

$$(3.241)$$

Hence it follows from Eq.(3.232) that the MPO fixed-point PEPS tensors in Eq.(3.240) satisfy the symmetry-enriched pulling through equation (3.237).

We remark that this MPO fixed-point construction yields the same PEPS tensor for all \mathcal{G} -extensions of an underlying MPO algebra \mathcal{C}_1 . This same tensor represents different SET phases, depending upon the choice of the on-site symmetry action. A similar phenomenon has previously been noted for the restricted case of SPT phases⁷⁰.

3.5.5 Abstracting the calculus of \mathcal{G} -graded MPO algebras to diagrams

At this point we have developed the theory of \mathcal{G} -graded MPO algebras, and seen that they represent \mathcal{G} domain walls of symmetric tensor networks. The characteristics of the domain wall MPOs within a tensor network are topological and do not have a strong dependence on local details, such as the number of sites within a certain region. In fact, the calculus of these MPOs within a tensor network can be abstracted further by not explicitly keeping track of the underlying lattice. This was described in detail in Eqs.(3.16) and (3.49).

To carrying out this abstraction, we first identify the tensor network ground state with the vacuum. This corresponds to the empty diagram

$$(3.242)$$

A loop on top of this background represents an MPO

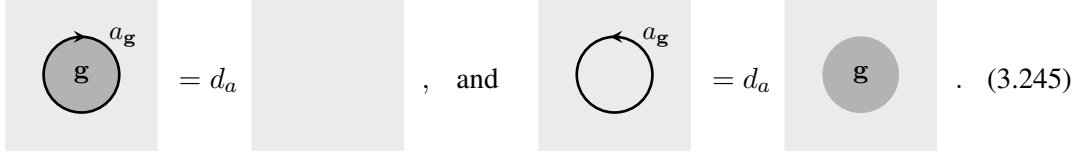
$$(3.243)$$

and the application of the on-site symmetry to all sites within a region is depicted as



$$\text{[Diagram: Gray square with a gray circle 'g' inside]} \quad (3.244)$$

Hence



$$\text{[Diagram: Gray square with a black circle 'a_g' and 'g' inside]} = d_a \text{ [Diagram: Gray square]} , \text{ and } \text{[Diagram: Black circle 'a_g' inside]} = d_a \text{ [Diagram: Gray square with a gray circle 'g' inside]} \quad (3.245)$$

When passing to the abstract diagrammatic calculus, we switched convention for the colour of MPO loops from red to black.

All of the properties satisfied by the \mathcal{G} -graded MPO algebras that were discussed throughout this section can be carried over to the abstract diagrammatic calculus. This realizes all consistent fusion diagrams, modulo local relations from the \mathcal{G} -graded unitary fusion category, and planar isotopy. In particular, restricting to the $\mathbf{1}$ -sector recovers the diagrammatic calculus^{203,217,218} of the unitary fusion category \mathcal{C}_1 . The full $\mathcal{C}_{\mathcal{G}}$ leads to a more general diagrammatic calculus, related to a 2-category, that was recently introduced in Ref. 222.

In this section we have adapted the theory of MPO algebras, presented in Ref. 64, to include a \mathcal{G} -grading. These MPOs form a representation of the domain walls of an SET ordered phase. Classifying the emergent SET order that arises from \mathcal{G} -graded MPO algebras corresponds to grouping them into graded Morita equivalence classes. Two \mathcal{G} -graded MPO algebras are equivalent if they give rise to the same symmetry-enriched \mathcal{G} -graded double, which is described by a UGxBFC. In the next section we will describe how to construct the symmetry-enriched double, and extract the gauge invariant physical data of the emergent SET.

This contains the classification of the underlying emergent topological order as a subproblem. This emergent topological order is given by the Drinfeld double (or center) of the fusion category corresponding to the MPO algebra and hence is nonchiral. Moreover, this construction can realize all nonchiral topological orders^{230,231}. The classification is then given by collecting MPO algebras into Morita equivalence classes that lead to the same topological order^{164,211}.

It was shown in Ref. 81, and later used in a condensed matter context by Refs. 32,33, that the symmetry-enriched double construction can realize all consistent symmetry actions of emergent anyons in an on-site manner. In the next section we will go further to construct the full SET on the lattice, including the theory of emergent symmetry defects.

3.6 The defect tube algebra and emergent symmetry-enriched topological order

In this section we generalize Ocneanu's tube algebra to an algebra of topological symmetries acting on each nontrivial monodromy \mathbf{g} -defect, appearing at the termination point of a \mathbf{g} -domain wall. We construct tensor network representations of the defect superselection sectors by block diagonalizing each \mathbf{g} -sector of this defect tube algebra. Furthermore, we find tensor network

3.6.1 Definition of the dube algebra

By a slight generalisation of Eq.(3.17) the \mathbf{g} -twisted cylinder is spanned by tensor networks that have been closed with an MPO from the \mathbf{g} -sector

We can repeat the analysis that lead to Eq.(3.120) by considering the virtual MPO symmetries in the $\mathbf{1}$ -sector that act on the punctures

Elements of the dube algebra are defined in the same way as for the tube algebra, except they now split into sectors according to the label of the horizontal MPO

which corresponds to the minimal tensor network

$$d_p^{\frac{1}{4}} d_r^{-\frac{1}{4}} \begin{array}{c} \begin{array}{c} \nearrow s \\ \rightarrow p \end{array} \\ \begin{array}{c} \leftarrow q \\ \nwarrow s \end{array} \end{array} . \quad (3.249)$$

We often refer to elements of the dube algebra simply as dubes*. We remark that there is a gauge freedom in the definition of the dube elements, similar to a 1-cochain.

Hence Eq.(3.247) can be rewritten as

$$\mathbb{1}_{\mathbf{g}} := \sum_{r_{\mathbf{g}}} \mathcal{T}_{r_{\mathbf{g}} r_{\mathbf{g}}}^0 = \frac{1}{\mathcal{D}_1^2} \sum_{\substack{p_{\mathbf{g}} q_{\mathbf{g}} \\ r_{\mathbf{g}} s_1}} (\mathcal{T}_{p_{\mathbf{g}} q_{\mathbf{g}} r_{\mathbf{g}}}^{s_1})^\dagger \mathcal{T}_{p_{\mathbf{g}} q_{\mathbf{g}} r_{\mathbf{g}}}^{s_1}, \quad (3.250)$$

where $\mathbb{1}_{\mathbf{g}}$ is the identity on the virtual level of the \mathbf{g} -twisted cylinder tensor network.

The definition of multiplication is given by stacking dubes, and is identical to the one given in Eq.(3.124). Similarly, the definition of Hermitian conjugation is given in Eq.(3.126). We remark that the \mathcal{G} -grading of the MPOs ensures that the dube algebra breaks into $|\mathcal{G}|$ orthogonal sectors, each of which is a C^* algebra. In particular, the $\mathbf{1}$ -sector of the dube algebra recovers the tube algebra of \mathcal{C}_1 .

3.6.2 Block diagonalizing sectors of the dube algebra with ICIs

Since the dube algebra breaks up into $|\mathcal{G}|$ decoupled C^* algebras, we can separately block diagonalize each of these sectors.

The sector generated by tubes of the form $\mathcal{T}_{p_{\mathbf{g}} q_{\mathbf{g}} r_{\mathbf{g}}}^{s_1}$ is referred to as the \mathbf{g} -dube algebra. It has dimension

$$D_{\mathbf{g}} = \sum_{p_{\mathbf{g}} q_{\mathbf{g}} r_{\mathbf{g}} s_1} \delta_{s_1 q_{\mathbf{g}}}^p \delta_{q_{\mathbf{g}} s_1}^r = \sum_{\underline{a}_{\mathbf{g}}} D_{a_{\mathbf{g}}} \times D_{a_{\mathbf{g}}}, \quad (3.251)$$

where the sum is over the irreducible blocks $\underline{a}_{\mathbf{g}}$ of the \mathbf{g} -dube algebra, and $D_{a_{\mathbf{g}}}$ is the dimension of the $\underline{a}_{\mathbf{g}}$ block (consisting of $D_{a_{\mathbf{g}}} \times D_{a_{\mathbf{g}}}$ -matrices).

The ICIs of each \mathbf{g} -sector are given by Hermitian projectors onto each irreducible $\underline{a}_{\mathbf{g}}$ block. The ICIs of the \mathbf{g} -sector determine the inequivalent superselection sectors for a disc filling a puncture at the termination point of a \mathbf{g} -domain wall. The ICIs can be found constructively by following the approach in Ref. 64. Expressions for the defect ICIs of the \mathcal{G} -graded dube algebra for $\mathcal{C}_{\mathcal{G}}$ can be derived from the ICIs of the tube algebra for $\mathcal{C}_{\mathcal{G}}$, this is discussed further in Section 3.8.

The \mathbf{g} -defect ICIs can be written as a linear combination of dubes from the \mathbf{g} -sector

$$\underline{a}_{\mathbf{g}} = \frac{1}{\mathcal{D}_1^2} \sum_{\substack{p_{\mathbf{g}} q_{\mathbf{g}} \\ r_{\mathbf{g}} s_1}} t_{a_{\mathbf{g}}}^{pqrs} \mathcal{T}_{p_{\mathbf{g}} q_{\mathbf{g}} r_{\mathbf{g}}}^{s_1}, \quad (3.252)$$

$$\begin{array}{c} \text{Diagram: A square box labeled } a_{\mathbf{g}} \text{ with four arrows pointing outwards (up, down, left, right).} \end{array} = \frac{1}{\mathcal{D}_1^2} \sum_{\substack{p_{\mathbf{g}} q_{\mathbf{g}} \\ r_{\mathbf{g}} s_1}} t_{a_{\mathbf{g}}}^{pqrs} \begin{array}{c} \text{Diagram: A vertex with four legs. Top-left leg labeled } p_{\mathbf{g}}, \text{ top-right leg labeled } s_1, \text{ bottom-left leg labeled } q_{\mathbf{g}}, \text{ bottom-right leg labeled } r_{\mathbf{g}}. \end{array}, \quad (3.253)$$

where the coefficients satisfy $t_{a_{\mathbf{g}}}^{pqrs} = \delta_{pr} t_{a_{\mathbf{g}}}^{pqps}$, as only dubes $\mathcal{T}_{p_{\mathbf{g}} q_{\mathbf{g}} r_{\mathbf{g}}}^{s_1}$ with $p_{\mathbf{g}} = r_{\mathbf{g}}$ can appear in the ICIs.

The $\mathbf{1}$ -sector of the dube algebra recovers the tube algebra of the underlying fusion category \mathcal{C}_1 . Hence the emergent topological order is described by $\mathcal{Z}(\mathcal{C}_1)$, see Section 3.4. The full set

*The process of constructing the defect tube algebra from a \mathcal{G} -graded MPO algebra is called *rolling a dube*.

of \mathbf{g} -sector ICIs lead to a description of the emergent SET order, which is denoted $\mathcal{Z}(\mathcal{C}_1)_{\mathcal{G}}$. The specifics of this construction, in particular how to extract the physical characteristics of the emergent theory, are described below.

For irreducible blocks of dimension $D_{a_{\mathbf{g}}} > 1$ the $\underline{a}_{\mathbf{g}}$ ICI further decomposes into a sum of $D_{a_{\mathbf{g}}}$ orthogonal irreducible idempotents $(\underline{a}_{\mathbf{g}})_{ii}$. Furthermore, there are $D_{a_{\mathbf{g}}}(D_{a_{\mathbf{g}}} - 1)$ nilpotent off diagonal elements $(\underline{a}_{\mathbf{g}})_{ij}$ for $i \neq j$

$$(\underline{a}_{\mathbf{g}})_{ij} = \frac{1}{\mathcal{D}_1^2} \sum_{\substack{p_{\mathbf{g}} q_{\mathbf{g}} \\ r_{\mathbf{g}} s_1}} t_{(\underline{a}_{\mathbf{g}})_{ij}}^{p_{\mathbf{g}} q_{\mathbf{g}} r_{\mathbf{g}} s_1} \mathcal{T}_{p_{\mathbf{g}} q_{\mathbf{g}} r_{\mathbf{g}} s_1}^{s_1}. \quad (3.254)$$

These elements span the $D_{a_{\mathbf{g}}} \times D_{a_{\mathbf{g}}}$ -matrix algebra of the $a_{\mathbf{g}}$ -block, hence the dubs in the \mathbf{g} -sector can be expanded in this basis

$$\mathcal{T}_{p_{\mathbf{g}} q_{\mathbf{g}} r_{\mathbf{g}} s_1}^{s_1} = \frac{1}{\mathcal{D}_1^2} \sum_{(\underline{a}_{\mathbf{g}})_{ij}} \bar{t}_{p_{\mathbf{g}} q_{\mathbf{g}} r_{\mathbf{g}} s_1}^{(\underline{a}_{\mathbf{g}})_{ij}} (\underline{a}_{\mathbf{g}})_{ij}. \quad (3.255)$$

The columns of this change-of-basis matrices are orthogonal

$$\frac{1}{\mathcal{D}_1^2} \sum_{p_{\mathbf{g}} q_{\mathbf{g}} r_{\mathbf{g}} s_1} \bar{t}_{p_{\mathbf{g}} q_{\mathbf{g}} r_{\mathbf{g}} s_1}^{(\underline{a}_{\mathbf{g}})_{ij}} (\bar{t}_{p_{\mathbf{g}} q_{\mathbf{g}} r_{\mathbf{g}} s_1}^{(b_{\mathbf{h}})_{kl}})^* = \delta_{ab} \delta_{ik} \delta_{jl} \frac{1}{|(\underline{a}_{\mathbf{g}})_{ij}|^2}, \quad (3.256)$$

for some positive weights $|(\underline{a}_{\mathbf{g}})_{ij}|$.

It follows from Eqs.(3.250) and (3.256) that

$$\mathbb{1}_{\mathbf{g}} = \sum_{(\underline{a}_{\mathbf{g}})_{ij}} \frac{1}{|(\underline{a}_{\mathbf{g}})_{ij}|^2} (\underline{a}_{\mathbf{g}})_{ij}^{\dagger} (\underline{a}_{\mathbf{g}})_{ij}, \quad (3.257)$$

where $\mathbb{1}_{\mathbf{g}}$ denotes the identity on the virtual level of the \mathbf{g} -twisted cylinder. Multiplying by $(\underline{a}_{\mathbf{g}})_{ii}$ implies

$$\sum_j \frac{1}{|(\underline{a}_{\mathbf{g}})_{ij}|^2} = 1, \quad \text{and hence} \quad \mathbb{1}_{\mathbf{g}} = \sum_{a_{\mathbf{g}}} \underline{a}_{\mathbf{g}}, \quad (3.258)$$

which is a partition of the identity on the virtual level of the \mathbf{g} -twisted cylinder by the $a_{\mathbf{g}}$ ICIs.

3.6.3 Projective group actions on the defect ICIs

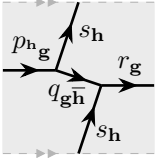
Beyond the topological symmetries acting on each \mathbf{g} -defect, there is also an action of each element of the physical symmetry group. This can be found by considering the action of the global symmetry on a \mathbf{g} -twisted cylinder tensor network

$$\begin{array}{c} \text{Diagram 1: A rectangle with a horizontal line through the middle. The top half is labeled } r_{\mathbf{g}} \text{ and the bottom half is labeled } \mathbf{h}. \end{array} = \frac{1}{d_s} \begin{array}{c} \text{Diagram 2: A rectangle with a horizontal line through the middle. The top half is labeled } r_{\mathbf{g}} \text{ and the bottom half is labeled } s_{\mathbf{h}}. \end{array} = \sum_{q_{\mathbf{gh}}} \sqrt{\frac{d_q}{d_r d_s^3}} \begin{array}{c} \text{Diagram 3: A rectangle with a horizontal line through the middle. The top half is labeled } r_{\mathbf{g}} \text{ and the bottom half is labeled } s_{\mathbf{h}}. \text{ There are vertical lines on the sides labeled } q_{\mathbf{gh}}. \end{array} \quad (3.259)$$

$$= \sum_{p_{\mathbf{hg}} q_{\mathbf{gh}}} \frac{1}{d_s^2} \sqrt{\frac{d_p}{d_r}} \begin{array}{c} \text{Diagram 4: A rectangle with a horizontal line through the middle. The top half is labeled } r_{\mathbf{g}} \text{ and the bottom half is labeled } s_{\mathbf{h}}. \text{ There are vertical lines on the sides labeled } p_{\mathbf{hg}} \text{ and } q_{\mathbf{gh}}. \end{array}, \quad (3.260)$$

where the darker shaded region denotes the application of the on-site physical action of $\mathbf{h} \in \mathcal{G}$.

The action of \mathbf{h} on a \mathbf{g} -defect involves tube elements of the form

$$\mathcal{T}_{p_{\mathbf{h}\mathbf{g}}q_{\mathbf{gh}}r_{\mathbf{g}}}^{s_{\mathbf{h}}} := d_p^{\frac{1}{4}} d_r^{-\frac{1}{4}} \left(\text{Diagram} \right). \quad (3.261)$$


These tubes match the set of elements of the tube algebra for $\mathcal{C}_{\mathcal{G}}$, however they are interpreted differently in light of the \mathcal{G} -grading structure.

Hence Eq.(3.259) can be written as

$$\mathbf{U}_{\mathbf{h}}[\mathbb{1}_{\mathbf{g}}] = \frac{1}{\mathcal{D}_{\mathbf{1}}^2} \sum_{\substack{p_{\mathbf{h}\mathbf{g}}q_{\mathbf{gh}} \\ r_{\mathbf{g}}s_{\mathbf{h}}}} (\mathcal{T}_{p_{\mathbf{h}\mathbf{g}}q_{\mathbf{gh}}r_{\mathbf{g}}}^{s_{\mathbf{h}}})^\dagger \mathcal{T}_{p_{\mathbf{h}\mathbf{g}}q_{\mathbf{gh}}r_{\mathbf{g}}}^{s_{\mathbf{h}}}, \quad (3.262)$$

where $\mathbf{U}_{\mathbf{h}}$ denotes the action of the global symmetry $\mathbf{h} \in \mathcal{G}$ to the physical level of the tensor network.

The action of an \mathbf{h} domain wall on an ICI $\underline{a}_{\mathbf{g}}$ is defined by projecting the collection of tubes with $s \in \mathcal{C}_{\mathbf{h}}$ onto the ICI

$$\mathcal{B}_{a_{\mathbf{g}}}^{\mathbf{h}} := K \left(\sum_{\substack{p_{\mathbf{h}\mathbf{g}}q_{\mathbf{gh}} \\ r_{\mathbf{g}}s_{\mathbf{h}}}} c_{a_{\mathbf{g}}}^{pqrs} \mathcal{T}_{p_{\mathbf{h}\mathbf{g}}q_{\mathbf{gh}}r_{\mathbf{g}}}^{s_{\mathbf{h}}} \right) \underline{a}_{\mathbf{g}}, \quad (3.263)$$

for arbitrary constants $c_{a_{\mathbf{g}}}^{pqrs} \neq 0$, and some normalization $K \neq 0$ that depends on the $c_{a_{\mathbf{g}}}^{pqrs}$. For simplicity of presentation we ignore some subtleties that may arise in the case of a degenerate block, the analysis presented can still be applied to the degenerate case with some care. We remark that the RHS of the above equation may be 0 for certain fine-tuned choices of $c_{a_{\mathbf{g}}}^{pqrs}$, we intend it to hold for generic choices, i.e. after adding a random perturbation to any given fine-tuned values.

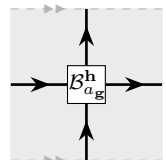
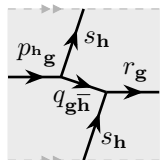
The normalization is fixed, up to a multiplicative phase factor, by the unitarity requirement

$$(\mathcal{B}_{a_{\mathbf{g}}}^{\mathbf{h}})^\dagger \mathcal{B}_{a_{\mathbf{g}}}^{\mathbf{h}} = \underline{a}_{\mathbf{g}}. \quad (3.264)$$

The domain walls are only defined up to a multiplicative 1-cochain $\varepsilon_{a_{\mathbf{g}}}^{\mathbf{h}} \in \text{U}(1)$. We always work with a choice of 1-cochain such that $\mathcal{B}_{a_{\mathbf{g}}}^{\mathbf{1}} = \underline{a}_{\mathbf{g}}$ and $\mathcal{B}_0^{\mathbf{g}} = \text{MPO}_{\mathbf{g}}$.

The domain walls on each sector can be expanded in the tube basis

$$\mathcal{B}_{a_{\mathbf{g}}}^{\mathbf{h}} = \frac{1}{\mathcal{D}_{\mathbf{1}}^2} \sum_{\substack{p_{\mathbf{h}\mathbf{g}}q_{\mathbf{gh}} \\ r_{\mathbf{g}}s_{\mathbf{h}}}} t_{\mathcal{B}_{a_{\mathbf{g}}}^{\mathbf{h}}}^{pqrs} \mathcal{T}_{p_{\mathbf{h}\mathbf{g}}q_{\mathbf{gh}}r_{\mathbf{g}}}^{s_{\mathbf{h}}}, \quad (3.265)$$

$$\left(\text{Diagram} \right) = \frac{1}{\mathcal{D}_{\mathbf{1}}^2} \sum_{\substack{p_{\mathbf{h}\mathbf{g}}q_{\mathbf{gh}} \\ r_{\mathbf{g}}s_{\mathbf{h}}}} t_{\mathcal{B}_{a_{\mathbf{g}}}^{\mathbf{h}}}^{pqrs} \left(\text{Diagram} \right). \quad (3.266)$$



Due to Eqs.(3.258), and (3.264) we have

$$\mathbf{U}_{\mathbf{h}}[\mathbb{1}_{\mathbf{g}}] = \sum_{a_{\mathbf{g}}} (\mathcal{B}_{a_{\mathbf{g}}}^{\mathbf{h}})^\dagger \mathcal{B}_{a_{\mathbf{g}}}^{\mathbf{h}}, \quad (3.267)$$

which corresponds to the intertwining of a physical \mathbf{h} action to the virtual level by the \mathbf{g} -twisted cylinder tensor network.

Permutation action on the defects

The action of the domain wall on the set of defects may result in a nontrivial permutation $\rho_h(a_g) = \mathbf{h}(a_g) = \underline{(\mathbf{h}a)}_{\mathbf{h}g}$. Which can be found as follows

$$\mathbf{h}(a_g) := \mathcal{B}_{a_g}^{\mathbf{h}} (\mathcal{B}_{a_g}^{\mathbf{h}})^\dagger, \quad \text{or equivalently} \quad \mathcal{B}_{a_g}^{\mathbf{h}} a_g = \mathbf{h}(a_g) \mathcal{B}_{a_g}^{\mathbf{h}}. \quad (3.268)$$

To reiterate, the permuted defect satisfies $\mathbf{h}(a_g) \in \mathcal{C}_{\mathbf{h}g}$, and even in the case $\mathbf{g}\mathbf{h} = \mathbf{h}\mathbf{g}$ there may still be a nontrivial permutation action of \mathbf{h} upon the defects within sector \mathbf{g} , captured by $\underline{(\mathbf{h}a)}_{\mathbf{g}}$. In particular, the potentially nontrivial permutation action of the global symmetry \mathcal{G} upon the emergent anyons (or $\mathbf{1}$ -defects) can be extracted.

By definition (3.263), we have $\mathcal{B}_{\mathbf{k}(a_g)}^{\mathbf{h}} \mathcal{B}_{a_g}^{\mathbf{k}} = C \mathcal{B}_{a_g}^{\mathbf{h}\mathbf{k}}$, for some constant C . Hence ρ is a homomorphism from \mathcal{G} to the permutation group on $\mathcal{C}_{\mathcal{G}}$

$$\mathbf{h}(\mathbf{k}(a_g)) = \mathbf{h}\mathbf{k}(a_g). \quad (3.269)$$

We remark that the action of the domain walls commutes with the T matrix, see Eqs.(3.146), and (3.283). Hence the topological spin of all superselection sectors in an orbit of the permutation action must match.

We refer to the set of all group elements that do not permute a given defect a_g as its centralizer

$$Z_{a_g} := \{\mathbf{h} \in \mathcal{G} \mid \mathbf{h}a_g = a_g\}, \quad (3.270)$$

which is a subgroup of \mathcal{G} . Note $\mathbf{g} \in Z_{a_g}$ as the T matrix, see Eq.(3.149), commutes with a_g .

The orbit of a defect a_g under the \mathcal{G} -action is denoted by

$$[a_g] := \{\mathbf{h}a_g \mid \mathbf{h} \in \mathcal{G}\}, \quad (3.271)$$

and a set of representatives for each right coset of Z_{a_g} is written as \mathcal{G}/Z_{a_g} , hence

$$[a_g] = \{\mathbf{h}a_g \mid \mathbf{h} \in \mathcal{G}/Z_{a_g}\}. \quad (3.272)$$

2-cocycle of the projective representation on a defect

We can go beyond the analysis of the previous section to work out precise composition rules of the domain walls. Since

$$\left(\sum_{a_g} (\mathcal{B}_{a_g}^{\mathbf{h}\mathbf{k}})^\dagger \mathcal{B}_{\mathbf{k}(a_g)}^{\mathbf{h}} \mathcal{B}_{a_g}^{\mathbf{k}} \right) \underline{b_g} = \underline{b_g} \left(\sum_{a_g} (\mathcal{B}_{a_g}^{\mathbf{h}\mathbf{k}})^\dagger \mathcal{B}_{\mathbf{k}(a_g)}^{\mathbf{h}} \mathcal{B}_{a_g}^{\mathbf{k}} \right), \quad (3.273)$$

$$\left(\sum_{a_g} (\mathcal{B}_{a_g}^{\mathbf{h}\mathbf{k}})^\dagger \mathcal{B}_{\mathbf{k}(a_g)}^{\mathbf{h}} \mathcal{B}_{a_g}^{\mathbf{k}} \right)^\dagger \left(\sum_{a_g} (\mathcal{B}_{a_g}^{\mathbf{h}\mathbf{k}})^\dagger \mathcal{B}_{\mathbf{k}(a_g)}^{\mathbf{h}} \mathcal{B}_{a_g}^{\mathbf{k}} \right) = \mathbf{1_g}, \quad (3.274)$$

by an application of Schur's lemma we have

$$\mathcal{B}_{\mathbf{k}(a_g)}^{\mathbf{h}} \mathcal{B}_{a_g}^{\mathbf{k}} = \eta_a(\mathbf{h}, \mathbf{k}) \mathcal{B}_{a_g}^{\mathbf{h}\mathbf{k}}, \quad (3.275)$$

for some phase $\eta_a(\mathbf{h}, \mathbf{k}) \in \text{U}(1)$. Due to the associativity of matrix multiplication, η_a must satisfy the twisted 2-cocycle equation

$$\eta_{\mathbf{k}a}(\mathbf{f}, \mathbf{h}) \eta_a(\mathbf{f}\mathbf{h}, \mathbf{k}) = \eta_a(\mathbf{f}, \mathbf{h}\mathbf{k}) \eta_a(\mathbf{h}, \mathbf{k}). \quad (3.276)$$

Since $\mathcal{B}_{a_g}^{\mathbf{k}}$ is only defined up to a multiplicative 1-chain, $\eta_a(\mathbf{h}, \mathbf{k})$ is only defined up to a 2-coboundary and hence each defect a_g carries a ρ -twisted projective representation in cohomology class $[\eta_a] \in \mathcal{H}_\rho^2(\mathcal{G}, \text{U}(1))$. Furthermore, each defect a_g transforms under a conventional projective representation of its own centralizer Z_{a_g} with cohomology class $[\eta_a] \in \mathcal{H}^2(Z_a, \text{U}(1))$. We assume these cocycles have been normalized such that

$$\eta_a(\mathbf{h}, \mathbf{1}) = \eta_a(\mathbf{1}, \mathbf{h}) = 1. \quad (3.277)$$

We remark that all defects in a \mathcal{G} -orbit $\mathbf{h}a_g \in [a_g]$ have isomorphic centralizer groups $Z_{a_g} \cong Z_{\mathbf{h}a_g}$, via the obvious isomorphism $\mathbf{k} \mapsto \mathbf{h}\mathbf{k}$. It was shown in Ref. 31 that the 2-cocycle of the projective rep of $Z_{\mathbf{h}a_g}$ acting on $\mathbf{h}a_g$ is related to the projective rep of Z_a acting on a_g by a coboundary

$$\eta_{\mathbf{h}a_g}(\mathbf{h}\mathbf{x}, \mathbf{h}\mathbf{y}) = d\varepsilon_a^{\mathbf{h}}(\mathbf{x}, \mathbf{y}) \eta_a(\mathbf{x}, \mathbf{y}), \quad \text{where} \quad \varepsilon_a^{\mathbf{h}}(\mathbf{x}) := \frac{\eta_a(\bar{\mathbf{h}}, \mathbf{h}\mathbf{x})}{\eta_a(\mathbf{x}, \mathbf{k})}, \quad (3.278)$$

hence $[\eta_{\mathbf{h}a_g}(\mathbf{h}\mathbf{x}, \mathbf{h}\mathbf{y})] = [\eta_a(\mathbf{x}, \mathbf{y})]$ give the same element in both $\mathcal{H}^2(Z_a, \text{U}(1))$ and $\mathcal{H}^2(Z_{\mathbf{h}a_g}, \text{U}(1))$.

Furthermore, this gives a canonical isomorphism between the $\eta_{\mathbf{h}a_g}$ -projective irreps of $Z_{\mathbf{h}a_g}$ and the η_a -projective irreps of Z_a , for a chosen representative $a \in [a]$, as follows

$$\pi_{\mathbf{h}a_g}^\mu(\mathbf{h}\mathbf{k}) = \varepsilon_a^{\mathbf{h}}(\mathbf{k}) \pi_a^\mu(\mathbf{k}). \quad (3.279)$$

Where π_a^μ is an irreducible projective representation of Z_a with cocycle η_a , labeled by μ .

3.6.4 Symmetry-twisted minimally entangled states and \mathcal{G} -crossed modular matrices

The representations of \mathbf{h} on the \mathbf{g} -defects $\mathcal{B}_{a_g}^{\mathbf{h}}$ yield all the (\mathbf{g}, \mathbf{h}) symmetry-twisted, minimally entangled states³¹ on the torus

$$|\mathcal{B}_{a_g}^{\mathbf{h}}\rangle = \frac{1}{D_a \mathcal{D}_1^2} \sum_{p_g q_{\bar{\mathbf{g}}\mathbf{h}} s_{\mathbf{h}}} t_{\mathcal{B}_{a_g}^{\mathbf{h}}}^{pqps} |p_g s_{\mathbf{h}} q_{\bar{\mathbf{g}}\mathbf{h}}\rangle. \quad (3.280)$$

Only tubes $\mathcal{T}_{p_{\mathbf{h}}q_{\bar{\mathbf{g}}\mathbf{h}}r_{\mathbf{g}}}^{s_{\mathbf{h}}}$ with $p = r$ lead to nonzero states, and hence nonzero symmetry-twisted sectors must satisfy $\mathbf{g}\mathbf{h} = \mathbf{h}\mathbf{g}$. Furthermore, only group elements with nonzero trace $\text{Tr}[\mathcal{B}_{a_g}^{\mathbf{h}}] \neq 0$ lead to nonzero states. By using Eq.(3.268), and the orthogonality of defect ICIs, this implies that nonzero symmetry-twisted MES must satisfy $\mathbf{h}a_g = a_g$. Hence the dimension of the (\mathbf{g}, \mathbf{h}) -sector equals the number of \mathbf{h} -invariant \mathbf{g} -defects.

Similarly, one can use the crossing tensors from the domain wall tensor networks $\mathcal{B}_{a_g}^{\mathbf{h}}$ — containing the weights $t_{\mathcal{B}_{a_g}^{\mathbf{h}}}^{pqps}$ — to construct general symmetry-twisted states on arbitrary oriented 2-manifolds, i.e. higher genus tori. Here we focus on the torus, as it already allows us to construct the \mathcal{G} -crossed S and T matrices that generate a representation of the modular group.

The action of the global, on-site symmetry upon the symmetry-twisted MES can be calculated by using Eq.(3.267)

$$\mathbf{U}_{\mathbf{k}} |\mathcal{B}_{a_g}^{\mathbf{h}}\rangle = |\mathcal{B}_{a_g}^{\mathbf{k}} \mathcal{B}_{a_g}^{\mathbf{h}} (\mathcal{B}_{a_g}^{\mathbf{k}})^\dagger\rangle = \frac{\eta_a(\mathbf{k}, \mathbf{h}) \eta_{\mathbf{k}a}(\mathbf{h}\mathbf{k}, \bar{\mathbf{k}})}{\eta_a(\bar{\mathbf{k}}, \mathbf{k})} |\mathcal{B}_{\mathbf{k}a_g}^{\mathbf{h}}\rangle. \quad (3.281)$$

Where, by Eq.(3.275), and Eq.(3.276), we have $\eta_a(\bar{\mathbf{k}}, \mathbf{k})(\mathcal{B}_{a_g}^{\mathbf{k}})^\dagger = \mathcal{B}_{\mathbf{k}a_g}^{\bar{\mathbf{k}}}$.

For calculational purposes it is often convenient to derive the permutation action on the defects $\mathbf{k}a_g$ directly from the MES. This can be done by intertwining the global $\mathbf{U}_{\mathbf{k}}$ action on the physical indices to $\text{MPO}_{\mathbf{k}}$ on the virtual indices, and fusing it into the 1-skeleton of the torus.

For $\mathbf{k} \in Z_h$, by Eq.(3.264), we have

$$\mathbf{U}_{\mathbf{k}} |\mathcal{B}_{a_g}^{\mathbf{h}}\rangle = \eta_{a_g}^{\mathbf{h}}(\mathbf{k}) |\mathcal{B}_{\mathbf{k}a_g}^{\mathbf{h}}\rangle, \quad \text{where} \quad \eta_{a_g}^{\mathbf{h}}(\mathbf{k}) = \frac{\eta_a(\mathbf{k}, \mathbf{h})}{\eta_a(\mathbf{h}, \mathbf{k})}, \quad (3.282)$$

which is the slant product. This phase is only gauge invariant for $\mathbf{k} \in Z_{\mathcal{B}_{a_g}^{\mathbf{h}}}$, which is defined to be the elements of Z_{a_g} that also commute with \mathbf{h} . In that case we find a group homomorphism $\eta_{a_g}^{\mathbf{h}} : Z_{\mathcal{B}_{a_g}^{\mathbf{h}}} \rightarrow \text{U}(1)$, due to the 2-cocycle Equation (3.276).

The \mathcal{G} -crossed modular S and T matrices are defined by the same action on tubes as the topological modular matrices, see Eq.(3.146). They satisfy

$$|S(\mathcal{B}_{a_g}^{\mathbf{h}})\rangle = \sum_{b_h} S_{a_g b_h} |\mathcal{B}_{b_h}^{\bar{\mathbf{g}}}\rangle, \quad |T(\mathcal{B}_{a_g}^{\mathbf{h}})\rangle = \theta_{\mathcal{B}_{a_g}^{\mathbf{h}}} |\mathcal{B}_{a_g}^{\mathbf{g}\mathbf{h}}\rangle, \quad (3.283)$$

where

$$S_{a_g b_h} = \frac{D_b \text{Tr}[(\mathcal{B}_{b_h}^{\bar{\mathbf{g}}})^\dagger S(\mathcal{B}_{a_g}^{\mathbf{h}})]}{D_a \text{Tr}[(\mathcal{B}_{b_h}^{\bar{\mathbf{g}}})^\dagger \mathcal{B}_{b_h}^{\bar{\mathbf{g}}}]}, \quad \theta_{\mathcal{B}_{a_g}^{\mathbf{h}}} \delta_{a,b} = \frac{D_b \text{Tr}[(\mathcal{B}_{b_h}^{\bar{\mathbf{g}}})^\dagger T(\mathcal{B}_{a_g}^{\mathbf{h}})]}{D_a \text{Tr}[(\mathcal{B}_{b_h}^{\bar{\mathbf{g}}})^\dagger \mathcal{B}_{b_h}^{\bar{\mathbf{g}}}]}, \quad (3.284)$$

and we have used that $\mathbf{g}a_g = a_g$, since the T matrix tube commutes with a_g , see Eq.(3.149).

This includes the special case of the topological spin of defect superselection sectors

$$|T(a_g)\rangle = \theta_{a_g} |\mathcal{B}_{a_g}^{\mathbf{g}}\rangle, \quad (3.285)$$

and due to Eq.(3.268) we have

$$\theta_{\mathcal{B}_{a_g}^{\mathbf{h}}} = \eta_a(\mathbf{g}, \mathbf{h}) \theta_{a_g}. \quad (3.286)$$

The \mathcal{G} -crossed modular matrices are broken down into sectors, outside of which they are identically zero. That is,

$$\langle \mathcal{B}_{b_x}^{\mathbf{y}} | S(\mathcal{B}_{a_g}^{\mathbf{h}}) \rangle =: \delta_{\mathbf{x}, \mathbf{h}} \delta_{\mathbf{y}, \bar{\mathbf{g}}} S_{a_g b_h}^{(\mathbf{g}, \mathbf{h})}, \quad \langle \mathcal{B}_{b_x}^{\mathbf{y}} | T(\mathcal{B}_{a_g}^{\mathbf{h}}) \rangle =: \delta_{\mathbf{x}, \mathbf{g}} \delta_{\mathbf{y}, \mathbf{g}\mathbf{h}} \delta_{a,b} T_{a_g a_g}^{(\mathbf{g}, \mathbf{h})}. \quad (3.287)$$

Since S and T are clearly invertible by definition, the dimension of the (\mathbf{g}, \mathbf{h}) and (\mathbf{h}, \mathbf{g}) sectors must match. This implies the number of \mathbf{h} -invariant \mathbf{g} -defects equals the number of \mathbf{g} -invariant \mathbf{h} -defects, where $\mathbf{g}\mathbf{h} = \mathbf{h}\mathbf{g}$. In particular, the number of \mathbf{g} -defects equals the number of \mathbf{g} -invariant anyons ($\mathbf{1}$ -defects). We also have that the (\mathbf{g}, \mathbf{h}) and $(\mathbf{g}, \mathbf{g}\mathbf{h})$ sectors must have the same dimension.

Similar to the case without symmetry, the S and T matrices are unitary. This is because the emergent theory describes a modular non-chiral topological order that has been enriched by a non-anomalous symmetry, and remarkably it has been shown that \mathcal{G} -extensions of modular theories are \mathcal{G} -crossed modular^{31,98,166}.

Unitarity of the T matrix follows directly from our definition, and we expect that unitarity of S can also be derived in similar fashion to the ungraded tube algebra. However, we will not give such a proof here.

The \mathcal{G} -crossed S and T matrices satisfy modular relations, similar to the ungraded case. For technical reasons³¹ we first rescale S by a complex phase $U_{\mathbf{h}}(a, \bar{a}; 0) \in \mathbf{U}(1)$ that arises from the group action on the fusion space, see Eq.(3.303),

$$\tilde{S}_{a_{\mathbf{g}}b_{\mathbf{h}}} := [U_{\mathbf{h}}(a, \bar{a}; 0)]^* S_{a_{\mathbf{g}}b_{\mathbf{h}}}. \quad (3.288)$$

Since the underlying topological order is a Drinfeld center $\mathcal{Z}(\mathcal{C}_1)$, the chiral central charge is trivial, and hence we have the modular relations

$$(\tilde{S}T)^3 = \tilde{S}^2, \quad \tilde{S}^4 = \mathbb{1}. \quad (3.289)$$

One can also verify these formulas by direct manipulation of MPOs, using the definitions of S and T given in Eq.(3.146).

We remark that $S_{a_{\mathbf{g}}b_{\mathbf{h}}}$ and $\theta_{\mathcal{B}_{a_{\mathbf{g}}}^{\mathbf{h}}}$ are not gauge-invariant, although they do contain gauge invariant data³¹. In particular, the S and T matrices of the underlying topological order are given by $S^{(1,1)}$ and $T^{(1,1)}$.

Furthermore, with the normalizations we have fixed for the $\mathcal{B}_{a_{\mathbf{g}}}^1, \mathcal{B}_0^{\mathbf{g}}$ domain walls, we can extract the normalized quantum dimensions of the defects using a similar approach to that which led to Eq.(3.153). The result

$$d_{a_{\mathbf{g}}} = \sum_{p_{\mathbf{g}}} \frac{d_{p_{\mathbf{g}}} t_{a_{\mathbf{g}}}^{p_{\mathbf{g}} p_{\mathbf{g}} p_{\mathbf{g}}^0}}{D_{a_{\mathbf{g}}}}, \quad (3.290)$$

follows from

$$\frac{d_{a_{\mathbf{g}}}}{\mathcal{D}_1^2} = S_{a_{\mathbf{g}}0} = \frac{\text{Tr}[(\mathcal{B}_0^{\mathbf{g}})^{\dagger} S(a_{\mathbf{g}})]}{D_a \text{Tr}[(\mathcal{B}_0^{\mathbf{g}})^{\dagger} \mathcal{B}_0^{\mathbf{g}}]} = \frac{1}{\mathcal{D}_1^2} \sum_{p_{\mathbf{g}} s_1} t_{a_{\mathbf{g}}}^{p_{\mathbf{g}} q_{\mathbf{g}} p_{\mathbf{g}} s_1} \frac{\text{Tr}[(\mathcal{B}_0^{\mathbf{g}})^{\dagger} S(\mathcal{T}_{p_{\mathbf{g}} q_{\mathbf{g}}})]}{D_a \text{Tr}[\underline{0}]} = \sum_{p_{\mathbf{g}}} \frac{d_p t_a^{p p p^0}}{\mathcal{D}_1^2 D_a}, \quad (3.291)$$

where we have used $S(\mathcal{T}_{p_{\mathbf{g}} q_{\mathbf{g}} p_{\mathbf{g}}}^{s_1}) \underline{0} = d_p \delta_{s_0} \delta_{p q} \mathcal{B}_0^{\mathbf{g}}$, which is implied by Eq.(3.298).

Since we have a \mathcal{G} -extension of $\mathcal{Z}(\mathcal{C}_1)$, and the total quantum dimension of the $\mathbf{1}$ -defect topological superselection sectors is given by $\mathcal{D}_{\text{out}} = \mathcal{D}_1^2$, the total quantum dimension of all defects is given by $\mathcal{D}_{\mathcal{G}, \text{out}} = \sqrt{|\mathcal{G}|} \mathcal{D}_1^2$.

3.6.5 Topological entanglement entropy of the defect superselection sectors

The topological entanglement entropy (TEE) of the defect superselection sectors can be calculated via the topological correction to the 0-Rényi entropy, similarly to the purely topological case considered in Section 3.4.4. The 0-Rényi entropy for the $a_{\mathbf{g}}$ defect superselection sector is calculated by taking the trace of the $a_{\mathbf{g}}$ ICI, of varying MPO length L , similar to Eq.(3.156).

By using Eq.(3.290) we recover a similar result to Eq.(3.157)

$$H_0 \approx \log(\lambda_0) L - \gamma_{a_{\mathbf{g}}}, \quad \text{where} \quad \gamma_{a_{\mathbf{g}}} = -\log \left(\sum_{p_{\mathbf{g}}} \frac{d_{p_{\mathbf{g}}} t_{a_{\mathbf{g}}}^{p_{\mathbf{g}} p_{\mathbf{g}} p_{\mathbf{g}}^0}}{D_{a_{\mathbf{g}}} \mathcal{D}_1^2} \right) = \log(\mathcal{D}_{\text{out}}) - \log(d_{a_{\mathbf{g}}}), \quad (3.292)$$

and $\mathcal{D}_{\text{out}} = \mathcal{D}_1^2$ is the quantum dimension of the underlying emergent topological order.

We argued in Section 3.4.4 that the topological correction to the entropy is independent of the Rényi index for an RG fixed point model, and that the topological entanglement entropy

is a robust quantity throughout a gapped phase of matter. The same arguments apply for the topological correction to the entropy of a defect superselection sector, and hence the quantity γ_{a_g} in Eq.(3.292) does indeed correspond to the TEE of a defect. Hence Eq.(3.292) provides a general method to calculate the TEE of defect superselection sectors directly on the lattice²⁰⁵.

3.6.6 \mathcal{G} -graded fusion

The fusion structure of the defect ICIs proceeds almost identically to the purely topological case, explained in Section 3.4.5. We briefly summarize the points of similarity, before moving on to discuss the interplay of fusion with the group action and domain walls, which are aspects that do not occur in the topological case.

We use a similar notation to that established in Section 3.4.5

$$\begin{array}{c} \text{Diagram 1: Junction of } p_g, q_g, r_g \text{ with sectors } s_1, s_1, s_1 \\ \text{Diagram 2: Loop with junction } p_g, q_g, r_g \text{ and sector } s_1 \end{array} = \begin{array}{c} \text{Diagram 3: Junction of } a_g, a_g \text{ with sector } 1 \\ \text{Diagram 4: Loop with junction } g, a, g \text{ and sector } 1 \end{array}, \quad (3.293)$$

where the group elements on the far right indicate the sector of the strings appearing in the definition of $\underline{a_g}$.

The fusion of defects $\underline{a_g}$ and $\underline{b_h}$ to sector $\underline{c_k}$ is captured by

$$\text{Diagram: Fusion vertex } \mu \text{ with strings } a, b, c \text{ and loops} \quad , \quad (3.294)$$

where

$$\text{Diagram: Fusion vertex } \mu := \sum_{p_g q_h r_{gh}} c_{\mu}^{pqr} d_p^{\frac{1}{4}} d_q^{\frac{1}{4}} d_r^{\frac{1}{4}} \text{Diagram: Junction of } p_g, q_h, r_{gh} \quad , \quad (3.295)$$

are fusion vertex tensors that lead to nonzero tensor networks. Due to the structure of the defect ICIs, $c_{\mu}^{p_g q_h r_k}$ contains the constraint $\delta_{gh,k}$ and hence the fusion is \mathcal{G} -graded.

The fusion space $V_{c_{gh}}^{a_g b_h}$ is spanned by states μ_{ab}^c in the support subspace of the projector described in Eq.(3.161). This is found using the same approach as in the purely topological case, by creating an MPO_1 loop projector between $\underline{c_{gh}}$ and $\underline{a_g}, \underline{b_h}$ and fusing it into the edges surrounding μ_{ab}^c .

By taking the trace of the projector in Eq.(3.161) we should find $N_{a_g b_h}^{c_{gh}}$, the dimension of its support subspace. After using the \mathcal{G} -crossed S -matrix to expand $\underline{a_g}, \underline{b_h}, \underline{c_{gh}}$ in a complimentary

basis, we find a formula that is very close to the \mathcal{G} -crossed Verlinde formula, recently introduced in Ref. 31

$$N_{a_g b_h}^{c_{gh}} = \sum_{x_1} \frac{S_{a_g x_1} S_{b_h x_1} S_{c_{gh} x_1}^*}{S_{0 x_1}} \eta_x(\bar{\mathbf{h}}, \bar{\mathbf{g}}). \quad (3.296)$$

This holds for any \mathcal{G} -crossed modular theory, which includes all the theories in our formalism as they are symmetry-enriched Drinfeld centers. We expect that with further work one could derive the exact \mathcal{G} -crossed Verlinde formula from our calculation, but we do not pursue this direction here.

Further properties of defect fusion that follow from a direct application of the methods described in Section 3.4.5 are briefly summarized below:

- If the ICIs $\underline{a_g}$, $\underline{b_h}$, $\underline{c_{gh}}$ are all nondegenerate, there is a unique fusion vertex μ_{ab}^c and one can absorb the \underline{c} ICI into \underline{a} , \underline{b} and μ , similar to Eq.(3.164).
- The antiparticle $\overline{\underline{a_g}}$ for each $\underline{a_g}$ is found using the same approach as in the topological case. That is, by finding the ICI $\overline{\underline{a_g}}$ that leads to nonzero cup and cap tubes, as defined in Eq.(3.171). The \mathcal{G} -grading of the fusion implies that $\overline{\underline{a_g}}$ lies in the $\bar{\mathbf{g}}$ -sector.
- The FS indicator \varkappa_{a_g} can then be calculated by multiplying a cup and cap tube as in Eq.(3.172). This is only gauge invariant for $\overline{\underline{a_g}} = \underline{a_g}$, which requires $\mathbf{g}^2 = 1$, and implies $\varkappa_{a_g} = \pm 1$.
- The F -symbols of the emergent theory are calculated using the same approach as in the topological case, see Eq.(3.173).

Similar to Eq.(3.267) we have

$$\sum_{s_h} \frac{d_s}{\mathcal{D}_1^2} \left[\text{Diagram: A box labeled } a_g \text{ with a horizontal line passing through it. Above the line, a tube labeled } s_h \text{ goes up and then right. Below the line, a tube labeled } s_h \text{ goes down and then right. The box is on the left, and the tubes extend to the right.} \right] = (\tilde{\mathcal{B}}_{a_g}^{\mathbf{h}})^\dagger \mathcal{B}_{a_g}^{\mathbf{h}} \quad (3.297)$$

For the special case $a_g = 0$ we recover a version of Eq.(3.232) for tubes

$$\sum_{s_g} \left[\text{Diagram: A box labeled } 0 \text{ with a horizontal line passing through it. Above the line, a tube labeled } s_g \text{ goes up and then right. Below the line, a tube labeled } s_g \text{ goes down and then right. The box is on the left, and the tubes extend to the right.} \right] = \sum_{s_g} \left[\text{Diagram: A box labeled } \mathcal{B}_0^{\mathbf{g}} \text{ with a horizontal line passing through it. Above the line, a tube labeled } s_g \text{ goes up and then right. Below the line, a tube labeled } s_g \text{ goes down and then right. The box is on the left, and the tubes extend to the right.} \right], \quad (3.298)$$

which corresponds to sliding a \mathbf{g} domain wall over an MPO_1 loop, thus transforming it into an $\text{MPO}_{\mathbf{g}}$ loop. This is similar to Eq.(3.232).

Eq.(3.297) follows from the following slight generalization of Eq.(3.267)

$$\sum_{\mathbf{g}, \mathbf{h}} \sum_{r_g s_h} \frac{d_s}{\mathcal{D}_1^2} \left[\text{Diagram: A box labeled } r_g \text{ with a horizontal line passing through it. Above the line, a tube labeled } s_h \text{ goes up and then right. Below the line, a tube labeled } s_h \text{ goes down and then right. The box is on the left, and the tubes extend to the right.} \right] = \frac{1}{\mathcal{D}_1^2} \sum_{\mathbf{g}, \mathbf{h}} \sum_{\substack{p_{\mathbf{h} \mathbf{g}} q_{\mathbf{g} \mathbf{h}} \\ r_{\mathbf{g} s_{\mathbf{h}}}}} (\tilde{\mathcal{T}}_{p_{\mathbf{h} \mathbf{g}} q_{\mathbf{g} \mathbf{h}} r_{\mathbf{g}}}^{s_{\mathbf{h}}})^\dagger \mathcal{T}_{p_{\mathbf{h} \mathbf{g}} q_{\mathbf{g} \mathbf{h}} r_{\mathbf{g}}}^{s_{\mathbf{h}}} = \sum_{\mathbf{g}, \mathbf{h}} (\tilde{\mathcal{B}}_{a_g}^{\mathbf{h}})^\dagger \mathcal{B}_{a_g}^{\mathbf{h}}, \quad (3.299)$$

where

$$(\tilde{\mathcal{T}}_{p_{\mathbf{g}}^{\mathbf{h}} q_{\mathbf{g}\bar{\mathbf{h}}} r_{\mathbf{g}}}^{s_{\mathbf{h}}})^\dagger = d_p^{\frac{1}{4}} d_r^{-\frac{1}{4}} \begin{array}{c} \xrightarrow{s_{\mathbf{h}}} \\ \xrightarrow{r_{\mathbf{g}}} \quad \xrightarrow{p_{\mathbf{h}\mathbf{g}}} \\ \xleftarrow{q_{\mathbf{g}\bar{\mathbf{h}}}} \\ \xleftarrow{s_{\mathbf{h}}} \end{array}, \quad (\tilde{\mathcal{B}}_{a_{\mathbf{g}}}^{\mathbf{h}})^\dagger = \frac{1}{\mathcal{D}_{\mathbf{I}}^2} \sum_{\substack{p_{\mathbf{h}\mathbf{g}} q_{\mathbf{g}\bar{\mathbf{h}}} \\ r_{\mathbf{g}} s_{\mathbf{h}}}} (t_{\mathcal{B}_{a_{\mathbf{g}}}^{\mathbf{h}}}^{pqrs})^* (\tilde{\mathcal{T}}_{p_{\mathbf{g}}^{\mathbf{h}} q_{\mathbf{g}\bar{\mathbf{h}}} r_{\mathbf{g}}}^{s_{\mathbf{h}}})^\dagger. \quad (3.300)$$

We also have the similar result

$$\sum_{s_{\mathbf{h}}} \frac{d_s}{\mathcal{D}_{\mathbf{I}}^2} \begin{array}{c} \xrightarrow{s_{\mathbf{h}}} \\ \xrightarrow{a_{\mathbf{g}}} \\ \xleftarrow{s_{\mathbf{h}}} \end{array} = (\mathcal{B}_{a_{\mathbf{g}}}^{\mathbf{h}})^\dagger \tilde{\mathcal{B}}_{a_{\mathbf{g}}}^{\mathbf{h}}. \quad (3.301)$$

Group action on the fusion space

The action of the on-site representation of \mathcal{G} on the fusion pair-of-pants tensor network can be calculated as follows

$$\begin{array}{c} \text{Diagram with legs } a, b, c \text{ and fusion vertex } \mu, \text{ shaded region } k \end{array} = \begin{array}{c} \text{Diagram with legs } \mathcal{B}_a^{\mathbf{k}}, \mathcal{B}_b^{\mathbf{k}}, \mathcal{B}_c^{\mathbf{k}} \text{ and fusion vertex } \mu, \text{ shaded region } k \end{array}. \quad (3.302)$$

Where the darker shaded region indicates the on-site action of \mathbf{k} on the fusion tensor network, and

$$\begin{array}{c} \text{Diagram with legs } \mu, \text{ shaded region } k \end{array} := \sum_{s_{\mathbf{k}}} \frac{\mathcal{D}^4}{d_s^2} \begin{array}{c} \text{Diagram with legs } \mathcal{B}_a^{\mathbf{k}}, \mathcal{B}_b^{\mathbf{k}}, \mathcal{B}_c^{\mathbf{k}} \text{ and fusion vertex } \mu, \text{ shaded region } s_{\mathbf{k}} \end{array} = \sum_{\nu} [U_{\mathbf{k}}(a, b; c)]_{\nu}^{\mu} \begin{array}{c} \text{Diagram with leg } \nu, \text{ shaded region } k \end{array}, \quad (3.303)$$

defines the group action $U_{\mathbf{k}}(a, b; c)$ on the fusion space.

We denote the pair-of-pants tensor network in Eq.(3.294) by $\mathcal{V}_{c_{\mathbf{g}\bar{\mathbf{h}}}}^{a_{\mathbf{g}} b_{\mathbf{h}}}$, hence

$$\mathbf{U}_{\mathbf{k}}[\mathcal{V}_{c_{\mathbf{g}\bar{\mathbf{h}}}}^{a_{\mathbf{g}} b_{\mathbf{h}}}] = (\mathcal{B}_c^{\mathbf{k}})^\dagger \mathcal{V}_{c_{\mathbf{g}\bar{\mathbf{h}}}}^{a_{\mathbf{g}} b_{\mathbf{h}}} \mathcal{B}_a^{\mathbf{k}} \otimes U_{\mathbf{k}}(a, b; c) \otimes \mathcal{B}_b^{\mathbf{k}}. \quad (3.304)$$

Since $\mathbf{U}_{\mathbf{k}}$ forms a representation and $\mathcal{B}_a^{\mathbf{k}}$ forms a projective representation we find that $U_{\mathbf{k}}(a, b; c)$ forms a projective representation

$$U_{\mathbf{x}}({}^{\mathbf{y}}a, {}^{\mathbf{y}}b; {}^{\mathbf{y}}c) U_{\mathbf{y}}(a, b; c) = \omega_{\mathbf{x}, \mathbf{y}}(a, b; c) U_{\mathbf{xy}}(a, b; c). \quad (3.305)$$

Where

$$\omega_{\mathbf{x}, \mathbf{y}}(a, b; c) = \frac{\eta_c(\mathbf{x}, \mathbf{y})}{\eta_a(\mathbf{x}, \mathbf{y}) \eta_b(\mathbf{x}, \mathbf{y})}, \quad (3.306)$$

is a $U(1)$ phase that satisfies the twisted 2-cocycle equation

$$\omega_{\mathbf{x},\mathbf{yz}}(a, b; c) \omega_{\mathbf{y},\mathbf{z}}(a, b; c) = \omega_{\mathbf{x},\mathbf{y}}(\mathbf{z}a, \mathbf{z}b; \mathbf{z}c) \omega_{\mathbf{xy},\mathbf{z}}(a, b; c). \quad (3.307)$$

For $\mathbf{x}, \mathbf{y} \in Z_{a,b,c}$ we find $[\omega(a, b; c)] \in \mathcal{H}^2(Z_{a,b,c}, U(1))$ as it is only defined up to a coboundary, corresponding to rephasing $U_{\mathbf{k}}(a, b; c)$.

Eq.(3.302) included an action of the symmetry within the \underline{a} , \underline{b} , and \underline{c} superselection sectors. To this end we consider closing the pair-of-pants tensor network via defect tensors T_a^-, T_b^-, T_c , where the $-$ indicates that the boundary of the puncture is negatively oriented. The defect tensors must transform under the on-site physical symmetry as follows

$$\mathbf{U}_{\mathbf{k}}[T_a] = T_{\mathbf{k}a} \mathcal{B}_a^{\mathbf{k}}, \quad \mathbf{U}_{\mathbf{k}}[T_a^-] = (\mathcal{B}_a^{\mathbf{k}})^\dagger T_{\mathbf{k}a}^-, \quad (3.308)$$

if they are to correctly capture the behaviour of the defect a_g . For the special case $T_a = \underline{a}$, we have $\mathbf{U}_{\mathbf{k}}[T_a] = \mathcal{B}_a^{\mathbf{k}}$.

Including the action of the physical symmetry upon the defect superselection sectors yields the following modification of Eq.(3.302)

$$\mathbf{U}_{\mathbf{k}}[T_c \mathcal{V}_{c_{gh}}^{a_g b_h} T_a^- \otimes \mathbb{1} \otimes T_b^-] = \mathbf{U}_{\mathbf{k}}[T_c] (\mathcal{B}_c^{\mathbf{k}})^\dagger \mathcal{V}_{k_{c_{gh}}}^{k_{a_g} k_{b_h}} \mathcal{B}_a^{\mathbf{k}} \mathbf{U}_{\mathbf{k}}[T_a^-] \otimes U_{\mathbf{k}}(a, b; c) \otimes \mathcal{B}_b^{\mathbf{k}} \mathbf{U}_{\mathbf{k}}[T_b^-] \quad (3.309)$$

$$= T_{\mathbf{k}c} \mathcal{V}_{k_{c_{gh}}}^{k_{a_g} k_{b_h}} T_{\mathbf{k}a}^- \otimes U_{\mathbf{k}}(a, b; c) \otimes T_{\mathbf{k}b}^-. \quad (3.310)$$

That is, the physical action of the symmetry compensates the action on each defect sector appearing in Eq.(3.302).

3.6.7 \mathcal{G} -crossed braiding

The process of exchanging defects differs from the exchange of anyons, as we must now also move the domain walls attached to the defects, which requires the application of the physical symmetry

$$= \sum_{s_h} \frac{D_1^2}{d_s} \quad (3.311)$$

During the exchange step we have applied the physical symmetry to the dark shaded region, and to the superselection sector, which resulted in the application of $(\mathcal{B}_a^{\mathbf{h}})^\dagger$ to the ICI $\underline{a}_{\mathbf{g}}$.

For nondegenerate $\underline{a}_{\mathbf{g}}$ and $\underline{b}_{\mathbf{h}}$ we have

$$R^{\mathbf{h}a_{\mathbf{g}}b_{\mathbf{h}}} := \text{Diagram} = \sum_{q_{\mathbf{gh}}} \frac{(t_{\mathcal{B}_a^{\mathbf{h}}}^{s_{\mathbf{h}}^a q s_{\mathbf{g}}^a s_{\mathbf{h}}^b})^*}{d_{s^b}}, \quad (3.312)$$

where s_a is defined by the equation $\underline{a}_{\mathbf{g}} \mathcal{T}_{ppp}^0 = \delta_{ps^a} \underline{a}_{\mathbf{g}}$.

The \mathcal{G} -crossed R -symbols $R_{c_{\mathbf{hg}}}^{\mathbf{h}a_{\mathbf{g}}b_{\mathbf{h}}}$ are defined by resolving the R -matrix into defect superselection sectors of definite topological charge. For nondegenerate defect ICIs $\underline{a}_{\mathbf{g}}$, $\underline{b}_{\mathbf{h}}$, $\underline{c}_{\mathbf{hg}}$, the fusion vertices μ_{ba}^c and ν_{ab}^c are unique, and we have

$$\text{Diagram} = R_{c_{\mathbf{hg}}}^{\mathbf{h}a_{\mathbf{g}}b_{\mathbf{h}}} \text{Diagram}, \quad (3.313)$$

as part of a larger fusion pair-of-pants tensor network $\mathcal{V}_{c_{\mathbf{gh}}}^{\mathbf{h}a_{\mathbf{g}}b_{\mathbf{h}}}$. An explicit expression for $R_{c_{\mathbf{hg}}}^{\mathbf{h}a_{\mathbf{g}}b_{\mathbf{h}}}$ can be derived directly from Eq.(3.312). These results can be generalized to degenerate defect ICIs by following a similar line of reasoning.

3.6.8 Shifting by 2 and 3 cocycles

In Section 3.5.2 we found that consistent fusion rules for a \mathcal{G} -graded MPO algebra correspond to an $\mathcal{H}^2(\mathcal{G}, \mathbb{Z}_1)$ torsor, while F -symbol associators that satisfy the pentagon equation correspond to $\mathcal{H}^3(\mathcal{G}, \mathbb{U}(1))$ -torsors. Hence one might consider the effect on the emergent theory, of shifting the MPO algebra by an element of $\mathcal{H}^2(\mathcal{G}, \mathbb{Z}_1)$ or $\mathcal{H}^3(\mathcal{G}, \mathbb{U}(1))$. Shifting the fusion rules by an element of $\mathcal{H}^2(\mathcal{G}, \mathbb{Z}_1)$ can totally change the structure of the \mathbf{g} -defect tube algebras for $\mathbf{g} \neq \mathbf{1}$. Beyond the $\mathbf{1}$ -sector, which remains the same, there is no obvious relation between the emergent theories before and after the shift. This is demonstrated in Example 3.9.1.

Shifting the F -symbol associators by an element of $\mathcal{H}^3(\mathcal{G}, \mathbb{U}(1))$ is more subtle, as it preserves the set of emergent defects, but it may change some of their properties. Except for the underlying emergent topological order, corresponding to the $\mathbf{1}$ -sector, which is left invariant. Specifically, we consider shifting by a nontrivial cocycle $[\alpha] \in \mathcal{H}^3(\mathcal{G}, \mathbb{U}(1))$

$$F_{def}^{a_{\mathbf{g}}b_{\mathbf{h}}c_{\mathbf{k}}} \mapsto \alpha(\mathbf{g}, \mathbf{h}, \mathbf{k}) F_{def}^{a_{\mathbf{g}}b_{\mathbf{h}}c_{\mathbf{k}}}, \quad (3.314)$$

which leads to an obvious change in the F -symbols of the emergent theory, via Eq.(3.173). The effect on the \mathcal{G} -crossed R matrices can also be derived.

The \mathcal{G} -crossed modular matrices are modified as follows

$$S_{a_{\mathbf{g}}b_{\mathbf{h}}} \mapsto \mathcal{N}_{\mathbf{g}}^* \alpha^{\mathbf{h}}(\mathbf{g}, \bar{\mathbf{g}})^* \frac{\alpha(\mathbf{h}, \mathbf{g}\bar{\mathbf{h}}, \mathbf{h})}{\alpha(\bar{\mathbf{g}}, \mathbf{h}\mathbf{g}, \bar{\mathbf{g}})} S_{a_{\mathbf{g}}b_{\mathbf{h}}}, \quad \theta_{\mathcal{B}_{a_{\mathbf{g}}}^{\mathbf{h}}} \mapsto \alpha(\mathbf{g}, \mathbf{h}, \mathbf{g})^* \frac{\alpha(\mathbf{h}, \mathbf{g}\bar{\mathbf{h}}, \mathbf{h})}{\alpha(\mathbf{g}\bar{\mathbf{h}}, \bar{\mathbf{h}}, \mathbf{g}\bar{\mathbf{h}})} \theta_{\mathcal{B}_{a_{\mathbf{g}}}^{\mathbf{h}}}. \quad (3.315)$$

The effects of the cocycle shift on the physically observable data are more apparent after gauging the symmetry, see Section 3.7. These effects are largely a consequence of the following transformations.

The Frobenius-Schur indicator transforms as follows

$$\mathcal{N}_{a_g} \mapsto \alpha(\mathbf{g}, \bar{\mathbf{g}}, \mathbf{g}) \mathcal{N}_{a_g}. \quad (3.316)$$

The 2-cocycle of the projective representation acting on the a_g defect transforms as

$$\eta_a(\mathbf{h}, \mathbf{k}) \mapsto \omega_g(\mathbf{h}, \mathbf{k}) \eta_a(\mathbf{h}, \mathbf{k}), \quad (3.317)$$

where

$$\omega_g(\mathbf{h}, \mathbf{k}) = \alpha^g(\mathbf{h}, \mathbf{k}) d\varepsilon^g(\mathbf{h}), \quad \alpha^g(\mathbf{h}, \mathbf{k}) = \frac{\alpha(\mathbf{h}, \mathbf{k}, \mathbf{g}, \mathbf{k})}{\alpha(\mathbf{h}\mathbf{k}, \mathbf{g}, \mathbf{h}, \mathbf{k}) \alpha(\mathbf{h}, \mathbf{k}, \mathbf{g})}, \quad (3.318)$$

$$d\varepsilon^g(\mathbf{h}, \mathbf{k}) = \frac{\varepsilon^g(\mathbf{k}) \varepsilon^{\mathbf{k}\mathbf{g}}(\mathbf{h}, \mathbf{k})}{\varepsilon^g(\mathbf{h}\mathbf{k})}, \quad \varepsilon^g(\mathbf{h}) = \alpha(\mathbf{h}, \mathbf{g}\bar{\mathbf{h}}, \mathbf{h}). \quad (3.319)$$

Hence the group action on the symmetry-twisted MES becomes

$$\eta_{a_g}^{\mathbf{h}}(\mathbf{k}) \mapsto \alpha^{\mathbf{g}, \mathbf{h}}(\mathbf{k}) \eta_{a_g}^{\mathbf{h}}(\mathbf{k}), \quad \text{where} \quad \alpha^{\mathbf{g}, \mathbf{h}}(\mathbf{k}) = \frac{\alpha^g(\mathbf{k}, \mathbf{h})}{\alpha^g(\mathbf{h}, \mathbf{k})}, \quad (3.320)$$

and $\mathbf{k} \in Z_{g, \mathbf{h}}$, with $\mathbf{g}\mathbf{h} = \mathbf{h}\mathbf{g}$. Finally the group action on the fusion vertices transforms as follows

$$U_{\mathbf{k}}(a_g, b_{\mathbf{h}}; c_{\mathbf{g}\mathbf{h}}) \mapsto \omega_{\mathbf{k}}(\mathbf{g}, \mathbf{h}) U_{\mathbf{k}}(a_g, b_{\mathbf{h}}; c_{\mathbf{g}\mathbf{h}}), \quad (3.321)$$

for $\mathbf{k} \in Z_{a_g, b_{\mathbf{h}}, c_{\mathbf{g}\mathbf{h}}}$.

We remark that shifting by a 3-cocycle cannot, in general, be absorbed by a change of gauge of the MPO data. For instance it is apparent that the projective representations acting on the defects are shifted when the 2-cocycle α^g lies in a nontrivial cohomology class. Hence one must assess whether shifting by a 3-cocycle actually changes the emergent UGxBFC on a case by case basis. In Section 3.8 we present some examples for which a 3-cocycle shift can be absorbed by a change of gauge, and some for which it cannot.

3.7 Gauging the global symmetry

In this section, we describe the effect of applying the state gauging procedure — developed in Refs. 71,93, Chapter 1 — to SET tensor networks. This corresponds to equivariantization in the category theory language used in Refs. 81,97,98. Our analysis focuses on the transformation of the \mathcal{G} -graded MPO symmetry algebra. Gauging effectively promotes the nontrivial \mathbf{g} -sectors into purely topological symmetries. From this we derive formulas for the ICIs of the gauged topological order. These gauged ICIs lead to expressions for the resulting S and T matrices, as well as the fusion degeneracies and quantum dimensions. Before addressing the general case, we focus on a simple example that captures many features of the gauging procedure.

3.7.1 Example: Gauging SPT orders

We begin by applying the gauging procedure to the simplest class of examples where a unitary, on-site SPT order is gauged to a twisted quantum double (Dijkgraaf-Witten) topological order^{19,72,73,93}.

MPO description of an SPT order

We consider a \mathcal{G} -graded MPO algebra with $|\mathcal{C}_1| = 1$. It was shown in Ref. 93 and Chapter 1 that this corresponds to a non-chiral, invertible topological order. Furthermore it was shown that $|\mathcal{C}_g| = 1, \forall g \in \mathcal{G}$, for a faithful MPO representation with $|\mathcal{C}_1| = 1$.

In this case the single block MPOs are simply labeled by group elements MPO_g , and their fusion is given by the group product $\text{MPO}_g \text{MPO}_h = \text{MPO}_{gh}$. Consequently, the associators are simply $U(1)$ phases $F_{ghk,gh,hk}^{g,h,k} = \alpha(g, h, k)$ that satisfy the 3-cocycle equation

$$\alpha(f, g, h)\alpha(f, gh, k)\alpha(g, h, k) = \alpha(fg, h, k)\alpha(f, g, hk), \quad (3.322)$$

due to the pentagon equation. The algebraic data of the MPO algebra is described by the UFC $\text{Vec}_{\mathcal{G}}^\alpha$, considered as a \mathcal{G} -graded category. The classification of such MPO algebras recovers the third cohomology classification of SPTs^{70,75,242}. In this case the \mathcal{G} -graded Morita equivalence class is given by a representative, up to a 1-cochain, since each sector consists of only one single block MPO. Fixed point representatives of these SPT phases are captured by a special case of the \mathcal{G} -graded string-net example, see Section 3.3.

The significance of the fact that F -symbol solutions are torsors can be understood in this case as follows: the classification of SPT phases is dependent upon the precise choice of physical symmetry, with respect to which the classification is done. As an explicit example, the well known CZX model⁷⁰ is in the trivial phase w.r.t. an on-site $X^{\otimes N}$ symmetry, but is in a nontrivial phase for the more complicated on site symmetry chosen in Ref. 70.

Since $|\mathcal{C}_g| = 1$ the dube algebras are all one dimensional. There is a single defect ICI for each sector, which is simply given by $\underline{g} = \mathcal{T}_{g,g,g}^1$.

When considering the group action on the defects we use the following choice of gauge

$$\mathcal{B}_g^h = \alpha^*(h, g\bar{h}, h)\mathcal{T}_{hg,gh,g}^h =: \mathcal{T}_g^h. \quad (3.323)$$

The permutation action is simply given by group conjugation, i.e. ${}^h\underline{g} = \underline{hgh}$.

Multiplication of domain walls is given by

$$\mathcal{B}_{k_g}^h \mathcal{B}_g^k = \frac{\alpha(h, {}^k\underline{g}, k)}{\alpha(hk\underline{g}, h, k)\alpha(h, k, g)} \mathcal{B}_g^{hk}, \quad \text{hence} \quad \eta_g(h, k) = \alpha^g(h, k). \quad (3.324)$$

The group action of $k \in Z_h$ on the MES is given by

$$U_k |\mathcal{B}_g^h\rangle = \alpha^{g,h}(k) |\mathcal{B}_{k_g}^h\rangle, \quad \text{where} \quad \alpha^{g,h}(k) = \frac{\alpha^g(k, h)}{\alpha^g(h, k)}. \quad (3.325)$$

The \mathcal{G} -crossed modular matrices are given by

$$\langle \mathcal{B}_x^y | S(\mathcal{B}_g^h) \rangle = \delta_{x,h} \delta_{y,\bar{g}} \delta_{g,h_g} \mathcal{Z}_g^* \alpha^h(g, \bar{g})^*, \quad (3.326)$$

$$\langle \mathcal{B}_x^y | T(\mathcal{B}_g^h) \rangle = \delta_{x,g} \delta_{y,gh} \delta_{g,h_g} \alpha(g, h, g)^*. \quad (3.327)$$

Fusion of the defect ICIs is again given by the group multiplication rule, and it is multiplicity free. Hence the group action on the fusion space is simply a $U(1)$ phase, which is only defined up to multiplication with a 1-cocycle. One can verify that the following is a valid choice⁶⁴

$$U_k(g, h; gh) = \alpha^k(g, h). \quad (3.328)$$

Even though U is a phase in this case, it cannot generally be absorbed into the gauge of the projective representation $\mathcal{B}_{\mathbf{g}}^{\mathbf{h}}$ as it is a function of three group variables.

The F -symbols of the defects are given by the 3-cocycle α of the underlying MPO algebra. Hence the FS indicators of the defects are given by $\varkappa_{\mathbf{g}} = \alpha(\mathbf{g}, \bar{\mathbf{g}}, \mathbf{g})$.

Gauging the global symmetry

It was shown in Ref. 93 and Chapter 1 that applying the lattice gauging procedure introduced in Ref. 71, for the full symmetry group \mathcal{G} , results in a tensor network with an MPO algebra where the \mathcal{G} -grading is essentially forgotten. That is, the 1-sector of the resulting MPO algebra is given by the full \mathcal{G} -graded MPO algebra of the ungauged model. The algebraic data describing this is again the UFC $\text{Vec}_{\mathcal{G}}^{\alpha}$, but without including the \mathcal{G} -grading. Hence the emergent topological order is $\mathcal{Z}(\text{Vec}_{\mathcal{G}}^{\alpha})$, which is a twisted quantum double model. See Section 3.3 for a description of the gauging map applied to the fixed point PEPS tensors.

After gauging, the former domain walls $\mathcal{B}_{\mathbf{g}}^{\mathbf{h}}$ become purely virtual operators that do not require a physical group action. These MPOs can now be thought of as fluctuating in the vacuum given by the tensor network representation of the ground state.

This produces a tube algebra for $\text{Vec}_{\mathcal{G}}^{\alpha}$ from the tube algebra of the \mathcal{G} -graded $\text{Vec}_{\mathcal{G}}^{\alpha}$, together with the former domain walls $\mathcal{B}_{\mathbf{g}}^{\mathbf{h}}$. Hence all the sectors in a conjugacy class $C_{\mathbf{g}}$ of the tube algebra are coupled by the domain wall tubes $\mathcal{B}_{\mathbf{g}}^{\mathbf{h}}$ and result in a $|C_{\mathbf{g}}| \times |\mathcal{G}|$ block of the gauged tube algebra.

An individual defect \mathbf{g} supports a projective representation of $Z_{\mathbf{g}}$ with 2-cocycle $\alpha^{\mathbf{g}}$. This contributes a block of size $|Z_{\mathbf{g}}|$ to the gauged tube algebra, which is block-diagonalized by idempotents that project onto the projective irreps $\pi_{\mathbf{g}}^{\mu}$

$$(\underline{\mathbf{g}}, \mu) := \frac{d_{\mu}}{|Z_{\mathbf{g}}|} \sum_{\mathbf{h} \in Z_{\mathbf{g}}} \bar{\chi}_{\mathbf{g}}^{\mu}(\mathbf{h}) \mathcal{B}_{\mathbf{g}}^{\mathbf{h}}, \quad (3.329)$$

where $\bar{\chi}_{\mathbf{g}}^{\mu}(\mathbf{h}) := \text{Tr}[\pi_{\mathbf{g}}^{\mu}(\mathbf{h})]^*$ is a complex conjugated character. Each $(\underline{\mathbf{g}}, \mu)$ projects onto a block of size d_{μ} , and since

$$\sum_{\mu} d_{\mu}^2 = |Z_{\mathbf{g}}|, \quad (3.330)$$

we see that the decomposition is complete.

These irreducible idempotents can be extended to the full $|C_{\mathbf{g}}| \times |\mathcal{G}|$ block, by summing over the orbit of (\mathbf{g}, μ) under conjugation

$$[\underline{\mathbf{g}}, \mu] = \sum_{\mathbf{k} \in \mathcal{G}/Z_{\mathbf{g}}} (\underline{\mathbf{k}\mathbf{g}}, \mathbf{k}\mu), \quad (3.331)$$

where the canonical isomorphism between projective irreps, given in Eq.(3.279), is used to define $(\underline{\mathbf{k}\mathbf{g}}, \mathbf{k}\mu)$. The resulting $[\underline{\mathbf{g}}, \mu]$ are ICIs that project onto $d_{\mu} \times |C_{\mathbf{g}}|$ dimensional blocks, and by counting one can verify that they give a complete decomposition.

After gauging, some states on the torus vanish. As discusses in Ref. 93, Chapter 1, only those states $|\mathcal{B}_{\mathbf{g}}^{\mathbf{h}}\rangle$ satisfying $\alpha^{\mathbf{g}, \mathbf{h}} \equiv 1$ survive the gauging process.

The gauged S and T can be derived from the \mathcal{G} -crossed modular matrices, leading to the formulas

$$S_{[\mathbf{g},\mu][\mathbf{h},\nu]}^{\mathcal{Z}(\text{Vec}_{\mathcal{G}}^{\alpha})} = \frac{1}{|\mathcal{G}|} \sum_{\substack{\mathbf{r} \in \mathcal{G}/Z_{\mathbf{g}} \\ \mathbf{s} \in \mathcal{G}/Z_{\mathbf{h}}}} \delta_{\mathbf{r}\mathbf{g}^{\mathbf{s}}, \mathbf{s}\mathbf{h}\mathbf{r}} \mathbf{r}\bar{\chi}_{\mathbf{g}}^{\mu}(\mathbf{s}\mathbf{h}) \mathbf{s}\chi_{\mathbf{h}}^{\nu}(\mathbf{r}\bar{\mathbf{g}}) \mathcal{Z}_{\mathbf{r}\mathbf{g}}^* \alpha^{\mathbf{s}\mathbf{h}}(\mathbf{r}\mathbf{g}, \mathbf{r}\bar{\mathbf{g}}), \quad (3.332)$$

$$T_{[\mathbf{g},\mu][\mathbf{h},\nu]}^{\mathcal{Z}(\text{Vec}_{\mathcal{G}}^{\alpha})} = \delta_{[\mathbf{g},\mu][\mathbf{h},\nu]} \frac{\chi_{\mathbf{g}}^{\mu}(\mathbf{g})}{\chi_{\mathbf{g}}^{\mu}(\mathbf{1})}, \quad (3.333)$$

where $\mathbf{r}\chi_{\mathbf{g}}^{\mu} := \chi_{\mathbf{r}\mathbf{g}}^{\mu}$. From the special case of the S matrix with $[\mathbf{h}, \nu] = [\mathbf{1}, 1]$, we find

$$d_{[\mathbf{g},\mu]} = \frac{|\mathcal{G}|d_{\mu}}{|Z_{\mathbf{g}}|}. \quad (3.334)$$

The fusion multiplicities can be derived from S via the Verlinde formulas, but they can also be obtained directly by considering the intertwining property of a defect pair-of-pants tensor network

$$\mathcal{B}_{\mathbf{gh}}^{\mathbf{k}} \mathbf{U}_{\mathbf{k}}[\mathcal{V}_{\mathbf{gh}}^{\mathbf{g},\mathbf{h}}] = \mathcal{V}_{\mathbf{gh}}^{\mathbf{g},\mathbf{h}} \alpha^{\mathbf{k}}(\mathbf{g}, \mathbf{h}) \mathcal{B}_{\mathbf{g}}^{\mathbf{k}} \otimes \mathcal{B}_{\mathbf{h}}^{\mathbf{k}}, \quad (3.335)$$

for $\mathbf{k} \in Z_{\mathbf{g},\mathbf{h}}$. After gauging there is no global group action $\mathbf{U}_{\mathbf{k}}$ remaining, hence the projector onto the $\pi_{\mathbf{gh}}^{\kappa}(\mathbf{k})$ projective rep is intertwined by the gauged pair-of-pants tensor network as follows

$$\frac{d_{\kappa}}{|Z_{\mathbf{gh}}|} \sum_{\mathbf{k} \in Z_{\mathbf{g},\mathbf{h}}} \bar{\chi}_{\mathbf{gh}}^{\kappa}(\mathbf{k}) \mathcal{B}_{\mathbf{gh}}^{\mathbf{k}} \mapsto \frac{d_{\kappa}}{|Z_{\mathbf{gh}}|} \sum_{\mathbf{k} \in Z_{\mathbf{g},\mathbf{h}}} \bar{\chi}_{\mathbf{gh}}^{\kappa}(\mathbf{k}) \alpha^{\mathbf{k}}(\mathbf{g}, \mathbf{h}) \mathcal{B}_{\mathbf{g}}^{\mathbf{k}} \otimes \mathcal{B}_{\mathbf{h}}^{\mathbf{k}}, \quad (3.336)$$

which projects onto the diagonal $\pi_{\mathbf{gh}}^{\kappa}(\mathbf{k})|_{\mathbf{k} \in Z_{\mathbf{g},\mathbf{h}}}$ irrep within $\left((\alpha^{\mathbf{k}}(\mathbf{g}, \mathbf{h}) \pi_{\mathbf{g}}^{\mu}(\mathbf{k}) \otimes \pi_{\mathbf{h}}^{\nu}(\mathbf{k})) \right)|_{\mathbf{k} \in Z_{\mathbf{g},\mathbf{h}}}$. To calculate the fusion multiplicity one must also sum over conjugacy classes C_g , C_h , and C_{gh} . This is implemented by summing over conjugates $(\mathbf{x}\mathbf{g}, \mathbf{y}\mathbf{h})$, where $\mathbf{x} \in \mathcal{G}/Z_g$, $\mathbf{y} \in \mathcal{G}/Z_h$, modulo left multiplication $(\mathbf{z}\mathbf{x}, \mathbf{z}\mathbf{y})$, since that leads to conjugation $\mathbf{z}(\mathbf{x}\mathbf{g}\mathbf{y}\mathbf{h})$ which remains within $C_{\mathbf{x}\mathbf{g}\mathbf{y}\mathbf{h}}$. The set of elements $\mathcal{G}/C_g \times \mathcal{G}/C_h$, modulo left multiplication, is known to be isomorphic to the double coset $Z_g \backslash \mathcal{G} / Z_h$.

After including the summations over conjugacy classes we find that the fusion multiplicity is given by

$$N_{[\mathbf{g},\mu][\mathbf{h},\nu]}^{[\mathbf{k},\kappa]} = \sum_{\substack{(\mathbf{x},\mathbf{y}) \in Z_g \backslash \mathcal{G} / Z_h \\ \mathbf{z} \in \mathcal{G}/Z_k}} \delta_{\mathbf{x}\mathbf{g}\mathbf{y}\mathbf{h}, \mathbf{z}\mathbf{k}} m \left(\mathbf{z}\pi_{\mathbf{k}}^{\kappa}(\cdot) \Big|_{Z_{\mathbf{x}\mathbf{g},\mathbf{y}\mathbf{h}}}, \alpha^{(\cdot)}(\mathbf{x}\mathbf{g}, \mathbf{y}\mathbf{h}) \Big|_{Z_{\mathbf{x}\mathbf{g},\mathbf{y}\mathbf{h}}} \mathbf{x}\pi_{\mathbf{g}}^{\mu}(\cdot) \Big|_{Z_{\mathbf{x}\mathbf{g},\mathbf{y}\mathbf{h}}} \otimes \mathbf{y}\pi_{\mathbf{h}}^{\nu}(\cdot) \Big|_{Z_{\mathbf{x}\mathbf{g},\mathbf{y}\mathbf{h}}} \right), \quad (3.337)$$

where

$$m(\pi, \rho) = \dim [\text{Hom}_{\mathcal{G}}(\pi, \rho)], \quad (3.338)$$

counts the dimension of the space of intertwiners between the π and ρ reps. For the special case of π an irrep. it counts the number of times π appears in the irrep decomposition of ρ . For a

further discussion of the m function, and how it can be computed in terms of projective characters, see Ref. 31. In Ref. 64 this multiplicity was evaluated explicitly in terms of projective characters

$$N_{[\mathbf{g}, \mu][\mathbf{h}, \nu]}^{[\mathbf{k}, \kappa]} = \frac{1}{|\mathcal{G}|} \sum_{\mathbf{x} \in \mathcal{G}/Z_{\mathbf{g}}} \sum_{\mathbf{y} \in \mathcal{G}/Z_{\mathbf{h}}} \sum_{\mathbf{z} \in \mathcal{G}/Z_{\mathbf{k}}} \delta_{\mathbf{x}\mathbf{g}\mathbf{y}\mathbf{h}, \mathbf{z}\mathbf{k}} \sum_{\mathbf{w} \in Z_{\mathbf{x}\mathbf{g}, \mathbf{y}\mathbf{h}}} \alpha^{\mathbf{w}}(\mathbf{x}\mathbf{g}, \mathbf{y}\mathbf{h}) \bar{\chi}_{\mathbf{g}}^{\mu}(\mathbf{w}) \bar{\chi}_{\mathbf{h}}^{\nu}(\mathbf{w}) \chi_{\mathbf{k}}^{\kappa}(\mathbf{w}). \quad (3.339)$$

3.7.2 The general case

Gauging a global symmetry can be implemented explicitly on a tensor network state using the prescription of Ref. 71. It was shown in Ref. 93, Chapter 1, that gauging a symmetric tensor network results in the removal of the \mathcal{G} -grading from the MPO algebra. That is, the $\mathbf{1}$ -sector of the gauged MPO algebra consists of all sectors of the ungauged \mathcal{G} -graded MPO algebra. The application of the gauging map to the fixed point SET string-net tensors is described explicitly in Section 3.3.

Since the $\mathbf{1}$ -sector of the gauged MPO algebra is $\mathcal{C}_{\mathcal{G}}$, the emergent superselection sectors are given by $\mathcal{Z}(\mathcal{C}_{\mathcal{G}})$ and can be constructed via the tube algebra. The total quantum dimension is given by $\mathcal{D}_{\text{out}} = \mathcal{D}_{\mathcal{G}}^2 = |\mathcal{G}| \mathcal{D}_{\mathbf{1}}^2$, see Eq.(3.230).

Rather than calculating the gauged ICIs directly with the tube algebra, we can derive them from the defect ICIs $a_{\mathbf{g}}$ and the domain walls $\mathcal{B}_{a_{\mathbf{g}}}^{\mathbf{h}}$ of the tube algebra. In this section, and the next, we demonstrate that the problem of finding the gauged ICIs is equivalent to finding the ungauged defect ICIs and domain walls.

After gauging, the former domain walls $\mathcal{B}_{a_{\mathbf{g}}}^{\mathbf{h}}$ are now included in the tube algebra. Hence the sectors of the tube algebra within a conjugacy class $C_{\mathbf{g}}$ are coupled by the domain walls $\mathcal{B}_{a_{\mathbf{g}}}^{\mathbf{h}}$, and contribute a block to the resulting tube algebra.

The projective representation of $Z_{\mathbf{g}}$, acting on each $a_{\mathbf{g}}$ defect, was constructed in Section 3.6. Idempotents of the gauged theory are given by Hermitian projectors onto projective irreps $\pi_{a_{\mathbf{g}}}^{\mu}$ with 2-cocycle $\eta_{a_{\mathbf{g}}}$

$$\underline{(a_{\mathbf{g}}, \mu)} := \frac{d_{\mu}}{|Z_{a_{\mathbf{g}}}|} \sum_{\mathbf{h} \in Z_{a_{\mathbf{g}}}} \bar{\chi}_{a_{\mathbf{g}}}^{\mu}(\mathbf{h}) \mathcal{B}_{a_{\mathbf{g}}}^{\mathbf{h}}. \quad (3.340)$$

The projector $\underline{(a_{\mathbf{g}}, \mu)}$ correspond to the identity on a block of dimension $d_{\mu} \times D_{a_{\mathbf{g}}}$.

The ICIs are then found by summing over the orbit of the defect $a_{\mathbf{g}}$ under the group action

$$[a_{\mathbf{g}}, \mu] = \sum_{\mathbf{k} \in \mathcal{G}/Z_{a_{\mathbf{g}}}} \underline{(\mathbf{k}a_{\mathbf{g}}, \mathbf{k}\mu)}, \quad (3.341)$$

which project onto blocks of dimension $d_{\mu} \times D_{a_{\mathbf{g}}} \times |\mathcal{G}|/|Z_{a_{\mathbf{g}}}|$. Similar to the SPT example⁹³, only states satisfying $\eta_{a_{\mathbf{g}}}^{\mathbf{h}} \equiv 1$ lead to nonzero gauged states.

The S and T matrices of the gauged theory can be calculated in terms of the \mathcal{G} -crossed

modular matrices by using Eqs.(3.150),(3.283),(3.341)

$$S_{ab} = \sum_{\substack{\mathbf{r} \in \mathcal{G}/Z_a \\ \mathbf{s} \in \mathcal{G}/Z_b}} \sum_{\substack{\mathbf{f} \in Z_{a_g} \\ \mathbf{k} \in Z_{s_{b_h}}}} \frac{D_{[b_h, \nu]} d_\mu d_\nu \bar{\chi}_{a_g}^\mu(\mathbf{f}) {}^s\chi_{b_h}^\nu(\mathbf{k}) \text{Tr}[(\mathcal{B}_{s_{b_h}}^{\mathbf{k}})^\dagger S(\mathcal{B}_{a_g}^{\mathbf{f}})]}{D_{[a_g, \mu]} |Z_{a_g}| |Z_{b_h}| \text{Tr}[b_h, \mu]} \quad (3.342)$$

$$= \sum_{\substack{\mathbf{r} \in \mathcal{G}/Z_a \\ \mathbf{s} \in \mathcal{G}/Z_b}} \frac{D_{b_h} d_\nu^2 \bar{\chi}_{a_g}^\mu(\mathbf{s}_h) {}^s\chi_{b_h}^\nu(\mathbf{r}_{\bar{\mathbf{g}}}) \text{Tr}[(\mathcal{B}_{s_{b_h}}^{\mathbf{r}_{\bar{\mathbf{g}}}})^\dagger S(\mathcal{B}_{a_g}^{\mathbf{s}_h})]}{D_{a_g} |Z_{b_h}|^2 \text{Tr}[b_h, \mu]} \quad (3.343)$$

$$= \sum_{\substack{\mathbf{r} \in \mathcal{G}/Z_a \\ \mathbf{s} \in \mathcal{G}/Z_b}} \frac{\bar{\chi}_{a_g}^\mu(\mathbf{s}_h) {}^s\chi_{b_h}^\nu(\mathbf{r}_{\bar{\mathbf{g}}}) S_{r_{a_g} s_{b_h}}}{|\mathcal{G}|}. \quad (3.344)$$

Where we have used that $\text{Tr}[(\mathcal{B}_{b_h}^{\mathbf{k}})^\dagger S(\mathcal{B}_{a_g}^{\mathbf{f}})]$ contains the delta condition $\delta_{\mathbf{k}, \bar{\mathbf{g}}} \delta_{\mathbf{f}, \mathbf{h}}$, and

$$\text{Tr}[b_h, \nu] = \sum_{\mathbf{s} \in \mathcal{G}/Z_{b_h}} \frac{d_\nu}{|Z_{b_h}|} \sum_{\mathbf{k} \in Z_{s_{b_h}}} {}^s\chi_{b_h}^\nu(\mathbf{k}) \text{Tr}(\mathcal{B}_{s_{b_h}}^{\mathbf{k}}) = \frac{|\mathcal{G}| d_\nu^2}{|Z_{b_h}|^2} \text{Tr}(b_h), \quad (3.345)$$

which follows from $\bar{\chi}_{b_h}^\nu(\mathbf{1}) = d_\nu$, $\text{Tr}(\mathcal{B}_{b_h}^{\mathbf{k}}) = \delta_{\mathbf{k}, \mathbf{1}} \text{Tr}(\mathcal{B}_{b_h}^{\mathbf{1}})$ and $\mathcal{B}_{s_{b_h}}^{\mathbf{1}} = b_h$.

Since it was shown in Eq.(3.148) that the T matrix simply results in a phase, it can be calculated by keeping track of the relative phase of the underlying defect ICI $\underline{a_g}$

$$T([a_g, \mu]) = \left(\sum_{\mathbf{k}, s_k} \mathcal{T}_{s_0 s}^s \right) \frac{d_\mu}{|Z_{a_g}|} \left(\bar{\chi}_{a_g}^\mu(\mathbf{1}) \underline{a_g} + \dots \right) \quad (3.346)$$

$$= \frac{d_\mu}{|Z_{a_g}|} \left(\bar{\chi}_{a_g}^\mu(\mathbf{1}) \frac{\chi_{a_g}^\mu(\mathbf{g})}{\chi_{a_g}^\mu(\mathbf{1})} \left(\frac{\chi_{a_g}^\mu(\mathbf{g})}{\chi_{a_g}^\mu(\mathbf{1})} \right)^* \theta_{a_g} \mathcal{B}_{a_g}^{\mathbf{g}} + \dots \right) \quad (3.347)$$

$$= \frac{\bar{\chi}_{a_g}^\mu(\mathbf{g})}{\chi_{a_g}^\mu(\mathbf{1})} \theta_{a_g} [a_g, \mu], \quad (3.348)$$

where we have used that $\frac{\chi_{a_g}^\mu(\mathbf{g})}{\chi_{a_g}^\mu(\mathbf{1})} \in \text{U}(1)$.

Hence we have³¹

$$S_{[a_g, \mu][b_h, \nu]}^{\mathcal{Z}(\mathcal{C}_G)} = \frac{1}{|\mathcal{G}|} \sum_{\substack{\mathbf{r} \in \mathcal{G}/Z_a \\ \mathbf{s} \in \mathcal{G}/Z_b}} \bar{\chi}_a^\mu(\mathbf{s}_h) {}^s\chi_b^\nu(\mathbf{r}_{\bar{\mathbf{g}}}) S_{r_{a_g} s_{b_h}}, \quad (3.349)$$

$$T_{[a_g, \mu][b_h, \nu]}^{\mathcal{Z}(\mathcal{C}_G)} = \delta_{[a_g, \mu][b_h, \nu]} \frac{\chi_a^\mu(\mathbf{g})}{\chi_a^\mu(\mathbf{1})} \theta_a. \quad (3.350)$$

These quantities are gauge invariant, as the variation of θ_{a_g} and $S_{r_{a_g} s_{b_h}}$ under a 2-coboundary is canceled by that of $\chi_{a_g}^\mu(\mathbf{g})$. In particular, the topological spins of the anyons ($\mathbf{1}$ -defects), after gauging, remain the same. Setting $[b_h, \nu] = [0, 0]$ in Eq.(3.349) we find the quantum dimensions of the gauged superselection sectors to be

$$d_{[a_g, \mu]} = \frac{|\mathcal{G}| d_\mu d_{a_g}}{|Z_{a_g}|}. \quad (3.351)$$

The fusion multiplicities can be derived from the S matrix, calculated in Eq.(3.349), by using the Verlinde formula. It is also possible to derive them directly, by using the intertwining

property of the pair-of-pants tensor network

$$\mathcal{B}_{c_{gh}}^{\mathbf{k}} \mathbf{U}_{\mathbf{k}}[\mathcal{V}_{c_{gh}}^{a_g, b_h}] = \mathcal{V}_{c_{gh}}^{a_g, b_h} \mathcal{B}_{a_g}^{\mathbf{k}} \otimes U_{\mathbf{k}}(a_g, b_h; c_{gh}) \otimes \mathcal{B}_{b_h}^{\mathbf{k}}, \quad (3.352)$$

for $\mathbf{k} \in Z_{a_g, b_h, c_{gh}}$. After gauging, there is no longer a physical group action, and hence the projector onto the $\pi_{c_{gh}}^{\kappa}$ rep is intertwined by the gauged pair-of-pants fusion tube as follows

$$\frac{d_{\kappa}}{|Z_{c_{gh}}|} \sum_{\mathbf{k} \in Z_{a_g, b_h, c_{gh}}} \bar{\chi}_{c_{gh}}^{\kappa}(\mathbf{k}) \mathcal{B}_{c_{gh}}^{\mathbf{k}} \mapsto \frac{d_{\kappa}}{|Z_{c_{gh}}|} \sum_{\mathbf{k} \in Z_{a_g, b_h, c_{gh}}} \bar{\chi}_{c_{gh}}^{\kappa}(\mathbf{k}) \mathcal{B}_{a_g}^{\mathbf{k}} \otimes U_{\mathbf{k}}(a_g, b_h; c_{gh}) \otimes \mathcal{B}_{b_h}^{\mathbf{k}}. \quad (3.353)$$

This projects onto the $\pi_{c_{gh}}^{\kappa}|_{Z_{a_g, b_h, c_{gh}}}$ rep within $(\pi_{a_g}^{\mu} \otimes U_{(\cdot)}(a_g, b_h; c_{gh}) \otimes \pi_{b_h}^{\nu})|_{Z_{a_g, b_h, c_{gh}}}$. To calculate the fusion multiplicity one must also include a summation over defect orbits $[a_g]$, $[b_h]$, $[c_{gh}]$. We implement this by summing over pairs $(^x a_g, ^y b_h)$, for $\mathbf{x} \in \mathcal{G}/Z_{a_g}$, $\mathbf{y} \in \mathcal{G}/Z_{b_h}$, modulo left multiplication $(\mathbf{z}\mathbf{x}, \mathbf{z}\mathbf{y})$, since that leads to defects $^z(^x a_g \times ^y b_h)$ in the same orbit. Hence

$$N_{[a_g, \mu][b_h, \nu]}^{[c_k, \kappa]} = \sum_{\substack{(\mathbf{x}, \mathbf{y}) \in Z_{a_g} \setminus \mathcal{G}/Z_{b_h} \\ \mathbf{z} \in \mathcal{G}/Z_{c_k}}} \delta_{^z a_g ^y b_h} m \left(^z \pi_{c_k}^{\kappa}|_{Z_{^z a_g, ^y b_h, ^z c_k}}, ^x \pi_{a_g}^{\mu}|_{Z_{^x a_g, ^y b_h, ^z c_k}} \right. \\ \left. \otimes U_{(\cdot)}(^x a_g, ^y b_h; ^z c_k)|_{Z_{^x a_g, ^y b_h, ^z c_k}} \otimes ^y \pi_{b_h}^{\nu}|_{Z_{^x a_g, ^y b_h, ^z c_k}} \right), \quad (3.354)$$

where m is the projective rep multiplicity counting function defined in Eq.(3.338).

3.8 Anyon condensation phase transitions dual to gauging

In this section, we study the $\text{Rep}(\mathcal{G})$ anyon condensation phase transition induced by breaking a \mathcal{G} -graded MPO symmetry down to the $\mathbf{1}$ -sector subalgebra^{236,237}. This corresponds to deequivariantization in the category theory language used in Ref. 81,97,98. These phase transition are dual to those induced by gauging a global \mathcal{G} symmetry, which were studied in the previous section. We recount how symmetry breaking perturbations to a local tensor lead to tensor network representations of an anyon condensate^{123,243,244}. Furthermore, we present a decomposition of these perturbations into topological charge sectors that identify which anyons are condensed by a given perturbation. A procedure to extract the defect superselection sectors and domain walls of the condensed theory from the topological superselection sectors of the original theory is explained. This allows one to identify which anyons split, which are identified, and which are confined during the condensation phase transition, as well as the full $U\mathcal{G}xBFC$ description of the resulting SET. We also outline how different — Morita equivalent — MPO algebras, that lead to the same emergent topological order, can be used to find different anyon condensation phase transitions. It is conjectured that this approach will recover all possible boson condensation transitions from a given nonchiral topological order.

3.8.1 MPO symmetry breaking perturbations and anyon condensation

We first explain how anyon condensation phase transitions, induced by a reduction of the topological MPO symmetry algebra, can be analyzed with superselection sector ICIs. The reduction

of the topological MPO symmetry algebra can either originate from explicit symmetry breaking^{236,243,244}, due to a non-symmetric perturbation to the local tensor, or from spontaneous symmetry breaking^{123,124,237}, where the local tensor is varied symmetrically until the boundary theory undergoes a phase transition.

For the case of explicit symmetry breaking, it was argued in Ref. 244 that perturbations to the local tensor can be classified according to the MPO symmetry they respect. The perturbations that are not even symmetric under the vacuum MPO_0 do not change the tensor network, while perturbations respecting MPO_0 lead to fluctuating anyons on top of the tensor network ground state vacuum. The full MPO algebra symmetry of the unperturbed tensor network implies that the fluctuating anyons satisfy a global charge constraint.

The perturbations respecting MPO_0 can be further divided into sectors corresponding to the subset of irreducible idempotents of the tube algebra that come attached to a vacuum string MPO_0 . The set of ICI sectors on which a perturbation has support identify the emergent anyons that it condenses.

We denote the set of irreducible idempotents that can be realized at the end of a vacuum MPO_0 string by $\{\underline{a}_0\}$. Hence we have

$$\underline{a}_0 = \frac{1}{\mathcal{D}^2} \sum_s t_{a_0}^{0s0s} \mathcal{T}_{0s0}^s = \frac{1}{\mathcal{D}^2} \sum_s t_{a_0}^{0s0s} \text{MPO}_s. \quad (3.355)$$

Each \underline{a}_0 corresponds to an internal state of a topological superselection sector satisfying $\underline{a} = (\underline{a}_0 + \dots)$. In particular the vacuum sector $\underline{0}$ always appears in this set of idempotents that occur at the end of MPO_0 .

Due to Eq.(3.143) any tensor perturbation V can be partitioned into a sum over \underline{a}_0 sectors

$$V = V_\times + \sum_{a_0} V_{a_0}, \quad (3.356)$$

where V_\times is orthogonal to MPO_0 and hence leads to a zero state, while V_{a_0} satisfies $V_{a_0} \underline{a}_0 = V_{a_0}$, and hence lies in the \underline{a} charge sector. The perturbations V_0 , satisfying $V_0 \underline{0} = V_0$, are symmetric under the full MPO algebra.

Let $|\Psi[T^{(i)}]\rangle$ denote the tensor network resulting from the contraction of tensors $T^{(i)}$ on every site i of some lattice. We assume the local tensor is symmetric under the full MPO algebra i.e. $T \underline{0} = T$. A perturbed tensor network is given by

$$\begin{aligned} |\Psi[(T + \varepsilon_\times V_\times + \sum_{a_0} \varepsilon_{a_0} V_{a_0})^{(i)}]\rangle &= |\Psi[T]\rangle + \sum_{a_0} \varepsilon_{a_0} \sum_v |\Psi[T^{(i \neq v)}, V_{a_0}^{(v)}]\rangle \\ &\quad + \sum_{a_0, b_0} \varepsilon_{a_0} \varepsilon_{b_0} \sum_{u, v} |\Psi[T^{(i \neq u, v)}, V_{a_0}^{(u)}, V_{b_0}^{(v)}]\rangle + \dots, \end{aligned} \quad (3.357)$$

where i, u, v are lattice sites. We remark that the first order perturbations, aside from V_0 , generically contribute a zero state for a closed manifold due to a global charge constraint. The resulting tensor network states can be interpreted as anyon condensates, as they involve a fluctuation of the charges a_0 with $\varepsilon_{a_0} \neq 0$ on top of the tensor network ground state vacuum.

We expect the case of spontaneous MPO symmetry breaking to follow a similar picture. That is, once the phase transition has been crossed the physical state becomes a cat (GHZ) state given by a sum of explicit MPO symmetry breaking tensor networks, each of which can be interpreted as an anyon condensate.

3.8.2 Extracting the SET order that results from $\text{Rep}(\mathcal{G})$ anyon condensation

Due to the additional structure appearing in the ICIs of a tube algebra derived from a graded MPO algebra $\mathcal{C}_{\mathcal{G}}$, it is possible to infer the defect ICIs and domain walls of the $\mathcal{C}_{\mathcal{G}}$ tube algebra from the anyon ICIs of the $\mathcal{C}_{\mathcal{G}}$ tube algebra. This procedure allows us to calculate the effect of condensing a bosonic $\text{Rep}(\mathcal{G})$ subtheory of $\mathcal{Z}(\mathcal{C}_{\mathcal{G}})$ that induces a phase transition to $\mathcal{Z}(\mathcal{C}_1)_{\mathcal{G}}$. While the anyon theory that results from this condensation transition is known³¹ to be $\mathcal{Z}(\mathcal{C}_1)$, which can simply be constructed by finding the ICIs of the \mathcal{C}_1 tube algebra, we go beyond this to explicitly derive the full SET defect theory $\mathcal{Z}(\mathcal{C}_1)_{\mathcal{G}}$. In particular we calculate which ICIs split, which become identified, and which become confined defect ICIs during the condensation phase transition²¹⁵. The resulting tube ICIs and domain walls can be used to construct the full UGxBFC description of the resulting SET, by following the procedure explained in Section 3.6.

We assume that the MPO algebra $\mathcal{C}_{\mathcal{G}}$ of the model under consideration admits a \mathcal{G} -grading. Hence there is a group element assigned to each of the single block MPOs $[a] \in \mathcal{G}$. The analysis of Refs. 243,244 can be extended to the case where the full virtual MPO symmetry $\mathcal{C}_{\mathcal{G}}$ is broken down to a nontrivial residual MPO symmetry, given by the $\mathbf{1}$ -sector subalgebra \mathcal{C}_1 . This corresponds to an anyon condensation transition from $\mathcal{Z}(\mathcal{C}_{\mathcal{G}})$ to a nontrivial topological phase $\mathcal{Z}(\mathcal{C}_1)$. To calculate the relationship between the $\mathcal{Z}(\mathcal{C}_{\mathcal{G}})$ theory and the condensate $\mathcal{Z}(\mathcal{C}_1)_{\mathcal{G}}$ we examine the implications of a \mathcal{G} -grading for the $\mathcal{C}_{\mathcal{G}}$ tube algebra ICIs. For an ICI of the $\mathcal{C}_{\mathcal{G}}$ tube algebra

$$\underline{a} = \frac{1}{\mathcal{D}^2} \sum_{pqs} t_a^{pqps} \mathcal{T}_{pp}^s, \quad (3.358)$$

we can separate out sectors according to the group elements $[p]$ and $[s]$

$$(\underline{a})_{\mathbf{g}}^{\mathbf{h}} := \frac{1}{\mathcal{D}^2} \sum_{pqs} \delta_{[p],\mathbf{g}} \delta_{[s],\mathbf{h}} t_a^{pqps} \mathcal{T}_{pp}^s, \quad (3.359)$$

we must have $\mathbf{gh} = \mathbf{hg}$ for a nonzero $(\underline{a})_{\mathbf{g}}^{\mathbf{h}}$.

Each ICI \underline{a} can be written as a sum of subidempotents

$$\underline{a} = \sum_{\mathbf{g} \in C} (\underline{a})_{\mathbf{g}}, \quad \text{where} \quad (\underline{a})_{\mathbf{g}} := \sum_{\mathbf{h} \in Z_{\mathbf{g}}} (\underline{a})_{\mathbf{g}}^{\mathbf{h}} \quad (3.360)$$

for some conjugacy class C .

Since the MPO symmetry has been broken down to \mathcal{C}_1 , the MPOs from the $\mathcal{C}_{\mathbf{g}}$ sectors for $\mathbf{g} \neq \mathbf{1}$ now correspond to immobile domain walls in the tensor network. Hence, tubes \mathcal{T}_{pp}^s with $[s] \neq \mathbf{1}$ should be dropped from the tube algebra. Furthermore, the remaining tubes \mathcal{T}_{pp}^s generate a \mathcal{G} tube algebra, that is graded by the sector $[p] = [q] = [r]$. By dropping the immobile domain walls from the topological symmetry algebra, the subidempotents of an ICI \underline{a} are mapped as follows

$$(\underline{a})_{\mathbf{g}} \mapsto (\underline{a})_{\mathbf{g}}^{\mathbf{1}}. \quad (3.361)$$

The resulting idempotents $(\underline{a})_{\mathbf{g}}^{\mathbf{1}}$ are attached to an MPO string in the \mathbf{g} -sector. For $\mathbf{g} \neq \mathbf{1}$ the idempotents correspond to confined defects, as they are connected to a physically observable \mathbf{g} -domain wall that is detected by the local terms of the PEPS parent Hamiltonian⁴⁶, and hence the energy penalty of a defect pair scales with their separation.

For a nontrivial conjugacy class $|C| > 1$ the ICI \underline{a} splits into multiple defects

$$\underline{a} \mapsto \{ K(\underline{a})_{\mathbf{g}}^{\mathbf{1}} \}_{\mathbf{g} \in C}, \quad (3.362)$$

for some positive constant normalization $K > 0$ such that $K(\underline{a})_{\mathbf{g}}^{\mathbf{1}}$ is a projector. We can also calculate which ICIs condense into the same defect, by looking for all \underline{a} and \underline{b} that satisfy

$$(\underline{a})_{\mathbf{g}}^{\mathbf{1}} = \widetilde{K}(\underline{b})_{\mathbf{g}}^{\mathbf{1}} \neq 0, \quad (3.363)$$

for some positive constant \widetilde{K} .

The centralizer $Z_{a_{\mathbf{g}}}$ of a defect $a_{\mathbf{g}}$ is given by the set of group elements \mathbf{h} that lead to a nonzero $(\underline{a})_{\mathbf{g}}^{\mathbf{h}}$, and the orbit of a defect $[(\underline{a})_{\mathbf{g}}^{\mathbf{1}}]$ is given by the set of defects $(\underline{a})_{\mathbf{k}\mathbf{g}}^{\mathbf{1}}$ that are nonzero.

The $(\underline{a})_{\mathbf{1}}^{\mathbf{1}}$ idempotents give the anyon ICIs of the condensed topological order. The procedure explained above allows one to determine the splitting and condensation relations between the anyons of $\mathcal{Z}(\mathcal{C}_{\mathcal{G}})$ and those of $\mathcal{Z}(\mathcal{C}_{\mathbf{1}})$. In particular, we can calculate the anyons that condense into the vacuum

$$\underline{0}_{\mathbf{1}} = \sum_s \delta_{[s], \mathbf{1}} \frac{d_s}{D_{\mathbf{1}}^2} \mathcal{T}_{0s0}^s, \quad (3.364)$$

by looking for those \underline{a} that satisfy $(\underline{a})_{\mathbf{1}}^{\mathbf{1}} = \frac{1}{|\mathcal{G}|} \underline{0}_{\mathbf{1}}$. For condensation induced by symmetry breaking down to the $\mathbf{1}$ -sector of a \mathcal{G} -graded MPO algebra, the ICIs that condense to vacuum are precisely given by $[0_{\mathbf{1}}, \mu]$, see Eq.(3.341). These superselection sectors correspond to bosonic \mathcal{G} -charges, which generate a $\text{Rep}(\mathcal{G})$ subtheory of $\mathcal{Z}(\mathcal{C}_{\mathcal{G}})$ that condenses to yield the resulting SET $\mathcal{Z}(\mathcal{C})_{\mathcal{G}}$.

Hence symmetry breaking perturbations to the local tensor can be divided into irreps, or \mathcal{G} -charges,

$$V = \varepsilon_{\times} V_{\times} + \sum_{\mu} \varepsilon_{\mu} V_{\mu}, \quad (3.365)$$

similar to Eq.(3.356). When a tensor network is built from a symmetric local tensor T with such a perturbation V — for $\varepsilon_{\mu} \neq 0$ — the \mathcal{G} -charges fluctuate and induce a $\text{Rep}(\mathcal{G})$ anyon condensation, see Eq.(3.357).

To construct a tensor network for the condensed SET, where the symmetry is realized on-site, we can modify the local tensor with a perturbation that is correlated to a newly introduced physical group variable

$$T \mapsto \sum_{\mathbf{g}} |\bar{\mathbf{g}}\rangle \otimes (T + V_0 \text{MPO}_{\mathbf{g}}). \quad (3.366)$$

One can verify that this tensor has the correct symmetry transformation under a physical group action, given by the left regular representation, acting on the newly introduced variable. This corresponds to ungauging a \mathcal{G} -gauge symmetry, or equivalently gauging a 1-form symmetry^{88,154,223}. We remark that the perturbations $V_0 \text{MPO}_{\mathbf{g}}$ can be constructed from a linear combination of the V_{μ} perturbations.

Beyond the defect ICIs, we can also extract the \mathcal{G} domain walls of the SET resulting from $\text{Rep}(\mathcal{G})$ condensation

$$\mathcal{B}_h^{a_{\mathbf{g}}} = K(\underline{a})_{\mathbf{g}}^{\mathbf{h}}, \quad (3.367)$$

where $\mathbf{gh} = \mathbf{hg}$, and $K > 0$ is a normalization fixed by the equation $(\mathcal{B}_h^{a_g})^\dagger \mathcal{B}_h^{a_g} = a_g$. These domain walls can be used to extract the second cohomology label of each defect $[\eta_a] \in \mathcal{H}_p^2(\mathcal{G}, \text{U}(1))$ that describes its projective transformation under the global symmetry.

Furthermore, the domain walls define the full set of symmetry-twisted MES on the torus $|\mathcal{B}_h^{a_g}\rangle$, from which the \mathcal{G} -crossed S and T matrices can be extracted, see Section 3.6.4. To calculate the permutation action on the defects, and symmetry twisted states, one can simply fuse an $\text{MPO}_{\mathbf{k}}$ loop into the skeleton of the torus

$$|\text{MPO}_{\mathbf{k}} \circ \mathcal{B}_{a_g}^{\mathbf{h}}\rangle \mapsto \frac{\eta_a(\mathbf{k}, \mathbf{h}) \eta_{\mathbf{k}_a}(\mathbf{kh}, \bar{\mathbf{k}})}{\eta_a(\bar{\mathbf{k}}, \mathbf{k})} |\mathcal{B}_{\mathbf{k}_{a_g}}^{\mathbf{k}\mathbf{h}}\rangle, \quad (3.368)$$

see Eq.(3.281).

3.8.3 Using Morita equivalences to find all anyon condensation phase transitions

The concept of Morita equivalence plays an important role in the search for all possible boson condensation transitions in the framework we have developed. Two MPO algebras \mathcal{C} , $\tilde{\mathcal{C}}$ are Morita equivalent, denoted $\mathcal{C} \sim \tilde{\mathcal{C}}$, precisely when they lead to the same emergent anyons ^{164,211}, $\mathcal{Z}(\mathcal{C}) \cong \mathcal{Z}(\tilde{\mathcal{C}})$. That is, when the physical properties derived from the ICIs of the tube algebras match.

Different, Morita equivalent, MPO algebras that lead to the same emergent topological order can exhibit different \mathcal{G} -gradings and different $\mathbf{1}$ -sectors \mathcal{C}_1 . Hence, by considering such different presentations of the same emergent topological order we can find different $\text{Rep}(\mathcal{G})$ condensation transitions from $\mathcal{Z}(\mathcal{C})$. Several examples of this phenomenon are given in Section 3.9.

By Ref. 81 all $\text{Rep}(\mathcal{G})$ condensation transitions from $\mathcal{Z}(\mathcal{C})$, which are dual to gauging an on-site \mathcal{G} symmetry on a nonchiral topological order, can be realized by considering Morita equivalent MPO algebras that lead to the $\mathcal{Z}(\mathcal{C})$ emergent topological order. To find Morita equivalent representations more explicitly would require a framework for invertible domain walls between different MPO algebras. This is more general than the \mathcal{G} -extension problem considered in Section 3.5.2, which only considered invertible domain walls between the same MPO algebra. We plan to address this in future work.

The process we have outlined for calculating the effects of anyon condensation, by breaking the MPO symmetry down to a nontrivial subalgebra, is straightforwardly generalized beyond the case of a \mathcal{G} -grading. The most general case corresponds to a grading by an algebra, note it is trivial that every MPO symmetry is graded by its own fusion algebra. Several examples of these more general condensations are given in Section 3.9.

Motivated by the \mathcal{G} -graded case, we conjecture that all possible boson condensation phase transitions from a nonchiral topological phase $\mathcal{Z}(\mathcal{C})$ can be realized by symmetry breaking down to the $\mathbf{1}$ -sector of some algebra-graded MPO symmetry algebra in the $\mathcal{Z}(\mathcal{C})$ Morita equivalence class. We plan to cover this generalization in more detail in a future work.

Beyond computing the effects of anyon condensation, the MPO symmetry breaking procedure leads to a simple method to derive the ICIs of a UFC \mathcal{C} from the ICIs of a modular extension of \mathcal{C} . This is because \mathcal{C} naturally forms a subcategory of any modular extension of \mathcal{C} . We expect this to prove useful as explicit formulas exist for the ICIs of a modular theory, making them particularly easy to find.

3.9 Further examples

In this section, we present several examples that demonstrate different aspects of the constructions explained throughout the paper. First, the \mathbb{Z}_2 -extension problem for $\text{Vec}_{\mathbb{Z}_2}$ is solved explicitly. Then, a Morita equivalent description of $\mathcal{Z}(\text{Vec}_{\mathbb{Z}_4})$ is used to study a $\text{Rep}(\mathbb{Z}_2)$ condensation phase transition to the doubled semion model $\mathcal{Z}(\text{Vec}_{\mathbb{Z}_2}^{\omega_1})$, induced by MPO symmetry breaking. Next, we study a condensation phase transition — not generated by a $\text{Rep}(\mathcal{G})$ subtheory — from the doubled Fibonacci model to the trivial phase. Finally, we use Morita equivalent descriptions of $\mathcal{Z}(\text{Vec}_{S_3})$ to study condensation phase transitions to $\mathcal{Z}(\text{Vec}_{\mathbb{Z}_3})$ and $\mathcal{Z}(\text{Vec}_{\mathbb{Z}_2})$, the latter of which is not generated by condensation of a $\text{Rep}(\mathcal{G})$ subtheory.

3.9.1 \mathbb{Z}_2 -extension of $\text{Vec}_{\mathbb{Z}_2}$ and symmetry-enriched toric codes

The \mathbb{Z}_2 -extension problem for an underlying UFC $\text{Vec}_{\mathbb{Z}_2} = \{0, \psi\}$ provides a simple and illustrative example of the extension procedure described in Section 3.5.2. It corresponds to classifying anomaly-free \mathbb{Z}_2 SET orders, where the underlying topological order is the toric code $\mathcal{Z}(\text{Vec}_{\mathbb{Z}_2})$. One of these extensions corresponds to the EM duality-enriched toric code, which was analyzed in detail in Section 3.2.

An extension is calculated in two stages, firstly we search for consistent \mathbb{Z}_2 -graded fusion rules containing $\text{Vec}_{\mathbb{Z}_2}$ as the trivial sector. Note the $\mathbb{Z}_2 = \{\mathbf{1}, \mathbf{x}\}$ action on the objects of $\text{Vec}_{\mathbb{Z}_2}$ must be trivial, as there is only a single nontrivial object. Since the total quantum dimension of each \mathbf{g} -sector must be the same we have $\mathcal{D}_{\mathbf{x}}^2 = \mathcal{D}_{\mathbf{1}}^2 = 2$. Hence the \mathbf{x} -sector can either consist of a single object σ with quantum dimension $\sqrt{2}$, or a pair of inequivalent objects σ_+, σ_- both with quantum dimension 1. We find consistent fusion rules for both of these cases, for which the potential obstructions in $H^3(\mathbb{Z}_2, \mathbb{Z}_2^2)$ disappear.

In the former case the fusion rules must be

$$\sigma \times \sigma = 0 + \psi, \quad (3.369)$$

and the action of the H^2 torsor, permuting 0 and ψ , is trivial. Hence the unique choice is given by the Ising fusion rules.

In the later case there is a trivial solution to the fusion rules

$$\sigma_{\pm} \times \sigma_{\pm} = 0, \quad \sigma_{\pm} \times \sigma_{\mp} = \psi, \quad (3.370)$$

which corresponds to $\mathbb{Z}_2 \times \mathbb{Z}_2$ fusion rules.

In this case the action of the H^2 torsor changes the fusion rules to an inequivalent choice

$$\sigma_{\pm} \times \sigma_{\pm} = \psi, \quad \sigma_{\pm} \times \sigma_{\mp} = 0, \quad (3.371)$$

which corresponds to \mathbb{Z}_4 fusion rules. This exhausts the different choices of consistent fusion rules.

The possible obstruction at the second stage also vanishes since $H^4(\mathbb{Z}_2, \text{U}(1)) = 0$. For each choice of fusion rule we can now look for solutions to the pentagon equation. These are $H^3(\mathbb{Z}_2, \text{U}(1))$ torsors, which can be realized through multiplication of a representative F -symbol with the nontrivial 3-cocycle function $\alpha(\mathbf{g}, \mathbf{h}, \mathbf{k}) = (-1)^{\mathbf{g}\mathbf{h}\mathbf{k}}$. That is

$$F_{def}^{a_g b_h c_k} \mapsto \alpha(\mathbf{g}, \mathbf{h}, \mathbf{k}) F_{def}^{a_g b_h c_k} \quad (3.372)$$

note the only nontrivial value of α is $\alpha(\mathbf{x}, \mathbf{x}, \mathbf{x}) = -1$.

Solutions to the pentagon equation for each choice of graded fusion rules are listed below, where we use the notation of Ref. 106,180 for the 3-cocycles ω_I, ω_{II} .

- Ising – For Ising fusion rules, the F -symbols in Eq.(3.37) solve the pentagon equation. In this case the FS indicator of σ is given by $\kappa_\sigma = 1$. As discussed in Section 3.2.1 this corresponds to the EM duality enriched toric code that gauges to the doubled Ising model, $\text{Ising}^{(1)} \boxtimes \overline{\text{Ising}}^{(1)}$.
- Multiplication with the 3-cocycle $\alpha(\sigma, \sigma, \sigma) = -1$ flips the phase of $F_{\sigma 00}^{\sigma \sigma \sigma}$ and hence yields $\kappa_\sigma = -1$. This corresponds to the EM duality enriched toric code with a pair of self-inverse defects with negative FS indicators. Gauging this leads to the Drinfeld center of the modified Ising model with $\kappa_\sigma = -1$, $\text{Ising}^{(3)} \boxtimes \overline{\text{Ising}}^{(3)}$.
- \mathbb{Z}_2^2 – For $\mathbb{Z}_2 \times \mathbb{Z}_2$ fusion rules, there is a trivial solution $F_{abc}^{ghk} = \delta_{ghk,a} \delta_{gh,b} \delta_{hk,c}$ which corresponds to a toric code tensor producted with a trivial paramagnet. This gauges to two copies of the toric code.
- Multiplying by $\alpha(\sigma_\pm, \sigma_\pm, \sigma_\pm) = -1$ leads to a \mathbb{Z}_2 -extension of $\text{Vec}_{\mathbb{Z}_2}$ with two self inverse defects that have negative FS indicator $\kappa_{\sigma_+} = \kappa_{\sigma_-} = -1$. This corresponds to a symmetry-enriched toric code that gauges to $\mathcal{Z}(\text{Vec}_{\mathbb{Z}_2 \times \mathbb{Z}_2}^{\omega_1^{(2)}})$.
- There is another distinct solution to the pentagon equation with these fusion rules, corresponding to a 3-cocycle $\omega_{I(1)} \omega_{II}$, which gives a toric code tensor producted with a nontrivial \mathbb{Z}_2 SPT. This gauges to a toric code tensor producted with a doubled semion model.
- Multiplying by $\alpha(\sigma_\pm, \sigma_\pm, \sigma_\pm) = -1$ in this case corresponds to relabeling σ_\pm , and hence yields the same solution.

The general F -symbol solutions for $\mathbb{Z}_2 \times \mathbb{Z}_2$ fusion rules are given by 3-cocycles representatives of the elements $H^3(\mathbb{Z}_2 \times \mathbb{Z}_2, \text{U}(1)) = \mathbb{Z}_2^3$, which are generated by $\omega_{I(1)}, \omega_{I(2)}, \omega_{II}$. For a fixed choice of \mathbb{Z}_2 subgroup, corresponding to \mathcal{C}_1 , there are four inequivalent 3-cocycles with a trivial restriction. Two of these 3-cocycles are captured by the first two cases above, while the other two are both captured by the third case.

- \mathbb{Z}_4 – For \mathbb{Z}_4 fusion rules, again there is the trivial solution, which corresponds to a toric code with two pairs of topologically distinct defects that are mutual inverses. This gauges to the \mathbb{Z}_4 quantum double model $\mathcal{Z}(\text{Vec}_{\mathbb{Z}_4})$.
- Multiplying by $\alpha(\sigma_\pm, \sigma_\pm, \sigma_\pm) = -1$ corresponds to a different symmetry-enriched toric code with two pairs of mutual inverse defects. This gauges to the ω_1^2 -twisted \mathbb{Z}_4 quantum double model $\mathcal{Z}(\text{Vec}_{\mathbb{Z}_4}^{\omega_1^2})$.

The general F -symbol solutions for \mathbb{Z}_4 fusion rules are given by 3-cocycles representatives of the elements $H^3(\mathbb{Z}_4, \text{U}(1)) = \mathbb{Z}_4$. There are two 3-cocycles that have trivial restriction to the \mathbb{Z}_2 subgroup. These correspond to the two cases above.

We remark that similar treatments of this example have appeared in Refs. 32,33.

3.9.2 Morita equivalent MPO algebras $\text{Vec}_{\mathbb{Z}_4} \sim \text{Vec}_{\mathbb{Z}_2 \times \mathbb{Z}_2}^{\omega_{\text{II}}}$ and condensation to the doubled semion model

In Ref. 237 a condensation phase transition from $\mathcal{Z}(\text{Vec}_{\mathbb{Z}_4})$ to the doubled semion model $\text{Vec}_{\mathbb{Z}_2}^{\omega_{\text{I}}}$ was described in terms of a boundary SPT phase under the MPO symmetry. Here we revisit this condensation with our framework, and by using a Morita equivalent description of the topological order $\mathcal{Z}(\text{Vec}_{\mathbb{Z}_4}) \cong \mathcal{Z}(\text{Vec}_{\mathbb{Z}_2 \times \mathbb{Z}_2}^{\omega_{\text{II}}})$ we find a reduction of the MPO symmetry that induces the same $\text{Rep}(\mathbb{Z}_2)$ condensation phase transition without any reference to a boundary SPT. This exemplifies the general fact, that all $\text{Rep}(\mathcal{G})$ condensation phase transitions can be realized through \mathcal{G} -graded MPO symmetry breaking. Hence any condensation phase transition corresponding to a boundary SPT phase in the language of Ref. 237, can be induced by symmetry breaking in some Morita equivalent MPO algebra using our framework. Our approach has the advantage that it captures all $\text{Rep}(\mathcal{G})$ condensation phase transition, while no such proof was given in Ref. 237.

There is a well known Morita equivalence $\text{Vec}_{\mathbb{Z}_4} \sim \text{Vec}_{\mathbb{Z}_2 \times \mathbb{Z}_2}^{\omega_{\text{II}}}$, see Ref. 106, and hence $\mathcal{Z}(\text{Vec}_{\mathbb{Z}_4}) \cong \mathcal{Z}(\text{Vec}_{\mathbb{Z}_2 \times \mathbb{Z}_2}^{\omega_{\text{II}}})$. Therefore, to describe an emergent $\mathcal{Z}(\text{Vec}_{\mathbb{Z}_4})$ topological order we may use an MPO algebra $\text{Vec}_{\mathbb{Z}_2 \times \mathbb{Z}_2}^{\omega_{\text{II}}}$.

let us first construct the tube algebra for $\text{Vec}_{\mathbb{Z}_2 \times \mathbb{Z}_2}^{\omega_{\text{II}}}$ and find its ICIs, from which one can verify the equivalence $\mathcal{Z}(\text{Vec}_{\mathbb{Z}_4}) \cong \mathcal{Z}(\text{Vec}_{\mathbb{Z}_2 \times \mathbb{Z}_2}^{\omega_{\text{II}}})$. Since the fusion rules are Abelian and all group elements are self inverse, the tubes appearing are of the form $\mathcal{T}_{g,g+h,g}^h$ and we use the shorthand notation $\mathcal{T}_g^h := \alpha(h, g+h, h) \mathcal{T}_{g,g+h,g}^h$, established in Eq.(3.323). This tube algebra has multiplication rules

$$\mathcal{T}_f^h \mathcal{T}_g^k = \delta_{f,g} \alpha^g(h, k) \mathcal{T}_g^{h+k}, \quad (3.373)$$

where α^g is the slant product defined in Eq.(3.318). The 3-cocycle is given by $\alpha \equiv \omega_{\text{II}}$ where

$$\omega_{\text{II}}(A, B, C) = (-1)^{a_0 b_1 c_1}, \quad \text{and} \quad A = (a_0, a_1). \quad (3.374)$$

Using the ICI formula for twisted gauge theory, given in Eq.(3.331), we find

Anyons	\mathcal{T}_{00}^{00}	\mathcal{T}_{00}^{01}	\mathcal{T}_{00}^{10}	\mathcal{T}_{00}^{11}	\mathcal{T}_{01}^{00}	\mathcal{T}_{01}^{01}	\mathcal{T}_{01}^{10}	\mathcal{T}_{01}^{11}	\mathcal{T}_{10}^{00}	\mathcal{T}_{10}^{01}	\mathcal{T}_{10}^{10}	\mathcal{T}_{10}^{11}	\mathcal{T}_{11}^{00}	\mathcal{T}_{11}^{01}	\mathcal{T}_{11}^{10}	\mathcal{T}_{11}^{11}
(00, ++)	1	1	1	1												
(00, +-)	1	-1	1	-1												
(00, -+)	1	1	-1	-1												
(00, --)	1	-1	-1	1												
(01, ++)					1	1	1	1								
(01, +-)					1	-1	1	-1								
(01, -+)					1	1	-1	-1								
(01, --)					1	-1	-1	1								
(10, ++)									1	-i	1	-i				
(10, +-)									1	i	1	i				
(10, -+)									1	-i	-1	i				
(10, --)									1	i	-1	-i				
(11, ++)													1	-i	1	-i
(11, +-)													1	i	1	i
(11, -+)													1	-i	-1	i
(11, --)													1	i	-1	-i

(3.375)

the table gives the elements t_i^j of the ICIs and should be read as follows

$$\underline{a}_i = \frac{1}{\mathcal{D}^2} \sum_j t_i^j (\mathcal{T}_h^g)_j, \quad (3.376)$$

where $\mathcal{D}^2 = 4$ in this case.

There are several \mathbb{Z}_2 -gradings of $\text{Vec}_{\mathbb{Z}_2 \times \mathbb{Z}_2}^{\omega_{\text{II}}}$ that we could consider for $\mathcal{C}_1 \oplus \mathcal{C}_{\mathbf{x}}$

$$\{00, 01\} \oplus \{10, 11\}, \quad \{00, 10\} \oplus \{01, 11\}, \quad \{00, 11\} \oplus \{01, 10\}. \quad (3.377)$$

The first two are equivalent and lead to a condensation to the toric code phase, while the third leads to a condensation to the doubled semion phase. This is because the restriction of the 3-cocycle ω_{II} to the $\{00, 11\}$ subgroup lies in the nontrivial cohomology class of $\mathcal{H}^3(\mathbb{Z}_2, \text{U}(1)) = \mathbb{Z}_2$. We remark that shifting by a ω_I cocycle on any of the \mathbb{Z}_2 subgroups rearranges which of the above \mathbb{Z}_2 -gradings corresponds to the doubled semion phase.

We choose the $\{00, 11\} \oplus \{01, 10\}$ grading for the MPO symmetry algebra. Then breaking the MPO symmetry down to \mathcal{C}_1 leads to a $\text{Rep}(\mathbb{Z}_2)$ condensation to a symmetry enriched

doubled semion phase described in the table below.

Sectors	Defects	Condensed anyons	\mathcal{T}_{00}^{00}	\mathcal{T}_{00}^{11}	\mathcal{T}_{11}^{00}	\mathcal{T}_{11}^{11}	\mathcal{T}_{01}^{00}	\mathcal{T}_{01}^{11}	\mathcal{T}_{10}^{00}	\mathcal{T}_{10}^{11}
1	0	(00, ++)	1	1						
		(00, --)	1	1						
	$s\bar{s}$	(00, +-)	1	-1						
		(00, -+)	1	-1						
	s	(11, ++)			1	$-i$				
		(11, --)			1	$-i$				
	\bar{s}	(11, +-)			1	i				
		(11, -+)			1	i				
x	σ_0	(01, ++)					1	1		
		(01, --)					1	1		
	σ_1	(01, +-)					1	-1		
		(01, -+)					1	-1		
	σ_2	(10, ++)							1	$-i$
		(10, --)							1	$-i$
	σ_3	(10, +-)							1	i
		(10, -+)							1	i

(3.378)

The domain walls for the nontrivial element **x** are given by

Sectors	Defects	\mathbb{Z}_2 -action							
		\mathcal{T}_{00}^{01}	\mathcal{T}_{00}^{10}	\mathcal{T}_{11}^{01}	\mathcal{T}_{11}^{01}	\mathcal{T}_{01}^{01}	\mathcal{T}_{01}^{10}	\mathcal{T}_{10}^{01}	\mathcal{T}_{10}^{10}
1	0	1	1						
	$s\bar{s}$	1	-1						
	s			1	i				
	\bar{s}			1	$-i$				
x	σ_0					1	1		
	σ_1					1	-1		
	σ_2							1	i
	σ_3							1	$-i$

(3.379)

where a normalization by $\mathcal{D}_1^2 = 2$ is implicit. For a more detailed guide to reading the tables, see Eq.(3.57).

Denote the \mathbb{Z}_2 generator on defect a by X_a , then $X_a^2 = 1$ for $a \in \{0, s\bar{s}, \sigma_0, \sigma_1\}$ and $X_a^2 = -1$ for $a \in \{s, \bar{s}, \sigma_2, \sigma_3\}$. We remark, in this case, the projective phase $X_a^2 = -1$ can be removed by a choice of coboundary. It is important, however, to keep track of the choice when calculating the effect of gauging the symmetry.

This example demonstrates that the topological data obtained by gauging an SET is not a faithful label. In particular one finds the same gauged data for the symmetry-enriched doubled semion, described in Eq.(3.378), and the symmetry-enriched toric code, described as the first case under \mathbb{Z}_4 in Section 3.9.1. For this example, the gauge invariant $S^{(1,1)}, T^{(1,1)}$ matrices of the SETs clearly distinguish the two SET phases, as they have different underlying topological orders.

We remark that even when the underlying topological order is the same, the gauged data still does not provide a faithful label. A well known example of this occurs for the trivial D_4 SPT and the type-III \mathbb{Z}_2^3 SPT, since $\mathcal{Z}(\text{Vec}_{D_4}) \cong \mathcal{Z}(\text{Vec}_{\mathbb{Z}_2^3}^{\omega_{\text{III}}})$ and the underlying topological orders are both trivial^{74,106,129}, see Chapter 2. In this case the SPTs are clearly distinguished by their different symmetry groups.

3.9.3 Doubled Fibonacci model

We now present the simplest nontrivial example of a condensation phase transition induced by MPO algebra symmetry breaking that does not originate from a \mathcal{G} -grading. The example is based on the Fibonacci fusion category. The fusion algebra is constructed from two objects, denoted $\{0, \tau\}$, with commutative multiplication rules

$$0 \times a = a, \quad \tau \times \tau = 0 + \tau, \quad (3.380)$$

for $a \in \{0, \tau\}$. Their quantum dimensions are $d_0 = 1$, $d_\tau = \phi$, and the nontrivial F -symbols are given by

$$[F_\tau^{\tau\tau\tau}]_i^j = \frac{1}{\phi} \begin{bmatrix} 1 & \sqrt{\phi} \\ \sqrt{\phi} & -1 \end{bmatrix}, \quad (3.381)$$

for $i, j \in \{0, \tau\}$. Where

$$\phi := \frac{1 + \sqrt{5}}{2} \quad \text{is the golden ratio,} \quad \phi^2 = 1 + \phi, \quad \text{and} \quad \mathcal{D}^2 = \phi\sqrt{5}. \quad (3.382)$$

The ICIs of the tube algebra are specified by the table below.

Anyons	\mathcal{T}_{000}^0	$\mathcal{T}_{0\tau 0}^\tau$	$\mathcal{T}_{\tau\tau\tau}^0$	$\mathcal{T}_{\tau 0\tau}^\tau$	$\mathcal{T}_{\tau\tau\tau}^\tau$
0	1	ϕ			
$\tau\bar{\tau}$	ϕ^2	$-\phi$	ϕ	ϕ	$\frac{1}{\sqrt{\phi}}$
τ			1	$e^{\frac{4i\pi}{5}}$	$\sqrt{\phi}e^{-\frac{3i\pi}{5}}$
$\bar{\tau}$			1	$e^{-\frac{4i\pi}{5}}$	$\sqrt{\phi}e^{\frac{3i\pi}{5}}$

(3.383)

Note the implicit normalization by \mathcal{D}^2 . The full two dimensional $\tau\bar{\tau}$ block is spanned by the elements

$$\tau\bar{\tau}_{00} = \frac{1}{\mathcal{D}^2} (\phi^2 \mathcal{T}_{000}^0 - \phi \mathcal{T}_{0\tau 0}^\tau) \quad \tau\bar{\tau}_{01} = \frac{\phi}{\mathcal{D}} \mathcal{T}_{0\tau\tau}^\tau \quad (3.384)$$

$$\tau\bar{\tau}_{10} = \frac{\sqrt{\phi}}{\mathcal{D}} \mathcal{T}_{\tau\tau 0}^\tau \quad \tau\bar{\tau}_{11} = \frac{1}{\mathcal{D}^2} \left(\phi \mathcal{T}_{\tau\tau\tau}^0 + \phi \mathcal{T}_{\tau 0\tau}^\tau + \frac{1}{\sqrt{\phi}} \mathcal{T}_{\tau\tau\tau}^\tau \right). \quad (3.385)$$

The other blocks are one dimensional.

The Fibonacci algebra clearly does not admit any nontrivial \mathcal{G} -grading. It does, however, admit the obvious grading by the fusion algebra itself. This statement in itself is vacuous. However, by breaking the MPO algebra down to the 0-sector — which consists only of MPO_0

— we can calculate the effects of a corresponding boson condensation transition.

Sectors	Defects	Condensed anyons	\mathcal{T}_{000}^0	$\mathcal{T}_{\tau\tau\tau}^0$
1	0	0 $\tau\bar{\tau}_{00}$	1 ϕ^2	
a	$\Delta_{\mathbf{a}}$	$\tau\bar{\tau}_{11}$ τ $\bar{\tau}$		ϕ 1 1

(3.386)

Where the fusion rules for $\{\mathbf{1}, \mathbf{a}\}$ are identical to the Fibonacci algebra

$$\mathbf{1} \times \mathbf{z} = \mathbf{z}, \quad \mathbf{a} \times \mathbf{a} = \mathbf{1} + \mathbf{a}, \quad \text{for} \quad \mathbf{z} \in \{\mathbf{1}, \mathbf{a}\}. \quad (3.387)$$

This example demonstrates that, unlike the \mathcal{G} -graded case, breaking an MPO symmetry according to an algebra-grading may induce a boson to split with only one of the resulting sectors condensing to the vacuum. Similar to the \mathcal{G} -graded case, MPOs in a nontrivial sector correspond to locally detectable domain walls after condensation. Hence, idempotents that appear at the end of MPOs in nontrivial sectors condense to extrinsic defects, which are confined. Unlike the \mathcal{G} -graded case, we do not expect it to be possible to move these domain walls by applying local unitaries to the physical system, as they are not generally invertible.

We remark that the resulting vacuum transforms under an action of the Fibonacci algebra generated by $\mathcal{T}_{0\tau 0}^\tau$, whereas the $\Delta_{\mathbf{a}}$ -defect transforms under a different algebra generated by $\{\mathcal{T}_{\tau\tau\tau}^\tau, \mathcal{T}_{\tau 0\tau}^\tau\}$. This algebra contains a copy of the Fibonacci algebra, generated by $(\phi^3 \mathcal{T}_{\tau 0\tau}^\tau + \phi^{3/2} \mathcal{T}_{\tau\tau\tau}^\tau)$, but also contains elements outside of this. One might like to think of this in analogy to the group case, where nontrivial defects may carry a projective representation of the symmetry group. However, here the difference between the the algebras in the two sectors is more extreme. There is also a \mathbb{Z}_2 action hopping between the 0 and $\Delta_{\mathbf{a}}$ defects generated by $\frac{\sqrt{\phi}}{\mathcal{D}}(\mathcal{T}_{\tau\tau 0}^\tau + \sqrt{\phi} \mathcal{T}_{0\tau\tau}^\tau)$. The precise physical meaning of the algebras under which the defects transform is unclear.

3.9.4 $\mathcal{Z}(\mathbf{Vec}_{S_3})$ and $\mathcal{Z}(\mathbf{Rep}(S_3))$

For a final example, we use another well known Morita equivalence $\mathbf{Vec}_{S_3} \sim \mathbf{Rep}(S_3)$ to study two different anyon condensation phase transitions from the emergent topological order $\mathcal{Z}(\mathbf{Vec}_{S_3}) \cong \mathcal{Z}(\mathbf{Rep}(S_3))$. We first use the \mathbb{Z}_2 -grading of \mathbf{Vec}_{S_3} to study a phase transition to $\mathcal{Z}(\mathbf{Vec}_{\mathbb{Z}_3})$. Next, we consider an algebra grading of $\mathbf{Rep}(S_3)$ to study a phase transition to $\mathcal{Z}(\mathbf{Vec}_{\mathbb{Z}_2})$.

We work with the following presentation of S_3

$$\langle s, r \mid s^2 = r^3 = (sr)^2 = 1 \rangle, \quad (3.388)$$

hence the set of group elements is given by $\{1, r, \bar{r}, s, sr, s\bar{r}\}$. Furthermore, we denote the irreducible representations of S_3 by $\{0, \psi, \pi\}$, correspond to the trivial, sign, and two-dimensional irrep, respectively.

The fusion rules of \mathbf{Vec}_{S_3} are given by S_3 multiplication, and the F -symbols are trivial. The anyons of $\mathcal{Z}(\mathbf{Vec}_{S_3})$ can be labeled by a conjugacy class, together with an irreducible representation of the centralizer of a representative from the conjugacy class. We use the notation $[g, \rho]$

to indicate the conjugacy class C_g and an irrep ρ of the centralizer Z_g . A formula for the ICIs is given in Eq.(3.331).

Anyons	\mathcal{T}_1^1	\mathcal{T}_1^r	$\mathcal{T}_1^{\bar{r}}$	\mathcal{T}_1^s	\mathcal{T}_1^{sr}	$\mathcal{T}_1^{s\bar{r}}$	\mathcal{T}_r^1	\mathcal{T}_r^r	$\mathcal{T}_r^{\bar{r}}$	\mathcal{T}_r^s	\mathcal{T}_r^{sr}	$\mathcal{T}_r^{s\bar{r}}$	\mathcal{T}_s^1	\mathcal{T}_s^r	$\mathcal{T}_s^{\bar{r}}$	\mathcal{T}_s^s	\mathcal{T}_s^{sr}	$\mathcal{T}_s^{s\bar{r}}$
$[1, 0]$	1	1	1	1	1	1												
$[1, \psi]$	1	1	1	-1	-1	-1												
$[1, \pi]$	4	-2	-2															
$[r, 1]$							2	2	2	2	2	2						
$[r, e^{\frac{2\pi i}{3}}]$							2	$2e^{-\frac{2\pi i}{3}}$	$2e^{\frac{2\pi i}{3}}$	2	$2e^{\frac{2\pi i}{3}}$	$2e^{-\frac{2\pi i}{3}}$						
$[r, e^{-\frac{2\pi i}{3}}]$							2	$2e^{\frac{2\pi i}{3}}$	$2e^{-\frac{2\pi i}{3}}$	2	$2e^{-\frac{2\pi i}{3}}$	$2e^{\frac{2\pi i}{3}}$						
$[s, +]$													3	3	3	3	3	3
$[s, -]$													3	-3	3	-3	3	-3

(3.389)

Note the implicit normalization of $\mathcal{D}^2 = 6$ in the above table.

The full two dimensional $[1, \pi]$, $[r, 1]$, $[r, e^{\frac{2\pi i}{3}}]$, and $[r, e^{-\frac{2\pi i}{3}}]$ blocks are given by

$$\begin{aligned}
 [1, \pi]_{00} &= \frac{1}{3} \left(\mathcal{T}_1^1 + e^{-\frac{2\pi i}{3}} \mathcal{T}_1^r + e^{\frac{2\pi i}{3}} \mathcal{T}_1^{\bar{r}} \right) & [1, \pi]_{01} &= \frac{1}{3} \left(\mathcal{T}_1^s + e^{\frac{2\pi i}{3}} \mathcal{T}_1^{sr} + e^{-\frac{2\pi i}{3}} \mathcal{T}_1^{s\bar{r}} \right) \\
 [1, \pi]_{10} &= \frac{1}{3} \left(\mathcal{T}_1^s + e^{-\frac{2\pi i}{3}} \mathcal{T}_1^{sr} + e^{\frac{2\pi i}{3}} \mathcal{T}_1^{s\bar{r}} \right) & [1, \pi]_{11} &= \frac{1}{3} \left(\mathcal{T}_1^1 + e^{\frac{2\pi i}{3}} \mathcal{T}_1^r + e^{-\frac{2\pi i}{3}} \mathcal{T}_1^{\bar{r}} \right),
 \end{aligned}
 \tag{3.390}$$

$$\begin{aligned}
 [r, 1]_{00} &= \frac{1}{3} \left(\mathcal{T}_r^1 + \mathcal{T}_r^r + \mathcal{T}_r^{\bar{r}} \right) & [r, 1]_{01} &= \frac{1}{3} \left(\mathcal{T}_r^s + \mathcal{T}_r^{sr} + \mathcal{T}_r^{s\bar{r}} \right) \\
 [r, 1]_{10} &= \frac{1}{3} \left(\mathcal{T}_r^s + \mathcal{T}_r^{sr} + \mathcal{T}_r^{s\bar{r}} \right) & [r, 1]_{11} &= \frac{1}{3} \left(\mathcal{T}_r^1 + \mathcal{T}_r^r + \mathcal{T}_r^{\bar{r}} \right),
 \end{aligned}
 \tag{3.391}$$

$$\begin{aligned}
 [r, e^{\pm \frac{2\pi i}{3}}]_{00} &= \frac{1}{3} \left(\mathcal{T}_r^1 + e^{\mp \frac{2\pi i}{3}} \mathcal{T}_r^r + e^{\pm \frac{2\pi i}{3}} \mathcal{T}_r^{\bar{r}} \right) & [r, e^{\pm \frac{2\pi i}{3}}]_{01} &= \frac{1}{3} \left(\mathcal{T}_r^s + e^{\pm \frac{2\pi i}{3}} \mathcal{T}_r^{sr} + e^{\mp \frac{2\pi i}{3}} \mathcal{T}_r^{s\bar{r}} \right) \\
 [r, e^{\pm \frac{2\pi i}{3}}]_{10} &= \frac{1}{3} \left(\mathcal{T}_r^s + e^{\mp \frac{2\pi i}{3}} \mathcal{T}_r^{sr} + e^{\pm \frac{2\pi i}{3}} \mathcal{T}_r^{s\bar{r}} \right) & [r, e^{\pm \frac{2\pi i}{3}}]_{11} &= \frac{1}{3} \left(\mathcal{T}_r^1 + e^{\pm \frac{2\pi i}{3}} \mathcal{T}_r^r + e^{\mp \frac{2\pi i}{3}} \mathcal{T}_r^{\bar{r}} \right).
 \end{aligned}
 \tag{3.392}$$

While the three dimensional $[s, +]$ and $[s, -]$ blocks are given by

$$\begin{aligned}
 [s, \pm]_{00} &= \frac{1}{2} \left(\mathcal{T}_s^1 \pm \mathcal{T}_s^s \right) & [s, \pm]_{01} &= \frac{1}{2} \left(\mathcal{T}_s^{\bar{r}} \pm \mathcal{T}_s^{s\bar{r}} \right) & [s, \pm]_{02} &= \frac{1}{2} \left(\mathcal{T}_s^r \pm \mathcal{T}_s^{sr} \right) \\
 [s, \pm]_{10} &= \frac{1}{2} \left(\mathcal{T}_s^r \pm \mathcal{T}_s^{s\bar{r}} \right) & [s, \pm]_{11} &= \frac{1}{2} \left(\mathcal{T}_s^1 \pm \mathcal{T}_s^{sr} \right) & [s, \pm]_{12} &= \frac{1}{2} \left(\mathcal{T}_s^{\bar{r}} \pm \mathcal{T}_s^s \right) \\
 [s, \pm]_{20} &= \frac{1}{2} \left(\mathcal{T}_s^{\bar{r}} \pm \mathcal{T}_s^{sr} \right) & [s, \pm]_{21} &= \frac{1}{2} \left(\mathcal{T}_s^r \pm \mathcal{T}_s^s \right) & [s, \pm]_{22} &= \frac{1}{2} \left(\mathcal{T}_s^1 \pm \mathcal{T}_s^{s\bar{r}} \right).
 \end{aligned}
 \tag{3.393}$$

Vec_{S_3} admits a \mathbb{Z}_2 -grading as follows $\{1, r, \bar{r}\} \oplus \{s, sr, s\bar{r}\}$. Breaking the MPO algebra

down to the **1**-sector induces a $\text{Rep}(\mathbb{Z}_2)$ condensation phase transition to $\mathcal{Z}(\text{Vec}_{\mathbb{Z}_3})$.

Sectors	Defects	Condensed anyons	\mathcal{T}_1^1	\mathcal{T}_1^r	$\mathcal{T}_1^{\bar{r}}$	\mathcal{T}_r^1	\mathcal{T}_r^r	$\mathcal{T}_r^{\bar{r}}$	$\mathcal{T}_{\bar{r}}^1$	$\mathcal{T}_{\bar{r}}^r$	$\mathcal{T}_{\bar{r}}^{\bar{r}}$	\mathcal{T}_s^1	\mathcal{T}_{sr}^1	$\mathcal{T}_{s\bar{r}}^1$
1	[1, 1]	[1, 0]	1	1	1									
		[1, ψ]	1	1	1									
	$[1, e^{\frac{2\pi i}{3}}]$	$[1, \pi]_{00}$	2	$2e^{-\frac{2\pi i}{3}}$	$2e^{\frac{2\pi i}{3}}$									
	$[1, e^{-\frac{2\pi i}{3}}]$	$[1, \pi]_{11}$	2	$2e^{\frac{2\pi i}{3}}$	$2e^{-\frac{2\pi i}{3}}$									
	$[r, 1]$	$[r, 1]_{00}$				2	2	2						
	$[\bar{r}, 1]$	$[r, 1]_{11}$							2	2	2			
	$[r, e^{\frac{2\pi i}{3}}]$	$[r, e^{\frac{2\pi i}{3}}]_{00}$				2	$2e^{-\frac{2\pi i}{3}}$	$2e^{\frac{2\pi i}{3}}$						
	$[\bar{r}, e^{-\frac{2\pi i}{3}}]$	$[r, e^{\frac{2\pi i}{3}}]_{11}$							2	$2e^{\frac{2\pi i}{3}}$	$2e^{-\frac{2\pi i}{3}}$			
	$[r, e^{-\frac{2\pi i}{3}}]$	$[r, e^{-\frac{2\pi i}{3}}]_{00}$				2	$2e^{\frac{2\pi i}{3}}$	$2e^{-\frac{2\pi i}{3}}$						
	$[\bar{r}, e^{\frac{2\pi i}{3}}]$	$[r, e^{-\frac{2\pi i}{3}}]_{11}$							2	$2e^{-\frac{2\pi i}{3}}$	$2e^{\frac{2\pi i}{3}}$			
x	Δ	$[s, +]$										3	3	3
		$[s, -]$										3	3	3

(3.394)

The three dimensional $\underline{\Delta}$ block is given by

$$\begin{aligned}
 \underline{\Delta}_{00} &= \mathcal{T}_s^1 & \underline{\Delta}_{01} &= \mathcal{T}_{sr}^{\bar{r}} & \underline{\Delta}_{02} &= \mathcal{T}_{s\bar{r}}^r \\
 \underline{\Delta}_{10} &= \mathcal{T}_s^r & \underline{\Delta}_{11} &= \mathcal{T}_{sr}^1 & \underline{\Delta}_{12} &= \mathcal{T}_{s\bar{r}}^{\bar{r}} \\
 \underline{\Delta}_{20} &= \mathcal{T}_s^{\bar{r}} & \underline{\Delta}_{21} &= \mathcal{T}_{sr}^r & \underline{\Delta}_{22} &= \mathcal{T}_{s\bar{r}}^1.
 \end{aligned} \tag{3.395}$$

The reader may find it amusing that this condensation transition actually increases the number of anyons from eight to nine.

The action of the nontrivial group element **x** upon the defect superselection sectors is given

by

Sectors	Defects	\mathbb{Z}_2 -action											
		\mathcal{T}_1^s	\mathcal{T}_1^{sr}	$\mathcal{T}_1^{s\bar{r}}$	\mathcal{T}_r^s	\mathcal{T}_r^{sr}	$\mathcal{T}_r^{s\bar{r}}$	$\mathcal{T}_{\bar{r}}^s$	$\mathcal{T}_{\bar{r}}^{sr}$	$\mathcal{T}_{\bar{r}}^{s\bar{r}}$	\mathcal{T}_s^s	\mathcal{T}_{sr}^{sr}	$\mathcal{T}_{s\bar{r}}^{s\bar{r}}$
1	$[1, 1]$	1	1	1									
	$[1, e^{\frac{2\pi i}{3}}]$	2	-1	-1									
	$[1, e^{-\frac{2\pi i}{3}}]$												
	$[r, 1]$				1	1	1						
	$[\bar{r}, 1]$							1	1	1			
	$[r, e^{\frac{2\pi i}{3}}]$				1	$e^{-\frac{2\pi i}{3}}$	$e^{\frac{2\pi i}{3}}$						
	$[\bar{r}, e^{-\frac{2\pi i}{3}}]$							1	$e^{\frac{2\pi i}{3}}$	$e^{-\frac{2\pi i}{3}}$			
	$[r, e^{-\frac{2\pi i}{3}}]$				1	$e^{\frac{2\pi i}{3}}$	$e^{-\frac{2\pi i}{3}}$						
	$[\bar{r}, e^{\frac{2\pi i}{3}}]$							1	$e^{-\frac{2\pi i}{3}}$	$e^{\frac{2\pi i}{3}}$			
x	Δ										3	3	3

(3.396)

where there is an implicit normalization by $\mathcal{D}_1^2 = 3$.

From these actions we can extract the permutation action upon the defects, summarized below.

$\rho_{\mathbf{x}}$	$\mathbf{x}[1, 1]$	$\mathbf{x}[1, e^{\frac{2\pi i}{3}}]$	$\mathbf{x}[1, e^{-\frac{2\pi i}{3}}]$	$\mathbf{x}[r, 1]$	$\mathbf{x}[\bar{r}, 1]$	$\mathbf{x}[r, e^{\frac{2\pi i}{3}}]$	$\mathbf{x}[\bar{r}, e^{\frac{2\pi i}{3}}]$	$\mathbf{x}[r, e^{-\frac{2\pi i}{3}}]$	$\mathbf{x}[\bar{r}, e^{-\frac{2\pi i}{3}}]$	$\mathbf{x}\Delta$
$[1, 1]$	1									
$[1, e^{\frac{2\pi i}{3}}]$		1								
$[1, e^{-\frac{2\pi i}{3}}]$			1							
$[r, 1]$				1						
$[\bar{r}, 1]$					1					
$[r, e^{\frac{2\pi i}{3}}]$						1				
$[\bar{r}, e^{\frac{2\pi i}{3}}]$							1			
$[r, e^{-\frac{2\pi i}{3}}]$								1		
$[\bar{r}, e^{-\frac{2\pi i}{3}}]$									1	
Δ										1

(3.397)

We now turn to the Morita equivalent $\text{Rep}(S_3)$ MPO algebra. The simple objects are given by the irreducible representations of S_3 which are $\{0, \psi, \pi\}$ as described above. The fusion

rules of this algebra are given by

$$0 \times a = a, \quad \psi \times \psi = 0, \quad \pi \times \psi = \psi, \quad \pi \times \pi = 0 + \psi + \pi, \quad (3.398)$$

while the nontrivial F -symbols are

$$[F_{\pi^{\pi\pi\pi}}]_i^j = \frac{1}{2} \begin{bmatrix} 1 & 1 & \sqrt{2} \\ 1 & 1 & -\sqrt{2} \\ \sqrt{2} & -\sqrt{2} & 0 \end{bmatrix}, \quad F_{\psi^{\pi\pi\pi}} = F_{\pi^{\psi\pi\pi}} = F_{\pi^{\pi\psi\pi}} = F_{\pi^{\pi\pi\psi}} = -1. \quad (3.399)$$

The emergent anyons can be labeled identically to those of $\mathcal{Z}(\text{Rep}(S_3))$, and the corresponding ICIs are given below.

Anyons	\mathcal{T}_{000}^0	$\mathcal{T}_{0\psi 0}^\psi$	$\mathcal{T}_{\psi\psi\psi}^0$	$\mathcal{T}_{\psi 0\psi}^\psi$	$\mathcal{T}_{0\pi 0}^\pi$	$\mathcal{T}_{\psi\pi\psi}^\pi$	$\mathcal{T}_{\pi\pi\pi}^0$	$\mathcal{T}_{\pi\pi\pi}^\psi$	$\mathcal{T}_{\pi 0\pi}^\pi$	$\mathcal{T}_{\pi\psi\pi}^\pi$	$\mathcal{T}_{\pi\pi\pi}^\pi$
$[1, 0]$ A \mathcal{P}_8	1	1			2						
$[1, \psi]$ B \mathcal{P}_2			1	1		-2					
$[1, \pi]$ C \mathcal{P}_6	2	2	2	2	-2	2					
$[s, +]$ D \mathcal{P}_7	3	-3					$\frac{3}{2}$	$\frac{3}{2}$	$\frac{3}{2}$	$\frac{3}{2}$	
$[s, -]$ E \mathcal{P}_3			3	-3			$\frac{3}{2}$	$\frac{3}{2}$	$-\frac{3}{2}$	$-\frac{3}{2}$	
$[r, 1]$ F \mathcal{P}_5							1	-1	1	-1	$\sqrt{2}$
$[r, e^{\frac{2\pi i}{3}}]$ G \mathcal{P}_4							1	-1	$e^{-\frac{2\pi i}{3}}$	$e^{\frac{\pi i}{3}}$	$\sqrt{2}e^{\frac{2\pi i}{3}}$
$[r, e^{-\frac{2\pi i}{3}}]$ H \mathcal{P}_1							1	-1	$e^{\frac{2\pi i}{3}}$	$e^{-\frac{\pi i}{3}}$	$\sqrt{2}e^{-\frac{2\pi i}{3}}$

(3.400)

Note the implicit normalization $\mathcal{D}^2 = 6$ in the above table. We have also included the anyon labels in the language of Refs. 64,204 to ease the comparison of our results.

The full two dimensional $[1, \pi]$, $[s, +]$, $[s, -]$ blocks are given by

$$\begin{aligned} [1, \pi]_{00} &= \frac{1}{3} (\mathcal{T}_{000}^0 + \mathcal{T}_{0\psi 0}^\psi - \mathcal{T}_{0\pi 0}^\pi) & [1, \pi]_{01} &= \frac{1}{\sqrt{3}} \mathcal{T}_{0\pi\psi}^\pi \\ [1, \pi]_{10} &= \frac{1}{\sqrt{3}} \mathcal{T}_{\psi\pi 0}^\pi & [1, \pi]_{11} &= \frac{1}{3} (\mathcal{T}_{\psi\psi\psi}^0 + \mathcal{T}_{\psi 0\psi}^\psi + \mathcal{T}_{\psi\pi\psi}^\pi), \end{aligned} \quad (3.401)$$

$$\begin{aligned} [s, +]_{00} &= \frac{1}{2} (\mathcal{T}_{000}^0 - \mathcal{T}_{0\psi 0}^\psi) & [s, +]_{01} &= \frac{1}{\sqrt{2}} \mathcal{T}_{0\pi\pi}^\pi \\ [s, +]_{10} &= \frac{1}{2} \mathcal{T}_{\pi\pi 0}^\pi & [s, +]_{11} &= \frac{1}{4} (\mathcal{T}_{\pi\pi\pi}^0 + \mathcal{T}_{\pi\pi\pi}^\psi + \mathcal{T}_{\pi 0\pi}^\pi + \mathcal{T}_{\pi\psi\pi}^\pi), \end{aligned} \quad (3.402)$$

$$\begin{aligned} [s, -]_{00} &= \frac{1}{2} (\mathcal{T}_{\psi\psi\psi}^0 - \mathcal{T}_{\psi 0\psi}^\psi) & [s, -]_{01} &= \frac{i}{\sqrt{2}} \mathcal{T}_{\psi\pi\pi}^\pi \\ [s, -]_{10} &= \frac{i}{2} \mathcal{T}_{\pi\pi\psi}^\pi & [s, -]_{11} &= \frac{1}{4} (\mathcal{T}_{\pi\pi\pi}^0 + \mathcal{T}_{\pi\pi\pi}^\psi - \mathcal{T}_{\pi 0\pi}^\pi - \mathcal{T}_{\pi\psi\pi}^\pi). \end{aligned} \quad (3.403)$$

$\text{Rep}(S_3)$ admits a grading by the Fibonacci algebra, see Eq.(3.387), as follows $\mathcal{C}_1 \oplus \mathcal{C}_a = \{0, \psi\} \oplus \{\pi\}$. The **1**-sector is nontrivial in this case, given by $\text{Rep}(\mathbb{Z}_2)$. Breaking the MPO symmetry down to the **1**-sector induces an anyon condensation phase transition to the toric code phase $\mathcal{Z}(\text{Rep}(\mathbb{Z}_2))$. The effects of condensation, including the resulting defects, are summa-

rized in the table below.

Sectors	Defects	Condensed anyons	\mathcal{T}_{000}^0	$\mathcal{T}_{0\psi 0}^\psi$	$\mathcal{T}_{\psi\psi\psi}^0$	$\mathcal{T}_{\psi 0\psi}^\psi$	$\mathcal{T}_{\pi\pi\pi}^0$	$\mathcal{T}_{\pi\pi\pi}^\psi$
1	0	$[1, 0]$	1	1				
		$[1, \pi]_{00}$	2	2				
	m	$[1, \psi]$			1	1		
		$[1, \pi]_{11}$			2	2		
	e	$[s, +]_{00}$	3	-3				
	em	$[s, -]_{00}$			3	-3		
a	π_+	$[s, +]_{11}$					$\frac{3}{2}$	$\frac{3}{2}$
		$[s, -]_{11}$					$\frac{3}{2}$	$\frac{3}{2}$
	π_-	$[r, 1]$					1	-1
		$[r, e^{\frac{2\pi i}{3}}]$					1	-1
		$[r, e^{-\frac{2\pi i}{3}}]$					1	-1

(3.404)

In this example, we see that the $[1, \pi]$ superselection sector splits, with only one of the resulting idempotents condensing to the vacuum, similar to what we saw in the Fibonacci example.

In the condensed theory, there is a copy of the Fibonacci algebra — generated by $\mathcal{T}_{0\pi 0}^\pi$ — acting on the 0 anyon. While the m anyon transforms under an algebra generated by $\mathcal{T}_{\psi\pi\psi}^\pi$, with multiplication $\mathbf{a} \times \mathbf{a} = \mathbf{1} - \mathbf{a}$. We remark that the identity on each anyon is given by the irreducible central idempotent for that anyon.

The π_+ defect supports a representation of \mathbb{Z}_2 generated by $\frac{1}{2}(\mathcal{T}_{\pi 0\pi}^\pi + \mathcal{T}_{\pi\psi\pi}^\pi)$, and the π_- defect transforms under an algebra generated by $\{\frac{1}{\sqrt{2}}\mathcal{T}_{\pi\pi\pi}^\pi, \frac{1}{2}(\mathcal{T}_{\pi\pi\pi}^0 - \mathcal{T}_{\pi\pi\pi}^\psi)\}$. The algebra also induces a \mathbb{Z}_2 hopping action between 0 and m generated by $\frac{1}{\sqrt{3}}(\mathcal{T}_{0\pi\psi}^\pi + \mathcal{T}_{\psi\pi 0}^\pi)$. Similarly there is a hopping between e and π_+ generated by $\frac{1}{2}(\mathcal{T}_{\pi\pi 0}^\pi + \sqrt{2}\mathcal{T}_{0\pi\pi}^\pi)$, and also between m and π_+ generated by $\frac{i}{2}(\mathcal{T}_{\pi\pi\psi}^\pi + \sqrt{2}\mathcal{T}_{\psi\pi\pi}^\pi)$. Again, the precise physical meaning of these actions is not clear.

3.10 Discussion and conclusions

In this work, we have established a description of emergent symmetry-enriched topological order in tensor network states in terms of \mathcal{G} -graded matrix product operator algebras. A classification of these \mathcal{G} -graded MPO algebras was given in terms of \mathcal{G} -extensions of an underlying topological MPO symmetry algebra. An extension of Ocneanu's tube algebra to nontrivial defect sectors was established, from which the physical data of the emergent SET order was extracted. This induced a \mathcal{G} -graded Morita equivalence relation on the \mathcal{G} -graded MPO algebras, relating those which led to the same emergent SET order. We described the effect that gauging the global \mathcal{G} symmetry had upon the MPO symmetry algebra, and found the relationship between the emergent SET and the topological order that results from gauging. The dual $\text{Rep}(\mathcal{G})$ anyon condensation process was also described in terms of the MPO symmetry algebra.

The results of Sections 3.4, 3.5, 3.6, 3.7, and 3.8 can be summarized succinctly with a

diagram

$$\begin{array}{ccccc}
 \mathcal{C}_1 & \xrightleftharpoons[\text{Restrict to } \mathcal{C}_1]{\mathcal{G}\text{-extension}} & \mathcal{C}_\mathcal{G} & & \\
 \downarrow \text{Double} & & \downarrow \mathcal{G}\text{-Double} & \searrow \text{Double} & \\
 \mathcal{Z}(\mathcal{C}_1) & \xrightleftharpoons[\text{Confine } \mathcal{G} \text{ defects}]{\text{Add } \mathcal{G} \text{ defects}} & \mathcal{Z}(\mathcal{C}_1)_\mathcal{G} & \xrightleftharpoons[\text{Condense Rep}(\mathcal{G})]{\text{Gauge } \mathcal{G} \text{ symmetry}} & \mathcal{Z}(\mathcal{C}_\mathcal{G}) .
 \end{array} \tag{3.405}$$

Where \mathcal{C}_1 is an MPO algebra (or UFC), $\mathcal{C}_\mathcal{G}$ is a \mathcal{G} -graded MPO algebra (or \mathcal{G} -graded UFC), $\mathcal{Z}(\mathcal{C}_1)$ and $\mathcal{Z}(\mathcal{C}_\mathcal{G})$ are emergent topological orders (or MTCs), and $\mathcal{Z}(\mathcal{C}_1)_\mathcal{G}$ is an emergent SET (or \mathcal{G} -crossed MTC). The theory of \mathcal{G} -graded MPO algebras $\mathcal{C}_\mathcal{G}$ was described in Section 3.5, the double construction was described in Section 3.4, \mathcal{G} -Double refers to the symmetry-enriched double construction described in Section 3.6, the gauging procedure was described in Section 3.7, and the condensation procedure was described in Section 3.8.

In summation, the results developed in this paper provide a comprehensive toolbox for the study of anomaly-free, nonchiral, SET orders under an on-site unitary group representation, on a lattice in two spatial dimensions. The tools thus developed were brought to bear on several examples: including an EM duality enriched toric code in Section 3.2, the symmetry-enriched string-nets in Section 3.3, and more in Section 3.9.

Moving forward, the work reported here has generated a number of outstanding questions and uncovered a number of promising paths toward future research.

For instance, it would be interesting — and extremely relevant — to incorporate anti-unitary symmetries such as time-reversal into our formalism. We remark symmetry-enriched string-net models with time reversal symmetry have been described in Ref. 33,112,222. Another immediate generalization would be the inclusion of spatial symmetries and lattice defects, for which tensor networks are naturally suited. We anticipate an approach similar to that presented in Ref. 245 would prove fruitful.

It would also be interesting to adapt our approach to systems with constituent fermion degrees of freedom. It is known that the fermionic parity symmetry can be gauged, and that this is dual to condensing an emergent fermion in the gauged system, which is made up of bosonic constituent degrees of freedom^{246–249}. The fermion parity defects can be interpreted singularities in a lattice spin structure^{250–252}.

A question that we have not answered is how to construct local isometry circuits between different symmetry-enriched phases with the same underlying topological order, which are expected to exist following the framework of Ref. 26. We remark that such circuits are simple to construct for the special case of SPT phases, see Refs. 75,93, Chapter 1 for example.

The \mathcal{G} -graded MPO algebras we have studied can be viewed as a construction of invertible gapped domain walls between a $\mathcal{Z}(\mathcal{C}_1)$ topological order and itself. More specifically, these are gapped domain walls between a specific representative of the $\mathcal{Z}(\mathcal{C}_1)$ Morita equivalence class, given by the MPO algebra \mathcal{C}_1 , and itself. A natural extension would be to consider invertible gapped domain walls between arbitrary representative MPO algebras from the $\mathcal{Z}(\mathcal{C}_1)$ Morita equivalence class. Such a gapped domain wall, between representative UFCs \mathcal{C}_A and \mathcal{C}_B , would correspond to an invertible \mathcal{C}_A - \mathcal{C}_B -bimodule^{216,253}. Developing the theory of these bimodules should allow us to understand the Morita equivalence relation more explicitly at the level of the local tensors of an MPO algebra.

Another extension would be to consider noninvertible gapped domain walls, which correspond to \mathcal{A} -graded MPO algebras, where \mathcal{A} is also an algebra. It was discussed in Section 3.8.3 how an \mathcal{A} -grading can be used to calculate the effects of an anyon condensation phase transition induced by breaking the MPO algebra down to the $\mathbf{1}$ -sector. Several examples demonstrating this procedure were given in Section 3.9. We conjectured that this captures all anyon condensation phase transitions between nonchiral topological orders in two spatial dimensions. It would be interesting to develop an \mathcal{A} -extension procedure, generalizing \mathcal{G} -extension, dual to these anyon condensations and to understand the connection between the \mathcal{A} algebra and the *algebra object* approach to anyon condensation^{246,253}. We expect \mathcal{A} -graded UFCs that admit a braiding can be used to generalize the Hamiltonian construction of topological phases presented in Ref. 254 and Chapter 4. The resulting phases of matter should correspond to a family of TQFTs known as *Dichromatic state sum models* recently defined in Ref. 255. We plan to expand on these directions in future work.

The even more general case of \mathcal{C}_A - \mathcal{C}_B -bimodules for arbitrary UFCs \mathcal{C}_A and \mathcal{C}_B (not necessarily Morita equivalent), describes all gapped domain walls between $\mathcal{Z}(\mathcal{C}_A)$ and $\mathcal{Z}(\mathcal{C}_B)$. This captures the gapped boundary conditions of $\mathcal{Z}(\mathcal{C}_A)$ via the special case where \mathcal{C}_B is trivial, $\mathcal{C}_B = \{0\}$, note the general case can be recovered by using the folding trick. We remark that a systematic study of this problem for string-net models was given in Ref. 253.

The tools we have developed also allow one to find and construct all possible transversal gates on topological quantum codes in two spatial dimensions. We remark that the results of Ref. 81 imply all locality preserving gates on topological quantum codes, that have an anomaly-free action on the superselection sectors of the topological order, can in fact be realized transversally. This may require one to use a different underlying model with the same emergent topological order. The symmetry-enriched string-nets^{32,33} suffice to realize all such transversal gates in local commuting projector topological quantum codes. We plan to explain this in more detail in a follow up work.

The boundary phases of an SET tensor network, and their phase transitions, can be classified in terms of the \mathcal{G} -graded MPO symmetry algebra. These phases are classified w.r.t. a symmetry given by the MPO algebra \mathcal{C}_1 , and \mathcal{G} plays the role of a group of dualities between the phases. Conversely, the framework developed in Section 3.5 allows one to construct the possible MPO algebra of dualities between the one dimensional \mathcal{C}_1 phases. These dualities can be used to find phase transitions, which are described by emergent conformal field theories (CFTs)^{191–194}. At the phase transition the dualities become symmetries and the topological superselection sectors of the CFT can be constructed using the approach described in Section 3.4, see Ref. 129 and Chapter 2 for example. The $(1 + 1)$ D quantum Euclidean path integrals, or 2D classical partition functions, of the boundary phases can be realized using a generalized strange correlator²⁵⁶, given by an overlap between a product state and the SET tensor network state. Generalized strange correlators derived from the symmetry-enriched string-nets can be used to construct many familiar lattice statistical mechanics models, including the Ising model and \mathbb{Z}_3 Potts model. Stable renormalization group fixed points on the boundary correspond to gapped phases and can be interpreted as gapped boundary conditions, while the unstable gapless fixed points correspond to CFTs.

It would be very interesting to find tensor networks that are symmetric under an anomalous symmetry in two spatial dimensions. Such anomalous symmetries can be expressed as tensor

network operators, that arise at the boundary of a (generalized) SPT phase in three spatial dimensions [155,238–241](#). We anticipate that such a tensor network could be found by following a similar approach to Ref. [129](#), Chapter [2](#). We plan to study this in a future work.

Acknowledgments — We thank Dave Aasen, Meng Cheng, Michaël Mariën, and Ryan Thorngren for many useful discussions and Jacob Bridgeman for sharing his tikz skillz.

Chapter 4

Hamiltonian models for topological phases of matter in three spatial dimensions

Synopsis:

We present commuting projector Hamiltonian realizations of a large class of (3+1)D topological models based on mathematical objects called unitary G -crossed braided fusion categories. This construction comes with a wealth of examples from the literature of symmetry-enriched topological phases. The spacetime counterparts to our Hamiltonians are unitary state sum topological quantum fields theories (TQFTs) that appear to capture all known constructions in the literature, including the Crane-Yetter-Walker-Wang and 2-Group gauge theory models. We also present Hamiltonian realizations of a state sum TQFT recently constructed by Kashaev whose relation to existing models was previously unknown. We argue that this TQFT is captured as a special case of the Crane-Yetter-Walker-Wang model, with a premodular input category in some instances.

Based on: [254](#)

Dominic J. Williamson and Zhenghan Wang,
[Ann. Phys. **377**, 311–344 \(2016\)](#), [arXiv:1606.07144](#).

Changes compared to published version: Minor corrections and formatting changes.

Contributions of the author: This project was a collaborative effort, the research direction was proposed by the second author, who also provided invaluable supervision through many stimulating discussions, whilst the calculation and writing was primarily done by the first author. This work contains a summary of Ref. [84](#), which was written by the first author.

4.1 Introduction

Theoretically, a topological phase of matter (TPM)^{9,257} without any symmetry protection is an equivalence class of local Hamiltonians^{19,25,26,258} whose low energy physics is modeled by a stable* unitary topological quantum field theory (TQFT)^{11–14,22,203,224}. Given a realistic Hamiltonian it is generally difficult to determine which TPM it is in. A fruitful approach is to reverse engineer Hamiltonians from known TQFTs. Famous examples include Kitaev’s toric code^{19,72} and Levin-Wen models^{24,108}.

Physical TQFTs are local and this is usually formulated by a set of axioms known as the gluing formulas^{220,221,259}. A more explicit form of locality is a state sum construction¹⁰⁸. It is generally believed that state sum TQFTs are in 1-1 correspondence with fully extended TQFTs and both admit local commuting projector Hamiltonian realizations. However this conjecture has not been rigorously proven in full generality largely due to an inability to drop restrictive symmetry assumptions on the input data and higher “j-symbols”. While it is difficult to algebraically formalize the fully extended TQFT framework without these assumptions some progress has been made for the state sum case in Ref. 84. An interesting example that clearly violates the symmetry assumptions is Kashaev’s state sum $(3+1)$ -TQFT^{82,260}, whose j-symbols strongly depend on the linear ordering of the vertices of a 4-simplex.

A basic principle in the study of state sum TQFTs is that the behavior of a local $(n+1)$ -TQFT restricted to a disk is encoded by some higher n -category \mathcal{C} ^{220,221,259}. Furthermore the partition functions and a local commuting projector Hamiltonian can be constructed from \mathcal{C} as illustrated by the Turaev-Viro and Levin-Wen models^{24,108} (generalized Kitaev models^{19,72}) in two spatial dimensions. The physical excitations in this general picture should be described by a special $(n+1)$ -category that is constructed by taking a generalized Drinfeld double of the n -category \mathcal{C} ^{164,211}. The major deficiencies of this general approach are the lack of a good algebraic definition for the appropriate weak n -categories and an absence of examples. This is in stark contrast to the well developed theory of fusion categories relevant to the $(2+1)$ D case^{165,216}.

In this paper our focus will be on three dimensional topological phases of matter and the associated $(3+1)$ -TQFTs. Many concrete constructions in three spatial dimensions have been proposed^{82,86,88,90,260–266}, but all seemingly fall short of capturing the full intricacies of $(3+1)$ D topological order. Looking back to $(2+1)$ D we note that state sum TQFTs constructed from unitary fusion categories (UFCs) are sufficiently general to achieve all non chiral topological orders^{24,108} (from the higher categorical point of view these should be understood as 2-categories that contain a single object). By analogy, we will refer to the most general input to $(3+1)$ D state sum TQFTs as unitary fusion 2-categories (which should correspond to 3-categories that contain a single object).

As a step towards a fully general unitary fusion 2-category construction, we focus on a case that is populated by a rich class of examples originating from the algebraic theory of defects in $(2+1)$ D symmetry enriched topological (SET) orders. These defects are described by mathematical objects known as unitary G-crossed braided fusion categories (UGxBFCs). We build on the work of Ref. 83 in which a large class of state sum $(3+1)$ -TQFTs were rigorously

*Stable can be understood as no spontaneous symmetry breaking. The technical definition is $Z[S^3 \times S^1] = 1$ which implies local operators act trivially within the ground space.

constructed from UGxBFCs that (with a small extension) seem to include almost all known examples of unitary state sum $(3 + 1)$ -TQFTs. In this paper we propose their Hamiltonian realization, generalizing the construction of Ref. 85. We note that a related construction of $(3 + 1)$ -TQFTs based on a proposed definition of spherical 2-category was given in Ref. 265 but it was shown in Ref. 83 that this definition was too restrictive to even capture the unitary G -crossed braided fusion categories (UGxBFC).

A family of models possibly outside this class of TQFTs are Kashaev's examples⁸². We also establish a Hamiltonian formulation of these $(3 + 1)$ -TQFTs. Moreover we pose, and provide evidence for, the following conjecture: Kashaev's TQFTs are equivalent to a subset of Crane-Yetter TQFTs with input categories that may be premodular, in particular $sVec$ for some instances (i.e. Walker-Wang models with fermionic string types).

4.2 Background

In this section we recount the definition of state sum TQFTs, and their associated Hamiltonians and tensor network ground states, before moving on to discuss two recently constructed classes of state sums; the UGxBFC and Kashaev's \mathbb{Z}_N models. To facilitate the discussion of these topics we first set up some basic conventions and terminologies that are used throughout the manuscript. From this point forward we also make free use of notation and constructions from combinatoric topology, for those unfamiliar with this topic the necessary points are summarized in Appendix 4.6.

We will define topological partition functions $Z[X]$ on space-time manifolds X of dimension $n + 1$, and Hilbert spaces $V[Y]$ on spatial n -manifolds Y that are equipped with triangulations¹³. But triangulation can mean many different things. For highly non-symmetric state sum TQFTs, we usually need a simplicial triangulation of the spatial manifold Y , but only a Δ -complex triangulation of the space-time manifold X .

A manifold M has a simplicial triangulation if M is homeomorphic to the realization or underlying space $|\mathcal{K}|$ of an abstract simplicial complex \mathcal{K} ²⁶⁷ (there are in fact extra technicalities, see the appendix). A simplicial complex \mathcal{K} is a collection of subsets of a finite set V , called the vertices of \mathcal{K} , with the property that if a subset σ of V is in \mathcal{K} then all subsets of σ are also in \mathcal{K} . The subset σ is called an i -simplex if σ has $(i + 1)$ vertices. A geometric realization $|\mathcal{K}|$ of \mathcal{K} can be built by associating each vertex $v \in V$ to a basis vector of the Euclidean space $\mathbb{R}^{|V|}$. An important technical point for our construction is that we assume V has a linear order. Therefore our simplicial triangulations always have induced branching structures by drawing an arrow on each edge from the lower numbered vertex to the higher one.

A manifold M of dimension m has a Δ -complex triangulation if the manifold M is constructed from a finite collection of m -simplices, which are glued together along the $(m - 1)$ -dimensional faces by simplicial maps. In particular a Δ -complex triangulation of a manifold can have a single vertex, for example the torus T^2 with two triangles.

4.2.1 State Sum TQFTs

An oriented unitary $(n + 1)$ -TQFT (V, Z) is technically a symmetric monoidal functor from $(n + 1)Cob$ to $Vec_{\mathbb{C}}$ ^{11,13}. This is nothing more than a very compact way of axiomatizing topological invariance of a field theory and can be broken down into a series of more elementary

statements. The TQFT assigns a topologically invariant partition function $Z[X^{n+1}] \in \mathbb{C}$ to each oriented closed $(n+1)$ -manifold and a finite dimensional Hilbert space $V[Y^n]$ to each oriented closed n -manifold. It furthermore assigns a linear map $Z[X^{n+1}] : V[Y_0^n] \rightarrow V[Y_1^n]$ to an oriented $(n+1)$ -manifold with boundary $\partial X^{n+1} = \bar{Y}_0 \sqcup Y_1$. Unpacking the definition leads to gluing formulas that ensure topological invariance amongst other technical axioms. Additionally for a unitary TQFT orientation reversal is mapped to complex conjugation. We do not delve any further into the general definition here, instead we move on to the more specific notion of a state sum TQFT.

The most general possible construction of state sum TQFTs is not yet rigorously formalized, due to technicalities in proving independence from the choice of branching structure, we will present an overview here. A state sum TQFT comes with a finite set of input labels $\{L^{(i)}\}_{i=0}^n$. For any triangulation \mathcal{K} of an $n+1$ -manifold X , we first choose a linear ordering of the vertices $\mathcal{K}^{(0)}$ (in fact a local ordering or branching structure will suffice). Then a configuration on the triangulated manifold is specified by a set of maps $s^{(i)} : \mathcal{K}^{(i)} \rightarrow L^{(i)}$, which color each i -simplex in $\mathcal{K}^{(i)}$ with a label from $L^{(i)}$. Moreover, to capture the most general solutions we allow each label l to have an associated “quantum dimension” $d_l \in \mathbb{C}^\times$. Finally in a configuration s each labeled $n+1$ -simplex Δ is evaluated to a “j-symbol” $\tau_{s(\Delta)}^{\sigma(\Delta)}$, where $\sigma(\Delta) = \pm$ is the orientation of the $n+1$ -simplex. The partition function is then

$$Z[X] = \sum_s \prod_{\Delta_{n+1}} \tau_{s(\Delta_{n+1})}^{\sigma(\Delta_{n+1})} \frac{\prod_{\Delta_{n-1}} d_{s(\Delta_{n-1})} \prod_{\Delta_{n-3}} d_{s(\Delta_{n-3})}}{\prod_{\Delta_n} d_{s(\Delta_n)} \prod_{\Delta_{n-2}} d_{s(\Delta_{n-2})}} \dots$$

note our quantum dimensions may be rescaled compared to the usual definition from a unitary fusion category (UFC).

This prescription extends to triangulated manifolds with boundary $\partial X = \bar{Y}_0 \sqcup Y_1$ ⁸⁴

$$Z[X] = \sum_s \prod_{\Delta_{n+1}} \tau_{s(\Delta_{n+1})}^{\sigma(\Delta_{n+1})} \frac{\prod_{\Delta_{n-1}} d_{s(\Delta_{n-1})}^{c(\Delta_{n-1})} \prod_{\Delta_{n-3}} d_{s(\Delta_{n-3})}^{c(\Delta_{n-3})}}{\prod_{\Delta_n} d_{s(\Delta_n)}^{c(\Delta_n)} \prod_{\Delta_{n-2}} d_{s(\Delta_{n-2})}^{c(\Delta_{n-2})}} \dots \bigotimes_{\Delta_j \in Y_1} |s(\Delta_j)\rangle \bigotimes_{\Delta_i \in Y_0} \langle s(\Delta_i)|$$

where $c(\Delta_i) = \frac{1}{2}$ if $\Delta_i \in \partial X$ and 1 if it is in the interior. Hilbert spaces $V[Y]$ are then defined to be the support subspace of the linear operator $Z[Y \times I]$ for a triangulation of $Y \times I$ that matches Y on both boundaries. Topological invariance of the state sum is more precisely an invariance of Z under piecewise linear (PL) homeomorphisms on the $(n+1)$ -manifold. PL homeomorphic manifolds are related by a sequence of local bistellar flips of the triangulation, drawn from a finite set known as the Pachner moves ²⁶⁸. This recasts topological invariance of the state sum into a finite set of equations that the j-symbol must satisfy ⁸⁴, corresponding to retriangulations of the $(n+1)$ -ball. This guarantees the partition function is independent of the choice of triangulation, moreover one must show the partition function is independent of the choice of vertex ordering.

4.2.2 Hamiltonians, Tensor Network Ground States and PEPO Symmetries

State sum TQFTs have a natural interpretation as tensor networks ^{84,108,269} (see Ref. 41 for an introduction to tensor networks). Copies of a single tensor are associated to each simplex and

contracted according to how the simplices are glued together. Topological invariance of the discrete partition functions is ensured if and only if the simplex tensor satisfies tensor equations corresponding to the Pachner moves²⁶⁸. There is a standard (although not widely known) construction to obtain a local real-space renormalization group (RSRG) fixed point commuting projector Hamiltonian that stabilizes the vector space of a state sum TQFT on a triangulated surface, generalizing that of Levin & Wen²⁴. The Hamiltonian is given by

$$H = \sum_v \mathbb{1} - Z[v' * \text{cl st}_v] \quad (4.1)$$

where v' is a copy of vertex v after one imaginary time step. For a definition of the operations $\{*, \text{cl}, \text{st}\}$ see Appendix.4.6. All the aforementioned properties of the Hamiltonian follow from the Pachner move invariance of the simplex tensor⁸⁴. A projected entangled pair state (PEPS)^{39,42,46,55} representation of a ground state wave function (GSWF) on a triangulated manifold (Y, \mathcal{K}) is given by $Z[v_0 * \mathcal{K}]$. Provided $Z[\{v_0, v_1\} * Y] > 0$ (which implies $\dim V[Y] = Z[Y \times S^1] > 0$) the resulting state is nonzero. This PEPS is a frustration free ground state as it satisfies $Z[v' * \text{cl st}_v]Z[v_0 * \mathcal{K}] = Z[v_0 * \mathcal{K}]$ following from the Pachner moves. This PEPS has a projected entangled pair operator (PEPO) symmetry which can be “pulled through” the virtual level^{59,62,63,66,93}, this is also ensured by the Pachner moves. The symmetry is indicative of topological order in the model via a bulk boundary correspondence given by taking the double of the algebra of tensor network operators on the boundary to construct the emergent physical excitations^{64,195,270}. The framework also yields a multiscale entanglement renormalization ansatz (MERA)⁴³ description of the ground space constructed by taking a triangulated identity bordism $(Y \times I, \mathcal{K}')$ such that the triangulation at the space manifold $(Y, 0)$ reduces to the physical lattice \mathcal{K} and we pick a minimal triangulation \mathcal{K}'' of $(Y, 1)$ at the ‘top’ of the MERA corresponding to the far IR scale. Then upon fixing a vector containing the fully coarse grained topological information $|t\rangle$ the MERA is given by

$$Z[\mathcal{K}'] |t\rangle \quad (4.2)$$

For physical lattice models it is important that the Hamiltonians output by our construction are Hermitian. This is ensured by a sufficient condition on the underlying tensor, namely that it is symmetric under simultaneous complex conjugation and orientation reversal. We note in the framework of Ref. 84 there is some technicality involved when dealing with weight functions associated to objects on lower dimensional strata of the triangulation.

4.2.3 Review of the UGxBFC TQFT

A new class of $(3+1)$ -TQFTs was constructed in Ref. 83 from unitary G -crossed braided fusion categories (UGxBFC) \mathcal{C}_G^\times ^{31,81,97,98}, where G is a finite group. These UGxBFCs can be thought of as special unitary fusion 2-categories. When G is trivial, a UGxBFC \mathcal{C}_G^\times reduces to a premodular category and the resulting TQFT is the Crane-Yetter TQFT^{86,261} whose Hamiltonian realization is described in Ref. 85. In general, a UGxBFC has $|G|$ sectors and the trivial sector is always a premodular category.

UGxBFC

A UGxBFC^{31,81,97,98} can roughly be thought of as a spherical fusion 1.5-category—it is a spherical fusion category with a G -crossed braiding, hence it does not seem to be a totally general

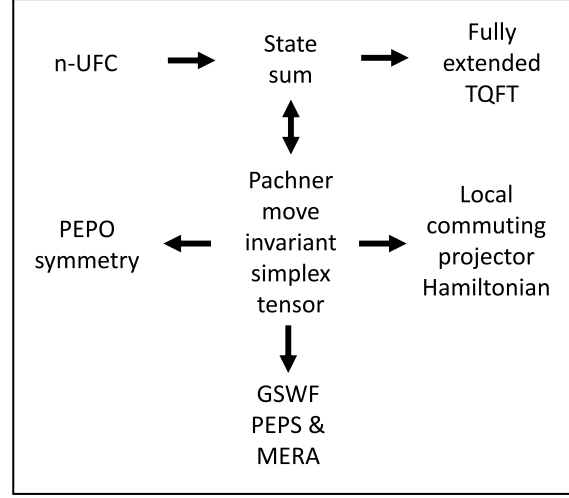


Figure 4.1: Summary of the results in Ref. 84.

spherical fusion 2-category. That being said there is no satisfactory agreed upon definition of a spherical 2-category in the literature. While a definition was proposed in Ref. 265 it was shown in Ref. 83 that this was too restrictive to even capture the UGxBFCs. Moving forward the UGxBFCs constitute a very important class of unitary fusion 2-categories as they provide a huge family of nontrivial examples, which have proved otherwise hard to come by.

For our purpose, the most convenient way to define a G -crossed braided fusion category is through a collection of symbols $\{N_{ab}^c, d_a, F_d^{abc}, R_c^{ab}, \varkappa_a, U_g(a, b; c), \eta_x(g, h)\}$ ³¹. This extends the description of a unitary premodular category through a collection of symbols $\{N_{ab}^c, d_a, F_d^{abc}, R_c^{ab}, \varkappa_a\}$ ²⁰³.

A UGxBFC is an abstract description of point like defects of a symmetry group G in a gapped phase of matter in $(2+1)$ D. Each defect carries a flux $g \in G$ but there may be multiple topologically distinct defects carrying the same G -flux, this is described by a G -graded category

$$\mathcal{C}_G = \bigoplus_{g \in G} \mathcal{C}_g$$

where each simple object is contained in some sector $a \in \mathcal{C}_g$. We follow the notation of Ref. 31 and use a_g as shorthand for $a \in \mathcal{C}_g$. Defects can be fused by physically bringing them together, this is described by a set of multiplicities N_{ab}^c counting the number of ways a and b can fuse to c . In particular the fusion $a \times b \rightarrow c$ is admissible iff $N_{ab}^c \neq 0$. The fusion should respect the grading, i.e.

$$a_g \times b_h = \sum_{c \in \mathcal{C}_G} N_{ab}^c c = \sum_{c \in \mathcal{C}_{gh}} N_{ab}^c c_{gh}.$$

The \mathcal{C}_1 sector is closed under fusion and contains the unique vacuum object that fuses trivially with everything else, thus forming a fusion subcategory.

The fusion of three defects is not strictly associative, two different fusion paths with result

d are related by an F -symbol associator $(a \times b) \times c \xrightarrow{F_d^{abc}} a \times (b \times c)$ more precisely

$$\begin{array}{c} a \quad b \quad c \\ \swarrow \quad \searrow \quad \nearrow \\ \alpha \quad e \quad \beta \\ \searrow \quad \nearrow \\ d \end{array} = \sum_{f\mu\nu} [F_d^{abc}]_{e\alpha\beta}^{f\mu\nu} \begin{array}{c} a \quad b \quad c \\ \swarrow \quad \searrow \quad \nearrow \\ \nu \quad f \quad \mu \\ \searrow \quad \nearrow \\ d \end{array} \quad (4.3)$$

Unitarity of the fusion category requires $[(F_d^{abc})^{-1}]_{f\mu\nu}^{e\alpha\beta} = ([F_d^{abc}]_{e\alpha\beta}^{f\mu\nu})^*$. For this associator to be consistent all paths between a pair of diagrams must agree, this is guaranteed by the well known pentagon equation

$$\sum_{\delta} [F_e^{fcd}]_{g\beta\gamma}^{l\delta\nu} [F_e^{abl}]_{f\alpha\delta}^{k\lambda\mu} = \sum_{h\sigma\psi\rho} [F_g^{abc}]_{f\alpha\beta}^{h\sigma\psi} [F_e^{ahd}]_{g\sigma\gamma}^{k\lambda\rho} [F_k^{bcd}]_{h\psi\rho}^{l\mu\nu} \quad (4.4)$$

this is depicted diagrammatically in Fig.4.2.

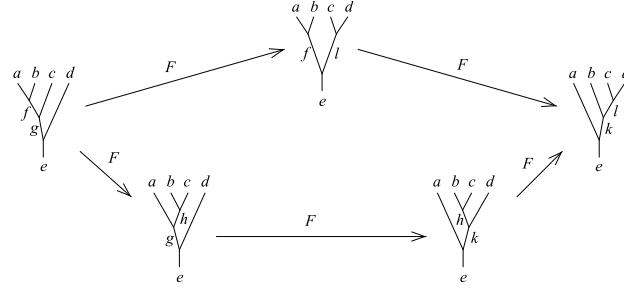


Figure 4.2: The pentagon equation.

The group G has an action on simple objects denoted by ${}^g a_h \in \mathcal{C}_{gh}$ where ${}^g h = ghg^{-1}$. Each simple object a_g has a unique conjugate $\bar{a} \in \mathcal{C}_{\bar{g}}$ that can fuse together to give the vacuum, where $\bar{g} = g^{-1}$. Flipping the direction of an edge is equivalent to conjugating the charge label

$$\begin{array}{c} \uparrow \\ a \end{array} = \begin{array}{c} \downarrow \\ \bar{a} \end{array}. \quad (4.5)$$

The element $[F_a^{a\bar{a}a}]_1^1 = \frac{\varkappa_a}{d_a}$ consists of a quantum dimension which arises from popping a bubble

$$d_a = d_{\bar{a}} = a \begin{array}{c} \circlearrowleft \end{array} \quad (4.6)$$

and a Frobenius-Shur (FS) indicator which arises when a cup and cap are canceled

$$\begin{array}{c} \uparrow \\ a \end{array} \begin{array}{c} \circlearrowleft \end{array} \begin{array}{c} \downarrow \\ a \end{array} = \varkappa_a \begin{array}{c} \uparrow \\ a \end{array}. \quad (4.7)$$

Note the FS indicator can be fixed to 1 via a gauge transformation unless $a = \bar{a}$ in which case $\varkappa_a = \pm 1$.

The total quantum dimension of \mathcal{C} is $\mathcal{D}^2 = \sum_{a \in \mathcal{C}} d_a^2$ and similarly for each sector \mathcal{C}_g , $\mathcal{D}_g^2 = \sum_{a \in \mathcal{C}_g} d_a^2$. The nonempty sectors form a subgroup $H \leq G$ and satisfy $\mathcal{D}_h = \mathcal{D}_1$ for $h \in H$. Note all defects in a given sector are related by fusion with objects in \mathcal{C}_1 .

The physical defects appear at the end of branch cuts and can be dragged around by adiabatically deforming the Hamiltonian. This leads to braided worldlines of the defects attached to worldsheets of the branch cuts. We follow the convention of Ref. 31 and depict the worldsheets going into the page. The worldsheet of a defect worldline acts on other defects which pass behind it. The G-crossed braiding is defined by several pieces of data, the R -symbol

$$\begin{array}{c} a_g \quad b_h \\ \diagdown \quad \diagup \\ \mu \\ \diagup \quad \diagdown \\ c_{gh} \end{array} = \sum_{\nu} [R_{c_{gh}}^{a_g b_h}]_{\mu}^{\nu} \begin{array}{c} a_g \quad b_h \\ \diagdown \quad \diagup \\ \nu \\ \diagup \quad \diagdown \\ c_{gh} \end{array} \quad (4.8)$$

and the U and η symbols, which arise due to symmetry actions as a defect is slid over or under a fusion vertex,

$$\begin{array}{c} a_g \quad b_h \\ \diagdown \quad \diagup \\ x_k \quad \mu \\ \diagup \quad \diagdown \\ \bar{k} \quad c_{gh} \end{array} = \sum_{\nu} [U_k(a, b; c)]_{\mu}^{\nu} \begin{array}{c} a_g \quad b_h \\ \diagdown \quad \diagup \\ c_{gh} \quad \nu \\ \diagup \quad \diagdown \\ x_k \quad \bar{k} \quad c_{gh} \end{array} \quad (4.9)$$

$$\begin{array}{c} a_g \quad b_h \quad \bar{h}\bar{g}x_k \\ \diagdown \quad \diagup \quad \diagup \\ x_k \quad \mu \\ \diagup \quad \diagdown \\ c_{gh} \end{array} = \eta_x(g, h) \begin{array}{c} a_g \quad b_h \quad \bar{h}\bar{g}x_k \\ \diagdown \quad \diagup \quad \diagup \\ x_k \quad \mu \\ \diagup \quad \diagdown \\ c_{gh} \end{array} \quad (4.10)$$

U corresponds to the action of the global symmetry on topological degrees of freedom, while η_x corresponds to the 2-cocycle of the projective representation carried by x .

For the data F_d^{abc} , R_c^{ab} , $U_g(a, b; c)$, $\eta_x(g, h)$ to define a consistent UGxBFC \mathcal{C}_G^{\times} the symbols must satisfy a number of conditions. The F -symbols must satisfy the pentagon equation in Fig.4.2. Equating the two different paths in Fig.4.3 yields a constraint corresponding to the action of $(kl)\bar{l}\bar{k}$ being trivial (technically a natural isomorphism)

$$\begin{aligned} [\kappa_{k,l}(a, b; c)]_{\mu}^{\nu} &= \sum_{\alpha\beta} [U_k^{-1}(a, b; c)]_{\mu}^{\alpha} [U_l^{-1}(\bar{k}a, \bar{k}b; \bar{k}c)]_{\alpha}^{\beta} \\ [U_{kl}(a, b; c)]_{\beta}^{\nu} &= \frac{\eta_a(k, l)\eta_b(k, l)}{\eta_c(k, l)} \delta_{\mu}^{\nu}. \end{aligned} \quad (4.11)$$

Associativity of the group action klm yields a further constraint on $\kappa_{k,l}$

$$\kappa_{l,m}(\bar{k}a, \bar{k}b; \bar{k}c) \kappa_{k,lm}(a, b; c) = \kappa_{k,l}(a, b; c) \kappa_{kl,m}(a, b; c).$$

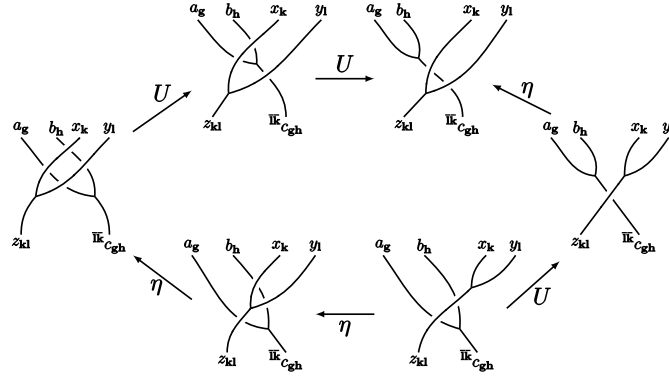


Figure 4.3: Consistency of the global symmetry action and projective phases.

Consistency of fusion and η leads to the equation

$$\eta_{\bar{g}x}(h, k)\eta_x(gh, k) = \eta_x(g, h)\eta_x(gh, k)$$

by equating the two paths in Fig.4.4. This ensures the symmetry fractionalization is not anomalous and can be realized in a standalone $(2 + 1)\text{D}$ system, corresponding to the vanishing of a $H^3(G, \mathcal{A})$ obstruction where \mathcal{A} is the group of abelian anyons. Similarly consistency of fusion

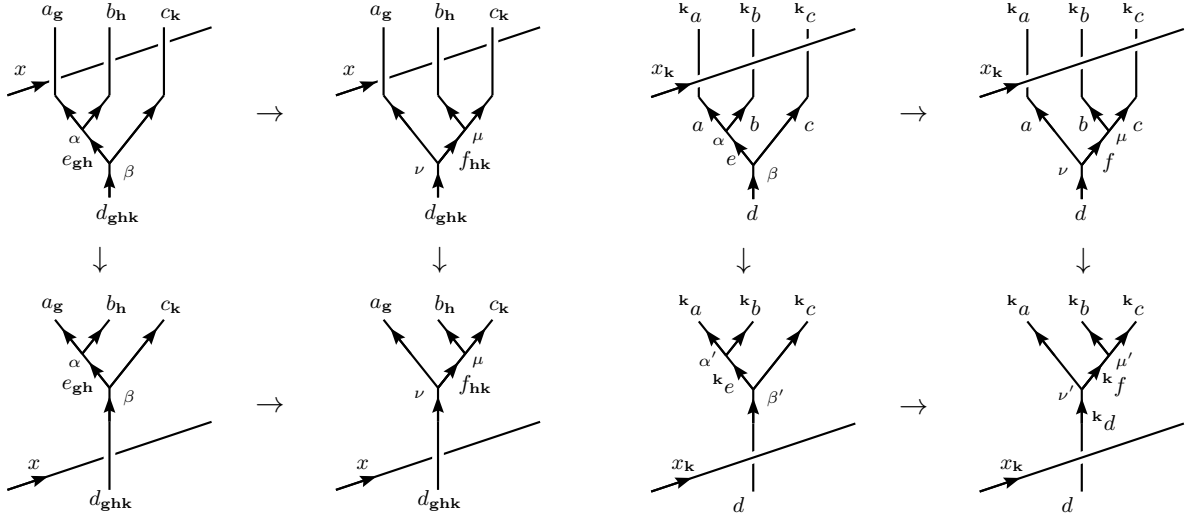


Figure 4.4: Consistency of fusion with: η (left), and U (right).

and U yields the equation

$$\sum_{\alpha'\beta'\mu'\nu'} [U_k(\bar{k}a, \bar{k}b; \bar{k}e)]_{\alpha}^{\alpha'} [U_k(\bar{k}e, \bar{k}c; \bar{k}d)]_{\beta}^{\beta'} [F_{\bar{k}d}^{\bar{k}a\bar{k}b\bar{k}c}]_{\bar{k}e\alpha'\beta'}^{\bar{k}f\mu'\nu'} [U_k^{-1}(\bar{k}b, \bar{k}c; \bar{k}f)]_{\mu}^{\mu'} [U_k^{-1}(\bar{k}a, \bar{k}f; \bar{k}d)]_{\nu}^{\nu'} = [F_d^{abc}]_{e\alpha\beta}^{f\mu\nu} \quad (4.12)$$

which corresponds to a symmetry condition on F under the group action.

The Yang-Baxter equation is no longer a strict equality in a UGxBFC and leads to a consistency equation between the dragging of a string over or under a crossing

$$\frac{\eta_{\bar{k}a}(\bar{k}h, k)}{\eta_{\bar{k}a}(k, h)} \sum_{\mu'\nu'} [U_k(kb, {}^{k\bar{h}}a; {}^k c)]_{\mu}^{\mu'} [R_c^{k a k b}]_{\mu'}^{\nu'} [U_k^{-1}(k a, {}^k b; {}^k c)]_{\nu'}^{\nu} = [R_c^{ab}]_{\mu}^{\nu} \quad (4.13)$$

which is a symmetry condition on R under the group action.

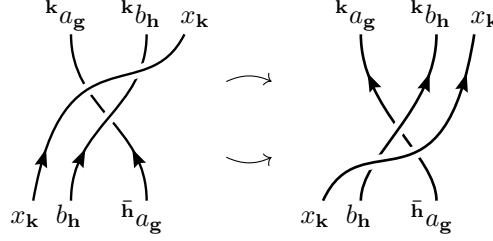


Figure 4.5: Yang-Baxter relation in a UGxBFC.

Finally there are consistency relations between F and R (also involving U and η) known as the heptagon equations, generalizing the well known hexagon equations for a UBFC, one each for right and left handed braiding (see Fig.4.6) as follows

$$\sum_{\lambda\gamma} [R_e^{ac}]_{\alpha}^{\lambda} [F_d^{ac\bar{k}b}]_{e\lambda\beta}^{m\gamma\nu} [R_m^{bc}]_{\gamma}^{\mu} = \sum_{f\sigma\delta\theta\psi} [F_d^{c\bar{k}a\bar{k}b}]_{e\alpha\beta}^{\bar{k}f\delta\sigma} [U_k(a, b; f)]_{\delta}^{\theta} [R_d^{fc}]_{\sigma}^{\psi} [F_d^{abc}]_{f\theta\psi}^{m\mu\nu} \quad (4.14)$$

$$\sum_{\lambda\gamma} [(R_e^{ca})^{-1}]_{\alpha}^{\lambda} [F_d^{a\bar{g}cb}]_{e\lambda\beta}^{m\gamma\nu} [(R_m^{cb})^{-1}]_{\gamma}^{\mu} = \sum_{f\sigma\delta\psi} [F_d^{cab}]_{e\alpha\beta}^{f\delta\sigma} \eta_c(g, h) [(R_d^{cf})^{-1}]_{\sigma}^{\psi} [F_d^{ab\bar{h}g}]_{f\delta\psi}^{g\mu\nu} \quad (4.15)$$

where the defect sectors are determined by a_g, b_h, c_k . For a unitary GxBFC it is required that

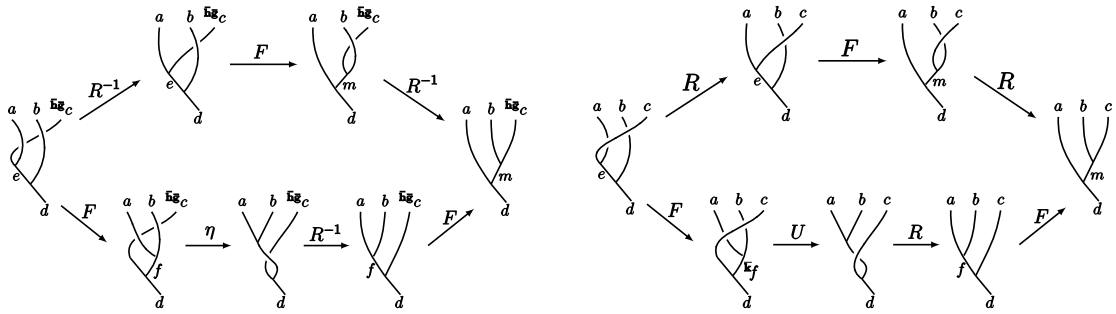


Figure 4.6: The left and right handed heptagon equations of a UGxBFC, respectively.

$[(R_c^{ab})^{-1}]_{\mu}^{\nu} = ([R_c^{ab}]_{\nu}^{\mu})^*$. Note the trivial sector \mathcal{C}_1 of a UGxBFC is itself a UBFC as the heptagon equations reduce to the hexagon equations in that case.

The consistency equations for a UGxBFC guarantee it is not anomalous and can be realized in a stand-alone (2+1)D system. Not all group actions on UBFCs can be extended to a UGxBFC as some are anomalous. The anomalies lie in $H^4(G, U(1))$, which is related to weakening the pentagon equation Fig.4.2, and $H^3(G, \mathcal{A})$ which is related to weakening the fractionalization constraint Fig.4.4.

Example: \mathbb{Z}_3 Tambara-Yamagami Category

A simple example of a UGxBFC known as the \mathbb{Z}_3 Tambara-Yamagami category can be constructed from a $\mathbb{Z}_3^{(1)}$ anyon theory $\{0, 1, 2\}$ with a \mathbb{Z}_2 symmetry that permutes 1 and 2. This theory is also known as $SU(3)_1$ which has central charge $c = 2$ and a \mathbb{Z}_2 particle-hole symmetry. Physically, this theory describes the topological order of a sector of the $\nu = \frac{1}{3}$ Laughlin FQH state.

The UGxBFC consists of two sectors $\mathcal{C}_{\mathbb{Z}_2}^\times = \mathcal{C}_0 \oplus \mathcal{C}_1$. The $\mathbb{Z}_3^{(1)}$ UBFC constitutes the \mathcal{C}_0 sector and is defined by the fusion rules $N_{ab}^c = \delta_{a+b=c \bmod 3}$, trivial F symbols and braiding $R_{a+b}^{ab} = e^{2\pi i ab/3}$. The nontrivial sector contains only a single defect $\mathcal{C}_1 = \{\sigma\}$. The fusion rules are thus

$$\begin{aligned}\sigma \times a &= a \times \sigma = \sigma \\ \sigma \times \sigma &= \sum_{a \in \mathcal{C}_0} a.\end{aligned}$$

The anyons in \mathcal{C}_0 each have quantum dimension 1, hence $d_\sigma = \sqrt{3}$. The nontrivial F symbols are then given by

$$\begin{aligned}[F_\sigma^{a\sigma b}]_\sigma^\sigma &= [F_b^{\sigma a \sigma}]_\sigma^\sigma = \chi(a, b) \\ [F_\sigma^{\sigma \sigma \sigma}]_a^b &= \frac{\varkappa_\sigma}{\sqrt{3}} \chi(a, b)^*\end{aligned}$$

where $\chi(a, b) = e^{2\pi i ab/3}$ is a symmetric bi-character. The G -crossed braidings involving σ are determined by

$$\begin{aligned}R_\sigma^{\sigma a} &= U_1(\sigma, \sigma, a)(-1)^a e^{-\pi i a^2/3}, & R_\sigma^{a\sigma} &= (-1)^a e^{-\pi i a^2/3} \\ R_a^{\sigma \sigma} &= \gamma(-1)^a e^{\pi i a^2/3}, & \gamma^2 &= \frac{\varkappa_\sigma}{\sqrt{3}} \sum_{a \in \mathcal{C}_0} (-1)^a e^{-\pi i a^2/3}\end{aligned}$$

where $U_1(\sigma, \sigma, a) = \pm 1$ and $\varkappa_\sigma = \pm 1$ are choices which yield slightly different UGxBFC extensions of \mathcal{C}_0 , note η is trivial in all cases.

State Sum from UGxBFC

The data of a UGxBFC \mathcal{C}_G^\times can be used as input to generate a family of $(3 + 1)$ D state sum TQFTs⁸³ generalizing the Crane-Yetter-Walker-Wang model. The label set is as follows $L^{(1)} = G$, $L^{(2)} = \mathcal{C}_G^\times$, $L^{(3)} = \text{Hom}(\mathcal{C}_G^\times \otimes \mathcal{C}_G^\times, \mathcal{C}_G^\times)$, where we are abusing notation by using \mathcal{C}_G^\times to denote the set of equivalence classes of simple objects. That is each edge is labeled by a group element g , each triangle is labeled by a defect a and each tetrahedron is labeled by a triple (a, μ, ν) of a defect and two degeneracy labels. The only configurations that have nonzero contributions to the state sum must satisfy the following constraints between the labels on the different strata: the defect on a simplex 012 must satisfy $a_{012} \in \mathcal{C}_{(dg)_{012}}$ where $(dg)_{012} = \bar{g}_{02}g_{01}g_{12}$ and the defect labels on the faces and body of a tetrahedra 0123 are subject to the constraints $N_{a_1 \bar{g}_{23} a_3}^{a_{0123}} \neq 0 \neq N_{a_2 \bar{a}_0}^{a_{0123}}$ (then μ, ν correspond to degeneracy labels of these fusion spaces).

The $15j$ -symbols are given by evaluating diagrams in the UGxBFC shown in Fig.4.7. The choice of diagram is determined by the configuration s and the vertex ordering on a pentachoron.

We use the compressed notation $F_{d;ef}^{abc} = [F_d^{abc}]_e^f$, explicit evaluation of the diagrams in Fig.4.7 yields

$$\begin{aligned} \mathsf{T}_{s(01234)}^+ &= \sum_{a,b} d_b F_{b;0234,a}^{024,234,\bar{34}\cdot\bar{23}012} \eta_{012}^{-1}(\bar{34},\bar{23}) R_a^{\bar{24}012,234} (F_{b;a,0124}^{024,\bar{24}012,234})^{-1} F_{b;0124,1234}^{014,124,234} \\ &\quad (F_{b;1234,0134}^{014,134,\bar{34}123})^{-1} F_{b;0134,\bar{34}0123}^{034,\bar{34}013,\bar{34}123} U_{\bar{34}}(023,\bar{23}012;0123) \\ &\quad U_{\bar{34}}^{-1}(013,123;0123) (F_{b;\bar{34}0123,0234}^{034,\bar{34}023,\bar{34}\cdot\bar{23}012})^{-1} \end{aligned} \quad (4.16)$$

$$\begin{aligned} \mathsf{T}_{s(01234)}^- &= \sum_{a,b} d_b (F_{b;a,0234}^{024,234,\bar{34}\cdot\bar{23}012})^{-1} \eta_{012}(\bar{34},\bar{23}) (R_a^{\bar{24}012,234})^{-1} F_{b;0124,a}^{024,\bar{24}012,234} \\ &\quad (F_{b;1234,0124}^{014,124,234})^{-1} F_{b;0134,1234}^{014,134,\bar{34}123} (F_{b;\bar{34}0123,0134}^{034,\bar{34}013,\bar{34}123})^{-1} \\ &\quad U_{\bar{34}}^{-1}(023,\bar{23}012;0123) U_{\bar{34}}(013,123;0123) F_{b;0234,\bar{34}0123}^{034,\bar{34}023,\bar{34}\cdot\bar{23}012} \end{aligned} \quad (4.17)$$

where each label Δ_i is to be read as $s(\Delta_i)$, we have omitted the explicit writing of s for brevity.

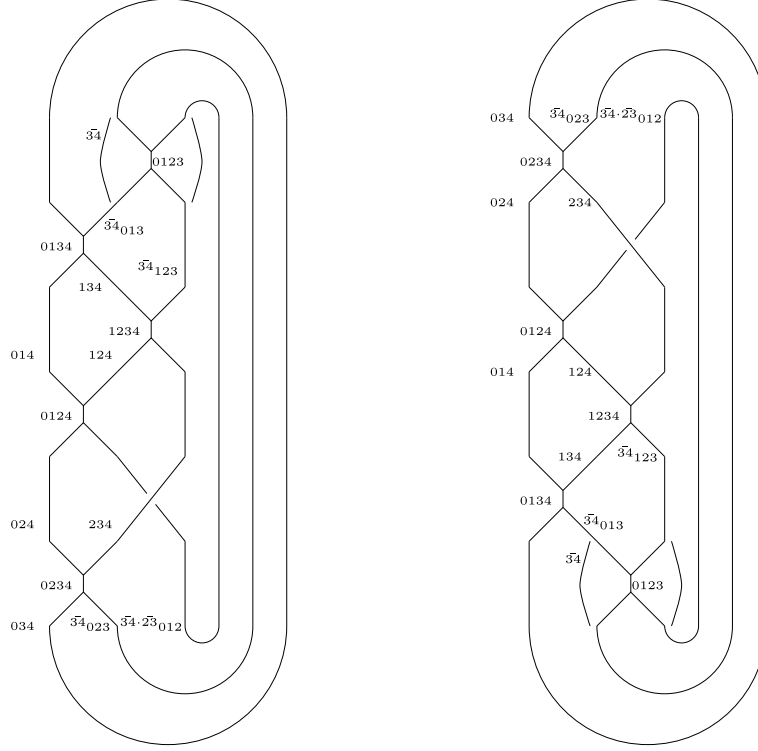


Figure 4.7: Diagrams in the UGxBFC that define the $15j$ -symbols $\mathsf{T}_{s(01234)}^+$ (left), and $\mathsf{T}_{s(01234)}^-$ (right)⁸³. It is intended that Δ_i should be read as $s(\Delta_i)$.

These $15j$ -symbols, together with the quantum dimensions, define the state sum partition function

$$Z[X] = \sum_s \prod_{\Delta_4} \mathsf{T}_{s(\Delta_4)}^{\sigma(\Delta_4)} \frac{\prod_{\Delta_2} d_{s(\Delta_2)} \prod_{\Delta_0} D^2/|G|}{\prod_{\Delta_3} d_{s(\Delta_3)} \prod_{\Delta_1} D^2}$$

where D is the total quantum dimension. It was shown in Ref. 83 that the partition function is a topological invariant, i.e. does not depend on the choice of vertex ordering or triangulation.

The latter condition is guaranteed by the equalities $Z[J] = Z[\Delta_5 \setminus J]$ for all 4-subcomplexes $J \subseteq \Delta_5$.

This state sum captures many known constructions as special cases:

- For $G = \{1\}$ the trivial group the UGxBFC $\mathcal{C}_G^\times = \mathcal{C}_1$ is a regular UBFC and the $15j$ -symbols match the construction of Crane and Yetter^{86,261}, hence $Z[X] = \text{CY}_{\mathcal{C}_1}(X)$ the Crane-Yetter partition function for \mathcal{C}_1 . This implies our lattice models include the Walker-Wang models⁸⁵.
- Another special case constructed from a categorical group (or crossed module) yields Yetter's homotopy 2-type invariant⁹⁰. Note this inclusion implies that our lattice models capture those of Ref. 89. Categorical groups are in 1-1 correspondence with crossed modules, we follow Ref. 83 and use the latter to build a UGxBFC. A crossed module is specified by the data (G, H, ρ, a) for G, H finite groups, $\rho : H \rightarrow G$ a group morphism and $a : G \times H \rightarrow H$ a group action of G on H subject to the conditions $\rho(a_g(h)) = {}^g\rho(h)$ and $a_{\rho(h')}(h) = {}^{h'}h$. A UGxBFC $\mathcal{C}(G, H, \rho, a) = \bigoplus_{g \in G} \mathcal{C}_g$ is constructed from the data as follows: the simple elements are $h \in H$, the grading is given by $h \in \mathcal{C}_{\rho h}$, fusion is given by multiplication in H , the G -action is given by a , the braiding and F symbols are trivial. The $15j$ -symbols are simply delta conditions on the configuration being admissible (i.e. face and tetrahedra constraints satisfied) and the partition function satisfies $Z[X] = Y(X)$ for the Yetter invariant⁹⁰ constructed from the categorical group corresponding to (G, H, ρ, a) . In the special case that $H = \{1\}$ is trivial, ρ & a are also trivial, then the triangle constraints become the flatness condition $dg = 0$ and the partition function recovers the untwisted Dijkgraaf-Witten theory for G , $Z[X] = \text{DW}_G(X)$ ⁷².
- The case where the only nontrivial sector is \mathcal{C}_1 , a UBFC, the triangle constraints imply the flatness condition $dg = 0$. If in addition the group action is trivial the group and anyon degrees of freedom decouple and the partition function factors into a product of CY and untwisted DW theory, $Z[X] = \text{DW}_G(X) \text{CY}_{\mathcal{C}_1}(X)$.

For the trivially graded case it is possible to introduce additional cocycle data to produce variants of the UGxBFC:

- Since the state sum only involves flat G -connections the 4 group variables $g_{i,i+1}$ fully specify the G configuration on a pentachoron. One may modify the $15j$ -symbol by multiplication with a 5-cocycle phase factor $[\omega] \in H^4(G, U(1))$ to produce $\hat{T}_{s(\Delta_4)}^\pm = T_{s(\Delta_4)}^\pm \omega^{\pm 1}(g_{01}, g_{12}, g_{23}, g_{34})$ which will give rise to a topologically invariant state sum. If in addition the group action is trivial the resulting partition function is given by a product of CY and twisted DW theories $Z[X] = \text{DW}_G^\omega(X) \text{CY}_{\mathcal{C}_1}(X)$.
- In the case that $\mathcal{C}_1 = H$ an abelian group, with trivial F and R symbols, and a group action $a : G \times H \rightarrow H$ the tetrahedra constraint reads $(d^a h)_{0123} = a_{g_{23}}(h_{\hat{1}}) + h_{\hat{3}} - h_{\hat{0}} - h_{\hat{2}} = 0$. One may introduce a twisted 3-cocycle $[\beta] \in H_a^3(G, H)$ modifying the flatness condition to $(d^a h)_{0123} = \beta(g_{01}, g_{12}, g_{23})$. The $15j$ -symbols are then delta conditions on the flatness of a 2-group connection defined by the data $\mathbb{G} = (G, H, a, \beta)$, following Ref. 88. Furthermore one may introduce a multiplicative cocycle $[\omega] \in H^4(B\mathbb{G}, U(1))$

to produce a new $15j$ -symbol $\hat{T}_{s(\Delta_4)}^\pm = T_{s(\Delta_4)}^\pm \omega^{\pm 1}(s(\Delta_4))$. The partition function then recovers the twisted 2-group gauge theory $Z[X] = 2\text{-DW}_\mathbb{G}^\omega(X)$.

No rigorous connection has been established between the aforementioned H^3 & H^4 co-cycles and the $H^3(G, \mathcal{A})$ & $H^4(G, U(1))$ anomaly classes of an SET. In these cases the SET theory \mathcal{C}_1 and group action cannot be extended to a UGxBFC. However we conjecture it will remain possible to construct an extension of the UGxBFC with a single sector whose $15j$ -symbol has an intrinsic H^3 & H^4 anomaly. We defer the details of this to future work²⁷¹. Note the possibility of adding an arbitrary H^3 & H^4 as discussed above suggest the intrinsic anomalies should be thought of as torsors. Furthermore we speculate that it should be possible to construct a unitary fusion 2-category generalizing the UGxBFC that describes extension of an anomalous SET to nontrivial defect sectors, and this construction may yield a state sum with $15j$ -symbols generalizing those of the UGxBFC.

It is not yet known how strong the UGxBFC state sum invariant is. Considering the special cases it contains it is clearly sensitive to homotopy 2-type and also the second Stiefel—Whitney class (as the anyons can be fermionic). It is unclear if the theory is able to detect any smooth structure, while it is known from general considerations that it cannot be sensitive to all smooth structure²⁷².

4.2.4 Review of Kashaev's TQFT

Kashaev's family of state sum TQFTs^{82,260} are indexed by a natural number $N \in \mathbb{N}$, they are specified by a tensor

$$Q = N^{-\frac{1}{2}} \sum_{k,l,m \in \mathbb{Z}_N} \omega^{km} |k\rangle \langle k+m| \otimes |l\rangle \langle l+m| \otimes |m\rangle \quad (4.18)$$

where $\omega \in U(1)$ is a primitive N th root of unity. A tensor Q (Q^\dagger) is assigned to each 4-

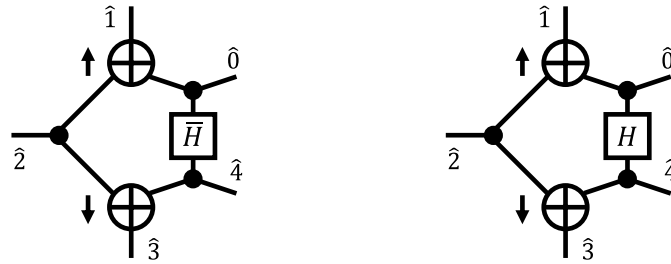


Figure 4.8: Kashaev's Q tensor (left) and its conjugate (right).

simplex in the triangulation where the orientation induced by the branching structure matches (is opposite to) the ambient orientation of the triangulated manifold. An N level qudit is associated to each 3-simplex facet of the 4-simplex tensor, they are written in the order given by taking the dual of the vertex order inherited from the branching structure. The full partition function on a triangulated 4-manifold (X, \mathcal{K}) is given by the evaluation of the tensor network times the normalization factors $N^{\frac{3}{2}\chi(X)}$ and $N^{-|\mathcal{K}_0|}$, where χ is the Euler characteristic and \mathcal{K}_0 is the number of vertices in the triangulation (with those on a boundary counted as half).

Kashaev has shown in Ref. 82 that the Q tensors satisfy the Pachner move invariance conditions, together with the Hermitian property of the tensors (i.e. parity reversal induces complex

conjugation) this implies the construction outlined in Ref. 84 gives rise to a local commuting projector Hamiltonian. The dimension of the (unfrustrated) zero energy eigenspace of the Hamiltonian on a spatial manifold Y is given by $Z[Y \times S^1]$. In particular the Hamiltonian is frustration free iff $Z[Y \times S^1]$ is nonzero. Partition functions have been calculated for a number of manifolds by Kashaev⁸² and for $S^1 \times T^3$ by the authors. These results are summarized in Table.4.1 and show that the TQFT is stable (i.e. the Hamiltonian does not exhibit spontaneous symmetry breaking). The final element of the table (highlighted in red) is the result of a new

X	$\chi(X)$	$\sigma(X)$	$Z_N[X]$
S^4	2	0	1
$S^2 \times S^2$	4	1	$\frac{3+(-1)^N}{2}$
$\mathbb{C}P^2$	3	1	$\frac{1}{\sqrt{N}} \sum_{k=1}^N \omega^{k^2}$
$S^3 \times S^1$	0	0	1
$S^2 \times S^1 \times S^1$	0	0	$\frac{3+(-1)^N}{2}$
$S^1 \times S^1 \times S^1 \times S^1$	0	0	$(\frac{3+(-1)^N}{2})^3$

Table 4.1: Partition functions of Kashaev's TQFT

calculation and yields the ground state degeneracy on the 3 torus for all N . Furthermore we have

$$\left| Z[\mathbb{C}P^2] \right|^2 = 1 + (-1)^{\frac{N}{2}} \frac{1 + (-1)^N}{2}.$$

Hence the data computed for the Kashaev theory is consistent with a modular CYWW model (an invertible TQFT) for N odd, and a premodular CYWW with transparent subcategory: \mathbb{Z}_2 with trivial braiding (topological order equivalent to toric code) for $N \equiv 0 \pmod{4}$, and $sVec$ for $N \equiv 2 \pmod{4}$ (as $Z[\mathbb{C}P^2] = 0$ the partition function can be seen to depend on spin structure in this case).

We conjecture that the general construction of Kashaev²⁶⁰ is dual to the Crane-Yetter TQFT, in a similar fashion to the duality between Kuperberg's $(2+1)$ -manifold invariants²⁷³ and the Turaev-Viro TQFT¹⁰⁸.

4.3 Lattice Model for Kashaev's TQFT

In this section we apply the framework developed in Ref. 84 to produce a translation invariant local commuting projector Hamiltonian for the theory on a particular 3-dimensional lattice.

4.3.1 The Hamiltonian

With the Q tensor from Eq.(4.18) one can explicitly construct a local commuting projector Hamiltonian of the form in Eq.(4.1) on any 3-manifold equipped with a triangulation and branching structure (Y, \mathcal{K}) by following the recipe outlined in Ref. 84. For concreteness we work with the body centered cubic (BCC) triangulation of T^3 or \mathbb{R}^3 which is dual to a tessellation by regular 4-permutohedra (also known as truncated octahedra). The branching structure is given for \mathbb{R}^3 by the rule that all edges not orthogonal to the \hat{z} axis are oriented along the $+\hat{z}$

direction, while those in an xy -plane point along the $+\hat{x}$ or $+\hat{y}$ direction (note these edges are always parallel to one of these axes). This also induces a branching structure on the triangulation of T^3 . Note this branching structure preserves the full translational symmetry along each of the spatial axes in addition to a translation symmetry generated by $(\frac{1}{2}, \frac{1}{2}, \frac{1}{2})$. Working on the

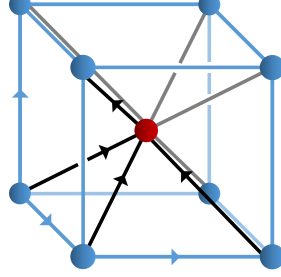


Figure 4.9: Triangulation and branching structure within a unit cell.

permutohedron cellulation dual to the triangulation the model is defined on a Hilbert space consisting of a qudit degree of freedom for each vertex $\mathcal{H} = \bigotimes_{v \in C} \mathbb{C}_v^N$. The Hamiltonian is a sum of identical terms each acting on 24 qudits in the boundary of a different permutohedron. To explicitly evaluate the Hamiltonian produced by the recipe of Ref. 84 we specify a numbering of the vertices on the boundary of a permutohedron depicted in Fig.4.10. The Hamiltonian is

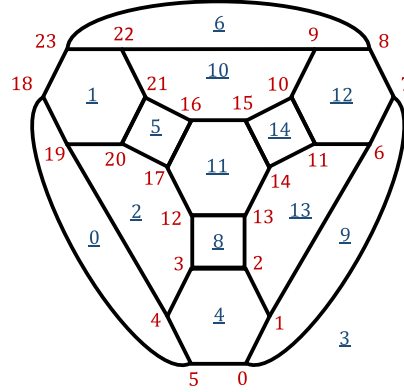


Figure 4.10: Ordering of the vertices (red) and dual vertices (underlined blue) on the boundary of a permutohedron flattened onto the plane.

given by

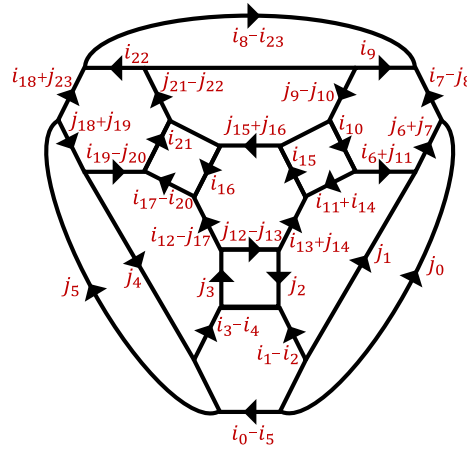
$$\begin{aligned}
 \langle \underline{j} | 1 - h_v | \underline{i} \rangle &= \frac{\omega^{\underline{i}_Z \cdot \underline{j}_X - \underline{i}_X \cdot \underline{j}_Z}}{N^{12}} \delta_{i_8 - i_9 + i_{22} + i_{23}} \delta_{i_{10} + i_{11} + i_{14} + i_{15}} \delta_{i_{16} + i_{17} - i_{20} + i_{21}} \delta_{i_0 - i_1 + i_2 + i_3 + i_4 - i_5} \\
 &\quad \delta_{-j_0 + j_1 + j_6 + j_7} \delta_{j_2 + j_3 + j_{12} - j_{13}} \delta_{j_4 + j_5 + j_{18} + j_{19}} \delta_{j_9 - j_{10} + j_{15} + j_{16} + j_{21} - j_{22}} \\
 &\quad \delta_{i_1 - i_2 + i_6 - i_{11} + i_{13} - i_{14} - j_1 - j_2 + j_{11} + j_{14}} \delta_{i_3 + i_4 + i_{12} + i_{17} - i_{19} - i_{20} + j_3 + j_4 - j_{17} + j_{20}} \\
 &\quad \delta_{i_6 + i_7 - i_9 + i_{10} + j_6 + j_7 - j_8 + j_9 - j_{10} + j_{11}} \delta_{-i_{12} + i_{13} + i_{15} + i_{16} + j_{12} - j_{13} + j_{14} + j_{15} + j_{16} + j_{17}} \\
 &\quad \delta_{-i_{18} + i_{19} + i_{21} + i_{22} + j_{18} + j_{19} - j_{20} + j_{21} - j_{22} - j_{23}}
 \end{aligned} \tag{4.19}$$

where the i_n and j_n labels are in either the X or Z basis as shown in Table.4.2 and by i in the X basis we mean $|\hat{i}\rangle := N^{-\frac{1}{2}} \sum_{k=0}^{N-1} \omega^{-i \cdot k} |k\rangle$. Also the notation \underline{i}_Z indicates the subset of i labels in the Z basis and similarly for j and X .

n	0	1	2	3	4	5	6	7	8	9	10	11	12	13	14	15	16	17	18	19	20	21	22	23
i_n	X	Z	Z	X	Z	Z	X	Z	X	Z	X	X	Z	X	X	X	Z	X	Z	Z	Z	X	X	Z
j_n	Z	X	X	Z	X	X	Z	X	Z	X	Z	Z	X	Z	Z	Z	X	Z	X	X	X	Z	Z	X

Table 4.2: Basis choices for $\underline{i}, \underline{j}$.

A matrix element of the Hamiltonian for fixed \underline{i} and \underline{j} as above gives rise to a tensor network multiplied by some nonzero weight. The tensor network is composed of delta tensors and X matrices and computes a delta condition on the flatness of the configuration shown in Fig. 4.11. Evaluating the delta flatness condition yields the Hamiltonian term in Eq.(4.19).

**Figure 4.11:** Configuration induced by fixing the input/output of a Hamiltonian term.

4.3.2 Degeneracy, Statistics, and the Ground State Wave Function

Thus far there is little known about the relation of the Kashaev TQFTs to other more established families of models. We conjecture that the Kashaev TQFTs and their Hamiltonian realizations are equivalent to Crane-Yetter-Walker-Wang (CYWW) models for \mathbb{Z}_N with a particular choice of braiding. In the case N is odd it is a nondegenerate braiding on \mathbb{Z}_N hence the CYWW model is an invertible TQFT and its partition functions depend only on Euler characteristic and signature. In the case of N even the relevant braiding on \mathbb{Z}_N is degenerate and hence the CYWW model is premodular.

The partition functions calculated for Kashaev's TQFT support our conjecture as they are consistent with an invertible modular CYWW model for N odd and consistent with a premodular CYWW in the even case, the simplest example being \mathbb{Z}_2 which we expect to be the CYWW model based on $sVec$. More generally we conjecture the even case is equivalent to a CYWW model based on a premodular category with transparent subcategory: \mathbb{Z}_2 (with trivial braiding) for $N = 0 \pmod 4$, and $sVec$ for $N = 2 \pmod 4$.

The partition function $Z[S^1 \times Y]$ equals the dimension of the ground space $V[Y]$ (note in this case normalization by Euler characteristic and signature are irrelevant as both are 0). The values of $Z[S^1 \times S^3]$ in the table indicate that Kashaev's TQFT is stable i.e. does not spontaneously break any symmetry.

In accordance with our conjecture we expect the topological excitations of the Kashaev model to match those of CYWW. In particular for N odd there are no deconfined particle like excitations in the bulk while there may be interesting loop like excitations. For N even there is a species of point like fermionic excitations in the bulk as well as loop like excitations. Explicitly comparing the 3 loop braiding statistics of the loop excitations in Kashaev and CYWW is an interesting problem which we leave for future work.

There is a PEPS representation of a ground state wave function for all Kashaev TQFTs which is obtained by following the procedure of Ref. 84. Due to the Pachner move symmetry of the tensors used to construct this PEPS it will have a closed surface PEPO topological symmetry on the virtual level^{59,62,63,84,93}. It should be possible to construct the excitations from this PEPO by following a higher dimensional generalization of the procedure laid out in Ref. 64 for $(2+1)\text{D}$. Note the procedure of Ref. 84 also yields a MERA representation of the ground state wave functions.

4.3.3 Example: \mathbb{Z}_2 Case

The explicit tensor for the $N = 2$ Kashaev TQFT is given by

$$Q = \frac{1}{\sqrt{2}} \sum_{k,l,m \in \mathbb{Z}_2} (-1)^{km} |k\rangle \langle k+m| \otimes |l\rangle \langle l+m| \otimes |m\rangle \quad (4.20)$$

We conjecture this $N = 2$ Kashaev model is described by the CYWW model for the premodular

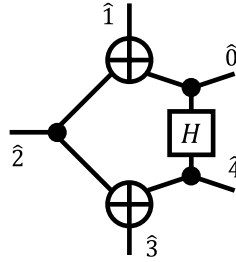


Figure 4.12: Kashaev's Q tensor for $N = 2$.

category $sVec$ consisting of a vacuum and fermion particle. Hence we expect the partition functions to depend on the possible spin structures of a manifold. This is supported by the observations that $Z[\mathbb{CP}^2] = 0$ which corresponds to \mathbb{CP}^2 not admitting a spin structure, and we proceed to show $Z[T^4] = 8$ corresponding to 8 spin structures on the space manifold T^3 .

Lemma 1. *For the commuting, projector, real-space blocking RG fixed point Hamiltonian term h_v we have $\dim V[T^3] = Z[T^4] = \text{Tr}[\pi Z[v' * \text{st}_v]] = \text{Tr}[\pi(\mathbb{1} - h_v)]$ for the permutation π given below.*

Proof. We consider the translation invariant BCC triangulation of T^3 (or \mathbb{R}^3) dual to a tiling by regular 4-permutohedra. For concreteness we fix the branching structure to be that of Fig.4.9 and the ordering of tetrahedra in st_v to be that of Fig.4.10. However note any branching structure that is consistent with periodic boundary conditions may be used, and the ordering is totally arbitrary. Considering the Hamiltonian term of Eq.4.19 we have $\mathbb{1} - h_v = Z[v' * \text{st}_v]$ and note this is a tensor network on the triangulation of a 4d hypercube. Conceptually it is clear that

taking closed boundary conditions yields the partition function of the 4d torus. The gluing map that corresponds to closing the boundary conditions is specified by the permutation

$$\begin{array}{cccccc}
 \pi: & 0 & \rightarrow & 13 & \rightarrow & 20 & \rightarrow & 9 & \rightarrow & 0 \\
 & 1 & \rightarrow & 18 & \rightarrow & 17 & \rightarrow & 10 & \rightarrow & 1 \\
 & 2 & \rightarrow & 19 & \rightarrow & 8 & \rightarrow & 15 & \rightarrow & 2 \\
 & 3 & \rightarrow & 6 & \rightarrow & 23 & \rightarrow & 16 & \rightarrow & 3 \\
 & 4 & \rightarrow & 7 & \rightarrow & 14 & \rightarrow & 21 & \rightarrow & 4 \\
 & 5 & \rightarrow & 12 & \rightarrow & 11 & \rightarrow & 22 & \rightarrow & 5
 \end{array} \tag{4.21}$$

abusing notation slightly we also use π to denote the linear operator $\sum_{\{i_n\}} |\{i_{\pi(n)}\}\rangle \langle \{i_n\}|$. Then we have $Z[T^4] = \text{Tr}[\pi Z[v' * \text{st}_v]] = \text{Tr}[\pi(\mathbb{1} - h_v)]$. \square

We furthermore conjecture that a similar relation holds in all dimensions, following from the basic facts that the regular $(n + 1)$ -permutohedron tiles n dimensional euclidean space (or the n dimensional torus) and that the join of its dual triangulation of the n -sphere with a line (including its two endpoints) is a triangulation of the $(n + 1)$ hypercube. By taking appropriate periodic boundary conditions, specified by a generalization of the permutation π we find a similar relation as in $(3 + 1)\text{D}$.

Proposition 1. *For Kashaev's model⁸² at $N = 2$, $\dim V[T^3] = Z[T^4] = 8$.*

Proof. We make use of Lemma 1 and calculate $\text{Tr}[\pi Z[v' * \text{st}_v]] = Z[T^4]$ using the tetrahedron labeling in Fig.4.10 and the branching structure in Fig.4.13. The quantity we want to compute

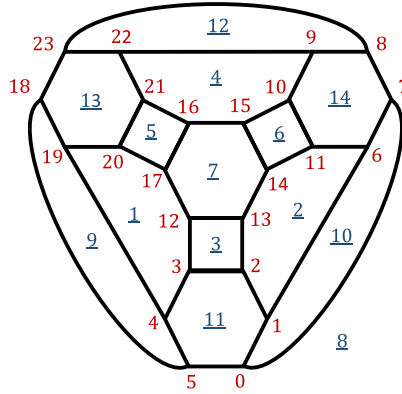


Figure 4.13: The branching structure used to calculate $Z[T^4]$.

is a sum over tensor networks on the 4-permutohedron graph

$$\text{Tr}[\pi Z[v' * \text{st}_v]] = \sum_{\{i_n\}} \langle \{i_n\} | Z[v' * \text{st}_v] | \{i_{\pi(n)}\} \rangle. \tag{4.22}$$

Each tensor has 5 indices, 2 exterior indices corresponding to $i_n, i_{\pi(n)}$ and 3 internal indices of the tensor network on the permutohedron. With the branching structure we have chosen the fixed exterior labels correspond to the 0 and 4 indices of each individual tensor, fixing these

labels we find the following 3 index tensor

$$\begin{array}{c} \text{Diagram 1: A central square node labeled } H \text{ with four external indices } \hat{1}, \hat{2}, \hat{3}, \text{ and } j. \end{array} = \frac{(-1)^{ij}}{\sqrt{2}} \begin{array}{c} \text{Diagram 2: A vertical line with two square nodes labeled } X^j \text{ and } X^i \text{ and external indices } \hat{1} \text{ and } \hat{3}. \end{array} \quad (4.23)$$

which consists of a delta tensor along with X matrices and a sign that is determined by the fixed external indices. From this equation it follows that the tensor network on the 4-permutohedron graph specifies a map $\sigma : \mathbb{Z}_2^{24} \rightarrow \mathbb{Z}_2^{36}$ from the fixed external indices to a \mathbb{Z}_2 configuration on the edges of the permutohedron, corresponding to the exponent of the X matrix on each edge. Contracting the tensor network yields a nonzero result only for those connections which are flat, i.e. the sum around each plaquette is 0. To describe this precisely we denote the map from a \mathbb{Z}_2 edge configuration to the induced flux through each plaquette by f then we have

$$\langle \{i_n\} | Z[v' * st_v] | \{i_{\pi(n)}\} \rangle = \frac{(-1)^{\mathbf{i} \cdot \pi(\mathbf{i})}}{2^{12}} \delta(\sigma \circ f(\mathbf{i}) = 0) \quad (4.24)$$

where $\mathbf{i} \cdot \pi(\mathbf{i}) = \sum_n i_n \cdot i_{\pi(n)}$ and the normalization factor comes from a product of $\frac{1}{\sqrt{2}}$ for each of the 24 tensors (See Eq.4.23), a factor $\frac{1}{2}$ from the normalization $N^{-|\mathcal{K}_0|}$, and a factor 2 from the contraction of delta tensors and X matrices on the permutohedron graph. We proceed to show that all flat configurations contribute with a +1 sign and hence the problem is to count the number of them. First we use the relation $\sum_k \delta_{i,j,k} \delta_{k,l,m} = \delta_{i,j,l,m}$ to remove 12 edges of the permutohedron tensor network by contracting them, precisely those on which an X never occurs, see Fig.4.14. Hence we can consider reduced \mathbb{Z}_2 maps $\sigma : \mathbb{Z}_2^{24} \rightarrow \mathbb{Z}_2^{24}$ and $f : \mathbb{Z}_2^{24} \rightarrow$

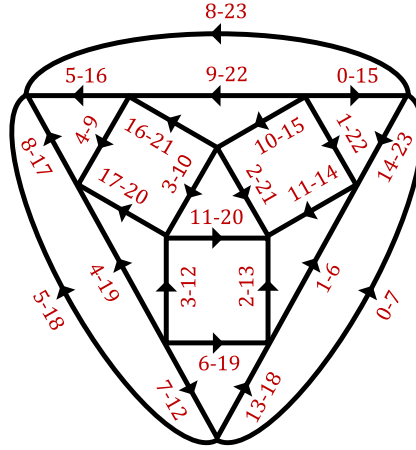


Figure 4.14: Configuration induced by the map σ . Value $n-m$ to be read as $i_n - i_m$.

\mathbb{Z}_2^{13} by noting there are 24 edges and 14 faces (one of which is redundant as its value equals the sum of all other faces). Since we are considering flat configurations on a cellulation of S^2 there is only a single homology class and furthermore an injective map $d : \mathbb{Z}_2^{11} \rightarrow \mathbb{Z}_2^{24}$ from \mathbb{Z}_2 values on the 12 vertices (with one vertex value fixed) to a \mathbb{Z}_2 configuration on edges such that

$\text{im } d = \ker f$. A full list of generators for $\ker \sigma \circ f$ is

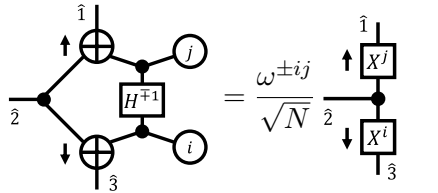
i	0	1	2	3	4	5	6	7	8	9	10	11	12	13	14
$g_{(\cdot)}^i = 1$	7	0	5	12	6	1	15	9	4	3	2	0	1	2	8
	18	23	8	19	13	14	22	16	17	20	11	7	6	13	17
												12	19	18	20
												3	4	5	11
												10	9	16	14
												15	22	21	23

(4.25)

one can verify that these are independent. Generators 11-14 correspond to the generators of $\ker \sigma$, while 0-10 lie in $(\ker \sigma)^\perp$ and their image under σ generates $\ker f$. Hence 2^{15} flat configurations contribute to the sum, and furthermore we have $\sum_n g_n^i \cdot g_{\pi(n)}^j = \sum_n g_n^j \cdot g_{\pi(n)}^i$. Any flat configuration $\underline{x} \in \ker \sigma \circ f$ is of the form $\underline{x} = \sum_i x_i \underline{g}^i$ and the corresponding phase factor is 1 as $\underline{x} \cdot \pi(\underline{x}) = 0$ hence all such configurations contribute with a positive sign. \square

4.3.4 Back to the general case

Our analysis of $Z[T^4]$ for $N = 2$ largely carries over to the case of general N , the main modifications required involve keeping track of orientations and complex conjugations. The calculation proceeds as above up to Eq.(4.23) at which point we find



(4.26)

where \pm depends on the orientation of the simplex to which the tensor is associated. This leads to new maps $\sigma : \mathbb{Z}_N^{24} \rightarrow \mathbb{Z}_N^{24}$ and $f : \mathbb{Z}_N^{24} \rightarrow \mathbb{Z}_N^{13}$ which can be understood in terms of flat \mathbb{Z}_N connections on a cellulation of S^2 , see Fig.4.14. In place of Eq.(4.24) we have

$$\langle \{i_n\} | Z[v' * \text{st}_v] | \{i_{\pi(n)}\} \rangle = \frac{\omega^{\mathbf{i} \cdot \pi(\mathbf{i})}}{N^{12}} \delta(\sigma \circ f(\mathbf{i}) = 0) \quad (4.27)$$

where the dot product has been altered as follows $\mathbf{i} \cdot \pi(\mathbf{i}) = \sum_n (-1)^n i_n \cdot i_{\pi(n)}$ and the normalization arises in the same way as above (with N in place of 2). Again we have a boundary map $d : \mathbb{Z}_N^{11} \rightarrow \mathbb{Z}_N^{24}$ that satisfies $\text{im } d = \ker f$ and the generators of $\sigma \circ f$ are the same as those given in Eq.(4.25), however now each has order N . Now N^{15} flat configurations contribute to the sum, the new complication being that they may take on different phase values. We still have the identities $\underline{g}^i \cdot \pi(\underline{g}^i) = 0$ and $\underline{g}^i \cdot \pi(\underline{g}^j) = \underline{g}^j \cdot \pi(\underline{g}^i)$ however they no longer guarantee the phase factors are trivial for $N > 2$. An arbitrary element $\underline{x} \in \ker \sigma \circ f$ is of the form $\underline{x} = \sum_i x_i \underline{g}^i$ and we have

$$\begin{aligned} \underline{x} \cdot \pi(\underline{x}) &= \sum_{i < j} 2x_i x_j \underline{g}^i \cdot \pi(\underline{g}^j) \\ &= 2(x_0(x_8 - x_5) + (x_1 - x_9)(x_4 - x_7) + (x_2 - x_{10})(x_6 - x_3)). \end{aligned}$$

Hence the overall summation becomes

$$Z[T^4] = \left(\sum_{i,j \in \mathbb{Z}_N} \frac{\omega^{2ij}}{N} \right)^3 \quad (4.28)$$

$$= \left(\sum_{i \in \mathbb{Z}_N} \delta(2i = 0 \bmod N) \right)^3 \quad (4.29)$$

which takes the value 1 for N odd and 8 for N even.

4.4 Lattice Model for UGxBFC TQFT

In this section we introduce tensor network and graphical calculus constructions of a class of commuting projector Hamiltonians for topological models based on the UGxBFC state sum TQFT.

Before discussing constructions of a Hamiltonian let us describe the Hilbert space on a general triangulation or equivalently the Poincaré dual simple polyhedra. Given a UGxBFC \mathcal{C}_G^\times and L the label set $L^{(1)} = G$, $L^{(2)} = \mathcal{C}_G^\times$, $L^{(3)} = \mathcal{C}_G^\times$. Suppose Y is an oriented spatial 3-manifold with a vertex ordered Δ -complex triangulation K . Γ_K denotes the dual simple polyhedron. We take a resolution of each 4-valent vertex in Γ_K into a pair of trivalent vertices where the edges dual to the faces $\hat{0}, \hat{2}$ and $\hat{1}, \hat{3}$ meet, denote the resulting polyhedron as Γ'_K . Let V, E, F denote the sets of vertices, edges, and faces of Γ'_K respectively. A configuration on Γ'_K is a labeling of each edge by a defect label $a \in \mathcal{C}_G^\times$, each face by a group element $g \in G$, and each vertex by a basis element in $\oplus_{(a,b,c) \in (\mathcal{C}_G^\times)^3} \mathbb{C}^{N_{ab}^c}$. Hence the total local Hilbert space is

$$\mathcal{H}(Y, K) = \bigotimes_E \mathbb{C}[\mathcal{C}_G^\times] \bigotimes_V \left(\bigoplus_{\substack{(a,b,c) \\ \in (\mathcal{C}_G^\times)^3}} \mathbb{C}^{N_{ab}^c} \right) \bigotimes_F \mathbb{C}[G]. \quad (4.30)$$

4.4.1 Tensor Network Approach

The recipe outlined in Ref. 84 constructs a local commuting projector Hamiltonian for the UGxBFC state sum on any triangulation from a set of $15j$ -symbols. The $15j$ -symbols for the UGxBFC $\mathbb{T}_{s(\Delta_4)}^\pm$ are shown in Fig.(4.7) they take as input a configuration $s = (g, a) : (K^{(1)}, K^{(2)} \cup K^{(3)}) \rightarrow (G, \mathcal{C}_G^\times)$ of group elements $g_e \in G$ on edges, and defects $a_\Delta, a_{\Delta_3} \in \mathcal{C}_G^\times$ on triangles and tetrahedra of a 4-simplex Δ_4 and return a value in \mathbb{C} . $\mathbb{T}_{s(\Delta_4)}^\pm$ only take nonzero values on admissible configurations, those satisfying the triangle constraints $a_\Delta \in \mathcal{C}_{dg_\Delta}$, where $dg_{012} = \bar{g}_{02}g_{01}g_{12}$, and the tetrahedra constraints $N_{a_1 \bar{g}_{23} a_3}^{a_{0123}} \neq 0 \neq N_{a_2 a_0}^{a_{0123}}$.

The Hamiltonian takes the form $H = \sum_v h_v$ where the term at vertex v is given by

$$h_v = \mathbb{1} - \frac{(D^2)^{-|(\text{st}_v)_1|}}{|G|} \sum_{\gamma, \alpha} \frac{\prod_{\Delta_2 \in J} d_{\alpha(\Delta_2)}}{\prod_{\Delta_3 \in J} d_{\alpha(\Delta_3)}} B_v^{\gamma, \alpha} \quad (4.31)$$

where $J = \text{int}(v' * \text{st}_v)$ can be thought of as a small piece of spacetime, with v' an auxiliary copy of vertex v at the next time step. The elements $\gamma \in G$, $\alpha : J^{(2)} \cup J^{(3)} \rightarrow \mathcal{C}_G^\times$ label the timelike edge, triangles and tetrahedra in J .

The individual summands are given by

$$B_v^{\gamma, \alpha} = \sum_{S, S'} \prod_{\substack{\Delta_i \in \text{lk}_v \\ i > 0}} \delta_{S(\Delta_i), S'(\Delta_i)} \frac{\prod_{\Delta_2 \in \text{st}_v} \sqrt{d_{a(\Delta_2)} d_{a'(\Delta_2)}}}{\prod_{\Delta_3 \in \text{st}_v} \sqrt{d_{a(\Delta_3)} d_{a'(\Delta_3)}}} \prod_{\Delta_4 \in J} T_{s(\Delta_4)}^{\sigma(\Delta_4)} \bigotimes_{e, \Delta, \Delta_3 \in \text{st}_v} |g'_e, a'_\Delta, a'_{\Delta_3}\rangle \langle g_e, a_\Delta, a_{\Delta_3}| \quad (4.32)$$

where $S = (g, a)$, $S' = (g', a')$ denote configurations on the triangulated spatial slices $\text{cl}(\text{st}_v)$, $v' * \text{lk}_v$ and s denotes the full spacetime configuration $\{S, S', (\gamma, \alpha)\}$ on $\text{cl}(J)$. Note the variables in lk_v are fixed control qudits for the operator $B_v^{\gamma, \alpha}$, while the variables in st_v fluctuate.

The Hamiltonian built in this way contains only vertex terms. These terms also enforce the flatness (admissibility) triangle and tetrahedra constraints on basis states with nonzero ground space overlap. Contrast this with the more conventional way of writing fixed point Hamiltonians as a sum of separate vertex fluctuation and plaquette flatness terms.

On the BCC triangulation with the branching structure chosen in Fig.4.9 the Hamiltonian is a translationally invariant sum with a single type of term. Note the case described explicitly above was assuming no multiplicity in the fusion of \mathcal{C}_G^\times , to include possible multiplicities one simply includes the corresponding fusion multiplicity labels together with the defect label on each tetrahedron.

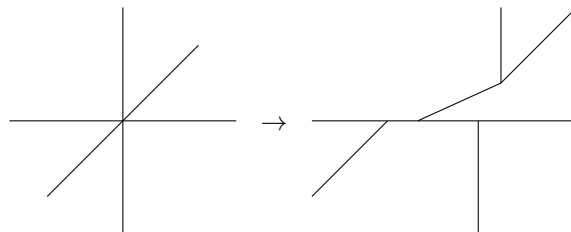
4.4.2 Graphical Calculus Approach

Another approach to constructing the Hamiltonian closer to that of Ref. 85 is to use the graphical calculus of the UGxBFC to define the local terms. First we consider two different cellulations of the 3-torus T^3 : the cellulation used in Ref. 85, and the simple polyhedron of the permutohedron cellulation dual to the BCC triangulation in Fig.4.9. Both cellulations have the full translational symmetry which keep the Hamiltonians relatively simple. We then explain the general construction on a simple polyhedra.

The Hamiltonian on the 3-Torus: resolved cubic lattice

We first focus on the simple case where G is abelian and all group elements and defects are self inverse, this removes the need to keep track of edge orientations. Note it is simple to generalize to the non self inverse case by keeping track of edge orientations, however extending to nonabelian G requires nontrivial work as the cellulation is not a simple polyhedra.

The cellulation Γ is given by the following resolution of the cubic lattice into trivalent vertices.



Group degrees of freedom live on the plaquettes of the cubic lattice, and defect degrees of freedom live on the edges of the resolved lattice. Hence the Hilbert space is given in Eq.(4.30).

The Hamiltonian is given by

$$H_\Gamma = - \sum_{v \in V} A_v - \sum_{e \in E} A_e - \sum_{f \in F} \sum_{\substack{g \in G, \\ a \in \mathcal{C}_g}} \frac{d_a}{D^2} B_f^{g,a} - \sum_{c \in C} \sum_{g \in G} B_c^g \quad (4.33)$$

where V, E, F, C are the vertices, edges, faces and 3-cells of Γ . The A_v term enforces the constraint that each triple of defects a, b, c meeting at a vertex is an admissible fusion $N_{ab}^c \neq 0$.

$$A_v \left(\begin{array}{c} | \\ c \\ \swarrow \quad \searrow \\ a \quad b \end{array} \right) = \delta_{ab}^c \begin{array}{c} | \\ c \\ \swarrow \quad \searrow \\ a \quad b \end{array}$$

A_e enforces the constraint that each defect lies in the sector given by the boundary of the group configuration on the adjacent faces i.e. $a_e \in \mathcal{C}_{(\partial g)_e}$.

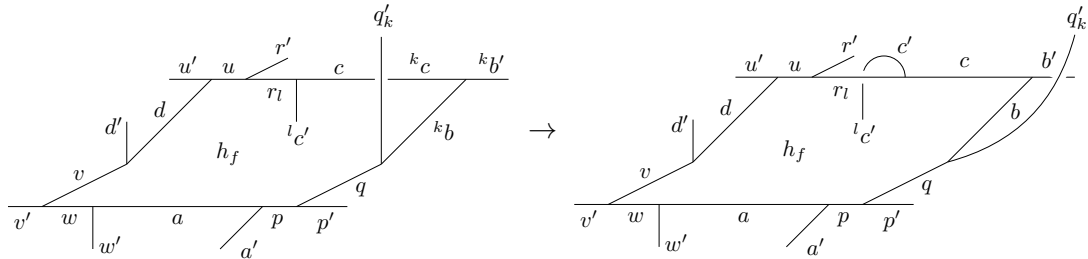
$$A_e \left(\begin{array}{c} | \\ h \\ \hline \begin{array}{ccc} g & a_x & k \\ \hline & l & \end{array} \end{array} \right) = \delta_{x,ghkl} \begin{array}{c} | \\ h \\ \hline \begin{array}{ccc} g & a_{ghkl} & k \\ \hline & l & \end{array} \end{array}$$

B_c^g fluctuates the group configuration adjacent to c in the conventional way $h_f g$, for $f \in \partial c$.

$$B_c^g \left(\begin{array}{c} \text{cube with faces } l, k, h \end{array} \right) = \begin{array}{c} \text{cube with faces } lg, kg, hg \end{array}$$

The $B_f^{g,a}$ term fluctuates the group and defect configuration adjacent to f by fusing a loop of defect a in to the defects on ∂f and simultaneously multiplying $h_f g$. This term is reminiscent of the plaquette term in the Walker-Wang model and matches it exactly in the case $G = \{1\}$.

We proceed to calculate the effect of the $B_f^{g,a}$ term using the diagrammatic calculus of the UGxBFC, we use the compressed notation $F_{d;ef}^{abc} = [F_d^{abc}]_e^f$. Consider an initial configuration σ_I depicted on the left; first the edges crossing f are moved aside



unlike the Walker-Wang model this invokes a factor of $U_k(b, c; b')$ on top of the braiding sym-

bolds $R_q^{q'kb} R_c^{lc'r}$. Now acting with $B_f^{g,a}$ introduces a loop of defect a onto plaquette f :

$$B_f^{g,a} \left(\begin{array}{c} \text{Diagram 1} \end{array} \right) = \begin{array}{c} \text{Diagram 2} \end{array}$$

Diagram 1: A lattice configuration with vertices labeled $v, w, a, p, p', q, b, c, b', q_k$ and edges labeled $u, u', d, d', r, r', l, l', c, b, a, p, p', q, b, c, b', q_k$. A loop of defect a is introduced onto plaquette f .

Diagram 2: The same lattice configuration as Diagram 1, but with the loop of defect a moved to a different position, labeled h_{fg} and s_g .

which we proceed to fuse in to ∂f :

$$\begin{array}{c} \text{Diagram 3} \end{array} \rightarrow \begin{array}{c} \text{Diagram 4} \end{array}$$

Diagram 3: A lattice configuration with vertices labeled $v, w, a'', p, p', q, b, c, b', q_k$ and edges labeled $u, u', d, d', r, r', l, l', c, b, a'', p, p', q, b, c, b', q_k$. A loop of defect a is introduced onto plaquette f .

Diagram 4: The same lattice configuration as Diagram 3, but with the loop of defect a moved to a different position, labeled h_{fg} and s_g .

this induces a factor $F_{a';ap''}^{a''sp} F_{p';pq''}^{p''sq} F_{q';qb''}^{q''sb} F_{b';bc''}^{b''sc} F_{c';cr''}^{c''sr}$. The next step induces a factor $\eta_{c'}(l, g)$

$$\begin{array}{c} \text{Diagram 5} \end{array} .$$

Diagram 5: A lattice configuration with vertices labeled $v, w, a'', p'', p', q'', b'', c'', b', q_k$ and edges labeled $u, u', d, d', r, r', l, l', c'', b'', a'', p'', p', q'', b'', c'', b', q_k$. A loop of defect a is introduced onto plaquette f .

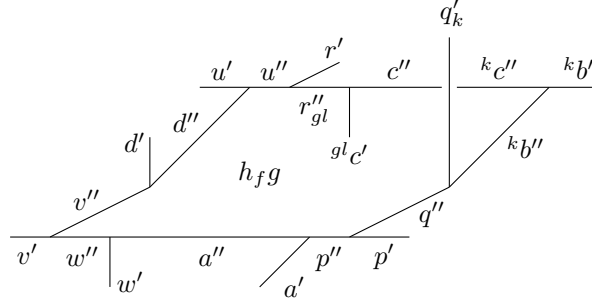
Then five more F -moves leads to

$$\begin{array}{c} \text{Diagram 6} \end{array}$$

Diagram 6: A lattice configuration with vertices labeled $v', w'', a'', a, a'', p'', p'$ and edges labeled $u', u'', d', d'', r', r'', l, l', c', c'', b', b'', q_k$. A loop of defect a is introduced onto plaquette f .

along with a factor $F_{r';ru''}^{r''su} F_{u';ud''}^{u''sd} F_{d';dv''}^{d''sv} F_{v';vw''}^{v''sw} F_{w';wa''}^{w''sa}$. Finally restoring the lattice to its orig-

inal position we find the final configuration σ_F shown below



along with a factor $U_k^{-1}(b'', c''; b') R_{q''}^{q' k b''} \overline{R_{c'}^{g l c' r''}}$ note $r'' \in \mathcal{C}_{gl}$. Hence the full plaquette term is

$$\begin{aligned} \langle \sigma_F | B_f^{g,a} | \sigma_I \rangle = & U_k(b, c; b') U_k^{-1}(b'', c''; b') \eta_{c'}(l, g) \overline{R_q^{q' k b}} R_c^{l c' r} R_{q''}^{q' k b''} \overline{R_{c''}^{g l c' r''}} \\ & F_{a'; ap''}^{a'' sp} F_{p'; pq''}^{p'' sq} F_{q'; qb''}^{q'' sb} F_{b'; bc''}^{b'' sc} F_{c'; cr''}^{c'' sr} F_{r'; ru''}^{r'' su} F_{u'; ud''}^{u'' sd} F_{d'; dv''}^{d'' sv} F_{v'; vw''}^{v'' sw} F_{w'; wa''}^{w'' sa} \end{aligned} \quad (4.34)$$

which differs noticeably from WW in the appearance of the factors $U_k(b, c; b') U_k^{-1}(b'', c''; b') \eta_{c'}(l, g)$.

The Hamiltonian on Simple Polyhedra

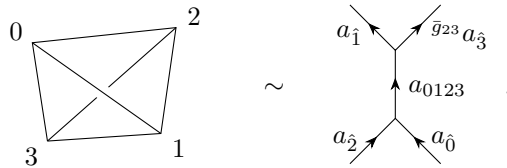
We now turn to the general case of an arbitrary finite G and a UGxBFC \mathcal{C}_G^\times , this requires a cellulation Γ_K dual to a triangulation K with branching structure and keeping track of edge orientations. Γ'_K is then the cellulation where each 4-valent vertex v has been resolved into a pair of trivalent vertices v^+, v^- , as in Eq.(4.30). The orientations of dual edges in Γ_K are specified as follows: for vertices dual to positively oriented tetrahedra, the dual $\hat{0}, \hat{2}$ edges point out and $\hat{1}, \hat{3}$ point in, and vice versa for vertices dual to negatively oriented tetrahedra. The extra edges introduced in Γ'_K point from the $\hat{0}, \hat{2}$ vertex to the $\hat{1}, \hat{3}$ vertex in a resolved vertex dual to a positively oriented tetrahedra, and vice versa for negative.

The Hamiltonian is similar to that in Eq.(4.33)

$$H_\Gamma = - \sum_{v \in V} (A_{v^+} + A_{v^-}) - \sum_{e \in E} A_e - \sum_{f \in F} \sum_{\substack{g \in G, \\ a \in \mathcal{C}_g}} \frac{d_a}{D^2} B_f^{g,a} - \sum_{c \in C} \sum_{g \in G} B_c^g \quad (4.35)$$

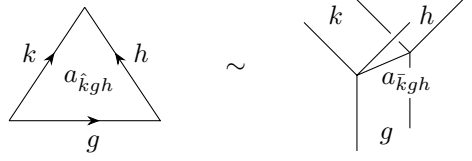
where V, E, F, C are the vertices, edges, faces, and 3-cells of Γ_K .

Writing 0123 for the tetrahedron dual to v then the A_{v^+} term enforces the admissibility of the fusion $N_{a_2 a_0}^{a_0 1 2 3} \neq 0$, while the A_{v^-} term enforces a twisted fusion constraint $N_{a_1 \bar{g} 2 3}^{a_0 1 2 3} \neq 0$. Both A_{v^+} and A_{v^-} terms project onto the subspace spanned by locally admissible configurations such as the following (depicted on a triangulation and its dual cellulation)

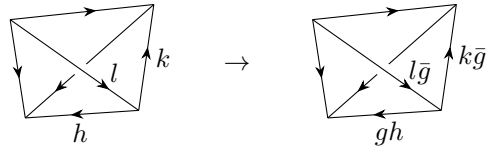


The operator A_e enforces the constraint that each defect lies in the sector specified by the difference of the adjacent group variables, for an edge e dual to the triangle 012 the constraint

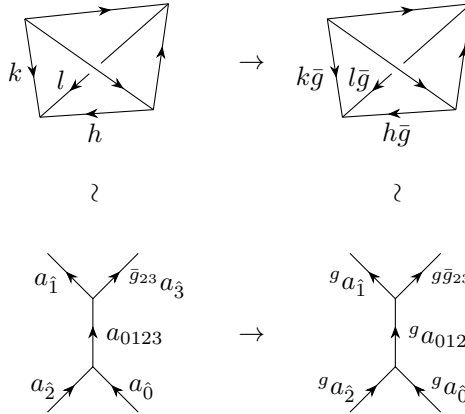
reads $a_{012} \in \mathcal{C}_{\hat{g}_{02}g_{01}g_{12}}$. Hence the A_e term projects onto the subspace spanned by admissible configurations such as:



The term B_c^g fluctuates the group configuration on faces $f \in \partial c$. To be more specific we work on the dual triangulation, then each group variable on an edge e^- pointing towards v_c (the vertex dual to c) transforms as $h_{e^-} \bar{g}$, while a group variable on an edge e^+ leaving v_c transforms as gh_{e^+} . Hence the operator B_c^g maps configurations as follows



Additionally the defects on the five edges associated to the dual of a tetrahedra having v_c as its highest ordered vertex (all edges pointing in) are acted upon by h as follows



when B_c^g is applied.

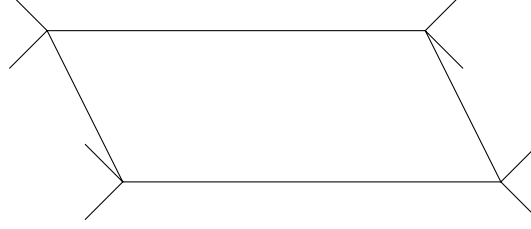
The plaquette term $B_f^{g,a}$ right multiplies the group variable on face f , resulting in $h_f \bar{g}$, and fuses a loop of defect $a \in \mathcal{C}_g$, oriented along the boundary of f , into the defects on edges $e \in \partial f$. The numerical amplitudes of $B_f^{g,a}$ are calculated according to the diagrammatic rules of the input UGxBFC.

The ground space of the Hamiltonian is supported on a subspace of states satisfying the vertex and edge constraints which is spanned by consistent diagrams from the UGxBFC. Naively these states and the Hamiltonian seem to depend on the choice of projection to the 2D plane of the picture, up to a local unitary gauge equivalence due to U and η . We note that such an apparent dependence does not appear when following the tensor network approach to produce a Hamiltonian which was described in Sec.4.4.1.

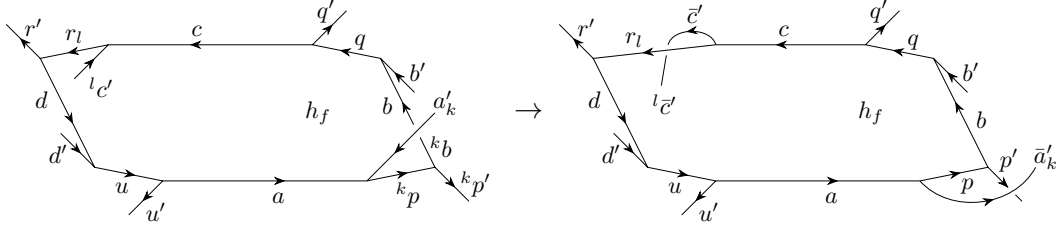
The Hamiltonian on the 3-Torus: BCC lattice

To explicitly construct an important special case of the Hamiltonian on simple polyhedra we pick Γ_K to be the regular cellulation of T^3 by permutohedra which is dual to the BCC triangulation K . We use the branching structure on K obtained from Fig.4.9 via translations. The

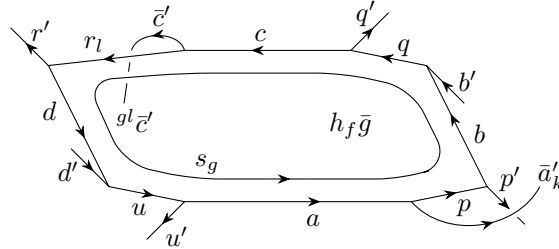
Hamiltonian is given in Eq.(4.35). We proceed to explicitly calculate the matrix elements of the plaquette term $B_f^{g,a}$ for the top face of a permutohedron by deriving the effect of fusing a defect loop a onto the lattice



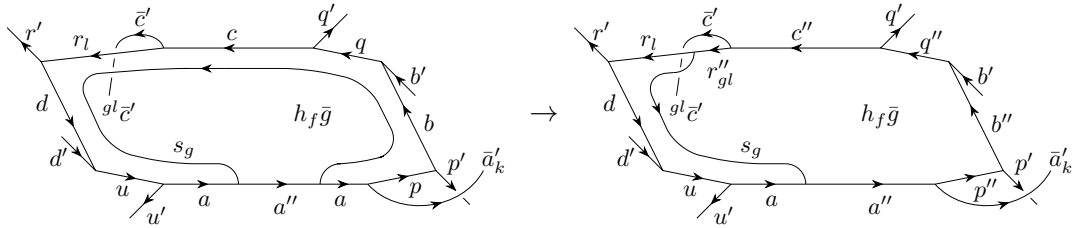
the other terms are calculated similarly. First the 4-valent vertices are resolved using our choice of branching structure. On the resolved lattice we have some initial configuration σ_I which is depicted on the left. Next the edges crossing f are moved aside:



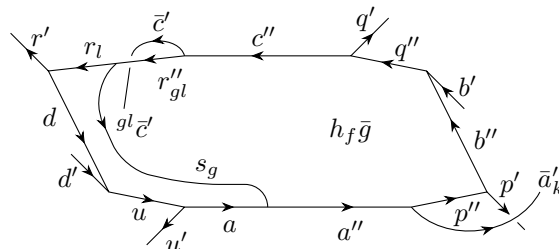
this introduces a factor $U_{k-1}^{-1}(\bar{b}, p; p') \overline{R_a^{p\bar{a}'}} R_c^{l\bar{c}'r}$. The plaquette term $B_f^{g,s}$ introduces a loop of defect s_g onto the face f :



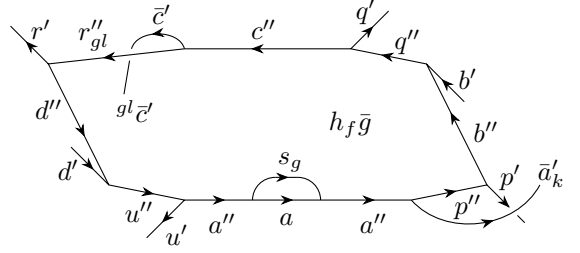
this is then fused into the lattice:



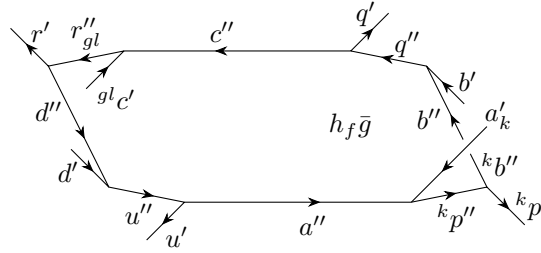
resulting in a factor $F_{a'; \bar{a}p''}^{\bar{a}''sp} F_{p'; \bar{p}q''}^{\bar{p}''sb} F_{b'; \bar{b}q''}^{\bar{b}''sq} F_{q'; \bar{q}c''}^{\bar{q}''sc} F_{c'; \bar{c}r''}^{\bar{c}''sr}$. Next we slide the c' line under a vertex



yielding a factor $\eta_{gl\bar{c}'}(g, l)$. Making three additional F -moves $F_{\bar{r}'; \bar{r}d''}^{\bar{r}''sd}$, $F_{d'; d''u''}^{\bar{d}''su}$, $F_{\bar{u}'; \bar{u}a''}^{\bar{u}''sa}$, leads to



Restoring the lattice to the initial position



yields the final configuration σ_F and a phase $U_{k-1}^{-1}(\bar{b}'', p''; p') R_{a''}^{p''\bar{a}'} \overline{R_{c''}^{gl\bar{c}'r''}}$. Hence the full matrix element of the plaquette term is given by:

$$\langle \sigma_F | B_f^{g,a} | \sigma_I \rangle = U_{k-1}^{-1}(\bar{b}, p; p') U_{k-1}^{-1}(\bar{b}'', p''; p') \eta_{gl\bar{c}'}(g, l) \overline{R_a^{p\bar{a}'}} R_c^{l\bar{c}'r} R_{a''}^{p''\bar{a}'} \overline{R_{c''}^{gl\bar{c}'r''}} \\ F_{a'; \bar{a}p''}^{\bar{a}''sp} F_{\bar{p}'; \bar{p}q''}^{\bar{p}''sb} F_{b'; \bar{b}q''}^{\bar{b}''sq} F_{\bar{q}'; \bar{q}c''}^{\bar{q}''sc} F_{c'; \bar{c}r''}^{\bar{c}''sr} F_{\bar{r}'; \bar{r}d''}^{\bar{r}''sd} F_{d'; \bar{d}u''}^{\bar{d}''su} F_{\bar{u}'; \bar{u}a''}^{\bar{u}''sa}. \quad (4.36)$$

4.4.3 Degeneracy, Statistics, and the Ground State Wave Function

The GSWF of the Hamiltonian in Eq.(4.31) admits a simple PEPS and MERA following the approach of Ref. 84. For a triangulated space manifold (Y, \mathcal{K}) the tensor network is given by

$$Z[\mathcal{K} * v_0] \quad (4.37)$$

where v_0 is an auxiliary vertex below the other vertices in the ordering. To normalize this state properly we use the convention that any weight associated to a simplex at the boundary $w(\Delta_i)$ is included in the state after taking a square root $\sqrt{w(\Delta_i)}$. This ensures that upon gluing along such a boundary the full weight is recovered. In particular

$$\langle Z[\mathcal{K} * v'_0] | Z[\mathcal{K} * v_0] \rangle = Z[\{v'_0, v_0\} * Y] \quad (4.38)$$

assuming the TQFT is unitary (Hermitian). Note in our models these weights are always positive real numbers and the positive square root is chosen, if these weights are negative (or complex) such a convention is not straightforward (for example this occurs in Ref. 274). Similarly for the MERA consider a triangulated identity bordism on some space manifold $(Y \times I, \mathcal{K}')$ such that the triangulation at the space manifold $(Y, 0)$ reduces to the physical lattice \mathcal{K} and we pick a minimal triangulation \mathcal{K}'' of $(Y, 1)$ at the ‘top’ of the MERA corresponding to the ultra IR scale. Then upon fixing a vector containing the fully coarse grained topological information $|t\rangle$ the MERA is given by

$$Z[\mathcal{K}'] |t\rangle \quad (4.39)$$

The PEPS built this way has a virtual PEPO symmetry, to extract the physical superselection sectors corresponding to point and loop like excitations we expect a generalization of Ocneanu's tube algebra can be constructed directly in the tensor network as has been achieved in $(2 + 1)\text{D}$ ⁶⁴.

There is an alternate approach to a tensor network description of the GSWF working directly with the diagrammatic representation of the anyons. For CYWW this yields roughly a 2.5D tensor network representation that is presented with a particular choice of projection down to a plane but transforms trivially under changing this choice²⁷⁵. This approach encounters complications for the UGxBFC model due to the nontrivial action of anyon worldlines upon configurations behind them³¹. Hence it appears this approach may only produce a gswf that transforms with a local unitary upon changing the plane of projection. Note a similar complication may occur for a figure 8 worldline in CYWW, however this can be corrected with a careful labeling of the writhe of each anyon worldline.

In Section 4.2 we discussed how special cases of the UGxBFC recover an uncoupled DW and CY theory, for trivial grading and group action, or a 2-group gauge theory, for a categorical group input. We also pointed out that one can add H^3 and H^4 cocycles to the data of the ungraded case to realize a general 2-group gauge theory with cohomology twist. This suggests an interpretation of the model (at least in the ungraded case) as a theory of anyons coupled to a 2-group gauge theory.

4.5 Discussion

In this section we aim to place the new models into the broader context of previously constructed state sum TQFTs^{82,86,88,90,260–266}. In doing so we sketch the general framework for state sum TQFTs and explain how the UGxBFC model fits into this. We also describe the relation of the UGxBFC model to other classes of $(3 + 1)\text{D}$ state sums and their boundary physics.

It is conventional wisdom that an n -category describes a local or fully extended TQFT restricted to the disc^{220,259,286}. This correspondence is materialized by the general prescription to construct an $(n + 1)\text{D}$ state sum model from an n -category⁸⁴. The recipe dictates that the i -simplices of a triangulation are labeled by i -morphisms of the n -category along with an $(n - 1)$ -associator for each $(n + 1)$ -simplex, a tensor satisfying the Pachner move equations. To make contact with familiar examples, first in $(1 + 1)\text{D}$, one can view the morphisms of a linear category with a single object as an associative algebra. Decorating the edges of a triangulated surface with these morphisms and assigning the structure coefficients to each triangle recovers the familiar Frobenius algebra TQFTs²⁷⁶. For $(2 + 1)\text{D}$ consider a 2-category with a single object, the 1-morphisms and 2-morphisms can be identified with the objects and morphisms of a fusion category respectively. Using these to label the edges and faces of a triangulated 3-manifold and assigning F-symbol associators to each tetrahedron recovers the Turaev-Viro TQFTs (Levin Wen string nets)^{24,108}. In $(3 + 1)\text{D}$ consider a 3-category with a single object and single 1-morphism, the 2- and 3- morphisms can be identified with the objects and morphisms of a braided fusion category. Using these to label the faces and tetrahedra of a triangulated 4-manifold and assigning a 15j-symbol to each 4-simplex recovers the Crane-Yetter TQFTs (Walker-Wang models)^{85,86,261}.

These examples display the general pattern that adding structure to an n -category is often

State Sum	Hamiltonian	Input data	ST Dimension D	Sensitivity	Physical excitations
Trivial/Invertible theory	Trivial paramagnet	-	all D	Classical local invariants: Euler characteristic, signature, ...	Local excitations, no nontrivial superselection sectors
GHZ TQFT (Includes all 2D TQFTs based on Frobenius Algebras ²⁷⁶)	Symmetry breaking	$n \in \mathbb{N}$	all D	π_0	Domain wall excitations
n-group Dijkgraaf-Witten gauge theory ^{72,88} or Yetter homotopy n-type ⁹⁰ (Includes Birmingham-Rakowski model ²⁷⁷ and Mackaay's group examples ²⁶⁴)	Higher group lattice gauge theory (includes twisted quantum doubles ^{19,105,278} , generalized toric codes, 2-group gauge theory ⁸⁹ and Yoshida's models ²⁷⁹)	n-group \mathbb{G} & D-cocycle $\alpha \in H^D(B\mathbb{G}, U(1))$	all $D \geq n$	n-homotopy type (or n-Postnikov system)	Gauge charges, fluxes etc..
Turaev-Viro (Barrett-Westbury) ^{108,219} (dropping semisimplicity assumption gives Kuperberg invariant ^{273,280} and ²⁸¹)	Levin-Wen string-net model ²⁴	UFC \mathcal{C} ²¹⁶	$(2 + 1) D$	PL homeomorphism	$Z(\mathcal{C})$ anyon theory
Crane-Yetter ^{86,261} (captures unitary Broda, Petit, Barenz-Barrett dichromatic state sums ^{255,282-284} via chainmail construction ²⁸⁵)	Walker-Wang model ⁸⁵	UBFC \mathcal{C} ²¹⁶	$(3 + 1) D$	π_1, w_2	Bosons and fermions and loop excitations (only for nonmodular \mathcal{C})
Crane-Frenkel ²⁶³ & Carter-Kauffman-Saito ²⁶²	?	Hopf category and cocycle	$(3 + 1) D$	homotopy ?	?
Kashaev TQFT ^{82,260}	Kashaev model	\mathbb{Z}_n	$(3 + 1) D$	π_1, w_2	Fermions (bosons) and loop excitations for $N = 2 (0) \bmod 4$ (trivial for N odd)
UGxBFC ⁸³ (includes Mackaay's spherical 2-category models ²⁶⁵)	UGxBFC Hamiltonian	UGxBFC \mathcal{C} ^{31,81,97,98}	$(3 + 1) D$	w_2 , homotopy 3-type ?	Bosons, fermions and loop excitations
Conjectural n-category TQFT (semisimplicity condition corresponds to having a single object)	$(n - 1)$ -membrane net Hamiltonian	Unitary n-category \mathcal{C}	all $D = (n + 1)$	PL homeomorphism (except for $D = 4$)	higher categorical center $Z(\mathcal{C})$

equivalent to shifting all the morphisms up a level while introducing a single object. From this point of view it is natural that to resolve the UV anomaly that prevents a $(2 + 1)D$ (commuting projector Hamiltonian) lattice realization of a chiral anyon theory one should consider the boundary of a $(3 + 1)D$ theory. This is precisely what the WW model achieves. It also suggests that to realize the most general $(3 + 1)D$ topological orders (with excitations described by a unitary braided fusion 2-category) with commuting projector Hamiltonians on the lattice one must similarly consider boundary theories of $(4 + 1)D$ state sums.

From the examples above the UGxBFC models appear to be the natural generalization of TV to $(3 + 1)D$ as they correspond to a 3-category with a single object (which can be thought of as a $(2 + 1)D$ topological phase) the 1-morphisms are identified with group elements (invertible gapped boundaries of the $(2 + 1)D$ phase), 2-morphisms between the 1-morphisms g_1 and g_2 correspond to defects in the sector $\mathcal{C}_{g_1^{-1}g_2}$ and 3-morphisms are the regular morphisms in the

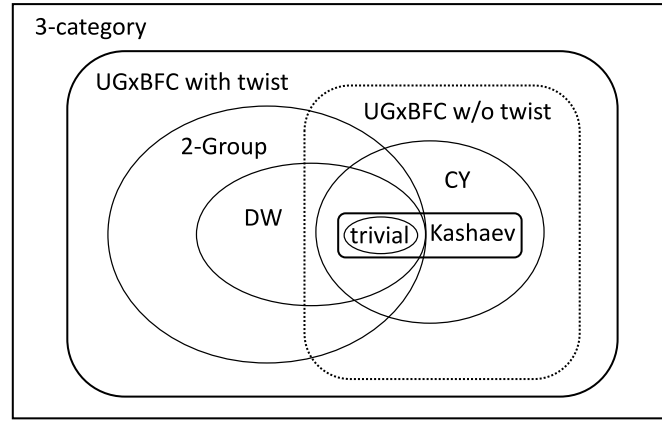


Figure 4.15: Conjectured relations of unitary $(3 + 1)$ D state sum TQFTs (“twist” refers to the addition of various cocycle functions).

UGxBFC. Following the recipe, edges are labeled by group elements, triangles by defects and tetrahedra by UGxBFC morphisms while 4-simplices come with a 15j-symbol.

Notice in all the examples thus far we have considered only n -categories with a single object, loosening this requirement seems to correspond to dropping the assumption of semi simplicity (or possibly simplicity of the unit object)^{273,287}. We conjecture all non chiral topological phases of finite spin models can be realized by a state sum construction from an n -category with a single object. One way to extend the UGxBFC model might be to include multiple objects in the 4-category, this naturally corresponds to considering boundaries between different topological phases rather than the same phase (this corresponds to a tricategory of bimodules which is a Gray category²⁸⁸).

Throughout the paper we have considered anomaly free SETs described by a UGxBFC (the state sums for these are rigorously constructed in Ref. 83), such SETs can be realized purely in $(2 + 1)$ D systems with ultra-local symmetry actions. From the perspective of using $(3 + 1)$ D models to realize anomalous boundary phases it is natural to consider extensions of the model to UGxBFCs with non vanishing H^3 and H^4 anomalies. In the case of a trivial grading (all nontrivial defect sectors empty) the labeling of the triangulation defines a flat 2-group connection. Using the language of Ref. 88 the 2 group specified by $\Pi_1 = G$, $\Pi_2 = \mathcal{A}$ (the abelian anyons) with a group action ρ inherited from the UGxBFC and trivial 3-cocycle. It is possible to augment this construction by adding in a 3-cocycle $\beta \in H^3_\rho(G, \mathcal{A})$, which alters the flatness condition to that of a different 2-group \mathbb{G} . Furthermore one may add in a 4-cocycle $H^4(B\mathbb{G}, U(1))$. Hence these trivially graded models can be understood as a theory of bosons or fermions coupled to a 2-group gauge field. This generalizes the picture of CYWW models as a theory of bosons or fermions coupled to a discrete group gauge field. We leave the details of this to future work²⁷¹.

From this perspective the ungraded UGxBFC models have a deequivariantized or ungauged counterpart given by a 2-group \mathbb{G} -SPT with ultra-local symmetry action. The boundaries of these models can support all anomalous $(2 + 1)$ D SET phases as the bulk serves to resolve the chiral, H^3 and H^4 anomalies¹⁵⁵. Upon gauging or equivariantizing the \mathbb{G} symmetry of these SET models one recovers the ungraded UGxBFC model. These possible additions suggest the intrinsic H^3 and H^4 classes of an anomalous UGxBFC should be treated as a torsor, as they

can be shifted by an arbitrary choice in the ungraded case, although it is unclear how this carries over to the general graded case.

Thus far we have explained how the 2-group and CYWW models are captured as subcases of the UGxBFC construction, furthermore we believe the Kashaev TQFT is equivalent to a subset of the CYWW model and hence is also captured. We have outlined what is conjectured to be the most general construction of a $(3 + 1)$ D state sum in terms of a 3-category. We made the case that restricting to models that have a single object is expected to capture all topological orders with a commuting projector Hamiltonian that admit a TQFT description. These topological orders are also known as gapped quantum liquids²⁸⁹ and they do not include models such as Haah's cubic code^{92,290} even though it admits a generalized gauge theory description^{87,223}, see Chapter 5. The UGxBFC model captures a very general case of the single object 3-category state sum construction, and most importantly the construction comes with a wealth of examples originating from SET phases in $(2 + 1)$ D^{29–31,81,97,98,100–102}.

To assess whether the UGxBFC model truly goes beyond the preexisting constructions one would ideally construct the irreducible excitations and compare their full set of physically accessible topological invariants. In general the construction of the excitations should correspond to taking the Drinfeld double or 2-categorical center of the input treated as a unitary fusion 2-category^{164,211}, this itself is not well understood. The resulting invariants are also not fully understood, although very interesting progress has been made^{291,292} particularly on the 3-loop braiding statistics^{182,293–295}. In principle these invariants should uniquely specify the unitary braided fusion 2-category describing the physical excitations, however it has not even been rigorously shown that the commonly used S and T matrices are in 1-1 correspondence with UBFCs in the $(2 + 1)$ D setting.

We may resort to comparing the boundary physics of the proposed UGxBFC models to previous constructions, but as we have seen the relevant boundaries can be understood as coming from a CYWW model coupled to a 2-group gauge field¹⁵⁵.

Another avenue is to focus on the closed manifold partition functions of the theory. This approach, for example, allows one to differentiate the Turaev-Viro models from Dijkgraaf-Witten in $(2 + 1)$ D as the former is sensitive to PL homeomorphism, while the latter depends only on homotopy. However in $(3 + 1)$ D the situation is complicated by the fact that it is fundamentally impossible for a unitary TQFT to detect all inequivalent smooth structures on homotopic or s-cobordant manifolds²⁷² (this is a consequence of the existence of 3D boundary diffeomorphisms that do not extend into the 4D bulk). Here we should note that the equality (equivalence) of all partition functions is not known to be a sufficient condition for two theories to be equivalent. That being said it has been suggested that the UGxBFC state sum depends on the homotopy 3-type of a manifold⁸³, it can also be seen to depend on some Stiefel-Whitney classes of a manifold as it includes the CYWW model which can involve fermions that are sensitive to a choice of spin structure. These dependencies are consistent with the interpretation of the UGxBFC model as bosons or fermions coupled to a higher group gauge theory. It is currently unclear if the UGxBFC models with nontrivial grading give rise to more general invariants, we plan to study this in future work²⁹⁶.

Finally let us clarify that for the UGxBFC models with non empty defect sectors, the TQFT constructed from the $15j$ -symbol does not depend on extra structure or decoration of the cobordism category (beyond possibly an orientation). That is to say the theory is not an SET involving

physical defects of some global symmetry. However it may be possible that the boundary theory can be thought of as an SET with a certain configuration of defects specified as a boundary condition.

Acknowledgments — The authors acknowledge Meng Cheng, Shawn Cui, Xie Chen, Sujeet Shukla, Jeongwan Haah, Maissam Barkeshli and Parsa Bonderson for helpful discussions and comments. We particularly thank Shawn Cui for sharing a draft of his unpublished thesis. DW acknowledges support from the Austrian Marshall Plan foundation. ZW was partially supported by NSF grants DMS-1108736 and DMS-1411212.

Supplementary Material

4.6 Elementary combinatoric topology

In this appendix we introduce some basic notions from the field of combinatorial topology that are used throughout the paper. We recommend Ref. 267 for further reading.

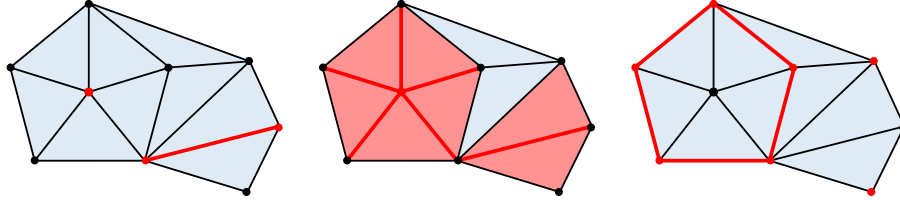


Figure 4.16: Red indicates the closure (left), star (middle) and link (right) of a vertex and an edge.

- An **n-simplex** $\Delta_n = [v_0 \dots v_n]$ is the convex hull of a set of $(n+1)$ points $v_0, \dots, v_n \in \mathbb{R}^{m \geq n}$ such that the vectors $v_1 - v_0, \dots, v_n - v_0$ are linearly independent. The orientation of a simplex can be defined as $\sigma(\Delta_n) := \text{sgn}(\det(v_1 - v_0, \dots, v_n - v_0))$ and satisfies $\sigma([v_0 \dots v_n]) = \text{sgn}(\pi)\sigma([v_{\pi(0)} \dots v_{\pi(n)}])$ for a permutation π . We focus on the combinatorial aspects of simplices, notice the convex hull of any subset of vertices $[v_{i_0} \dots v_{i_j}]$, for $0 \leq j \leq n$, is a j -subsimplex of Δ_n . Hence Δ_n contains $\binom{n+1}{j+1}$ j -subsimplices.
- A **simplicial complex** K is a union of simplices loosely defined as a subset of the power set of $(N+1)$ points $P\{v_0, \dots, v_N\}$ such that $\Delta \in K \implies P(\Delta) \subseteq K$. We exclusively deal with homogeneous simplicial complexes of some dimension D , which can be thought of as a union of D -simplices, in which all K -simplices, for $\dim K < D$, appear as a subsimplex of a D -simplex. The usual definition of simplicial complex requires the intersection of any pair of simplices $\Delta_p \cap \Delta_q$ to be a subsimplex of Δ_p and Δ_q . We also use a weaker notion referred to as a Δ -complex in which the intersection of a pair of simplices may consist of multiple subsimplices.
- The **underlying space** of a simplicial complex K is given by the union of all its simplices (treated as a topological space) denoted by $|K|$.
- The **k-skeleton** of a simplicial complex K , denoted K_k is the union of j -subsimplices $\Delta_j \in K$ with $j \leq k$.
- We often assume the vertices of a simplicial complex have been ordered, this induces an orientation on the edges of the 1-skeleton from lesser to greater adjacent vertex. This orientation is a **branching structure** since the edges on the boundary of a triangle never form a similarly oriented cycle. In fact our arguments only require a branching structure which is a local condition slightly weaker than a global ordering, although we will sometimes assume a global ordering for convenience.
- The **boundary** of a D -simplicial complex K is a $(D-1)$ -simplicial complex ∂K consisting of all $\Delta_{D-1} \in K$ that are the subsimplex of a single D -simplex within K . Note $\partial \circ \partial = 0$.

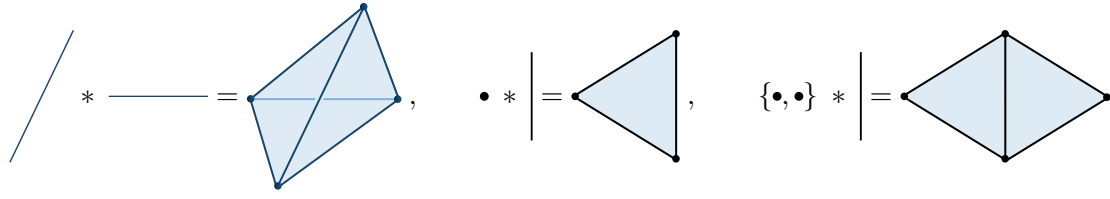


Figure 4.17: The join of two edges (left), cone of an edge (middle) and suspension of an edge (right).

- The **closure** of a collection of simplices $J \subseteq K$ is given by cl_J the minimal subcomplex of K containing J .
- The **interior** of a subcomplex $J \subseteq K$ is given by $\text{int } J := \text{cl}_J \setminus J$.
- The **star** of a subcomplex $J \subseteq K$ is given by st_J the union of simplices in K which have a subsimplex contained in J .
- The **link** of a subcomplex $J \subseteq K$ is given by $\text{lk}_J := \text{cl}_{\text{st}_J} \setminus \text{st}_{\text{cl}_J}$.
- The **join** of two simplices $\Delta_n = [v_0 \dots v_n], \Delta_m = [v_{n+1}, \dots, v_{n+m+1}]$ is the simplex $\Delta_n * \Delta_m = [v_0 \dots v_{n+m+1}] \simeq \Delta_{n+m+1}$. The join of two simplicial complexes K, J is given by $K * J$ the union of all $\Delta_i * \Delta_j, \forall \Delta_i \in K, \forall \Delta_j \in J$ (note this includes joins with the empty simplex $\emptyset * \Delta_j = \Delta_j$). Note the join is associative and commutative (possibly up to orientation reversal). There is a simple relation for any simplex $\Delta_i \in K$ given by $\text{st}_{\Delta_i} = \Delta_i * \text{lk}_{\Delta_i}$.
- The **cone** of a simplicial complex K is its join with a point v given by $v * K$.
- The **suspension** of a simplicial complex K is its join with two points v, v' given by $\{v, v'\} * K$.
- A **bistellar flip (Pachner move)** on any k -simplex $\Delta_k \in K$ is constructed from an auxiliary $(n-k)$ -simplex $\Delta_{n-k} \notin K$ by taking $(K \setminus \text{st}_{\Delta_k}) \cup \text{lk}_{\Delta_k} (\partial \Delta_k * \Delta_{n-k})$ with the identification $\text{lk}_{\Delta_k} \simeq \partial \Delta_k * \partial \Delta_{n-k}$.

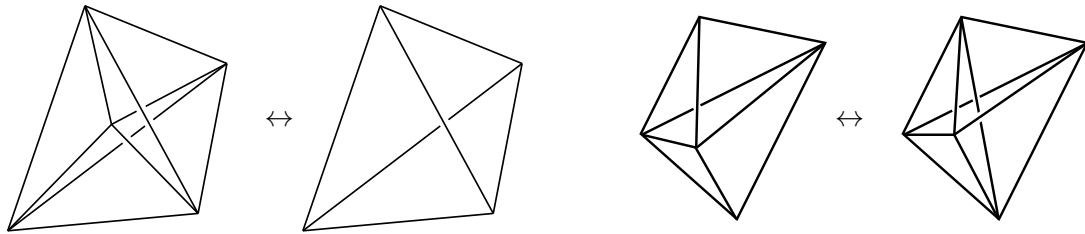


Figure 4.18: The bistellar (Pachner) moves in 3D.

- The **Poincaré dual** of an n -dimensional simplicial complex is an n -dimensional simple polytope with an $(n-k)$ -cell for each k -simplex of the simplicial complex. To construct

this dual one can start by associating a vertex v^i to each simplex $\Delta_n^i \in K$ then iteratively adding a j -cell σ_j for $j = 1, \dots, n$ for each $(n-j)$ -simplex $\Delta_{n-j} \in K$. For $\Delta_{n-j}^i \in K$ we add a j -cell σ_j^i with k_l $(j-1)$ faces, where k_l is the number of $(n-j+1)$ -simplices that intersect $\Delta(n-j)$ in K . Each $(j-1)$ face of σ_j^i is glued to the $(j-1)$ -cell that is dual to the corresponding $(n-j+1)$ -simplex intersecting Δ_{n-j} .

- A piecewise linear (PL) manifold is a topological space equipped with an atlas of coordinate charts such that the transition functions between charts are piecewise linear. Similarly a smooth manifold is a topological space with an atlas of coordinate charts such that the transition functions are smooth. **(Top, PL, Smooth)** is the category of (topological, PL, smooth) manifolds and (continuous, PL continuous, differentiable) maps between them, a (homeomorphism, PL homeomorphism, diffeomorphism) between spaces defines an equivalence. Not all topological manifolds admit a PL structure, an example of minimal dimensionality being Freedman's E_8 4-manifold, and those which do may admit infinitely many inequivalent PL structures, lowest dimensional examples are exotic \mathbb{R}^4 's due to Freedman, Donaldson and Taubes. Note the existence of exotic 4-spheres is unknown and would provide a counter example to the 4D smooth Poincaré conjecture. Similarly not all PL manifolds admit a smoothing, examples of minimal dimension 8 were discovered by Ells, Kuiper and Tamura, and those which do may admit multiple inequivalent smooth structures, minimal dimensional examples given by Milnor's exotic 7-spheres. In general we have $\text{Smooth} \subseteq \text{PL} \subseteq \text{Top}$, while for $D \leq 6$ $\text{Smooth} \simeq \text{PL}$, for $D = 7$ the inclusion $\text{Smooth} \subseteq \text{PL}$ is surjective but not injective and for $D \geq 8$ the inclusion is neither injective nor surjective. For $D \leq 3$ $\text{PL} \simeq \text{Top}$ while for $D \geq 4$ the inclusion is neither injective nor surjective.
- A **triangulation** of a topological manifold X is a simplicial complex K together with a homeomorphism $\phi : |K| \rightarrow X$.
- A **PL triangulation** of a topological manifold X is a simplicial complex K together with a homeomorphism $\phi : |K| \rightarrow X$, satisfying the extra constraint that the link of any vertex lk_v , $v \in K$ is homeomorphic to a PL $(n-1)$ -sphere (not merely a homotopy sphere). For $D \leq 4$ all triangulations are PL, while for $D \geq 5$ one can construct a non PL triangulation by taking two (or more) suspensions of a triangulated Poincaré sphere. According to the discussion above all smooth manifolds admit unique PL triangulations, while topological manifolds admit unique PL triangulations for $D \leq 3$ and may admit anywhere from 0 up to an infinite family of inequivalent PL triangulations for $D \geq 4$. For $D \geq 5$ it was shown by Manolescu that there are manifolds that do not admit PL triangulations but do admit the weaker notion of triangulation.

Chapter 5

Fractal symmetries: ungauging the cubic code

Synopsis:

Gauging is a ubiquitous tool in many-body physics. It allows one to construct highly entangled topological phases of matter from relatively simple phases and to relate certain characteristics of the two. Here we develop a gauging procedure for general submanifold symmetries of Pauli Hamiltonians, including symmetries of fractal type. We show a relation between the pre- and post-gauging models and use this to construct short-range entangled phases with fractal-like symmetries, one of which is mapped to the cubic code by the gauging.

Based on: [223](#)

Dominic J. Williamson,

[Phys. Rev. B **94**, 155128 \(2016\)](#), [arXiv:1603.05182](#).

Changes compared to published version: Minor corrections and formatting changes.

Contributions of the author: This research was carried out and written up by the author. The idea for this research emerged from stimulating discussions with Jeongwan Haah, Norbert Schuch, and Frank Verstraete.

5.1 Introduction

The study of topological order^{9,10} intertwines many rich areas of physics: strongly correlated quantum many-body condensed-matter systems^{24,203}, quantum codes^{19,297,298}, topological quantum field theory (TQFT)^{12,13,220}, and modular tensor categories¹⁶⁶ (and their higher categorical generalizations^{84,259,286,299}). By viewing the same physics through these complementary lenses valuable insights have been gained.

In two dimensions a concise and deep understanding of topological order has solidified in terms of the theory of anyonic excitations^{14,18,63,64,203,300–302} described mathematically by modular tensor categories¹⁶⁶ known to be equivalent to (3-2-1)-extended topological quantum field theories¹⁶⁵. The theory of stabilizer codes in two dimensions is also well understood^{303,304}. It is known that all two-dimensional (2D) stabilizer Hamiltonians possess stringlike logical operators and hence are not self-correcting quantum memories at finite temperature³⁰⁵, and furthermore that they are equivalent to some number of copies of the toric code^{306,307}.

In three dimensions the landscape of possibilities remains shrouded in mystery. Progress has been made via the construction of families of fixed point Hamiltonians^{85,254} and the development of novel tools such as the 3-loop braiding statistics²⁹⁴ (which primarily apply to gauge theories with a possibly anomalous 2D topological boundary) but a general understanding is still lacking. On the other hand novel contributions have been made in assessing the possibility of self-correcting three dimensional (3D) quantum memories^{92,308,309} but a definitive consensus has not been reached. For a nice overview of progress on this topic see the recent review article Ref. 310. Most significantly this search has revealed models^{92,290} that satisfy conventional definitions of topological order and stability and yet are not described by any (conventional) TQFT. Rather than being fixed points under real space blocking renormalization group flow they may bifurcate into multiple copies of themselves³¹¹.

The idea of gauging pervades the literature on topological order in condensed matter systems^{71,73,213,214}. This process makes global symmetries local while allowing one to relate certain physical properties of the pre- and post-gauged systems^{71,73,93}. This is most commonly applied to a truly global and on site symmetry, although it has also been adapted to higher form symmetries^{154,279} that are important in the classification of higher dimensional phases of matter^{155,299}.

In this paper we develop a framework for gauging submanifold symmetries, including those of fractal type, using the language of translationally invariant stabilizer Hamiltonians^{91,312,313}. We then demonstrate relations between physical characteristics of the pre- and post- gauged models. Our formalism includes exotic examples such as Haah’s cubic code⁹² and more conventional examples such as generalized toric codes. We go on to use the tools developed to construct novel cluster states with fractal-type symmetries.

The results presented here share many similarities with those in the concurrent work Ref. 87. In Ref. 87 the authors also develop a gauging duality map and apply it to study what they call fracton topological orders, meaning those with pointlike excitations that are not created by stringlike operators. The fundamental idea underlying the construction of their gauging map, which they call “ F - S ” duality, is the introduction of gauge degrees of freedom to mediate many-body interactions. This is identical to the ideology of our approach, although the execution and applications differ. They explicitly describe their gauging duality for many examples of classi-

cal spin models with what they call subsystem symmetries (which we refer to as submanifold symmetries) including Haah's cubic code⁹² and the model due to Chamon, Bravyi, Leemhuis and Terhal^{314,315}. While the set of examples they consider differs from those here, they are all equally well described using our formalism. Moreover the gauging duality map of Ref. 87 is defined only for classical Ising models and does not allow any local symmetries, which excludes them from gauging the 1-form symmetry of the toric code for example. An advantage of our approach is that it allows one to gauge any quantum model that is described by a spatially local Hamiltonian with a given submanifold symmetry; this goes beyond the classical (diagonal in the computational basis) Ising models considered in Ref. 87.

5.2 Background

In this section we recount several basic notions from the polynomial formalism developed in Refs. 91,313.

Our focus is on Pauli Hamiltonians that are local, translation invariant and consist of a sum of terms that are each tensor products of exclusively Pauli X or Z matrices (We shall loosen the last requirement somewhat in the next section). We use the language of polynomials developed by Haah in Refs. 91,313 as it provides a succinct description of the operators in this setting. In Haah's formalism a Pauli operator is specified by a column of polynomials over \mathbb{Z}_2 . For a translationally invariant system with d spatial dimensions each lattice site is specified by a vector $\mathbf{i} \in \mathbb{Z}^d$; when there are Q qubits per site a single qubit is specified by a pair (\mathbf{i}, q) for $q \in \{1, \dots, Q\}$. A general Pauli operator is then mapped to a column of length $2Q$ with a multivariate polynomial over \mathbb{Z}_2 in each entry as follows:

$$\bigotimes_{\mathbf{i},q} X_{\mathbf{i},q}^{p_{\mathbf{i}}^q} \bigotimes_{\mathbf{i},q} Z_{\mathbf{i},q}^{r_{\mathbf{i}}^q} \mapsto \begin{pmatrix} \mathbf{p} \\ \mathbf{r} \end{pmatrix} \quad (5.1)$$

where $\mathbf{p} = (p^1, \dots, p^Q)$ is a column consisting of entries p^q which are multivariate polynomials over \mathbb{Z}_2 whose $\underline{x}^{\mathbf{i}}$ coefficient is given by $p_{\mathbf{i}}^q \in \{0, 1\}$ (we are using multi-index notation) i.e.

$$p^q = \sum_{\mathbf{i} \in \mathbb{Z}^d} p_{\mathbf{i}}^q x_1^{i_1} \cdots x_Q^{i_Q} \quad (5.2)$$

with similar notation for \mathbf{r} . For example on a two dimensional lattice with two types of qubits r, b per site the operator $X_{(0,0),r} X_{(0,1),r} X_{(1,1),b} Z_{(1,0),r}$ is specified by the polynomial $(1 + y, xy, |x, 0)$ as shown in by

$$\begin{array}{cc} \textcolor{red}{X}\textcolor{blue}{I} - \textcolor{blue}{I}\textcolor{red}{X} & y - xy \\ | & | \\ \textcolor{red}{X}\textcolor{blue}{I} - \textcolor{blue}{Z}\textcolor{red}{I} & 1 - x \end{array} \quad (5.3)$$

A pair of Pauli operators $\begin{pmatrix} \mathbf{p} \\ \mathbf{r} \end{pmatrix}, \begin{pmatrix} \mathbf{s} \\ \mathbf{v} \end{pmatrix}$ commutes iff their symplectic inner product is zero, i.e.

$$\left[\begin{pmatrix} \bar{\mathbf{s}}^T & | & \bar{\mathbf{v}}^T \end{pmatrix} \lambda_Q \begin{pmatrix} \mathbf{p} \\ \mathbf{r} \end{pmatrix} \right]_{\underline{0}} = 0 \quad (5.4)$$

where $\lambda_Q := (ZX) \otimes \mathbb{1}_Q$ is the relevant symplectic form, \bar{s} is the antipode map (sending each monomial summand to its inverse) and the subscript $[\cdot]_0$ denotes the constant term of the polynomial. For convenience we also define the conjugation operation $\left(\frac{\mathbf{s}}{\mathbf{v}}\right)^\dagger := (\bar{\mathbf{s}}^T | \bar{\mathbf{v}}^T)$.

In Haah's formalism the Hamiltonian is identified with a module generated by the stabilizers on the unit cell. More specifically let F be a free module of rank T , think of this as the set of position labels for individual stabilizer terms, and P be the module of Pauli matrices on the lattice. The Hamiltonian module with T types of local interaction terms $\left\{ \begin{pmatrix} \mathbf{p}_t \\ \mathbf{r}_t \end{pmatrix} \right\}_t$ is generated by

$$\sigma := \begin{pmatrix} \mathbf{p}_1 & \dots & \mathbf{p}_T \\ \mathbf{r}_1 & \dots & \mathbf{r}_T \end{pmatrix}$$

which maps $\sigma : F \rightarrow P$. Its symplectic conjugate $\epsilon := \sigma^\dagger \lambda_Q$ maps $\epsilon : P \rightarrow E$, that is from the Pauli module P to the virtual excitation module E ; think of this as the positions of various stabilizer terms that anticommute with a given Pauli operator. The condition that the Hamiltonian is commuting and hence defines a stabilizer code is simply $\epsilon\sigma = 0$ which is equivalent to the sequence

$$F \xrightarrow{\sigma} P \xrightarrow{\epsilon} E$$

forming a complex. It was shown in Refs. 91,313 that the stabilizer Hamiltonian is topologically ordered if the aforementioned sequence is exact, i.e. $\text{im}(\sigma) = \ker(\epsilon)$.

In the case of Calderbank-Shor-Steane (CSS) codes this complex breaks up into a direct sum since we have $\sigma = \sigma_X \oplus \sigma_Z$ and the commutation condition becomes $\sigma_Z^\dagger \sigma_X = 0 = \sigma_X^\dagger \sigma_Z$.

In terms of the bipartite interaction graph of the Hamiltonian, σ can be thought of as mapping from a Hamiltonian node to the qubit nodes in its support (as an operator) and ϵ can be thought of as mapping from a qubit node to the adjacent Hamiltonian nodes with which a Pauli operator on that qudit anticommutes. Note we in fact need to add extra structure to distinguish the X and Z terms in the interaction graph above, alternatively if the Hamiltonian is CSS we can consider separate X and Z interaction graphs, corresponding to σ_X and σ_Z , and the only relevant operators are then either Z or X respectively.

5.3 Gauging

In this section we build up a procedure for gauging submanifold symmetries and analyze the important properties of this gauging map. We start by specifying the type of translationally invariant, symmetric, local Hamiltonians we treat. We then move on to the definition of the gauging procedure and proofs of several results that demonstrate its key features. Finally we describe the relationship between the gauging procedure and translationally invariant, local, CSS stabilizer Hamiltonians and give a construction of cluster state³¹⁶ models with submanifold symmetries.

5.3.1 Hamiltonian construction

Consider a system of “matter” degrees of freedom (Q qubits per site) with Hilbert space \mathbb{H}_m governed by a translationally invariant local Hamiltonian

$$H_m = \sum_{\mathbf{i} \in \mathbb{Z}^d} \sum_k h_{\mathbf{i},k}$$

with a family of on-site symmetry operators generated by a tensor product of X on qubits contained in each closed submanifold of some fixed but arbitrary dimension, possibly fractals with noninteger dimension (note these manifolds only appear as discretizations with a minimum length scale cutoff).

We only consider hypercube local Hamiltonian terms, hence the X symmetry can be specified by hypercube local constraints expressed as products of Z fields that commute with any symmetry operator. These Z constraints can be understood as locally checking whether an operator, which is a tensor product of X s, has the shape of an appropriate submanifold on which it is a symmetry. Associated with these checks is a fundamental object in our framework, the map

$$\eta : F_T \rightarrow P$$

from F_T , a free module of rank T , to P , the Pauli module (T is the number of independent local Z constraints).

In addition to sums and products of these Z constraint fields, a symmetric Hamiltonian may contain arbitrary X perturbations. There are two important irreducible types of X fields, single site X fields and hypercube local X fields that commute with the Z constraints. Hence the set of symmetric field perturbations we consider break up into the local Z constraint fields described by η , the single X terms described by $\mathbb{1}_Q$ and possibly a number S_X of additional X fields described by a map

$$\phi : F_{S_X} \rightarrow P$$

from a free module of rank S_X to the Pauli module, which satisfies $\phi^\dagger \lambda_Q \eta = 0$. These local X fields that commute with the Z constraints are in fact local symmetries of the model, we will largely ignore them for the time being as they become trivial after gauging.

In summary we are considering Hamiltonians that commute with a set of tensor product X operators which might best be described as a *locally defined* symmetry. Such symmetries are concretely defined in terms of a chain complex

$$F_{S_X} \xrightarrow{\phi} P \xrightarrow{\eta^\dagger \lambda_Q} F_T \quad (5.5)$$

with local symmetries given by the image of ϕ and equivalence classes of global symmetries given by the distinct homology classes of the sequence. Note this homology description of a locally defined, tensor product X symmetry is very general and does not rely on a translationally invariant structure or a fixed spatial dimension. This may prove interesting for future work.

An illustrative example is a generalized toric code in d spatial dimensions with qubits on k -cells, X stabilizers on $(k-1)$ -cells and Z stabilizers on $(k+1)$ -cells. This model has $(d-k)$ -manifold (k -form) X symmetry, specified by the local Z stabilizer constraints on the unit cell and their translations (note this analysis extends to an arbitrary cellulation of a closed d -manifold). See Sec. 5.4.1 for a more detailed description of the 2D case.

5.3.2 Gauging procedure

In this section we follow and generalize the approach of Ref. 71 to produce a (nearly) unambiguous gauging procedure for quantum states and operators with submanifold symmetry.

To gauge the Hamiltonian H_m we must first specify the gauge degrees of freedom. We extend the canonical choice for gauging a conventional k -form symmetry, given by associating a gauge field to each $(k+1)$ -cell, with a recipe that also deals with more exotic cases. The gauge and matter Hilbert space $\mathbb{H}_m \otimes \mathbb{H}_g$ is built by tensoring in a gauge qubit for each Z constraint field, i.e. each label in F_T . The locality of this system is described by the bipartite interaction graph of the Z constraint fields, which is generated by η . Hence η can now be thought of as the map from gauge qubits to neighbouring matter qubits, $\eta : F_T \rightarrow F_Q$, we will continue to use this definition below.

The next ingredient in the gauging procedure is a set of local constraints that project onto states satisfying a \mathbb{Z}_2 ‘‘Gauss law’’. This law states that the charge on each matter qubit equals the sum of the fields on the neighbouring gauge qubits. The local gauge constraints are generated by the map

$$\pi := \begin{pmatrix} \mathbb{1}_Q \\ \eta^\dagger \\ 0 \\ 0 \end{pmatrix}. \quad (5.6)$$

Specifically each constraint is given by a projector

$$P_{\mathbf{i},q} := \frac{1}{2}(P_{\mathbf{i},q}(0) + P_{\mathbf{i},q}(1))$$

onto the $+1$ eigenspace of the Pauli operator $\pi \mathbf{x}^\dagger \hat{e}_q$, which is identified with $P_{\mathbf{i},q}(1)$, where \hat{e}_q is the column with a 1 in the q th entry and zeros elsewhere and $P_{\mathbf{i},q}(0) := \mathbb{1}$. The full projector onto the gauge invariant subspace is then given by the product of these local projectors

$$P = \prod_{\mathbf{i},q} P_{\mathbf{i},q}.$$

The state gauging map $G : \mathbb{H}_m \rightarrow \mathbb{H}_m \otimes \mathbb{H}_g$ is given by

$$G|\psi\rangle := P|\psi\rangle \otimes |0\rangle^{\otimes NT}$$

where N is the number of unit cells in the system.

The local projection of an operator onto the gauge invariant subspace is given by

$$\mathcal{P}_\Gamma[\cdot] := \sum_{\mathcal{S}_\Gamma} \bigotimes_{\mathbf{i},q} P_{\mathbf{i},q}(s_{\mathbf{i}}^q) \big|_\Gamma [\cdot] \bigotimes_{\mathbf{i},q} P_{\mathbf{i},q}(s_{\mathbf{i}}^q) \big|_\Gamma$$

where $\big|_\Gamma$ denotes the restriction of an operator onto the qubits within the region Γ and the sum is over the set of variables $\mathcal{S}_\Gamma := \{s_{\mathbf{i}}^q\} \in \{0,1\}^{|\Gamma|}$. Then the corresponding operator gauging map is defined by

$$\mathcal{G}[O] := \mathcal{P}_\Gamma[O \bigotimes_{v \in \Gamma} |0\rangle \langle 0|_v]$$

where Γ is a (minimal) region containing $\text{supp}(O)$ that is generated by a set of points corresponding to gauge qubits in the interaction graph and their neighbours under η .

The matter Hamiltonian is gauged in a locality preserving way as follows:

$$H_m^{\mathcal{G}} := \sum_{\mathbf{i}, k} \mathcal{G}[h_{\mathbf{i}, k}].$$

To construct the full gauged Hamiltonian in a nontrivial way we must also specify some fields H_B that describe dynamics of the gauge spins. We will introduce these fields in the zero gauge coupling limit where the gauge degrees of freedom are frozen to have ‘zero magnetic flux’ (this is analogous to a flatness condition on a finite group connection) perturbations away from this point are considered later. Note the H_B fields are only defined within the gauge invariant subspace and so should commute with all local gauge constraints. The Z fields commuting with all $P_{\mathbf{i}, q}$ are precisely those described by polynomials in the kernel of η , in addition we require them to be a set of independent generators that are local to a hypercube and are hence described by a map μ which generates the kernel of η .

The full gauged Hamiltonian is then given by

$$H_{\text{full}} := H_m^{\mathcal{G}} + \Delta_B H_B + \Delta_P H_P$$

where $\Delta_B, \Delta_P > 0$ and H_P is the sum of all local gauge projectors. From the definitions of the various Hamiltonian terms one can see that

$$[H_m, H_B] = [H_B, H_P] = [H_P, H_m] = 0.$$

For Δ_P sufficiently large the low energy subspace of this Hamiltonian is gauge invariant, with a true gauge theory being recovered in the limit $\Delta_P \rightarrow \infty$. When Δ_B is also sufficiently large the states relevant to the low energy physics are those within the gauge invariant subspace that also have ‘flat’ gauge connections (specified by the μ constraints).

This full gauged Hamiltonian is equivalent, via a constant depth circuit U_D of local isometries, to another Hamiltonian where the gauge has been fixed to remove the local gauge constraints thus restoring a clear tensor product structure to the gauge invariant physics. The circuit is constructed from a product of controlled- X gates from each matter qubit to each of its adjacent gauge qubits (under the map η^\dagger). Note this unitary disentangles each local gauge constraint $P_{\mathbf{i}, q}$ such that it becomes a projector onto the $|+\rangle$ -state of the single qubit at site (\mathbf{i}, q) . Hence the full disentangling isometry U_D is given by

$$U_D := \bigotimes_{\mathbf{i}, q} \langle + | \prod_{\mathbf{i}, q} \prod_{\mathbf{x}^{\mathbf{i}} \hat{e}_t \in \eta^\dagger \mathbf{x}^{\mathbf{i}} \hat{e}_q} CX_{(\mathbf{i}, q) \rightarrow (\mathbf{j}, t)}. \quad (5.7)$$

Now the disentangled Hamiltonian, which acts purely on the gauge qubits remaining, is given by

$$U_D H_{\text{full}} U_D^\dagger = \hat{H}_m^{\mathcal{G}} + \Delta_B H_B$$

where $\hat{H}_m^{\mathcal{G}} = \sum_{\mathbf{i}, k} U_D \mathcal{G}_{\Gamma_{\mathbf{i}}}^k[h_{k, \mathbf{i}}] U_D^\dagger$ is again a sum of local terms.

We close the section by giving a summary of the full gauging and disentangling procedure in terms of its effect on local symmetric Pauli terms. In the polynomial language these are as follows

$$\mathbf{x}^{\mathbf{i}} \hat{e}_q \mapsto \eta^\dagger \lambda_Q \mathbf{x}^{\mathbf{i}} \hat{e}_q \quad (5.8)$$

$$\eta \mathbf{x}^{\mathbf{i}} \hat{e}_t \mapsto \mathbf{x}^{\mathbf{i}} \hat{e}_t. \quad (5.9)$$

Eq.(5.8) describes the mapping of a single qubit X to a product of X terms on the neighbouring gauge qubits and Eq.(5.9) describes the mapping of a minimal symmetric Z field (which is necessarily generated by η) to a single Z on the corresponding gauge qubit. Note these mappings suffice to describe the transformation of all local symmetric tensor products of Pauli matrices. In general the choice of \mathbf{p} generating a set of symmetric Z fields $\eta\mathbf{p}$ may not be unique since the kernel of η may be nontrivial. The exact term obtained is determined by the local support set Γ that is chosen when gauging the symmetric Z fields. All choices for gauging this term are related by some local fields in $H_{\mathcal{B}}$ since it is generated by μ which also generates the kernel of η . Hence all such choices have an equivalent action upon the ground space provided $\Delta_{\mathcal{B}}$ is sufficiently large.

In summary we have constructed a bipartite graph determined by the X symmetry which is specified in the polynomial language by η . The gauging procedure sends single site X terms to a product of X s on the neighbouring gauge bits and symmetric Z terms (which necessarily lie in the image of η) to a local term in their preimage under η . Additional local Z fields were also introduced in terms of the map μ which generates the kernel of η . Hence we have a CSS stabilizer Hamiltonian specified by the *gauging complex*

$$F \xrightarrow{\sigma} P \xrightarrow{\epsilon} E \quad (5.10)$$

where $\sigma = \eta^\dagger \oplus \mu$ and $\epsilon = \sigma^\dagger \lambda_Q$. Note the additional Z terms are noncommuting perturbations to this code Hamiltonian.

5.3.3 Basic properties of the gauging procedure

The mantra of gauging is ‘global symmetry to local symmetry’. This is made precise in the gauging procedure above as follows; any symmetry specified by a subset of qubits M of the original model

$$X(M) := \bigotimes_{(\mathbf{i},q) \in M} X_{\mathbf{i},q}$$

can be reconstructed from the local symmetries of the gauged model, i.e.

$$\prod_{(\mathbf{i},q) \in M} P_{\mathbf{i},q}(1) = X(M) \otimes \mathbb{1}_g$$

where g indicates the gauge subsystem.

Gauging in the zero coupling limit (described above in terms of the maps G, \mathcal{G}) provides an equivalence between the gauged and ungauged models in that the operator gauging map is invertible (in a sense) and furthermore all symmetric expectation values are preserved. We proceed to show this below. For the remainder of the section we use the labeling convention that (\mathbf{j}, t) are gauge qubits while (\mathbf{i}, q) are matter qubits.

Proposition 14. *The operator gauging map is invertible for symmetric operators O in the following sense: $\text{Tr}_{(\mathbf{j},t) \in \Gamma} (\mathcal{G}[O] \cdot \bigotimes_{(\mathbf{j},t) \in \Gamma} |0\rangle \langle 0|) = O$.*

Proof. This is simply a calculation

$$\begin{aligned} \text{Tr}_{(\mathbf{j},t) \in \Gamma} \left(\mathcal{G}[O] \cdot \bigotimes_{(\mathbf{j},t) \in \Gamma} |0\rangle \langle 0| \right) &= \sum_{\mathcal{S}_\Gamma} \bigotimes_{(\mathbf{i},q) \in \Gamma} X_{\mathbf{i},q}^{s_{\mathbf{i}}^q} O \bigotimes_{(\mathbf{i},q) \in \Gamma} X_{\mathbf{i},q}^{s_{\mathbf{i}}^q} \prod_{(\mathbf{j},t) \in \Gamma} \delta \left(\sum_{\eta^\dagger \underline{\mathbf{x}}^{\mathbf{i}} \hat{e}_q \ni \underline{\mathbf{x}}^{\mathbf{j}} \hat{e}_t} s_{\mathbf{i}}^q \right) \\ &= O \end{aligned}$$

the only nontrivial step is realizing that whenever the variables $s_{\underline{i}}^q$ satisfy the δ condition the operator $\bigotimes_{(\underline{i},q) \in \Gamma} X_{\underline{i},q}^{s_{\underline{i}}^q}$ is a symmetry and hence commutes with O by assumption. \square

Lemma 2. *The operator $G^\dagger G$ projects onto the symmetric subspace.*

Proof. Again this is simply a calculation

$$G^\dagger G = \sum_{S_\Lambda} \sum_{\bar{S}_\Lambda} \bigotimes_{(\underline{i},q) \in \Lambda} X_{\underline{i},q}^{s_{\underline{i}}^q + \bar{s}_{\underline{i}}^q} \prod_{(\underline{j},t) \in \Gamma} \delta \left(\sum_{\eta^\dagger \underline{x}^{\underline{i}} \hat{e}_q \ni \underline{x}^{\underline{j}} \hat{e}_t} s_{\underline{i}}^q + \bar{s}_{\underline{i}}^q \right)$$

where Λ is the full interaction graph (note the sums are only over matter qubits (\underline{i}, q) and the product is over the gauge qubits (\underline{j}, t)). Observe that due to the δ condition this is by definition the sum over all symmetries of the model. \square

Lemma 3. *The identity $\mathcal{G}[O]G = GO$ holds for any symmetric local operator O .*

Proof. Once again this is simply a calculation

$$\begin{aligned} \mathcal{G}[O]G &= \sum_{\bar{S}_\Gamma} \bigotimes_{(\underline{i},q) \in \Gamma} X_{\underline{i},q}^{\bar{s}_{\underline{i}}^q} O \bigotimes_{(\underline{i},q) \in \Gamma} X_{\underline{i},q}^{\bar{s}_{\underline{i}}^q} \bigotimes_{(\underline{j},t) \in \Gamma} \left| \sum_{\eta^\dagger \underline{x}^{\underline{i}} \hat{e}_q \ni \underline{x}^{\underline{j}} \hat{e}_t} \bar{s}_{\underline{i}}^q \right\rangle \\ &\quad \times \left\langle \sum_{\eta^\dagger \underline{x}^{\underline{i}} \hat{e}_q \ni \underline{x}^{\underline{j}} \hat{e}_t} \bar{s}_{\underline{i}}^q \right| \sum_{S_\Lambda} \bigotimes_{(\underline{i},q) \in \Lambda} X_{\underline{i},q}^{s_{\underline{i}}^q} \bigotimes_{(\underline{j},t) \in \Lambda} \left| \sum_{\eta^\dagger \underline{x}^{\underline{i}} \hat{e}_q \ni \underline{x}^{\underline{j}} \hat{e}_t} s_{\underline{i}}^q \right\rangle \\ &= \sum_{\bar{S}_\Gamma} \sum_{S_\Lambda} \bigotimes_{(\underline{i},q) \in \Lambda} X_{\underline{i},q}^{s_{\underline{i}}^q} \bigotimes_{(\underline{i},q) \in \Gamma} X_{\underline{i},q}^{s_{\underline{i}}^q + \bar{s}_{\underline{i}}^q} O \bigotimes_{(\underline{i},q) \in \Gamma} X_{\underline{i},q}^{s_{\underline{i}}^q + \bar{s}_{\underline{i}}^q} \prod_{(\underline{j},t) \in \Gamma} \delta \left(\sum_{\eta^\dagger \underline{x}^{\underline{i}} \hat{e}_q \ni \underline{x}^{\underline{j}} \hat{e}_t} s_{\underline{i}}^q + \bar{s}_{\underline{i}}^q \right) \\ &\quad \bigotimes_{(\underline{j},t) \in \Lambda} \left| \sum_{\eta^\dagger \underline{x}^{\underline{i}} \hat{e}_q \ni \underline{x}^{\underline{j}} \hat{e}_t} s_{\underline{i}}^q \right\rangle \\ &= GO \end{aligned}$$

where the final step follows from the δ condition and the symmetry of O . \square

Proposition 15. *Any matrix element of a local symmetric operator O taken with respect to a symmetric state $|\psi_0\rangle$ and an arbitrary state $|\psi_1\rangle$ is preserved by the gauging procedure i.e. $\langle \psi_0 | O | \psi_1 \rangle = \langle \psi_0 | G^\dagger \mathcal{G}[O] G | \psi_1 \rangle$.*

Proof. We have

$$\begin{aligned} \langle \psi_0 | G^\dagger \mathcal{G}[O] G | \psi_1 \rangle &= \langle \psi_0 | G^\dagger G O | \psi_1 \rangle \\ &= \langle \psi_0 | O | \psi_1 \rangle \end{aligned}$$

where the first equality follows from Lemma 3 and the second from Lemma 2. \square

Lemma 4. *The states $\{G|\lambda\rangle\}$, for a basis $\{|\lambda\rangle\}$ of H_m , span the ground space of $\Delta_B H_B + \Delta_P H_P$ with $\Delta_B, \Delta_P > 0$.*

Proof. As discussed in Section 5.3.2 the ground space of H_P is spanned by the states $\{P|\lambda\rangle \otimes |\psi\rangle\}$ for bases $\{|\lambda\rangle\}, \{|\psi\rangle\}$ of $\mathbb{H}_m, \mathbb{H}_g$ respectively. To restrict to the ground space of H_B we consider the computational basis for \mathbb{H}_g which consists of states $|\mathcal{S}_\Lambda\rangle = \bigotimes_{\mathbf{i},q} X_{\mathbf{i},q}^{s_{\mathbf{i}}^q} |0\rangle^{\otimes |\Lambda|}$. Since each local field in H_B commutes with P the combined ground space is spanned by states $\{P|\lambda\rangle \otimes |\mathcal{S}_\Lambda\rangle\}$ where $[\bigotimes_{\mathbf{i},q} X_{\mathbf{i},q}^{s_{\mathbf{i}}^q}, H_B] = 0$; i.e. the X terms correspond to polynomials in the kernel of μ^\dagger . We only treat the exact case where $\ker(\mu^\dagger) = \text{im}(\eta^\dagger)$ (this is always true for our constructions from topologically ordered CSS codes see Sec. 5.3.5, if this assumption is loosened one must deal more carefully with the ground space⁹³ see Chapter 1) then the only relevant states in \mathbb{H}_g are generated by a Pauli operator of the form $\eta^\dagger \mathbf{p}$.

Note we have the relation $PP_{\mathbf{i},q}(1) = P$ hence

$$PP_{\mathbf{i},q}(1)|_g = PP_{\mathbf{i},q}(1)|_m \quad (5.11)$$

where $|_g|_m$ denotes the restriction of the operator onto the gauge or matter qubits respectively. Since any Pauli operator specified by $\eta^\dagger \mathbf{p}$ is of the form $\prod_{\mathbf{i},q} P_{\mathbf{i},q}(1)|_g$ the ground space of $\Delta_B H_B + \Delta_P H_P$ is spanned by states

$$\begin{aligned} P|\lambda\rangle \otimes \prod_{\mathbf{i},q} P_{\mathbf{i},q}(1)|_g |0\rangle^{\otimes |\Lambda|} &= P \prod_{\mathbf{i},q} P_{\mathbf{i},q}(1)|_m |\lambda\rangle \otimes |0\rangle^{\otimes |\Lambda|} \\ &= G \prod_{\mathbf{i},q} P_{\mathbf{i},q}(1)|_m |\lambda\rangle \end{aligned}$$

where we have used Eq.(5.11). Hence the ground space is spanned by states of the form $\{G|\lambda\rangle\}$. \square

Proposition 16. *The gauging procedure preserves a gap; i.e. if H_m has a uniform constant energy gap then H_{full} does too, provided the constants Δ_B, Δ_P are sufficiently large.*

Proof. By Lemma 4, for $\Delta_B, \Delta_P > 0$ sufficiently large, the ground space of H_{full} is spanned by states of the form $\{G|\lambda\rangle\}$. Since $H_m^G = \sum_{\mathbf{i},k} \mathcal{G}_{\Gamma_{\frac{1}{2}}}^k[h_{\mathbf{i},k}]$ is a sum of gauged local operators Lemma 3 implies that, for any matter eigenstate $H_m|\lambda\rangle = \lambda|\lambda\rangle$, we have $H_m^G G|\lambda\rangle = \lambda G|\lambda\rangle$. Hence H_{full} has the same lowest eigenvalue as H_m (assuming a symmetric ground state) and gap $\Delta_{\text{full}} \geq \min(\Delta_m, \Delta_B, \Delta_P)$. \square

We remark that Proposition 16 implies that gauging defines a function from the set of gapped phases of the ungauged model into the set of gapped phases of the gauged model. That is, Hamiltonians from the same symmetry protected phase must land in the same phase of the gauged model.

5.3.4 Properties of the gauging complex

Recall the *gauging complex*

$$F \xrightarrow{\sigma} P \xrightarrow{\epsilon} E \quad (5.12)$$

defined in terms of the maps involved in the gauging procedure $\sigma = \eta^\dagger \oplus \mu$. By focusing on the maps in the gauging complex one can infer interesting relationships between quantities pre- and post- gauging.

Firstly any product of the generating symmetric Z fields which multiplies to identity in the initial model gives an element $\mathbf{p} \in \ker(\eta)$ and hence a Z symmetry of the gauged model. Furthermore when the gauging complex is exact and the gauged model is topologically ordered $\ker(\eta)$ is generated by the map μ and hence $\mathbf{p} = \mu \mathbf{r}$, $\exists \mathbf{r}$. Then μ describes the minimal local Z -fields that commute with the gauged X terms.

Secondly any X symmetry of the initial model is an element $\mathbf{p} \in \ker(\eta^\dagger)$ which specifies a product of X stabilizers equal to the identity, i.e. a redundant X stabilizer, in the gauged model. This is relevant in the calculation of the number of qubits encoded into the ground space of the gauged model, which also requires information about redundant Z stabilizers.

Notice that the gauging procedure is in fact a duality map, in that applying it twice takes us back to the original model. To achieve this duality we consider gauging the Z symmetry, generated by μ , of the gauged model. The local X fields commuting with this symmetry are generated by η^\dagger , any product of them equal to identity is in $\ker(\eta^\dagger)$ by definition and gives a symmetry of the twice gauged model. Let ϕ be a local map generating $\ker(\eta^\dagger)$, then ϕ describes the independent local X fields that commute with the Z stabilizers of the twice gauged model. These twice gauged Z terms are given by η . Note these are precisely the local commuting Z and X fields in the the initial stabilizer Hamiltonian. This suggests an addition to the picture of the gauging complex, completing the circle of gauging

$$\begin{array}{ccccc}
 F & \xrightarrow{\sigma} & P & \xrightarrow{\epsilon} & E \\
 \parallel & & & & \parallel \\
 \hat{E} & \xleftarrow{\hat{\epsilon}} & \hat{P} & \xleftarrow{\hat{\sigma}} & \hat{F}
 \end{array} \tag{5.13}$$

where $\hat{\sigma} := \phi \oplus \eta$, & $\hat{\epsilon} = \hat{\sigma}^\dagger \lambda_Q$.

Collecting these facts together, we note the number of encoded qubits in the ungauged model is

$$N[Q - T + S_Z - S_X] + C_m$$

where N is the number of unit cells, Q is the number of matter qubits per site, $T = \text{rank}(\eta)$ is the number of local Z stabilizers, $S_Z = \text{rank}(\mu)$ is the number of redundant Z stabilizers locally, $S_X = \text{rank}(\phi)$ is the number of independent local X symmetries and C_m accounts for global products of X and Z stabilizers that multiply to the identity upon taking closed boundary conditions for the matter model. The number of encoded qubits in the gauged model is given by

$$N[T - Q + S_X - S_Z] + C_g$$

where T now corresponds to the number of gauge qubits per site, Q is the number of local X stabilizers, S_X is the number of redundant X stabilizers locally, S_Z is the number of independent local Z stabilizers and again C_g accounts for global products of X and Z stabilizers that multiply to the identity upon taking closed boundary conditions for the gauged model.

5.3.5 A construction from CSS stabilizer Hamiltonians

In light of the above discussion it is clear that from a complex corresponding to a topological CSS stabilizer code

$$F \xrightarrow{\sigma} P \xrightarrow{\epsilon} E \quad (5.14)$$

where $\sigma = \sigma_X \oplus \sigma_Z$, one can read off a gauging duality. This duality is specified in our language by the maps $\eta = \sigma_X^\dagger$ and $\mu = \sigma_Z$. Hence the ungauged Hamiltonian is generated by $\phi \oplus \sigma_X^\dagger$ (with $\text{im}(\phi) = \ker(\sigma_X)$) with local symmetric X field perturbations ($\mathbb{1}_Q, |0\rangle$).

From this analysis we see that if $\ker(\sigma_X)$ is locally trivial, in the sense that it contains no local elements, then the ungauged Hamiltonian possesses only global symmetries and the stabilizers are all Z fields (see the examples in Section 5.4). This point highlights a difference between the cubic code and generalized toric codes, while both the respective ungauged variants may have a growing number of global X symmetries (one for each redundant X stabilizer) the former has no local symmetries whereas the latter has an extensive number. This is relevant to the distinct behaviours of their ground state degeneracies. We speculate that it is indicative of spatially extended vs. isolated pointlike excitations

5.3.6 Cluster state construction & gauging

We now go slightly beyond CSS stabilizers and consider cluster state models built on bipartite graphs specified by the map η from the gauging procedure for some CSS Hamiltonian. By construction this cluster state inherits the X symmetry of the input ungauged model (corresponding to $\ker(\eta^\dagger)$) on one sublattice and an X symmetry on the other sublattice in the position of each Z symmetry of the input gauged model. This cluster model is clearly short-range entangled (SRE) since it can be mapped to a trivial decoupled model via a local circuit of CZ s. However this disentangling does not respect the symmetries. Hence these cluster states are candidates for higher form or fractal symmetry-protected topological (SPT) ^{27,35,36,56,242} states.

Several different approaches could be taken when gauging these cluster models. We take advantage of the natural bipartite structure of the system and treat the two disjoint sublattices separately. Since the terms appearing on a single sublattice are either single X s or products of Z s, generated by η or η^\dagger respectively, one can instantly read off the effect of gauging one sublattice. Specifically it results in a doubling of the qubits on the remaining sublattice with each X, Z field on that lattice now accompanied by a Z, X term, respectively, on the new partner qubit.

Z fields generated by either μ or ϕ , depending on the sublattice gauged, are also added to the new qubits. These intermediate models can possess topological order since they are equivalent to either the input gauged or ungauged model under a local circuit of CZ s. However these gates do not respect the symmetry on the remaining sublattice, which is indicative of the possibility of symmetry-enriched topological (SET) ^{29–31,97,98,100,101} order.

Once both sublattices have been gauged one can easily see that the model is mapped to itself up to local swaps and Hadamards.

5.4 Fractal Symmetries

In this section we present several examples which consist of pairs of models that are dual under gauging and support interesting symmetries.

5.4.1 2D toric code - Ising model

The toric code is a CSS code that is known to be equivalent to a \mathbb{Z}_2 gauge theory (see Section 3 of Ref. 19 and also Ref. 317). In the polynomial language the toric code is generated by $\sigma_X = (x + xy, y + xy)$, $\sigma_Z = (1 + x, 1 + y)$, graphically

$$\begin{array}{cc} IX & \cdot & XX \\ | & & | \\ II & - & XI \end{array} \quad \begin{array}{cc} IZ & - & II \\ | & & | \\ ZZ & - & ZI \end{array} . \quad (5.15)$$

The map $\eta = \sigma_X^\dagger$ determined by the X stabilizers corresponds to the 2D Ising model, generated by the terms $(0, 1 + y)$, $(0, 1 + x)$

$$\begin{array}{cc} Z & - & I \\ | & & | \\ Z & - & I \end{array} \quad \begin{array}{cc} I & - & I \\ | & & | \\ Z & - & Z \end{array} \quad (5.16)$$

with X perturbations generated by $(1, 0)$.

Note that when gauging the Ising model one encounters a situation in which $\ker(\eta)$ is non-trivial and is generated by σ_Z as expected. To see this explicitly consider a product of terms from Eq.(5.16) around a plaquette that yields the identity.

5.4.2 3D cubic code - fractal symmetry Ising model

The cubic code is a 3D CSS code generated by

$$\sigma_X = \begin{pmatrix} x + y + z + xyz \\ 1 + y + xy + yz \end{pmatrix} \quad \sigma_Z = \begin{pmatrix} x + y + xy + xyz \\ 1 + xy + yz + xz \end{pmatrix}$$

or graphically

$$\begin{array}{ccc} IX & \text{---} & XI \\ / & & / \\ XI & \text{---} & II \\ | & & | \\ & XX & \\ | & & | \\ IX & \text{---} & XI \end{array} \quad \begin{array}{ccc} IZ & \text{---} & ZI \\ / & & / \\ ZI & \text{---} & ZZ \\ | & & | \\ & II & \\ | & & | \\ IZ & \text{---} & ZI \end{array} \quad (5.17)$$

the gauging map η specifies the ungauged cubic code, a type of ‘Ising’ model, with Z stabilizers generated by

$$(0, 1 + xy + xz + yz), (0, x + z + xz + xyz) \quad (5.18)$$

$$\begin{array}{ccc} Z & \text{---} & I \\ / & & / \\ I & \text{---} & Z \\ | & & | \\ & I & \\ | & & | \\ Z & \text{---} & I \end{array} \quad \begin{array}{ccc} I & \text{---} & Z \\ / & & / \\ Z & \text{---} & Z \\ | & & | \\ & I & \\ | & & | \\ I & \text{---} & Z \end{array}$$

and single qubit X perturbations. This model has a fractal X symmetry for each product of stabilizers equal to the identity in the cubic code.

5.4.3 Self dual cluster models

The first cluster model is derived from the 2D toric code and has stabilizers

$$\begin{array}{ccc}
 \begin{array}{c} IZ \cdots II \\ | \quad | \\ \cdots (X) \cdots \\ | \quad | \\ ZZ \cdots ZI \end{array} &
 \begin{array}{c} Z \cdots I \\ | \quad | \\ \cdots (XI) \cdots \\ | \quad | \\ Z \cdots I \end{array} &
 \begin{array}{c} I \cdots I \\ | \quad | \\ \cdots (IX) \cdots \\ | \quad | \\ Z \cdots Z \end{array}
 \end{array} \quad (5.19)$$

where the matter sublattice has a single qubit per site (blue) and the gauge sublattice has two (red). This model has a 1D (1-form) X symmetry on the red sublattice and a global (0-form) X symmetry on the blue sublattice.

The previous example fits into a broad class of cluster states in arbitrary dimension d with qubits on $(k-1)$ - and (k) - cells. These cluster states are constructed on the bipartite adjacency graph of these cells and possess $(d-k)$ - and $(k-1)$ - form X symmetry.

The second cluster state model comes from the cubic code and has stabilizers

$$\begin{array}{ccc}
 \begin{array}{c} IZ \quad \quad ZI \\ \diagdown \quad \diagup \\ ZI \quad \quad ZZ \\ | \quad | \\ \cdots X \cdots \\ | \quad | \\ II \quad \quad IZ \\ \diagup \quad \diagdown \\ IZ \quad \quad ZI \end{array} &
 \begin{array}{c} Z \cdots I \\ | \quad | \\ I \cdots I \\ | \quad | \\ \cdots XI \cdots \\ | \quad | \\ Z \cdots Z \\ | \quad | \\ Z \cdots I \end{array} &
 \begin{array}{c} I \cdots Z \\ | \quad | \\ Z \cdots I \\ | \quad | \\ \cdots IX \cdots \\ | \quad | \\ Z \cdots Z \\ | \quad | \\ I \cdots I \end{array}
 \end{array} \quad (5.20)$$

using the same sublattice conventions as above. One can see by inspecting the pictures that all translations of these terms commute.

This model supports fractal X symmetries on each sublattice. It inherits an X symmetry on the red sublattice for each X symmetry of the cubic code and an X symmetry on the blue sublattice for each X symmetry of the ungauged cubic code.

5.5 Conclusions

In this paper we have defined a gauging procedure for general submanifold symmetries, including those of fractal type, within the framework of Pauli Hamiltonians. We demonstrated relations between the pre- and post- gauging models reminiscent of those obtained via the conventional gauging procedure. Using the tools developed in this process we constructed short-range entangled Ising and cluster models with fractal symmetries and examined their transformation under gauging.

This gauging procedure constitutes a small step towards adapting the standard tools from the condensed matter toolbox for application to more exotic 3D topological orders, including

cases where the common sense assumptions leading to a TQFT description are not satisfied³¹¹. We are optimistic that this path leads to a cache of strange and exotic phases of matter beyond (conventional) TQFTs, citing Haah's cubic code⁹² as a demonstrative example.

Our approach opens the door to more general constructions and a possible relation between SRE fractal-symmetric and exotic topological phases similar to the well known connection between SPT phases and Dijkgraaf-Witten theories^{72,93}. In particular the gauging procedure applied to a subgroup of the global symmetry allows one to construct and study fractal SET phases. The fractal symmetries in this context may play a role in understanding the most general transversal gates in topological codes^{204,206} and a connection of these phases of matter to quantum computation^{134,136}.

Acknowledgments — The author acknowledges Frank Verstraete, Norbert Schuch and especially Jeongwan Haah for helpful discussions (and for the use of his figures), Jacob Bridgeman and Sam Roberts for comments, trivia with the CB and is grateful to the Berkeley Simons Institute and the organizers of the Quantum Hamiltonian Complexity program where this work originated and also to the quantum theory group at the University of Sydney where it was written up.

Discussion and outlook

In this thesis we have established a powerful approach to the extraction of emergent physical properties of a quantum state from the local entanglement structure of its constituent degrees of freedom. Our approach was founded on the principles of locality, linearity and symmetry, which were brought together in the study of the MPO symmetry algebra of local PEPS tensors. From these MPO symmetries, which constrain the pattern of local correlations in the resulting quantum states, we outlined how the emergent SET order could be extracted.

In Chapter 1 we introduced a formalism for the description of global symmetry in PEPS in terms of MPO group representations and the symmetry-enriched pulling through condition. We applied our formalism to SPT phases, and provided a detailed description of the emergent physical data. This included the anomalous action of the symmetry upon the edge degrees of freedom, and a construction of the topological order that results from gauging the global symmetry. We also explained a method to introduce symmetry twists and monodromy defects into a symmetric PEPS and calculated the projective action of the global symmetry upon a monodromy defect.

In Chapter 2 we focused on the $(1 + 1)$ D edge theories of $(2 + 1)$ D SPTs. In these models MPO group representations appear as dualities between gapped phases, which become symmetries at a gapless phase transition point. We used the MPOs to construct topological superselection sectors of the gapless models, which contain nonlocal scaling fields of the emergent CFT. We demonstrated our approach with an example, which was shown to support a gapless phase, protected by an MPO symmetry.

In Chapter 3 we further developed the framework introduced in Chapter 1, culminating in a construction of the defect superselection sectors of a symmetric PEPS. To achieve this, we established a close connection between graded MPO algebras and graded UFCs. We explained how the emergent physical data of an SET phase could be extracted from our representations of the superselection sectors. We also studied the relationship between SET phases and topological phases that are related by the dual processes of gauging a global symmetry, or condensing a bosonic subtheory.

In Chapter 4 we utilized two recent constructions of state sum TQFTs^{82,83} to write down new fixed point commuting projector Hamiltonians for topological phases of matter in $(3 + 1)$ D. We calculated the ground state degeneracies of Kashaev's models⁸² on the 3-torus, which formed the basis for our conjecture that these models fall into a subset of the topological phases realized by the CYWW models^{85,86}. We also discussed how the UGxBFC models⁸³ — with a small modification — capture previous constructions, including the CYWW models, Dijkgraaf-Witten theories⁷² and their 2-group generalizations^{88,90}, and how these models fit into a general framework based on unitary fusion 2-categories.

In Chapter 5 we extended the quantum state gauging procedure, introduced in Ref. 71, to generalized global symmetries that act on subsets of the lattice. This allows the tools of lattice gauge theory to be applied to exotic fracton topological phases of matter⁸⁷. General results about the connection between models before and after gauging were derived. In particular, it

was shown that a gapped Hamiltonian is mapped to a gapped Hamiltonian. As an example we found a modified Ising model, with a generalized global symmetry, that is mapped to Haah's cubic code by the gauging process.

Together, these results exemplify the utility of tensor networks for the description of topological phases of matter. We have used them not only to construct ground states, but also complicated fixed point Hamiltonians for new topological phases, and local symmetries on the entanglement degrees of freedom of a PEPS, which were used to find topological superselection sectors. Key elements in our formalism were the fusion tensors, that locally implement multiplication of the MPO symmetry algebra, and the associator tensors, that relate different orders of multiplication. We further described how this hierarchical structure could be extended to higher dimension⁸⁴. A particular emphasis was placed on the fact that emergent properties of a phase of matter can be extracted from the local TNO symmetries.

Our approach lends itself to a plethora of natural generalization: An immediate, although significant, generalization is the extension of the tube algebra and the derivation of superselection sectors, to a *cube algebra* in $(3 + 1)$ D. This could be significantly complicated by the higher categorical nature of emergent excitations in $(3 + 1)$ D, since the superselection sectors for regions of different topology behave in fundamentally different ways. While the pointlike particles are relatively simple, as they must be either bosons or fermions, a general construction of looplike excitations has not been given, although interesting progress was made in this direction recently³¹⁸. For a complete theory we expect one must also consider the cutting and gluing of superselection sectors with boundaries, highlighting the higher categorical nature of the emergent excitations, which are expected to be described by a modular tensor 2-category. The analysis is also complicated by the fact that domain walls of 1-form symmetries may appear in the looplike superselection sectors^{210,318}.

Alongside the construction of the cube algebra, it would be interesting to find the most general $(3 + 1)$ D state sum TQFTs and their local commuting projector Hamiltonian realizations, as discussed in Chapter 4. We anticipate that such models will arise from unitary fusion 2-categories, although no satisfactory algebraic definition of such objects has yet been established. Perhaps the most significant aspect of this endeavor, is the search for new concrete examples. In particular, we would like to establish whether the Hamiltonian models we described in Chapter 4 capture topological phases beyond 2-group gauge theories and Walker-Wang models. At this point it remains unclear whether there are any $(3 + 1)$ D topological phases not captured by 2-group gauge theory coupled to a Walker-Wang model, and Ref. 319 provides some preliminary arguments indicating that there may not be. Even if there is nothing beyond this class of topological phases, we expect that the finer classification of higher form SET phases will go beyond 2-group gauge theory and Walker-Wang models. To this end we have identified a simple subclass of our models which appear to capture novel 1-form SET phases, including the recently introduced 2-Ising theory²⁴⁸. We plan to explore the properties of these models in more detail in a future work.

One approach to finding new state sum models in $(3 + 1)$ D is to look for tensor solution to the Pachner move equations described in Ref. 84 and Chapter 4. It was shown that such tensors naturally give rise to a tensor network operator (TNO) symmetry algebra. By using a dimension reduction procedure, higher levels of categorical structure can be accessed directly in the tensor networks. Exploring these TNO algebras further could yield promising tools in the search for

new models.

Another immediate avenue for generalization would be to incorporate antiunitary and spatial symmetries, and their associated lattice defects, into our framework for SET phases. Tensor networks provide a natural environment for the construction of such defects, and we expect an approach similar to Ref. 245 could be combined with our defect tube algebra to classify emergent SET phases on the lattice, see Chapter 3.

It would also be interesting to consider anomalous symmetries in two spatial dimensions and extend the approach taken in Chapter 2 to find symmetric PEPS or MERA tensor networks. A closely related direction is the development of a general, cohesive framework for the description of chiral topological orders in PEPS. Both anomalous symmetries and chiral anomalies occur at the boundary of WW models and their generalizations described in Chapter 4. Hence, the problem of constructing chiral and anomalous symmetric tensor networks is related to finding those with the relevant TNO symmetries. This approach could lead to interesting gapless phases of matter, and may shed light on why the chiral tensor networks found thus far are ground states of gapless Hamiltonians.

We expect that the tools we have developed will prove useful in the study of topological quantum codes and computation. For instance, we plan to apply our general framework for SET order in PEPS to produce a construction of all non-anomalous locality preserving gates in two-dimensional lattice topological codes in a forthcoming work. In our formalism these gates are all realized transversally, making precise the connection between non-anomalous SET phases and transversal gates in topological codes. We also plan to use our construction of emergent superselection sectors in PEPS to derive effective noise models, for topological degrees of freedom, from realistic noise models on the physical degrees of freedom. We also anticipate that our isolation of topological degrees of freedom, concretely in a tensor network representation, could lead to improved schemes for topological quantum computation on the lattice.

Our analysis of MPO dualities in one-dimensional phases in Chapter 2 can be extended to the more general class of dualities considered in Refs. 193,194. These MPOs can be used to construct the topological superselection sectors, and nonlocal scaling fields of emergent RCFTs that describe symmetric critical points. These sectors allow one to pick out the primary fields and derive their set of scaling dimensions, which describe the universality class of the phase transition. The mathematical framework for group extensions of MPO algebras, developed in Chapter 3, can be applied to classify $(1+1)$ D phases and their phase transitions in terms of an algebra of MPO symmetries and dualities.

For all of the aforementioned future directions it would be interesting to also include constituent fermionic degrees of freedom, some work along these lines has already been done in Refs. 66,126,320.

A final, far reaching future direction would be to adapt our approach to emergence in condensed matter systems — by analyzing the entanglement structure — to the problem of emergence in quantum gravity. We remark that other ideas from quantum information have proven extremely fruitful in recent applications to quantum gravity^{321–323}, and a captivating dialog is ongoing.

In summary, this thesis constitutes a modest addition to the grand story of how the macroscopic world emerges from an intricate tapestry of correlations in the underlying microscopic degrees of freedom.

Bibliography

- [1] J. M. Kosterlitz and D. J. Thouless, Ordering, metastability and phase transitions in two-dimensional systems, [J. Phys. C: Solid State Phys.](#) **6**, 1181 (1973).
- [2] F. Haldane, Continuum dynamics of the 1-d heisenberg antiferromagnet: Identification with the $o(3)$ nonlinear sigma model, [Phys Lett. A](#) **93**, 464 (1983).
- [3] F. D. M. Haldane, Nonlinear Field Theory of Large-Spin Heisenberg Antiferromagnets: Semiclassically Quantized Solitons of the One-Dimensional Easy-Axis Néel State, [Phys. Rev. Lett.](#) **50**, 1153 (1983).
- [4] N. D. Mermin and H. Wagner, Absence of ferromagnetism or antiferromagnetism in one- or two-dimensional isotropic heisenberg models, [Phys. Rev. Lett.](#) **17**, 1133 (1966).
- [5] K. v. Klitzing, G. Dorda, and M. Pepper, New method for high-accuracy determination of the fine-structure constant based on quantized hall resistance, [Phys. Rev. Lett.](#) **45**, 494 (1980).
- [6] R. B. Laughlin, Quantized hall conductivity in two dimensions, [Phys. Rev. B](#) **23**, 5632 (1981).
- [7] D. J. Thouless, M. Kohmoto, M. P. Nightingale, and M. den Nijs, Quantized hall conductance in a two-dimensional periodic potential, [Phys. Rev. Lett.](#) **49**, 405 (1982).
- [8] X.-G. Wen, Vacuum degeneracy of chiral spin states in compactified space, [Phys. Rev. B](#) **40**, 7387 (1989).
- [9] T. Einarsson, Fractional statistics on a torus, [Phys. Rev. Lett.](#) **64**, 1995 (1990).
- [10] X.-G. Wen, Topological Orders in Rigid States, [Int. J. Mod. Phys. B](#) **04**, 239 (1990).
- [11] G. B. Segal, The definition of conformal field theory, in [Differential Geometrical Methods in Theoretical Physics](#), edited by K. Bleuler and M. Werner (Springer Netherlands, Dordrecht, 1988) pp. 165–171.
- [12] E. Witten, Topological quantum field theory, [Commun. Math. Phys.](#) **117**, 353 (1988).
- [13] M. Atiyah, Topological quantum field theories, [Inst. Hautes Études Sci. Publ. Math.](#) **68**, 175 (1988).
- [14] G. Moore and N. Seiberg, Classical and quantum conformal field theory, [Commun. Math. Phys.](#) **123**, 177 (1989).
- [15] L. P. Kadanoff, Scaling laws for Ising models near T_c , [Physics](#) **2**, 263 (1966).
- [16] K. G. Wilson, The renormalization group: Critical phenomena and the Kondo problem, [Rev. Mod. Phys.](#) **47**, 773 (1975).

- [17] V. F. Jones, A polynomial invariant for knots via von neumann algebras, [Bulletin of the American Mathematical Society](#) **12**, 103 (1985).
- [18] E. Witten, Quantum field theory and the jones polynomial, [Commun. Math. Phys.](#) **121**, 351 (1989).
- [19] A. Kitaev, Fault-tolerant quantum computation by anyons, [Ann. Phys.](#) **303**, 2 , [arXiv:quant-ph/9707021](#) (2003).
- [20] R. Walter Ogburn and J. Preskill, Topological quantum computation, in [Quantum Computing and Quantum Communications: First NASA International Conference, QCQC'98 Palm Springs, California, USA February 17–20, 1998 Selected Papers](#), edited by C. P. Williams (Springer Berlin Heidelberg, Berlin, Heidelberg, 1999) pp. 341–356.
- [21] M. Freedman, A. Kitaev, M. Larsen, and Z. Wang, Topological quantum computation, [Bull. Am. Math. Soc.](#) **40**, 31, [arXiv:quant-ph/0101025](#) (2003).
- [22] C. Nayak, S. H. Simon, A. Stern, M. Freedman, and S. Das Sarma, Non-abelian anyons and topological quantum computation, [Rev. Mod. Phys.](#) **80**, 1083, [arXiv:0707.1889](#) (2008).
- [23] Z. Wang, [Topological quantum computation](#), 112 (American Mathematical Soc., 2010).
- [24] M. A. Levin and X.-G. Wen, String-net condensation: A physical mechanism for topological phases, [Phys. Rev. B](#) **71**, 045110, [arXiv:cond-mat/0404617](#) (2005).
- [25] M. B. Hastings and X.-G. Wen, Quasiadiabatic continuation of quantum states: The stability of topological ground-state degeneracy and emergent gauge invariance, [Phys. Rev. B](#) **72**, 045141, [arXiv:cond-mat/0503554](#) (2005).
- [26] X. Chen, Z.-C. Gu, and X.-G. Wen, Local unitary transformation, long-range quantum entanglement, wave function renormalization, and topological order, [Phys. Rev. B](#) **82**, 155138, [arXiv:1004.3835](#) (2010).
- [27] X. Chen, Z.-C. Gu, and X.-G. Wen, Classification of gapped symmetric phases in one-dimensional spin systems, [Phys. Rev. B](#) **83**, 035107, [arXiv:1008.3745](#) (2011).
- [28] P. Bonderson and C. Nayak, Quasi-topological phases of matter and topological protection, [Phys. Rev. B](#) **87**, 195451, [arXiv:1212.6395](#) (2013).
- [29] A. Mesaros and Y. Ran, Classification of symmetry enriched topological phases with exactly solvable models, [Phys. Rev. B](#) **87**, 155115, [arXiv:1212.0835](#) (2013).
- [30] L.-Y. Hung and X.-G. Wen, Quantized topological terms in weak-coupling gauge theories with a global symmetry and their connection to symmetry-enriched topological phases, [Phys. Rev. B](#) **87**, 165107, [arXiv:1212.1827](#) (2013).
- [31] M. Barkeshli, P. Bonderson, M. Cheng, and Z. Wang, Symmetry, defects, and gauging of topological phases, preprint, [arXiv:1410.4540](#) (2014).

- [32] C. Heinrich, F. Burnell, L. Fidkowski, and M. Levin, Symmetry-enriched string nets: Exactly solvable models for set phases, [Phys. Rev. B **94**, 235136](#), [arXiv:1606.07816](#) (2016).
- [33] M. Cheng, Z.-C. Gu, S. Jiang, and Y. Qi, Exactly solvable models for symmetry-enriched topological phases, preprint, [arXiv:1606.08482](#) (2016).
- [34] Z.-C. Gu and X.-G. Wen, Tensor-entanglement-filtering renormalization approach and symmetry-protected topological order, [Phys. Rev. B **80**, 155131](#), [arXiv:0903.1069](#) (2009).
- [35] F. Pollmann, A. M. Turner, E. Berg, and M. Oshikawa, Entanglement spectrum of a topological phase in one dimension, [Phys. Rev. B **81**, 064439](#), [arXiv:0910.1811](#) (2010).
- [36] X. Chen, Z.-C. Gu, Z.-X. Liu, and X.-G. Wen, Symmetry protected topological orders and the group cohomology of their symmetry group, [Phys. Rev. B **87**, 155114](#), [arXiv:1106.4772](#) (2013).
- [37] A. Kitaev and J. Preskill, Topological entanglement entropy, [Phys. Rev. Lett. **96**, 110404](#), [arXiv:hep-th/0510092](#) (2006).
- [38] M. Levin and X.-G. Wen, Detecting Topological Order in a Ground State Wave Function, [Phys. Rev. Lett. **96**, 110405](#), [arXiv:cond-mat/0510613](#) (2006).
- [39] F. Verstraete, J. I. Cirac, and V. Murg, Matrix product states, projected entangled pair states, and variational renormalization group methods for quantum spin systems, [Adv. Phys. **57**, 143](#), [arXiv:0907.2796](#) (2009).
- [40] R. Orús, A practical introduction to tensor networks: Matrix product states and projected entangled pair states, [Ann. Phys. **349**, 117](#), [arXiv:1306.2164](#) (2014).
- [41] J. C. Bridgeman and C. T. Chubb, Hand-waving and interpretive dance: an introductory course on tensor networks, [J. Phys. A **50**, 223001](#), [arXiv:1603.03039](#) (2017).
- [42] F. Verstraete and J. I. Cirac, Matrix product states represent ground states faithfully, [Phys. Rev. B **73**, 094423](#), [arXiv:cond-mat/0505140](#) (2006).
- [43] G. Vidal, Entanglement renormalization, [Phys. Rev. Lett. **99**, 220405](#), [arXiv:cond-mat/0512165](#) (2007).
- [44] M. B. Hastings, Entropy and entanglement in quantum ground states, [Phys. Rev. B **76**, 035114](#), [arXiv:cond-mat/0701055](#) (2007).
- [45] D. Pérez-García, F. Verstraete, M. M. Wolf, and J. I. Cirac, Matrix product state representations, [Quantum Info. Comput. **7**, 401](#), [arXiv:quant-ph/0608197](#) (2007).
- [46] D. Pérez-García, F. Verstraete, M. M. Wolf, and J. I. Cirac, Peps as unique ground states of local hamiltonians, [Quantum Info. Comput. **8**, 650](#), [arXiv:0707.2260](#) (2008).
- [47] R. B. Laughlin, Anomalous quantum hall effect: An incompressible quantum fluid with fractionally charged excitations, [Phys. Rev. Lett. **50**, 1395](#) (1983).

- [48] G. Moore and N. Read, Nonabelions in the fractional quantum hall effect, [Nuclear Physics B](#) **360**, 362 (1991).
- [49] S. R. White, Density matrix formulation for quantum renormalization groups, [Phys. Rev. Lett.](#) **69**, 2863 (1992).
- [50] S. Östlund and S. Rommer, Thermodynamic Limit of Density Matrix Renormalization, [Phys. Rev. Lett.](#) **75**, 3537, [arXiv:cond-mat/9503107](#) (1995).
- [51] J. Dukelsky, M. A. Martín-Delgado, T. Nishino, and G. Sierra, Equivalence of the variational matrix product method and the density matrix renormalization group applied to spin chains, [EPL](#) **43**, 457, [arXiv:cond-mat/9710310](#) (1998).
- [52] M. B. Hastings, An area law for one-dimensional quantum systems, [J. Stat. Mech.](#) **2007**, P08024, [arXiv:0705.2024](#) (2007).
- [53] I. Affleck, T. Kennedy, E. H. Lieb, and H. Tasaki, Rigorous results on valence-bond ground states in antiferromagnets, [Phys. Rev. Lett.](#) **59**, 799 (1987).
- [54] A. Klümper, A. Schadschneider, and J. Zittartz, Matrix Product Ground States for One-Dimensional Spin-1 Quantum Antiferromagnets, [EPL](#) **24**, 293, [arXiv:cond-mat/9307028](#) (1993).
- [55] M. Fannes, B. Nachtergaele, and R. F. Werner, Finitely correlated states on quantum spin chains, [Commun. Math. Phys.](#) **144**, 443 (1992).
- [56] N. Schuch, D. Pérez-García, and I. Cirac, Classifying quantum phases using matrix product states and projected entangled pair states, [Phys. Rev. B](#) **84**, 165139, [arXiv:1010.3732](#) (2011).
- [57] T. Nishino, Y. Hieida, K. Okunishi, N. Maeshima, Y. Akutsu, and A. Gendiar, Two-Dimensional Tensor Product Variational Formulation, [Progr. Theor. Phys.](#) **105**, 409, [arXiv:cond-mat/0011103](#) (2001).
- [58] F. Verstraete and J. I. Cirac, Renormalization algorithms for quantum-many body systems in two and higher dimensions, [arXiv:cond-mat/0407066](#) (2004).
- [59] N. Schuch, I. Cirac, and D. Perez-Garcia, Peps as ground states: Degeneracy and topology, [Ann. Phys.](#) **325**, 2153, [arXiv:1001.3807](#) (2010).
- [60] J. Dubail and N. Read, Tensor network trial states for chiral topological phases in two dimensions and a no-go theorem in any dimension, [Phys. Rev. B](#) **92**, 205307, [arXiv:1307.7726](#) (2015).
- [61] T. B. Wahl, H.-H. Tu, N. Schuch, and J. I. Cirac, Projected Entangled-Pair States Can Describe Chiral Topological States, [Phys. Rev. Lett.](#) **111**, 236805, [arXiv:1308.0316](#) (2013).
- [62] O. Buerschaper, Twisted injectivity in projected entangled pair states and the classification of quantum phases, [Ann. Phys.](#) **351**, 447, [arXiv:1307.7763](#) (2014).

- [63] M. B. Şahinoğlu, D. Williamson, N. Bultinck, M. Mariën, J. Haegeman, N. Schuch, and F. Verstraete, Characterizing topological order with matrix product operators, preprint, [arXiv:1409.2150](#) (2014).
- [64] N. Bultinck, M. Mariën, D. Williamson, M. B. Şahinoğlu, J. Haegeman, and F. Verstraete, Anyons and matrix product operator algebras, *Ann. Phys.* **378**, 183 , [arXiv:1511.08090](#) (2017).
- [65] J. Bridgeman, S. T. Flammia, and D. Poulin, Detecting Topological Order with Ribbon Operators, *Phys. Rev. B* **94**, 205123, [arXiv:1603.02275](#) (2016).
- [66] D. J. Williamson, N. Bultinck, J. Haegeman, and F. Verstraete, Fermionic Matrix Product Operators and Topological Phases of Matter, preprint, [arXiv:1609.02897](#) (2016).
- [67] J. Cirac, D. Pérez-García, N. Schuch, and F. Verstraete, Matrix product density operators: Renormalization fixed points and boundary theories, *Ann. Phys.* **378**, 100 , [arXiv:1606.00608](#) (2017).
- [68] D. Pérez-García, M. M. Wolf, M. Sanz, F. Verstraete, and J. I. Cirac, String Order and Symmetries in Quantum Spin Lattices, *Phys. Rev. Lett.* **100**, 167202, [arXiv:0802.0447](#) (2008).
- [69] D. Pérez-García, M. Sanz, C. E. González-Guillén, M. M. Wolf, and J. I. Cirac, Characterizing symmetries in a projected entangled pair state, *New J. Phys.* **12**, 025010, [arXiv:0908.1674](#) (2010).
- [70] X. Chen, Z.-X. Liu, and X.-G. Wen, Two-dimensional symmetry-protected topological orders and their protected gapless edge excitations, *Phys. Rev. B* **84**, 235141, [arXiv:1106.4752](#) (2011).
- [71] J. Haegeman, K. Van Acoleyen, N. Schuch, J. I. Cirac, and F. Verstraete, Gauging quantum states: from global to local symmetries in many-body systems, *Phys. Rev. X* **5**, 011024, [arXiv:1407.1025](#) (2015).
- [72] R. Dijkgraaf and E. Witten, Topological gauge theories and group cohomology, *Commun. Math. Phys.* **129**, 393 (1990).
- [73] M. Levin and Z.-C. Gu, Braiding statistics approach to symmetry-protected topological phases, *Phys. Rev. B* **86**, 115109, [arXiv:1202.3120](#) (2012).
- [74] J. C. Wang, L. H. Santos, and X.-G. Wen, Bosonic anomalies, induced fractional quantum numbers, and degenerate zero modes: The anomalous edge physics of symmetry-protected topological states, *Phys. Rev. B* **91**, 195134, [arXiv:1403.5256](#) (2015).
- [75] D. V. Else and C. Nayak, Classifying symmetry-protected topological phases through the anomalous action of the symmetry on the edge, *Phys. Rev. B* **90**, 235137, [arXiv:1409.5436](#) (2014).
- [76] A. Kapustin and R. Thorngren, Anomalies of discrete symmetries in various dimensions and group cohomology, preprint, [arXiv:1404.3230](#) (2014).

- [77] X. Chen, F. Wang, Y.-M. Lu, and D.-H. Lee, Critical theories of phase transition between symmetry protected topological states and their relation to the gapless boundary theories, *Nucl. Phys. B* **873**, 248 , [arXiv:1302.3121](#) (2013).
- [78] G. Evenbly and G. Vidal, Algorithms for entanglement renormalization, *Phys. Rev. B* **79**, 144108, [arXiv:0707.1454](#) (2009).
- [79] G. Evenbly, P. Corboz, and G. Vidal, Nonlocal scaling operators with entanglement renormalization, *Phys. Rev. B* **82**, 132411, [arXiv:0912.2166](#) (2010).
- [80] A. Feiguin, S. Trebst, A. W. W. Ludwig, M. Troyer, A. Kitaev, Z. Wang, and M. H. Freedman, Interacting anyons in topological quantum liquids: The golden chain, *Phys. Rev. Lett* **95**, 160409, [arXiv:cond-mat/0612341](#) (2007).
- [81] P. Etingof, D. Nikshych, and V. Ostrik, Fusion categories and homotopy theory, preprint, [arXiv:0909.3140](#) (2009).
- [82] R. Kashaev, A simple model of 4d-tqft, preprint, [arXiv:1405.5763](#) (2014).
- [83] S. X. Cui, *Higher Categories and Topological Quantum Field Theories*, Ph.D. thesis, University of California, Santa Barbara, [arXiv:1610.07628](#) (2016).
- [84] M. B. Sahinoglu, M. Walter, and D. J. Williamson, A tensor network framework for topological order in any dimension, [preprint, available at https://sites.google.com/site/dominicjw/papers](#) .
- [85] K. Walker and Z. Wang, (3+1)-tqfts and topological insulators, *Front. Phys.* **7**, 150, [arXiv:1104.2632](#) (2012).
- [86] L. Crane and D. Yetter, A categorical construction of 4d topological quantum field theories, in *Quantum Topology* (WORLD SCIENTIFIC, 2011) pp. 120–130, [arXiv:hep-th/9301062](#) .
- [87] S. Vijay, J. Haah, and L. Fu, Fracton topological order, generalized lattice gauge theory, and duality, *Phys. Rev. B* **94**, 235157, [arXiv:1603.04442](#) (2016).
- [88] A. Kapustin and R. Thorngren, Higher symmetry and gapped phases of gauge theories, preprint, [arXiv:1309.4721](#) (2013).
- [89] A. Bullivant, M. Calçada, Z. Kádár, P. Martin, and J. a. F. Martins, Topological phases from higher gauge symmetry in 3 + 1 dimensions, *Phys. Rev. B* **95**, 155118, [arXiv:1606.06639](#) (2017).
- [90] D. N. Yetter, Tqft's from homotopy 2-types, *J. Knot Theor. Ramif.* **02**, 113 (1993).
- [91] J. Haah, Commuting pauli hamiltonians as maps between free modules, *Commun. Math. Phys.* **324**, 351, [arXiv:1204.1063](#) (2013).
- [92] J. Haah, Local stabilizer codes in three dimensions without string logical operators, *Phys. Rev. A* **83**, 042330, [arXiv:1101.1962](#) (2011).

- [93] D. J. Williamson, N. Bultinck, M. Mariën, M. B. Şahinoğlu, J. Haegeman, and F. Verstraete, Matrix product operators for symmetry-protected topological phases: Gauging and edge theories, *Phys. Rev. B* **94**, 205150, [arXiv:1412.5604](#) (2016).
- [94] N. Schuch, D. Poilblanc, J. I. Cirac, and D. Pérez-García, Topological order in the projected entangled-pair states formalism: Transfer operator and boundary hamiltonians, *Phys. Rev. Lett.* **111**, 090501, [arXiv:1210.5601](#) (2013).
- [95] S. Yang, T. B. Wahl, H.-H. Tu, N. Schuch, and J. I. Cirac, Chiral projected entangled-pair state with topological order, *Phys. Rev. Lett.* **114**, 106803, [arXiv:1411.6618](#) (2015).
- [96] T. B. Wahl, S. T. Haßler, H.-H. Tu, J. I. Cirac, and N. Schuch, Symmetries and boundary theories for chiral projected entangled pair states, *Phys. Rev. B* **90**, 115133, [arXiv:1405.0447](#) (2014).
- [97] V. Turaev, Homotopy field theory in dimension 3 and crossed group-categories, preprint, [arXiv:math/0005291](#) (2000).
- [98] A. Kirillov Jr, On g -equivariant modular categories, preprint, [arXiv:math/0401119](#) (2004).
- [99] V. Drinfeld, S. Gelaki, D. Nikshych, and V. Ostrik, On braided fusion categories i, *Selecta Mathematica* **16**, 1, [arXiv:0906.0620](#) (2010).
- [100] H. Bombin, Topological order with a twist: Ising anyons from an abelian model, *Phys. Rev. Lett.* **105**, 030403, [arXiv:1004.1838](#) (2010).
- [101] N. Tarantino, N. H. Lindner, and L. Fidkowski, Symmetry fractionalization and twist defects, *New J. Phys.* **18**, 035006, [arXiv:1506.06754](#) (2016).
- [102] J. C. Teo, T. L. Hughes, and E. Fradkin, Theory of twist liquids: gauging an anyonic symmetry, *Ann. Phys.* **360**, 349, [arXiv:1503.06812](#) (2015).
- [103] D. J. Williamson, N. Bultinck, J. Haegeman, and F. Verstraete, Symmetry-enriched topological order in tensor networks: gauging and anyon condensation, In preparation .
- [104] R. Dijkgraaf, V. Pasquier, and P. Roche, Quasi hopf algebras, group cohomology and orbifold models, *Nucl. Phys. B* **18**, 60 (1991).
- [105] Y. Hu, Y. Wan, and Y.-S. Wu, Twisted quantum double model of topological phases in two dimensions, *Phys. Rev. B* **87**, 125114, [arXiv:1211.3695](#) (2013).
- [106] M. de Wild Propitius, *Topological interactions in broken gauge theories*, Ph.D. thesis, University of Amsterdam, [arXiv:hep-th/9511195](#) (1995).
- [107] S. Jiang and Y. Ran, Symmetric tensor networks and practical simulation algorithms to sharply identify classes of quantum phases distinguishable by short-range physics, *Phys. Rev. B* **92**, 104414, [arXiv:1505.03171](#) (2015).
- [108] V. Turaev and O. Viro, State sum invariants of 3-manifolds and quantum 6j-symbols, *Topology* **31**, 865 (1992).

- [109] S. Flammia, A. Hamma, T. Hughes, and X.-G. Wen, Topological entanglement Renyi entropy and reduced density matrix structure, *Phys. Rev. Lett.* **103**, 261601, [arXiv:0909.3305](#) (2009).
- [110] J. I. Cirac, D. Poilblanc, N. Schuch, and F. Verstraete, Entanglement spectrum and boundary theories with projected entangled-pair states, *Phys. Rev. B* **83**, 245134, [arXiv:1103.3427](#) (2011).
- [111] S. Yang, L. Lehman, D. Poilblanc, K. Van Acoleyen, F. Verstraete, J. I. Cirac, and N. Schuch, Edge theories in projected entangled pair state models, *Phys. Rev. Lett.* **112**, 036402, [arXiv:1309.4596](#) (2014).
- [112] X. Chen and A. Vishwanath, Towards gauging time-reversal symmetry: A tensor network approach, *Phys. Rev. X* **5**, 041034, [arXiv:1401.3736](#) (2015).
- [113] L.-Y. Hung and X.-G. Wen, Universal symmetry-protected topological invariants for symmetry-protected topological states, *Phys. Rev. B* **89**, 075121, [arXiv:1311.5539](#) (2014).
- [114] C.-Y. Huang and T.-C. Wei, Detecting and identifying two-dimensional symmetry-protected topological, symmetry-breaking, and intrinsic topological phases with modular matrices via tensor-network methods, *Phys. Rev. B* **93**, 155163, [arXiv:1512.07842](#) (2016).
- [115] Y. Zhang, T. Grover, A. Turner, M. Oshikawa, and A. Vishwanath, Quasiparticle statistics and braiding from ground-state entanglement, *Phys. Rev. B* **85**, 235151, [arXiv:1111.2342](#) (2012).
- [116] H. Moradi and X.-G. Wen, Universal wave-function overlap and universal topological data from generic gapped ground states, *Phys. Rev. Lett.* **115**, 036802, [arXiv:1401.0518](#) (2015).
- [117] X.-G. Wen, Symmetry-protected topological invariants of symmetry-protected topological phases of interacting bosons and fermions, *Phys. Rev. B* **89**, 035147, [arXiv:1301.7675](#) (2014).
- [118] M. P. Zaletel, Detecting two-dimensional symmetry-protected topological order in a ground-state wave function, *Phys. Rev. B* **90**, 235113, [arXiv:1309.7387](#) (2014).
- [119] O. Buerschaper, M. Aguado, and G. Vidal, Explicit tensor network representation for the ground states of string-net models, *Phys. Rev. B* **79**, 085119, [arXiv:0809.2393](#) (2009).
- [120] Z.-C. Gu, M. Levin, B. Swingle, and X.-G. Wen, Tensor-product representations for string-net condensed states, *Phys. Rev. B* **79**, 085118, [arXiv:0809.2821](#) (2009).
- [121] L.-Y. Hung and Y. Wan, String-net models with Z_N fusion algebra, *Phys. Rev. B* **86**, 235132, [arXiv:1207.6169](#) (2012).
- [122] J. I. Cirac, S. Michalakis, D. Pérez-García, and N. Schuch, Robustness in projected entangled pair states, *Phys. Rev. B* **88**, 115108, [arXiv:1306.4003](#) (2013).

- [123] J. Haegeman, V. Zauner, N. Schuch, and F. Verstraete, Shadows of anyons and the entanglement structure of topological phases, *Nat. Commun.* **6**, 10.1038/ncomms9284, [arXiv:1410.5443](#) (2015).
- [124] M. Mariën, J. Haegeman, P. Fendley, and F. Verstraete, Condensation-driven phase transitions in perturbed string nets, preprint, [arXiv:1607.05296](#) (2016).
- [125] C. V. Kraus, N. Schuch, F. Verstraete, and J. I. Cirac, Fermionic projected entangled pair states, *Phys. Rev. A* **81**, 052338, [arXiv:0904.4667](#) (2010).
- [126] N. Bultinck, D. J. Williamson, J. Haegeman, and F. Verstraete, Fermionic matrix product states and one-dimensional topological phases, *Phys. Rev. B* **95**, 075108, [arXiv:1610.07849](#) (2017).
- [127] Z.-C. Gu and X.-G. Wen, Symmetry-protected topological orders for interacting fermions: Fermionic topological nonlinear σ models and a special group supercohomology theory, *Phys. Rev. B* **90**, 115141, [arXiv:1201.2648](#) (2014).
- [128] M. Cheng, Z. Bi, Y.-Z. You, and Z.-C. Gu, Towards a complete classification of symmetry-protected phases for interacting fermions in two dimensions, preprint, [arXiv:1501.01313](#) (2015).
- [129] J. C. Bridgeman and D. J. Williamson, Anomalies and entanglement renormalization, preprint, [arXiv:1703.07782](#) (2017).
- [130] L. D. Landau and E. M. Lifshitz, *Course of theoretical physics* (Pergamon Press, 1965).
- [131] F. J. Wegner, Duality in generalized Ising models and phase transitions without local order parameters, *J. Math. Phys.* **12**, 2259 (1971).
- [132] A. Miyake, Quantum Computation on the Edge of a Symmetry-Protected Topological Order, *Phys. Rev. Lett.* **105**, 040501, [arXiv:1003.4662](#) (2010).
- [133] J. M. Renes, A. Miyake, G. K. Brennen, and S. D. Bartlett, Holonomic quantum computing in symmetry-protected ground states of spin chains, *New J. Phys.* **15**, 025020, [arXiv:1103.5076](#) (2013).
- [134] D. V. Else, I. Schwarz, S. D. Bartlett, and A. C. Doherty, Symmetry-protected phases for measurement-based quantum computation, *Phys. Rev. Lett.* **108**, 240505, [arXiv:1201.4877](#) (2012).
- [135] D. V. Else, S. D. Bartlett, and A. C. Doherty, Symmetry protection of measurement-based quantum computation in ground states, *New J. Phys.* **14**, 113016, [arXiv:1207.4805](#) (2012).
- [136] D. J. Williamson and S. D. Bartlett, Symmetry-protected adiabatic quantum transistors, *New J. Phys.* **17**, 053019, [arXiv:1408.3415](#) (2015).
- [137] R. N. C. Pfeifer, O. Buerschaper, S. Trebst, A. W. W. Ludwig, M. Troyer, and G. Vidal, Translation invariance, topology, and protection of criticality in chains of interacting anyons, *Phys. Rev. B* **86**, 155111, [arXiv:1005.5486](#) (2012).

- [138] C. Gils, E. Ardonne, S. Trebst, D. A. Huse, A. W. W. Ludwig, M. Troyer, and Z. Wang, Anyonic quantum spin chains: Spin-1 generalizations and topological stability, [*Phys. Rev. B* **87**, 235120](#), [arXiv:1303.4290](#) (2013).
- [139] R. N. C. Pfeifer, P. Corboz, O. Buerschaper, M. Aguado, M. Troyer, and G. Vidal, Simulation of anyons with tensor network algorithms, [*Phys. Rev. B* **82**, 115126](#), [arXiv:1006.3532](#) (2010).
- [140] R. König and E. Bilgin, Anyonic entanglement renormalization, [*Phys. Rev. B* **82**, 125118](#), [arXiv:1006.2478](#) (2010).
- [141] L. H. Santos and J. Wang, Symmetry-protected many-body Aharonov-Bohm effect, [*Phys. Rev. B* **89**, 195122](#), [arXiv:1310.8291](#) (2014).
- [142] X.-G. Wen, Classifying gauge anomalies through symmetry-protected trivial orders and classifying gravitational anomalies through topological orders, [*Phys. Rev. D* **88**, 045013](#), [arXiv:1303.1803](#) (2013).
- [143] A. Kapustin and R. Thorngren, Anomalous Discrete Symmetries in Three Dimensions and Group Cohomology, [*Phys. Rev. Lett.* **112**, 231602](#), [arXiv:1403.0617](#) (2014).
- [144] A. Kapustin, Symmetry protected topological phases, anomalies, and cobordisms: beyond group cohomology, preprint, [arXiv:1403.1467](#) (2014).
- [145] J. Wang and X.-G. Wen, A Lattice Non-Perturbative Hamiltonian Construction of 1+ 1D Anomaly-Free Chiral Fermions and Bosons-on the equivalence of the anomaly matching conditions and the boundary fully gapping rules, preprint, [arXiv:1307.7480](#) (2013).
- [146] G. 't Hooft, Naturalness, chiral symmetry, and spontaneous chiral symmetry breaking, [*Recent Developments in Gauge Theories* , 135](#) (1980).
- [147] S. C. Furuya and M. Oshikawa, Symmetry Protection of Critical Phases and a Global Anomaly in 1 + 1 Dimensions, [*Phys. Rev. Lett.* **118**, 021601](#), [arXiv:1503.07292](#) (2017).
- [148] S. Singh, R. Pfeifer, and G. Vidal, Tensor network decompositions in the presence of a global symmetry, [*Phys. Rev. A* **82**, 050301](#), [arXiv:0907.2994](#) (2010).
- [149] R. Pfeifer, G. Evenbly, and G. Vidal, Entanglement renormalization, scale invariance, and quantum criticality, [*Phys. Rev. A* **79**, 040301](#), [arXiv:0810.0580](#) (2009).
- [150] P. Ginsparg, in *Fields, Strings and Critical Phenomena*, Les Houches 1988, Session XLIX, edited by E. Brézin and J. Z. Justin (North-Holland, Amsterdam, 1990) [arXiv:hep-th/9108028](#) .
- [151] P. Di Francesco, *Conformal field theory* (Springer, New York, 1997).
- [152] S. Ryu, J. E. Moore, and A. W. W. Ludwig, Electromagnetic and gravitational responses and anomalies in topological insulators and superconductors, [*Phys. Rev. B* **85**, 045104](#), [arXiv:1010.0936](#) (2012).

- [153] J. C. Wang, Z.-C. Gu, and X.-G. Wen, Field-Theory Representation of Gauge-Gravity Symmetry-Protected Topological Invariants, Group Cohomology, and Beyond, [Phys. Rev. Lett. **114**, 031601, arXiv:1405.7689](#) (2015).
- [154] D. Gaiotto, A. Kapustin, N. Seiberg, and B. Willett, Generalized global symmetries, [J. High Energy Phys. **2015**, 172, arXiv:1412.5148](#) (2015).
- [155] R. Thorngren and C. von Keyserlingk, Higher SPT's and a generalization of anomaly in-flow, preprint, [arXiv:1511.02929](#) (2015).
- [156] J. Wess and B. Zumino, Consequences of anomalous ward identities, [Phys. Lett. B **37**, 95](#) (1971).
- [157] S. Weinberg, *The quantum theory of fields. Vol. 2: Modern applications* (Cambridge University Press, 2013).
- [158] G. Evenbly and G. Vidal, in *Strongly Correlated Systems-Numerical Methods*, Springer Series in Solid-State Sciences, Vol. 176, edited by A. Avella and F. Mancini (Springer, Berlin New York, 2013) pp. 99–130, [arXiv:1109.5334](#) .
- [159] M. Hauru, G. Evenbly, W. W. Ho, D. Gaiotto, and G. Vidal, Topological conformal defects with tensor networks, [Phys. Rev. B **94**, 115125, arXiv:1512.03846](#) (2016).
- [160] D. Aasen, R. S. K. Mong, and P. Fendley, Topological Defects on the Lattice I: The Ising model, [J. Phys. A **49**, 354001, arXiv:1601.07185](#) (2016).
- [161] P. Christe and M. Henkel, *Introduction to Conformal Invariance and Its Applications to Critical Phenomena* (Springer-Verlag, Berlin, 1993) [arXiv:cond-mat/9304035](#) .
- [162] V. Drinfel'd, Quantum groups, [Proc. Int. Congr. Math. **1**, 798](#) (1986).
- [163] D. Evans and Y. Kawahigashi, On Ocneanu's theory of asymptotic inclusions for subfactors, topological quantum field theories and quantum doubles, [Int. J. Math. **6**, 205](#) (1995).
- [164] M. Muger, From subfactors to categories and topology II: The quantum double of tensor categories and subfactors, [J. Pure Appl. Algebr. **180**, 159](#) , [arXiv:math/0111205](#) (2003).
- [165] B. Bakalov and A. A. Kirillov, *Lectures on tensor categories and modular functors*, Vol. 21 (American Mathematical Soc., 2001).
- [166] P. Etingof, D. Nikshych, and V. Ostrik, On fusion categories, [Ann. Math. , 581](#)[arXiv:math/0203060](#) (2005).
- [167] L. Tsui, H.-C. Jiang, Y.-M. Lu, and D.-H. Lee, Quantum phase transitions between a class of symmetry protected topological states, [Nucl. Phys. B **896**, 330](#) , [arXiv:1503.06794](#) (2015).
- [168] L. Tsui, F. Wang, and D.-H. Lee, Topological versus landau-like phase transitions, preprint, [arXiv:1511.07460](#) (2015).

- [169] L. Tsui, Y.-T. Huang, H.-C. Jiang, and D.-H. Lee, Which conformal field theories can describe phase transitions between bosonic symmetry protected topological states?, preprint, [arXiv:1701.00834](#) (2017).
- [170] A. Kubica and B. Yoshida, Precise estimation of critical exponents from real-space renormalization group analysis, [arXiv:1402.0619](#) (2014).
- [171] A. O'Brien, S. D. Bartlett, A. C. Doherty, and S. T. Flammia, Symmetry-respecting real-space renormalization for the quantum Ashkin-Teller model, [Phys. Rev. E **92**, 042163](#), [arXiv:1507.00038](#) (2015).
- [172] T. Kennedy and H. Tasaki, Hidden $\mathbb{Z}_2 \times \mathbb{Z}_2$ symmetry breaking in Haldane-gap antiferromagnets, [Phys. Rev. B **45**, 304](#) (1992).
- [173] D. V. Else, S. D. Bartlett, and A. C. Doherty, The hidden symmetry-breaking picture of symmetry-protected topological order, [Phys. Rev. B **88**, 085114](#), [arXiv:1304.0783](#) (2013).
- [174] S.-K. Yang, Modular invariant partition function of the Ashkin-Teller model on the critical line and $N=2$ superconformal invariance, [Nucl. Phys. B **285**, 183](#) (1987).
- [175] M. Baake, G. von Gehlen, and V. Rittenberg, Operator content of the Ashkin-Teller quantum chain-superconformal and Zamolodchikov-Fateev invariance: II. Boundary conditions compatible with the torus, [J. Phys. A: Math. Gen. **20**, 6635](#) (1987).
- [176] F. C. Alcaraz, M. Baake, U. Grimm, and V. Rittenberg, Operator content of the XXZ chain, [J. Phys. A: Math. Gen. **21**, L117](#) (1988).
- [177] F. C. Alcaraz, M. N. Barber, and M. T. Batchelor, Conformal invariance, the XXZ chain and the operator content of two-dimensional critical systems, [Ann. Phys. **182**, 280](#) (1988).
- [178] J. C. Bridgeman, *Effective Edge States of Symmetry Protected Topological Systems*, [Master's thesis](#), Perimeter Institute (2014).
- [179] J. C. Bridgeman, A. O'Brien, S. D. Bartlett, and A. C. Doherty, Multiscale entanglement renormalization ansatz for spin chains with continuously varying criticality, [Phys. Rev. B **91**, 165129](#), [arXiv:1501.02817](#) (2015).
- [180] M. de Wild Propitius, (Spontaneously broken) Abelian Chern-Simons theories, [Nucl. Phys. B **489**, 297](#), [arXiv:hep-th/9606029](#) (1997).
- [181] C. Goff, G. Mason, and S.-H. Ng, On the Gauge Equivalence of Twisted Quantum Doubles of Elementary Abelian and Extra-Special 2-Groups, [J. Algebra **312**, 849](#), [arXiv:math/0603191](#) (2007).
- [182] J. Wang and X.-G. Wen, Non-Abelian String and Particle Braiding in Topological Order: Modular $SL(3, \mathbb{Z})$ Representation and $3 + 1D$ Twisted Gauge Theory, [Phys. Rev. B **91**, 035134](#), [arXiv:1404.7854](#) (2015).

- [183] H. He, Y. Zheng, and C. von Keyserlingk, Field theories for gauged symmetry-protected topological phases: Non-Abelian anyons with Abelian gauge group $\mathbb{Z}_2^{\otimes 3}$, *Phys. Rev. B* **95**, 035131, [arXiv:1608.05393](#) (2017).
- [184] S. Trebst, E. Ardonne, A. Feiguin, D. A. Huse, A. W. W. Ludwig, and M. Troyer, Collective States of Interacting Fibonacci Anyons, *Phys. Rev. Lett.* **101**, 050401, [arXiv:0801.4602](#) (2008).
- [185] C. Gils, S. Trebst, A. Kitaev, A. W. Ludwig, M. Troyer, and Z. Wang, Topology-driven quantum phase transitions in time-reversal-invariant anyonic quantum liquids, *Nat. Phys.* **5**, 834, [arXiv:0906.1579](#) (2009).
- [186] B. Bauer, L. D. Carr, H. Evertz, A. Feiguin, J. Freire, S. Fuchs, L. Gamper, J. Gukelberger, E. Gull, S. Guertler, A. Hehn, R. Igarashi, S. Isakov, D. Koop, P. Ma, P. Mates, H. Matsuo, O. Parcollet, G. Pawłowski, J. Picon, L. Pollet, E. Santos, V. Scarola, U. Schollwöck, C. Silva, B. Surer, S. Todo, S. Trebst, M. Troyer, M. Wall, P. Werner, and S. Wessel, The ALPS project release 2.0: Open source software for strongly correlated systems, *J. Stat. Mech.* **2011**, P05001, [arXiv:1101.2646](#) (2011).
- [187] M. Dolfi, B. Bauer, S. Keller, A. Kosenkov, T. Ewart, A. Kantian, T. Giamarchi, and M. Troyer, Matrix Product State applications for the ALPS project, *Comput. Phys. Commun.* **185**, 3430, [arXiv:1407.0872](#) (2014).
- [188] G. von Gehlen and V. Rittenberg, The Ashkin-Teller quantum chain and conformal invariance, *J. Phys. A: Math. Gen* **20**, 227 (1987).
- [189] D. Aasen *et al.*, in preparation .
- [190] M. Buican and A. Gromov, Anyonic Chains, Topological Defects, and Conformal Field Theory, preprint, [arXiv:1701.02800](#) (2017).
- [191] R. S. K. Mong, D. J. Clarke, J. Alicea, N. H. Lindner, and P. Fendley, Parafermionic conformal field theory on the lattice, *J. Phys. A* **47**, 452001, [arXiv:1406.0846](#) (2014).
- [192] J. Fuchs, I. Runkel, and C. Schweigert, Tft construction of rcft correlators i: Partition functions, *Nucl. Phys. B* **646**, 353, [arXiv:hep-th/0204148](#) (2002).
- [193] J. Fröhlich, J. Fuchs, I. Runkel, and C. Schweigert, Kramers-wannier duality from conformal defects, *Phys. Rev. Lett.* **93**, 070601, [arXiv:cond-mat/0404051](#) (2004).
- [194] J. Fröhlich, J. Fuchs, I. Runkel, and C. Schweigert, Duality and defects in rational conformal field theory, *Nucl. Phys. B* **763**, 354, [arXiv:hep-th/0607247](#) (2007).
- [195] T. Lan and X.-G. Wen, Topological quasiparticles and the holographic bulk-edge relation in $(2 + 1)$ -dimensional string-net models, *Phys. Rev. B* **90**, 115119, [arXiv:1311.1784](#) (2014).
- [196] J. Haah, An invariant of topologically ordered states under local unitary transformations, *Commun. Math. Phys.* **342**, 771, [arXiv:quant-ph/1407.2926](#) (2016).

- [197] Y. Hu, N. Geer, and Y.-S. Wu, Full Dyon Excitation Spectrum in Generalized Levin-Wen Models, [arXiv:cond-mat.str-el/1502.03433](#) (2015).
- [198] G. Evenbly and G. Vidal, Tensor Network Renormalization, [Phys. Rev. Lett. **115**, 180405](#), [arXiv:1412.0732](#) (2015).
- [199] G. Evenbly, Algorithms for tensor network renormalization, [Phys. Rev. B **95**, 045117](#), [arXiv:1509.07484](#) (2017).
- [200] S. Yang, Z.-C. Gu, and X.-G. Wen, Loop optimization for tensor network renormalization, [Phys. Rev. Lett **118**, 110504](#), [arXiv:1512.04938](#) (2017).
- [201] M. Bal, M. Mariën, J. Haegeman, and F. Verstraete, Renormalization group flows of Hamiltonians using tensor networks, preprint, [arXiv:1703.00365](#) (2017).
- [202] R. N. C. Pfeifer, J. Haegeman, and F. Verstraete, Faster identification of optimal contraction sequences for tensor networks, [Phys. Rev. E **90**, 033315](#), [arXiv:1304.6112](#) (2014).
- [203] A. Kitaev, Anyons in an exactly solved model and beyond, [Ann. Phys. **321**, 2](#), january Special Issue, [arXiv:cond-mat/0506438](#) (2006).
- [204] S. Beigi, P. W. Shor, and D. Whalen, The quantum double model with boundary: Condensations and symmetries, [Commun. Math. Phys. **306**, 663](#), [arXiv:1006.5479](#) (2011).
- [205] B. J. Brown, S. D. Bartlett, A. C. Doherty, and S. D. Barrett, Topological entanglement entropy with a twist, [Phys. Rev. Lett. **111**, 220402](#), [arXiv:1303.4455](#) (2013).
- [206] B. Yoshida, Gapped boundaries, group cohomology and fault-tolerant logical gates, [Ann. Phys. **377**, 387](#), [arXiv:1509.03626](#) (2017).
- [207] F. Pastawski and B. Yoshida, Fault-tolerant logical gates in quantum error-correcting codes, [Phys. Rev. A **91**, 012305](#), [arXiv:1408.1720](#) (2015).
- [208] S. Bravyi and R. König, Classification of topologically protected gates for local stabilizer codes, [Phys. Rev. Lett. **110**, 170503](#), [arXiv:1206.1609](#) (2013).
- [209] M. E. Beverland, O. Buerschaper, R. Koenig, F. Pastawski, J. Preskill, and S. Shjher, Protected gates for topological quantum field theories, [J. Math. Phys. **57**, 022201](#), [arXiv:1409.3898](#) (2016).
- [210] B. Yoshida, Topological color code and symmetry-protected topological phases, [Phys. Rev. B **91**, 245131](#), [arXiv:1503.07208](#) (2015).
- [211] M. Müger, From subfactors to categories and topology i: Frobenius algebras in and morita equivalence of tensor categories, [J. of Pure Appl. Algebr. **180**, 81](#), [arXiv:math/0111204](#) (2003).
- [212] D. E. Evans and Y. Kawahigashi, *Quantum symmetries on operator algebras*, Vol. 147 (Clarendon Press Oxford, 1998).
- [213] K. G. Wilson, Confinement of quarks, [Phys. Rev. D **10**, 2445](#) (1974).

- [214] J. Kogut and L. Susskind, Hamiltonian formulation of wilson’s lattice gauge theories, *Phys. Rev. D* **11**, 395 (1975).
- [215] F. A. Bais and J. K. Slingerland, Condensate-induced transitions between topologically ordered phases, *Phys. Rev. B* **79**, 045316, [arXiv:0808.0627](#) (2009).
- [216] P. Etingof, S. Gelaki, D. Nikshych, and V. Ostrik, *Tensor categories*, Vol. 205 (American Mathematical Soc., 2015).
- [217] A. Joyal and R. Street, The geometry of tensor calculus, i, *Advances in Mathematics* **88**, 55 (1991).
- [218] A. Joyal and R. Street, Braided tensor categories, *Advances in Mathematics* **102**, 20 (1993).
- [219] J. Barrett and B. Westbury, Invariants of piecewise-linear 3-manifolds, *Trans. Am. Math. Soc.* **348**, 3997, [arXiv:hep-th/9311155](#) (1996).
- [220] K. Walker, On witten’s 3-manifold invariants & tqfts, [preprints, available at http://canyon23.net/math](#) (1991,2006).
- [221] M. Freedman, C. Nayak, K. Walker, and Z. Wang, On picture $(2 + 1)$ -tqfts, in *Topology and Physics* (WORLD SCIENTIFIC, 2011) pp. 19–106, [arXiv:0806.1926](#).
- [222] M. Barkeshli, P. Bonderson, C.-M. Jian, M. Cheng, and K. Walker, Reflection and time reversal symmetry enriched topological phases of matter: path integrals, non-orientable manifolds, and anomalies, preprint, [arXiv:1612.07792](#) (2016).
- [223] D. J. Williamson, Fractal symmetries: Ungauging the cubic code, *Phys. Rev. B* **94**, 155128, [arXiv:1603.05182](#) (2016).
- [224] G. Moore and N. Seiberg, Polynomial equations for rational conformal field theories, *Phys. Lett. B* **212**, 451 (1988).
- [225] S. Mac Lane, *Categories for the working mathematician*, Vol. 5 (Springer, 2013).
- [226] Z.-X. Luo, E. Lake, and Y.-S. Wu, The structure of fixed-point tensor network states characterizes pattern of long-range entanglement, preprint, [arXiv:1611.01140](#) (2016).
- [227] C. Fernández-González, R. S. K. Mong, O. Landon-Cardinal, D. Pérez-García, and N. Schuch, Constructing topological models by symmetrization: A projected entangled pair states study, *Phys. Rev. B* **94**, 155106, [arXiv:1608.00594](#) (2016).
- [228] D. Aasen, private communication .
- [229] Y. Zhang, T. Grover, A. Turner, M. Oshikawa, and A. Vishwanath, Quasiparticle statistics and braiding from ground-state entanglement, *Phys. Rev. B* **85**, 235151, [arXiv:1111.2342](#) (2012).
- [230] A. Davydov, M. Müger, D. Nikshych, and V. Ostrik, The witt group of non-degenerate braided fusion categories, *Journal für die reine und angewandte Mathematik* **2013**, 135, [arXiv:1009.2117](#) (2013).

- [231] A. Davydov, D. Nikshych, and V. Ostrik, On the structure of the witt group of braided fusion categories, *Selecta Mathematica* **19**, 237, [arXiv:1109.5558](#) (2013).
- [232] X.-L. Qi, H. Katsura, and A. W. W. Ludwig, General relationship between the entanglement spectrum and the edge state spectrum of topological quantum states, *Phys. Rev. Lett.* **108**, 196402, [arXiv:1103.5437](#) (2012).
- [233] V. Pasquier, Operator content of the ade lattice models, *Journal of Physics A: Mathematical and General* **20**, 5707 (1987).
- [234] E. Verlinde, Fusion rules and modular transformations in 2d conformal field theory, *Nuclear Physics B* **300**, 360 (1988).
- [235] S. Jiang and Y. Ran, Anyon condensation and a generic tensor-network construction for symmetry-protected topological phases, *Phys. Rev. B* **95**, 125107, [arXiv:1611.07652](#) (2017).
- [236] J. Garre-Rubio, S. Iblisdir, and D. Pérez-García, Symmetry reduction induced by anyon condensation: a tensor network approach, preprint, [arXiv:1702.08759](#) (2017).
- [237] K. Duivenvoorden, M. Iqbal, J. Haegeman, F. Verstraete, and N. Schuch, Entanglement phases as holographic duals of anyon condensates, *Phys. Rev. B* **95**, 235119, [arXiv:1702.08469](#) (2017).
- [238] L. Fidkowski and A. Vishwanath, Realizing anomalous anyonic symmetries at the surfaces of 3d gauge theories, preprint, [arXiv:1511.01502](#) (2015).
- [239] L. Fidkowski, X. Chen, and A. Vishwanath, Non-abelian topological order on the surface of a 3d topological superconductor from an exactly solved model, *Phys. Rev. X* **3**, 041016, [arXiv:1305.5851](#) (2013).
- [240] F. J. Burnell, X. Chen, L. Fidkowski, and A. Vishwanath, Exactly soluble model of a three-dimensional symmetry-protected topological phase of bosons with surface topological order, *Phys. Rev. B* **90**, 245122, [arXiv:1302.7072](#) (2014).
- [241] X. Chen, F. J. Burnell, A. Vishwanath, and L. Fidkowski, Anomalous symmetry fractionalization and surface topological order, *Phys. Rev. X* **5**, 041013, [arXiv:1403.6491](#) (2015).
- [242] X. Chen, Z.-C. Gu, Z.-X. Liu, and X.-G. Wen, Symmetry-protected topological orders in interacting bosonic systems, *Science* **338**, 1604, [arXiv:1301.0861](#) (2012).
- [243] X. Chen, B. Zeng, Z.-C. Gu, I. L. Chuang, and X.-G. Wen, Tensor product representation of a topological ordered phase: Necessary symmetry conditions, *Phys. Rev. B* **82**, 165119, [arXiv:1003.1774](#) (2010).
- [244] S. K. Shukla, M. B. Şahinoğlu, F. Pollmann, and X. Chen, Boson condensation and instability in the tensor network representation of string-net states, preprint, [arXiv:1610.00608](#) (2016).

- [245] R. Thorngren and D. V. Else, Gauging spatial symmetries and the classification of topological crystalline phases, preprint, [arXiv:1612.00846](#) (2016).
- [246] K. Walker, Codimension-1 defects, categorified group actions, and condensing fermions, [talk at IPAM workshop](#) (Jan. 26-30, 2015).
- [247] L. Bhardwaj, D. Gaiotto, and A. Kapustin, State sum constructions of spin-tfts and string net constructions of fermionic phases of matter, [J. High Energy Phys.](#) **2017**, 96, [arXiv:1605.01640](#) (2017).
- [248] A. Kapustin and R. Thorngren, Fermionic spt phases in higher dimensions and bosonization, preprint, [arXiv:1701.08264](#) (2017).
- [249] Y. Wan and C. Wang, Fermion condensation and gapped domain walls in topological orders, [J. High Energy Phys.](#) **2017**, 172, [arXiv:1607.01388](#) (2017).
- [250] D. Gaiotto and A. Kapustin, Spin tqfts and fermionic phases of matter, [Int. J. Mod. Phys. A](#) **31**, 1645044, [arXiv:1505.05856](#) (2016).
- [251] N. Tarantino and L. Fidkowski, Discrete spin structures and commuting projector models for two-dimensional fermionic symmetry-protected topological phases, [Phys. Rev. B](#) **94**, 115115, [arXiv:1604.02145](#) (2016).
- [252] B. Ware, J. H. Son, M. Cheng, R. V. Mishmash, J. Alicea, and B. Bauer, Ising anyons in frustration-free majorana-dimer models, [Phys. Rev. B](#) **94**, 115127, [arXiv:1605.06125](#) (2016).
- [253] A. Kitaev and L. Kong, Models for gapped boundaries and domain walls, [Commun. Math. Phys.](#) **313**, 351, [arXiv:1104.5047](#) (2012).
- [254] D. J. Williamson and Z. Wang, Hamiltonian models for topological phases of matter in three spatial dimensions, [Ann. Phys.](#) **377**, 311, [arXiv:1606.07144](#) (2017).
- [255] M. Bärenz and J. Barrett, Dichromatic state sum models for four-manifolds from pivotal functors, preprint, [arXiv:1601.03580](#) (2016).
- [256] Y.-Z. You, Z. Bi, A. Rasmussen, K. Slagle, and C. Xu, Wave function and strange correlator of short-range entangled states, [Phys. Rev. Lett.](#) **112**, 247202, [arXiv:1312.0626](#) (2014).
- [257] X. G. Wen and Q. Niu, Ground-state degeneracy of the fractional quantum hall states in the presence of a random potential and on high-genus riemann surfaces, [Phys. Rev. B](#) **41**, 9377 (1990).
- [258] S. Bravyi, M. B. Hastings, and S. Michalakis, Topological quantum order: Stability under local perturbations, [Journal of Mathematical Physics](#) **51**, 093512, [arXiv:1001.0344](#) (2010).
- [259] J. C. Baez and J. Dolan, Higher-dimensional algebra and topological quantum field theory, [Journal of Mathematical Physics](#) **36**, 6073, [arXiv:q-alg/9503002](#) (1995).

- [260] R. M. Kashaev, On realizations of pachner moves in 4d, *J. Knot Theor. Ramif.* **24**, 1541002, [arXiv:1504.01979](#) (2015).
- [261] L. Crane, L. H. Kauffman, and D. N. Yetter, State-sum invariants of 4-manifolds, *J. Knot Theor. Ramif.* **06**, 177, [arXiv:hep-th/9409167](#) (1997).
- [262] J. S. Carter, L. H. Kauffman, and M. Saito, Structures and diagrammatics of four dimensional topological lattice field theories, *Adv. in Math.* **146**, 39, [arXiv:math/9806023](#) (1999).
- [263] L. Crane and I. B. Frenkel, Four-dimensional topological quantum field theory, hopf categories, and the canonical bases, *J. Math. Phys.* **35**, 5136, [arXiv:hep-th/9405183](#) (1994).
- [264] M. Mackaay, Finite groups, spherical 2-categories, and 4-manifold invariants, *Adv. in Math.* **153**, 353, [arXiv:math/9903003](#) (2000).
- [265] M. Mackaay, Spherical 2-categories and 4-manifold invariants, *Advances in Mathematics* **143**, 288, [arXiv:math/9805030](#) (1999).
- [266] A. Kapustin and R. Thorngren, Topological field theory on a lattice, discrete theta-angles and confinement, *Adv. Theor. Math. Phys.* **18**, 1233, [arXiv:1308.2926](#) (2014).
- [267] A. Hatcher, *Algebraic topology. 2002*, Vol. 606 (Cambridge UP, Cambridge).
- [268] U. Pachner, P.l. homeomorphic manifolds are equivalent by elementary shellings, *European J. Combin.* **12**, 129 (1991).
- [269] R. Koenig, G. Kuperberg, and B. W. Reichardt, Quantum computation with turaev–viro codes, *Ann. Phys.* **325**, 2707, [arXiv:1002.2816](#) (2010).
- [270] L. Fidkowski, M. Freedman, C. Nayak, K. Walker, and Z. Wang, From string nets to nonabelions, *Commun. Math. Phys.* **287**, 805, [arXiv:cond-mat/0610583](#) (2009).
- [271] M. Cheng, S. X. Cui, D. J. Williamson, and Z. Wang, In preparation .
- [272] M. H. Freedman, A. Kitaev, C. Nayak, J. K. Slingerland, K. Walker, and Z. Wang, Universal manifold pairings and positivity, *Geometry & Topology* **9**, 2303, [arXiv:math.GT/0503054](#) (2005).
- [273] G. Kuperberg, Involutory hopf algebras and 3-manifold invariants, *Int. J. Math.* **02**, 41, [arXiv:math/9201301](#) (1991).
- [274] M. H. Freedman and M. B. Hastings, Double semions in arbitrary dimension, *Commun. Math. Phys.* **347**, 389, [arXiv:1507.05676](#) (2016).
- [275] D. J. Williamson *et. al.*, In preparation .
- [276] M. Fukuma, S. Hosono, and H. Kawai, Lattice topological field theory in two dimensions, *Commun. Math. Phys.* **161**, 157, [arXiv:hep-th/9212154](#) (1994).
- [277] D. Birmingham and M. Rakowski, State sum models and simplicial cohomology, *Commun. Math. Phys.* **173**, 135, [arXiv:hep-th/9405108](#) (1995).

- [278] Y. Wan, J. C. Wang, and H. He, Twisted gauge theory model of topological phases in three dimensions, *Phys. Rev. B* **92**, 045101, [arXiv:1409.3216](#) (2015).
- [279] B. Yoshida, Topological phases with generalized global symmetries, *Phys. Rev. B* **93**, 155131, [arXiv:1508.03468](#) (2016).
- [280] J. W. Barrett and B. W. Westbury, The equality of 3-manifold invariants, *Math. Proc. Cambridge Philos. Soc.* **118**, 503–510, [arXiv:hep-th/9406019](#) (1995).
- [281] S. X. Cui and Z. Wang, State sum invariants of three manifolds from spherical multi-fusion categories, preprint, [arXiv:1702.07113](#) (2017).
- [282] B. Broda, Surgical invariants of four-manifolds, preprint, [arXiv:hep-th/9302092](#) (1993).
- [283] J. Roberts, Refined state-sum invariants of 3-and 4-manifolds, *Geometric Topology (Athens, GA, 1993)*, *AMS/IP Stud. Adv. Math.* **2**, 217 (1996).
- [284] J. PETIT, The dichromatic invariants of smooth 4-manifolds, *Global Journal of Pure and Applied Mathematics* **4** (2008).
- [285] J. Roberts, Skein theory and turaev-viro invariants, *Topology* **34**, 771 (1995).
- [286] J. Lurie, On the classification of topological field theories, *Current Developments in Mathematics* **2008**, 129, [arXiv:0905.0465](#) (2009).
- [287] L. Chang, M. Cheng, S. X. Cui, Y. Hu, W. Jin, R. Movassagh, P. Naaijken, Z. Wang, and A. Young, On enriching the levin–wen model with symmetry, *J. Phys. A* **48**, 12FT01, [arXiv:1412.6589](#) (2015).
- [288] N. Carqueville, C. Meusburger, and G. Schaumann, 3-dimensional defect tqfts and their tricategories, preprint, [arXiv:1603.01171](#) (2016).
- [289] B. Zeng and X.-G. Wen, Gapped quantum liquids and topological order, stochastic local transformations and emergence of unitarity, *Phys. Rev. B* **91**, 125121, [arXiv:1406.5090](#) (2015).
- [290] B. Yoshida, Exotic topological order in fractal spin liquids, *Phys. Rev. B* **88**, 125122, [arXiv:1302.6248](#) (2013).
- [291] H. Moradi and X.-G. Wen, Universal topological data for gapped quantum liquids in three dimensions and fusion algebra for non-abelian string excitations, *Phys. Rev. B* **91**, 075114, [arXiv:1404.4618](#) (2015).
- [292] J. Wang, X.-G. Wen, and S.-T. Yau, Quantum statistics and spacetime surgery, preprint, [arXiv:1602.05951](#) (2016).
- [293] S. Jiang, A. Mesaros, and Y. Ran, Generalized modular transformations in $(3 + 1)d$ topologically ordered phases and triple linking invariant of loop braiding, *Phys. Rev. X* **4**, 031048, [arXiv:1404.1062](#) (2014).
- [294] C. Wang and M. Levin, Braiding statistics of loop excitations in three dimensions, *Phys. Rev. Lett.* **113**, 080403, [arXiv:1403.7437](#) (2014).

- [295] C. Wang and M. Levin, Topological invariants for gauge theories and symmetry-protected topological phases, *Phys. Rev. B* **91**, 165119, [arXiv:1412.1781](#) (2015).
- [296] S. X. Cui, Z. Wang, and D. J. Williamson, In preparation .
- [297] P. W. Shor, in *Proceedings of 37th Conference on Foundations of Computer Science* (1996) pp. 56–65, [arXiv:quant-ph/9605011](#) .
- [298] J. Preskill, Reliable quantum computers, *P. Roy. Soc. Lond. A Mat.* **454**, 385, [arXiv:quant-ph/9705031](#) (1998).
- [299] L. Kong and X.-G. Wen, Braided fusion categories, gravitational anomalies, and the mathematical framework for topological orders in any dimensions, preprint, [arXiv:1405.5858](#) (2014).
- [300] F. Wilczek, Magnetic flux, angular momentum, and statistics, *Phys. Rev. Lett.* **48**, 1144 (1982).
- [301] F. Wilczek, Remarks on dyons, *Phys. Rev. Lett.* **48**, 1146 (1982).
- [302] V. G. Turaev, *Quantum invariants of knots and 3-manifolds*, Vol. 18 (Walter de Gruyter, 1994) [arXiv:hep-th/9409028](#) .
- [303] B. Yoshida, Classification of quantum phases and topology of logical operators in an exactly solved model of quantum codes, *Ann. Phys.* **326**, 15, january 2011 Special Issue, [arXiv:1007.4601](#) (2011).
- [304] H. Bombín, Structure of 2d topological stabilizer codes, *Commun. Math. Phys.* **327**, 387, [arXiv:1107.2707](#) (2014).
- [305] S. Bravyi and B. Terhal, A no-go theorem for a two-dimensional self-correcting quantum memory based on stabilizer codes, *New Journal of Physics* **11**, 043029, [arXiv:0810.1983](#) (2009).
- [306] H. Bombin, G. Duclos-Cianci, and D. Poulin, Universal topological phase of two-dimensional stabilizer codes, *New J. Phys.* **14**, 073048, [arXiv:1103.4606](#) (2012).
- [307] A. Kubica, B. Yoshida, and F. Pastawski, Unfolding the color code, *New J. Phys.* **17**, 083026, [arXiv:1503.02065](#) (2015).
- [308] C. G. Brell, A proposal for self-correcting stabilizer quantum memories in 3 dimensions (or slightly less), *New Journal of Physics* **18**, 013050, [arXiv:1411.7046](#) (2016).
- [309] S. Bravyi and J. Haah, Quantum self-correction in the 3d cubic code model, *Phys. Rev. Lett.* **111**, 200501, [arXiv:1112.3252](#) (2013).
- [310] B. J. Brown, D. Loss, J. K. Pachos, C. N. Self, and J. R. Wootton, Quantum memories at finite temperature, *Rev. Mod. Phys.* **88**, 045005, [arXiv:1411.6643](#) (2016).
- [311] J. Haah, Bifurcation in entanglement renormalization group flow of a gapped spin model, *Phys. Rev. B* **89**, 075119, [arXiv:1310.4507](#) (2014).

- [312] D. Gottesman, Stabilizer codes and quantum error correction, PhD thesis [arXiv:quant-ph/9705052](#) (1997).
- [313] J. Haah, *Lattice quantum codes and exotic topological phases of matter*, Ph.D. thesis, California Institute of Technology, [arXiv:1305.6973](#) (2013).
- [314] C. Chamon, Quantum glassiness in strongly correlated clean systems: An example of topological overprotection, *Phys. Rev. Lett.* **94**, 040402, [arXiv:0404182](#) (2005).
- [315] S. Bravyi, B. Leemhuis, and B. M. Terhal, Topological order in an exactly solvable 3d spin model, *Ann. Phys.* **326**, 839, [arXiv:1006.4871](#) (2011).
- [316] H. J. Briegel and R. Raussendorf, Persistent entanglement in arrays of interacting particles, *Phys. Rev. Lett.* **86**, 910, [arXiv:quant-ph/0004051](#) (2001).
- [317] A. Kitaev and C. Laumann, Topological phases and quantum computation, Exact Methods in Low-dimensional Statistical Physics and Quantum Computing: Lecture Notes of the Les Houches Summer School: Volume 89, July 2008 **89**, 101, [arXiv:0904.2771](#) (2010).
- [318] D. V. Else and C. Nayak, Cheshire charge in $(3+1)$ -d topological phases, preprint, [arXiv:1702.02148](#) (2017).
- [319] T. Lan, L. Kong, and X.-G. Wen, A classification of $(3+1)$ d bosonic topological orders (i): the case when point-like excitations are all bosons, preprint, [arXiv:1704.04221](#) (2017).
- [320] N. Bultinck, D. J. Williamson, J. Haegeman, and F. Verstraete, Fermionic projected entangled-pair states and topological phases, In preparation .
- [321] P. Hayden and J. Preskill, Black holes as mirrors: quantum information in random subsystems, *J. High Energy Phys.* **2007**, 120, [arXiv:0708.4025](#) (2007).
- [322] F. Pastawski, B. Yoshida, D. Harlow, and J. Preskill, Holographic quantum error-correcting codes: toy models for the bulk/boundary correspondence, *Journal of High Energy Physics* **2015**, 149, [arXiv:1503.06237](#) (2015).
- [323] A. Kitaev, <http://online.kitp.ucsb.edu/online/entangled15/kitaev/> (2015).

Lebenslauf

Persönliche Daten

Name: Dominic Joseph Williamson MSc
Geburtsdatum: 31. December 1990
Geburtsort: Westmead, Australia
Nationalität: Australian

Ausbildung und Tätigkeiten

09 / 2013 – 09 / 2017 PhD in Physics at the University of Vienna
03 / 2013 – 03 / 2014 Master of Science in Physics at the University of Sydney
03 / 2009 – 11 / 2012 Bachelor of Science (Honours) in Physics and Mathematics
at the University of Sydney
11 / 2008 Graduated from Baulkham Hills High School

Publikationsliste

- D. J. Williamson, N. Bultinck, J. Haegeman, & F. Verstraete,
Symmetry-enriched topological order in tensor networks: gauging and anyon condensation,
in preparation.
- N. Bultinck, D. J. Williamson, J. Haegeman, & F. Verstraete,
Fermionic projected entangled-pair states and topological phases,
in preparation.
- M. B. Sahinoglu, M. Walter & D. J. Williamson,
A tensor network framework for topological order in any dimension,
preprint, available at <https://sites.google.com/site/dominicjw/papers>.
- J. C. Bridgeman & D. J. Williamson,
Anomalies and entanglement renormalization,
submitted, [arXiv:1703.07782](https://arxiv.org/abs/1703.07782).
- N. Bultinck, D. J. Williamson, J. Haegeman, & F. Verstraete,
Fermionic matrix product states and one-dimensional topological phases,
[Phys. Rev. B **95**, 075108 \(2017\)](https://arxiv.org/abs/1610.07849), [arXiv:1610.07849](https://arxiv.org/abs/1610.07849).
- D. J. Williamson, N. Bultinck, J. Haegeman, & F. Verstraete,
Fermionic matrix product operators and topological phases of matter,
preprint, [arXiv:1609.02897](https://arxiv.org/abs/1609.02897).

- D. J. Williamson & Z. Wang,
Hamiltonian models for topological phases of matter in three spatial dimensions,
[Ann. Phys. **377**, 311–344 \(2016\)](#), [arXiv:1606.07144](#).
- D. J. Williamson,
Fractal symmetries: ungauging the cubic code,
[Phys. Rev. B **94**, 155128 \(2016\)](#), [arXiv:1603.05182](#).
- N. Bultinck, M. Mariën, D. J. Williamson, M. B. Sahinoglu, J. Haegeman, & F. Verstraete,
Anyons and matrix product operator algebras,
[Ann. Phys. **378**, 183–233 \(2017\)](#), [arXiv:1511.08090](#).
- D. J. Williamson, N. Bultinck, M. Mariën, M. B. Sahinoglu, J. Haegeman, & F. Verstraete,
Matrix product operators for symmetry-protected topological phases: gauging and edge theories,
[Phys. Rev. B **94**, 205150 \(2016\)](#), [arXiv:1412.5604](#).
- M. B. Sahinoglu, D. J. Williamson, N. Bultinck, M. Mariën, J. Haegeman, N. Schuch, & F. Verstraete,
Characterizing topological order with matrix product operators,
submitted, [arXiv:1409.2150](#).
- D. J. Williamson & S. D. Bartlett,
Symmetry-protected adiabatic quantum transistors,
[New J. Phys. **17**, 053019 \(2015\)](#), [arXiv:1408.3415](#).
- Y. Tyshetskiy, D. J. Williamson, R. Kompaneets, & S. V. Vladimirov,
Dispersion and damping of potential surface waves in a degenerate plasma,
[Phys. Plasmas **19**, 032102 \(2012\)](#), [arXiv:1111.6723](#).
- R. C. McPhedran, L. C. Botten, D. J. Williamson, & N.-A. P. Nicorovici,
The Riemann hypothesis and the zero distribution of angular lattice sums,
[Proc. R. Soc. A, **rspa20100566** \(2011\)](#), [arXiv:1007.4111](#).